- Oil and water -

Fibrous illite diagenesis and the onset of hydrocarbon charge in the petroleum systems of the Northern North Sea

Andrew James Cavanagh

Thesis submitted for the degree of Doctor of Philosophy

University of Edinburgh, May 2002

This thesis has been composed by myself and has not been submitted in any previous application for a degree. The work presented is my own except where acknowledged.

- Abstract -

Fibrous illite clay is common in deep-buried sandstones in the North Sea and other hydrocarbon basins. This clay, a poorly structured form of muscovite, and other types of illite exist in sandstones. However, the fibrous habit dramatically reduces sandstone permeability by factors of up to 10^5. This has a detrimental effect on oil recovery, and economics. Consequently, the nature of fibrous illite genesis has been much studied, though remains surprisingly unresolved.

A unique aspect of fibrous illite is the radiometric dating of K-Ar isotopes; the first North Sea application of this method by Sommer (1978), suggested a link of growth timing to hydrocarbon charge. Illite dating typically yields a single age for an individual oil field. The significance of such ages is controversial. Uniformitarian advocates propose a simple burial-temperature threshold, dependent on solute supply from feldspar dissolution. Catastrophist advocates propose episodic events associated with fluid changes in the basin, such as the arrival of porewater-displacing oil. Discriminating between opposing and entrenched arguments pertaining to a single data set has been the focus of the following thesis.

The set of all published illite data for the East Shetland Basin, Northern North Sea, was reviewed and plotted on a structural geographic base map. Fibrous illite growth clearly took place over a period spanning 70 Ma to 20 Ma. A simple regional pattern exists, with old 70 Ma ages near the deep graben, and young 20 Ma ages along the western and northern shallows of the basin terraces. This is consistent with the generally understood timing of oil charge for the region, based upon organic maturity modelling. The geographic pattern does not, however, in itself exclude the possibility of thermodynamic control. And yet no zero Ma ages have been observed: a phenomenon inconsistent with thermodynamic illite growth at the present day.

Anomalous ages of 90 Ma were reported from Magnus, on the northwest extremity of the basin, prompting a new study of illite diagenesis in the neighbouring Penguin field. This complex array of four hydrocarbon traps consists of a western flank genetically identical to the Upper Jurassic reservoir of the Magnus field, a central Triassic horst, and two Middle Jurassic traps on the fringe of the Brent province. The field is also juxtaposed between the petroleum systems of the Northern North Sea and Møre Basin. The Penguin illite ages are unusual relative to Magnus and the wider East Shetland Basin population. Ages range from 120 Ma to 30 Ma. Similar data elsewhere in the region has without exception been interpreted as an artefact of contamination resulting from disaggregation.

The Penguin clay separates appear to be of high quality after characterisation by XRD and TEM analysis. An alternative geological model is proposed to explain these unusual ages - fibrous illite diagenesis in the Penguin field records the onset of oil migration in local kitchen areas and deeper kitchen areas associated with the Atlantic Margins. The model is supported by oxygen and deuterium stable isotope data. East Shetland Basin illite ages are reinterpreted in light of this.

Two-dimensional basin models of a small petroleum system based on the geology of the Magnus and Penguin fields, province and local kitchen areas, examine this interpretation. A simple model, the Magnus model, supports the hypothesis that hydrocarbon charge controls the growth of fibrous illite within oil fields. A calibrated Magnus model is extrapolated to examine the likely critical moment of oil charge for the Viking Graben and Møre Basin. The Magnus model supports a simple geological explanation for the entire Northern North Sea data set, including the absence of zero-age illite.

Fibrous illite diagenesis records the critical moment of hydrocarbon charge to oil fields from local kitchen areas - a fundamentally catastrophic phenomenon. A modified formulation of Sommer's original hypothesis is presented. The implications of this robust and highly relevant model are considered in light of recent oil exploration on the Atlantic Margins. An equally significant outcome is the potential value of this method as a palaeocalibration tool for basin models.

Firstly, I wish to acknowledge Stuart Haszeldine for his generosity of spirit and deep scientific understanding, gifted as he is with an unusual mind as well as a mercurial ability to be both friend and mentor. It seems like only other postgraduates read these things nowadays. So, if he is your supervisor, take heart.

The thesis and my understanding of all things diagenetic have benefited greatly from discussions with Mark Wilkinson and Gavin England – two great sparring partners. Thank you both. And Gary Couples for introducing me to the curious world of basin modelling. Thanks also to the following -

The old school - Bill, Roddy and Big John. Mike Russell, Ian Allison and a pirate crew of postgrads, especially Dave and Chris, who remained a fine example and source of inspiration when things got tough. And the new school - John, Justin, Shane, Helena, Gordon and all the fine people at the Edinburgh University Geology department. It has been a pleasure.

SUERC, NERC and Shell UK for their funding, support and interest in the work.

To my fellow inmates, Em and Theo, Magnus, Chris, Ira, Noah, Pete, Matt and Rich.
It has been great fun getting to know you. Last one out, turn off the lights.

Thanks to Tez Sawicki for your sage insight and friendship. It has been a joy.
And to Susie Jackson, likewise. For helping to restore my health and peace of mind.

Holly, Yoshi and T'ai. Magic.

Heartfelt thanks to Mossina, Rob, Shelagh and Stephen. Amy, Maddy and Nico. Phil, Willow and Kay. And also to Ian Cameron, Tadeusz, Adrian, Andreas and Alex. For your warmth, generosity and encouragement.

The away crew - David, Allison, Neil, Nico, Matt, Wilson, Hilary and Peter. For a bunch of Scottish, American and French lunatics, you made a lot of sense to me.

The home crew - Wing, Paolo, Rob, Tim, Woody, Monica, Marina and Fuzzy. And their parents for tea, food, wisdom, and the occasional place to crash. And Louie, for some timely advice.

Lana Asfour, Hubert Berger, John Lapthorn, Mr Cobham, Jed Delaney, Robert and Barry Anderson.

Finally, thanks to my family. Mum and Dad, Simon and James, Helen and Sophie. For incredible reserves of strength, faith and love. Especially Mum and Dad for knowing a thing or two about qualifications. And for what it takes to hold station in adversity. Thank you for this. I couldn't have done it without you.

—

Just as a man serving a long sentence in prison will begin to live in despair about the time he recognises that the effort to keep his sanity is going to leave him less of a man, so a fighter goes through something like the same calculation. The prisoner or the fighter must give up some part of what is best in him, since what is best for any human is no more designed for prison – or training – than an animal for the zoo. Sooner or later the fighter recognises that something in his psyche is paying too much for the training. Boredom is not only deadening his personality but killing his soul.

Norman Mailer, The Fight

Illite diagenesis and petroleum systems
Rationale, aims and objectives of the research project

'Twas brillig, and the slithy toves
Did gyre and gimble in the wabe;
All mimsy were the borogoves,
And the mome raths outgrabe.

"It seems very pretty," she said when she had finished it,
"but it's rather hard to understand."

This chapter presents the rationale, underlying philosophy and initial aims and objectives of the Ph.D. The conflicting ideas and initial hypotheses that resulted in the final body of research are set out and followed by a brief overview of the work undertaken as emulated in the thesis structure.

Figures

1.0 Rationale

The quality of Jurassic sandstone reservoirs in the Northern North Sea is adversely affected by the presence of illite clay. Illite, as a diagenetic mineral, occurs in petroleum sandstone reservoirs. Authigenic illite is one of a suite of minerals that have been the focus of diagenetic studies related to basinal fluid evolution in the North Sea over the last decade (Brint *et al.* 1988; Glasmann *et al.* 1989, Bjorlykke *et al.*1992) which has built on earlier research by workers such as Sommer (1978), Kantorowicz (1984), Haszeldine *et al.* (1984), Liewig *et al.* (1987) and Hamilton *et al.* (1987). These are amongst the first detailed studies of diagenesis in the North Sea. Such minerals make up the cement fraction of reservoirs, and as such are of considerable interest to industry and academia alike, as they are both an important control on reservoir quality and related production economics, while signifying the burial and fluid-flow history of petroleum systems in this important resource region.

This thesis intends to augment the body of diagenetic research on the Northern North Sea by examining the relationship between authigenic illite, as occurring in Jurassic sandstone reservoirs of the East Shetland Basin, and conceptual models of basinal fluid flow, as pertaining to such reservoirs and their related petroleum systems – Figure 1.1.

1.1 Aims and Objectives

The five principle aims of this research project are as follows:

• to review the occurrence of illite in the Northern North Sea by compiling maps, cross-sections and stratigraphic compilations of illite age data available in the public domain for the East Shetland Basin, Viking Graben and Norwegian Shelf.

• to formulate hypotheses of illite growth mechanisms in Jurassic sandstone reservoirs of the East Shetland Basin by the analysis and synthesis of data collated in the review of the Northern North Sea

• to test the validity of predictions based on the Northern North Sea data synthesis by sampling and experimentally dating sandstone cores from the reservoir compartments of an East Shetland Basin oil field, namely the Penguin field.

• to examine rival hypotheses of illite formation for the Penguin oil field by two-dimensional mathematical modelling of the associated petroleum system, including the adjacent Magnus field.

• to synthesise the results of the petroleum system model, local experimental study, and regional data interpretation into an original conceptual model of the relationship between illite diagenesis and fluid flow history for the East Shetland Basin, Northern North Sea.

1.2 Context

The principal experimental laboratory method employed in this research project is K-Ar age dating of illite clay particles. In the context of this thesis, illite is defined as 'a non-expanding, dioctahedral, aluminous, potassium mica-like mineral which occurs in the clay-size fraction' (Srodon & Eberl, 1984), as extracted from sandstone reservoirs. The rare occurrence of smectite in the chosen study area, (Bjorlykke *et al.*, 1992), further limits the working definition to fibrous diagenetic illite crystallising out of solution onto a substrate of sandstone pore surfaces, consisting of the sand grain matrix and earlier cement phases. A succinct summary of the K-Ar age dating method can be found in Hamilton *et al.* (1989).

The principle experimental modelling method employed is built around commercial basin modelling software i.e. the BasinMod® 2-D code (Platte River Associates 1995). This sophisticated computational package is a means of integrating diverse information suites, in order to visualise likely basin scale dynamics, as a result of extrapolating or up-scaling from pore space observations and bore hole measurements to the regional systems apparent in seismic surveys.

Illite diagenesis

The fibrous habit of illite, combined with the common occurrence of the mineral in pore throats, is highly detrimental with regard to the fluid connectivity of the pore network. The fibres grow across pore throats, acting as a baffle, impeding the flow of solutes and hydrocarbons. This lowers the reservoir permeability by as much as an extraordinary four orders of magnitude i.e. in the region of one ten thousandth of the flow rate, and so acts as an important control on reservoir quality and production economics. Illite happens to be a potassium-aluminosilicate; as such it is of considerable interest to diagenetic researchers and petroleum geologists alike, as the unstable K-Ar system present in the crystal lattice provides a radiometric age. Questions arising from this detrimental effect on reservoir quality and experimentally amenable chemistry are as follows: what is the significance of the radiometric age? Is there a simple relationship between the timing of illite diagenesis and the dynamics of the petroleum system within which the fibres grow? Can an understanding of illite diagenesis help prediction of reservoir quality during exploration and appraisal? Resolving these questions depends on a classical geological division as outlined below.

Early work and opposing philosophies

Early work by Aronson & Burtner (1983) identified the potential this common reservoir cement offered in the elucidation of the relationship between the oil field diagenesis and the evolving petroleum system responsible for the accumulation of hydrocarbons. The interest this generated was due largely to the poor constraints on geological fluid flow dynamics. An interest that has evolved into a pressing need with the advent of sophisticated petroleum system simulations.

Whereas sequence stratigraphy and section balancing give reasonably accurate constraints on the basin dynamics of rock masses during the significant periods of hydrocarbon generation, migration and trapping, there are surprisingly few geological constraints on the subtle fluid flow history of petroleum basin evolution. As such, the strategic aim of many illite diagenesis studies has been to relate potassium-argon illite ages to specific events in petroleum systems – a fundamentally catastrophic approach.

The opposing uniformitarian lobby has sustained an argument that illite diagenesis is the result of closed-system, equilibrium chemistry in response to changing pressure and temperature with burial. In other words, that the apparent event associations of illite ages may in fact be nothing more than the signature of an uneventful chemical threshold for illite nucleation.

Two schools - three popular hypotheses

The above arguments can be summarised by three commonly held hypotheses for the significance of illite growth. One and two are not unrelated in respect to the underlying vision of illite genesis. The third hypothesis, however, is representative of a distinct and radically opposing school of thought.

- illite grows in response to large-scale changes in basin hydrodynamics.
- illite grows in response to the small scale phenomenon of reservoir oil charging.
- illite grows as a result of the interaction between pressure, temperature and solid-fluid chemistry, primarily driven by burial history.

The first two arguments are intrinsically fluid flow conceptual models, whereas the third is a chemical conceptual model independent of fluid flow considerations. The null hypothesis driving the research for this study, as stated below, is a formulation sympathetic to the fluid flow conceptual model.

The null hypothesis

Fibrous, pore-filling diagenetic illite, as found in oil fields, is fundamentally a response to shifts in regional hydrodynamics – specifically the onset of oil migration within the petroleum system. As such, K-Ar illite ages record the onset of oil charge to a trap structure.

Hypothesis testing

It is conceptually straightforward to test these rival hypotheses of fluid-flow dynamics and temperature dependant chemistry. The density of cored exploration and appraisal wells in the Northern North Sea have turned this industrial region into a fascinating natural laboratory – Figure 1.2. Indeed, a number of such studies have been made in the East Shetland Basin in the last twenty years (e.g. Hamilton *et al.* 1989). However, it has remained possible to infer the influence of either fluid flow or thermodynamic controls in each of these case studies.

1.3 Recent work and reservations

Recent investigations have served to illuminate the complexity of the relationship between diagenesis and petroleum systems (Wilkinson & Haszeldine 2002), with the hoped for causal links remaining ambiguous and conclusions parochial in their limitations to the immediate study area. This prompts the question, to what extent is the nature of the system intrinsically ambiguous? Is it apparent that the technical constraints of the experimental method play an important role in limiting the understanding of the true nature of the system? With regard to radiometric age-dating, the ever-present risk of sample contamination by potassium feldspars, mica and detrital illite, combined with the difficulty of quantifying resultant errors in age estimation have prompted both Fallick *et al.* (1998) and Liewig & Clauer (1998) to emphasise the need for experimental rigour when acquiring illite data and caution in application of already published data. The mitigating factors of contamination and related prevention strategies are discussed at length in chapter 4.

1.4 A regional study - criticism and apprehension

It is in this context of apprehension and criticism that the thesis reviews illite data available in the public domain, leading to an original interpretation of illite ages for the East Shetland Basin – Figure 1.3. This new synthesis of illite ages is used as a platform to consider currently held conceptual models of the relationship between oil field diagenesis and petroleum system dynamics, while questioning the reliability of published data in light of the experience of workers to date.

1.5 A complimentary experimental study

Numerous illite diagenesis studies have been published in their own right or as a part of multi-disciplinary studies of the East Shetland Basin over the last decade, the earliest by Sommer (1978) - Figure 1.4. Most of these studies have sampled Middle Jurassic Brent Group sandstones. However, the close juxtaposition of the Magnus oil field to the Penguin structure, allied with the wide representation of stratigraphic and structural traps contained within the Penguin structure - Triassic, Middle Jurassic and Upper Jurassic, horst, half graben and onlap - makes the Penguin an ideal candidate for extending the investigation of the Magnus diagenetic system to the east, while also acting as a bridging study between the phenomenon of illite diagenesis in the Upper Jurassic turbidite sandstone reservoirs of the Magnus province and the ubiquitous Middle Jurassic sandstone reservoirs associated with the deltaic sediments of the Brent province – Figure 1.5.

The thesis presents new isotopic data for authigenic illite from the Penguin structure, Northern North Sea. The Penguin study is similar to other illite diagenetic investigations published for the North Sea - for instance, Darby *et al.* (1997); Hogg *et al.* (1993); Glassman *et al.* (1989) and the original paper, Sommer (1975). However, the study area is a valid addition to previous generic studies due to the diverse nature of the structural and stratigraphic traps that make up the Penguin accumulation.

1.6 Conceptual and mathematical modelling

The regional review and parochial experimental study are used as a basis for the selection and construction of a small size-scale conceptual model of a petroleum system within the Northern North Sea: the Magnus model. Similar modelling scenarios have been used by workers such as Swarbrick (1994), Darby *et al.* (1996, 1998) and Fleming (1998) to investigate aspects of basinal fluid evolution throughout the North Sea. It is in this context that the thesis presents a conceptual model driven by a mathematical engine, BasinMod® 2-D (Platte River Associates 1995), comparing simulations of fluid flow evolution with illite age data for the Magnus oil field. The model is used to critique two independent diagenetic studies of the Magnus oil field by Macaulay *et al.* (1992, 1993) and Emery *et al.* (1990) and recent work by Barclay *et al.* (2000), as well as new data for the Penguin oil field presented for the first time in this thesis.

1.7 A new synthesis

The findings of the regional review, Penguin study and Magnus models form the basis for an original interpretation of the relationship between illite diagenesis and petroleum systems of the Northern North Sea. This synthesis is discussed in the context of relevant diagenetic and modelling studies already published for the East Shetland Basin (Hogg *et al.* 1993; Wilkinson *et al.* 1997; Fallick *et al.* 1998; Worden *et al.* 1998), while citing recent work on the influences of the Early Cretaceous North Atlantic opening on the Northern North Sea as expounded by Doré (1991), Booth *et al.* (1992) and Barclay *et al.* (2000), and significant diagenetic and modelling studies representative of the Central North Sea (Zeigler *et al.* 1994; Darby *et al.* 1996, 1997, 1998). The thesis ends with a review of the aims set out in this chapter and a discussion of the significance of illite diagenesis in light of the evidence presented below. A brief suggestion for further work arising concludes the study.

1.8 Structure of the thesis

The six chapters that follow describe the background, regional review, experimental study, modelling and synthesis of the results of this research project respectively. The rationale, aims and objectives of the work are outlined above. The thesis structure emulates the project development.

• Chapter one presents the rationale, underlying philosophy and initial aims and objectives of the study. The conflicting ideas and initial hypotheses that resulted in the final body of research are set out and a simple null hypothesis stated. This is followed by a brief overview of the work undertaken as emulated in the thesis structure.

• Chapter two reviews the geological and conceptual framework to diagenetic and modelling studies of the Northern North Sea from a selection of the background literature, in order to provide the reader with a robust context in which to place the work presented in the following chapters.

• Chapter three presents an original synthesis and interpretation of illite age data for the East Shetland Basin, Northern North Sea, from a regional review of published diagenetic studies.

• Chapter four presents the results of an original experimental study of the Penguin oil field, Northern North Sea i.e. isotopic data for illite samples extracted from cored sections of the Penguin reservoir intervals. This new data set is interpreted in light of the regional study outlined in chapter three and forms the basis of a comparative data set for the modelling study outlined in chapter five.

• Chapter five presents conceptual and mathematical models of the Magnus oil field and related petroleum system, Northern North Sea, which examine a hypothesis of illite diagenesis and fluid flow formulated as a result of the work discussed in chapter three.

• Chapter six presents an alternative and ultimately unsustainable hypothesis for unusually early illite diagenesis in the Penguin field area. This antithesis to the open system formulation of the null hypothesis is dependent on a highly unorthodox interpretation of the Penguin B horst structure.

• Chapter seven presents a new regional framework for the relationship between basinal fluid flow and illite diagenesis in sandstone reservoirs of the Northern North Sea, incorporating the implications of the experimental, modelling and regional studies outlined in chapters five, four and three respectively. The thesis closes with a review of aims and consideration of further work arising from the project.

1.9 Summary

In summary, the thesis combines a well proven approach to illite diagenesis with sophisticated basin model simulations in order to address the parochial and provisional findings of similar studies in the Northern North Sea region. Illite studies pertaining to the East Shetland Basin are reviewed, and simple predictions made relating to the simple null hypothesis formulation presented in chapter one. As a consequence of this review, the Magnus and Penguin oil fields are chosen as the best candidates for further investigation, and as such, form the crucible for laboratory and modelling studies related to illite diagenesis and petroleum system dynamics. The resultant data appears to thoroughly test the null hypothesis and drives a new conceptual model for illite diagenesis, which is found to be applicable to both the Brent and Magnus provinces of the East Shetland Basin region, as well as implying unusual exploration scenarios for basins out-with the Northern North Sea paradigm.

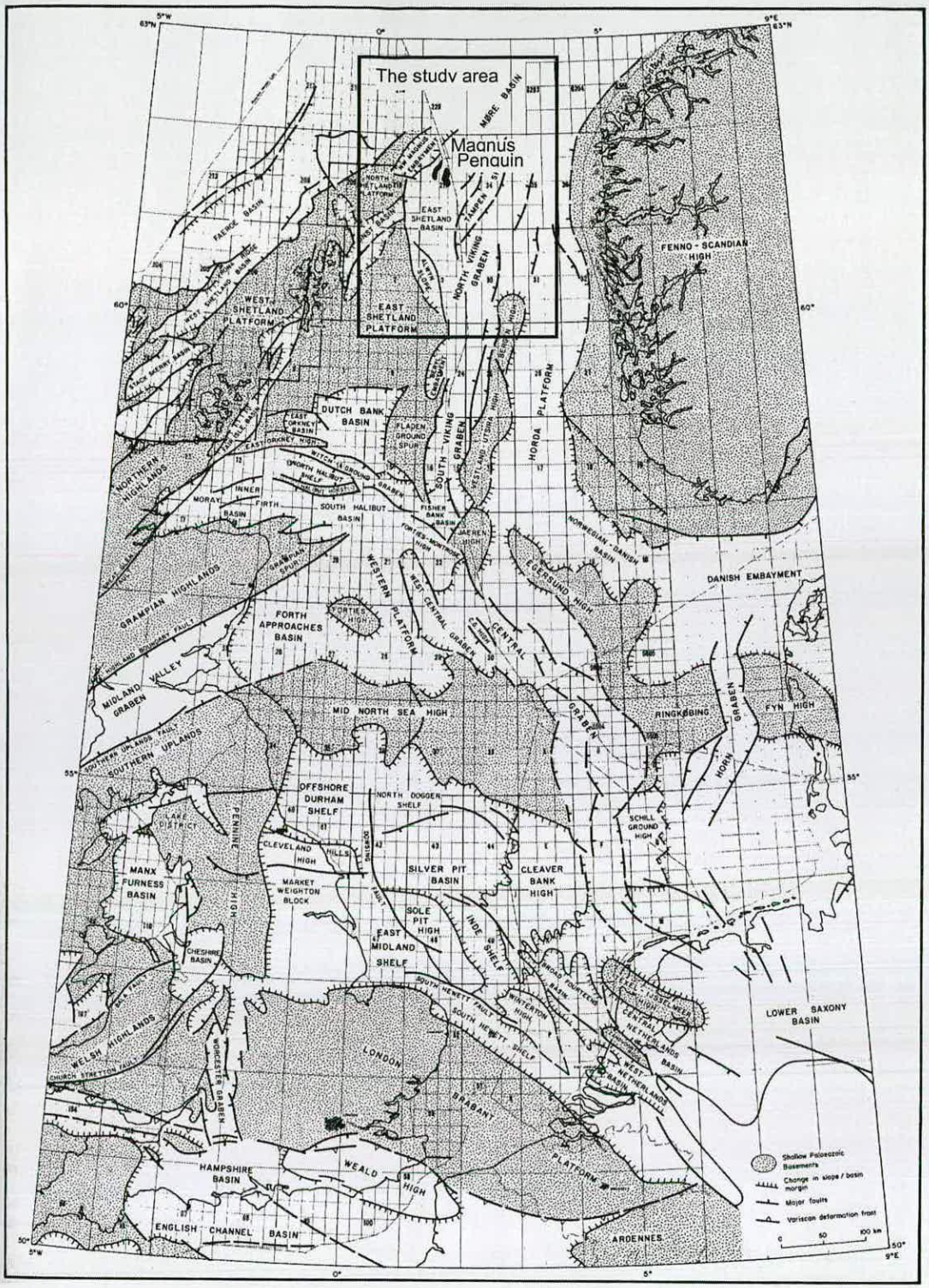

Figure 1.1 The principal hydrocarbon basins of the North Sea. The area of the Northern North Sea related to this study is highlighted, placing the size of the study in context with respect to the vast North West European tableaux of prospective basins, including the emergent plays of the Atlantic Margins (after Brennand *et al.* 1990).

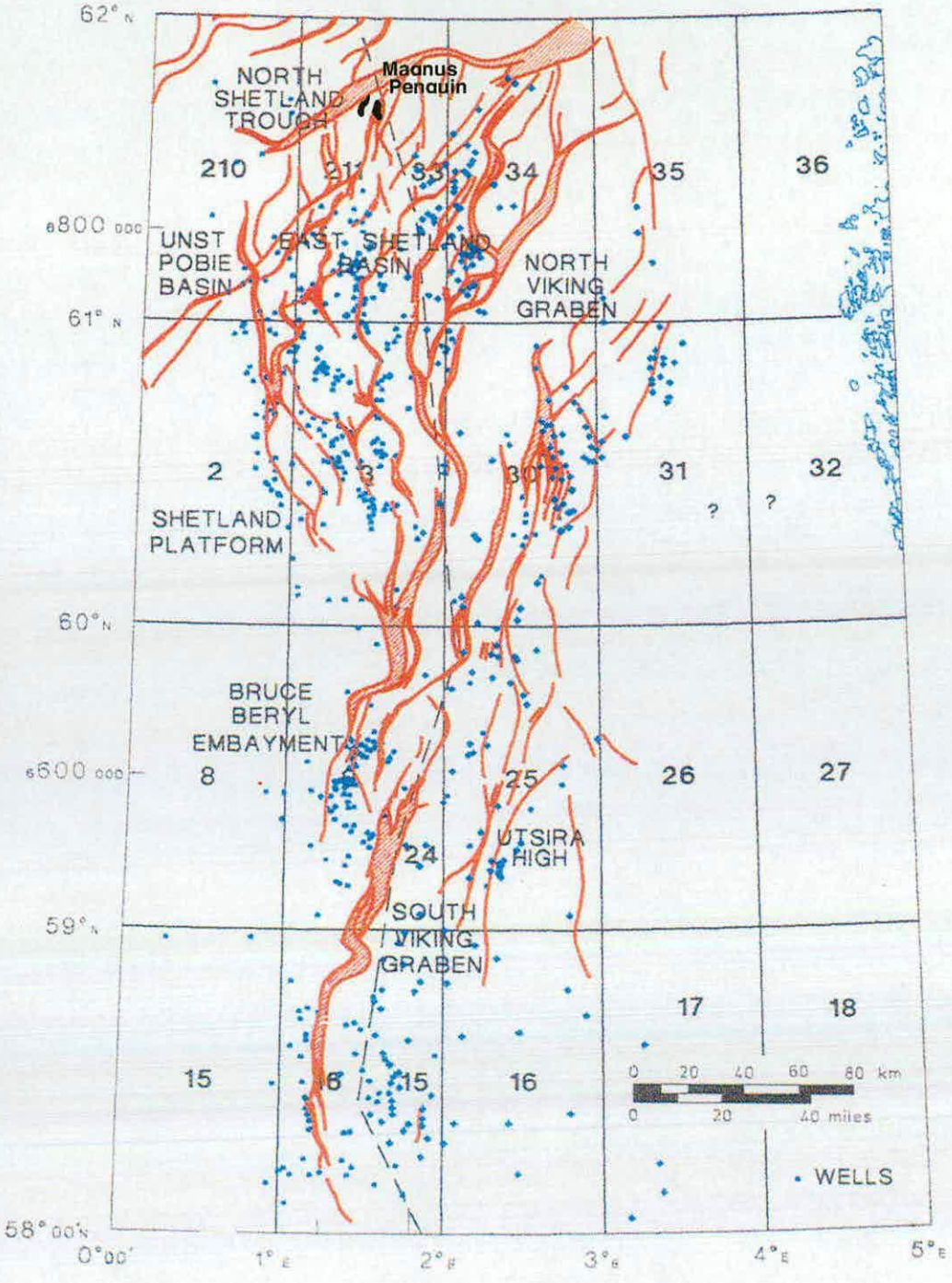

Figure 1.2 Exploration and appraisal well database for petroleum regions in the Northern North Sea province. Note the high density of wells on the East Shetland Basin and Troll terraces relative to the deep areas of the Viking Graben and North Shetland Trough (after Mitchener *et al.* 1992).

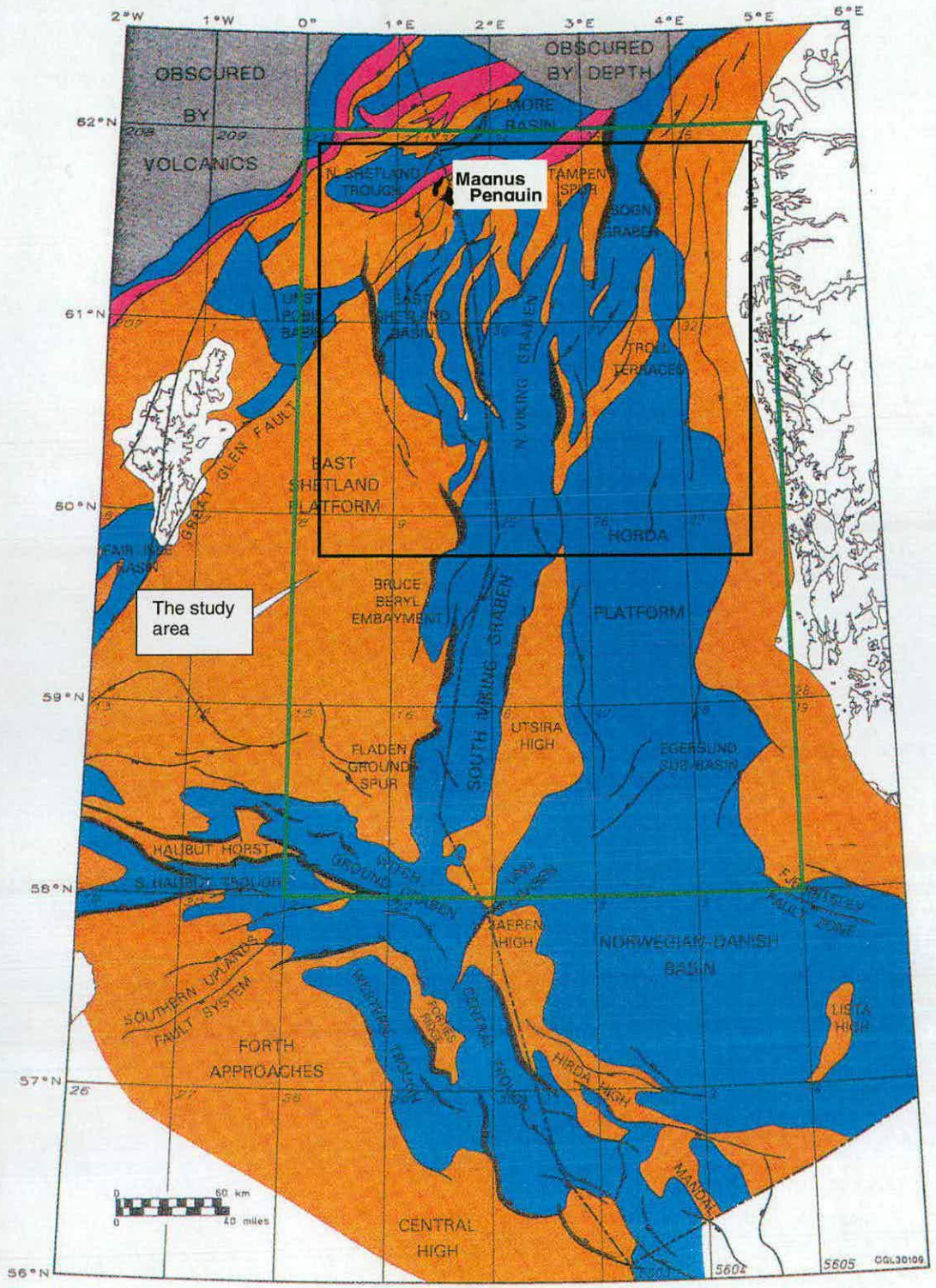

Figure 1.3 The Northern North Sea, highlighted in green. The study area, consisting of the East Shetland Basin, North Viking Graben and Troll Terraces, is highlighted in black, and the principle tectonic elements shown in colour. Black scarps are Mesozoic North Sea features. Red scarps are associated with a later post-Jurassic generation of faulting along the northern boundary of the East Shetland Basin related to the North Atlantic extension (after Mitchener *et al.* 1992).

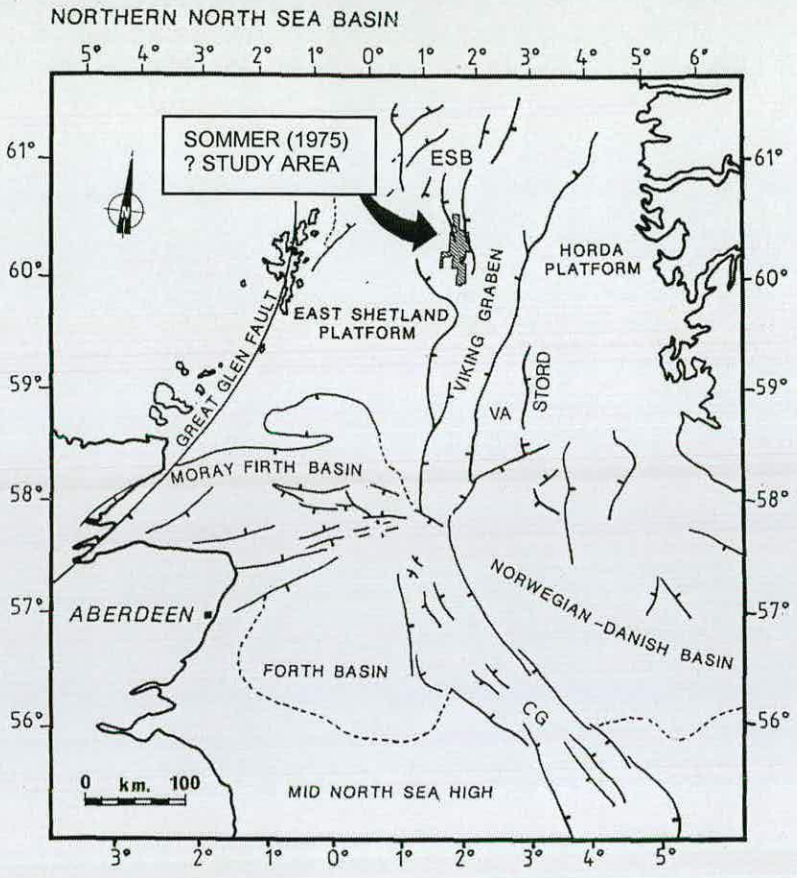

Figure 1.4 The Alwyn field, Northern North Sea - the area of the East Shetland Basin most likely to have been the origin of Sommer's original findings (Sommer 1975), and the subject of two further studies involving the Frenchman (after Hogg *et al.* 1992).

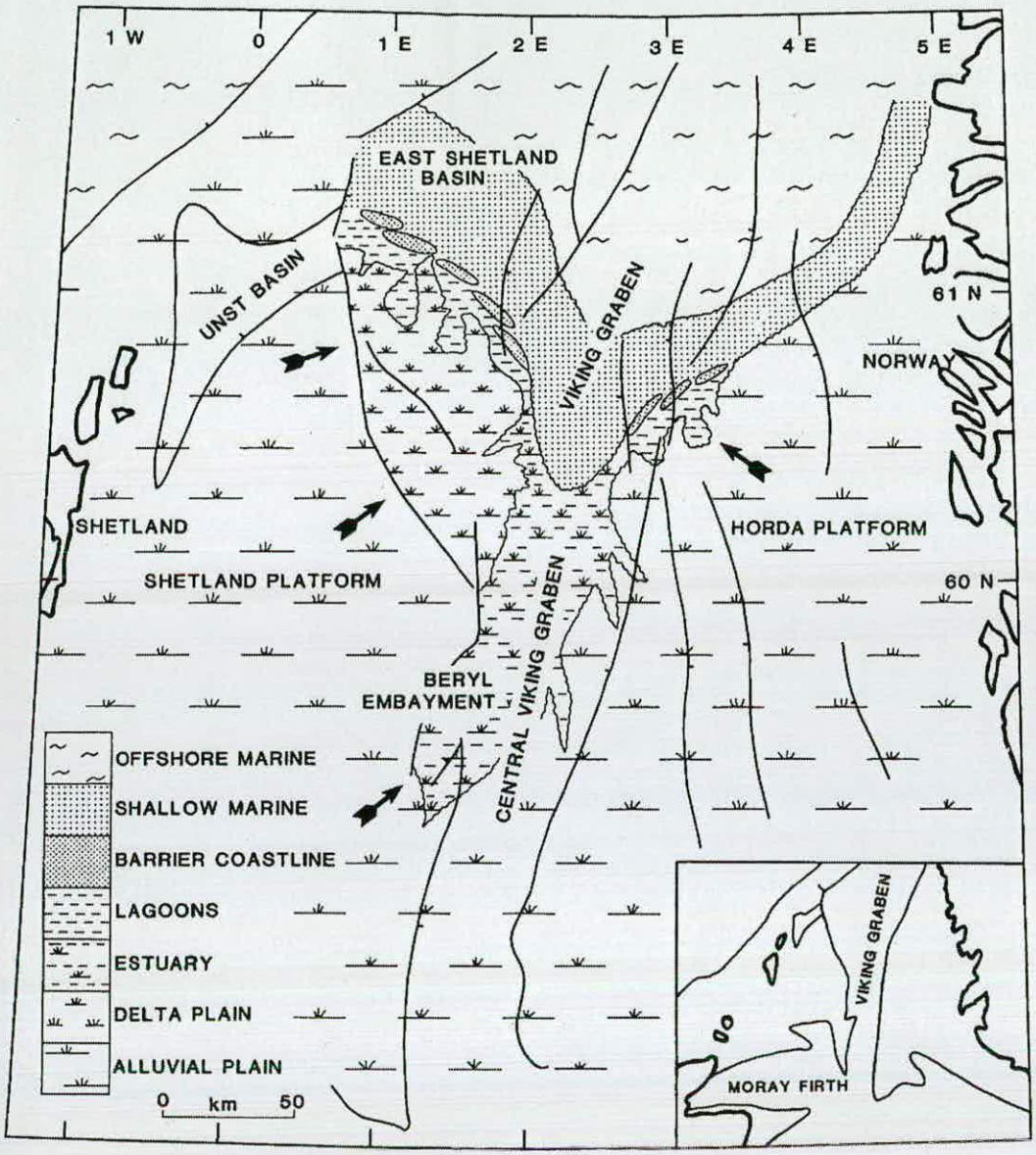

Figure 1.5 The Brent delta – a simple palaeogeographic model of deposition during the Aalenian to earliest Bajocian, prior to maximum progradation. While the model is in accord with the generally accepted view of Central North Sea doming as the background to delta progradation., the local topography is seen as a significant control on facies thickness and distribution (after Richards 1992).

A literature review

Geological, diagenetic and modelling studies of the Northern North Sea

nothing, neither among the elements nor within the system,
is anywhere ever simply present or absent; there are only,
everywhere, differences and traces of traces

This chapter reviews the geological and conceptual framework of diagenetic and modelling studies in the Northern North Sea, from a selection of the background literature, to provide the reader with a robust context in which to place work presented in the following chapters.

Figures

2.0 A Selective review of three topics

The regional scope and multidisciplinary nature of the study presented in this thesis requires a broad context for the general reader. The following review is selective and restricted to areas of petroleum geology, diagenesis and basin modelling relevant to the work in the following chapters.

Petroleum Geology - the petroleum geology of the study area is described in relation to the structural style and sedimentary-tectonic evolution of the Northern North Sea. A widely accepted model for petroleum systems is presented and complications in the style of trapping are considered.

Diagenesis - the diagenetic evolution of Northern North Sea Jurassic sandstone reservoirs is outlined, and a more detailed consideration of illite diagenesis is given within this context.

Modelling - a short review of basin modelling studies undertaken in the North Sea is presented and discussed with regard to important aspects of modelling studies. The modelling software chosen for this study is discussed in this context.

2.1 Petroleum Geology of the Northern North Sea

The Northern North Sea is a component of the larger North Sea rift system - Figure 2.1. The North Sea region is comprehensively reviewed by Glennie (1990, 1998). A general review of the relationship between the structural styles of the North Sea and hydrocarbon habitats has been undertaken by Spencer & Larsen (1990) and related kinematic models for the North Sea rift system are discussed by Roberts *et al.* (1993). A synopsis of this work in the context of the thesis is presented below.

The Northern North Sea

Chapter one defined the Northern North Sea province as the area between 58°N and 62°N, 0°E and 5°E i.e from the Jaeren High to the Møre Basin, after Mitchener *et al.* (1992) – Chapter 1, Figure 1.2. The petroleum geology of the Northern North Sea is distinct from that of the Central North Sea, as Late Proterozoic- Early Palaeozoic structural differences in the substratum of the two regions have controlled the differential deposition of Mesozoic source and reservoir sediments and subsequent structural evolution. Elements of the structural style and tectonic evolution specific to the Northern North Sea have also controlled the later timing of maturation, migration, trap formation and seal integrity in the area during the Late Mesozoic and Cenozoic eras.

Rattey & Hayward (1993) suggest the southern boundary of the Northern North Sea is equivalent to the speculated southern boundary of the Caledonian basement along an arcuate lineament, which includes the Tornquist Line and Fjerritslev fault zone. The northern boundary of the Northern North Sea and East Shetland Basin Sea is marked abruptly by the 'End of the World' fault – Figure 2.1. The

North Shetland Trough, Møre Basin and Atlantic Margins to the north of this fault are indicative of a profound change in the tectonic stress regime of the area. During the Late Jurassic to Early Cretaceous, the focus of rifting leapt west from the failed North Sea axis to the embryonic North Atlantic opening.

The resultant hydrocarbon habitats of the Northern North Sea are dominated by clean sandstone sequences associated with Permian and Triassic continental environments, Lower-Middle Jurassic coastal deltas and Upper Jurassic submarine turbidites. The abundant, high-quality reservoir rocks are augmented by the ubiquitous Kimmeridge Clay Formation source rock – principally a result of massive algal blooms in the surface currents of seas that encroached the area during the onset of post-rift subsidence during the Late Jurassic. The segmentation of the widespread sandstone units into gently dipping fault blocks with steep footwall terminations during the Late Jurassic, associated turbidite deposition, and subsequent burial under thick sequences of Cretaceous mudstones resulted in ideal trap and seal conditions. Together, these factors contributed to the Northern North Sea as an economically significant global hydrocarbon province numbering over 110 discoveries, with the greatest accumulation of oil occurring on the terraces of the East Shetland Basin - Figure 2.2.

The East Shetland Basin

The East Shetland Basin is a Mesozoic extensional feature, with predominantly north-northeast trending westerly-dipping fault blocks, typical of the region. The principal play, with over 75% of finds, occurs in the pre-rift Triassic-Middle Jurassic reservoirs that make up the Brent province. A smaller syn-rift play, the Magnus province, occurs in Upper Jurassic reservoirs on the northern edge of the East Shetland Basin. A post-rift play occurs in Paleogene sands to the south of the area, and at present the exploration challenge is on increasingly more subtle traps in this mature province (Spencer *et al.* 1999). The reader is referred to a recent review by Knag *et al.* (1995) for a more in-depth discussion.

The sedimentary and tectonic evolution of the region is widely accepted as consisting of two failed rifting events: the first phase during the Permian-Triassic; the second phase during the Late Jurassic-earliest Cretaceous. Subsequent subsidence and thick post-rift sedimentation during the Mesozoic and Cainozoic completes the basin evolution - Figure 2.3. A wealth of 3-D seismic surveys, integrated stratigraphic well data, core analysis and associated literature for the east Shetland Basin contribute to an information archive on one of the most intensively studied regions of the earth's sub-surface.

Pre-Mesozoic geology

However, even in this intensively studied area there are many persistent gaps in understanding related to the Pre-Mesozoic geology. The depth to pre-Mesozoic sediments is about 7 km in the Viking Graben (Hospers & Ediriweera 1991), decreasing to about 3 km in areas of the East Shetland Basin, yet there are few well penetrations as the basement is of little economic interest. What is inferred

about the pre-Mesozoic geology of the region is mostly reliant on the reasonable assumption that outcrop exposures on the northern Scottish mainland and south-east Scandinavian mainland are a direct analogue of the East Shetland Basin basement (Klemperer 1988).

It is assumed therefore that the oldest crustal basements associated with East Shetland Basin geology are remnants of the Iapetus margins of Baltica and Laurentia (Andersen 1991), i.e. Precambrian meta-sedimentary and igneous allochthons and terranes, typical of pre-Caledonian poly-deformation of which the last episode occurred during the Grenville Orogeny (Coward 1990). These deep crustal elements were sutured by diachronous, oblique and orthogonal collision during the Caledonian Orogeny, resulting in an estimated 500 kilometres of crustal shortening (Hossack & Cooper 1986) and a distinct regional north-east grain.

The Caledonian north-east grain of the region has been identified in Northern North Sea basement by deep seismic reflection profiles (e.g. Beach *et al.*1987). This is thought to combine with the north-westerly Tornquist trend, controlling the primary structural grain (Rattey & Hayward 1993). Intermontane basin formation under Caledonian structural control during the Devonian orogenic collapse (Glennie 1998) is likely to have been the first significant episode of sedimentary deposition in the region. The Variscan orogeny and related Carboniferous inversion of Devonian basins along northeast-southwest Caledonian faults (Roberts *et al.* 1999) is thought to have removed much of the Devonian sediment. Hence, the first significant occurrence of reservoir units in the region is associated with Permian stability and an expansion of the North Permian Basin (Ziegler 1982). The onset of Late Permian – Early Triassic rifting marks the beginning of the common currency in the understanding of East Shetland Basin geology.

Mesozoic geology

Two artefacts of pre-existing compressional basement structural evolution controlled failure of the East Shetland Basin during the Mesozoic rifting phases: Caledonian northeast-southwest and north-south lineaments; and Variscan east-west lineaments (Lee & Hwang 1993). The Viking Graben had undergone two cycles of rifting and quiescence by the Ryazanian (Rattey & Hayward 1993). Lithospheric failure and stress relief eventually transferred to the west with the advent of North Atlantic opening during the earliest Cretaceous – Figure 2.4.

Rifting phase I comprises of Late Palaeozoic and Early Mesozoic extension. The dynamics of rift I are poorly constrained for the East Shetland Basin due to the overprint of Late Jurassic extension (Lervik *et al.* 1989). However, regional evidence for a basal Triassic unconformity indicates Late Permian extension, followed by a shift from marine to continental conditions during the Early Triassic with the advent of red beds (Roberts *et al.* 1993). Backstripping estimates of ß value for the event vary from 1.05 (White 1989) to 1.4 (Roberts *et al.* 1993) for the East Shetland Basin.

Post-rifting thermal subsidence, sag and drowning occur from the Middle Triassic onwards with continental strata passing into the coastal Banks Group. Triassic to Early Jurassic lithostratigraphy has recently been revised by Richards *et al.* (1993). The drowning theme continues into the Lower Jurassic with the marine Dunlin Group indicating base level fluctuations (Steel 1993) and Middle Jurassic Brent Group sediments thickening into the Viking Graben (Yielding *et al.* 1992).

The first motions of rift II (Yielding *et al.* 1992) are marked by the top of the Dunlin Group at the end of the Toarcian (Partington *et al.* 1993). Prior to extension, a general base level shallowing occurs with a shift from marine to deltaic environments as the North Sea thermal dome develops to the south (Underhill & Partington 1993). This accounts for thickness fluctuations of Brent Group units across major faults, prior to rifting (Richards *et al.* 1988; Badley *et al.* 1988), as the Brent delta progrades north during the Middle Jurassic, depositing a diachronous sequence of fan delta, shoreface, back barrier and delta plain sediments (Budding and Inglin 1981).

The second rift, stratigraphically constrained in the East Shetland Basin to onset in Late Bajocian and cessation in Early Ryazanian (Mitchener *et al.* 1992; Partington *et al.* 1993), actively controlled sedimentation as a function of extension from the Tarbert Formation onwards (Mitchener *et al.* 1992). Syn-rift Tarbert Formation and Humber Group deposits are found in hanging wall basins (Badley *et al.* 1988), with the characteristic half graben geometry of cantilever fault blocks, as preserved below Cretaceous-Tertiary-Quaternary post-rift cover - Figure 2.5. Debate over quantification of rift II extension continues. Roberts *et al.* (1995) estimates a ß factor of around 1.15 for the East Shetland Basin, placing Late Jurassic extension on a par with the earlier Triassic rift event, in contrast to earlier modelling estimates by White (1989) and White & Latin (1993).

The Early Cretaceous saw an end to active extension in the East Shetland Basin, (Badley *et al.* 1988; Rattey & Hayward 1993), the last episode of which was confined to Magnus province, in response to the new regime affecting the Møre Basin and emergent Atlantic Margins – Figure 2.4. The Northern North Sea entered the subsidence phase of thinned continental lithosphere i.e. slow flexure in response to thermal cooling and sediment loading (Marsden *et al.* 1990). Approximately 3.5 km of marls, chalks and clastics accumulated with a typical 'Steer's head' geometry in accordance with lithospheric models devised by White & McKenzie (1988) – Figure 2.5. Rapid subsidence outpaced sedimentation (Bertram & Milton 1989) throughout the Cretaceous, as the eustatic sea level rose (Haq *et al.* 1987), maintaining deep-water conditions. Normal faulting where present is planar, non-extensional, and above existing basement anisotropies (Badley *et al.* 1988).

Cainozoic geology

The general background subsidence continued throughout the Tertiary with a brief episode of volcanism and associated thermal bulge during the Paleocene. Forward and reverse subsidence history modelling (Joy 1992) indicates departure from the McKenzie (1978) model of thermal subsidence. A

transient uplift appears to be superimposed on the background (Nadin & Kuznir 1995). Dynamic support of the lithosphere during the Paleocene by the Icelandic plume to north west (Brodie & White 1994; Nadin *et al.* 1995) has been proposed to explain the anomaly. This appears to have been followed by rapid subsidence and flooding during the Eocene (Bertram & Milton 1989). With the exception of this Early Tertiary curiosity, uneventful subsidence has continued up to the present day, presumably driven by sediment loading, compaction, and a component of thermal decay associated with underplated crustal cooling.

2.2 Petroleum systems of the Northern North Sea

System analysis of petroleum provinces has become increasingly popular in the last two decades. Essentially the elements alluded to below - source area, migration pathway, reservoir, trap and seal, have been understood as co-dependent for much of the last century. The shift in emphasis with a systems approach is towards a more dynamic process-based understanding, largely as a consequence of powerful computer applications and related visualisation techniques such as modelling, 3-D seismic surveys and real-time well data processing.

> *'A petroleum system is a natural system that encompasses a pod of active source rock and all the related oil and gas and which includes all the geological elements and processes that are essential if a hydrocarbon accumulation is to exist' (Magoon & Dow 1994).*

The East Shetland Basin is not a petroleum system, but rather a discrete region within the Northern North Sea petroleum province. The province itself, though often discussed in terms of a petroleum system driven by the Viking Graben kitchen area, encompasses considerable complexity and diversity within its boundaries, the consequence of a number of interacting systems. The following passages describe the petroleum geology of the East Shetland Basin and the basic elements of the petroleum systems active in the region.

Source rock – all significant hydrocarbon accumulations in the East Shetland Basin are believed to be a result of organic maturation within the predominant source rock in the region i.e the Kimmeridge Clay Formation shale of the Upper Jurassic and Ryazanian (Glennie 1998). A prolific oil shale with a total organic carbon content (TOC) somewhere between 5 % and 10%, consisting of type II kerogen, Kimmeridgian shale underwrites the petroleum systems of the Northern North Sea. Locally, the Lower Cretaceous Cromer Knoll Group has been found to reach the much lower TOC value of 1% and appears to be gas prone (Kirk 1980). However, it is generally accepted that condensates as they occur in areas of the Northern North Sea are the result of late-mature generation from the abundant Kimmeridgian shales (Glennie 1998).

Generation – the principle phase of oil generation takes place at temperatures around 70°C to 100°C. Assuming an average geothermal gradient, the oil window occurs over a depth of 2 km - 3.5 km (Tucker 1991). With an uneventful post-rift burial history for the region, generation in deeply buried sub-basins potentially occurred from the Late Cretaceous onwards, passing into a late-mature gas-prone phase in deep areas of the graben during the Early Tertiary. However, a commonly held perception of the region is that the onset of widespread oil generation did not occur until the Eocene, with significant gas generation limited to the Neogene onwards (Goff 1983; Pegrum & Spencer 1991). The typical hydrocarbon associated with Northern North Sea kitchen areas is a low-sulphur, medium gravity, naptheno-paraffinic oil, 34°-38° API (Cornford 1990).

Migration – the abundance of a single source rock, the prevalence of the same source rock in a number of active kitchen areas, and the diverse potential migration pathways laterally and vertically through sandstones and along faults, has left the mapping of secondary migration and related assignation of specific kitchen areas to accumulations a subtle and elusive quarry. It seems that sophisticated tracer geochemistry may yet resolve the problem (Larter *et al.* 1997, 2000). However, at present there is considerable ambiguity as to the distance over which hydrocarbons migrate in the east Shetland Basin. Additionally, it is difficult to ascertain whether or not oils are sourced directly from kitchen areas or arrive via fill-spill pathways and episodes of residence in other trap structures.

Reservoir – The host strata for East Shetland Basin hydrocarbon accumulations are Mesozoic sedimentary rocks. Significant volumes occur in the pre-rift II play: Triassic sandstones and the high quality Lower to Middle Jurassic reservoirs of the Brent Group. Syn-rift II turbidites also provide excellent reservoirs in the Late Jurassic.

Trap – the simplest trap structures in the East Shetland Basin are typically a combination of fault blocks and related unconformities, as a result of an erosional surface developing with footwall emergence during the Late Jurassic –Early Cretaceous rifting event. The largest accumulations, such as the Brent field, were quickly identified and targeted by this simple configuration. As the production from these giant fields begins to ebb, considerable effort has been directed towards the identification of by-passed oil within fields, and subtle traps such as downfaulted compartments, as well as uniquely stratigraphic traps such as Upper Jurassic submarine fan complexes and hanging wall sedimentation pods (Davies *et al.* 1999).

Seal – the Mesozoic trap structures of the East Shetland Basin are stratigraphically followed by the thick accumulations of Cretaceous mudstones, siltstones and shale. While it is difficult to precisely quantify the vertical permeability of these important seal lithologies, their effectiveness is empirically established by the presence of significant hydrocarbon columns - 98 meters of gas and 146 meters of oil in the case of the Brent field – and the absence of a viable alternative seal.

These elements and their interplay contribute to the dynamics of the petroleum system; the timing of generation, charging and trapping; the basin heat flow, pressure regime and burial history - all interact with reservoir sandstones, altering the diagenetic evolution of oil fields, leaving traces of their ebb and flow.

2.3 Oil field diagenesis

Reservoir sandstone diagenesis has been the subject of intense study over the last twenty years as the need for conceptual and quantitative understanding of reservoir quality to predict porosity and permeability has grown with the advent of predictive modelling. Sampling tends to be limited to cored intervals, often biasing studies towards the most productive units of reservoir sandstone bodies. Standard petrographic techniques (optical thin section, SEM and XRD) are often supplemented by isotopic analysis of whole rock and separate fractions.

Despite the large body of research in recent years, as Haszeldine *et al.* (2000) point out, there has been surprisingly little resolution of the differing and apparently fixed viewpoints held by distinct academic camps. In part, this is due to the complexity and range of natural cementation patterns found in sandstones and their distant, implicit indication of porefluid processes at the time of diagenesis. As such, there has been ample room for confusion and divergence in approaches to diagenetic studies, leaving the oil industry prone to data-rich but overly cautious interpretation, whereas academia has been open to criticisms of data-poor speculation.

Perhaps it worth reiterating that what remains clear about the North Sea, and for that matter, global sandstone reservoirs in general, are the following two relationships:

- the first-order control on reservoir quality is depositional facies i.e. reservoir porosity and permeability are a function of grain size and sorting (Beard and Weyl 1973; Bryant *et al.* 1993).

- the second-order control on reservoir quality is also related to provenance and deposition - the mineralogical mix of the sediment prior to diagenesis. This will be the significant determinant of physical and chemical changes once burial begins and diagenesis commences.

Oil companies such as Exxon and BP are now using generic models based on these two relationships to successfully predict cementation (Smalley *et al.* 1998), however such models continue to require adjustments via iteration with known data sets for each parochial case study. This is probably due to distinctions between the clearly documented effects of sequence stratigraphy and sedimentary facies on shallow diagenesis and the less well understood rock-fluid interactions of deep-burial diagenesis which play a vital role in predictive, quantitative modelling of cementation and porosity loss.

These deep fluid-rock diagnetic systems are often widely and conflictingly interpreted. A North American school is prevalent in its advocation of long-distance solute transfer and associated regional patterns of fluid flow (Bethke & Marshak 1990; Garven *et al.* 1993) – perhaps reflecting the scale and nature of processes occurring in the foreland and cratonic basins on which much of their early work was focused. By contrast, a largely European group of North Sea researchers favour a closed system approach to deep sandstone diagenesis. The sediment is perceived as interacting with density-layered porewaters, where the principle controlling factors are pressure and temperature (Aagard *et al.* 1990; Bjorkum *et al.* 1998). Other workers in the North Sea region tend to favour case-specific models incorporating a number of features of both schools – Figure 2.6, such as paleofluid flow along faults (Clauer *et al.* 1996), lateral solute transfer (Coleman 1999) and locally sourced cementation (Macaulay *et al.* 1992).

The context of this thesis is rock-fluid interaction and deep-burial diagenesis in as much as illite appears to be a late-stage cement in the evolution of reservoir sandstones; as evident in its occurrence on the surface of other recognisable deep-burial cements such as feldspar and quartz. The brief overview of quartz and feldspar studies below is followed by a detailed discussion of illite diagenesis.

Quartz and feldspar

Quartz and feldspar account for much of the body of work published on North Sea sandstone reservoir diagenesis, in part due to the ease with which they can be identified in thin section, making them amenable to quantitative analysis; and in part due to their associations with reservoir depletion and enhancement respectively. Quartz cement volumes may decrease reservoir porosity as rapidly as 30%-80% per km (Emery *et al.* 1993), whereas dissolution of feldspars can enhance reservoir quality significantly if the resultant secondary porosity is preserved, as it appears to be in the Fulmar Formation of the Central North Sea, with porosity in excess of 25% at 4.7 km. A causal mechanism has been proposed for the latter phenomenon by Wilkinson *et al.* (1997) involving overpressured pore fluids. Concerning the elusive processes underlying unusually high levels of quartz cementation, Marchand *et al.* (2001) and Lander & Walderhaug AAPG (1999) seem to have shown that locally sourced quartz resulting from grain-to-grain dissolution, and gradual diagenesis may be the cause.

2.4 Illite diagenesis in the oil fields of the East Shetland Basin

Illite, as a mineral, was first identified in 1937 by workers in the Illinois Basin (De Segonzac, 1970). Since then it has been found to occur as a diagenetic, metamorphic and detrital mineral in assemblages as diverse as metamorphic rocks and deltaic sediments. In the context of this thesis, illite as found in sandstone reservoirs is taken to be the 'non-expanding, dioctehedral, aluminous, potassium mica-like mineral which occurs in the clay-size fraction' (Srodon & Eberl 1984). The rare occurrence of smectite in the East Shetland Basin, further limits the working definition to fibrous illite, crystallising out of solution onto a substrate of sandstone grain surfaces and related cement phases.

Quartz and illite

Illite notoriously lowers reservoir permeability and has a commonly perceived coeval genesis with authigenic quartz overgrowths - the important porosity-impairing cement phase. Additionally, fibrous illite, as a K-Ar radiometric decay system, offers the tempting possibility of chronologically pinpointing the timing of major damage to reservoir quality as a result of porosity and permeability reduction. This would link quartz overgrowths, illite diagenesis, and the resultant impairment of the reservoir to a geological event. Relating this to the petroleum system would have important implications for industrial exploration and production strategies.

The relationship of illite to petroleum systems

Illite, as a pore lining, fibrous, diagenetic mineral in sandstone oil reservoirs, has been of considerable academic interest to petroleum geologists over the last two decades. Early work by Sommer (1975, 1978), Jourdan et al. (1987) and Hamilton *et al.* (1987, 1989) amongst others, identified the possible relationship between late diagenesis and the onset of oil migration, field charge and hydrocarbon accumulation. Further studies have failed to clarify the precise nature of illite diagenesis or unequivocally support the proposal that fibrous illite growth is a response to specific changes within the petroleum system. Furthermore, criticism has increasingly focused upon the susceptibility of the K-Ar age dating method of fibrous illite to contamination (Liewig *et al.* 1987). As the K-Ar method requires physically pure illite aliquot extraction from sandstones, the presence of contaminant phases such as feldspar, muscovite, and sericite poses a significant problem if the associated K and Ar isotopes are relatively old.

With regard to current thinking, two dominant conceptual approaches to illite diagenesis research follow the closed system-open system paradigm discussed above – section 2.3. In the former, reservoir quality as affected by fibrous illite is considered the result of interaction between pressure, temperature and solid--fluid chemistry, primarily envisaged as a function of burial history, for instance by Matthews *et al.* (1994). While simplification of the diagenetic system is apposite, this over simplistic conceptual modelling was probably a result of limitations in computer hardware during the late 1980's. The limited mathematical modelling software of 1-dimensional paradigms tended to overemphasise the role of burial history in the evolution of reservoir diagenesis. The apparent geographical and geological separation between reservoir and source area in most case studies, including Matthews *et al.* (1994), requires the system to be modelled as open with respect to solute and fluid phases, while indicating similar boundary conditions for heat flow and pressure transfer.

It is not surprising, therefore, that with the advent of increasingly more sophisticated multi-dimensional mathematical models in recent years, most workers have favoured an open-system conceptual framework for hypothesis formulation. As a result, reservoir diagenesis, and illite growth in particular, has been linked to various palaeodynamic fluid-flow models.

Open system paradigm

In the open-system modeller's paradigm, candidates for palaeodynamic fluid-flow models range from meteoric flushing at the surface during emergence and exposure of the reservoir (Macaulay *et al.* 1992), and subsurface meteoric flushing as a result of a distant topographic head (Haszeldine *et al.* 1992; Fleming 1996), to hydrocarbon migration under both hydropressured and overpressured conditions, as result of both liquid and gaseous hydrocarbon phases (Glasmann *et al.*1989; Swarbrick 1994; Darby *et al.* 1996).

The breadth of age arrays attained from illite separates, even for samples taken from a single well horizon (Glasmann *et al.* 1989) have also evoked conceptual models reliant on multiple hydrocarbon and meteoric charges, pressure fluctuations and structural inversion of the reservoir to account for differences in the apparent ages of illite fractions. Certainly, there is convincing evidence that oil reservoirs may continue to evolve diagenetically through more than one hydrocarbon charge (Karlsen *et al.* 1993), though not if the field is filled by, and retains the first oil charge (Marchand *et al.* 2000). Contamination is also commonly cited to account for such variation in illite data and unusually old ages (Hamilton *et al.* 1987, Emery *et al.* 1990, & Matthews *et al.* 1994).

Illite hypothesis

As can be seen, the plethora of different conceptual models relating to illite diagenesis that are under discussion in the literature at present gives a fair impression of this vigorously contested and recently emerged area of scientific research. However, this provokes the banal though apt observation that the deep diagenetic system is potentially influenced by all the various facets of basin evolution. It is plausible that aspects of the closed system, such as burial history and porewater evolution, and the open system, such as fluid flow dynamics, are capable of being the primary controlling factors on reservoir diagenesis, depending on the nature of the study in question. It is perhaps a paradox that both the strength and weakness of the Popperian scientific method lies in reducing a complex system to a resolvable hypothesis and anti-hypothesis whereas the natural world does not necessarily resolve into polarised phenomena.

With this in mind, the aim of this study is to consider illite diagenesis in the East Shetland Basin at the largest possible scale, both with respect to space and time, in order to formulate a valuable hypothesis suitable for scientific investigation within the resource and time constraints of the project. The nature of illite diagenesis is further examined in the following two chapters, providing the basis of work presented in chapter three and informing the strategy for sampling in chapter four.

2.5 Conceptual and mathematical modelling

Intellectual environments as diverse as economics, management, social and the physical sciences have undergone a remarkable evolution in computational modelling and simulation of complex systems

over the last two decades (Neelamkavil 1991). Petroleum geology is no exception - modelling has rapidly asserted itself as a useful problem-solving tool alongside the more traditional techniques of field observation and laboratory experiment. This study attempts to synthesise the unique problem solving skills of modelling with regional field observations and experimental data in order to investigate the link between illite diagenesis and petroleum system dynamics.

Petroleum geology and modelling

In many respects, computational modelling is ideally suited to the process-based understanding required by petroleum geologists (Darby 1995) of the system within which they explore and develop hydrocarbon resources (Dewers & Ortoleva 1994). Not surprisingly, considering the cost of offshore field development, the local data set of cored rock samples is sparse and highly biased towards a non-representative sample set from the most prospective units of trap reservoirs. Regional petroleum geology, on the other hand, is part of a wider dynamic system consisting of multiple variables, many of which are sensed remotely, interacting in a number of processes that represent the basin hydrogeology.

Modelling solutions

A commonplace if naive criticism levelled at modelling studies usually implies that a model can be used to generate any number of required solutions depending on the skill and moral ambivalence of the operator. It is worth emphasising that the purpose of geological modelling is to aid the analysis, understanding and prediction of a system which cannot be observed in real-time, and is spatially and temporally too large to usefully replicate in a laboratory. Although optimum solutions may exist for problems pertaining to such systems, modelling studies are primarily directed towards finding a 'satisfactory solution' to a given problem (Neelamkavil 1991). If all the feasible solutions for a defined system occupy a multi-dimensional space and the modelled solution exists within that space close to the optimum solution, then the solution is deemed to be satisfactory - Figure 2.5. If the observed data for the system plots within the solution space the simulation is deemed to be empirically adequate.

Commercial codes

Commercial modelling codes have been developed to simulate the basin paleohydrology, dependent on calibration with respect to the available data. The codes are used to reproduce the present, in order to implicate the past. Such retrodiction provides quantitative criticism of observational hypotheses and provokes new quantifiable hypotheses in order to further guide data acquisition. Both of these simple techniques are used in the Magnus modelling study.

Styles of fluid flow modelling

Considerable thought has been given as to the type of model best suited to investigating the relationship between illite diagenesis and petroleum systems in the Northern North Sea. Static models and basin models are the two dominant conceptual models used to simulate dynamic fluid flow in geological environments.

Static models - the static model uses a rigid, unchanging computational grid. The underlying tenet is that the subsurface geology is a structural framework of rock types and fault zones that does not evolve spatially throughout the duration of geological time investigated by the model e.g. *Oilgen* (Garven 1989). This style of modelling is ideal for examining phenomena such as groundwater flow through the subsurface at the present day and is suitable for relatively short-term (10^5 - 10^6 years) geological predictions of environmental evolution e.g. Haszeldine & McKeown (1995). The longevity of the petroleum systems envisaged for the Northern North Sea and their probable relationship to the spatial evolution of the basin precludes the use of static models for this study.

Basin models - basin models are conceptually designed to simulate the spatial evolution of basins and the co-dependant relationship between this evolution and the fluid flow systems operating within the basin on geological timescales of 10^7 - 10^9 years. Basin models come in two styles, both highly dependent on mathematical descriptions of burial history during basin evolution.

Physical basin models - such models rely on the premise that compactional rates are slow i.e. slow enough to allow fluids to remain at chemical equilibrium with the host rock during movement (Magara 1987). This allows the model design to envisage the basin evolution as an entirely physical system with the one caveat that a temperature-dependant geochemical calculation is used in order to calculate the timing of oil and gas phases entering the system as a result of source rock maturation. Physical models have evolved primarily in response to the needs of the petroleum industry and as such have evolved within the context of large petroleum province sedimentary basins such as the North Sea and Gulf of Mexico, e.g. (Bethke 1986; Burrus *et al.* 1991; Audet & Fowler 1992).

Physical-geochemical basin models -these have an entirely different and younger bloodline to physical basin models. Though both calculate basin evolution primarily as a function of burial history, physical-geochemical models use an inorganic geochemical description in order to calculate compaction. This younger style of modelling evolved predominantly within the academic community of the U.S.A. in order to investigate intracratonic basin evolution within the North American plate e.g. Park & Ortoleva (1999); Payne *et al.* (1998).

Adaptability and adequacy

Interestingly, physical basin models have been readily adapted to cratonic basin studies by Burrus *et al.* (1996). A physical-geochemical model has also been successfully applied to the Viking Graben (Payne *et al.* 1994). As Darby (1995) points out, the successful application of both basin modelling styles in their alien domains indicates that the underlying conceptualisation for both models provides an adequate representation of the observed basin hydrogeology.

Favoured modelling software

The early evolution, low hardware requirements and economic tailoring of physical basin models to the petroleum industry has resulted in basin models being the dominant modelling package used for sedimentary basin modelling. Physical basin modelling software was chosen to investigate the petroleum systems of the East Shetland Basin for this study for two principle reasons. This style of software has been sympathetically developed with respect to modelling petroleum systems within generically young, actively subsiding sedimentary basins (Darby 1995) as exemplified by the Viking Graben and East Shetland Basin. Secondly, physical basin models have a proven track record of successful application to the environs of the North Sea (e.g. Mudford *et al.* 1991; Burrus *et al.* 1992; Darby *et al.* 1996).

The software package chosen for this study is the widely-used BasinMod® 2-D, under license from Platte River Associates (Platte River Associates 1998). While a number of commercial software packages are on the market, and further confidential in-house packages exist within the petroleum industry, in some respects physical basin models are much alike, conforming to the same physical methodology and mathematical descriptions inherent within this style of coding. BasinMod® 2-D is typical of physical models in this respect.

Grey box - an important aspect in favour of the chosen software, BasinMod® 2-D, has been the grey box approach taken to marketing the software: while the BasinMod® 2-D gridding algorithms are commercially confidential, the underlying conceptualisation is described in detail in the user's handbook (Platte River Associates 1998). This includes a description of the geological algorithms used to simulate the basin. Figure 2.8 graphically illustrates the mathematical basis for the model.

Widely critiqued - as a result the various aspects of this commonly used code have been critically appraised in numerous publications (e.g. Williamson and Smyth 1992; Cornford 1994; Swarbrick 1994; Ziegler *et al.* 1994). A critical awareness and understanding of these geological equations is essential in order to evaluate the validity of solutions supplied by the software. The demonstrated applicability of this software to a number of basins including those of the North Sea is a good initial indication that the code is suitable for the purposes of this study.

One dimensional models

Many published studies have found one-dimensional modelling to be a useful agent provocateur with respect to formulating new qualitative hypotheses with regard to basin dynamics. However, one-dimensional models have generally been found to be inadequate for quantifying petroleum systems (Darby 1995). In the late 1980's limitations in computer hardware restricted mathematical modelling to one dimension. An important artefact of this was a strong conceptual bias towards a closed system approach to reservoir diagenesis as mentioned above. Diagenetic studies require the trap structure to be modelled as a potentially open system with respect to pressure, temperature and fluid (Darby 1995).

Two and three dimensions

Two-dimensional versions of the BasinMod® code exist, and three-dimensional basin model studies are beginning to emerge. This study has favoured a two-dimensional approach, as this encapsulates the structural complexity of the seal-trap-conduit-kitchen juxtapositions that mediate the lateral fluid flow within simple petroleum systems without the added complexity and hardware requirements of three-dimensional modelling.

A more detailed consideration of the BasinMod® 2-D code, two-dimensional modelling in general and related issues such as calibration and sensitivity analysis can be found in chapter five.

Summary

In summary, the geology of the Northern North Sea is well constrained with respect to Mesozoic and Cainozoic tectonics and stratigraphy, as these form the framework for the predominant petroleum system in the region. However, this knowledge base is highly biased towards the trap structures that result in oil fields, to the detriment of detailed understanding with regard to migration pathways and field-specific kitchen areas. The fluid dynamics of the petroleum systems are also often subject to weak generalisations, as the traces of these subtle aspects of basin geology are difficult to interpret. However, with the recent advent of sophisticated basin modelling packages and continued growth in the complimentary research field of deep diagenesis, there has emerged a new and exciting inter-disciplinary approach to petroleum geology. Of all the various common diagenetic phases associated with Northern North Sea sandstone reservoirs, quartz, feldspar and illite are explicitly associated with reservoir quality. Fibrous illite, an unusual permeability-destroying phase, has inspired a large body of research on oil fields flanking the Viking Graben. The mineral chemistry offers the possibility of potassium–argon age dating the time of fibrous crystal growth, a phenomenon that is often associated with a specific event within the petroleum system. However, the technique is notoriously vulnerable to contamination, and, furthermore, some workers postulate that this cement phase grows in response to thermodynamic and chemical changes within a closed system, unrelated to fluid dynamics in the wider basin. These different conceptual models, issues of contamination and general development of illite diagenesis research in the Northern North Sea form the basis of the chapter three, which presents a new synthesis of potassium-argon illite ages for the Northern North Sea.

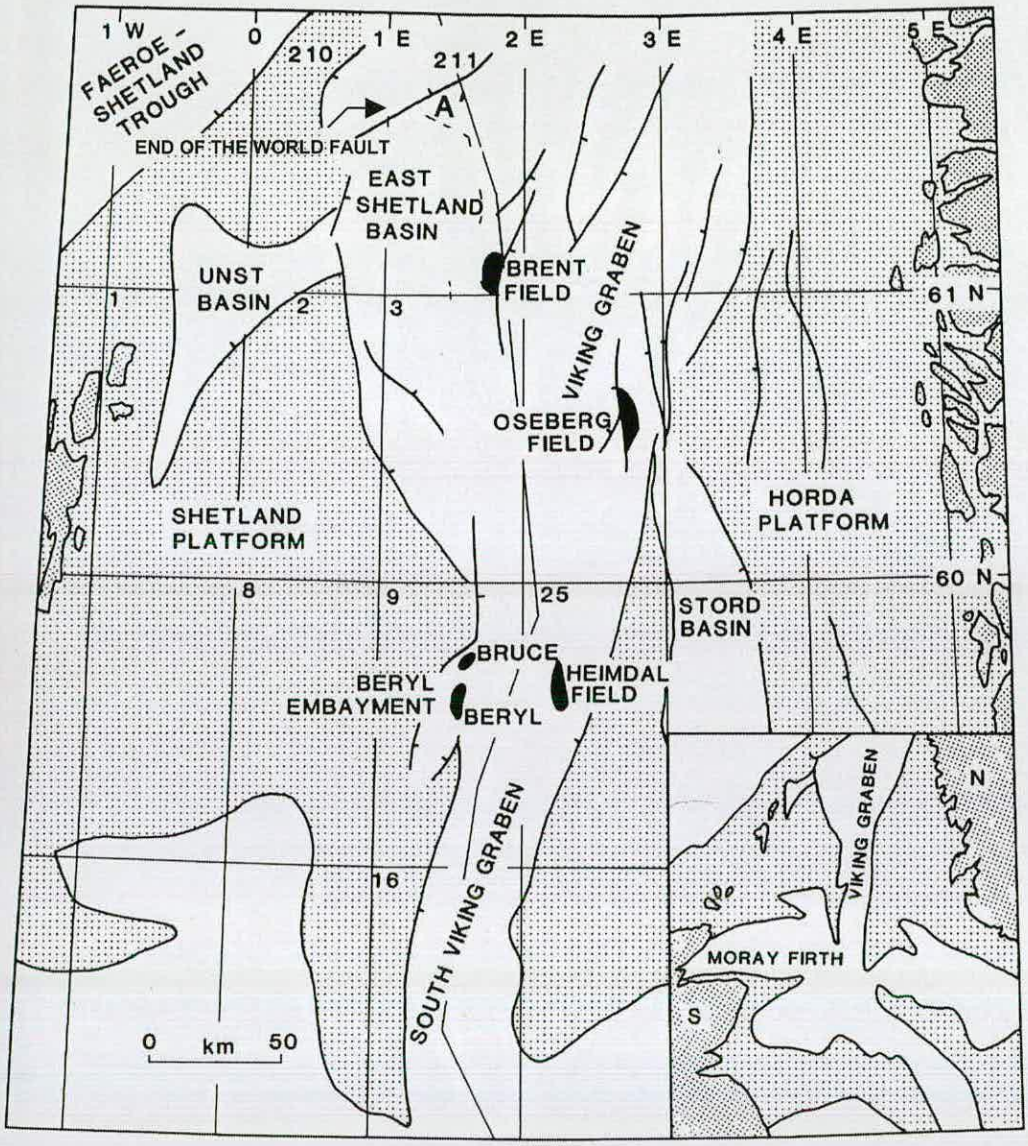

Figure 2.1 The study area – comprised principally of oil field diagenesis research, largely confined to the Brent province of the East Shetland Basin and a small number of fields on the eastern Troll Terraces associated with the Horda Platform. These areas flank the North Viking Graben. Note the abrupt termination of the East Shetland Basin at the 'End of the World' fault (after Richards 1992).

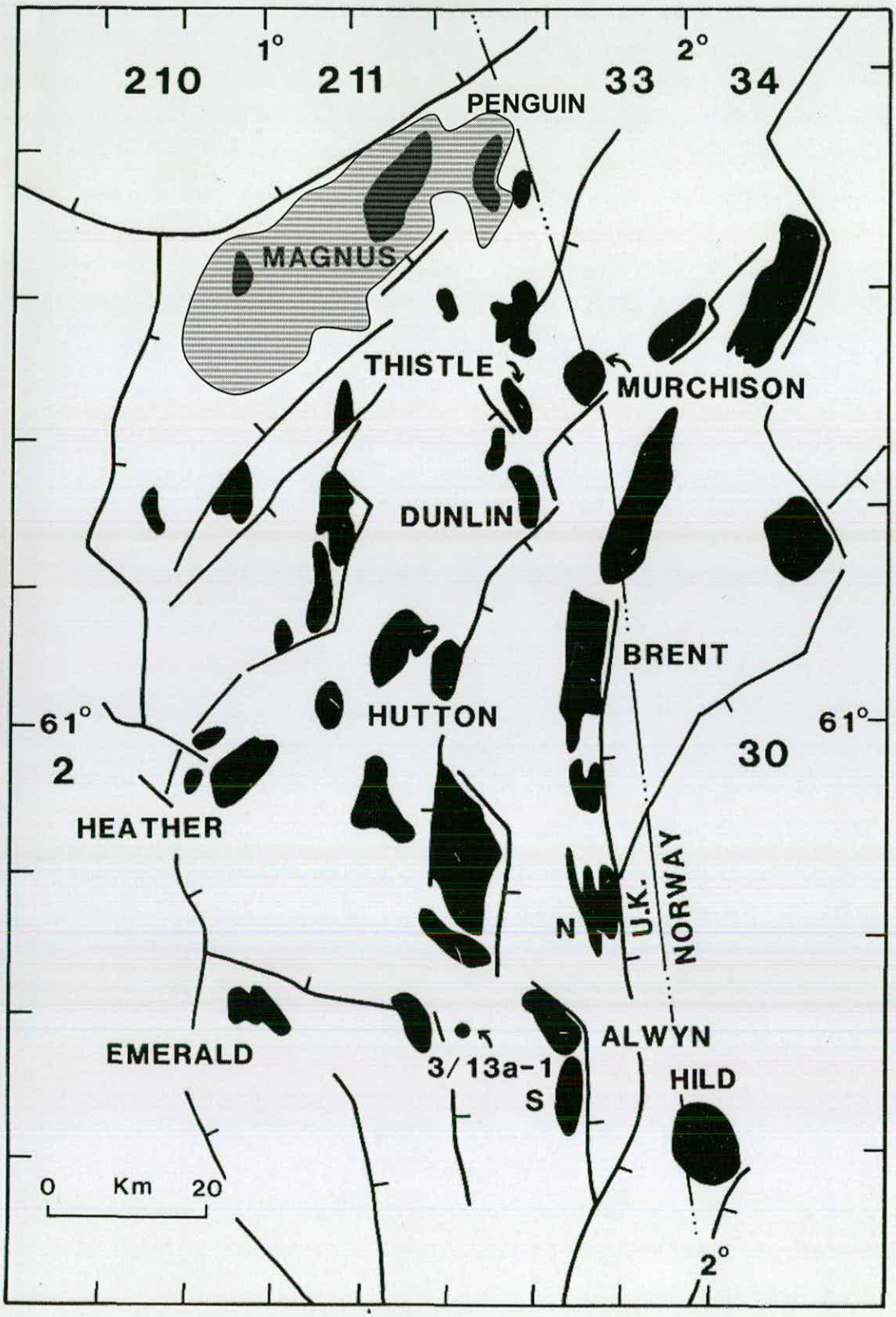

Figure 2.2 The East Shetland Basin. Significant fields associated with this study are the Magnus and Penguin fields on the northern fringes of the basin, the Alwyn fields to the south and Heather on the western margin of the terraces. The grey area encompasses the Magnus Province, an upper Jurassic turbidite play, in stark contrast to the rest of the basin, which is dominated by a middle Jurassic deltaic play (modified from Haszeldine *et al.* 1992).

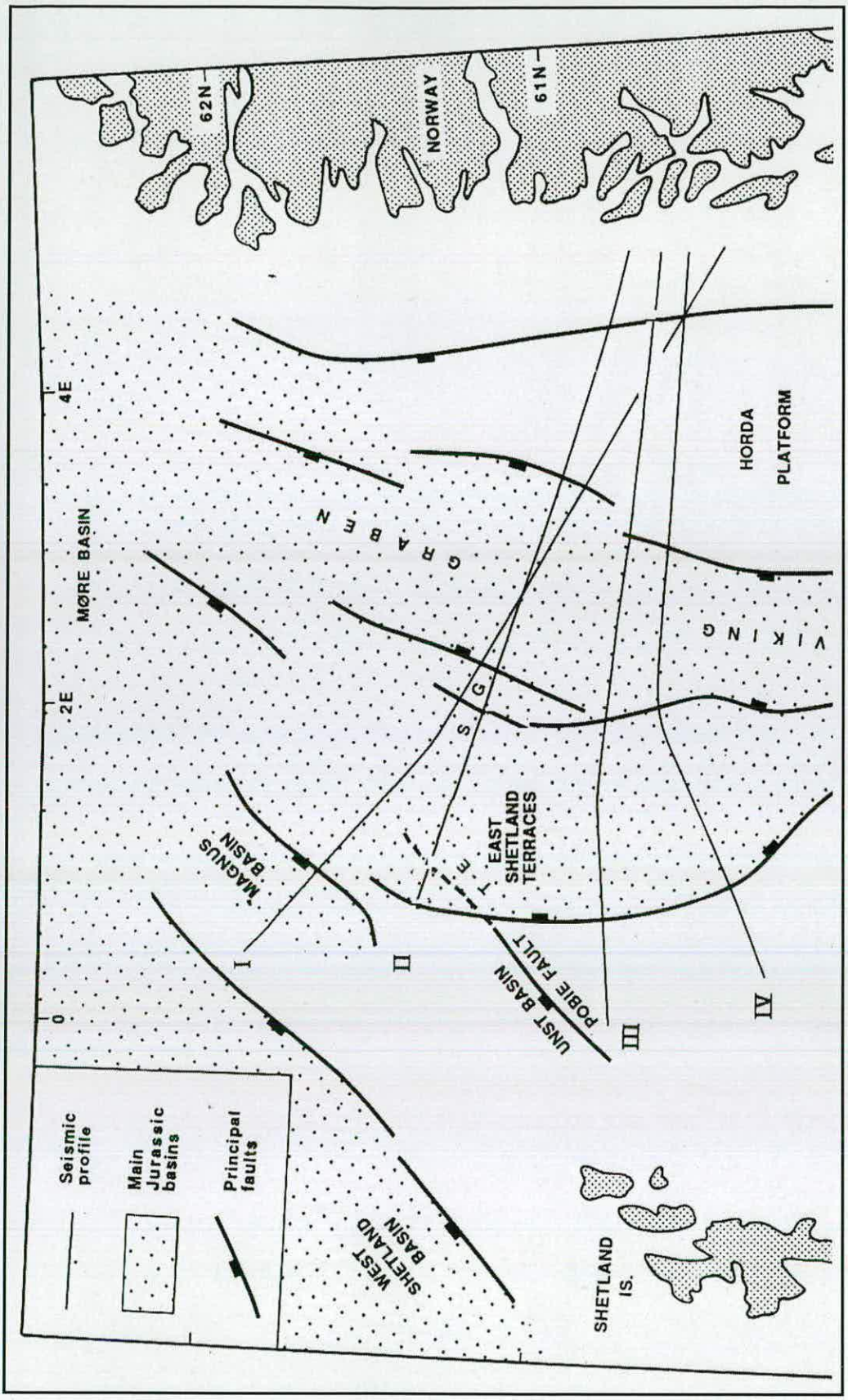

Figure 2.3a Cross-section location map. Jurassic deltaic play (modified from Yielding *et al.* 1992).

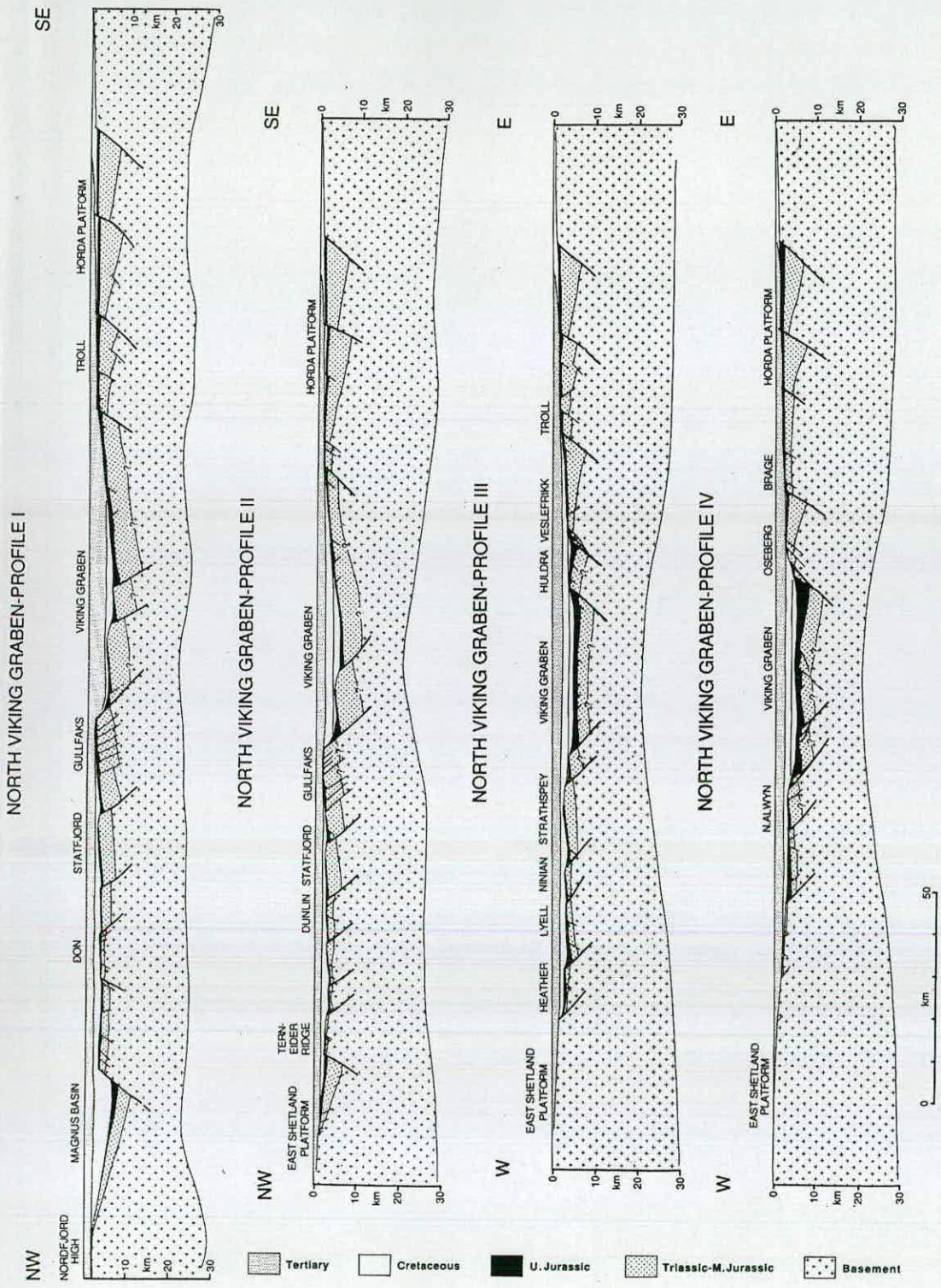

Figure 2.3b Cross-section profiles of the North Viking Graben from regional seismic lines. Note the depth of the Magnus Basin, aka the North Shetland Trough, relative to the Viking Graben margin. The crustal response to lithospheric stretching has resulted in cantilever fault blocks, associated with the largest oil fields in the region. The terraces and graben are overlain by thick post-rift sedimentation (modified from Yielding *et al.* 1992).

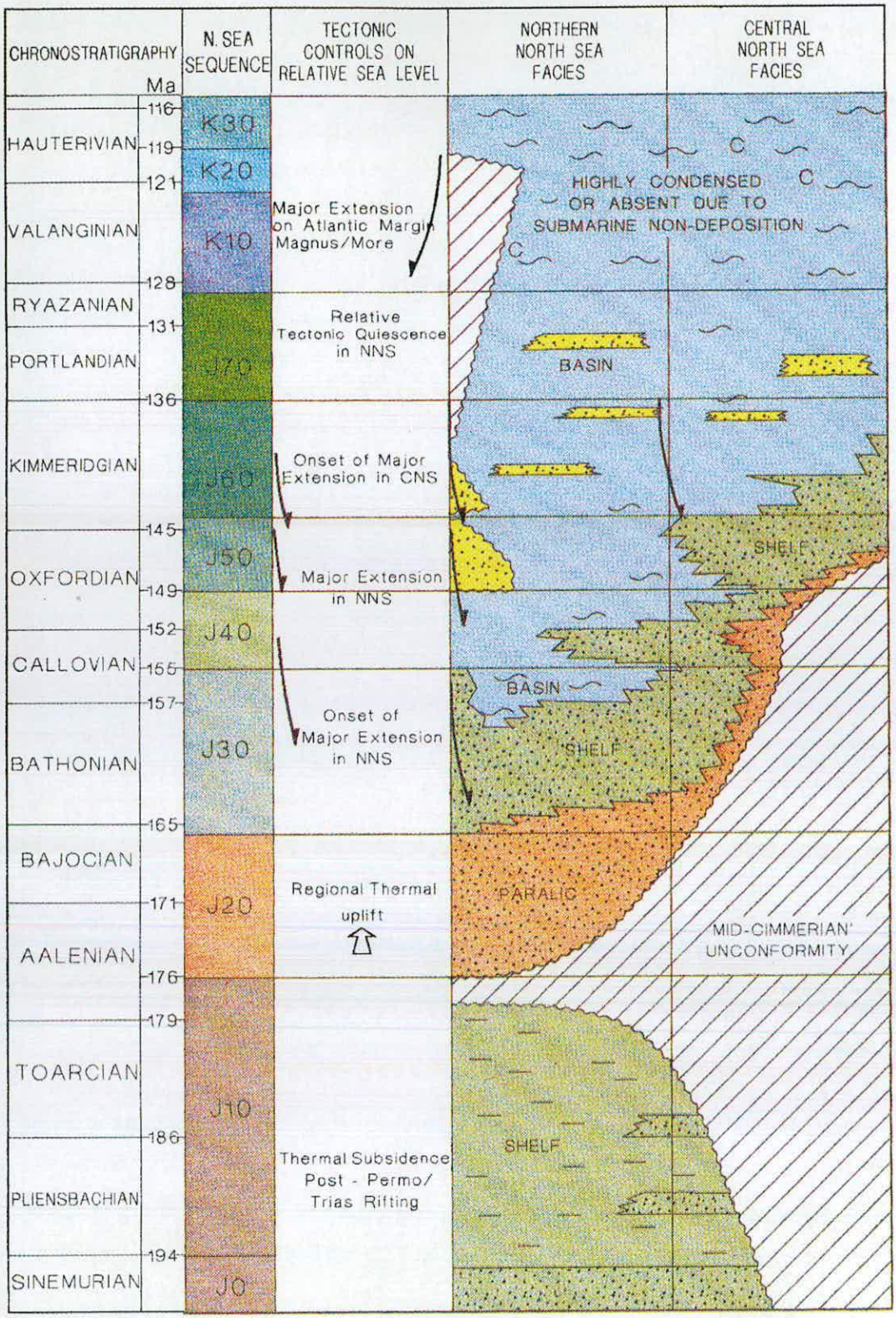

Figure 2.4 Stratigraphy of the Northern North Sea relative to the Central North Sea. Note the occurrence of major extension during J70 and K20, associated with the Atlantic Margin, Møre Basin, and Magnus province only. The Northern North Sea is commonly only associated with two rifting events during the Permo-Triassic and Middle Jurassic periods (Rattey and Hayward 1993).

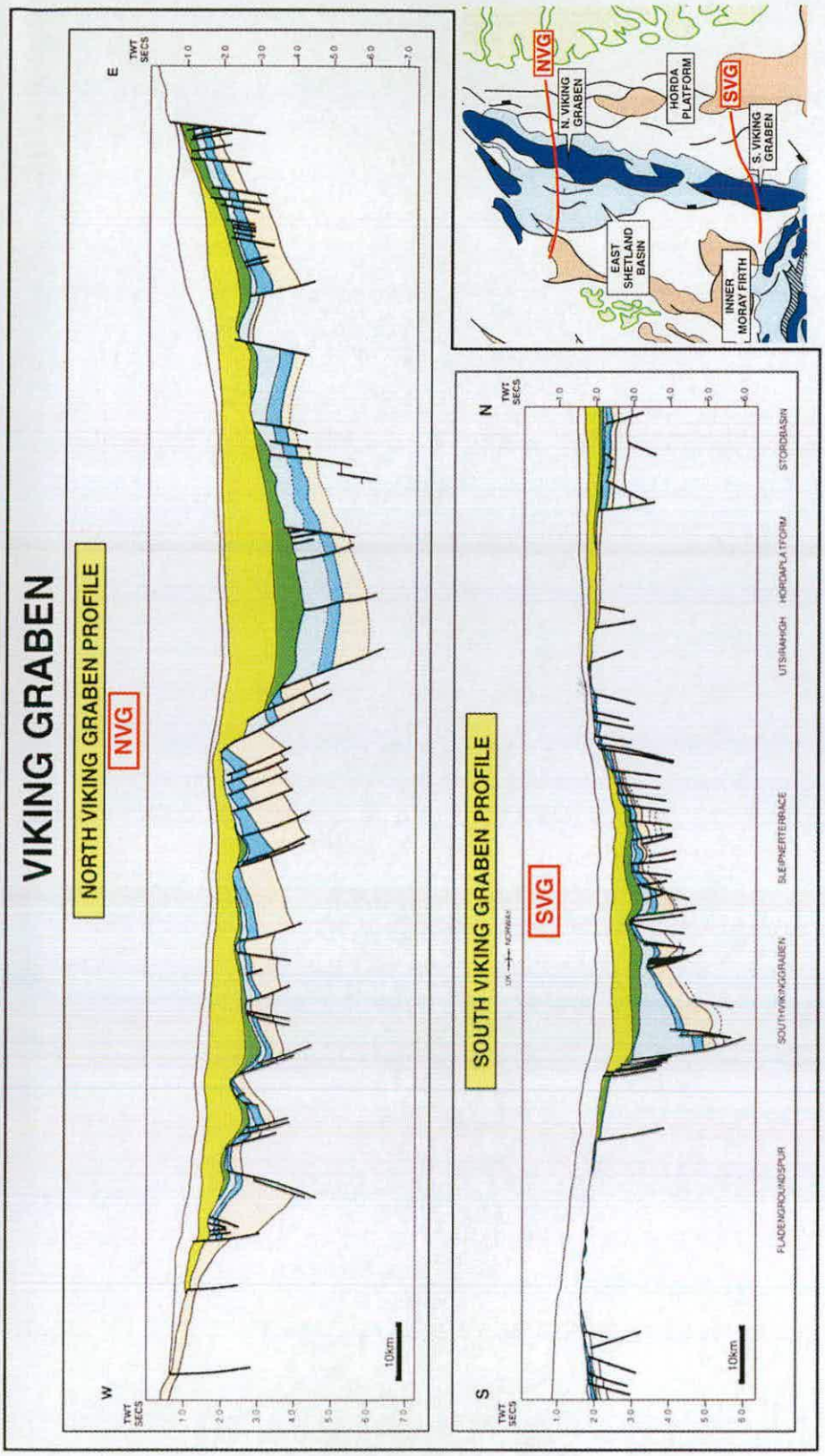

Figure 2.5 Cross-sections of the Viking Graben showing the thickness of post-rift sedimentation of the Cretaceous-Tertiary-Quaternary cover, and interesting asymmetry of the graben (Erratt *et al.* 1999).

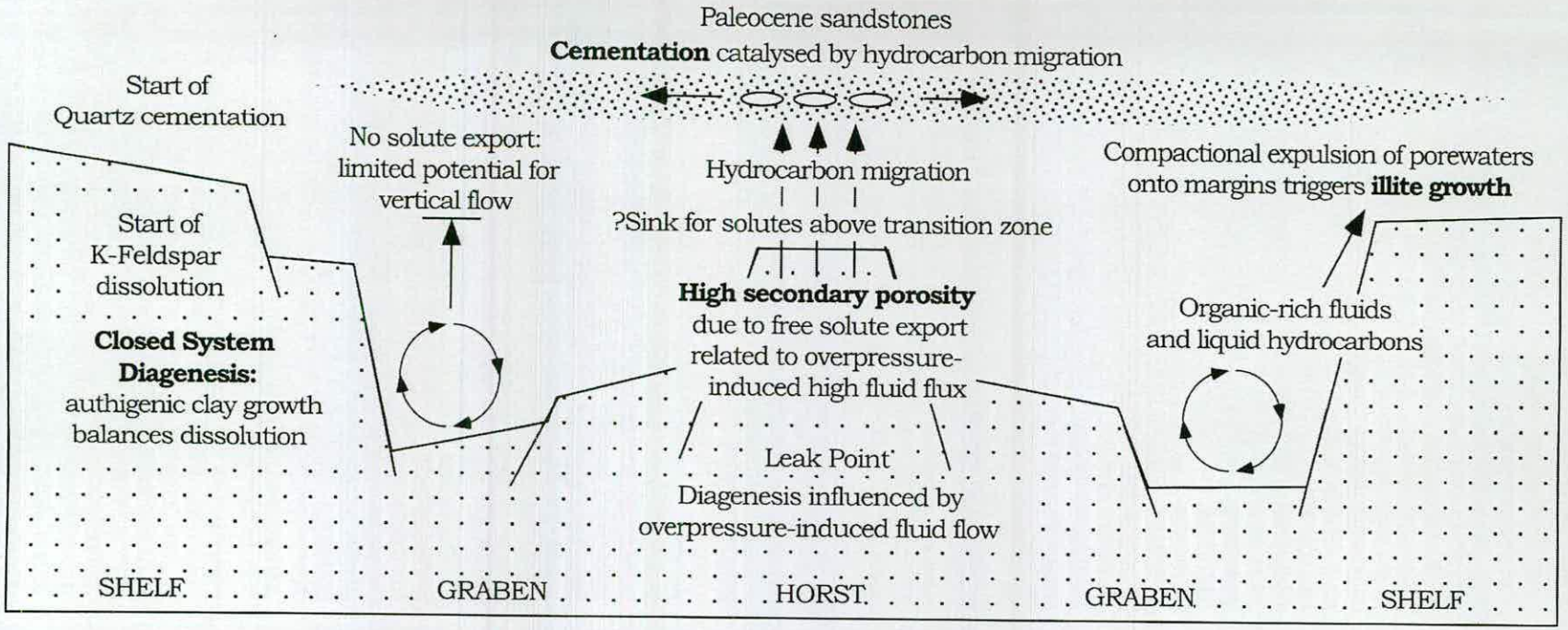

Figure 2.6 An eclectic model for deep sandstone diagenesis in the Central Graben, North Sea. This regional-scale approach to diagenesis associates this suite of phenomena with various dynamic events within the open system, such as overpressure, hydrocarbon migration and compaction hydrology, as well as with closed system equilibrium on the flanks of the graben. The model targets the paragenesis of quartz, potassium feldspar and illite i.e. the principle phases affecting reservoir quality (after Haszeldine *et al.* 1999).

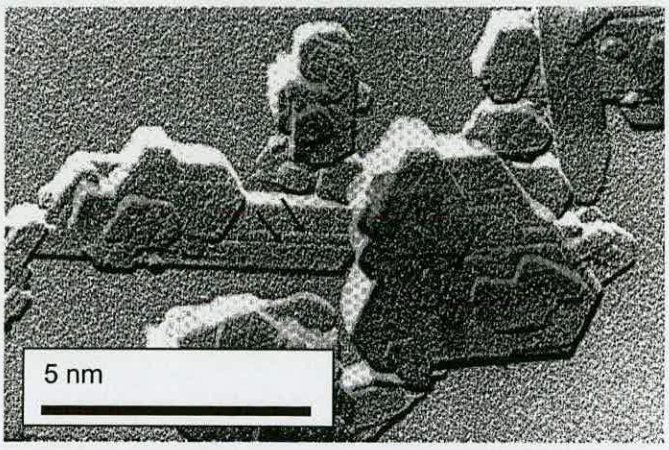

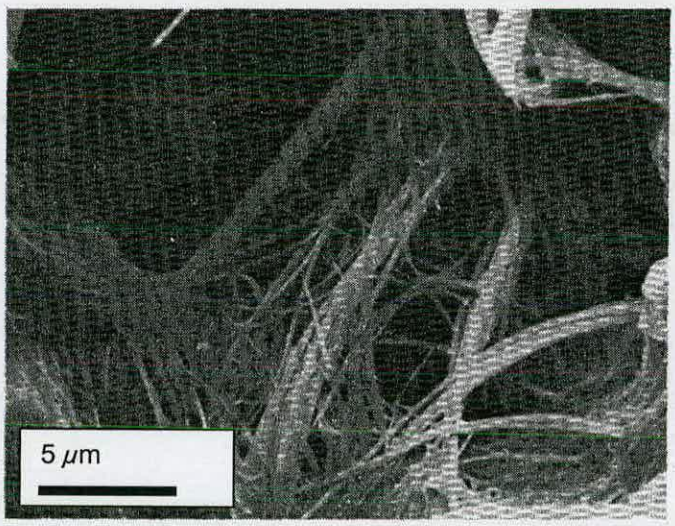

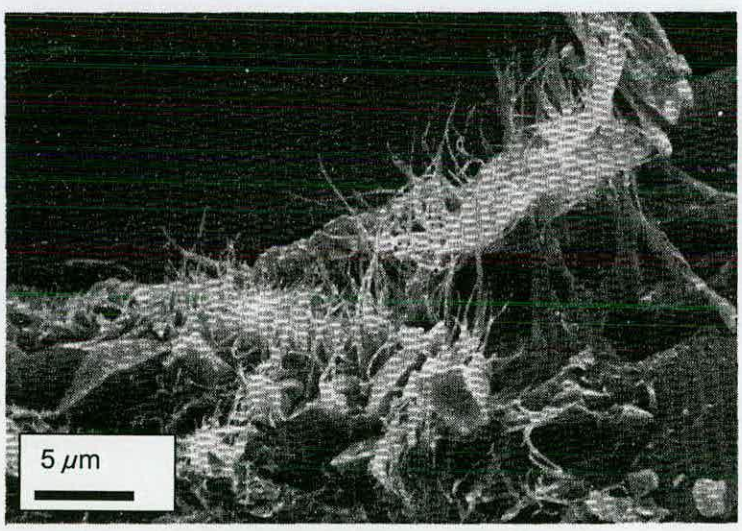

Figure 2.7 High magnification images of illite. The illite fundamental particles, imaged by TEM are typical of high purity aliquots used in K-Ar dating (from Wilkinson & Haszeldine 2002). The SEM images indicates the natural occurrence of fibres in situ within pore volumes of quartz cemented sandstones (from Sommer 1978).

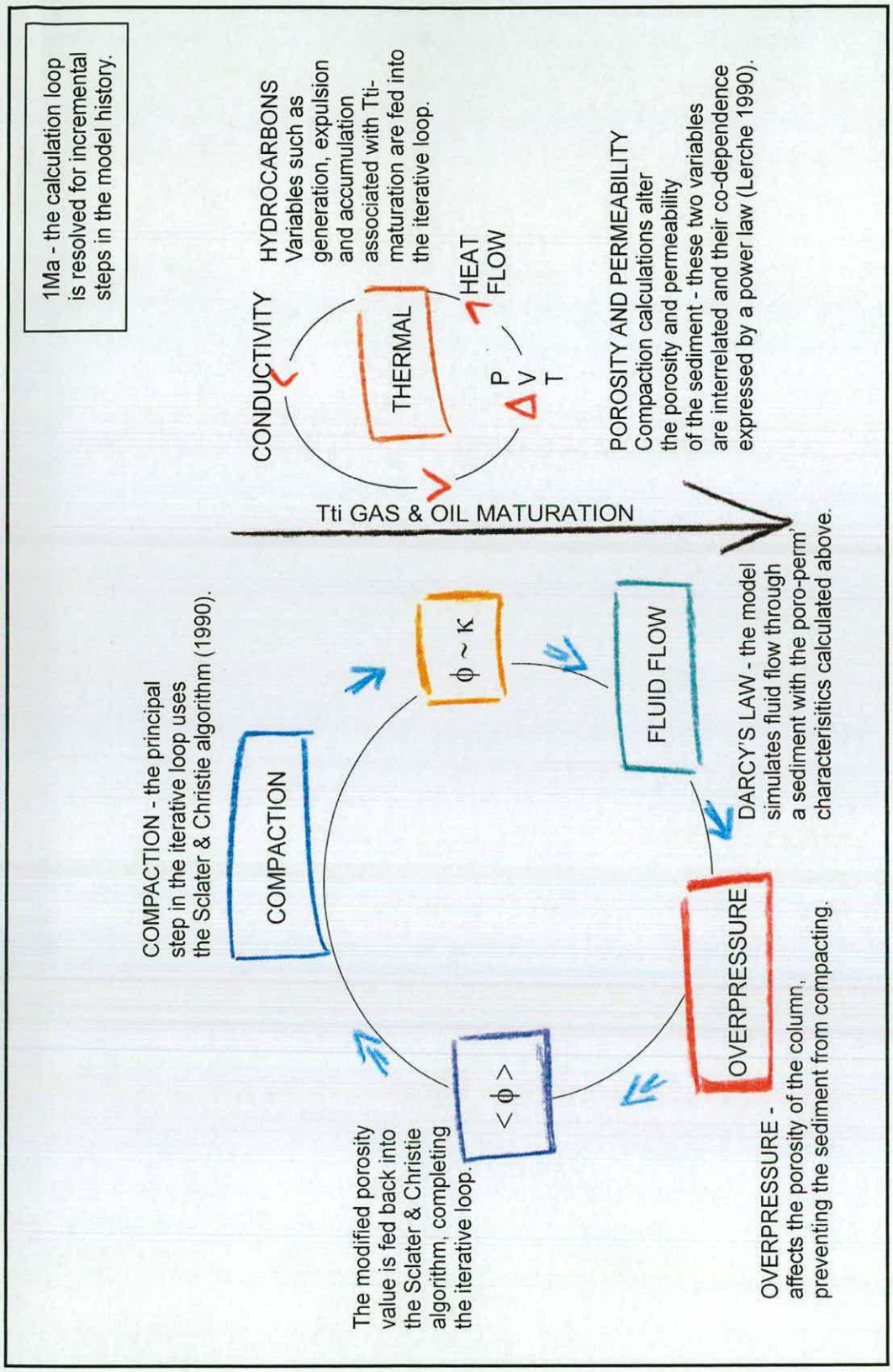

Figure 2.8 Calculation loops for BasinMod® 2-D. This simplified expression of the BasinMod® engine demonstrates the principal variables required for the loop (Platte River Associates 1998).

Empiricism and rationalism

Illite diagenesis in the petroleum systems of the East Shetland Basin

Mock on, Mock on Voltaire, Rousseau:
Mock on, Mock on: 'tis all in vain!
You throw the sand against the wind,
And the wind blows it back again.

And every sand becomes a Gem
Reflected in the beams divine;
Blown back they blind the mocking Eye,
But still in Israel's paths they shine.

This chapter presents an original synthesis and interpretation of illite age data for the East Shetland Basin, from a regional review of published diagenetic studies. Rival hypotheses regarding illite diagenesis in the Northern North Sea are discussed, and relevant examples from the wider context of the North Sea cited. The data synthesis is used to formulate three simple scenarios for illite diagenesis, which reflect the common strategies used to rationalise illite age data.

Figures

Tables

3.0 Aims and objectives

The aim of this chapter is to establish a thorough evaluation of illite diagenesis in the Northern North Sea in order to formulate useful observational hypotheses regarding the nature and timing of fibrous illite diagenesis in the petroleum systems of the East Shetland Basin. As a consequence, the two principal objectives of this chapter are as follows:

• to review the occurrence of illite in the Northern North Sea by compiling tables, maps and depth compilations of illite age data available in the public domain for the East Shetland Basin, Viking Graben and Norwegian Shelf.

• to formulate rival hypotheses of illite growth mechanisms in Jurassic sandstone reservoirs of the East Shetland Basin by the analysis and synthesis of the data collated in the Northern North Sea review.

The first objective is met through manipulating spreadsheets of published data - Appendix 3.1. This forms the basis of the results for this chapter. The second objective requires detailed consideration of previous research into illite diagenesis. Both the technical and geological aspects of illite data interpretation are examined in the discussion that follows below.

3.1 Illite diagenesis and the Northern North Sea

The following extracts and short reviews are intended to furnish the reader with a good introduction to key workers and basic concepts in the field of illite diagenesis. This includes the original East Shetland Basin study by Jourdan (1975, 1978), as well as case studies for each of the four principal geographic data clusters within the Northern North Sea - north (Emery *et al.* 1993); south (Hogg *et al.*, 1987); east (Glasmann *et al.*, 1989); and west (Hamilton *et al.*, 1992). As such, it is the endeavour of this synopsis to provide the reader with the background necessary to critically evaluate the implications of the data interpretation and hypotheses presented at the end of this chapter.

A new method

One of the earliest examples of K-Ar age dating of illite occurred in the Southern North Sea during the mid-1980's (Lee & Savin 1985). The method was applied to cements within the Rotliegend aeolian sandstones, as these clean, quartz-rich sandstones appeared likely to meet the technical ideal of low mineral contamination. The encouraging results established a paradigm associating illite with hydrocarbon charge, and depth profiles of illite ages with the style of filling history.

The first published study of diagenesis in the Northern North Sea to include K-Ar illite age dating was authored by Sommer (1975, 1978). Prior to this, Weaver (1960) and Burst (1969) had suggested that diagenetic clays might be useful in characterising petroleum systems, having conducted preliminary studies on Gulf Coast sediments. By the early 1970's a number of researchers were looking to apply

these new techniques to the rapidly expanding province of the Northern North Sea and the Brent Group in particular. These clean and extensive sandstone reservoirs were deeply buried, suffering significant degradation in quality due to the growth of diagenetic minerals, including illite.

Early workers

In the years that followed, numerous authors published papers on oil field diagenesis in the East Shetland Basin (e.g. Whitaker & Blanche 1978; Glasmann *et al.* 1989; Hogg *et al.* 1992; Hamilton *et al.* 1992). A favoured hypothesis at the time associated fibrous illite diagenesis with the onset of oil migration and the associated changes in chemistry of basinal waters. A common consequent prediction of this hypothesis was that illite diagenesis resulted from the descending oil-water contact. Both arguments depended heavily on event-related diagenesis coupled to petroleum system dynamics. For instance, Hancock & Taylor (1978) postulated that, on the basis of paleotemperature modelling, large volumes of oil migration would result in illite from such fields yielding ages of around 40 Ma to 20 Ma i.e. Oligocene-Miocene epochs.

1978 onwards

However, in retrospect it is clear that Sommer's paper (1978) became the archetype for illite studies in the region. The work effectively establishes the damage illite diagenesis inflicts on sandstones as a result of permeability reduction – Figure 3.1. Additionally, illite fractions from the Brent Group were dated at around 55 and 45 Ma; the problems of analysis and contamination were broached; and an unequivocal statement linking ages and illite diagenesis to oil migration was published in the abstract.

> *One of the three main diagenetic phases during the evolution of sand bodies of the Brent Formation, Viking Graben, is late illitization contemporaneous with the migration of hydrocarbons and associated water....Migration is dated as probably occurring during Lower Eocene times (Sommer 1978).*

The paper goes on to state that illite diagenesis was found to be more complicated than expected and makes three distinct points relating to this issue, as summarised below:

• the saturation of pore space by hydrocarbons in the oil zone inhibits diagenesis. As a result, fibrous illite is rare or absent above the Oil Water Contact. Where fibrous illite is present, high levels of bound water occur, probably as a result of the large surface area of illite crystals.

• fibrous, authigenic illite is prolific in the transition zone of the Oil Water Contact, where oil saturation drops from 40% to 15%.

• clean, water-bearing sandstone bodies below the Oil Water Contact transition zone typically have no illite. This potentially reflects the isolation of these strata from migrating oil and associated waters. It appears that only sandstone bodies exposed to migration are affected.

It is worth noting that Norbert Clauer was responsible for the illite analyses published in the Viking Graben study (Sommer 1978). Clauer is now widely recognised as an authority on illite diagenesis, and has devised new clay separation techniques to minimise the risk of contamination when age dating illite fractions (Liewig *et al.* 1987). Nine years after the study, Sommer co-authored two further papers relating to illite in East Shetland Basin oil fields (Jourdan *et al.* 1987; Liewig *et al.* 1987). Both papers supported and expanded on the initial findings as summarised in the above review.

The Magnus field

In the early 1990's Emery and co-authors published two papers on the Magnus oil field, both concentrating on the diagenesis of this Upper Jurassic sandstone reservoir. The first paper clearly states the case for subaerial exposure of the field and associated meteoric water incursion during the earliest Cretaceous (Emery *et al.* 1990). The second paper postulates that the principal late phases of diagenesis are synchronous with oil migration, and assumes that K-Ar ages for Magnus illite fractions date the timing of this oil charge to a brief period of ten million years i.e. from about 70 Ma to 60 Ma. A concurrent PhD thesis and associated papers by Macaulay and supervisors reached similar conclusions with respect to meteoric incursion, illite diagenesis and oil charge, though Macaulay's ages indicated a slightly more diffuse period of oil charge i.e. from about 65 Ma to 45 Ma (Macaulay 1990; Macaulay et al. 1992). Interestingly, with regard to this study, both research groups independently record an illite age in excess of 80 Ma, i.e. 83 Ma for Macaulay (1990) and 88 Ma for Emery *et al.* (1993). Both reject this data point on the grounds that it is either 'too old' for the supposed time of oil charge to the field, or 'too old' with respect to the supposed temperature of formation. Both studies infer contamination.

> *'If the oldest sample, which gives an age of 87.7 Ma, is ignored then the mean age is reduced to 66 Ma.... This procedure is probably reasonable because the sample is distinctly older, and most likely contaminated,' (Emery et al. 1993).*

> *'For a minimum assumed illite formation temperature of 100°C, constraints on illite formation suggest that, in the past, geothermal gradients may have been significantly higher in the Magnus basin,' (Macaulay 1990).*

If the older, suspect ages do bear credence, then fine illite fractions may yield diachronous ages, indicating distinct episodes of illite diagenesis, related to separate diagenetic events. This would invite the reasonable proposition that oil fields are potentially heterogeneous diagenetic environments.

A southern style

Hogg published a refined study of the Alwyn area work presented by Jourdan *et al.* (1987) and Sommer (1978), associating high levels of late quartz cementation in the Alwyn South field with a relatively brief period of illite diagenesis coupled to oil charge at around 45 Ma to 55 Ma (Hogg 1989). Thermal modelling based on quartz overgrowths indicated that growth took place at around

110°C (Hogg *et al.* 1992; 1995). Coupled with stable isotope data, these findings all pointed towards a simple reservoir history with respect to pore fluid evolution, and appeared to indicate that fibrous illite growth occurred either at or immediately prior to hydrocarbon charge (Hogg *et al.* 1995).

Norwegian waters

Glasmann and co-workers widened the net with the first illite isotope analyses of Brent Group sandstones on the eastern side of the Viking Graben (Glasmann *et al.* 1989). The study of oil fields on the Bergen High found that feldspar dissolution appeared to be associated with quartz overgrowths and illite cementation. Glasmann and co-workers also concluded that fibrous illite diagenesis was closely linked to the timing of maturation in the main Viking Graben kitchen area, and related charging of traps located on structural highs. The researchers differentiated between the neighbouring Veslefrikk and Huldra fields on the basis of stable isotope and fluid inclusion data, inferring a significant movement of deep basinal brines into the latter, displacing paleometeoric waters retained since the Cimmerian exposure, and a discrete hydrocarbon phase migration into the former, free of associated compactional waters (Glasmann *et al.* 1989). This distinction is sympathetic to conceptual models of Northern North Sea petroleum systems that distinguish between local hydrocarbon charge and fill-spill cascades associated with regional charge.

Western margins

Scotchman and co-workers' lucid description of paragenesis in the NW Hutton field on the western terraces of the East Shetland Basin falls short of relating the onset of illite diagenesis to oil migration, though comments that illite diagenesis appeared 'to have ceased soon after the main migration of hydrocarbon fluids into the structure' at around 49 Ma to 39 Ma (Scotchman *et al.* 1989). Research by Hamilton and co-workers on NW Hutton concurred with these findings, returning a slightly wider spectrum of ages i.e. 56 Ma to 34 Ma (Hamilton et al. 1992). They also noted the unusual occurrence of an older age from a finer fraction, 'the reverse of what might be expected' (Hamilton *et al.* 1992). The same study found a similar inversion of the expected trend in the Cormorant field, with the finest fraction yielding an age of 41 Ma, and the coarser fraction, an age of 34 Ma.

The Hamilton paper goes on to note the occurrence of conspicuous patterns of age decrease with depth for the Heather, Pelican and Hutton fields, as seen elsewhere in the region. Both Cormorant and NW Hutton were found to show an inversion of this typical age profile. The paper concludes that the general population of data correlates well with the onset of migration in local kitchen areas, though is candid in pointing out that inverse patterns and younger ages for coarser fractions are puzzling, contradict the model of local hydrocarbon charge, and imply contamination of the samples in question (Hamilton *et al.* 1992). However, recent diagenetic research on Cormorant by Wilkinson *et al.* (in press) indicates that the field has been exposed to multiple hydrocarbon charges, filling specific levels in the trap structure diachronously. Anomalous age arrays in general are considered below and this study in particular is discussed at length in chapter seven.

Summary

Perhaps what is most apparent from all of the studies that followed on from these early beginnings is that the simple hypothetical model of illite diagenesis and oil migration presented by Sommer (1978) has continued to be applied, but has also continued to attract criticism. This is due in part to a somewhat justifiable scepticism around K-Ar illite ages relating to the issue of contamination, mode of precipitation and also to the continued elusive nature of source area and migration pathway mapping.

> *'K-Ar datings of diagenetic illite have been used by various authors to attempt to date the emplacement of hydrocarbons, based on the assumption that the age of the finest diagenetic illite fraction approximates to the timing of hydrocarbon emplacement.' (Giles et al. 1992)*

As this citation suggests in its qualifications of the method by the terms 'attempt' and 'assumption', these investigations have served to further illuminate the complexity of the relationship, with the hoped-for causal link remaining ambiguous and conclusions parochial in their limitations to the study area. Figure 3.2 demonstrates variations typical of the estimated timing for oil incursion relative to the position of illite diagenesis in the paragenetic sequence of East Shetland Basin oil field sandstones.

3.2 Technical constraints

The question arises, to what extent is the nature of the system intrinsically ambiguous? It is apparent that the technical constraints of the method play an important role in limiting the precision of age dating. However, it is accuracy rather than precision that will lead to a valid understanding of the system. This is entirely dependent on the quality of clay separation:

> *'Clay-sized feldspar dissolution fragments are often present in size fractions smaller than 0.5μm and result in serious contamination of illite K-Ar ages (Glasmann et al. 1989a, Liewig et al. 1987); however, size fractions smaller than 0.1μm typically consist of mineralogically pure illite (Glasmann et al. 1989c, Hamilton et al. 1989).' (Glasmann 1992)*

The destructive physical processing of core samples required to extract fibrous diagenetic illite results in an unavoidable risk of sample contamination by various phases present in the host rock. The most significant contaminant phases are detrital illite, feldspar and mica fragments due to their potassium content and potentially old age relative to the diagenetic fraction.

> *'...Liewig et al. (1987) samples were variably contaminated with feldspar, and gave apparent ages of 35-129 Ma that broadly correlate with the illite to feldspar ratio. Extrapolation of this contamination trend to zero feldspar yields an age of c. 40 Ma.' (Hamilton et al. 1992)*

'Only about 6% of muscovite of Caledonian provenance i.e. K-Ar age about 300-430 Ma, is required in the coarser fraction to generate this 14 Ma age difference.' (Hamilton et al. 1992)

Figure 3.3 illustrates the high sensitivity of illite K-Ar age data to K-rich contaminant phases as described by Hamilton *et al.* (1992). Figure 3.4 illustrates a data set with considerable age spread i.e. 120 Ma – 40 Ma, which has been interpreted as contaminated. Contamination volume, type and probable age were estimated in an attempt to extrapolate the data from old, 'mixed' ages to younger uncontaminated ages, inferred to be about 40 Ma (Liewig *et al.* 1987). Attempts to improve the sample processing technique are discussed at length in chapter four.

It is worth noting that the presence and nature of contamination can be screened for with the aid of XRD and Transmission Electron Microscope analytical tools. However, these techniques are semi-quantitative at best, with contamination remaining a ubiquitous problem in the generation of illite K-Ar age data. In light of this, both Fallick (1996) and Clauer (1996) emphasise the need for a rigorous approach to acquiring illite K-Ar data and caution in the use of data already published in the literature.

3.3 Geological constraints

Over the last twenty years, some basic geological constraints have been established with regard to fibrous illite diagenesis. For instance, there appear to be spatial, temporal and thermodynamic limits to the window for illite growth in basinal sandstones.

'Depth plots indicate that illite is not common until the depth exceeds 10 000 ft equivalent to 100°C. Illite dominates the clay mineral assemblage of the <2μm clay fraction below 12 000 ft...115°C. By about 13 000 ft, 125°C, K-feldspars, the source of the K^+ for illite growth, have generally been consumed.' (Giles et al. 1992)

There certainly appears to be maximum and minimum depth limitations to the occurrence of illite. However, though fibres are commonly found below 3000 m, shallower samples do exist; Oseberg, Veslefrikk and Cormorant are all such examples, as cited by Giles et al. (1992). Hence, with Brent Group fields as shallow as 2500 m returning fibrous illite, this appears to be a minor consideration.

Note the implication in the above statement that illite diagenesis is dependent on K-feldspar dissolution. This is another commonly held assumption regarding illite diagenesis:

'Huang et al. (1986) have suggested a possible link between feldspar dissolution and illite formation based on experiments carried out at 200°C. Such a link is also explicit in the work of Bjorkum and Glesvik (1987).' (Giles et al. 1992)

Giles *et al.* (1992) go on to state that the only solute requirement for illite diagenesis is the presence of K^+ ions, assuming the likely presence of aluminium and silica ions in abundance. This is a more reasonable proposition, allowing for the potential relevance of species other than K-feldspar i.e. muscovite, volcanic lithics and glass, when considering both illite growth and contamination.

> *'With increased burial, providing sufficient potassium is available, the pore fluid compositions will move into the stability field of illite.' (Giles et al. 1992)*

The above statement raises two important points:

- where sandstone reservoirs are in the stability field of illite and potassium ions are present illite diagenesis is likely to occur i.e. the controlling factor may be solute chemistry.

- assuming that feldspar is unstable at very shallow burial depths or another suitable source of potassium ions exists, the principal control on the growth of illite may be the illite stability field. This implies that temperature may be an important factor in the timing of illite diagenesis i.e. thermodynamics may be the principal control.

In other words, in the above paradigm, where solute chemistry and temperature are the dominant controls, assuming that the youngest illite habit is fibrous and the reservoir has only recently entered the illite stability field with respect to solutes and temperature, and with the added caveat that the finest clay fraction from such reservoirs is genuinely isolated by extraction techniques, it is likely that illite ages would approach zero. However, 'zero-age illite' is conspicuous by its absence. Solute chemistry, temperature and the zero age anomaly are addressed in turn below.

Solute chemistry

Firstly, the apparent instability of feldspars at shallow depths and related pH conditions has led recent researchers to conclude that feldspar dissolution is unlikely to be a first order control on the inception of illite diagenesis, and will only effect the cessation of illite diagenesis if it is the only significant source of potassium ions in the pore water system.

> *Experimental data on feldspar decomposition (Giles & de Boer 1990) indicates that feldspars will decompose not just in acid waters as is popularly believed ...and suggested for Brent Group sediments by Scotchman et al. (1989) but also in neutral or alkaline pore waters.' (Giles et al. 1992)*

Wilkinson *et al.* (2001) have come to the conclusion that feldspar dissolution takes places consistently over such a depth interval that it is unlikely to be a first order control on the episodic nature of illite diagenesis, as associated basinal porewaters are commonly abundant in K^+ ions.

'Petrographic data from reservoir sandstones from both the U.S. Gulf Coast and the UK North Sea indicate that feldspar dissolution is a continuous process taking place over a considerable depth interval, while illite K-Ar ages indicate that illite growth is an episodic process.' (Wilkinson et al. 2001)

Temperature

This raises the second point, namely that the principal control for the onset of illite diagenesis may be a temperature threshold with regard to the thermodynamic constraints of illite precipitation. Estimated temperatures for precipitation are commonly cited in papers concerning illite diagenesis.

However, the apparent timing of illite diagenesis with respect to temperature varies widely depending on the locality of the study, and has gradually eroded the cooler limit of fibrous illite precipitation from a perceived 100°C in the late 1980's to a chilly 50 - 60°C by the early 1990's.

'Depth plots indicate that illite is not common until the depth exceeds 10 000 ft, equivalent to 100°C...Illite dominates the clay mineral assemblage of the <2μm clay fraction below 12 000 ft...115°C.' (Giles et al. 1992)

'The timing of illite diagenesis in the Oseberg field corresponds with calculated reservoir temperatures in the range of about 50-60°C...considerably cooler than temperatures associated with deeper fields' (Glasmann 1992)

'Bjorkum & Gjelsvik (1988) suggest a temperature for the onset of illite growth of less than 100°C and possibly as low as 50°C for initiation of this reaction.' (Hamilton et al. 1992)

This has also eroded the reasoning for a significant thermal control on timing of illite precipitation within the East Shetland Basin. As Glasmann (1992) points out, a measure of the uncertainty in the perceived temperature threshold results from uncertainties in the construction of thermal history for the sampled sandstone.

'The variation in range of initial illitization temperature may reflect inaccuracies in paleotemperature reconstruction....' (Glasmann 1992)

With such uncertainty existing in the reconstruction of paleotemperatures for the proposed timing of illite diagenesis, it is conceivable that even the lowest temperatures currently estimated for the onset of illite precipitation are too high. The measure of shallow burial illite diagenesis, and by implication, low temperature illite diagenesis is the presence or otherwise of fibrous illite in the cored sections of the shallow fields in question. It is conceivable that the assumed paucity of illite diagenesis above 3000 metres may bias future investigation targets towards deeper oil fields, despite successful sampling from existing wells as shallow as 2500 metres (Giles *et al.* 1992).

Indeed, for most first-order chemical reactions, such as the precipitation of illite, the rate of reaction is related to the temperature by the Arhennius rate equation. In simple terms, the rate doubles for each 10°C of temperature increase. Fibrous illite abundance in sandstone reservoirs is likely to follow this pattern – Figure 3.5. Hence, it is possible that illite may grow at cool temperatures, but at a relatively slow rate, generating small volumes of grain rimming illite that are difficult to detect in thin-section. It would follow that fibrous illite may have been present, but overlooked, in shallow reservoirs unless in excess of 3% of the rock volume.

Zero-age illite

The most intriguing mystery regarding illite diagenesis in the East Shetland Basin and petroleum provinces of the world is the lack of so called 'zero-age' illite i.e. recently formed illite which, if dated, would present a K-Ar age of 0 Ma, theoretically indicative of present-day growth.

> *'K-Ar dates from diagenetic illites within the Brent Group have not yet yielded recent ages....there is no apparent reason why illite growth in the Brent province should have ceased.' (Giles et al. 1992)*

> *'Near zero ages might be encountered where illite formation had only just begun. However, in such circumstances, as the initial growth rates are not likely to be high, there would be the practical difficulty of obtaining enough illite to date.' (Hamilton et al. 1992)*

The lack of zero age illite and the episodic nature of illite age occurrence in oil fields may be an artefact of the analytical method or sample bias in the studies. However, with no obvious thermal control or solute-supply effect on the temporal and spatial occurrence of illite, workers have continued to link the episodic nature of illite ages with geological events within the petroleum basin. By contrast, some Norwegian researchers (Bjorlykke pers comm. 2002) remain convinced that illite continues to grow at the present day, and infer that zero-age illite does exist, explaining the absence of measured examples as the artefact of ubiquitous contamination of all samples to levels resulting in mixed ages of at least 30 Ma.

Overpressure

An interesting variation on the common hypothesis of illite diagenesis and oil migration in the Northern North Sea as first elucidated by Sommer (1978), has been the association of illite ages with overpressure dynamics in the Central North Sea by Swarbrick (1994) and Darby *et al.* (1997; 1998). The latter study sampled sandstones from overpressured reservoirs of the Fulmar Formation to find that the graben margins yielded relatively old ages, approximately 80 - 60 Ma, compared to younger, 30 Ma ages for the graben axis.

Darby *et al.* (1998) concluded that the older ages were a response to pore fluid expulsion with the onset of rapid subsidence i.e. predating and unrelated to the petroleum system. The younger ages were found to post-date the principal episode of subsidence in the axial area, appearing to match calibrated basin model simulations of overpressure. It is worth noting, however, that Darby's recent position on the younger ages is equivocal relative to the stand taken in his thesis (Darby *et al.* 1997 versus Darby 1995) allowing for an oil charge interpretation with respect to axial illite growth.

Critical nucleation

An unusual approach to the problem by Wilkinson & Haszeldine (2002) has highlighted the role of nucleation kinetics in controlling what amounts to a strange crystalline morphology, namely fibrous illite. In effect, fibrous illite has a high threshold, or critical nucleation value, relative to other common diagenetic phases such as kaolin, quartz, and feldspar. Crystallisation requires unusually high energy conditions in order to precipitate fundamental particles of illite. These fundamental particles, in turn have a flawed ultrastructure, as a result of rapid, low entropy fibrous growth in supersaturated conditions. This inhibits sustained cascades of growth, unless critical nucleation conditions are maintained. As a consequence, fibrous illite diagenesis is an exceptional form of reservoir cementation, dependent on the high threshold conditions associated with critical nucleation. It is perhaps then unsurprising that fibrous illite appears to grow in an episodic fashion and has been implicated in event-driven diagenesis. Wilkinson & Haszeldine (2002) go on to state that this atypical mode of crystallisation may account for the lack of 'zero-age' illite, suggesting that the events responsible for illite diagenesis in the Northern North Sea may not have occurred in the last 20 My. The remit of the paper is quite specific and so remains silent on the subject of what these events might be. The implication, however, is clearly that fluid motion is a vital factor, providing the change in conditions necessary to breach the threshold conditions of illite nucleation, possibly as a result of the increase flux in ions. Such a paradigm is highly sympathetic to the hydrocarbon charge – illite diagenesis hypothesis, as oil migration and trap incursion would displace the resident porewaters, providing the necessary fluid flux event.

Summary

This states the case as to the commonly perceived parameters for the illite diagenetic system with regard to spatial and temporal occurrence, temperature, pressure, solute supply, nucleation chemistry and interaction with the petroleum systems and hydrodynamics of the East Shetland Basin. A brief consideration of the conceptual models that have resulted from investigation of these parameters follows.

3.4 Illite diagenetic studies and conceptual models

Illite is a favoured target of conceptual models as it has an often-perceived coeval genesis with the important porosity-impairing phase, authigenic quartz. The ability to date this clay fraction, using the K-Ar radiometric decay system, offers the tempting possibility of being able to chronologically pinpoint the timing of major diagenetic damage to reservoir quality as a result of porosity and permeability reduction, thus linking this impairment to a single geological event. The correlation of an absolute age to a geological event within a petroleum system also potentially establishes a palaeo-calibration point for basin model simulations.

3.5 Illite age-event models

Candidates for diagenetically significant geological events in the dynamic modeller's paradigm range from meteoric flushing at the surface during unconformity-related emergence of the reservoir (Haszeldine *et al.* 1992), and subsurface meteoric flushing as a result of a distant topographic head (Macaulay *et al.* 1993; Fleming 1995), to hydrocarbon migration under both hydropressured and overpressured conditions (Swarbrick 1994; Darby *et al.* 1998); both as a result of liquid and gaseous hydrocarbon phases (Glasmann *et al.* 1992; Haszeldine *et al.* 2000). These models are applied variously, depending upon the physical and chemical limits of the illite stability field inferred for each study area.

Conceptual bias

Reservoir quality as affected by diagenetic evolution has also been considered to be the result of a closed system interaction between pressure, temperature and solid-fluid chemistry, primarily envisaged as a function of burial history, for instance by Matthews *et al.* (1994) and Bjorkum *et al.* (1998). While simplification of the diagenetic system is apposite, overly simplistic conceptual modelling is likely to have been a result of limitations in computer hardware during the late 1980's which limited mathematical modelling software to one-dimensional paradigms, over-emphasising the role of burial history as a control on reservoir diagenesis. The apparent geographical and geological separation between reservoir and source area in most case studies, including Matthews *et al.* (1994), requires the system to be modelled as open with respect to solute and fluid phases, while implicating similar boundary conditions for heat flow and pressure transfer.

Recent conceptual shift

It is not surprising then, that with the advent of increasingly more sophisticated multi-dimensional mathematical models in recent years most workers have favoured an open-system conceptual framework for hypothesis formulation. Reservoir diagenesis, and illite growth in particular, has been linked to various palaeodynamic fluid-flow models.

3.6 Complex natural systems and duality - the need for a regional review

The diversity of conceptual models under consideration in the literature at present gives an accurate impression of this vigorously contested and newly emerged area of scientific research. The banal though pertinent observation apparent from the published literature is that the diagenetic system is probably representative of many facets of basin evolution. It is highly plausible that aspects of the closed system, such as burial history, and the open system, such as fluid flow dynamics, are capable of being significant variables controlling reservoir diagenesis, depending on the focus of the study in question. In this respect, it is perhaps a paradox of Popperian scientific method that the strength and weakness of this school of analysis lies in reducing a complex system to a refutable dualism, i.e. a null hypothesis and antithesis. With this in mind, the system under investigation is initially considered at the largest possible scale, both with respect to space and time, in order to formulate a valuable hypothesis suitable for scientific investigation of a parochial system within the resource limitations and time constraints of this study.

Context of review

The following review encompasses all known published illite ages for the Northern North Sea, prior to the selection of a single oil field for further illite sampling and related testing of the conceptual models outlined above. The understandable apprehension and criticism associated with the technical limitations of K-Ar age dating illite and the lively debate as to the geological significance of illite ages are the critical context within which this chapter presents a new compilation of illite data from ages available in the public domain. This new synthesis of illite ages is used to stimulate a reconsideration of currently held hypotheses on the relationship between oil field diagenesis and petroleum system dynamics, while questioning the reliability of data available in the public domain in light of the experience of workers to date.

3.7 Results – illite age data for the Northern North Sea

There are numerous diagenetic studies published for the region, which by their nature tend to be similar in methodology. For the sake of brevity, a short synopsis of specific illite diagenesis studies relevant to this work has been presented above. The data compilation that follows below derives from fourteen first authors and seventeen papers, relating to twenty-four oil fields and three regional studies. These are representative of the principal schools of thought and studies conducted on oil field diagenesis in the Northern North Sea. – Table 3.1.

1978-1987		*1988-1989*	
Sommer 1978	*East Shet' Basin*	Brint *et al.* 1988	*Murchison*
		Brint *et al.* 1988	*Thistle*
Thomas 1986	*Heimdal*		
Thomas 1986	*25/4*	Glasmann *et al.* 1989	*Heather*
		Glasmann *et al.* 1989	*Huldra*
		Glasmann *et al.* 1989	*Hutton*
Hamilton *et al.* 1987	*Brent Province*	Glasmann *et al.* 1989	*Veslefrikk*
Hamilton *et al.* 1987	*Thistle*		
		Harris 1989	*Hutton*
Haszledine *et al.* 1987	*Murchison*		
		Hogg 1989	*Alwyn North*
Hogg *et al.* 1987	*Alwyn South*	Hogg 1989	*Alwyn South*
Jourdan *et al.* 1987	*Alwyn North*		
Liewig *et al.* 1987	*Alwyn*	Scotchman *et al.* 1989	*Hutton NW*

1992		*1992-1993*	
Giles *et al.* 1992	*Magnus*	Hamilton *et al.* 1992	*Penguin*
Giles *et al.* 1992	*Tern*		
		Macaulay *et al.* 1992	*Magnus*
Glasmann *et al.* 1992	*Hild*		
Glasmann *et al.* 1992	*Oseberg*	Emery *et al.* 1993	*Magnus*
Glasmann *et al.* 1992	*Viking Graben*		
Hamilton *et al.* 1992	*3/8*		
Hamilton *et al.* 1992	*211/7*		
Hamilton *et al.* 1992	*211/11*		
Hamilton *et al.* 1992	*Cormorant*		
Hamilton *et al.* 1992	*Grtr Don Area*		
Hamilton *et al.* 1992	*NW Hutton*		
Hamilton *et al.* 1992	Pelican		

Table 3.1 First authors and study areas for illite age data relating to the Northern North Sea.

Parameter variation

There are numerous parameters relating to K-Ar age dates for illite clay separates. Information cited varies markedly from publication to publication depending on the emphasis of the study. In order to make the data more manageable published ages were retabulated with respect to five basic parameters: location, depth, stratigraphic unit, K-Ar age, and size-fraction - Table 2. The first author name is cited for ease of cross-reference to the original data set - Appendix 3.1.

Presentation

Histograms, comparative depth diagrams, and map presentation of the data set are used to aid analysis of the data for trends, patterns and anomalies in K-Ar ages for the Brent and Magnus provinces of the East Shetland Basin. The map is a simple template of major faults and fields (after Alastair Beach Associates/Geco map 1989) - Figure 3.6. The spread of illite data on the map can be conveniently split into four geographic groups relating to the four cardinal directions: north, south, east and west –

Table 3.3. A description of the data occurring in each of these quarters, as presented on the map, follows below. These groups are also used to display the data as histograms of frequency versus age - Figures 3.7 to 3.11, and for comparative depth diagrams - Figures 3.12 to 3.15. It is worth noting that these subsets and their presentation as comparative depth diagrams do not infer geological or hydro-geological characteristics to the groups.

Old ages of the Northern Group

Strictly speaking, the oldest undisputed age in the Northern North Sea area occurs in the Alwyn North field, quadrant 3/4 at 75 Ma. However, older ages occur in the Magnus field, Northern Group – Figure 3.11. Ages in excess of 80 Ma were measured by two separate studies (Macaulay *et al.* 1992; Emery *et al.* 1993) – Table 3.2. Both research teams considered these ages to be the result of contamination. In the case of Emery *et al.* (1992), it would appear that the rejection of an age of 82 Ma was based partly on the observation that the data point was exceptional with respect to other data for the same study, and partly due to the failure of this age to compliment the favoured conceptual model for illite diagenesis. The evidence is perhaps less equivocal in the case of Macaulay *et al.* (1992). Here an age of 83 Ma is accompanied by a younger age, 55 Ma, for a finer fraction of the same sample – Figure 3.6. Both researchers are assuming that contamination has resulted in the unusually old ages. Note, however the similarity in rejected ages for two distinct samples from the same field by two separate research teams.

Older ages, in excess of 120 Ma, occur elsewhere in the basin; for instance, 147 Ma for the Cormorant field, Western Group (Hamilton *et al.* 1992) – Figure 3.6 and Figure 3.9. Such ages are understandably interpreted as contamination artefacts. In the case of Liewig *et al.* (1987), there is clear and convincing evidence that coarser size fractions returned older ages in keeping with increased concentrations of a contaminant phase - Figure 3.4. In this case, the trend implies that a true age of about 35 Ma can be extrapolated from a maximum apparent age of 120 Ma.

In light of this, the candidate threshold for the oldest acceptable ages in the Northern Group quadrant would appear to be approximately 75 Ma – Figure 3.11. This age generally holds true for the entire region, occurring as it does in both the northern and southern quadrants, and not exceeded to the west, nor to the east. In fact, these ages are conspicuous by their absence in both the Western Group and Eastern Group – Figure 3.11.

Location	Author	Depth (ft)	Stratigraphy	Zone	Size (μm)	Age (Ma)
Wendy-Magnus-Penguin-Don						
211/7- '	Hamilton et al.	11243	Tarbert	Oil	0.1-0.5	36.5
'K'	Hamilton et al.	11285	Etive	Water	<0.1	24
'K'	Hamilton et al.	11325	Etive	Water	<0.1	17
211/12a-9	Macaulay et al.	10448	MSM	Water	<0.1	55
211/12a-9	Macaulay et al.	10448	MSM	Water	0.1-0.5	83
211/12a-9	Macaulay et al.	10704	MSM	Water	0.1-0.5	46
211/12a-11	Emery et al.	*10318*	MSM	?oil	-	68
211/12a-11	Emery et al.	*10430*	MSM	?water	-	88
211/12a-11	Emery et al.	*10486*	MSM	?water	-	72
211/12a-11	Emery et al.	*10512*	MSM	?water	-	63
211/12a-11	Emery et al.	*10574*	MSM	?water	-	64
211/13- 'X'	Hamilton et al.	11621	Etive	Oil	0.3-0.1	34
211/13- 'X'	Hamilton et al.	11621	Etive	Oil	<0.1	28
211/13- 'X'	Hamilton et al.	11710	Etive	Oil	0.3-0.1	28
211/13- 'X'	Hamilton et al.	11710	Etive	Oil	<0.1	22
'Z'	Hamilton et al.	13322	Tarbert	Oil	<0.1	54
Murchison-Thistle-Dunlin						
211/19-4	Haszeldine et al.	10202	Rannoch	-	<0.1	59
M'son/This -	Hamilton et al.	-	Brent Group	-	-	-
M'son/This -	Brint et al.	*8694-9514*	Brent Group	-	-	-

Table 3.2 Published ages for the Northern Group, East Shetland Basin - Appendix 3.2.

Bimodality in the Eastern Group

In this case, although the data set is small, the age spread appears to be distinctly bimodal, around the ages 35 Ma to 30 Ma, and 60 Ma to 55 Ma – Figure 3.8. Interestingly, both suites occur in a single field, in the case of Huldra - Table 3.3. A trend apparent elsewhere in the region is the increase in age with depth within the field e.g. Huldra and Veslefrikk – Figure 3.12. An age indicative of the younger mode, 37 Ma, bucks this simple trend for the Huldra field. Note that the separation in measured ages upon which these observations are based can be as small as 1 My. Questions concerning resolvability of the data are addressed below – Section 3.9.

Location	Author	Depth (ft)	Stratigraphy	Zone	Size (µm)	Age (Ma)
Huldra-Oseberg-Veslefrikk-Brage						
Huldra -	Glasmann et al.	*12139*	Brent Group	-	-	59
Huldra -	Glasmann et al.	*12467*	Brent Group	-	-	37
Huldra -	Glasmann et al.	*13451*	Brent Group	-	-	55
Huldra -	Glasmann et al.	*13451*	Brent Group	-	-	56
Huldra -	Glasmann et al.	*13451*	Brent Group	-	-	57
Oseberg-	Glasmann	*9186*	Brent Group	Water	-	53
Veslefrikk -	Glasmann et al.	*9514*	-	-	-	31
Veslefrikk -	Glasmann et al.	*9843*	-	-	-	32

Table 3.3 Published ages for the Eastern Group, Bergen High area - Appendix 3.2.

Southern ages

The range of ages in the Southern Group is surpassed only by the Northern Group – Table 3.4. Liewig *et al.* (1987), Jourdan *et al.* (1987) and Hogg et al. (1992) all contributed to the pioneering work of Sommer (1978), who was a published co-worker on the two papers published in 1987. This concerted research effort resulted in a comprehensive suite of ages for the Alwyn area complex – Figure 3.6 and Table 3.4.

Location	Author	Depth (ft)	Stratigraphy	Zone	Size (µm)	Age (Ma)
Alwyn-Alwyn.Nth-Alwyn.Sth-Hild						
3/4 - 3/9-	Hogg	-	-	-	-	74
3/4-8; 3/9a-1-4	Jourdan et al.	-	Brent Group	-	<0.2	75
'3/9-6	Jourdan et al.	-	Brent Group	-	<0.2	35-45
'3/14-3-4-6-7-8-11;3/15-2-4	Jourdan et al.	-	Brent Group	-	<0.2	45-55
Alwyn -	Liewig et al.	-	Brent Group	-	-	-
Alwyn -	Liewig et al.	10636	Brent Group	OWC	<0.6	35
Alwyn -	Liewig et al.	10625	Brent Group	OWC	<0.6	44
Alwyn -	Liewig et al.	-	Brent Group	OWC	<0.6	129-35
'3/8-4;3/14-9-10-12	Jourdan et al.	-	Brent Group	-	<0.2	35-45
3/14a-7-8-9	Hogg et al.	-	Brent Group	-	-	-
Alwyn South -	Hogg et al.	-	Brent Group	-	1.0-0.5	45-56
Alwyn South -	Hogg	-	Brent Group	-	0.5-0.1	45-56
Alwyn South -	Hogg	-	Brent Group	-	-	48
Alwyn South -	Hogg	-	Brent Group	-	-	50
Hild -	Glasmann et al.	*12795*	Brent Group	-	-	60
Hild -	Glasmann et al.	*12795*	Brent Group	-	-	64

Table 3.4a Published ages for the Southern Group, East Shetland Basin - Appendix 3.2.

Location	Author	Depth (ft)	Stratigraphy	Zone	Size (μm)	Age (Ma)
Ninian-Columba						
Well 2	Hamilton et al.	12176	Tarbert	oil	<0.1	62
Well 2	Hamilton et al.	12308	Etive	oil	<0.1	45
Well 1	Hamilton et al.	13532	Ness	oil	0.5-0.1	59

Table 3.4b Published ages for the Southern Group, East Shetland Basin - Appendix 3.2.

Early statements concerning the timing of illite diagenesis for the area were expressed as range estimations. However, three modalities are apparent from the collated pool of ages i.e. 35 Ma to 50 Ma, 60 Ma to 65 Ma and 75 Ma – Figure 3.9. These ages suggest that the 45 Ma to 55 Ma age range published without location in Sommer's original study (Sommer 1975, 1978), originated from this area. However, the older and younger modalities apparent from the later data sets indicate that while the area is unlikely to be suitable to a closed system interpretation, the hydrocarbon migration model favoured by Sommer (1978) would require multiple charges to the traps in the area, either associated with distinct, local kitchen areas, or as the result of fill-spill pathways.

Western Group trends and contradictions

The range of ages found in the Western Group are similar to those published for the Eastern group, at 25 Ma – 55 Ma, with the exception of the apparently-contaminated age, 147 Ma, associated with the Cormorant field – Table 3.5. The frequency histogram indicates three modalities, i.e. 25 Ma to 35 Ma, 40 Ma to 45 Ma and 55 Ma – Figure 3.10. Interestingly, the quadrant has more than one example where the coarser fractions have returned younger ages than their finer illite counterparts e.g. 56 Ma and 45 Ma for NW Hutton (Hamilton *et al.* 1992); 34 Ma and 32 Ma for Heather (Glasmann *et al.* 1989). Though this may be a resolution issue, the exceptions buck the generally observed trend of younger ages for finer fractions. Additionally, the area yields consistently young ages relative to the rest of the region, with the exception of the unusual quadrant 211/11.

Location	Author	Depth (ft)	Stratigraphy	Zone	Size (μm)	Age (Ma)
Tern-Eider-Cormorant						
Tern 'I'	Giles et al.	8350	Etive	-	-	-
211/26-CA30	Hamilton et al.	9942	Etive	water	0.3-0.1	147
211/26-CA30	Hamilton et al.	9942	Etive	water	<0.1	36
211/26-CA30	Hamilton et al.	9966	Etive	water	0.3-0.1	34
211/26-CA30	Hamilton et al.	9966	Etive	water	<0.1	41

Table 3.5a Published ages for the Western Group, East Shetland Basin - Appendix 3.2.

Location	Author	Depth (ft)	Stratigraphy	Zone	Size (μm)	Age (Ma)
Hutton-N.W.Hutton-Pelican-Heather						
Hutton -	Harris	-	Brent Group	-	-	45
Hutton -	Glasmann	*11483*	Brent Group	-	-	45
Hutton -	Glasmann	*12139*	Brent Group	-	-	44
N.W.Hutton-X	Hamilton et al.	12618	Etive	water	0.5-0.1	35
N.W.Hutton-X	Hamilton et al.	12618	Etive	water	<0.3	33
N.W.Hutton-X	Hamilton et al.	12467	Ness	oil	0.5-0.1	45
N.W.Hutton-X	Hamilton et al.	12467	Ness	oil	<0.3	56
N.W.Hutton-Y	Scotchman et al.	-	Brent Group	oil	-	av.43
N.W.Hutton-Y	Scotchman et al.	-	Brent Group	water	-	av.41
Well C	Hamilton et al.	10780	Ness	oil	0.5-0.1	44
Well C	Hamilton et al.	10780	Ness	oil	<0.1	35
Well C	Hamilton et al.	10906	Etive	oil	0.3-0.1	27
Well B	Hamilton et al.	11071	Etive	oil	0.5-0.1	27
Well A	Hamilton et al.	11602	Ness	oil	0.5-0.1	55
Well A	Hamilton et al.	11602	Ness	oil	<0.1	41
Well A	Hamilton et al.	11761	Etive	oil	0.5-0.1	25
Heather -	Glasmann et al.	9750	Broom	-	-	40
Heather -	Glasmann et al.	*9843*	Brent Group	-	-	41
Heather -	Glasmann et al.	10875	Tarbert	-	-	40
Heather -	Glasmann et al.	10950	Broom	-	-	51
Heather -	Glasmann et al.	11025	Ness	-	<0.1	31
Heather -	Glasmann et al.	11025	Ness	-	-	34
Heather -	Glasmann et al.	*11155*	Brent Group	-	-	32
Heather -	Glasmann et al.	11175	Etive	-	<0.1	28
Heather -	Glasmann et al.	11175	Etive	-	-	31
Heather -	Glasmann et al.	*11483*	Brent Group	-	-	27
Heather -	Glasmann et al.	11700	Etive	-	-	27
Heather -	Glasmann et al.	11775	Broom	-	-	35
Heather -	Glasmann et al.	*11811*	Brent Group	-	-	34
Heather -	Glasmann et al.	11850	Broom	-	-	32
Heather -	Glasmann et al.	11850	Tarbert	-	<0.1	34
Heather -	Glasmann et al.	11850	Tarbert	-	-	39
Heather -	Glasmann et al.	11925	Etive	-	-	30

Table 3.5b Published ages for the Western Group, East Shetland Basin - Appendix 3.2.

The modality of the Western Group appears slightly more complex than the Eastern Group. This may be simply a result of the data set being larger. However, note the strongly developed trend of younger ages with increasing stratigraphic depth of the sample e.g. Heather. This is sympathetic to the observation of slight indications of such a pattern in the Eastern Group, and clearly developed examples for the Northern Group generally. However, the Cormorant field, Western Group, contradicts this younging of illite ages with depth, as discussed earlier – section 3.17.

3. 8 Interpretation

The following interpretation is drawn from the data set discussed above, covering various aspects of the diverse studies relating to the field area and illite diagenesis in general, collated from publications over the period 1978-2002.

Mind the Gaps

Of the seven or so oil fields on the extremities of the East Shetland Basin that make up the Northern Group, only Magnus, Penguin, Don, Wendy, Murchison, and associated blocks have published illite age data. It is possible that no data exists for Snorre, Zeta and related areas, due to a lack of illite growth or dearth of analytical research – Figure 3.6.

The shallowness of such structures, as indicated in maps and cross sections for the area (Spencer & Larsen 1990), implies reservoir temperatures may be too low for illite diagenesis. Assuming these fields, and others in the region that are absent from the data set, have reasonable poro-perm characteristics and appeared clear with respect to fibrous illite when examined with standard petrophysical equipment, it is unlikely that researchers would have attempted illite separation on their related core. However, with the continued lowering of thermodynamic boundaries on illite stability, it may be that illite occurs as a minor volume within the fields, and has been overlooked.

A second gap, as apparent from the clustering of data around oil fields, is the lack of illite sampling out-with the boundaries of discovered fields. This is obviously in part due to the operator bias i.e. most wells are drilled and cored on discoveries. However, there are enough wildcats, dry holes and misdirected terminations in a large petroleum province to make off-field sampling a viable option. Perhaps the lack of data is then representative of the bias towards researching oil fields rather than source areas and migration pathways. A third, geological explanation, however, is that, as Sommer observed, fibrous illite concentrations drop markedly below the oil-water contact and are absent in clean, water filled sandstones (Sommer 1978). The latter argument, and lack of data pertaining to off-field illite would suggest that illite diagenesis is indeed related to oil charge associated with trap structures, and not to changes in fluid composition and temperature with burial, as favoured by closed system advocates. If the latter were the case, fibrous illite would be widely distributed throughout the sandstones of the basin.

The oldest illite occurs at the crest

The generally observed decrease in age of illite samples with burial depth within a single field, e.g. Heather, Magnus, Veslefrikk and Alwyn – Figures 3.12 - 3.15, would support the commonly proffered hypothesis of illite diagenesis in response to a descending oil-water contact. This suggests that Sommer's original findings (Sommer 1978) may have been parochial and peculiar to the dynamics of the field in question – Section 3.13. However, the pattern is occasionally reversed e.g. NW Hutton and Cormorant – Figure 3.15, perhaps indicating that these fields have similar, renegade dynamics with respect to illite diagenesis, possibly in accord with Sommer's original hypothesis that illite grows in the vicinity of discrete migration pathways associated with hydrocarbon incursion (Sommer 1978), and not as a response to the descending oil-water contact, as commonly seen elsewhere.

Young ages on the flanks and in the shallows

In contradiction to Darby's Central North Sea findings (Darby *et al.* 1998), the largest group of young ages in the East Shetland Basin occur furthest away from the central axis of the graben, on the high, peripheral fields of Heather and Pelican. Similarly, the oldest ages are generally found in fields closest to the graben – Figure 3.16. As a consequence, three likely scenarios arise:

• As the basin has deepened along the axis more rapidly than the terraces, illite diagenesis may simply be a function of burial, associated with temperature increase and thermodynamic thresholds in the reservoir i.e. a chemical artefact indicative of a closed system paradigm.

Alternatively, in an open system event-related paradigm the onset of oil migration would be expected to occur in the graben first and on the terraces last. This prompts the two remaining possibilities.

• illite diagenesis is driven by the deep kitchen area of the Viking Graben and the various ages are in response to the delay in arrival of this regional charge as a result of temporary reservoiring and long residence times in large fields along the fill-spill pathway.

• illite diagenesis is associated with local kitchen areas, growing at different times throughout the basin in response to the onset of local charges as small kitchen areas become active. This would then be a function of local fault dynamics and subsidence, independent of the graben axis subsidence rate.

Age resolution

It is worth considering the resolution of ages as they occur in the Northern North Sea. Illite ages, in common with all experimentally derived data, are subject to error as a result of the method employed. In the case of illite K-Ar ages this may be as low as ±1 My. Typically, the ages are good to within ±5 My. A second, and discrete error, however, is geological in nature, and specific to the vulnerability of the method to potassium contamination by phases such as feldspar, mica and detrital illite. This aspect of the error is widely recognised as unquantifiable, beyond the semi-quantitative methods of assessing sample purity. As such, the contamination error is often assumed to be in excess of the experimental error. As a consequence, illite ages are conservatively deemed to be at best resolvable

to ±5 My. This obviously is a hindrance to high-resolution interpretations of synthesised data sets as employed in this chapter. However, it seems reasonable to approach the data in this fashion when examining the various aspects of illite diagenesis as they are presented and debated in the literature.

Renegade ages

Instances of distinctly different ages occurring in otherwise coherent arrays are not uncommon in the Northern North Sea region. The statistical significance of such ages is refutable, in light of the likely geological error, ±10 My, as discussed above. However, these ages appear to be conspicuously older as in the Heather field, 40 Ma – *50 Ma* – 30 Ma – 25 Ma, or more controversially the Magnus field, 70 Ma – *80 Ma* – 70 Ma – 65 Ma – Figures 3.15 and 3.12 respectively. By contrast, the ages may equally be younger as in Huldra, 60 Ma – *35 Ma* – 55 Ma, and Ninian, 60 Ma – *45 Ma* – 60 Ma – Figures 3.13 and 3.14. These outliers do seem to occur within the general trend of ages and occasionally form their own discrete arrays as in the deeper samples for the Heather field, 40 Ma –30 Ma –25 Ma – *35 Ma* – *30 Ma* – Figure 3.15. These are perhaps indicative of discrete modalities, indicating multiple events affecting different horizons within the reservoir. This interpretation is dependent on two assumptions: firstly, an event-related diagenetic model of fibrous illite being adopted or reasonable in light of standing hypotheses; secondly, a lenient application of error estimation with respect to the K-Ar ages in question. The first assumption will either be sustained or collapse in lieu of the principal hypothesis driving this thesis. The latter assumption is discussed briefly above and given further consideration in chapter 4.

Coarser fractions yielding younger ages

The latter phenomenon, as apparent in the Western Group – Figure 3.6, is usually attributed to either sequential growing or contamination, or alternatively dismissed as unresolvable given the limitations of the method. However a reversal of the norm would suggest that coarser fractions may represent distinct and valid ages independent of the finer fraction, and possibly indicative of discrete events associated with coarser sandstone carrier beds experiencing earlier episodes of oil charge. While this is amenable to the status quo when coarser fractions return slightly younger ages as in the above cited examples, the implication of this pattern is that the coarser fraction may also be a true age when older. This would support a reconsideration of the Magnus field data.

Generalities of the big picture

A simple generalisation of the distribution of ages in the region is that the older modalities, 70 Ma to 60 Ma, occur close to the deeper parts of the Viking Graben – Figure 3.16. The younger modalities occur peripherally on both the west and east flanks. The 60 Ma – 30 Ma bimodal pattern in the Eastern Group occurs in fields juxtaposed between the graben and eastern terraces. This argument is tenuous, though, due to the small amount of data in the Norwegian sector. The pattern in the UK sector is more developed and generally decreases towards the fringe of the basin, 60 Ma – 40 Ma – 20 Ma. As discussed in the accompanying interpretation, there are a number of distinct and unusual

exceptions to this simplistic model. However, it is accurate enough to promote questions concerning the large-scale dynamics of the basin that may or may not be underlying illite diagenesis. Such a simple conceptual view lends itself to both closed and open system interpretations.

The anomalies of the northern arrays

Perhaps the most intriguing and challenging area for consideration of these three simple models is the Northern Group quadrant, as it presents both the youngest and oldest ages in the basin. The principal component of the Northern Group quadrant is the Magnus Province.

• At 17 Ma and 24 Ma, quadrant 211/11 of this province appears to record the last fibrous illite growth in the East Shetland Basin. The position of the younger age below the older age in this small array, as well as the Magnus field and Penguin field arrays, is counter-intuitive to the expected supra-position of illite growth in the closed system model as a result of early growth in the deepest parts of the reservoir. Early growth high in the trap structure is far more sympathetic to the dynamics of an open system approach, as both the local and regional models are amenable to the descending oil-water contact explanation of this phenomenon.

• The Magnus field also yields ages typical of intermediate modalities i.e. about 40 Ma to 60 Ma. Similar ages are found in all four cardinal groups – Figure 3.6, and as such are loosely representative of the Northern North Sea. Indeed, for published data where locations were withheld at the time of publication to protect commercial interests, all return similar ages e.g. 45 Ma to 55 Ma, 54 Ma to 56 Ma and 45 Ma to 60 Ma – Table 3.6. In as much as these unattached ages are true to the mean, they are misleading in their failure to address the boundaries of onset and cessation, as well as the complexities of arrays associated with specific fields.

Location	Author	Depth (ft)	Stratigraphy	Zone	Size (µm)	Age (Ma)
Brent Province north–ESB–Viking Gbn						
Brent Pr'nce -	Hamilton et al.	X to x+109	Rannoch	-	c'rse-fine	60-45
Brent Pr'nce -	Hamilton et al.	X to x+109	Rannoch	-	<0.05	59-46
ESB -	Sommer	-	Brent Group	-	-	45-55
Wendy-Magnus-Penguin-Don						
'Z'	Hamilton et al.	13322	Tarbert	Oil	<0.1	54
VG -	Glasmann	*14764*	Brent Group	-	-	54
VG -	Glasmann	*14764*	Brent Group	-	-	55
VG -	Glasmann	*14764*	Brent Group	-	-	56

Table 3.6 Unallocated ages for the Northern North Sea - Appendix 3.2.

• following on from the previous point, and in light of the oldest though apparently unacceptable ages of 83 Ma and 88 Ma for the Magnus Province, an event-driven model would need to go beyond satisfying the norm, accounting for both the diversity and complexity of ages as they occur in the Northern Group and other groups of the region. It is not enough to satisfy the mean in this respect, but

vital to question the assumptions implicit in marshalling the boundaries of the illite diagenesis paradigm. Why is there no zero-age illite? Is it necessary to restrict the conceptual model to a minimum age of approximately 20 Ma? Equally, what controls the upper limits of acceptable illite ages? Why is an upper limit of 75 Ma preferable to 70 Ma or 80 Ma? Or 90 Ma?

Shifting the boundaries

It is the intention of this thesis and the following experimental and basin modelling chapters to address these questions by testing the null hypothesis that:

> *fibrous, pore-filling diagenetic illite, as found in oil fields, is fundamentally a response to shifts in regional hydrodynamics – specifically the onset of oil migration within the petroleum system. K-Ar illite ages record the onset of oil charge into a trap structure (Chapter 1, section 1.24).*

Furthermore, it is the intention of this thesis to experimentally challenge this hypothesis in the unusual crucible of the Northern Group i.e. the Magnus and Penguin fields and associated petroleum systems. This area represents the full spectrum of illite ages in the region, from the lack of zero ages, through the youngest and mid-range modalities, to controversially old ages.

3.9 Summary and conclusions

In summary, it would appear that the general pattern of Northern North Sea illite age data favours an open system event-driven diagenetic model, where hydrocarbon charge appears to be the prime suspect. As a consequence, the following chapters have to meet two challenges.

• firstly to establish whether such a conceptual model can stand in the light of new data and petroleum system simulation by computational modelling.

• secondly to distinguish between the regional Viking Graben charge hypothesis with its related implications of long-distance migration and fill-spill cascades and the alternative hypothesis of local charge from small, but numerous kitchen areas.

It is the intention of this thesis to attempt to redefine the boundaries of the illite diagenesis paradigm in order to establish reasonable age limits for illite diagenesis in the Northern North Sea, explain the lack of recent illite growth, and propose a conceptual model that accounts for the complexities as well as the generalities of fibrous illite diagenesis. To whit, a brief synopsis of the principal conclusions drawn from this regional review and synthesis of published ages follows below.

Fibrous illite growth is common in the deeply buried sandstone reservoirs of Northern North Sea oil fields. The K-Ar age dating technique has been widely applied to these fields since its inception as a tool for establishing the timing of hydrocarbon migration in 1978.

The key processes controlling fibrous illite growth are elusive, and much debated in published work. These are namely pore fluid control; temperature control; hydrocarbon migration control.

Different schools of thought exist regarding the significance of illite diagenesis, and have remained trenchant since the 1970's.

A compilation of published age dates for the Northern North Sea shows two simple patterns:

• firstly, older ages occur at the top of trap structures, becoming younger with depth. This is compatible with oil filling and well shown in the Heather, Magnus, Pelican and Alwyn fields.

• secondly, a regional pattern indicates that old ages occur near the graben axis and progressively young towards the peripheral, and shallow terraces of the western margins of the East Shetland Basin. This is unexpectedly simple. The pattern is compatible with the progressive maturation of Kimmeridge Clay source rocks in local hydrocarbon kitchens, starting in the deep Viking Graben, and gradually transferring west, as the East Shetland Basin subsided during the Tertiary.

There are no zero Ma ages, as would be commensurate with a simple thermodynamic control of illite growth. It is probable that illite grows at temperatures as cool as 50°C, though in such small volumes that it is difficult to detect, separate and analyse using routine petrographic techniques.

The morphology of fibrous illite is unusual, i.e. not a typical outcome of standard high-entropy crystal growth. As a consequence, the conditions required for nucleation may restrict fibrous illite to growing under highly unusual porewater conditions, i.e. the onset of hydrocarbon charge into trap structures.

Anomalous age arrays exist for the far northern extremities of the East Shetland Basin, in particular the Magnus and Penguin fields.

The simplest interpretation is similar to the first published ideas on the phenomenon: fibrous illite grows in response to hydrocarbon charge, with no temperature threshold for growth. The unusual hydrogeological dynamics of porewaters at such times are responsible for the catastrophic diagenetic response. When the hydrocarbon charge ceases, illite growth stops. The East Shetland Basin is geologically and hydronamically old and inactive, and has been for nearly twenty million years. This is the reason for the lack of recent fibrous illite growth.

In conclusion, it was proposed that on the basis of the aforementioned evidence, a detailed analytical and experimental study of the Penguin field, Magnus Province and associated petroleum systems be undertaken in order to establish a combined case study of fibrous illite diagenesis and hydrocarbon charge timing for the Northern North Sea. This research is presented in the following two chapters.

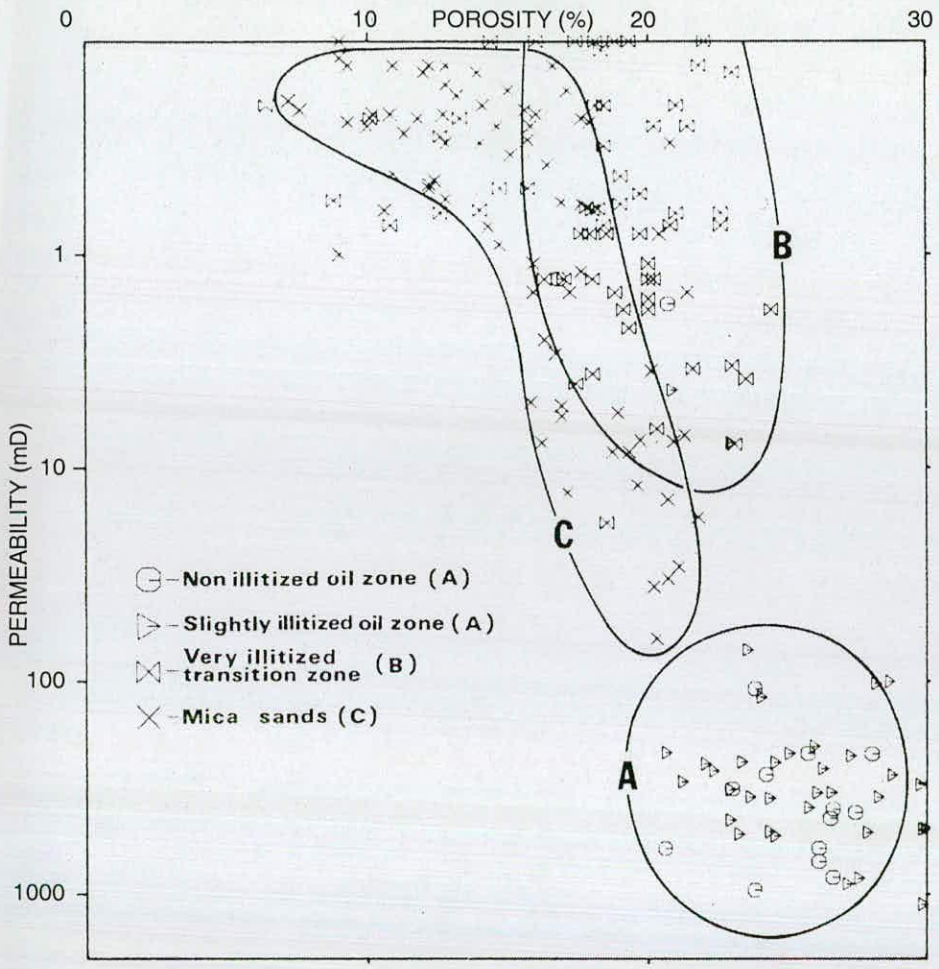

Figure 3.1 Permeability reduction as a result of illite diagenesis. These results from the Alwyn area indicate three fields of permeability. The presence of illite is seen to have a drastic effect on reservoir quality as evident in the relatively high porosities and dramatically low permeabilities of set B (from Sommer 1978).

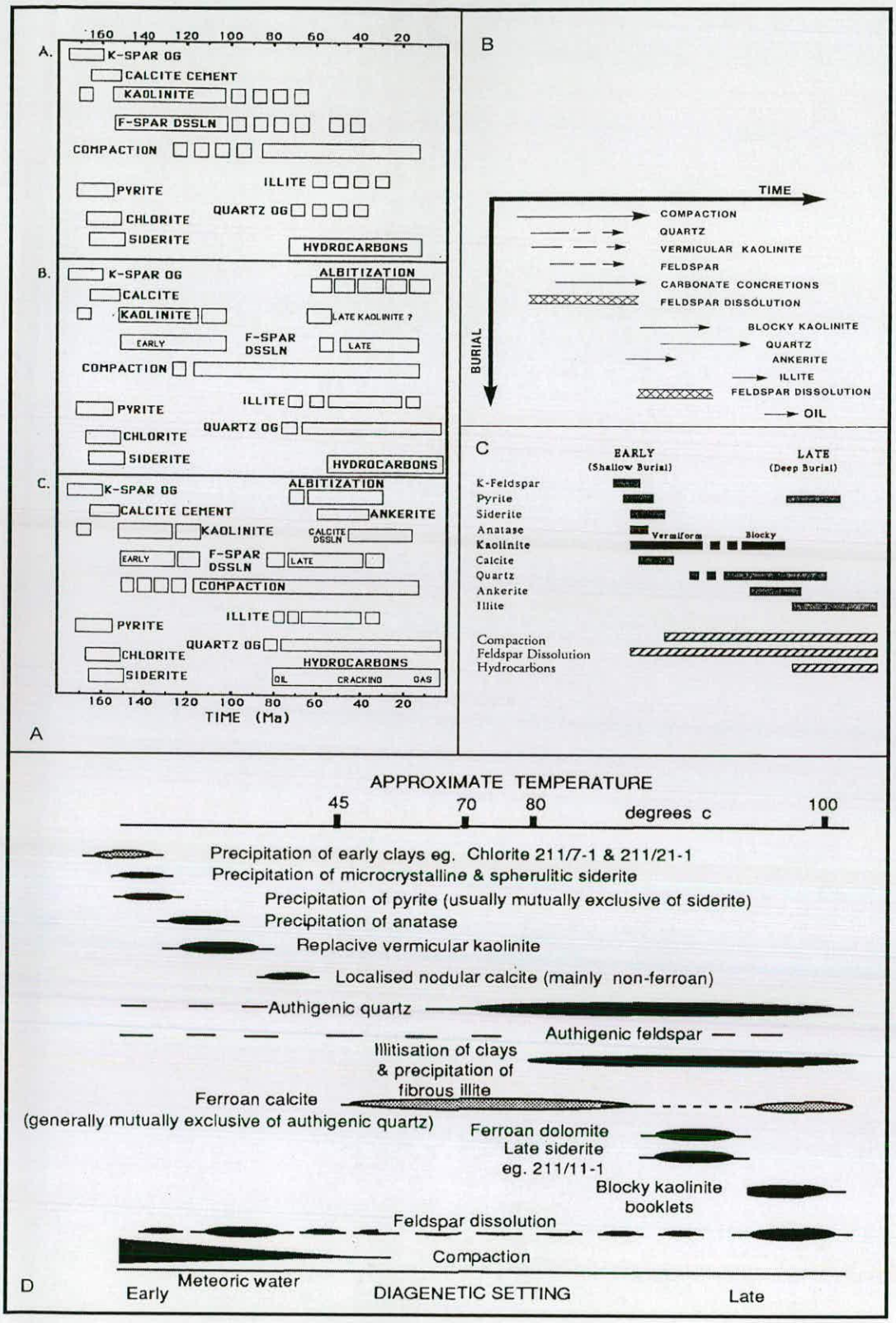

Figure 3.2 Illite paragenesis and associated estimates for the timing of hydrocarbon charge in Brent Group oil fields. A - shallow, medium and deep field profiles (Glasmann 1992); B & C – general descriptions (Haszledine et al. 1992; Osborne et al. 1994); D – temperature associations (Giles et al. 1992). Note the ubiquitous late association of a single hydrocarbon charge to paragenesis.

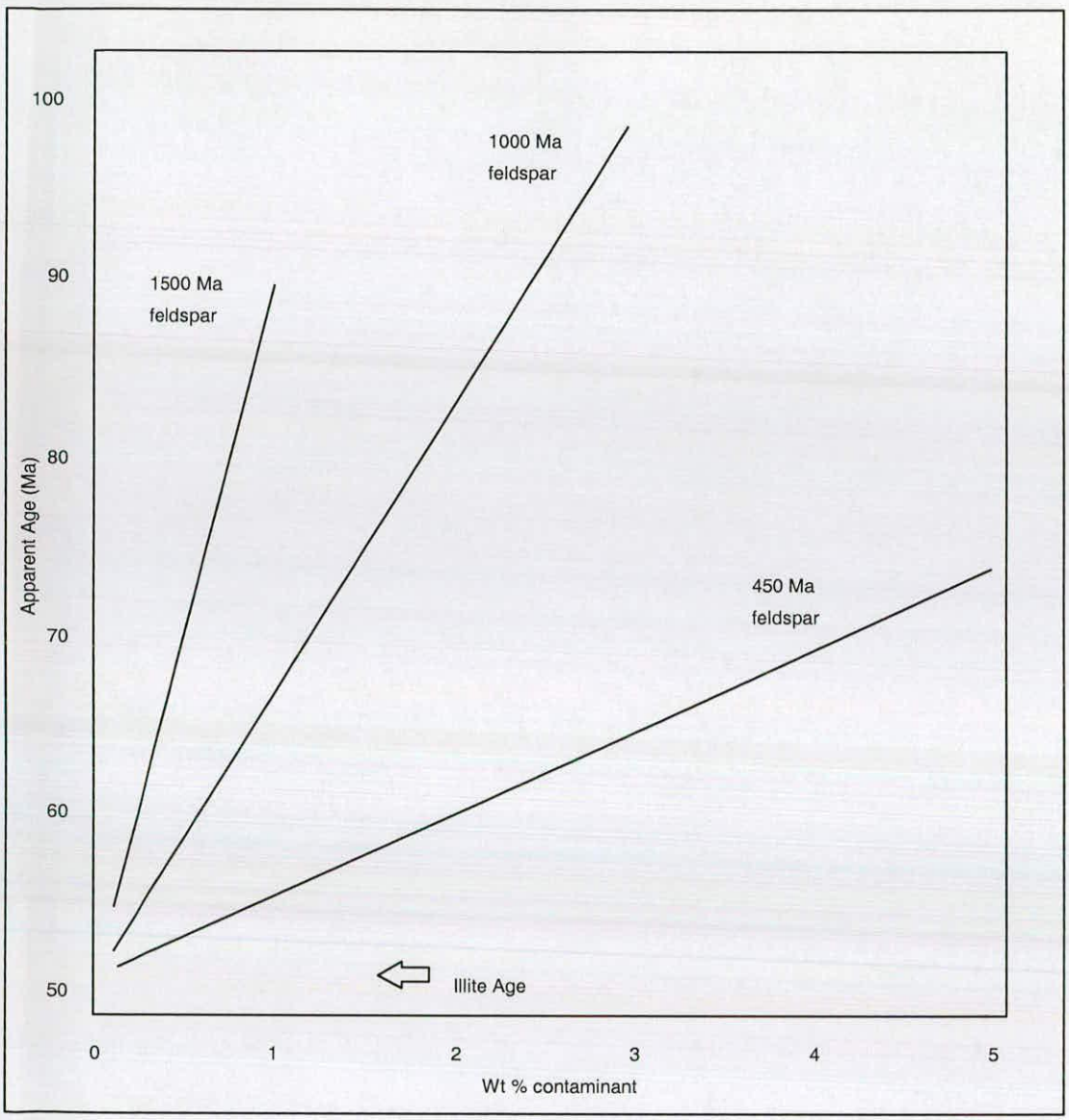

Figure 3.3 A crossplot for likely contaminant phases present in illite K-Ar analyses. The resultant apparent age of K-Ar data from such aliquots is highly sensitive with respect to the weight percentage of contaminant present and the provenance of the potassium-bearing contaminant phase. The three lines represent potential orogenies associated with sediment source areas (after Hamilton et al. 1992).

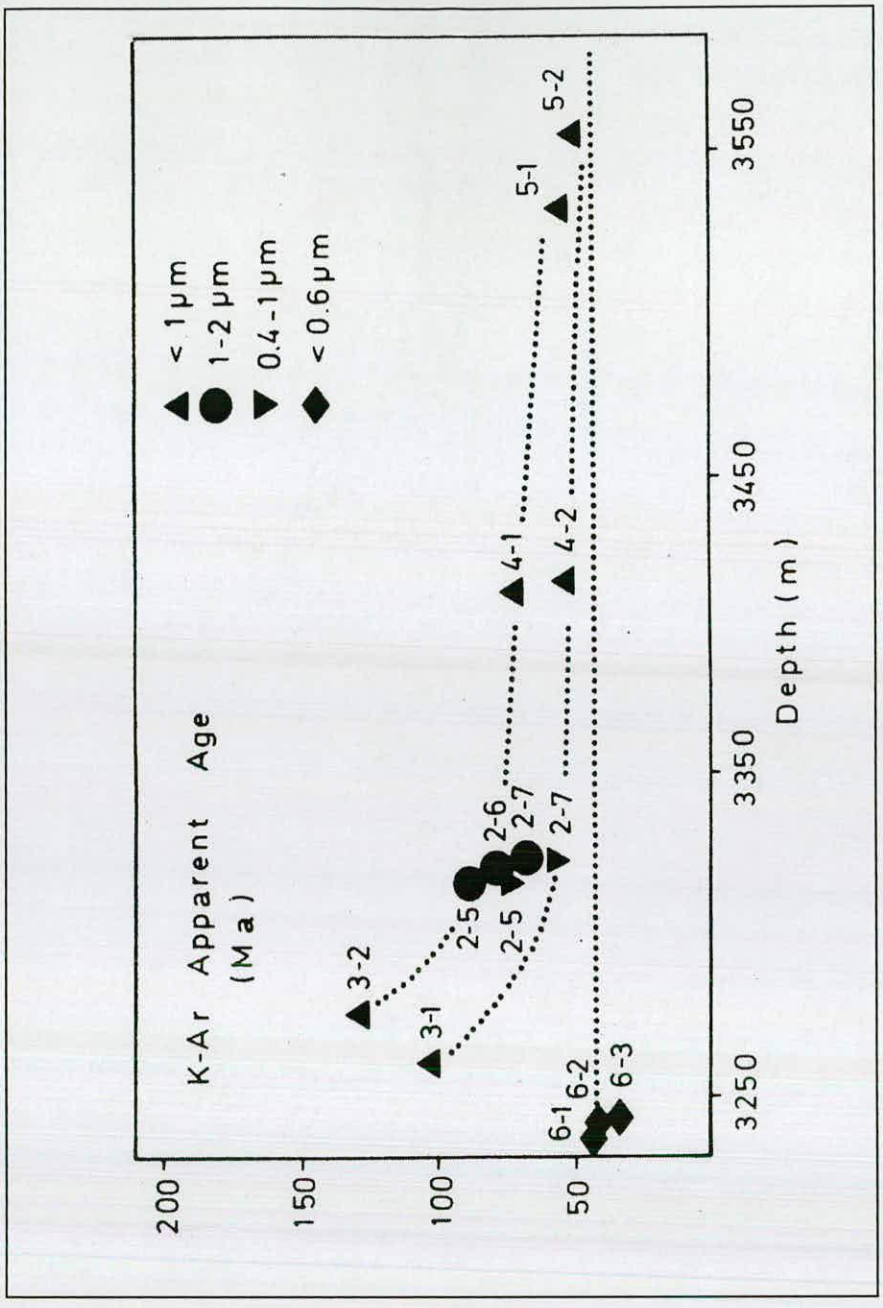

Figure 3.4 Extrapolation of illite ages from a contaminated data set (Liewig *et al.* 1987). Note that the coarser samples tend to yield older ages – a trait indicative of contamination. All the data is from a single field and appears to resolve to an age of about 40 Ma.

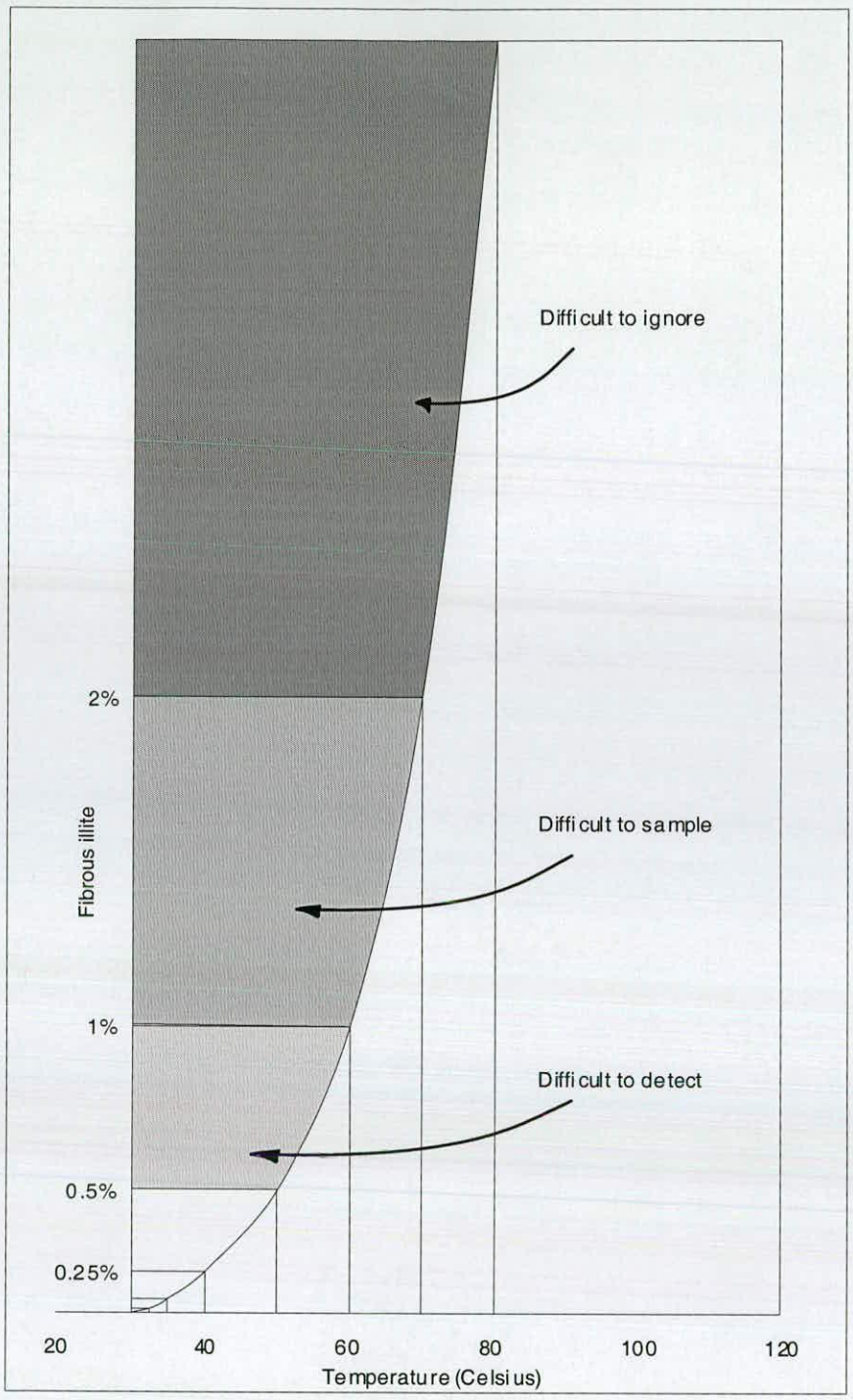

Figure 3.5 Illite abundance and visibility with respect to temperature. Assuming the premise that the rate of reaction approximately doubles with each 10°C temperature increase, after Arhennius, the apparent scarcity of fibrous illite at low temperatures is simply a function of chemistry. However, the curve illustrates that commonly cited 'threshold' temperatures for fibrous illite precipitation may simply be artefacts of the low concentration of this diagenetic phase in the reservoirs studied.

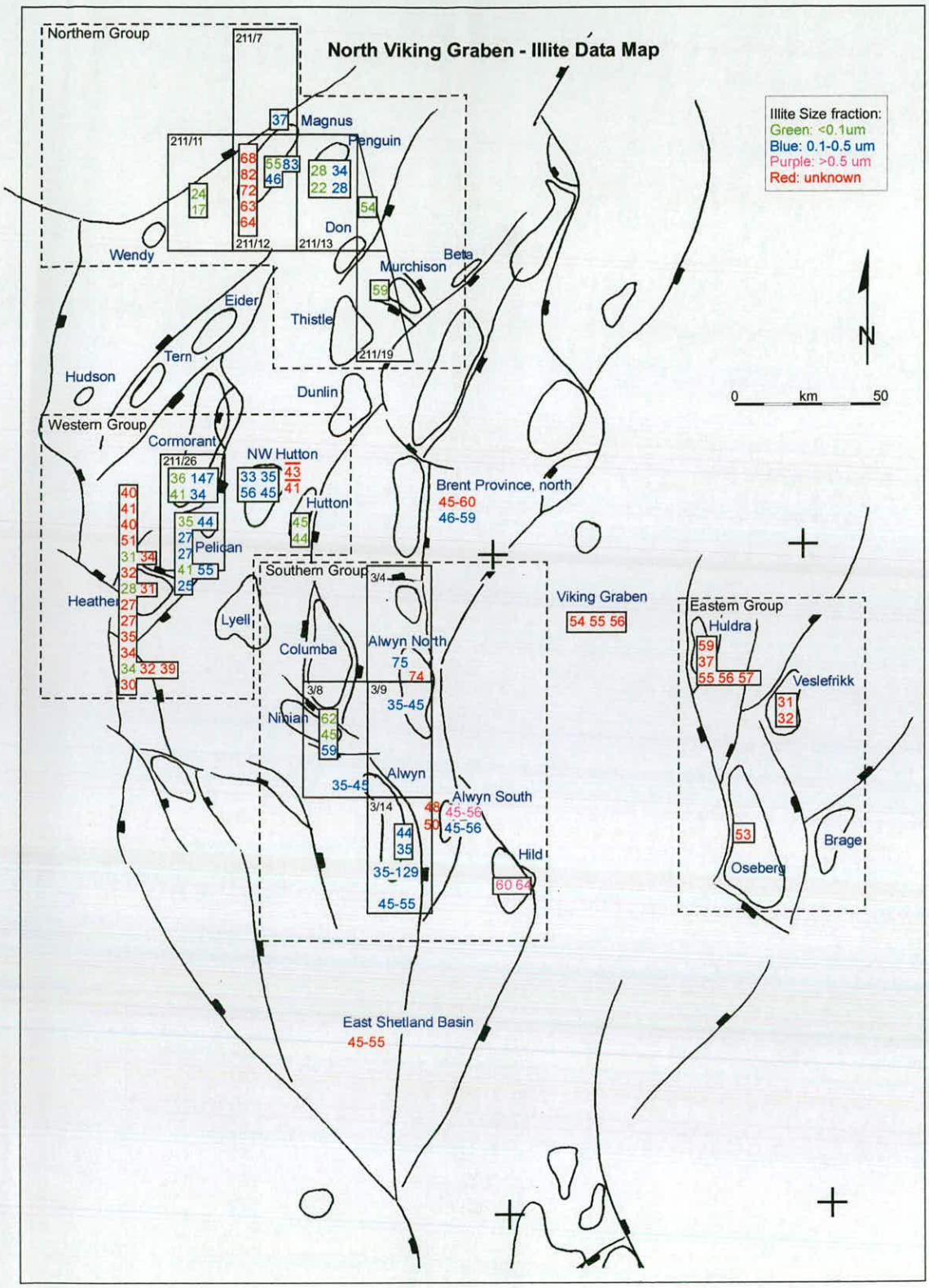

Figure 3.6 Illite age compilation map for the Northern North Sea. The map is divided into four arbitrary areas consisting of grouped data for the four cardinal directions. Colour coding of illite ages identifies the size fraction of aliquots. Data displayed within a box has been correlated to a specific depth; a small bar over an age indicates a mean value; two hyphenated ages indicate a range. The underlying map is a simple structural map indicating the principal fault geometries and field locations after Geco/Prakla (1985)

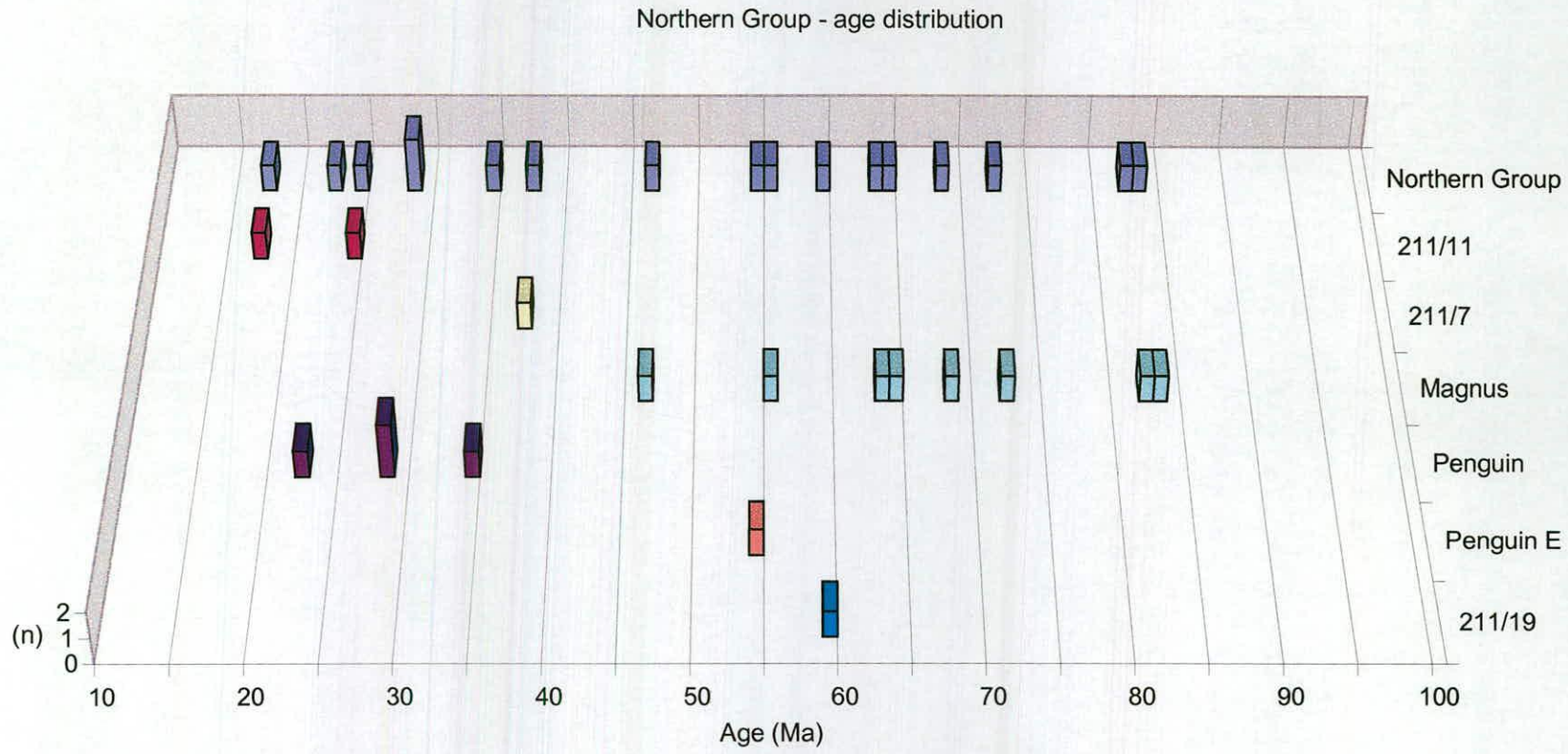

Figure 3.7 A histogram of fibrous illite ages for the Northern Group quadrant. The figure shows that the Northern Group has an unusually wide spread of ages, representing both the youngest and oldest published data for the Northern North Sea, as well as more typical modalities associated with fields throughout the East Shetland Basin. The predominant studies in the area focus on the Magnus field.

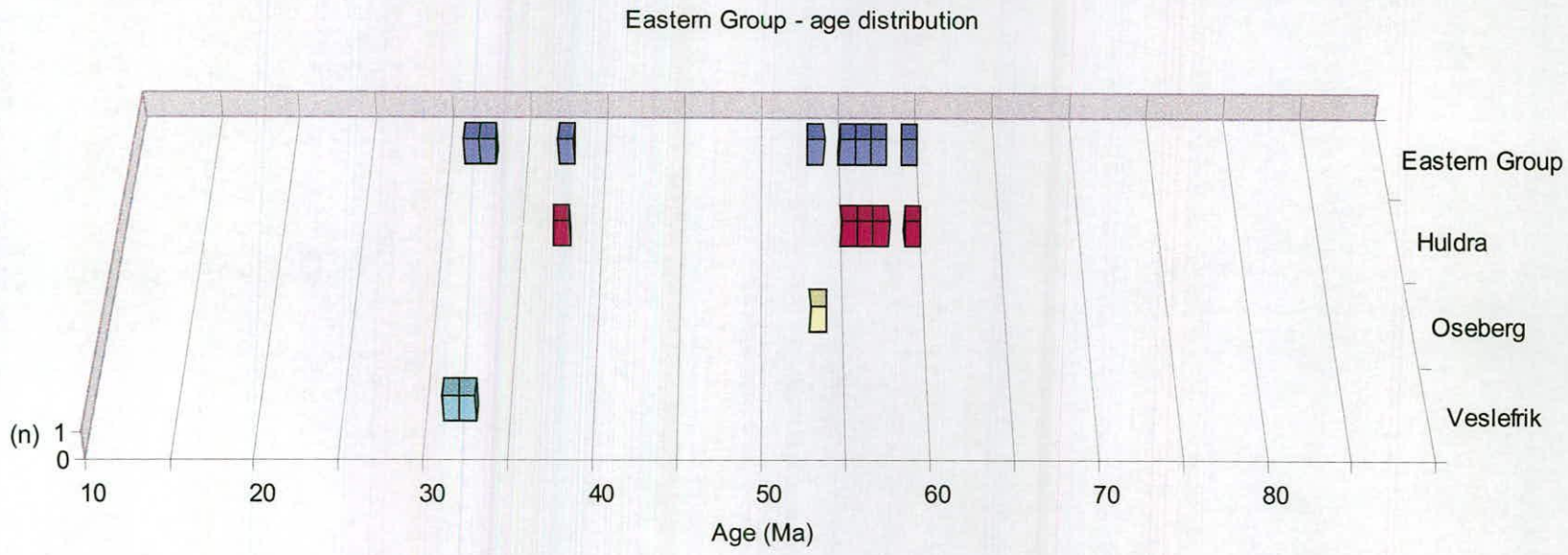

Figure 3.8 A histogram of fibrous illite ages for the Eastern Group quadrant. Although the data set is relatively small, there appears to be a distinct bimodality to the age distribution. Huldra has seemingly undergone two episodes of illite growth. The younger modality is also present in the Veslefrik field. Likewise, the older modality occurs in the Oseberg field.

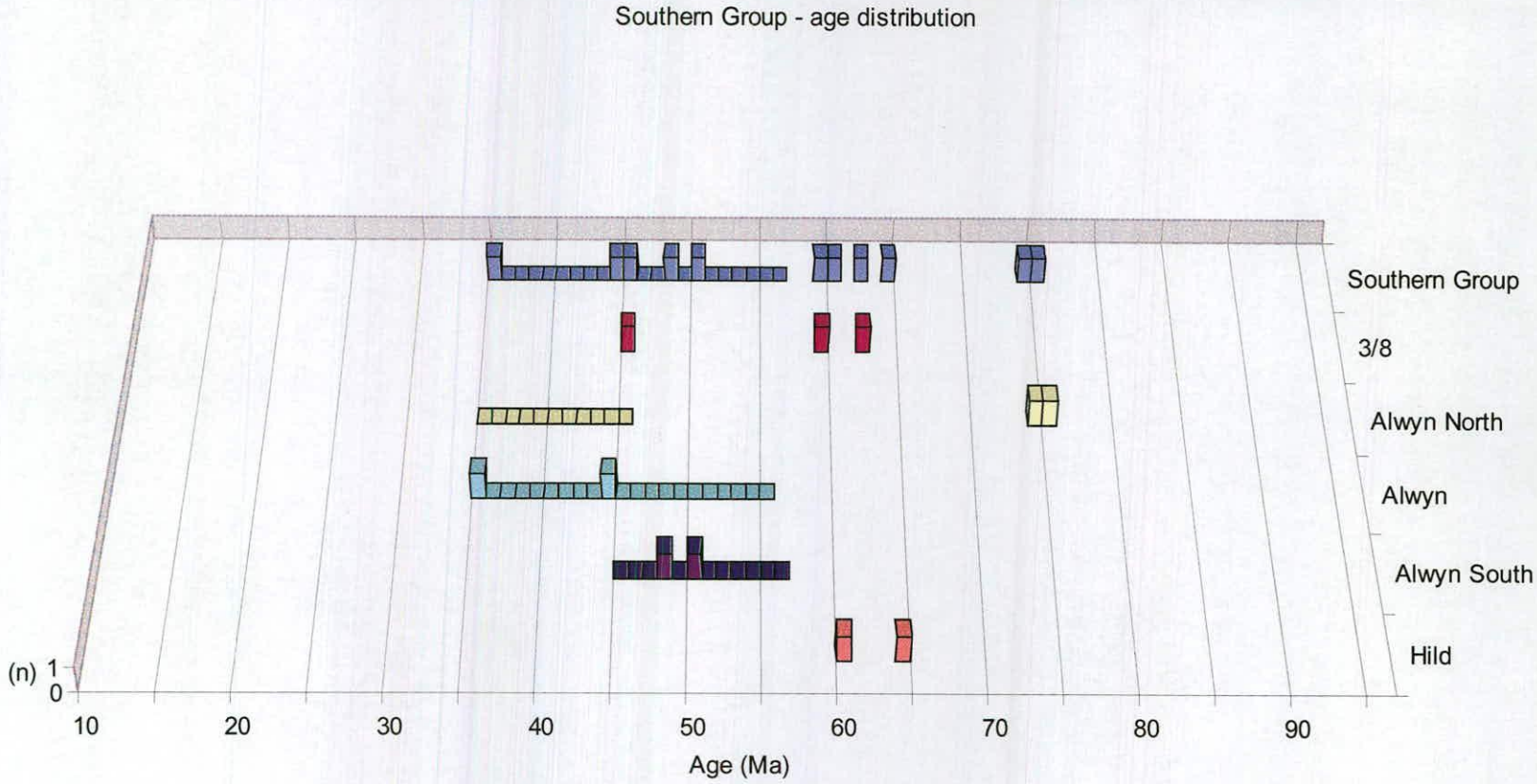

Figure 3.9 A histogram of fibrous illite ages for the Southern Group quadrant. The southern age distributions tend to have been published with ranges, hence the empty bands associated with the Alwyn area. This is an artefact of the early publication style adopted by Sommer (1978) and later co-workers (Jourdan *et al.* 1987) and Hogg *et al.* (1992). Note that these ranges tend to skew the data array towards older ages. This is a consequence of the assumption that such results are contaminated by older potassium-bearing phases. However, in general, the data appears to demonstrate older to mid-range modalities.

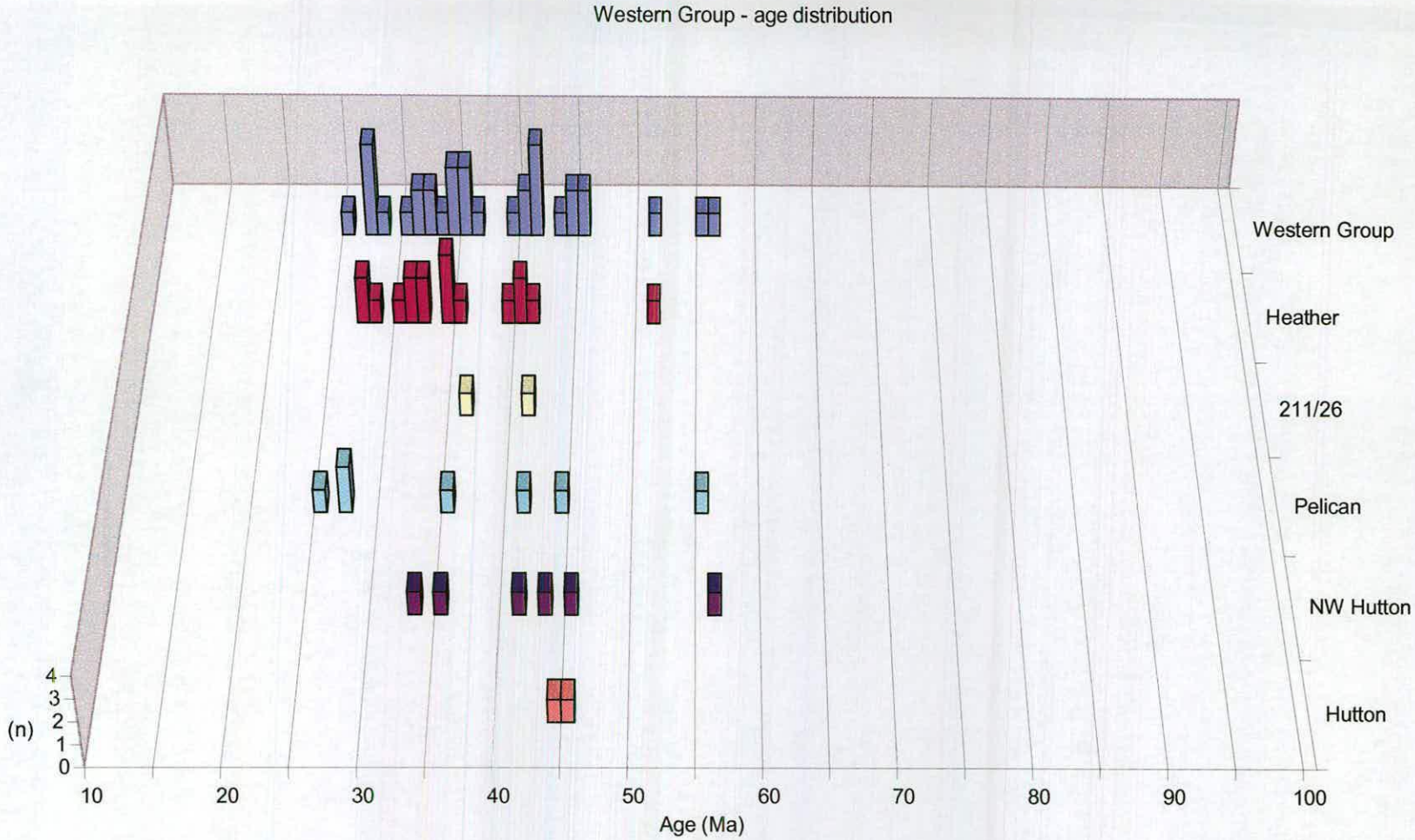

Figure 3.10 A histogram of fibrous illite ages for the Western Group quadrant. This area on the western shallows and terraces of the East Shetland Basin contains young to mid-range modalities, in contrast to the Southern Group. Though the data sets are small and age resollution is a moot point, the fields appear to show four distinct modalities: three young clusters between 25 Ma and 45 Ma, and an older modality around 55 Ma. Interestingly, the Heather field appears to have all four modalities present in its age array.

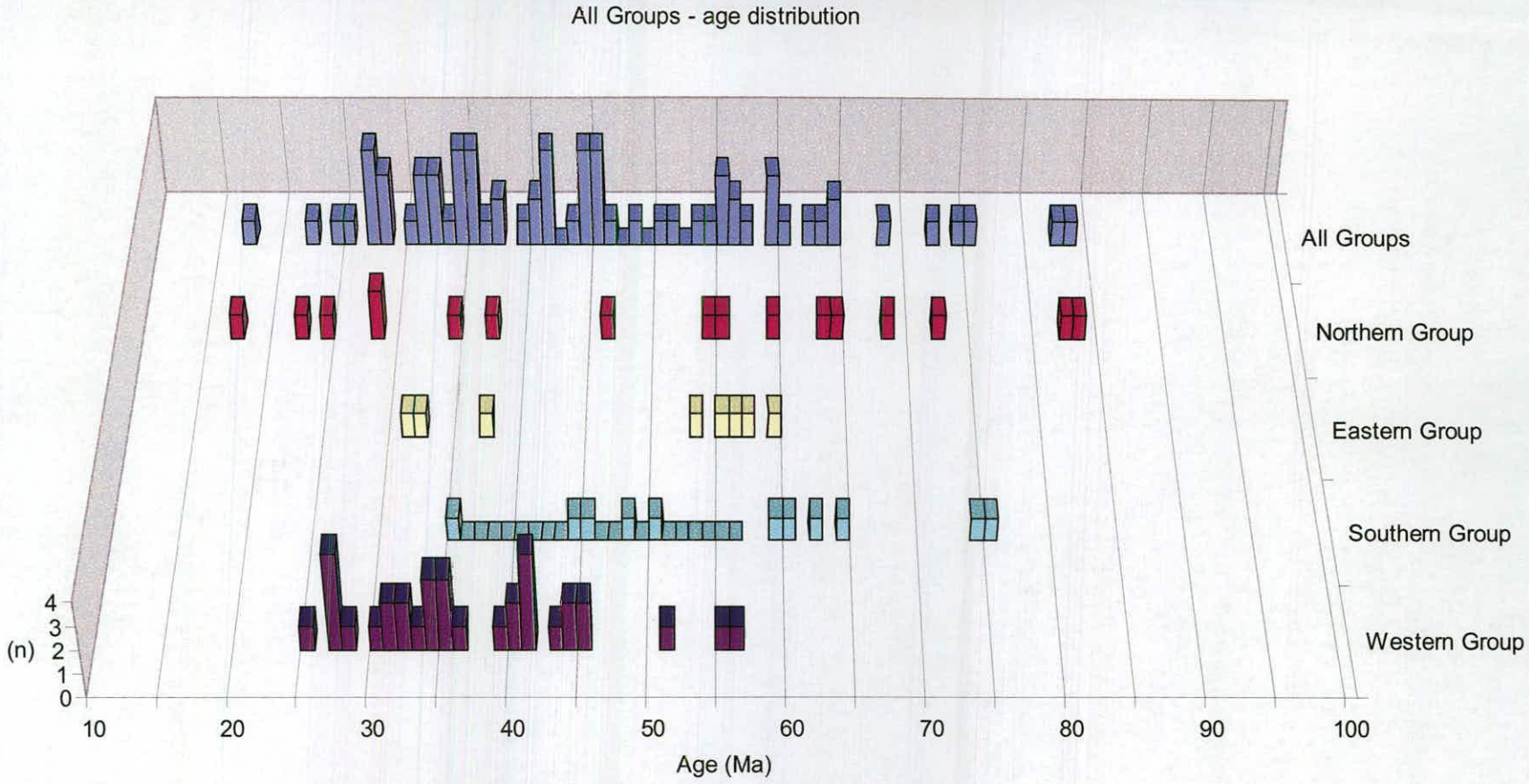

Figure 3.11 A histogram of fibrous illite ages for all four quadrants studied in the Northern North Sea. The composite figure shows that while there are two principal clusters of data around the 25 Ma to 45 Ma period of time, there are also saignificant clusters or modes associated with 55 Ma to 65 Ma, and 70 to 75 Ma. Ages in excess of 80 Ma and less than 20 Ma appear to be outliers with respect to the main body of data. Note the conspicuous absence of ages less than 15 Ma.

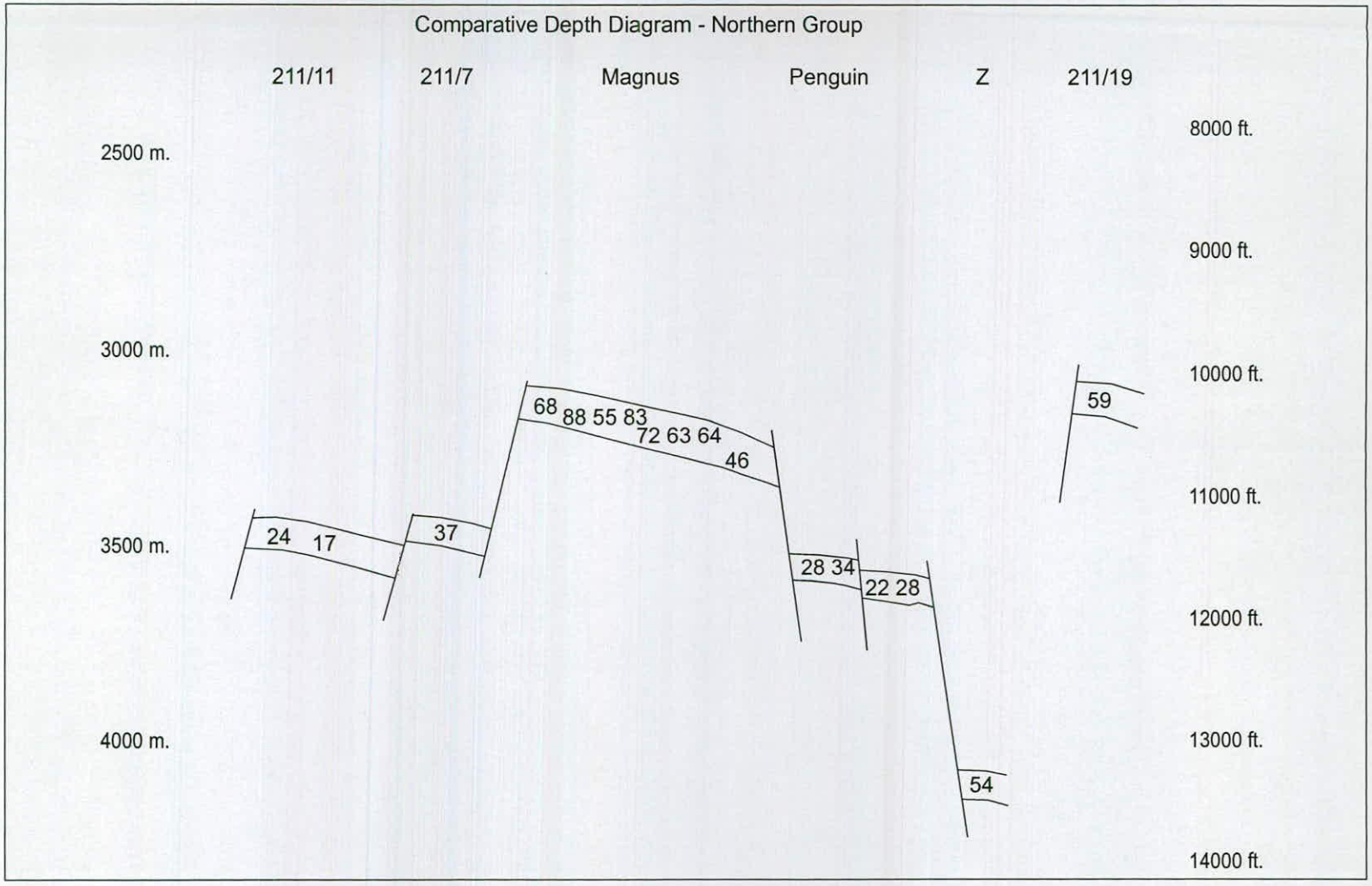

Figure 3.12 A comparative depth diagram for the Northern Group data. The presentation does not infer geological or hydro-geological characteristics to the groups. Note that ages tend to get younger with depth both within field arrays and in absolute terms.

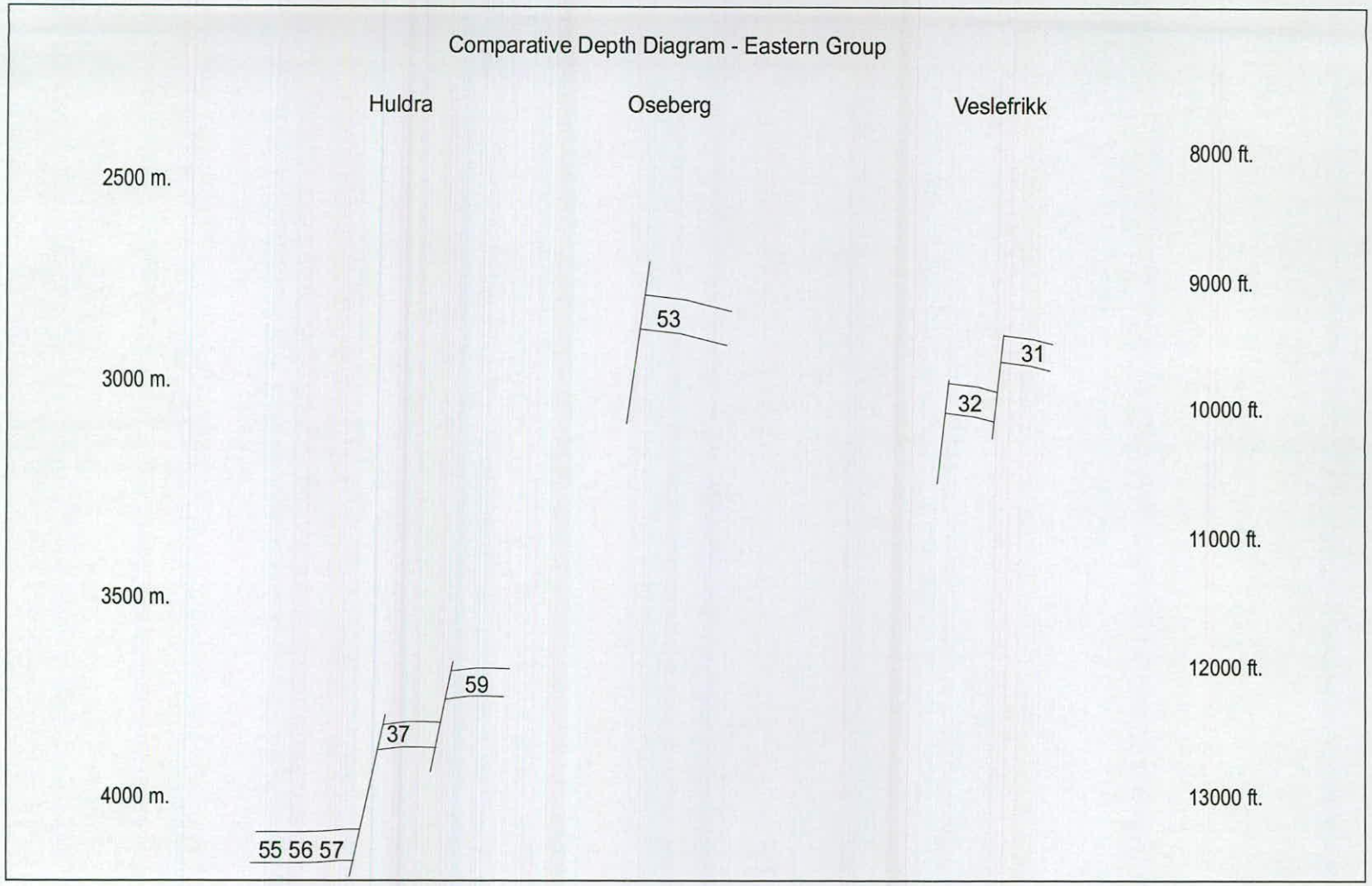

Figure 3.13 A comparative depth diagram for the Eastern Group data. The presentation does not infer geological or hydro-geological characteristics to the groups. Note the bimodality of ages for the Eastern Group quadrant.

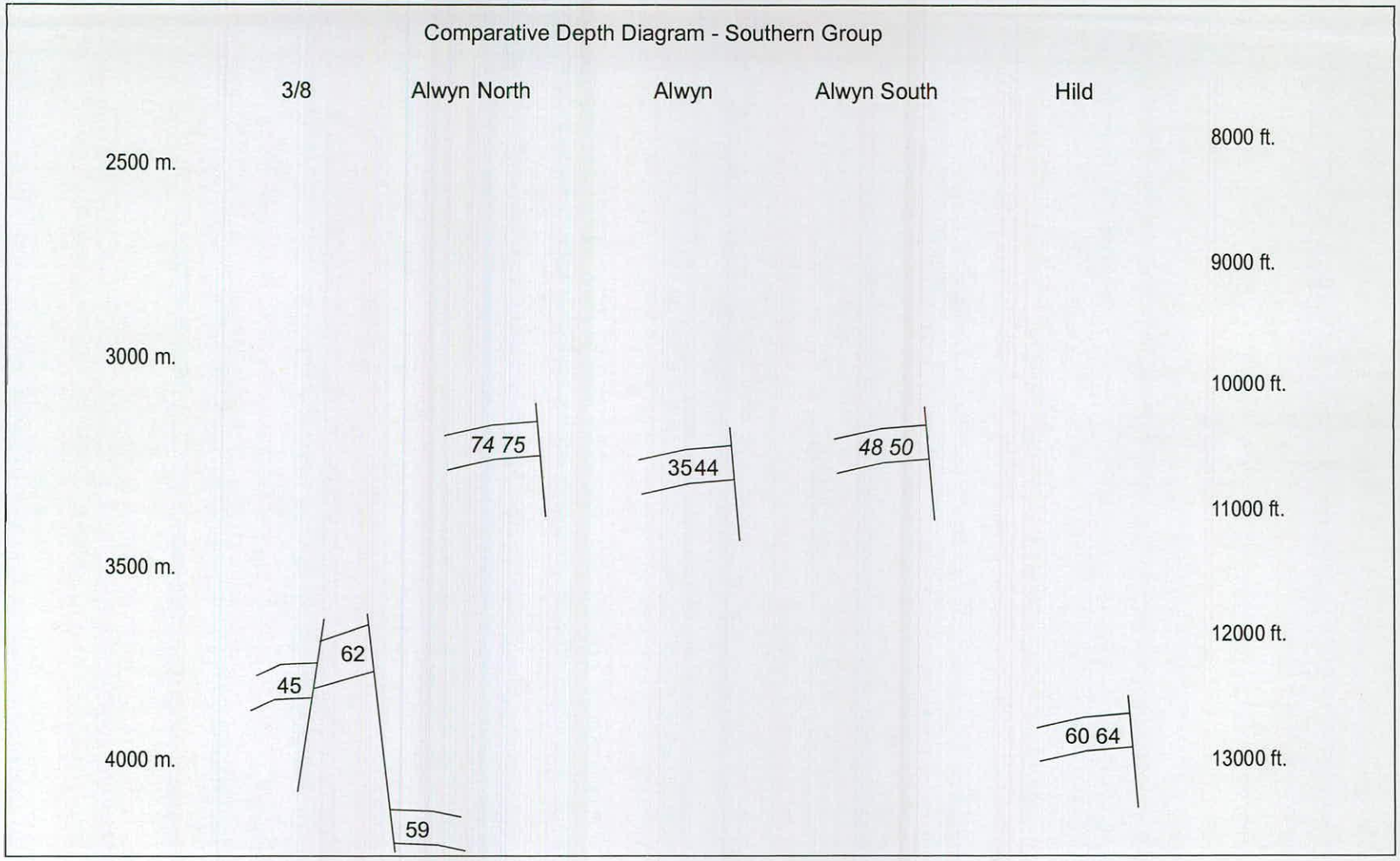

Figure 3.14 A comparative depth diagram for the Southern Group data. The presentation does not infer geological or hydro-geological characteristics to the groups. The Alwyn area presents a diverse range of ages for fields of a similar depth. 3/8 appears to exhibit bimodality.

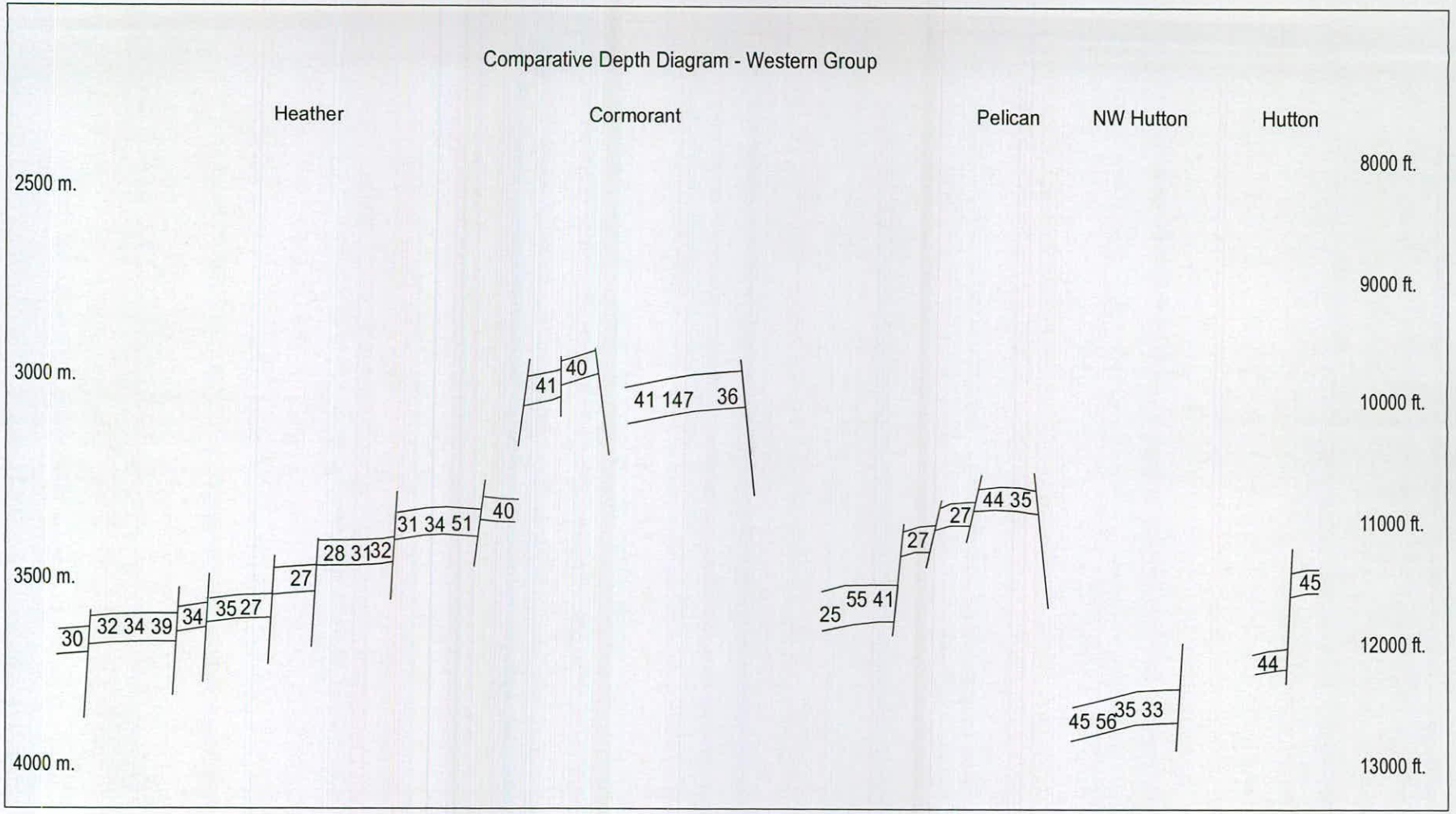

Figure 3.15 A comparative depth diagram for the Western Group data. The presentation does not infer geological or hydro-geological characteristics to the groups. The data arrays for this quadrant are complex, and discussed at length in the main body of the text.

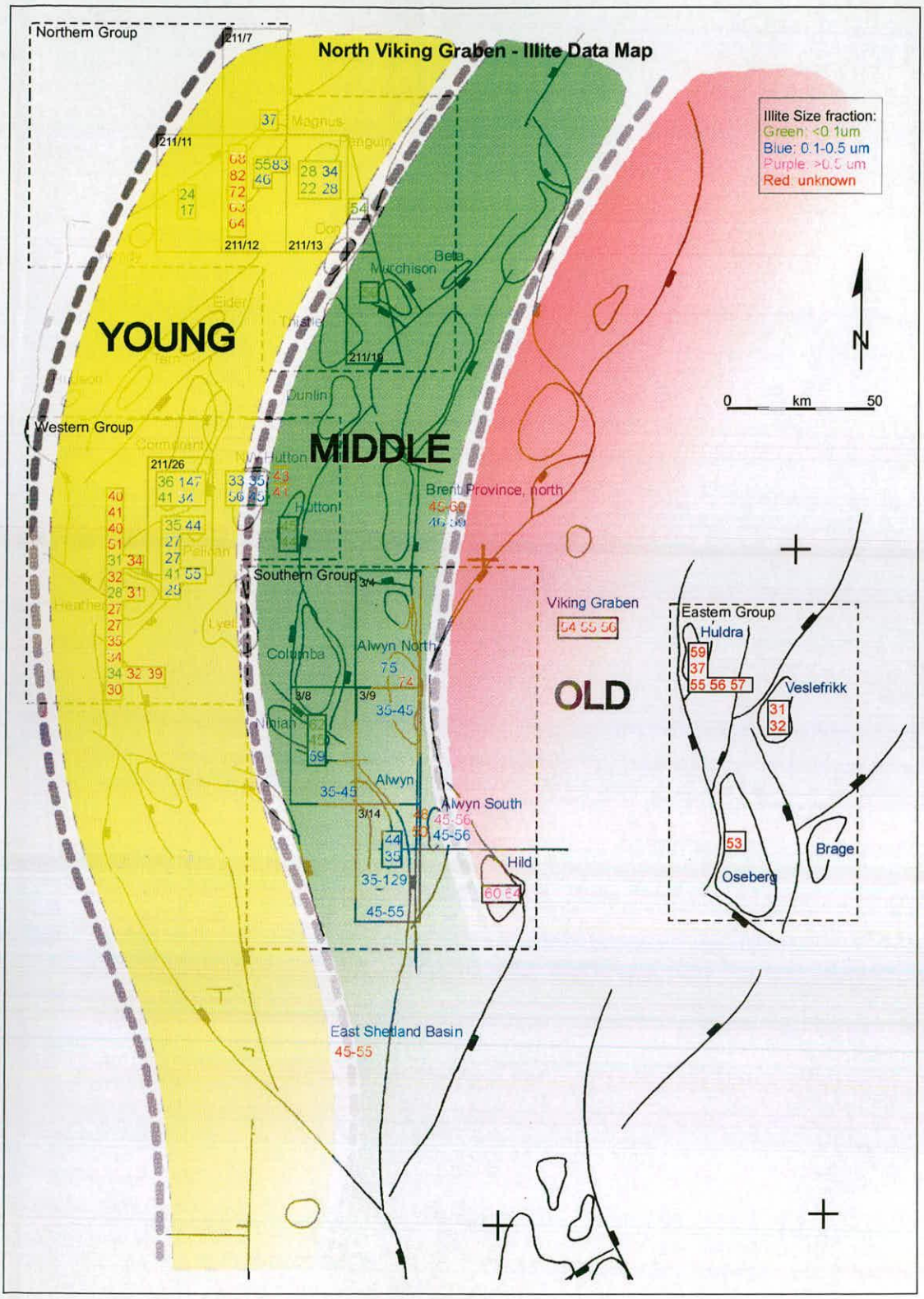

Figure 3.16 Illite ages for the Northern North Sea - an interpretation. This highly simplistic scenario equates the oldest ages to the deepest, graben-associated areas of the East Shetland Basin, middle ages to the intra-terraces of the basin, and youngest ages to the peripheral shallows. While this addresses the general picture and appears amenable to both closed and open system hypotheses concerning illite diagenesis, the closed system scenario fails to account for the ubiquitous complexities of illite age arrays in the region. Open system formulations are more sustainable in the face of such complexity.

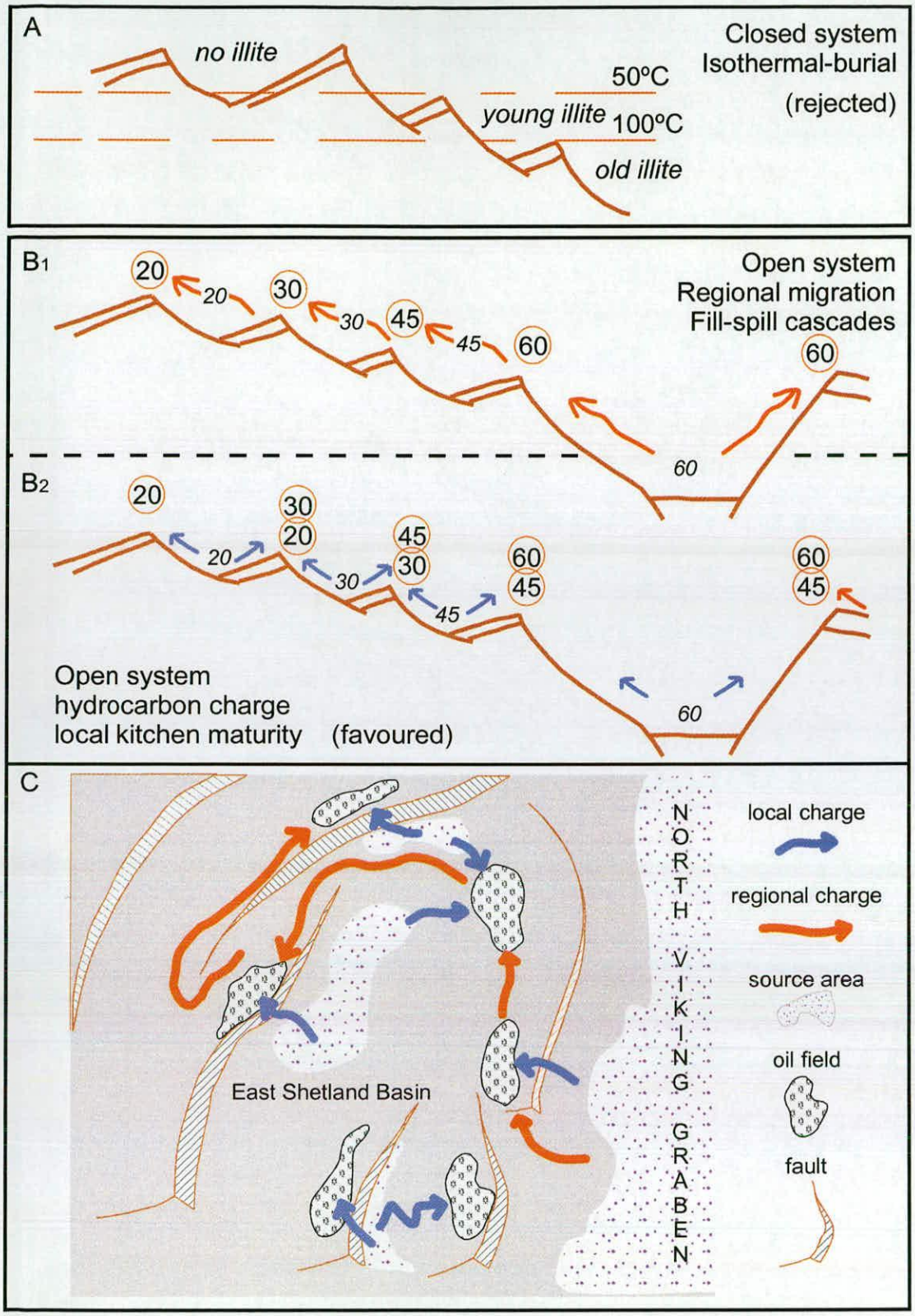

Figure 3.17 Simple hypothetical scenarios for illite diagenesis in oil fields. A- the closed system formulation, which is highly dependant on burial-related temperature thresholds, and fails to account for complexity in the data. B - two open system formulations. These differ in the nature and extent of hydrocarbon migration. C - as the map indicates, the two scenarios are not mutually exclusive. However, the thesis favours the local-charge variation of the null hypothesis, as discussed in the text.

The Penguin study

Isotopic analysis of illite samples for the Penguin field, Northern North Sea

don't it always seem to go
that you don't know what you've got
'til it's gone

This chapter presents the results of an original experimental study of the Penguin oil field, Northern North Sea: isotopic data for illite samples extracted from cored sections of Penguin reservoir intervals. This new data set is interpreted in the context of the regional study outlined in chapter three and forms the basis of a comparative data set for the modelling study outlined in chapter five. These analyses enable inference of at least three periods of illite growth, relating to older oil charges, now gone, and recharging by the present-day hydrocarbons.

Figures

Appendices

4.0 Aims and Objectives

It has been established in chapter 3 that there is a simple pattern to illite ages from the East Shetland Basin. This pattern supports the commonly cited hypothesis that illite diagenesis is a response to the petroleum system - either as a result of change in the pore waters with the onset of generation; or charging of the trap structures during migration; or a combination of these factors.

This is further borne out by present day maps for regional source rock distributions and proposed maps for the timing of oil maturation - Figure 4.1. Note, however that the Möre Basin is exceptionally deep with respect to the Northern North Sea, and that the significant burial phase was earlier - Figure 4.1a. Note also that the onset of early-mid-late oil maturity phases in the Northern North Sea are diachronous and provincial as a result of the extensive Jurassic terracing and related palaeotopography of the regional subsurface - Figure 4.1b.

The generally accepted association of fields in the East Shetland Basin to local source areas - Figure 4.2, would tend to favour a local generation-charge version of the illite-oil hypothesis over a regional fill-spill trapping scenario. In this respect, the Penguin study is ideally suited to discriminating between these two candidates, as the field is both in close proximity to the deep Möre Basin, and distally located at the end of likely Brent field fill-spill pathways.

The above reasoning suggests that the apparent regional illite-age pattern and associated implications of the illite-oil hypothesis have a predictive potential. To this effect, chapter 4 aims to provide an isotopic analysis of illite samples for the Penguin field, Northern North Sea: an authigenic illite data set for the Penguin field similar to that already existing for the Magnus field – Figure 4.3. This will establish whether illite diagenesis in the Penguin oil field is consistent with interpretations put forward for fibrous illite growth in the Magnus field, and East Shetland Basin as a whole.

In summary, the aim is to extend the interpretation of Magnus field isotopic studies (Macaulay *et al.* 1992, Emery *et al.* 1990, Barclay *et al.* 2000) to this nearby, geologically-related oil field. Diagenetic studies tend to be parochial in nature by their limitation to a field-specific data set. The Magnus case study is unusual in this respect, in that a suitable candidate for extension of the study exists in close proximity to the study area.

This experimental study tests the hypothesis that illite diagenesis in these two fields is similar and potentially related to the same geological events. This essentially relates to the principal hypothesis: fibrous illite diagenesis is caused by hydrocarbon charge to trap structures. If this is the case, these two neighbouring oil fields, subject to hydrocarbon charges from the same petroleum system, will yield similar fibrous illite diagenetic histories.

Alternatively, if illite grew in response to burial-related temperature changes within the reservoir sandstones, much younger ages would be predicted for Penguin with respect to Magnus, reflecting a slower and shallower burial history.

To meet this aim the experimental study assays the isotopic properties of fine clay fractions from core samples of Penguin field sandstones. Additionally, the origin and nature of the isolated clay samples are established in order to place the analytical data in context. Standard petrographic analysis informs the diagenetic analysis - Appendix 4.1. In this respect, the objectives of this chapter are as follows:

- to select sandstone core samples representative of the Penguin trap structures.
- to extract the clay content of the sandstones.
- to determine the mineral content of the clay fractions.
- to analyse the clays for K-Ar, δO and δD.
- to assess the purity of fractions with regard to fibrous illite.
- to interpret the data set within the context of the Penguin field.
- to compare the Penguin data set with that established for the Magnus field.
- to discuss the new data set with regard to illite ages for the East Shetland Basin.
- to propose further work in light of the new Penguin field isotopic data set.

4.1 Penguin

The Penguin oil field is located in North Sea blocks 211/13 and 211/14, 170 km north-east of the Shetland Islands, close to the Magnus oil field on the northern edge of the East Shetland Basin – Figure 4.4. The Penguin field consists of four distinct reservoir compartments: Penguin A lies to the west of Penguin B, a horst, and is flanked to the southeast by Penguin C and Penguin D – Figure 4.5.

Four fields

The Penguin oil field is unique amongst the oil fields of the East Shetland Basin, containing traps representative of disparate Northern North Sea structural and stratigraphic elements in one small area: an Upper Jurassic turbidite sandstone reservoir typical of the Magnus province - Penguin A; two Middle Jurassic deltaic sandstone reservoirs typical of the Brent province - Penguins C and D; The intervening horst structure contains a Triassic sandstone reservoir, Penguin B. The juxtaposition of these distinct trap structures, and their relative position with respect to the Magnus oil field are shown in detail in both map and cross-section – Figures 4.6 and 4.7. In this regard, Penguin provides a link between the hydrocarbon systems of the East Shetland Basin, the Magnus province, and potentially the Atlantic Margin.

It is this unusual juxtaposition of hydrocarbon accumulations coupled with Penguin's proximity to the Magnus oil field which make the field such an excellent candidate for testing the applicability of the

Magnus model and regional East Shetland Basin model to reservoirs of the northern North Sea and Atlantic Margin. Furthermore, the experimental Penguin study examines the hypothesis that illite diagenesis is primarily a response to hydrocarbon charging the reservoir, largely independent of sedimentary facies and structural considerations.

Geological setting

There is sparse information in the public domain directly concerning Penguin (Purvis 1995, Booth *et al.* 1992). However, the provincial geological context can be constrained from regional reviews and the extensive number of studies published for the Magnus oil field. A general stratigraphic framework, based on Richards *et al.* (1993) as outlined in chapter 2, is used throughout - Figure 4.8.

Reservoir and trap configuration

The Penguin field subdivisions are discussed individually below. As a group, they are typical of the northern North Sea in that they consist of Triassic-Jurassic sediments deposited within half grabens controlled by the regional structural grain. A combination of NE-SW trending faults relate to Caledonian tectonics and SE-NW trending faults relate to the arcuate lineament defined by the Tornquist line and Fjerritslev fault zone (Rattey & Hayward 1993). These small Mesozoic sedimentary basins are probably floored by crystalline Caledonian basement (Barclay al. 2000), though no wells have penetrated basement in the Penguin area.

The description of field configuration is restricted to the Upper and Middle Jurassic reservoirs in Penguin A, C and D, as befits the experimental sample horizons. For a detailed description of the Lower Jurassic Nansen and Statfjord Formation reservoirs refer to Purvis (1995). The depths of quoted reservoir units are in Driller's Depth to the nearest metre, as taken from composite logs.

Penguin A is an Upper Jurassic submarine turbidite sandstone, encountered below 3383 metres in 211/13-3. The reservoir unit is stratigraphically bounded by older and younger Kimmeridge Clay Formation shales, dipping gently to the West towards the axis of the Magnus province syncline and shaling out to the East at the hanging wall of the Penguin B structure.

Penguin B is a Triassic sandstone, classified as Cormorant formation. The sandstone occupies a horst block which terminates in an erosive contact with the overlying highly condensed Lower Cretaceous shales at 2682 metres, and is flanked to the East and West by Penguin A and C respectively. The discovery well, 211/13-1, terminates in Triassic sandstone at 3932 metres.

Penguin C is a Middle Jurassic Brent-type reservoir, at the northern limit of the Brent Delta, comprised of Etive and Rannoch Formations in the south-west part of the structure, as present in 211/14-4RE. The Etive unit thins to the north-east, leaving only Rannoch as the reservoir unit in 211/13-6. The reservoir is overlain by Humber Group shales at approximately 3414 metres and

floored by Dunlin Group shales and siltstones. The Penguin B structure dips steeply away to the east and is tectonically bound to the west and south by normal faults.

Penguin D is a Middle Jurassic Brent-type reservoir. The Etive and Rannoch Formation sandstones make up the principal reservoir unit, and occupy a fault bounded terrace as encountered at a depth of 3444 metres in wells 211/14-1 and 211/14-3. The southern extreme of Penguin D, penetrated by well 211/14-2, consists of a separate terraced compartment at 3414 metres. The Penguin D structure lies to the south of Penguin C and to the north-west of the Don field.

Hydrocarbon sources

The probable hydrocarbon source rocks for the reservoirs are the organic-rich Kimmeridge Clay Formation mudstones that envelop Penguin A in the Magnus province (Fallick *et al.* 1993) and lie above Penguin C and D in the Brent province. However, the diverse nature of the accumulated hydrocarbons at the present day – black oil in Penguin A, condensate in Penguin B, mixed oil and condensate in Penguin C and D- indicate that kitchen areas in addition to those occurring locally have contributed to the reservoir filling history. Deeper source areas potentially exist to the north-west, the Magnus Embayment; the north, More Basin; and the east, the Viking Graben. These basins may additionally contribute hydrocarbons from atypical northern North Sea source rocks such as the Cromer Knoll Group.

Early burial history

Tectonic uplift during the Early Cretaceous (Rattey and Hayward 1993) resulted in erosion of the Penguin B horst block down to sediments of Triassic age. Suspected meteoric water penetration into Lower Jurassic sandstones in Penguin A and D (Purvis 1995), is thought to be similar to meteoric incursion recorded for the Magnus field (De'Ath and Schuyleman 1981, Emery *et al.* 1990, Macaulay *et al.* 1992). A thin highly-condensed Lower Cretaceous shale cover over Penguin A and Penguins C and D, to either side of the horst indicates basin starvation as rifting transferred to the Atlantic Margin to the North West (Rattey & Hayward 1993).

Late burial history

Upper Cretaceous mudstones in excess of one kilometre thick over Penguin B provide a seal, and are overlain by a thick sequence of Cainozoic mudstones, indicative of rapid burial in the Late Tertiary. The field's current burial depth varies from about 2700 metres in Penguin B to approximately 3400 metres in Penguin A, C and D.

Diagenesis

Penguin A is thought to have undergone a diagenetic evolution similar to the Magnus field, with the singular exception of an early diagenetic episode of alteration in the Magnus as a result of local meteoric water incursion. With this qualification in mind, the generally accepted view is that both the

Magnus reservoir interval and the Penguin A reservoir interval are genetically related to the same sub-sea depositional system, and have similar burial histories, post-inversion (Late Jurassic - Early Cretaceous, as indicated by an erosional surface which truncates the crest of the Magnus field), resulting in comparable mid-to-late diagenetic evolutions for the two fields.

• the position of Penguin A, in the deepest part of the half graben against the hanging wall, has left the sediment unaffected by erosion, and probably diagenetically unaltered, subject to the scale of penetration of meteoric water during the Magnus emergence.

• Penguin B, a Triassic horst, is thought to have eroded prior to Magnus emergence in the Late Jurassic. However, it has also been subject to a second phase of shallow burial and diagenesis at the same time as the Magnus structure unroofed and subsided.

• Penguin C and D are typical shallow marine Brent deposits, though they display a condensed section as a result of being at the distal margin of a delta complex. Neither of these structures have been eroded, or exposed to surficial weathering, displaying a typical Brent-style paragenetic sequence.

All four Penguin structures and Magnus share a common late diagenetic indicator: fibrous illite. As a potassium-rich aluminosilicate with a high surface area to volume ratio, illite is highly susceptible to surficial weathering, probably related to the depth of meteoric incursion i.e. in the order of $10^0 - 10^1$ metres, and has not, as yet, been reported at surface outcrop. It is reasonable, therefore, to presume that K-Ar ages from fibrous illite samples post-date the last exposure of the structures to surficial weathering by at least the amount of burial required for illite to become thermodynamically stable.

4.2 Analytical focus

True to the aim of the experiment, all analytical work has been focused on fulfilling the principal objective: providing an illite data set comparable to that established for the Magnus. As considerable experimental work has already been undertaken on the general petrography, detrital and diagenetic mineralogy of Penguin by the parent oil company, Shell UK, this data has been used to establish the geological and diagenetic framework described above, within which this study has been placed.

4.3 Sampling strategy

The initial strategy for sampling was to gather a representative selection of core from the Penguin field area in order to produce an illite data set that was comprehensive with respect to field stratigraphy, burial depth, trap configuration and hydrocarbon accumulation. On this basis, thirty Penguin core intervals were identified as suitable. However, due to the destructive nature of the analytical procedure and the relatively large amount of core involved at about twenty kilograms, the CASE partner, Shell UK, requested that the strategy be modified.

Sample selection

A final selection of ten core intervals was accepted by Shell UK. This provided for two samples from the hydrocarbon leg of each of the four principal Penguin structures and two 'control' samples located off-structure in the south-west quadrant of the Penguin field area – Table 4.1. The final strategy gives a general sample spectrum across the Penguin field area, while allowing for comparative analysis of two related samples from each individual structure - Figure 4.9.

I.D.	Location	Well label	Core	Box	Depth Interval (m)
PO	Penguin C	211/13-6	2	-	3451.45 - 3451.60
P1	off-structure	211/13-5A	1	2/4	3615.08 - 3615.23
P2	Penguin A	211/13-3	2	1/2	3439.21 - 3439.36
P3	Penguin A	211/13-3	4	3/6	3467.71 - 3467.86
P4	Penguin B	211/13-1	1	2/5	2686.05 - 2686.20
P5	Penguin B	211/13-1	3	1/6	2855.45 - 2855.60
P6	Penguin C	211/14-4RE	1	-	3504.90 - 3505.05
P7	Penguin D	211/14-3	1	1/7	3454.30 - 3454.45
P8	Penguin D	211/14-1	1	4	3406.14 - 3406.29
P9	Penguin D	211/14-2	2	4	3441.88 - 3442.03
P10	Penguin A	211/13-7	2	-	3665.22 - 3665.37

Table 4.1 Sample set for isotope analysis of illite from Penguin

4.4 Prediction

Consistent with the aim of the experiment, predictions were made prior to analysis for expected ages from illite extractions, obtained from Penguin reservoir compartments - Figure 4.10.

• Penguin A: similar to Magnus i.e. two age groups: old and young, representing shallow and deep charging histories form local kitchen areas associated with the Magnus province.

• Penguin B - older than Penguin A as suggested by present-day condensate accumulation. This indicates the horst is plumbed into the deepest parts of the basin, probably to the north of the Horst area, suggesting a very early hydrocarbon filling history and complimentary old illite as seen in the deepest parts of the East Shetland Basin: regional review, chapter three.

• Penguin C and D - old, middle and young? The presence of mixed hydrocarbons in these two structures, their shallow position at the fringe of the Brent delta and on the peripheral terraces of the East Shetland Basin suggest they may have experienced a complex filling history indicative both of the deep kitchen area directly to the North, and the shallow local kitchen areas similar to the Magnus

province while potentially experiencing the most recent charge to trap structures in the East Shetland Basin that occur at the end of hypothetical fill-spill migration pathways in the Brent province.

In summary, the predictions for the analytical age results from the Penguin field are based on the expected hydrocarbon filling histories of the various structures. The resultant expectations are that the simplest age profile will occur in Penguin B, where gas condensates imply the earliest hydrocarbon charge and oldest ages will occur. More complex profiles are expected in Penguin C and D where mixed ages are expected, indicative of their mixed hydrocarbon accumulations, resulting from juxtaposition close to both deep and shallow kitchen areas and their Brent province position at the end of expected fill-spill migration pathway. Penguin A is expected to give a similar bimodal age profile to that of Magnus, resulting from two separate charges to the trap structure by shallow and deep kitchen areas in the Magnus province and the Magnus Embayment respectively.

A unimodal prediction for the Penguin field, assuming only one episode of filling would simplify the model to mid-range ages for Penguin A, in accord with the bulk of ages for the Magnus field; an old age for Penguin B as stated above, and a young age for Penguin C and D, commensurate with charge from the south associated with a Brent province fill-spill cascade – Figure 4.11.

4.5 Destructive Analytical Procedure

All potassium-argon illite age data in the literature related to the East Shetland Basin result from careful breaking, crushing, milling and sieving of sandstone cores. This destructive analytical procedure is thought to be the principal source of error associated with illite K-Ar ages. However, in recent years Norbert Clauer (1996) has pioneered a more sophisticated approach to illite separation.

This new technique, *freeze-thaw disaggregation*, has refined and altered established methods of illite sample preparation in order to address the prime source of error. As is commonly acknowledged, the uncertainty in K-Ar age analyses principally results from a necessarily destructive separation procedure, required to liberate the fine illite crystals from the sandstone matrix. The breaking, crushing and sieving of samples, potentially powders small amounts of the predominant phases that make up the arkosic sandstone host rock, including potassium-rich feldspar grains. The significance of small amounts of K-rich feldspar contamination is considerable and dealt with at length below.

Freeze-thaw disaggregation

The high risk of contamination requires routine screening of illite aliquots for purity. This potentially allows for a correction factor to be estimated. However, the significant gains in data-enhancement are dependent primarily on contamination-prevention during the destructive analytical procedure. Freeze thaw disaggregation aims to minimise contamination as a result of extraction. A brief description of the new technique follows.

• a prepared sandstone core sample is sealed in polythene while under low pressure.

• the polythene seal is then breached in a vat of 1M NaCl salt solution. The salt solution is chosen to maximise the volume expansion between the solution's liquid state and frozen state.

• the saturated sandstone is then cycled through extremes of temperature in order to repetitively freeze and thaw the solution. The maximum temperature of the cycle is about 80°C in order not to compromise retention of argon in the illite crystals. The intention is to gently disaggregate the sandstone core in a similar, albeit accelerated way to the diurnal weathering desert sandstones undergo.

The method is hypothetically gentler on the sandstone sample; however it is difficult to assess the effect of this technique on friable, deteriorated K-feldspar laths that are the prime suspect for contamination. K-Ar age results emanating from the technique have not been directly compared with milled separates. When considering ages obtained for various illite studies with those published for the new method there appears to be little difference in the reasoning for confidence in the data i.e. apparently low levels of contaminant phases in obtained aliquots.

The significant disadvantage of the technique, with respect to the banal constraints of this project, was found to be the time required disaggregating samples. Trial studies indicated that each sample would take in excess of two months to disaggregate. For ten samples, a projected run-time of twenty to thirty months was considered prohibitive. The time required for milled samples was less than one month, by comparison.

In summary, where practical it may be advisable to disaggregate samples by the thermal stressing method devised by Clauer *et al.* (1997). This gentle form of disaggregation is advantageous in that it separates the cement and matrix fractions by rapidly fluctuating a wet core sample through freeze-thaw cycles over an extended period of time in a specially designed environmental chamber. This hypothetically lowers the risk of contamination from mechanically broken detrital grains as a result of impacts. However, the effect of ice-crystal expansion on weathered feldspars is not yet well established. Additionally, the experimental run time is in the order of months for each sample.

Methodology

The analytical method for the extraction and analysis of fine size fractions of illite from oil field sandstones has been well established and extensively refined by diagenetic researchers in recent years. Useful discussions of the method can be found in Darby *et al.* (1997); Clauer *et al.* (1997); Hogg *et al.* (1993); and Hamilton *et al.* (1989).

The destructive analytical procedure employed in this study is similar in method and detail to that employed in the aforementioned published work, and so only a brief synopsis of the method follows below - Figure 4.12. However, the extensive experimental guide to soil science separation by Jackson (1956) and aforementioned discussions specific to illite are recommended to the reader. A guide to initial preparation procedures and a complete listing of equipment and related chemical agents can be found in Farrant (1996).

Two stages

The method can basically be treated as two separate stages - a preliminary sample preparation stage where quality control is of primary importance, followed by an analytical stage where quality assessment is integral to the acquirement of analytical data suitable for interpretation.

Stage one - preparation and quality control

The preparation of samples for isotopic analysis is a sample-intensive and destructive procedure. The primary aim of this stage is to extract high quality illite separates from the core, leaving the remaining material to be archived for future research.

Sample size

The sample size is controlled by the likely amount of illite clay in the rock, ~0.1% rock mass. A large sample, 1 kg, has to be processed to yield the small amount of authigenic illite, 100 mg, required to gain a satisfactory result from the principal analytical technique: K-Ar isotope dating of fibrous illite.

Archive

An archive photograph was taken for each sample, showing the condition of the core and location of the sample site in the composite log used for selection of the sample - Figure 4.13.

Initial preparation

The core was cleaned with a stiff wire brush and washed to remove drilling mud. A small cut was removed for thin section work – Figure 4.14. In addition to this a small chip of the sample cut was taken for initial Scanning Electron Microscope (SEM) analysis - Figure 4.15. Energy Dispersive Spectrometer (EDS) analyses of fibrous cement phases confirmed the likely presence of illite in the core samples – Figure 4.16.

Disaggregation

The sample was mechanically disaggregated. This is a high-risk process where the quality of the final separates can be compromised by inorganic contamination. Specifically, the risk is that detrital material and cement fractions can be broken into the fine size fractions occupied by the targeted sample range of illite fibres in the final stages of the separation procedure. Contamination theory is discussed in more detail in section 4.6.

The initial stages of disaggregation are crude, requiring the core to be broken by a rock vice into cobbles small enough to enter a rock crusher, which in turn compressively shocks the core into gravel and finer particles. The final stage of disaggregation uses a rolling crown mill with a finely adjustable aperture and a set of calibrated sieves to reduce the core to an aggregate of clay, silt and sand with a maximum grain size of 1 mm. diameter - Figure 4.17.

Aggregate monitoring

Small amounts of sample were removed throughout the disaggregation process for SEM analysis, to monitor the quality of the clay fraction separated from the bulk sample, and to look for indications of crushing and powdering of the coarser fraction material - Figure 4.18 and Figure 4.19.

Suspension and chemical treatment

The disaggregated sample is slurried with pure water and the resultant suspension is subjected to a number of chemical baths. This decontaminates the clay fraction with respect to organic and salt impurities and defloculates the clay particles, increasing the purity and quantity of separates obtained from the finest fraction of the clay spectrum.

Fine fraction separation

The slurry is suspended and decanted to remove the coarsest fractions of the sample, and the resultant mix of silt and clay is subjected to progressively more intensive gravitational fields in a high speed centrifuge in order to isolate the finest fractions of clay particles separated during the sample processing for quality assessment and isotopic analysis. The morphology and size of illite fibres constrain the size fraction of measurable clay aliquots to less than 2 microns. Subdivisions of this fraction are arbitrary, though precision is expected to increase with finer size fractions, as these favour the concentration of fibrous illite over distinct morphologies of contaminant species. The finest size fraction dated is constrained by the mass of sample required for analysis i.e. about 10 mg.

Stage two - quality assessment and isotopic analysis

The resultant dry separates represent a fraction of a percent of the initial volume of core that entered the analytical procedure. Quality assessment is required before proceeding with the isotopic analysis to establish the purity of these fractions with respect to illite, whilst also screening the samples for residual inorganic and organic compounds, using Transmission Electron Microscopy and Infa-Red Spectroscopy respectively.

This establishes the veracity of isotope data by assuring that the fine fraction separation has isolated the illite fibres, excluding other species such as smectite, chlorite and contaminant phases such as potassium feldspars, while assuring no damage to the sensitive analytical equipment by trace organic compounds, as discussed below.

Organic contamination

As the core samples are from the hydrocarbon legs of the various structures, there is a risk that residual organics may adhere to the clay surface of the sample fractions despite the prolonged exposure to hydrogen peroxide during stage one of the analytical procedure. The separates are screened for the presence of long and short chain hydrocarbon groups by Infrared Spectroscopy (IRS) of a fine fraction sample aliquot.

Sample purity and inorganic contamination

Analysing the X-Ray Diffraction (XRD) patterns of fine fraction sample aliquots qualitatively assesses the presence of illite and other major crystalline phases. This preliminary assessment of the fine fraction samples indicated the presence of illite and contamination phases, predominantly quartz, kaolinite and feldspar. High purity samples are required for K-Ar age analysis. Hence, fine fraction aliquots were photographed using an Analytical Transmission Electron Microscope (ATEM) to establish the level of sample purity - Figure 4.20. The ATEM was also used to obtain individual crystal XRD spectra in order obtain a qualitative assessment of the nature of contamination present. A complete library of ATEM photographs from this study is presented in Appendix 4.2.

4.6 Contamination

Previous workers have addressed the susceptibility of the method to contamination particularly with respect to K-Ar analysis (Hamilton *et al* 1989). Associated with this experimental error is the difficulty of quantitatively assessing the degree of contamination resulting from sample processing. Common inorganic contaminants found in illite aliquots are representative of the principal detrital and cement phases present in the bulk rock analysis. These are thought to enter the sample fraction during the early stages of processing as a result of the need for the whole core sample to be disaggregated in order to extract the illite cement fraction.

Sample disaggregation options

As mentioned earlier – paragraph 4.51, there are two common disaggregation methods currently employed: mechanical and thermal stressing. The former method was chosen for this study and has been described at length in the above section – section 4.5.

Analytical sensitivity to mineral phases

Hamilton *et al.* (1989) discusses the likely mineral phases of inorganic contamination at length. In the mineral systems of the sample set used in this study, these are principally quartz, feldspar, kaolinite and other clays. With the exception of potassium feldspar, muscovite and detrital illite clay, these phases are relatively inert with respect to K-Ar isotopic analysis, and only cause significant error to the calculated age for illite diagenesis when present in abundance i.e. greater than 10% sample volume.

Potassium feldspar contamination

The method is highly sensitive to detrital potassium feldspar contamination. As Hamilton *et al.* (1989) discuss at length, low levels of detrital potassium feldspar contamination (less than 5%) can potentially cause a significant shift in the calculated age of the sample illite towards an older false age for illite diagenesis. For example, if a diagenetic illite sample with a known age of 50 Ma was contaminated by one weight percent Precambrian potassium feldspar (1,500 Ma), the theoretical result would be a 90 Ma apparent age for the timing of illite diagenesis, an error of 40 Ma – Figure 4.21.

Contaminant source dependence

It is important to note, however, that the margin of error is dependent on the source terrain of feldspar contamination. Hence, in the previous example, if five times the amount of contamination had been present as Caledonian feldspar (450 Ma), the resultant error would theoretically be halved to 20 Ma. In the context of the sample set - Middle and Upper Jurassic arkosic sandstones- Appendix 4.1, the likely feldspar source area is the uplifted Caledonian hinterland that is still evident along the Caledonian trend from North America to Norway via the Scottish mainland. Hence, the likely age of potassium feldspar contamination where evident in the samples, is likely to be no older than 450 Ma.

Experimental age sensitivity

This implies that for an apparent experimental age of 160 Ma, a 15 My error in the age, equivalent to a true illite age of 145 Ma, would result from only 5 wt% contamination by Caledonian potassium feldspar. By comparison, an experimental age of 50 Ma would have a true age of 29 Ma if contaminated to the same degree. The younger the illite the more sensitive the age is to contamination.

Practical implications of contamination theory

In summary, the practical implication of the above discussion is that significant amounts of contamination occur at levels below 5 wt% for ages within the general remit of this study. Such low levels of contamination are qualitatively identifiable with an ATEM analysis of sample purity. However the quantification of contaminant error in individual samples, and discrimination between, say, 3% and 5% contamination is beyond the financial and practical limitations of this study. Even if this was a feasible methodology, any resultant correction factor would be dependent on the assumption that the contaminant phase was homogeneous and of known progeny.

Therefore, it is unreasonable to set limits on the probable contaminant error for the set on the basis of the ATEM analysis. This experimental study, in common with other illite studies from the North Sea, is dependent for its validity on the strength of the geological model proffered to explain the data array.

Argon and Deuterium – alternative indicators of contamination

As 5% feldspar contamination is potentially significant, may not always be detectable by XRD, and would need high levels of resolution by ATEM, other indicators of sample purity need to be

considered. Both argon and deuterium data derived from pure clay separates implicitly indicate levels of illite purity. High argon values are indicative of contamination by old feldspar. Low argon levels indicate argon loss either prior to, or as a result of sample processing. Additionally, high deuterium returns from aliquots imply high levels of adhered water molecules. This is also potentially indicative of low purity. Neither of these indicators allows for a precise quantification of contamination. However, they can provide sensitive and precise indicators of relative differences between samples in a coherent, related group of clays from a single area or structure. Consequently, the principal explicit assessment of illite purity remains the ATEM characterisation.

4.7 DAP results - sample quality

The original core samples all yielded fine fraction separates suitable for isotopic analysis, with the exception of sample P1 from well 211/13-5A. P1, the off-structure sample, was rejected during the cleaning and separation stage due to a low clay content and high levels of organic contamination.

In addition to yielding aliquots suitable for analysis, all the field core samples had clear indications of fibrous illite diagenesis when examined by Scanning Electron Microscope and X-Ray Diffraction. Furthermore, the samples appeared to be pure with respect to organic contamination, despite their provenance, when screened by Infra-Red Spectroscopy. Finally, the high quality of separation was confirmed using an Analytical Transmission Electron Microscope. Despite the difficulties in quantitatively assessing the levels of potassium-bearing contaminant phases, the general indications from the ATEM work were of aliquots in the region of 95% pure euhedral, fibrous illite crystals, with atypical morphologies being predominantly quartz and kaolinite – both harmless contaminant phases.

In summary, the quality of samples were found to be high and the sample set appeared likely to yield a useful and geologically-valid isotopic data set.

4.8 Isotopic analytical results

Following separation, the clay aliquots were prepared at the Scottish Universities Environmental Research Centre under the supervision of Professor Anthony E Fallick. The samples yielded four sets of isotopic data. The first two sets, potassium and argon, were combined to derive an unusual array of K-Ar ages - Table 4.2. The last two sets consisted of conventional δ18O and δD values - Table 4.3. The three data sets are presented independently, and then compared to each other below.

Potassium-Argon

A standard analytical protocol was followed for establishing the potassium - argon age of the clay fractions (Brint *et al.* 1990). A small aliquot, approximately 10 mg of the clay fraction, was used for analysis after degassing overnight at 100°C to remove adsorbed water.

Potassium variation

The ^{40}K ratio was measured on a wet flame photometry line with a sodium buffer and lithium standard. Isotope dilution is a common method, employed to ensure the assumed $^{40}K/K$ ratio is accurate. Each result was duplicated at the time of measurement. A second run conducted two weeks later recorded distinctly different ^{40}K values. Once again, the results were duplicated at the time of measurement. Sample heterogeneity was ruled out as a potential cause of variation on the basis of ATEM indications that sample purity was reasonably high. The likely principal factor in the variable output was agreed to be the wet flame photometry line.

For the second run, most of the clays returned K^+ values within 10% of the initial run values. However, notable variations occurred on samples JAC8, JAC9 and JAC11 – Table 4.2. A third run and comparisons with a control group resulted in similar data, which was then accepted as satisfactory.

These differences in potassium values are significant, increasing the error on the measured ages from ±2 My to ±5 My for small variations in K^+ ions and ±20 My for samples JAC9 and JAC11. Assuming the analytical equipment is in good order and the protocols are followed, the two principal causes for variations result from subtle differences in the clay samples with each run:

• *Surface charge* - for homogeneous clays, small variations can occur as a result of distinct surface charges associated with different crystal lath shapes. This does not account for the large variations seen in samples JAC9 and JAC11.

• *Sample heterogeneity* - potassium variation may also result from sample heterogeneity i.e. low levels of contamination by a potassium-free agent such as kaolinite. BP researchers have found such heterogeneity at the milligram mass scale. However, the small aliquots analysed in this study are below such detection limits. Qualitative appraisal of the samples by ATEM, discussed below, does indicate the presence of small amounts of contaminant phases (less than 5%). Such low levels of heterogeneity would not result in the variations seen in samples JAC9 and JAC11.

In order to assess the consistency of the analytical procedure, the potassium ion line was tested with an homogeneous control group, Habisch clays. The Habisch clay K^+ results were found to show similar levels of variation. It is likely, therefore, that the data variation is an analytical-instrumental problem. Despite attempts to stabilise temperature and humidity levels in the laboratory environment, as well as thorough checks of the electronic and mechanical equipment, the variation in K^+ results persisted.

Although the K^+ results vary, the spread of data does not fundamentally compromise the integrity of the data set and the resultant ages. However it does significantly increase the age error on two of the samples to about ±20 My. From a pragmatic view point, the analysis is required to address an argument relating the timing of illite diagenesis to shifts in the dynamics of a petroleum system i.e.

migration, hydrocarbon accumulation and overpressure. Modelling constraints on the timing of these phenomena are at best ±10 My. The body of illite age data lies within the error bars of the least constrainable phenomenon and so, even JAC9 and JAC11 result in ages that are resolvable against the background of simulated events for the modelled petroleum system. The clay analysis is sufficiently precise.

An additional point is that Potassium content is thought to be an authigenic indicator if a sample is of high purity. Values in excess of 4% tend to indicate the clay is authigenic. Notably, JAC7, the aliquot with the oldest age at 136 Ma, has a depressed K value with respect to the rest of the data set – Table 4.2. This does not invalidate the data point. However, the implication that JAC7 may contain detrital illite, or be of low purity, combined with its status as a left-field sample with respect to age, makes this aliquot a prime contender for intensive scrutiny under a transmission electron microscope.

Implications of potassium variation

Note that while K value variation has resulted in expanded error bars with respect to the resultant ages, this error is confined to the analytical procedure. Additionally, although two of the aliquots, JAC4 and JAC7, have K values less than 4.0%, the actual K levels, 3.98% and 2.70% respectively, are acceptable values for authigenic illite age analysis. The low value for JAC7 merely indicates that TEM analysis is required to assess the nature of the aliquot in question.

The minutiae of variation in the required factors for the age equation have simply required that the analytical technique be scrutinised, while confirming that the fine fractions of clay extracted from the sandstone core samples are yielding data typical of illite analyses in general. While it is not possible to quantitatively assess potential contamination within the aliquots used for this data set, these issues can be adequately addressed by examining the samples under a transmission electron microscope.

Argon

The ^{40}Ar ratio was measured on standard argon-argon Mass Spectrometry line. The samples were pre-baked to remove atmospheric argon; the argon content released by fusion in vacuo; purified and added to a ^{38}Ar spike prior to mass-spectrometer analysis.

A significant source of error in potassium-argon age determinations is commonly held to be argon leakage (Brownlow 1996). As a noble gas, argon does not chemically bond within a mineral. The crystal lattice physically imprisons radiogenic argon atoms, and tends to leak argon as lattice vibrational energies increase with temperatures associated with metamorphism. However, diagenetic minerals such as illite potentially retain their argon and yield a reliable age. Correction for initial argon content is usually unnecessary as only minerals formed under the very high pressures of extreme metamorphism have significant levels of original ^{40}Ar.

The argon results are encouraging, at about 90%, of expected content, indicating both very low levels of original, trapped atmospheric argon, and present-day atmospheric argon associated with poor degassing as well as low levels of organic contamination, that mimic ^{36}Ar.

Potassium-Argon ages

The K-Ar age was established from the resultant values by using the internationally accepted value for the half-life of ^{40}K and assuming the provisos of unstable isotopic dating (Fauré *et al.* 1986). The radiometric geochronometer for K-Ar decay in years, with accepted values for λ_K and λ_β, 0.581 x 10^{-10} and 4.962 x 10^{-10} respectively, is summarised mathematically below, where '*t*' is time elapsed in years (Brownlow 1996).

$$t = 1.804 \times 10^{9} \ln\left(1 + 9.540 \frac{^{40}Ar}{^{40}K}\right)$$

The analysis yielded a set of values for the clay aliquots, which, if attributed to fibrous illite and event-related diagenesis, yield a K-Ar age for a significant geological event associated with the sandstones in the Penguin fields. The ages are presented below – Table 4.2

ID	WELL	SIZE	% 40Ar	K wt% (I)	K wt% (II)	(II)/(I)	Age (Ma)	± (My)
JAC12	211/13-3	O	93	4.01	4.27	106%	**99**	± 6
JAC8	211/13-3	o	92	4.55	3.87	85%	**85**	± 13
JAC10	211/13-1 Shallow	O	93	4.39	4.04	92%	**127**	± 10
JAC5	211/13-1	o	89	4.66	4.84	104%	**117**	± 5
JAC11	211/13-1 Deep	O	92	4.06	5.88	145%	**80**	± 36
JAC6	211/13-1	o	91	5.35	5.32	99%	**108**	± 1
JAC4	211/13-6	o	89	3.98	4.03	101%	**72**	± 1
JAC9	211/14-4	o	92	5.88	4.02	71%	**88**	± 26
JAC1	211/14-3	0	95	5.75	5.33	93%	**71**	± 5
JAC2	211/14-3	O	92	6.30	5.99	95%	**44**	± 1
JAC3	211/14-3	o	87	6.64	6.27	94%	**33**	± 2
JAC7	211/14-1	o	93	2.78	2.70	97%	**136**	± 4

Scale: 0 1-2 microns O 0.5-1.0 microns o 0.1-0.5 microns

Table 4.2 Potassium-Argon data for Penguin core samples.

The K-Ar ages for the sample set range from 34 Ma to 145 Ma. The associated error bar, resulting from analytical variation varies from as little as ±1 My to ±36 My. This wide variation in uncertainty is a result of variable reproducibility for the potassium content of the aliquots. In general the error is less than ±10 My, with two notable exceptions for wells 211/14-4 and 211/13-1 - Table 4.2.

δ18O oxygen values

A standard analytical protocol (Brint *et al.* 1990) was followed for establishing δ18O values of the clay fractions on a VG Isogas SIRA-10 mass spectrometer. The results of δ18O analysis are presented relative to the Standard Mean Ocean Water value, SMOW (Craig, 1961).

• the δ18O values were measured by oxidising a small aliquot (~10 mg) of the clay fraction with ClF_3 in a nickel vessel at 650°C prior to cleansing and reduction to CO_2 in a vacuum extraction line. The CO_2 was then analysed by mass spectrometry. An NBS standard was used to calibrate the results.

δD hydrogen values

A standard analytical protocol was followed for establishing δD values of the clay fractions (Brint *et al.* 1990). The δD analysis was conducted on a VG Isotopes Mircromass 602B mass spectrometer. The δD analyses are presented relative to Standard Mean Ocean Water, SMOW (H Craig, 1961).

• the δD values were measured by placing a small aliquot (~30 mg) of the clay in a platinum crucible, previously heated to 1500°C for three hours. The aliquot and crucible were then degassed at 120°C in vacuo overnight prior to further heating to release bound hydrogen, principally as water. The water vapour was reduced by reaction with hot uranium and the resultant hydrogen gas analysed in a mass spectrometer to establish the deuterium ratio. An NBS standard was used to calibrate the results.

The stable isotope results are presented below - Table 4.3. Note that a number of samples have no δD values as the volumes of clay separates were only sufficient for the K-Ar and δ18O analyses.

ID	WELL	SIZE	Age (Ma)	± (My)	$\delta^{18}O$ (SMOW)	δD (SMOW)
JAC12	211/13-3	O	99	± 6	**14.9**	**-55**
JAC8	211/13-3	O	85	± 13	**15.1**	-
JAC10	211/13-1 Shallow	O	127	± 10	**16.2**	**-52**
JAC5	211/13-1	O	117	± 5	**14.2**	**-53**
JAC11	211/13-1 Deep	O	80	± 36	**15.7**	**-52**
JAC6	211/13-1	o	108	± 1	**14.6**	**-55**
JAC4	211/13-6	o	72	± 1	**15.3**	**-53**
JAC9	211/14-4	o	88	± 26	**13.8**	**-52**
JAC1	211/14-3	0	71	± 5	**12.3**	**-66**
JAC2	211/14-3	O	44	± 1	**12.9**	**-55**
JAC3	211/14-3	o	33	± 2	**13.6**	-
JAC7	211/14-1	o	136	± 4	**13.4**	-

Scale: 0 1-2 microns O 0.5-1.0 microns o 0.1-0.5 microns

Table 4.3 K-Ar and stable isotope data for Penguin core samples.

Results presentation

• A graph of K-Ar ages with respect to field and clay fraction size shows a tendency for finer fractions to return younger ages, though aliquot JAC11 - well 211/13-1, is the exception - Figure 4.22. The geological and geographical juxtaposition of Penguin K-Ar ages - Figure 4.23, provides the basis for testing the predictions made from Magnus field studies and the regional review of East Shetland Basin illite data, as discussed in the aims and objectives of this study.

• Map comparisons of δD and δ18O with K-Ar ages are presented to place the stable isotopic data in context with respect to the ages and field positions – Figure 4.24 and Figure 4.25.

• The δ18O value of a mineral is dependent on two factors: the ambient temperature at the time of growth and the δ18O value of the pore water. This relies on the following assumptions: precipitation occurs at a given temperature; isotopic equilibrium is reached; and no further isotopic exchange occurs after precipitation (Savin and Lee, 1988). The relationship, as a function of $1/T^2$, is typical of fractionation for the isotopes of most elements, and is expressed mathematically below (Savin & Lee 1988). A graph of $\delta^{18}O_{WATER}$ versus T_{WATER} for distinct values of $\delta^{18}O_{ILLITE}$ allows one factor to be calculated, assuming conditions for the other – Figure 4.26.

$$1000\ln\alpha^{OXYGEN}_{ILLITE\ -\ WATER} = a/T^2 + b$$

$$\delta^{18}O_{ILLITE} - \delta^{18}O_{WATER} = a/T^2 + b$$

δ18O $a = 2.39 \times 10^6$ $b = -4.19$ (Land & Dutton 1978)

• The same assumptions apply for δD values. The equation differs in the case of hydrogen, however, due to the high vibrational frequencies of the hydroxyl bond; the related isotopic fraction equation is a linear function of 1/T (Yeh 1980). The resulting deuterium isotope curves allow comparisons to be made for potential water-temperature conditions during illite diagenesis – Figure 4.27.

$$1000\ln\alpha^{HYDROGEN}_{ILLITE\ -\ WATER} = a/T + b$$

$$\delta D_{ILLITE} - \delta D_{WATER} = a/T + b$$

δD $a = -19.6 \times 10^3$ $b = 25$ (Yeh 1980)

The numerical constants 'a' and 'b' are empirically derived for clay minerals and are specific to illite.

• A cross-plot of δ18O and δD provides a way of visualising the position of the mineral with respect to both stable isotopes in a space defined by a porewater-temperature grid. As both isotopic equations have the same two unconstrained variables, the cross-plot gives a unique position for the mineral with respect to temperature and formation waters at the time of crystallisation –Figure 4.28.

4.9 Interpretation

Considering the data as a whole, the K-Ar ages differ considerably from the predictions outlined at the beginning of this chapter – Section 4.4 and Figure 4.10. The result is an unusual and unexpected array. The data is more complex than predicted and covers a wider range of geological time - Figure 4.29. The stable isotope data, however, presents a small cluster indicative of reasonable temperature and formation water values for the Penguin fields - Figures 4.24 and 4.25. Additionally, the stable isotope data mirrors the structural and geographic location of the samples, and gives further confidence that the samples are uncontaminated, indicating that the K-Ar ages are true geological phenomena.

The defining test of the principal hypothesis requires the unambiguous association of K-Ar ages to event-related illite diagenesis coupled to a petroleum system. A simple data array, matching the prediction would have supported the local interpretation for illite diagenesis in the Magnus field, and indicated that the Penguin field met the general picture of illite diagenesis for the East Shetland Basin as outlined in chapter 3. This new array of ages precipitates two distinct and opposing conclusions:

• the illite samples have yielded erroneous 'ages' as a result of contamination.

• the ages require an unusual petroleum system for the illite-oil hypothesis to stand.

Contamination

Contamination concerns arising from K-Ar analysis have been discussed at length in sections 4.5 and 4.6. Other workers have also treated this matter extensively e.g. Hamilton *et al.* (1989) on authigenic and detrital illite. As a result of this, a sceptical position is easy to adopt when considering new K-Ar ages. In effect, once a model is established relating to K-Ar ages, studies that complement the norm are readily accepted whereas unusual ages are treated with a measure of suspicion, particularly when the shift is towards older ages. As a result, it is quite difficult to challenge the established paradigm.

Perhaps the strongest line of evidence to support the sceptical view is that two of the ages have large error bars. However, the error is experimental and attributable to the potassium analysis. Additionally, one of these data points, JAC11, 80 Ma ± 36, is from well 211/13-1, with three other tightly constrained data points of similar age to each other at around 110Ma -120 Ma. The other data point, JAC9, 88 Ma ± 26, is from the Penguin C field, which has another well data point of a similar age with a low experimental error: JAC4, 211/13-6, 72 Ma ± 1.

The principal indication that contamination may be a significant factor is the occurrence of ages in excess of the oldest ages found elsewhere in the East Shetland Basin. For example, JAC7 - 211/14-1, is dated at 136 Ma ± 4; Penguin B records ages around 110 –120 Ma; Penguin A returned an age of about 90 Ma. Not only is the data set consistently older than for elsewhere in the East Shetland Basin, but the ages exceed the predicted onset of earliest oil migration for the region – Figures 4.1 and 4.2.

Furthermore, Penguin A yields an age in excess of the body of data for the related Magnus field – Figure 4.3, though the data is highly supportive of the oldest ages measured for the Magnus field, which have in the past been dismissed as contamination effects. The Penguin data set also yields one of the youngest ages for the East Shetland Basin, at 33 Ma ± 2. This is coincidentally from the same structural block as the oldest age, Penguin D.

Coherent age array

Considering the data set as a whole, the Penguin field complex contains the entire span of ages for the East Shetland Basin. Although the absolute ages are all older than predicted, it is very noteable that the geographic pattern of relative ages is a very good match to that predicted – Figure 4.29. Penguin D yields a young age, matching the original prediction. Penguin C yields mid-range ages at about 70 Ma. Penguin B also yields the oldest ages for the field complex. This is in agreement with the original reasoning underlying the prediction for Penguin B to be older than the other fields. As stated above, Penguin A yields an age which, though old, matches the nearby Magnus data.

In general the age data presents a coherent geographical pattern, and is supported by highly plausible stable isotope data from the same illite aliquots that yielded the K-Ar ages. Contaminated data would be less coherent, and unlikely to show internal consistency – for example, the consistent results in Penguin B or the general trend of decreasing age with finer fractions in Penguin A, B, C and D, typical of illite growth.

Stable isotope pattern

Although the K-Ar ages are surprising in their antiquity, they show a coherent spatial pattern of relative ages similar to that originally predicted. The δD and $\delta^{18}O$ illite analyses also show a coherent and plausible geographical pattern. This gives strong credibility to the position that the analyses are accurate and free of significant contamination. Such contamination would affect both K-Ar ages and δD and $\delta^{18}O$ values, shifting the authigenic signature towards values more typical of detrital minerals. For example, a $\delta^{18}O$ value of +15 ‰ would shift towards +0 ‰. The weighting of contamination artefacts would differ for each element, making coherent correlations between K-Ar, δD and $\delta^{18}O$ highly unlikely. However, the returned data is found to be entirely consistent with illite precipitation from porewaters that are isotopically a mix of Cretaceous meteoric water and Jurassic sea water - Figures 4.26 and 4.27. Additionally, the δD and $\delta^{18}O$ values are mutually supportive, indicating no contamination by igneous or metamorphic detritus – Figure 4.28.

With regard to spatial distribution, the Penguin illite δD and $\delta^{18}O$ values show a coherent pattern related to structural position - Figures 4.24 and 4.25, that varies in a similar way to the younger K-Ar ages. These ages are inferred to form at deeper burial depths commensurate with the uniform, prograde, post-Jurassic burial history of the region. With increased depths of burial, porewaters would generally be considered to be warmer, resulting in more evolved, less negative porewater $\delta^{18}O$ values. The more negative δD and $\delta^{18}O$ values in Penguin C and D, compared with those for Penguin B, are consistent with this artefact of warm and evolving porewater.

Hence, the stable isotope evidence indicates that the fibrous illite grew in porewaters that lay somewhere between Jurassic seawater and Early Cretaceous meteoric water. This fits the established provincial geology of local meteoric incursion related to an episode of uplift during a Jurassic-Cretaceous shift in basin dynamics (Dawers & Underhill 2000, Macaulay *et al.* 1992). The stable isotope evidence also indicates a temperature range for illite growth of about 30°C to 80°C – Figure 4.28. This is entirely in accord with the current understanding of thermodynamic controls on illite growth (Small *et al.* 1992; Haszledine *et al.* 2000; Wilkinson *et al.* 2002) and further supports the age data profile of a complex, multi-phase growth history for illite diagenesis in the Penguin field.

Finally, the orthodox approach to separation, the careful monitoring of samples throughout the procedure and rigorous assessment of sample nature prior to aliquot analysis, as documented above, all increase confidence in the quality of the resultant data. While it is nigh impossible to conclusively rule out the presence of contaminant phases and their effects, such are limitations of the method, it seems reasonable to argue that this data set is a genuine representation of a geological phenomenon.

Geological solution

The problem remaining is to find a reasonable geological explanation for the data array. If the principal hypothesis is to stand i.e. fibrous illite diagenesis results from hydrocarbon charge to trap structures, a new paradigm will need to accommodate the ages measured for Penguin B, which at 120 Ma, are the oldest ages yet found in the East Shetland Basin. Such a geological solution would also imply that fibrous illite grows at much shallower depths and lower temperatures than previously thought, as the cover over Penguin B at 120 Ma is thought to have been about 30 metres at most.

Paradigm shift

A new conceptual model would be dependent on testing the assumption that hydrocarbon charges from a petroleum system match the fibrous illite diagenetic histories established for the Penguin field. Assuming the finest fractions are representative of the most recent illite growth (Macaulay 1992), a model of such a petroleum system would require the following:

• the Magnus field needs to have been charged twice: once at approximately 90 Ma and again, over an extended period from 70 to 40 Ma. This potentially implies two kitchen areas for the system.

• The Penguin B horst block, and potentially Penguin D terrace, was charged at about 120 Ma: an extraordinarily early age, considering current thinking on the East Shetland Basin petroleum systems.

• Penguin C and D have been charged at about 70 Ma and 35 Ma respectively. This is similar to the charge range required for the second phase of fibrous illite growth recorded in the Magnus province.

Modelling

A conceptual drawing of such a petroleum system emphasises the role of distinct hydrocarbon source areas in the filling history of the Penguin and Magnus fields - Figure 4.30. These kitchen areas may be geographically distant or in close proximity to the trap structures. Treating the system as a set of discrete kitchen area-field area couplings similar to pairings already hypothesised for the East Shetland Basin - Figure 4.2, makes the conceptual model a suitable candidate for two-dimensional basin modelling. Such modelling would be a reasonable test of the argument that the illite-oil hypothesis is not only compatible with the illite ages measured for the Penguin and Magnus fields, but also requires a paradigm shift associated with petroleum systems affecting the East Shetland Basin.

4.10 Conclusion

In conclusion, the aims for this chapter have been met. The Penguin oil field was chosen as a suitable candidate for K-Ar analysis due to its proximity to the Magnus field, and related data set, as well as the diverse nature of the four structures that make up the Penguin field, and their location within the East Shetland Basin.

Fine fraction clays were extracted, analysed and assessed for purity from ten wells associated with the Penguin field. The resultant data set is judged to be internally consistent with regard to the patterns of δD and $\delta^{18}O$ data. The K-Ar ages are also found to be coherent, despite being significantly older than predicted. Even so, the relative geography of K-Ar ages are similar to the original prediction. Consequently, the K-Ar ages can be interpreted with respect to the Penguin field and its environs, and with specific regard to the Magnus field and East Shetland Basin as a whole.

Further work has been suggested in order to test whether the illite-oil hypothesis stands in light of an unexpectedly old and complex data array. Namely, the nature and timing of oil migration in the Penguin area is to be examined using two dimensional computer simulations of petroleum systems.

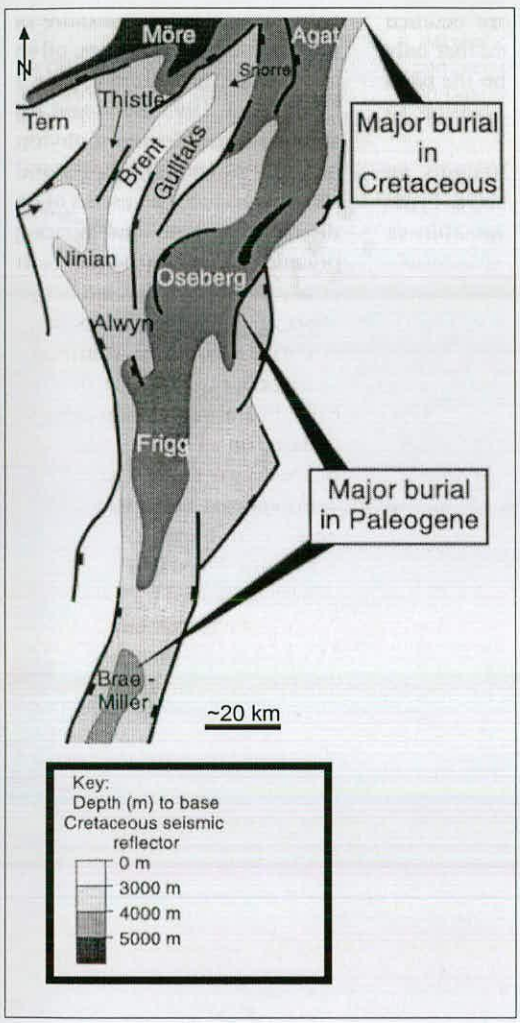

Figure 4.1a

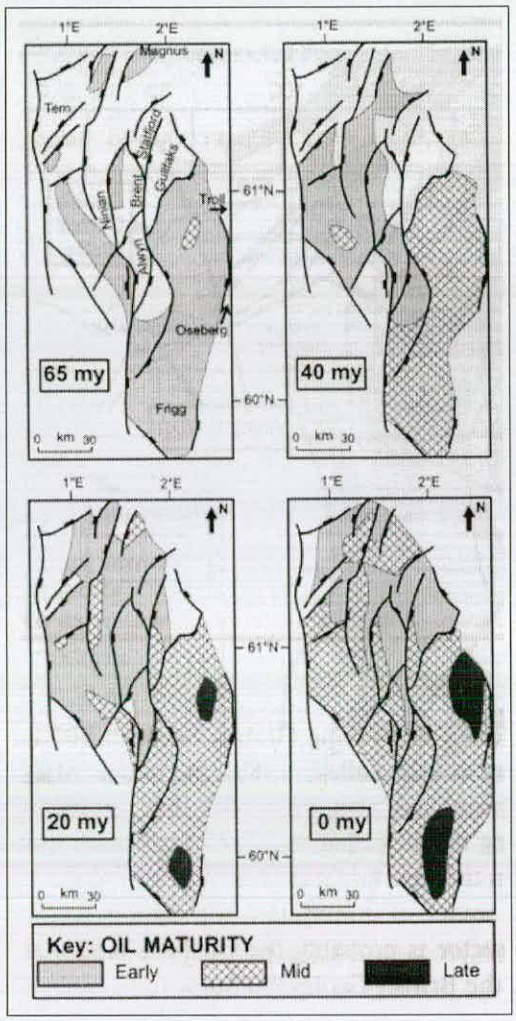

Figure 4.1b

Figure 4.1a - a schematic map of the East Shetland Basin, indicating the approximate depth of burial of the source rocks at the present day; 4.1b - schematic maps of the East Shetland Basin showing developing oil maturity in the source rocks. (Adapted from K. W. Glennie 1998).

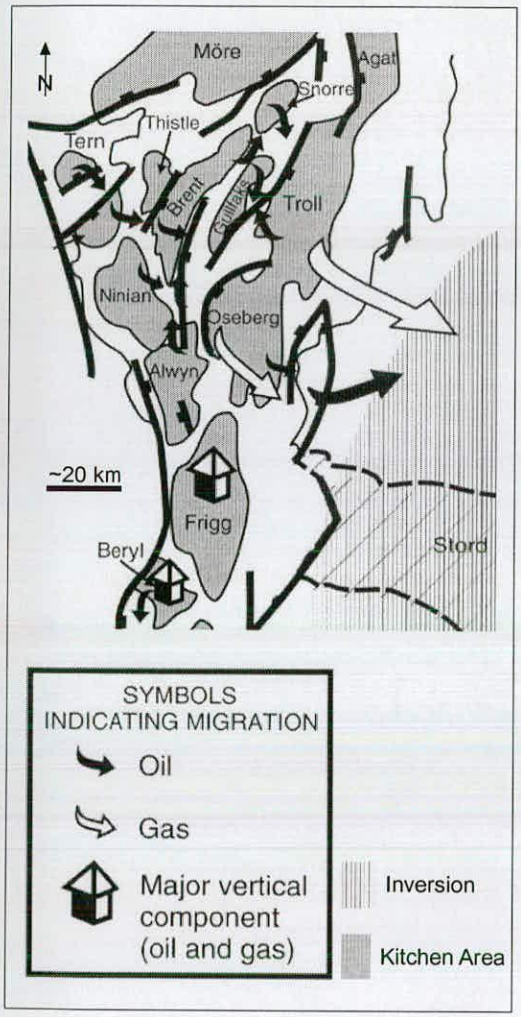

Figure 4.2a

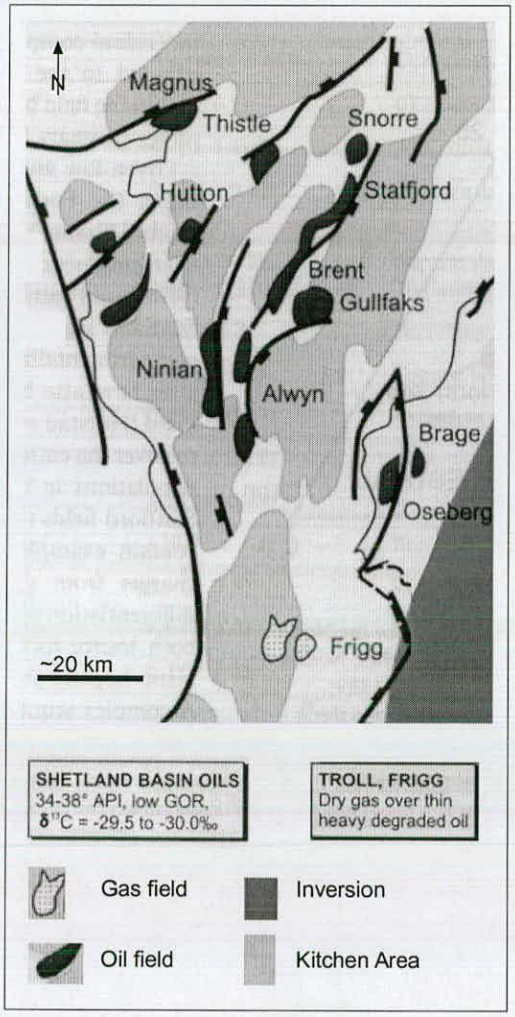

Figure 4.2b

Figure 4.2a - A schematic map of the East Shetland Basin, showing the accepted pattern of hydrocarbon migration from kitchen areas to oil and gas fields. 4.2b - A schematic map of the East Shetland Basin, indicating the general relationship between fields and kitchen areas. Both maps are adapted from K. W. Glennie (1998).

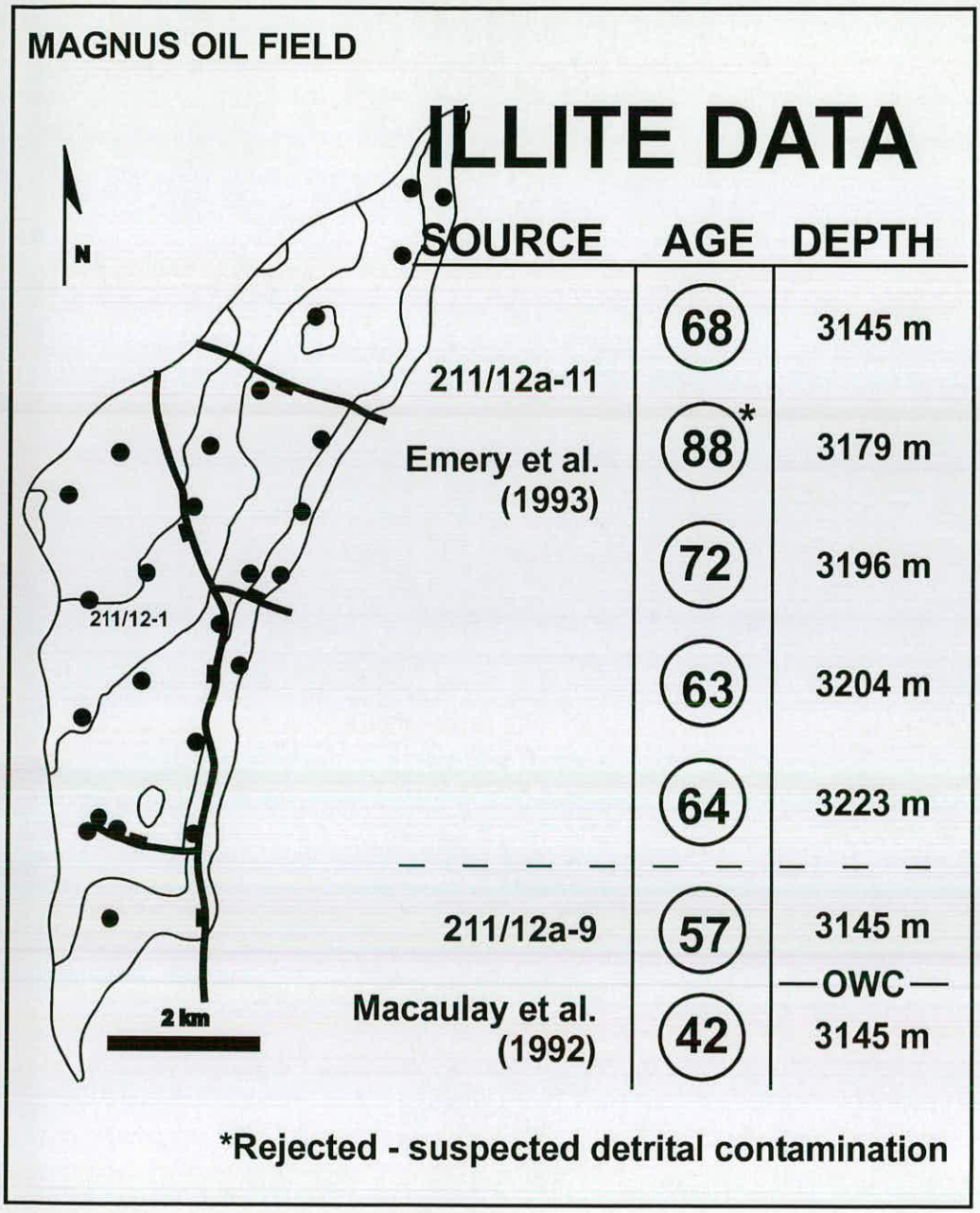

Figure 4.3 Illite ages for the Magnus oil field. The larger set, published by Emery *et al.* (1993), includes an illite age thought to be significantly older than expected ages for the field. As such, the age was rejected on grounds of suspected contamination. The illite ages for Magnus published by Macaulay *et al.* (1992) are suplemented by a further age in the doctoral thesis (Macaulay 1990).

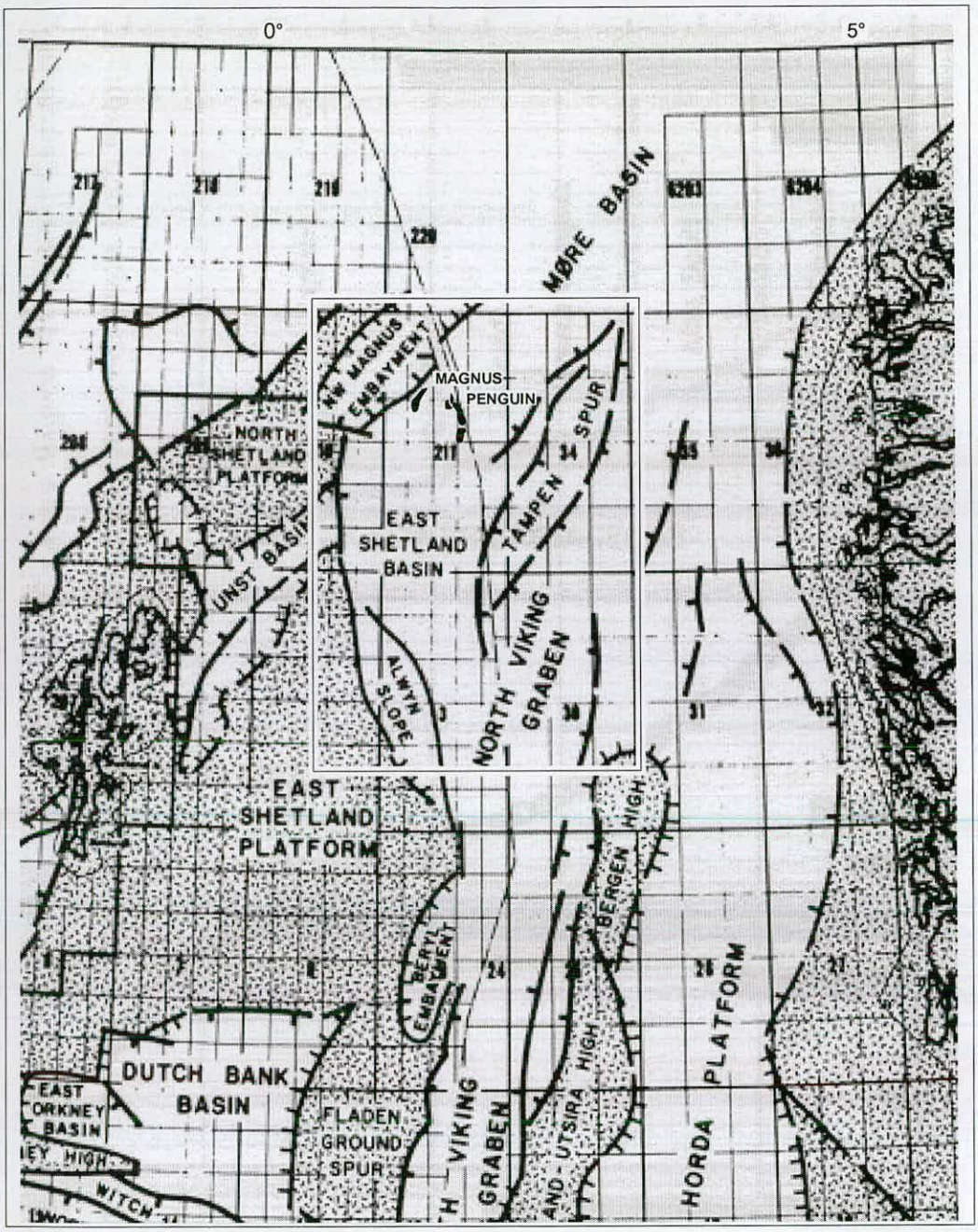

Figure 4.4 The Penguin and Magnus oil fields and their relationship to the Northern North Sea.

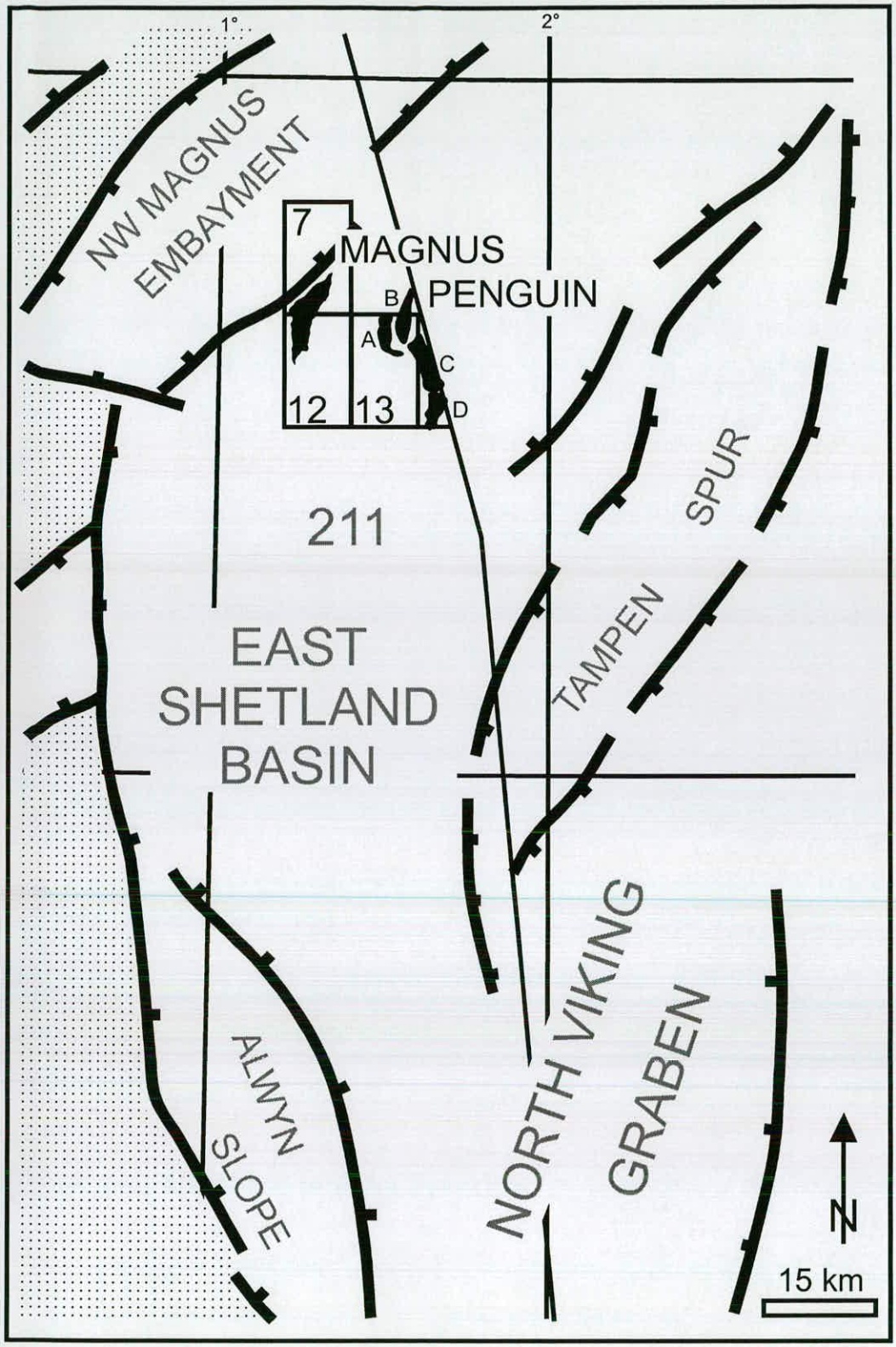

Figure 4.5 The Penguin oil field in relationship to Magnus and the East Shetland Basin area.

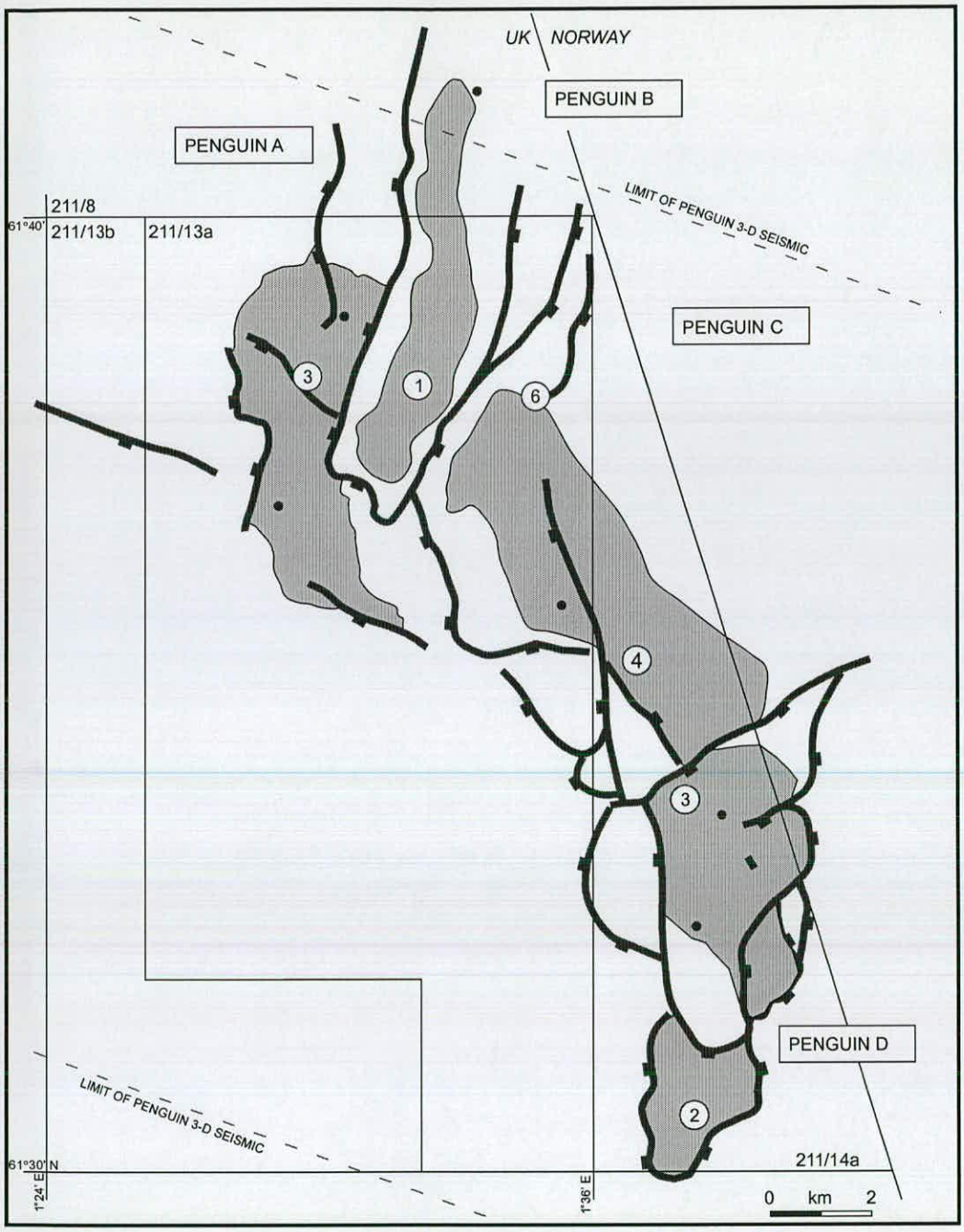

Figure 4.6 The Penguin oil field. The map view clearly shows Penguin 'A' lieing in a half graben to the west of a fragmented fault array, consisting of the Penguin 'B' horst, which is flanked to the southeast by the Penguin 'C' and Penguin 'D' compartments. Circled figures are sampled wells. Quadrant identification can be found on the map (Shell UK 1995).

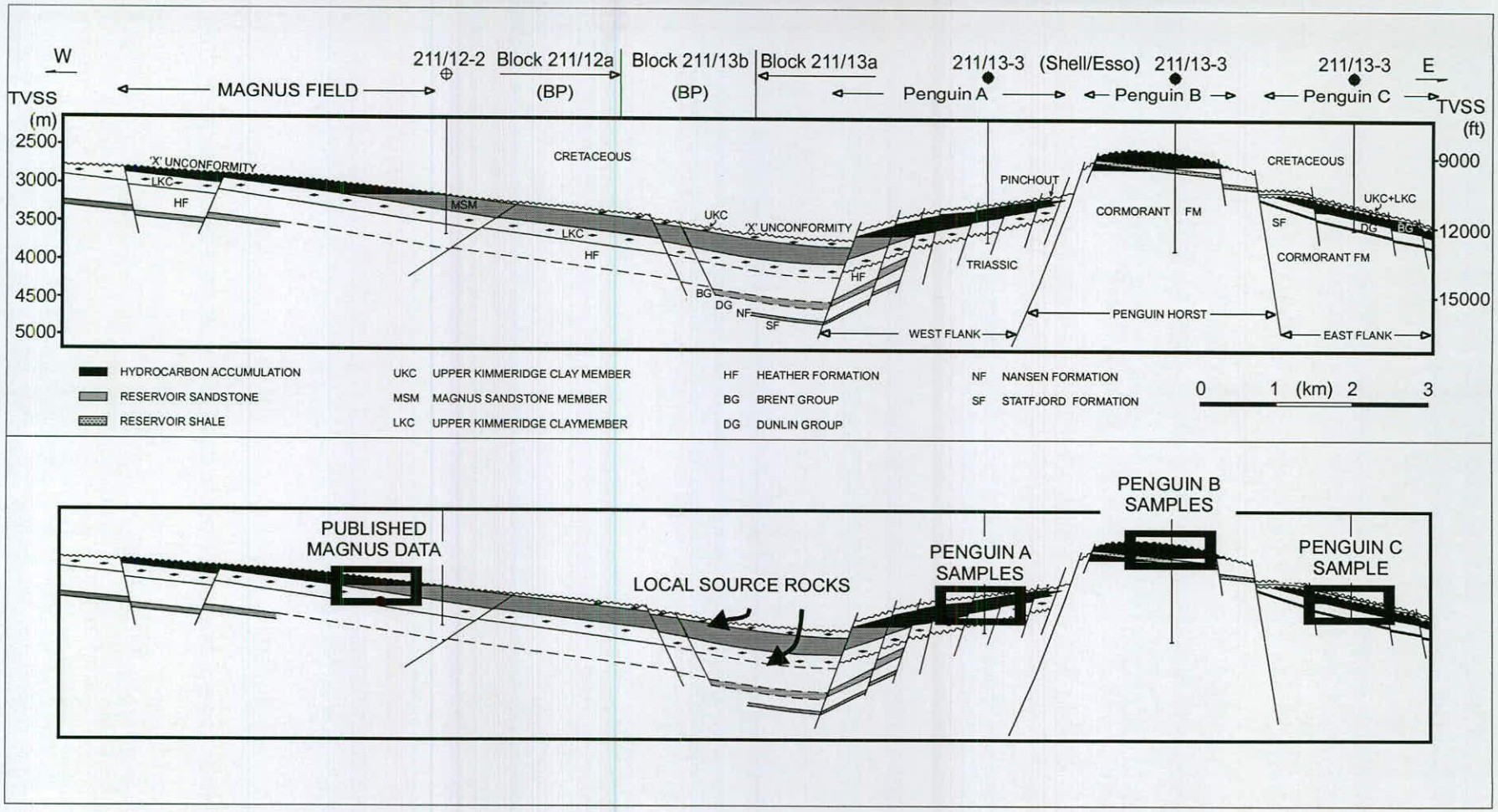

Figure 4.7 A cross-section from the Magnus crest to the eastern flank of the Penguin horst. Penguin D is not shown as it lies out of section. The approximate position of published data for the Magnus field and the selected sample sites for Penguin A, B and C are indicated by boxed areas.

Figure 4.8 A stratigraphic column for the Magnus Province. The left-hand column shows a generalised stratigraphy for the area. The detailed column to the right is specific to the Magnus field, based on BP data (after Barclay *et al.* 2000).

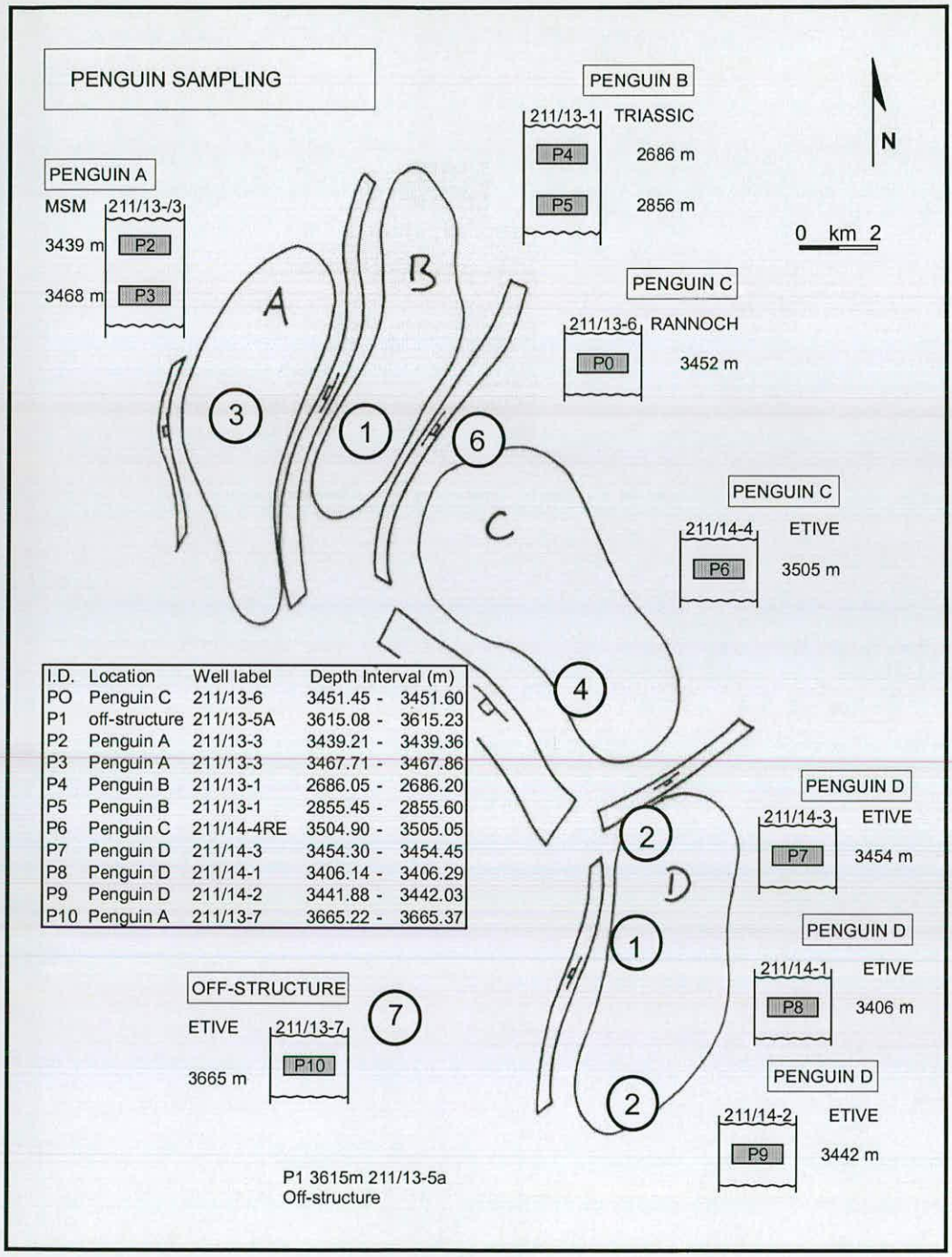

I.D.	Location	Well label	Depth Interval (m)	
PO	Penguin C	211/13-6	3451.45 -	3451.60
P1	off-structure	211/13-5A	3615.08 -	3615.23
P2	Penguin A	211/13-3	3439.21 -	3439.36
P3	Penguin A	211/13-3	3467.71 -	3467.86
P4	Penguin B	211/13-1	2686.05 -	2686.20
P5	Penguin B	211/13-1	2855.45 -	2855.60
P6	Penguin C	211/14-4RE	3504.90 -	3505.05
P7	Penguin D	211/14-3	3454.30 -	3454.45
P8	Penguin D	211/14-1	3406.14 -	3406.29
P9	Penguin D	211/14-2	3441.88 -	3442.03
P10	Penguin A	211/13-7	3665.22 -	3665.37

Figure 4.9 A map of sandstone sample locations for illite analyis from the Penguin oil field. All samples consisted of 15 cm, half-core lengths, weighing approximately one kilogram.

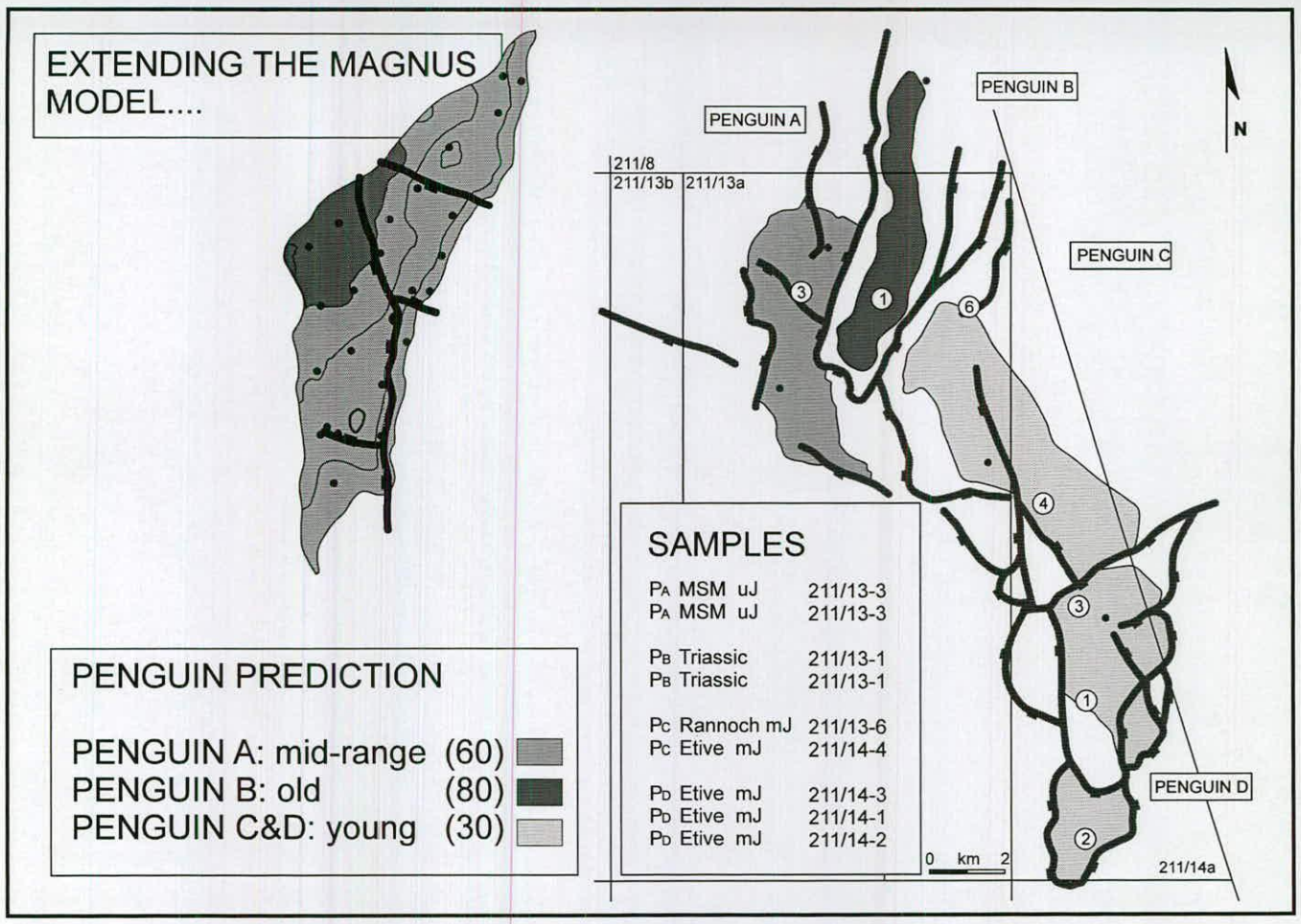

Figure 4.10 A map of predictions for illite ages from the Penguin field based on observations from Magnus. Well locations are shown for Penguin core samples. The predictions are unimodal and related to the expected origin of migrating hydroacrbons.

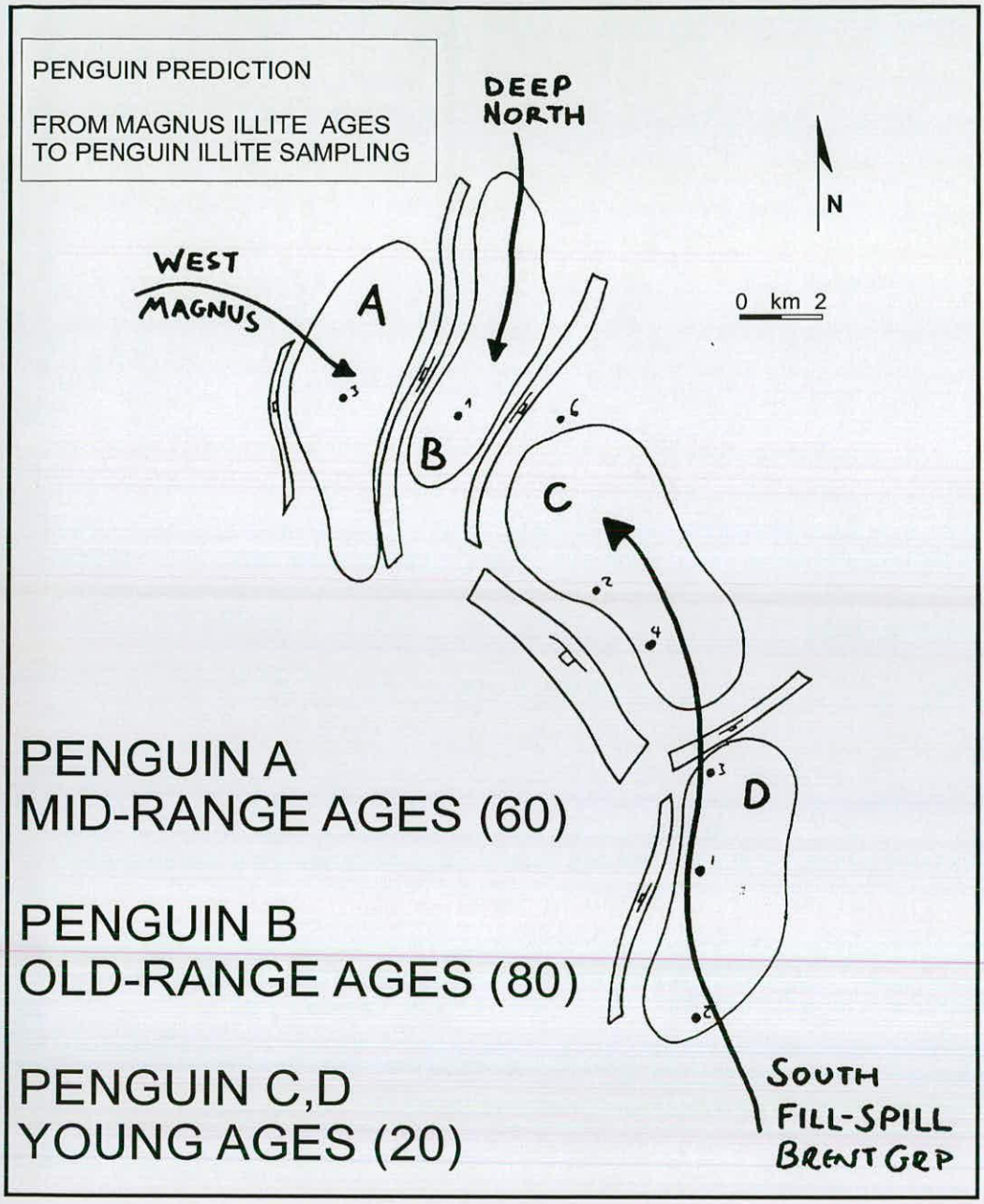

Figure 4.11 A prediction for illite ages from Penguin oil field samples. The map view indicates that PenguinA is thought to fill from the west, and is closely related to Magnus in this respect. The Penguin B condensate - thought to be indicative of a deeper source rock, is associated with the deep Möre basin to the north. Penguin C and D are Brent-type reservoirs, representative of the northern edge of the deltaic complex. As such, these two reservoirs are expected to fill last, at the end of a fill-spill sequence. The predicted ages reflect these hypothetical migration pathways.

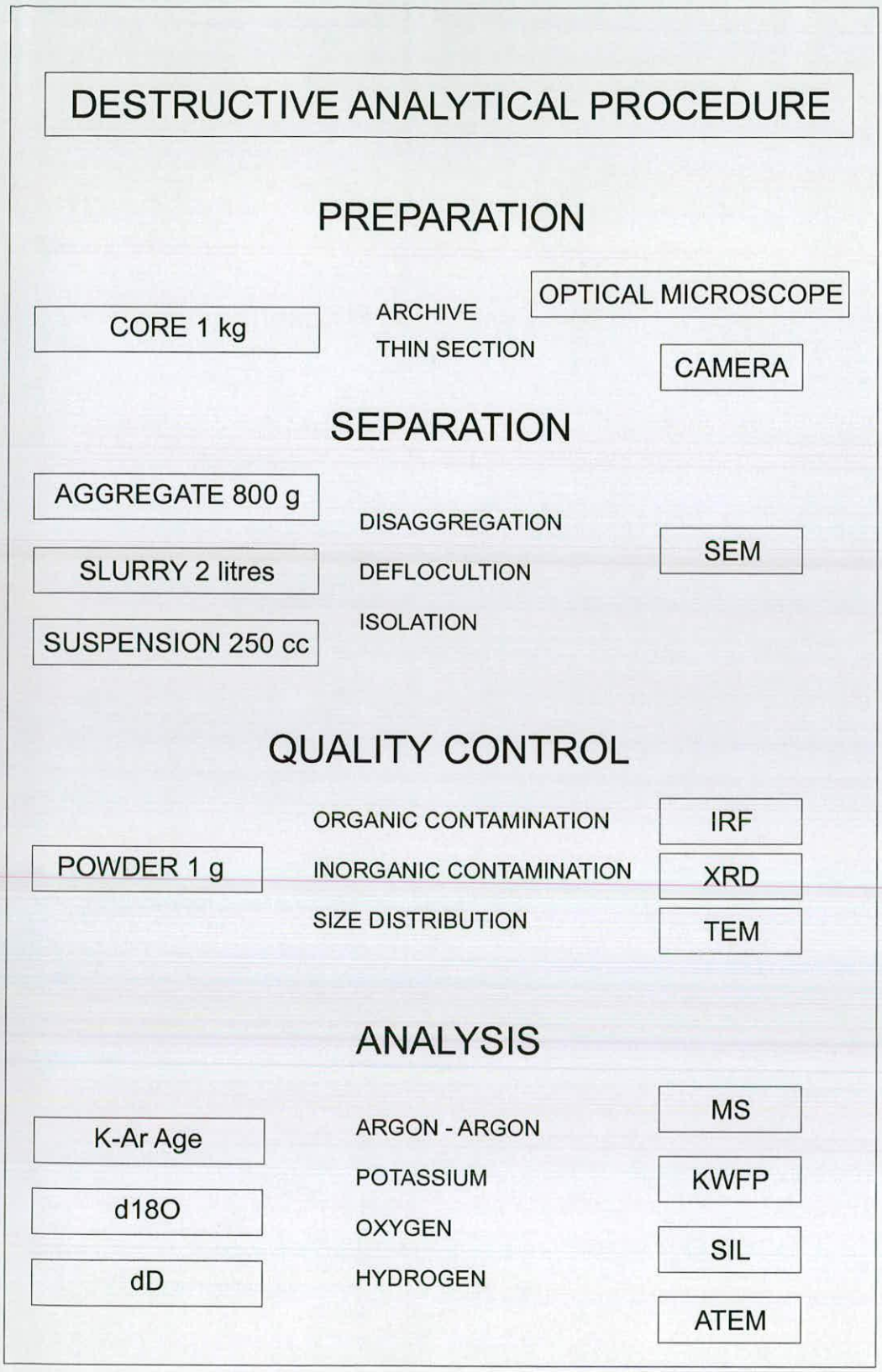

Figure 4.12 A flow chart detailing the destructive analytical procedure followed to extract, qualitatively assess and quantify illite ages from the Penguin field, Northern North Sea. Note that a large core sample, ~ 1 kg, yields a very small illite aliquot, ~ 1 g. IRF - Infared Fluorescence, KWFP - Potassium Wet Flame Photometry, SIL - Stable Isotope Line.

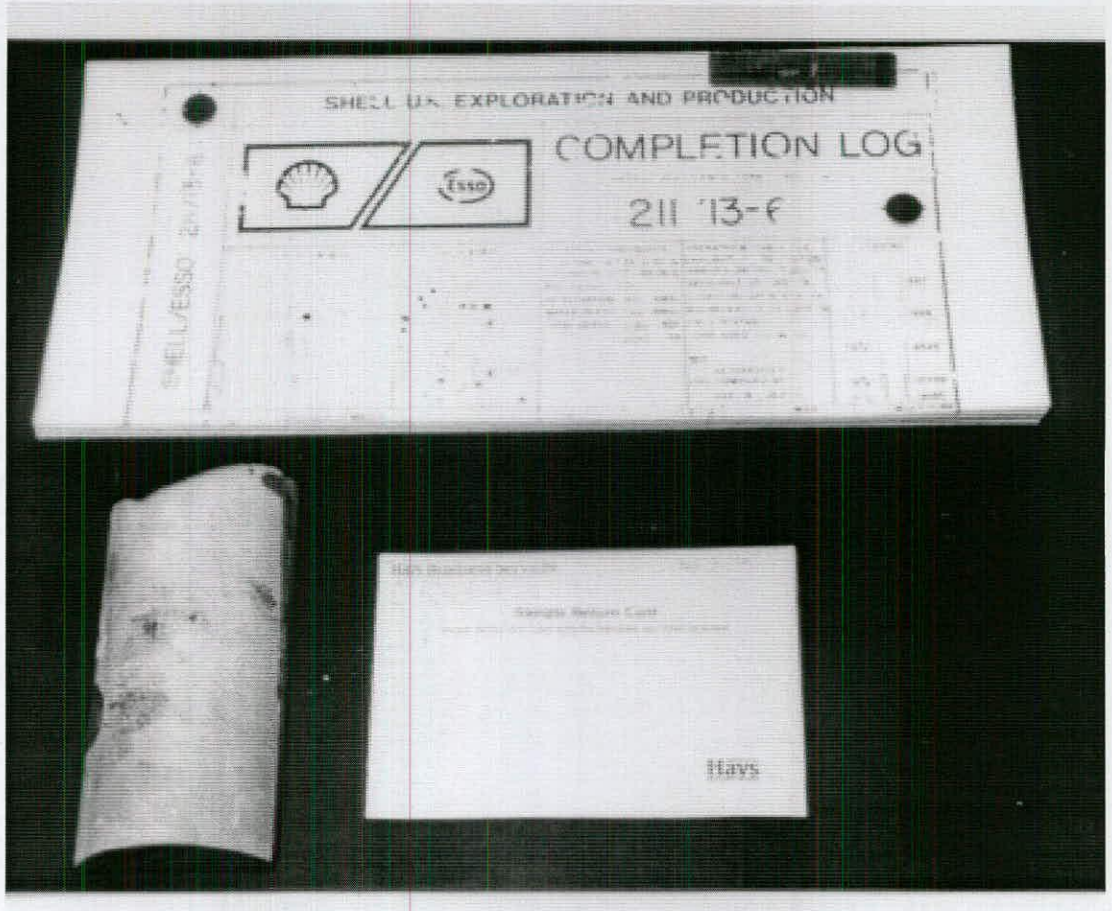

Figure 4.13 A sandstone core sample, 'P0', from Penguin C, well 211/13-6.
The completion log and archive card are included for scale. The sample weighs about 1 kg.

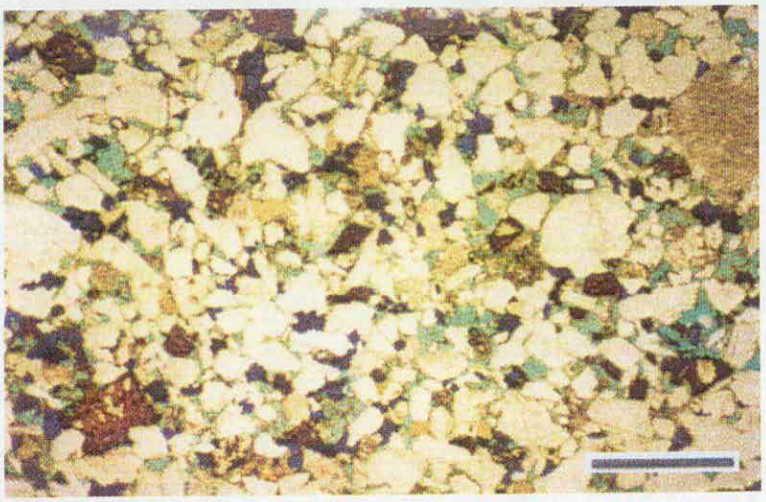

211/13-3
PENGUIN A

scale bar: 1 mm

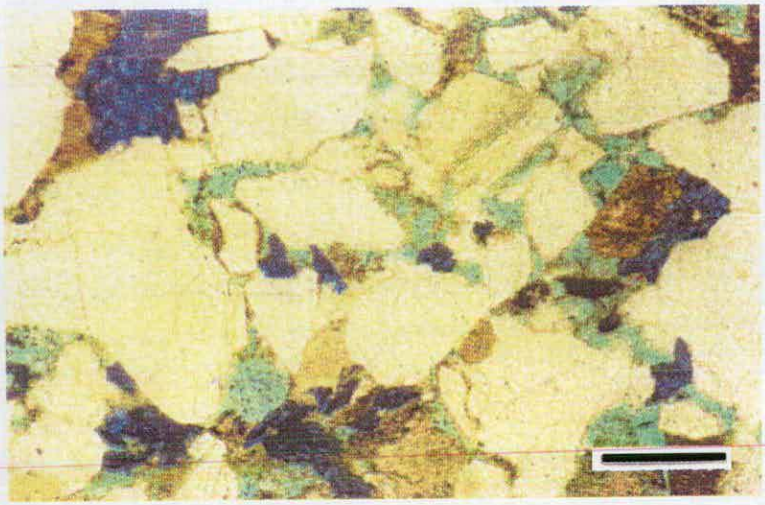

211/13-3
PENGUIN A

scale bar: 0.25 mm

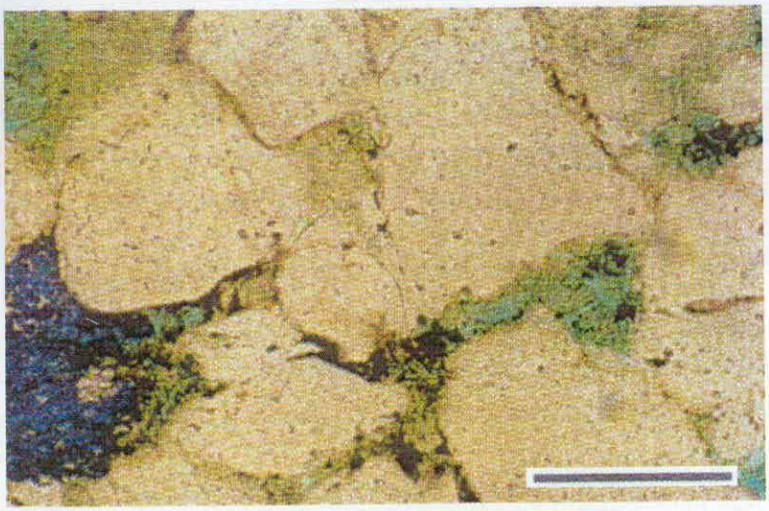

211/14-1
PENGUIN D

scale bar: 0.1 mm

Figure 4.14 Thin section photographs from Penguin trap structures A and D. The sand grains in Penguin A are typically angular to sub-angular and poorly sorted, in contrast to the rounded, well-sorted grains of Penguin D. These attributes are indicative of provenance and the mode of deposition: a turbidite sequence in Penguin A and a distal deltaic sequence in Penguin D.

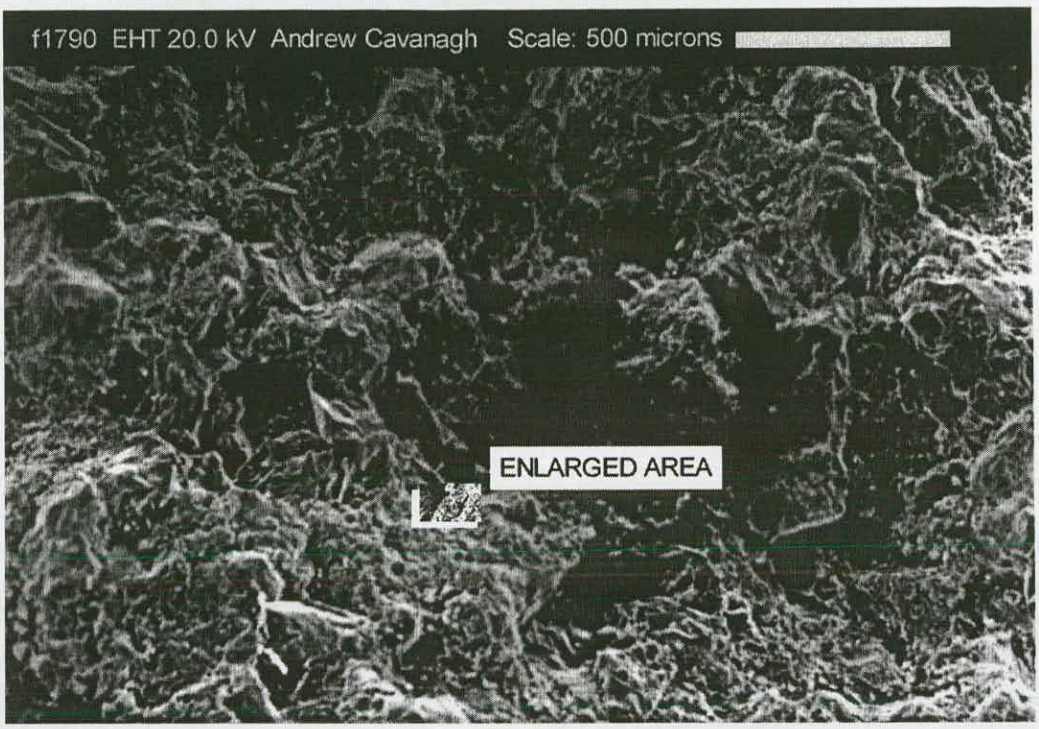

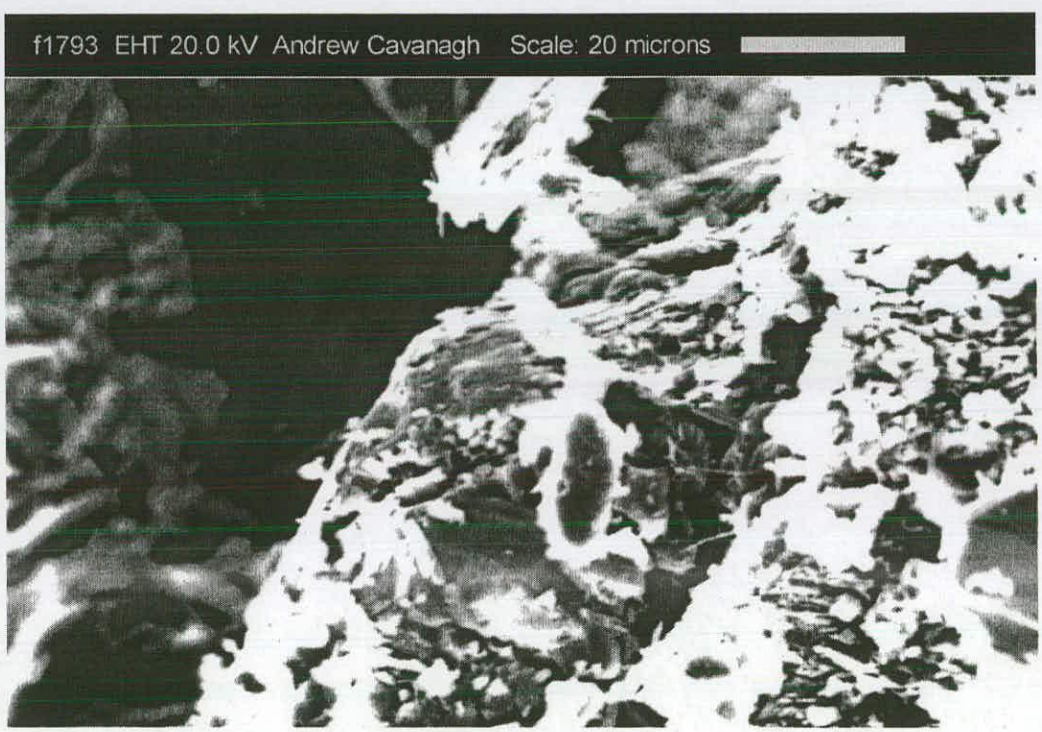

Figure 4.15 A low magnification Scanning Electron Microscope photograph (f1970) of a core sample from the Penguin A field. The generally observable morphology of sand grains is slightly obscured by a pervasive shroud of diagenetic material. The enlarged area (f1793) clearly exhibits fine strands of crystalline material, coating what appears to be earlier phases of euhedral, diagnetic material. This is consistent with a late phase of fibrous illite cementation.

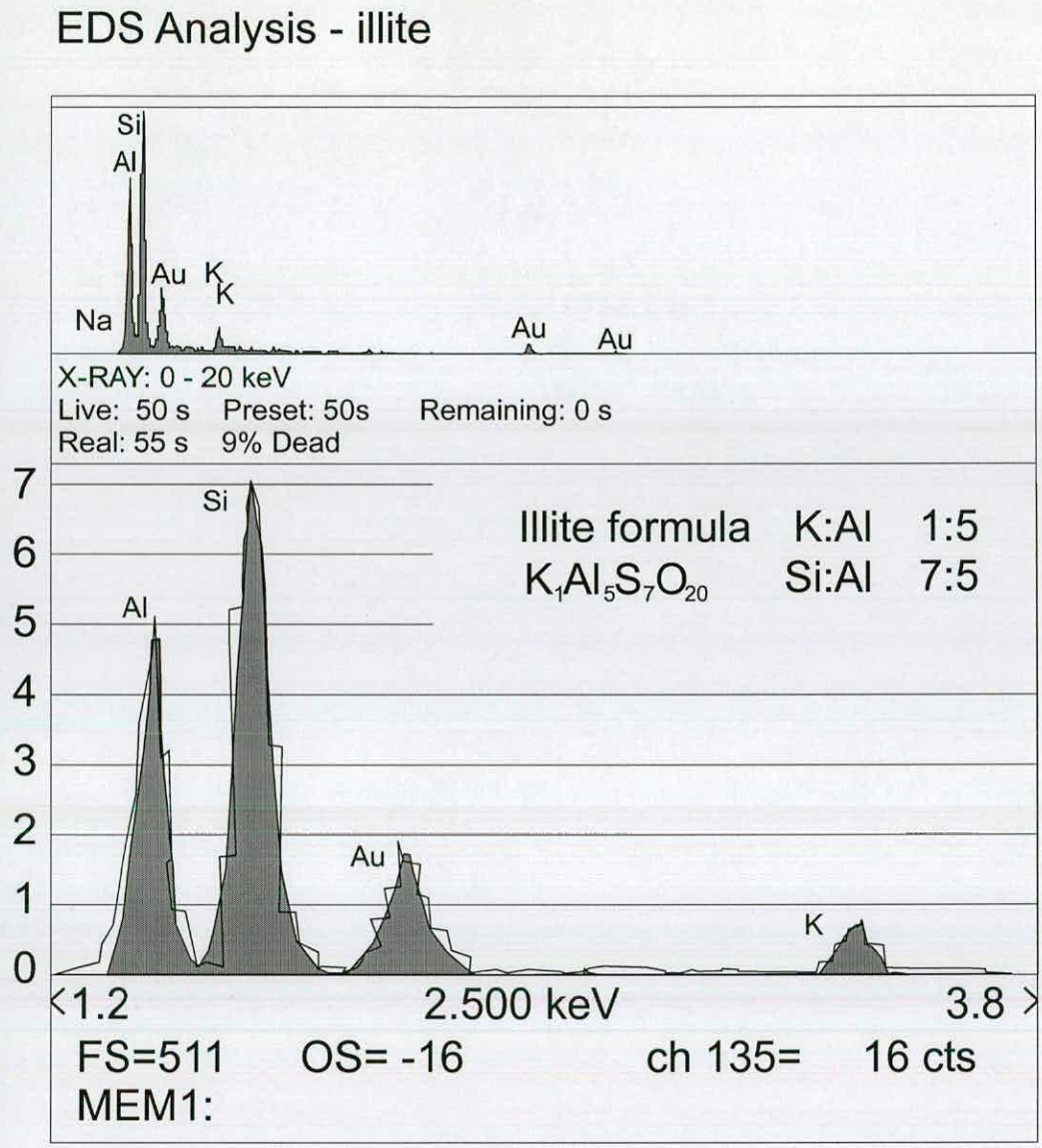

Figure 4.16 EDS analyis on suspected illite crystals, as observed in SEM photograph, f1476 - see Figure 4.14. The general spectrum indicates that the crystal is an aluminosilicate containing potassium. An enlargement of the spectrum shows that the relative proportions of elements, K:Al and Si:Al, is in accord with the formulaic ratio for the mineral illite. The traces of gold result from sample preparation.

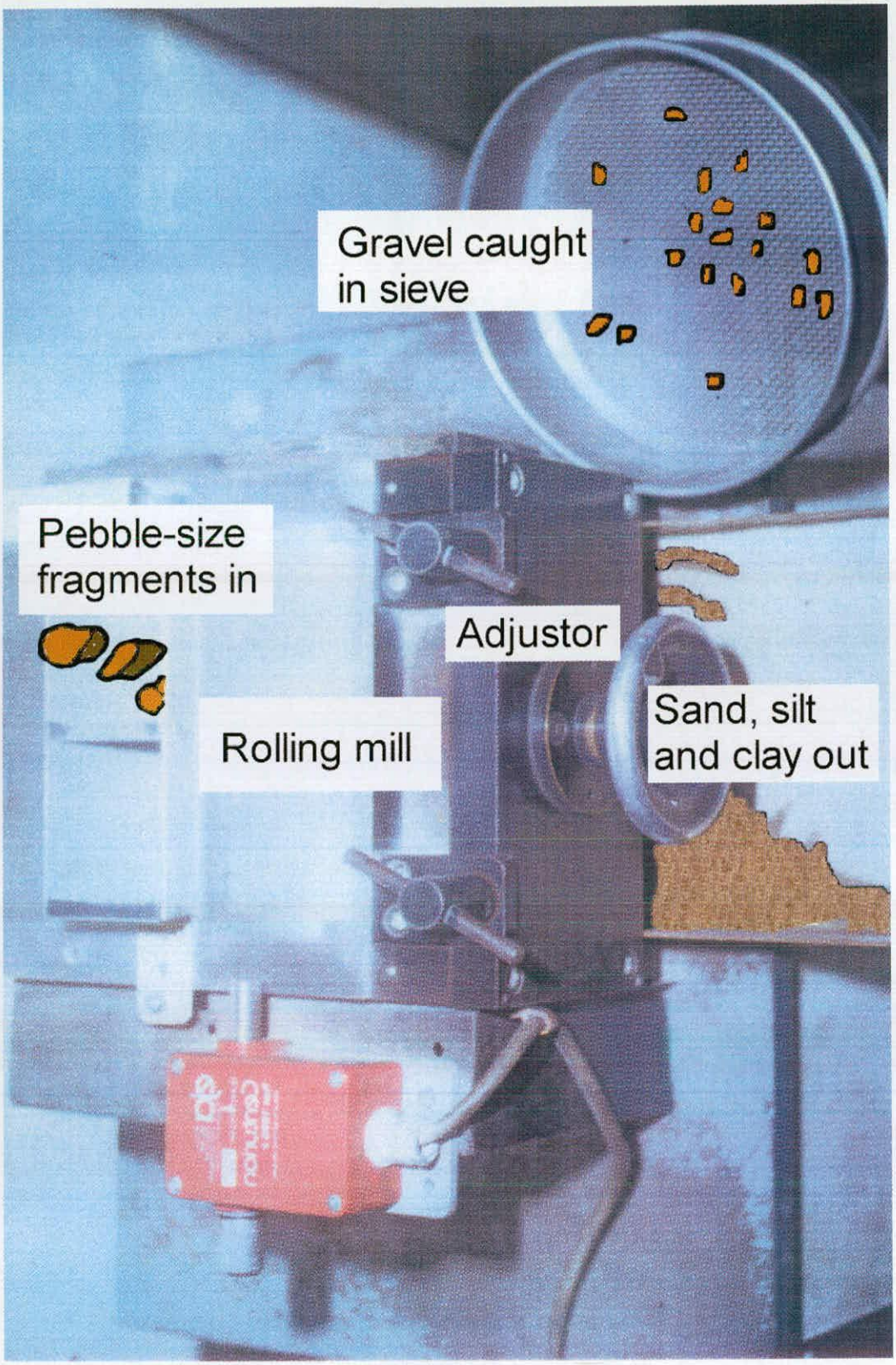

Figure 4.17 A crown mill, used to disaggregate sandstone core samples. The core is broken into cobbles with a rock splitter, then reduced to pebble-size fragments with a cold chisel. The pebbles are fed into a crown mill. The aggregate is sieved for sand, silt and clay, which are set aside for wet processing. The adjustable aperture on the crown mill is reduced, and then the gravel reprocessed until all the sample has been disaggregated to sand, silt and clay fractions.

Figure 4.18 A Scanning Electron Microscope image of a disaggregated sample from one of the Penguin cores. Note that the discrete larger grains in the image are intact sand grains complete with diagenetically altered surfaces. Fine silt and clay particles are also present and generally display the angular, euhedral morphologies expected of cement crystals. These morphologies indicate that the disaggregation technique has not significantly damaged or powdered the delicate crystals present. The result is likely to be adequately clean, low-contamination illite aliquots.

Figure 4.19 A high magnification SEM photograph of the aggregate sample from Penguin 211/13-6. Remnant spars of an old feldspar crystal occupy the central field of the photograph. Spar fragments of relict feldspars like this one are the principal contaminant hazard when analysing illite aliquots, due to their relatively old age with respect to the timing of illite diagenesis.

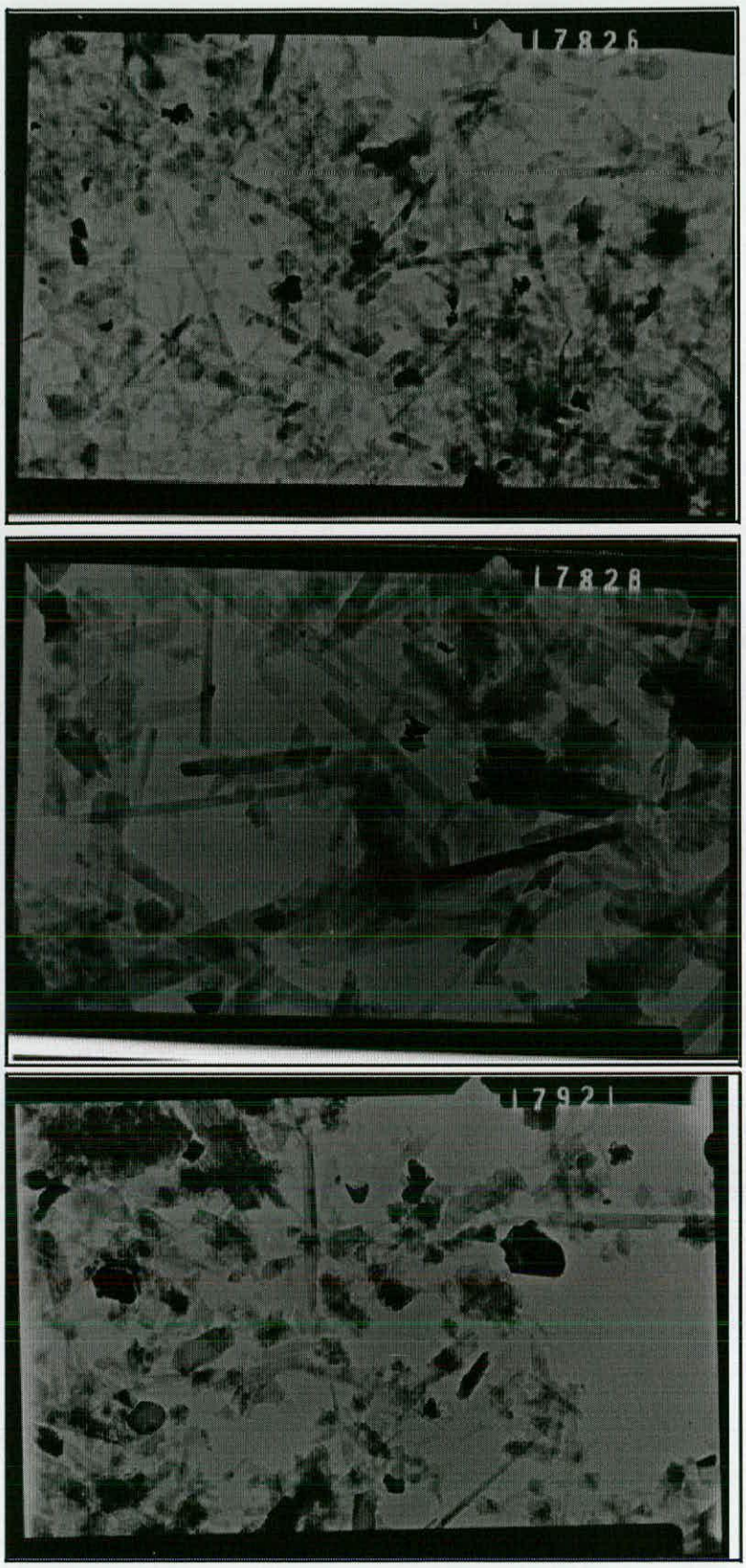

Figure 4.20 Three Transmission Electron Microscope photographs of clay aliquots extracted from the Penguin samples. All clay fractions show a predominant acicular morphology. Fibrous mats of acicular crystals are also common. Irregular morphologies and darker, electron-dense material are likely to be contaminant phases.

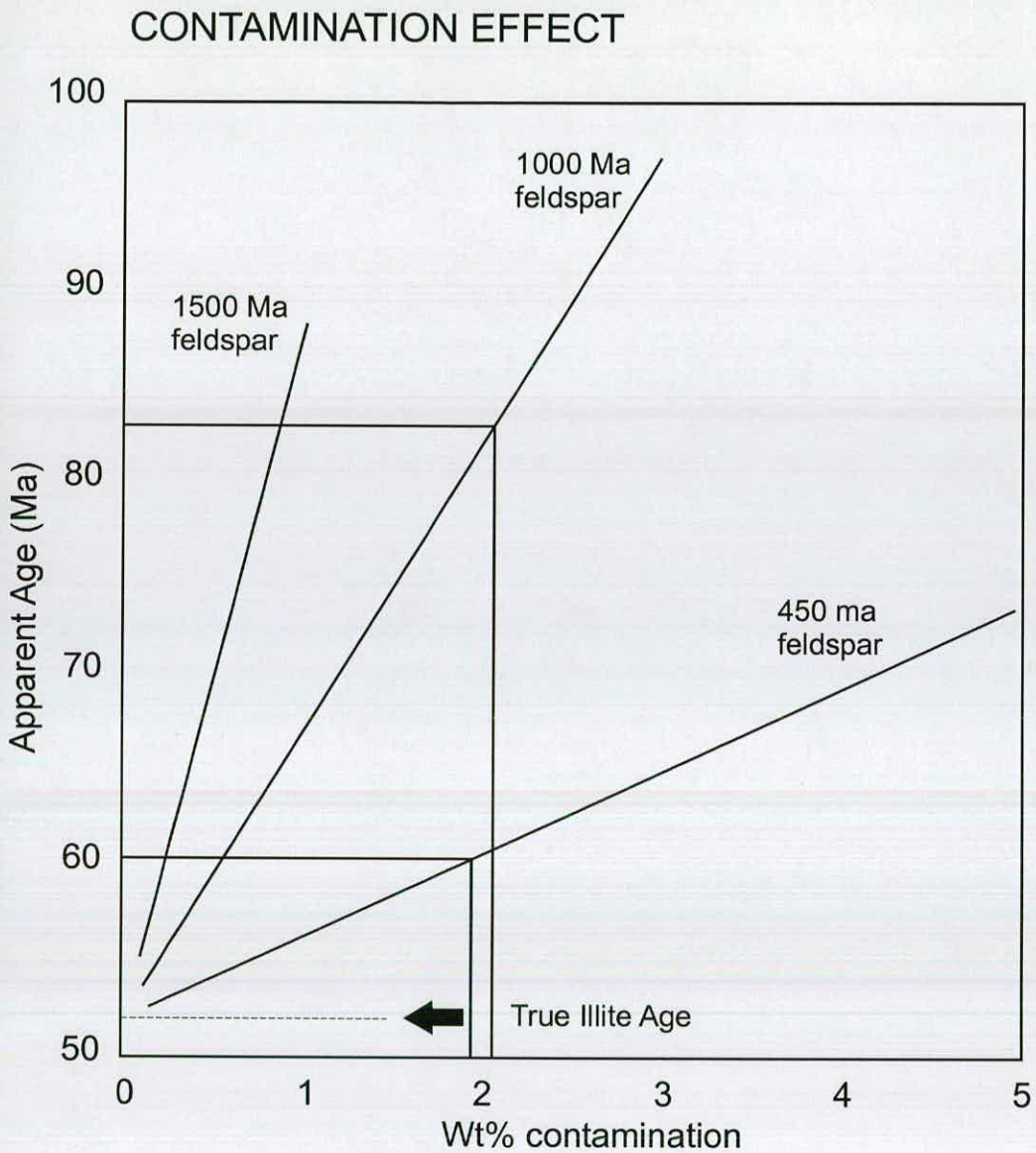

Figure 4.21 A cross-plot of apparent age versus contamination by feldspars of various ages. The feldspar ages all represent common provenance ages for feldspar sources. Depending on the type of feldspar contamination, a very low weight % can result in a significant error in the true illite age. The nature and degree of contamination are the principle factors in ascertaining the reliability of illite ages.

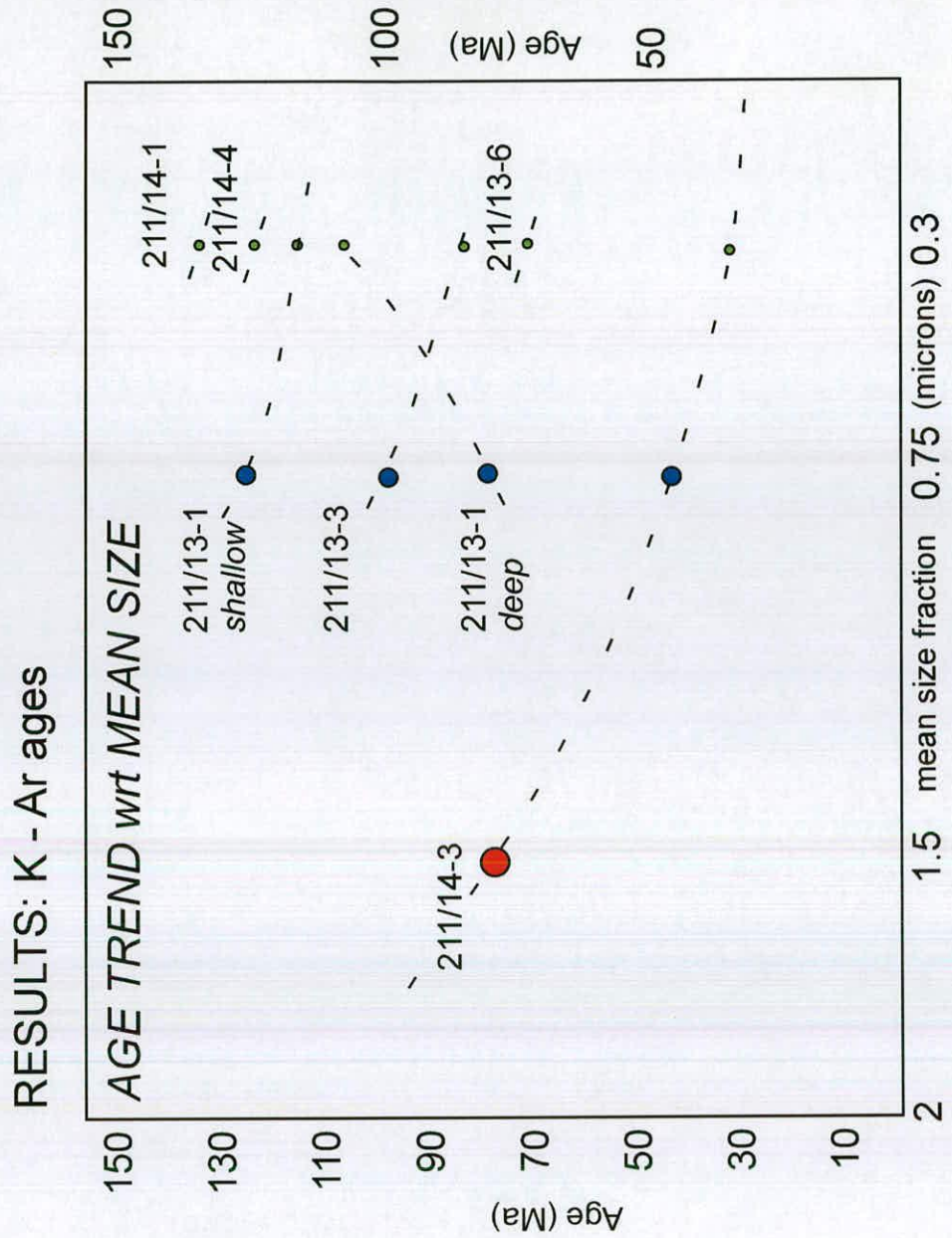

Figure 4.22 A cross-plot of illite ages versus mean size fraction. Sample 211/14-3 yielded three aliquots, which exhibit an increase in age with size fraction. This trend of younger ages with finer aliquots holds true for well 211/13-3 and the shallow sample from 211/13-1. The deep sample from 211/13-1 goes against the general trend. Additionally, note that the finest size fraction aliquots yield a broad range of ages, ranging from 30 Ma to 130 Ma.

RESULTS: K - Ar ages

Well	Fraction	Age (Ma)
211/13-3	○	99 ±6
211/13-3	∘	85 ±13
211/13-1 SHALLOW	○	127 ±10
211/13-1 SHALLOW	∘	117 ±5
211/13-1 DEEP	○	80 ±36
211/13-1 DEEP	∘	108 ±1
211/13-6	∘	72 ±1
211/14-4	∘	88 ±26
211/14-3	◯	71 ±5
211/14-3	○	44 ±1
211/14-3	∘	33 ±2
211/14-1	∘	136 ±4

Size fraction (microns)
◯ >1.0 ○ 1.0-0.5 ∘ 0.5-0.1

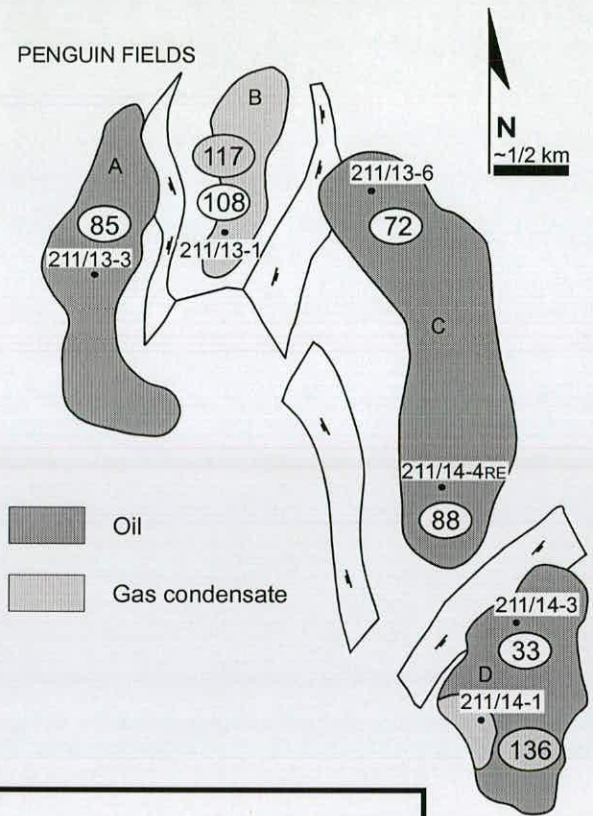

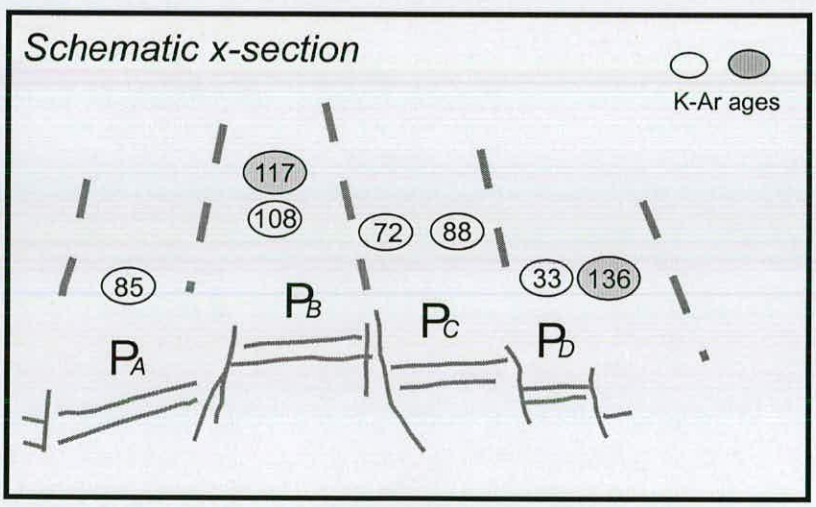

Figure 4.23 A map of K-Ar ages for Penguin illite aliquots. The map shows a coherent geographical pattern to the distribution of ages for the finest aliquots. All data points are displayed in the adjoining table. Illite from the Penguin B horst is unexpectedly old at around 120 Ma. The two flanking structures, Penguin A and C, have returned illite similar to ages published for the Magnus field. Penguin D puzzlingly retruns both the youngest and oldest ages for the data array. Note that ages in excess of 100 Ma are associated with condensate accumulations in Penguin B and Penguin D. A schematic x-section of K-Ar ages further illustrates the simple geographical associations of ages to trap structures.

RESULTS: K - Ar ages vs δ18O

Well	Fraction	Age (Ma)	δ18O
211/13-3	○	99 ±6	14.9
211/13-3	o	85 ±13	15.1
211/13-1	○	127 ±10	16.2
211/13-1 SHALLOW	o	117 ±5	14.2
211/13-1	○	80 ±36	15.7
211/13-1 DEEP	o	108 ±1	14.6
211/13-6	o	72 ±1	15.3
211/14-4	o	88 ±26	13.8
211/14-3	○	71 ±5	12.3
211/14-3	○	44 ±1	12.9
211/14-3	o	33 ±2	13.6
211/14-1	o	136 ±4	13.4

Size fraction (microns)
○ >1.0 ○ 1.0-0.5 o 0.5-0.1

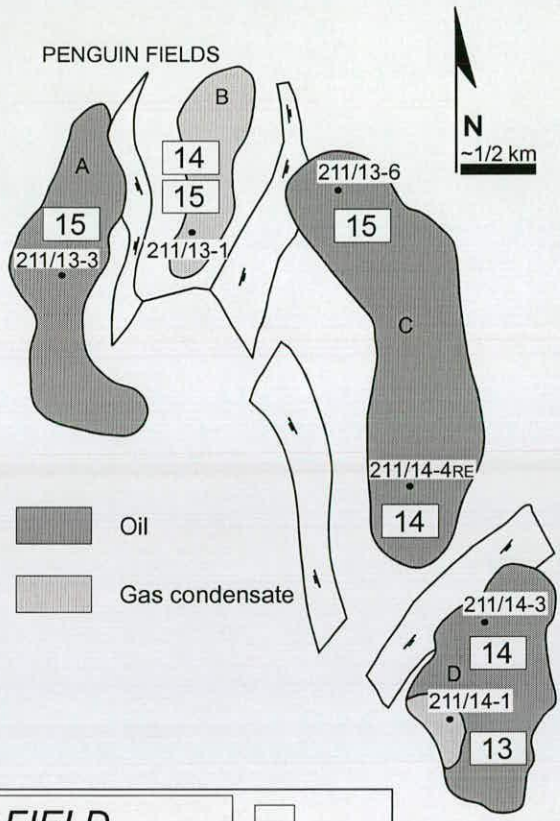

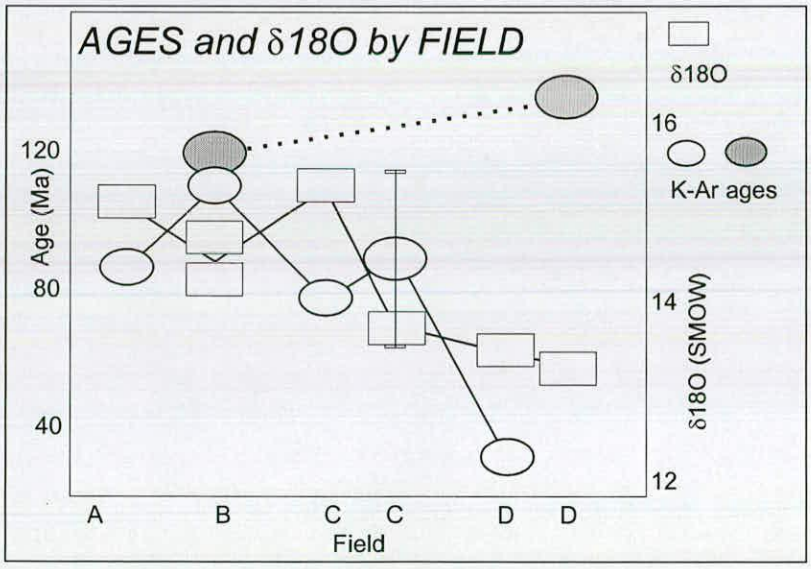

Figure 4.24 A comparison of K-Ar ages to δ18O values for the same aliquots. The map shows a distinct geographical pattern to the distribution of δ18O values for the finest aliquots. All data points are displayed in the adjoining table. A chart of K-Ar ages and δ18O data by field further illustrates the correlation between oxygen isotope values and ages for illite aliquots from the Penguin field. The older ages and heavie r δ18O results occur in or close to Penguin B. Younger ages and lighter δ180 values occur in Penguin fields C and D. The oldest ages appear to be independent of δ18O results from the same samples.

RESULTS: K - Ar ages vs δD

Well	Fraction	Age (Ma)		δ18O	δD
211/13-3	○	99	±6	14.9	-55
211/13-3	o	85	±13	15.1	-
211/13-1	○	127	±10	16.2	-52
211/13-1 *SHALLOW*	o	117	±5	14.2	-53
211/13-1	○	80	±36	15.7	-52
211/13-1 *DEEP*	o	108	±1	14.6	-55
211/13-6	o	72	±1	15.3	-53
211/14-4	o	88	±26	13.8	-52
211/14-3	○	71	±5	12.3	-66
211/14-3	○	44	±1	12.9	-55
211/14-3	o	33	±2	13.6	-
211/14-1	o	136	±4	13.4	-

Size fraction (microns)
○ >1.0 ○ 1.0-0.5 o 0.5-0.1

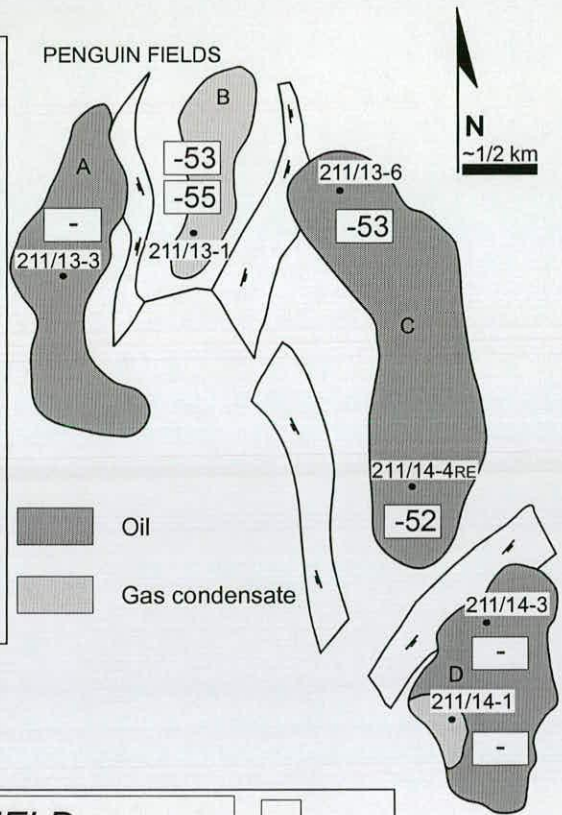

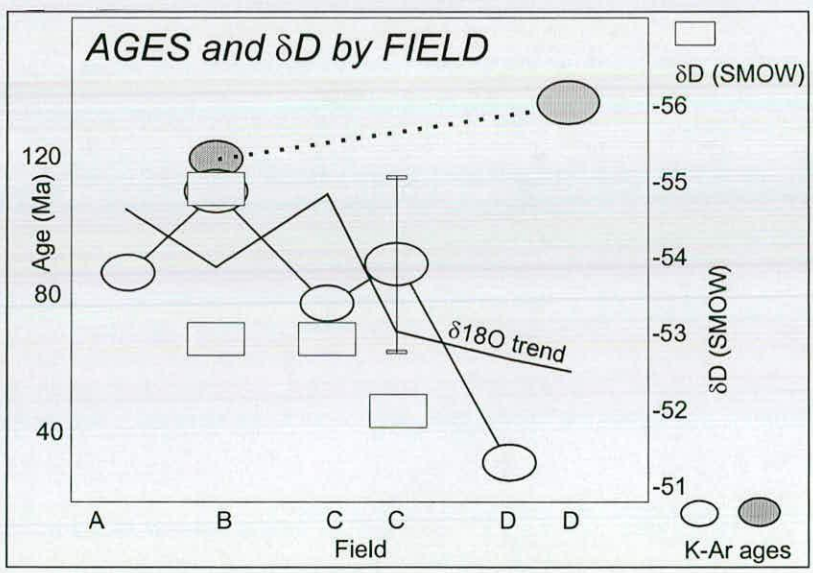

Figure 4.25 A comparison of K-Ar ages to δD values for the same aliquots. The map shows a the geographical distribution of δD values for the finest aliquots. All data points are displayed in the adjoining table. A chart of K-Ar ages and δD data by field includes the trend for oxygen isotope values from the Penguin field. Although the data is restricted to only four points for fine fraction aliquots, there is a similarity in the trend between the ages, oxygen and deuterium isotopes.

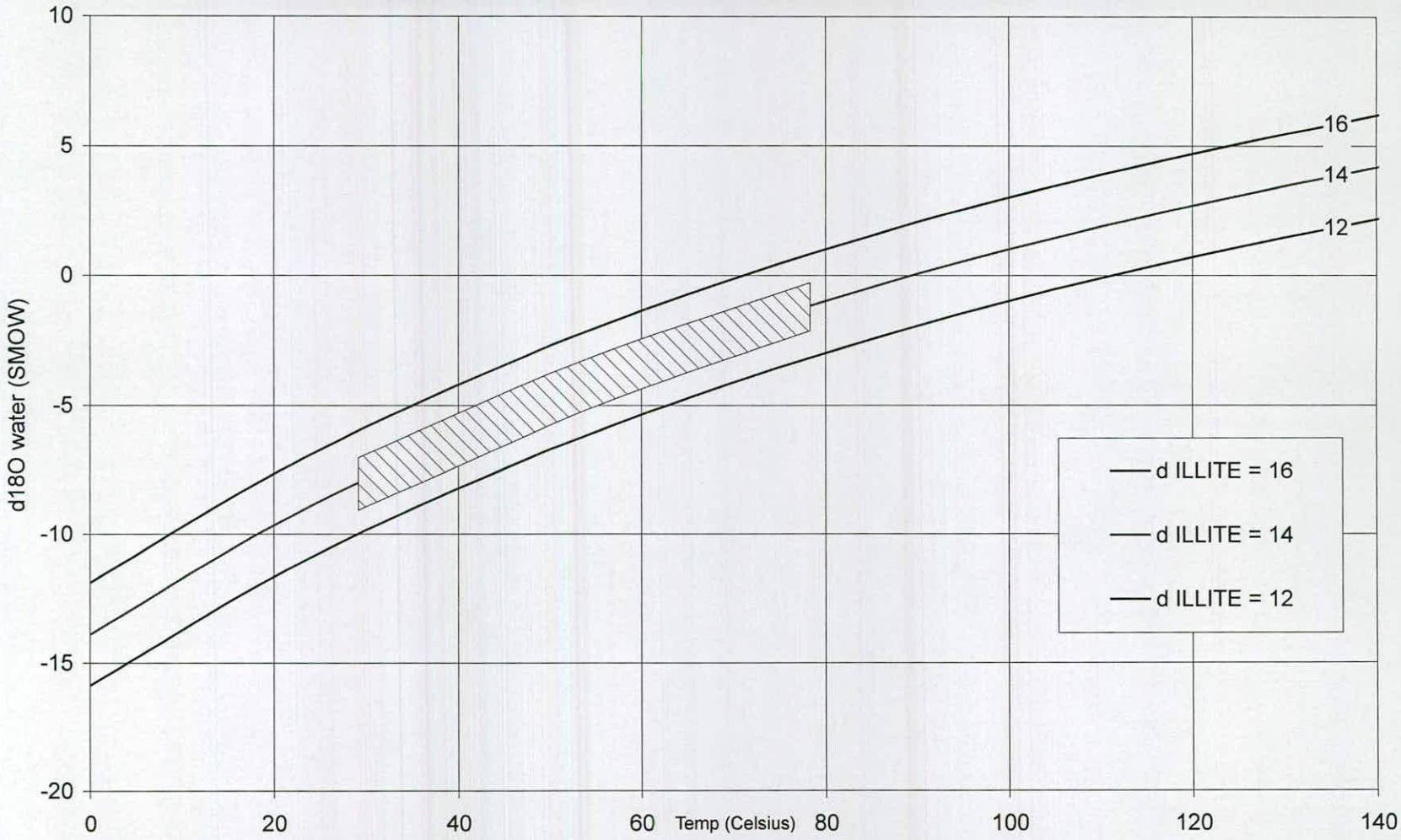

Figure 4.26 δO curves for illite with respect to porewater δO and temperature. The stiple area indicates the interpreted growth field for illite from Penguin.

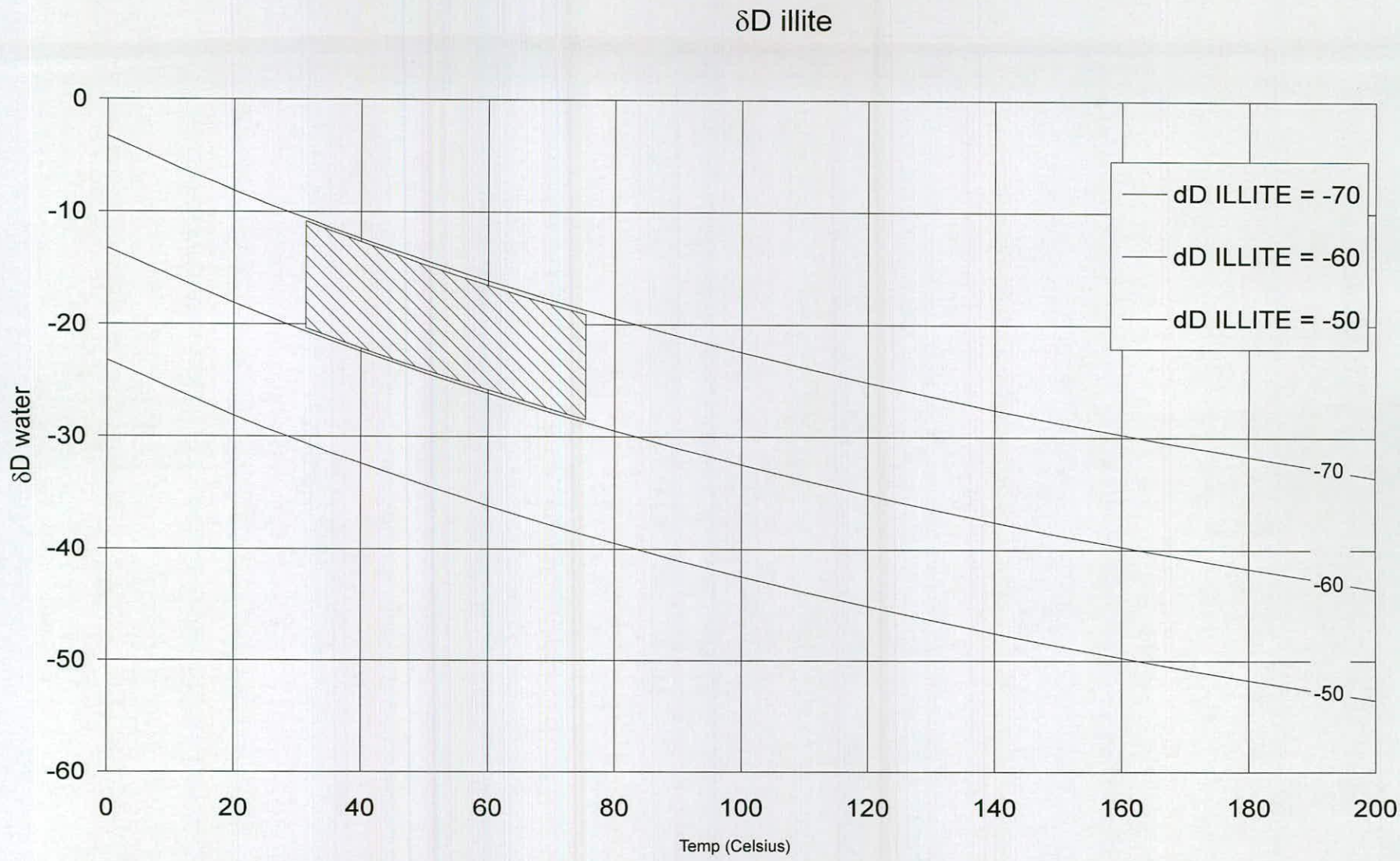

Figure 4.27 δD curves for illite with respect to porewater δD and temperature (after Yeh 1980). The stiple area indicates the interpreted growth field for Penguin illites.

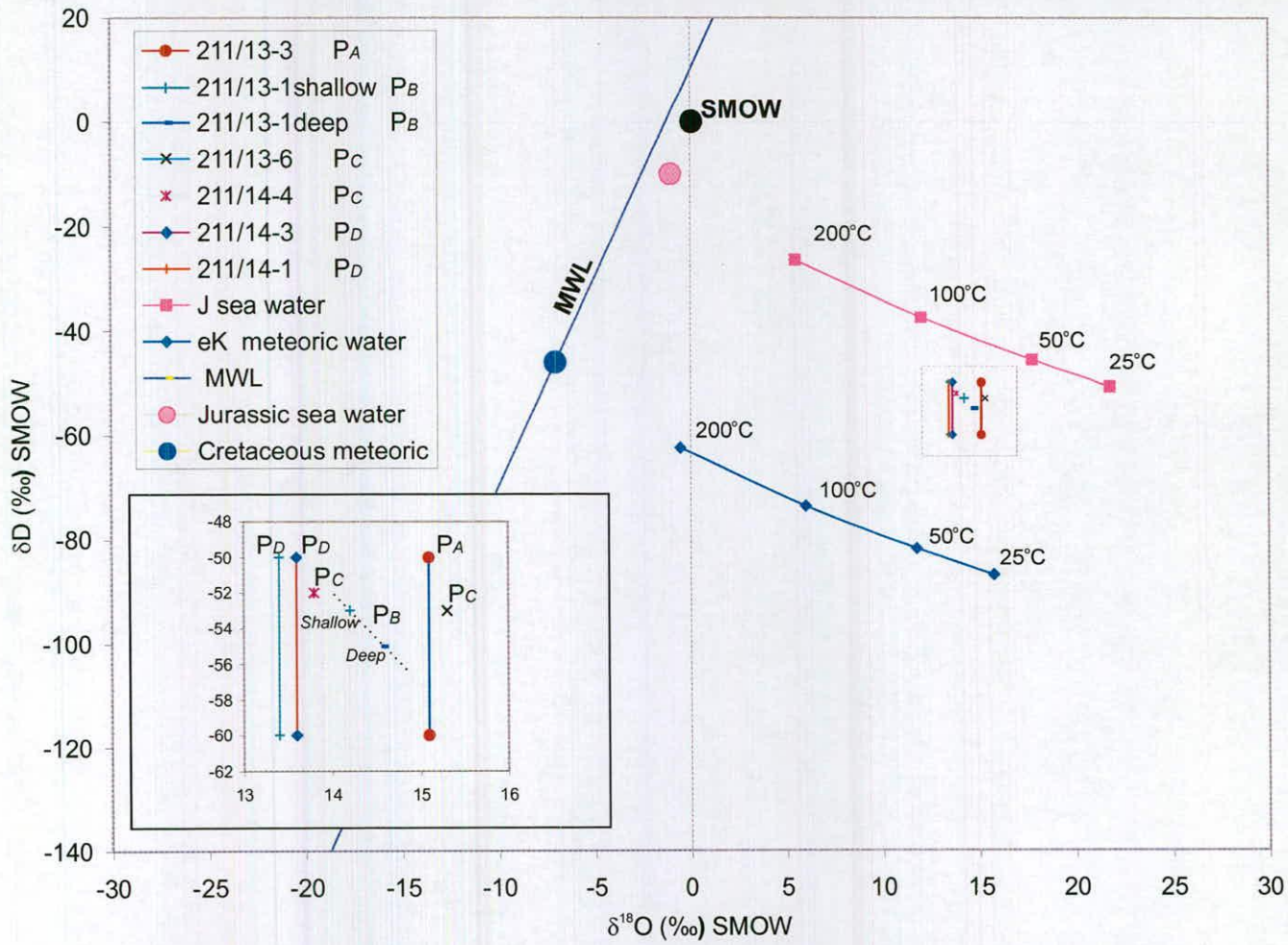

Figure 4.28 a cross-plot of D and 18O values for fine fraction illites. The graph shows a meteoric water line, a Jurassic sea water evolution curve, and an early Cretaceous meteroic water evolution curve for context. An enlargement of the data cluster is also included.

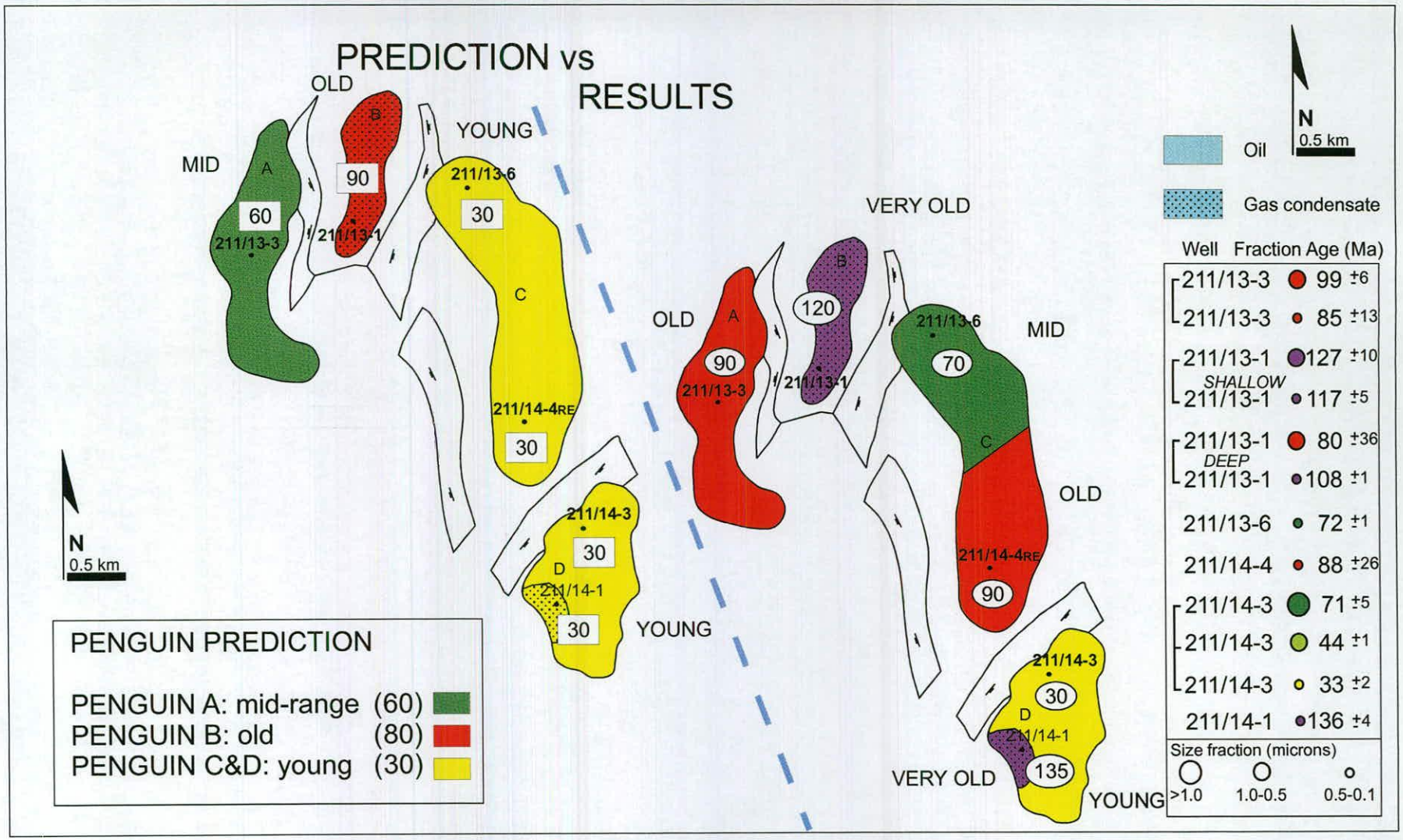

Figure 4.29 A schematic map of the initial predictions for Penguin illite ages versus the eventual results. Note that the results are generally older but similar in trend.

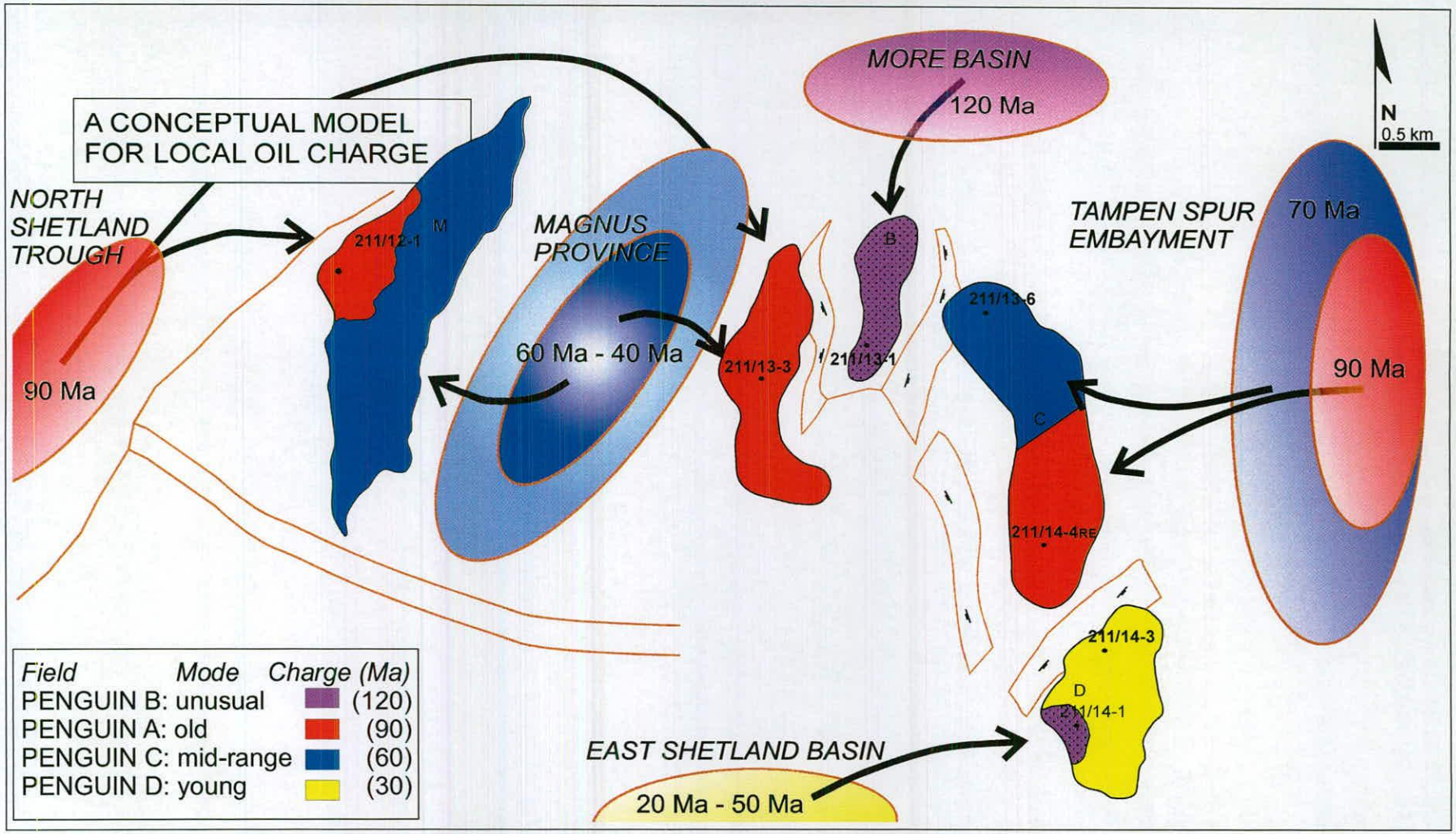

Figure 4.30 A simple model for oil charge from provincial kitchen areas in the vicinity of the Magnus and Penguin fields. This provides the premise for the 2-D basin modelling study that follows in chapter five. The Penguin fibrous illite data is interpreted as indicating charge from five kitchen areas. Active basins associated with charge are shown in shaded hues; associated hydrocarbon accumulations are in monochrome. Timings are thematic.

Oil and water
Modelling basinal fluid flow in the Magnus petroleum system

Oil and water do not mix
nor is it to be doubted that as such a procedure can do no harm, it may possibly be of no contemptible advantage; considering that oil and water are hostile; that oil is a sliding thing....

This chapter presents conceptual and mathematical models of the Magnus oil field and related petroleum system, Northern North Sea, which examine a hypothesis of illite diagenesis and fluid flow formulated as a result of the work discussed in chapter three and chapter four.

Figures

Appendices

5.0 Aims and Objectives

The aim of this chapter is to quantitatively examine the hypothesis that there is a link between the timing of illite diagenesis within East Shetland Basin oil fields and the evolution of fluid flow in the Northern North Sea, with particular respect to hydrocarbon movements. This chapter tests this hypothesis by relating basin modelling simulations of fluid flow systems to fibrous illite K-Ar ages obtained from sandstone reservoirs where oil has accumulated. This aim essentially addresses the principal question: what evidence is there to support the often-proposed linking of late-stage illite diagenesis within oil fields to the filling histories of those hydrocarbon accumulations? Secondly, this chapter also aims to critically consider alternative models e.g. overpressure (Darby et al. 1996, 1997); fault conduit fluid flow, (Clauer et al. 1996) to the favoured model of oil charge, postulated for illite growth within the context of the East Shetland Basin (Glasmann et al. 1989) – Figure 5.1. A tertiary aim of the modelling study is to provoke new hypotheses regarding the puzzling lack of illite ages younger than 15 Ma.

To meet these aims the modelling study must adequately simulate the basic elements of the East Shetland Basin petroleum system. However, the simulated system must be simple enough to allow an investigation of the inter-relationships between the primary attributes of the system. In this respect, the objectives of this chapter are as follows:

- to simplify the East Shetland Basin to a two-dimensional flow system.

- to simulate this system using a basin modelling code which can be calibrated to present day conditions and is suitable for analysing the sensitivity of simulations to geological variables.

- to interpret the results of the modelling in the light of all available data, and with particular regard to illite ages from oil fields represented within the simulation. A modelling study will establish whether or not measured K-Ar illite ages, extracted from East Shetland Basin oil fields, coincide with model ages for simulated hydrocarbon maturation, migration and accumulation from this area of the Northern North Sea.

- to propose further work in light of quantitative modelling of East Shetland Basin type flow systems.

5.1 Petroleum system modelling

It is in the nature of modelling that the natural system represented must be simplified to suit the limitations of the data pertaining to the system, the hardware and software used to run the model simulation, and the aims and objectives of the study. These compromising factors have to be accommodated within a modelling study without eclipsing the need to adequately evaluate the system.

Limitations - turning a cube into a square

Within the context of this thesis, the two main processes under investigation are the later diagenesis and petroleum accumulations of the Northern North Sea - as exemplified by the East Shetland Basin. The geographic and geological complexity of the East Shetland Basin - Figure 5.2, including fault terraces, the potential for variation with regard to oil-field sourcing from local and remote kitchen areas, fill-spill migration, and the timing of trap and seal efficacy, makes an adequate three-dimensional simulation of the East Shetland Basin beyond the limitations of time and software available to this research project. It is therefore necessary to meet the aims and objectives of this study within the limitations of a two-dimensional study.

Hydrodynamic processes

The challenge is how to simplify the observed complexity of the East Shetland Basin paradigm to two dimensions while still encapsulating the essence of the flow systems. Essentially, what is required is a simple two-dimensional section across the East Shetland Basin that follows the hypothesised direction of principal fluid flow. In the simplest scenario, with a buoyancy-driven fluid such as oil, this is in the up-dip direction perpendicular to the strike of the fluid conduit, though this may be modified by hydrodynamic gradients. By adapting this simple concept, local and regional cross sections can be constructed by adapting available seismic sections to represent the structural framework and distribution of rock units for the proposed flow system – Figure 5.3.

Systems, sub-systems and closed systems

The simplest system to model is a "closed" system. In other words, all aspects pertaining to the behaviour of the fluids within the system are accounted for within the boundaries of the system, or by specifying fluxes on the boundaries for attributes such as heat flow. As a result, although no system is truly closed by definition, small sub-systems with constrained boundary conditions can be usefully modelled within large complex natural systems such as the East Shetland Basin.

5.2 Geological data

A further consideration when choosing a suitable case study is the availability of geological data. The study in question requires two detailed data sets:

• the first data set pertains specifically to the petroleum system. Seismic data, well log information and petrographical analysis provide the means to construct the basic structural framework, allocate likely kitchen areas, migration pathways, and trap structures, source rock, migration, reservoir and seal lithologies. The data set also constrains the likely temperature, pressure and burial history.

• the second data set consists of diagenetic information, pertaining specifically to the nature and timing of illite diagenesis within the oil field. This provides an independent data set against which the simulation results can be compared.

Data sources

The primary source of geological data for this research project comes from the CASE partner, Shell UK. This operator has relatively extensive, but far from comprehensive, acreage within the East Shetland Basin – Figure 5.4. The acreage location is an important factor influencing the choice of a case study. However, the Shell UK information is significantly augmented by data released into the public domain. The need for pertinent diagenetic data also limits candidate case studies to areas containing oil fields with extant K-Ar data. A suitable case study must provide K-Ar illite ages and related diagenetic data, as well as a suite of geological data pertaining to the petroleum system. A well-orientated and interpreted seismic profile is required, incorporating essential aspects of the East Shetland Basin petroleum system: source rocks, migration pathways, trap, seal and structural styles.

5.3 Magnus - a suitable candidate

The Magnus oil field is unique within the environs of the East Shetland Basin in that other discoveries of equivalent volumetric magnitude have usually heralded further satellite discoveries. With the exception of a small Magnus-South compartment, the Penguin A structure, and minor shows in nearby wildcats, the Magnus field stands alone. This supports the geologically unusual possibility, within the context of the northern Viking Graben, that the Magnus field is part of a relatively simple, closed petroleum system unlike the potentially large and open system of the Brent Province. The high quality of geological data and parameter characterisation relating to the Magnus area is supplemented by published illite age data for the field. The combination of a simple closed petroleum system, observed and constrained geological parameter values, and a comprehensively investigated diagenetic system makes Magnus an ideal candidate for a modelling study. The study applies basin modelling, and the extrapolation of a calibrated basin model to related petroleum systems within the East Shetland Basin.

Field profile

The Magnus field is named after the patron saint of the Orkney Isles, despite being geographically closer to the Shetland Isles, which lie about 160 km to the south west of the discovery well, 211/12-1. The discovery well, spudded in March 1974, found an unusual play on the most northerly fringe of the East Shetland Basin, (latitude 61° 37' N), which is bounded immediately to the north by a deep Cretaceous trough. Well 211/12-1 encountered a 63 metre column of oil-bearing sandstones approximately 3000 metres sub sea in a water depth of 186 meters. This giant oil field, with a plan area of 33 km^2 and estimated reserves in excess of 500 MMBBL, was highly unusual for the East Shetland Basin, in that it consisted of a suite of Upper Jurassic submarine fan sandstones, dipping gently at about 11° to the east. This is in contrast to the predominant oil-bearing stratigraphies of the East Shetland Basin: middle Jurassic deltaic sandstones and Triassic continental sandstones.

The Magnus Petroleum System

The regional petroleum geology of the Magnus area has been extensively researched and discussed by a number of authors (e.g. Emery et al. 1990; Macaulay et al. 1992; and Shepherd et al. 1990). Despite the superficial differences in the stratigraphic location of the Magnus accumulation relative to other large fields within the East Shetland Basin, the Magnus petroleum system as a whole is remarkably representative of the larger petroleum systems operating in the Brent province of the East Shetland Basin. A simplified representation of the geological setting of the Magnus field is shown in Figure 5.5. This figure illustrates how the essential aspects of large-scale petroleum systems thought to be operating within the East Shetland Basin are manifest at a smaller scale in the Magnus area.

• As with most oil fields within the East Shetland Basin, more than one kitchen area is implicated for the charging history of the field. A shallow kitchen area lies directly down-dip to the east south east of the trap structure. The Magnus Sandstone Member provides a straightforward secondary migration pathway along a carrier bed, which in turn becomes the field reservoir. Immediately up-dip from the field the trap structure terminates at a bounding fault with potential fracture connections to a relatively deep kitchen area in the hanging wall of the normal fault to the north west. This juxtaposition of shallow and deep locations for a single source rock, and potentially multiple kitchen areas for field charge is typical of the East Shetland Basin as a whole.

• Both kitchen areas are characterised by organic-rich mudstones (5%-10% Total Organic Content) of the Kimmeridge Clay Formation, the principal source rock for the whole of the East Shetland Basin.

• The field itself is typical of other East Shetland Basin fields, in that the trap structure occurs as a structural high on the crest of a tilted fault block and shows the regionally common phenomenon of late Jurassic-earliest Cretaceous erosion of that crest, producing a local unconformity over the field.

• The trap structure is laterally and vertically sealed by a combination of late Jurassic and early Cretaceous shales. The seal is overlain by a thick accumulation of Cretaceous, Tertiary and Quaternary shales. A thin Palaeocene tuff occurs as a clear marker horizon close to the K-T boundary in well log 211/12-1 and provides a strong regional reflector in seismic sections for the area. Weak hydrocarbon shows in Palaeocene sands indicate some vertical migration of hydrocarbons through the thick Cretaceous shale sequences.

These essential aspects of the petroleum system for the Magnus area, and for petroleum systems of the Brent Province in general, form the basis for the modelling case study. Published work relating to the regional geology of the Magnus Province, and detailed research on the Magnus Field itself are used to constrain the parameters required for modelling - Appendix 5.1.

One and two dimensional constraints on the Magnus system

The published regional section by Emery et al. (1990) provides the basis for construction of the two dimensional framework for the model - Figure 5.6. The burial history for the Magnus field is constrained by the composite log for well 211/12-1. Figure 5.7 illustrates the general stratigraphy for the Magnus province. The deep and shallow kitchen areas are not directly penetrated by wells and therefore have ambiguous burial histories. This ambiguity is additionally present in the unconstrainable burial, hiatus and erosion episodes implicit in the unconformities logged throughout the well profiles. However, the extensive analysis of the regional geological evolution by the likes of Emery, Shepherd, and Macaulay, coupled with the high quality of interpreted seismic sections (Emery et al. 1990) and detailed log data for wells on these sections, have reasonably constrained the present-day depths. As a result, the probable burial histories for the two kitchen areas can be constructed by projecting pseudo wells onto relevant positions and deducing the inferred stratigraphy.

Illite age data constraints on the Magnus system

Importantly, there is illite age data for the Magnus field provided by two independent studies by Macaulay (1990) and Emery et al. (1993) - Figure 5.8. Note the occurrence of relatively old ages in both populations. The Macaulay age of 83 Ma is derived from a coarse size fraction: 0.1 - 0.5 microns. This 83 Ma age is comparatively at odds with a younger age, 57 Ma, extracted from a finer fraction of sample i.e. clay crystals < 0.1 microns (Macaulay 1990). In the case of Emery et al. (1993) the old age, 88 Ma, occurs alone and was dismissed by Emery *et al.* on the grounds of suspected contamination. The nature of contamination has been briefly addressed in chapter two and is more extensively discussed in chapter five. The important point to note here is that whereas there are comparative grounds for Macaulay to challenge old ages, the Emery data is independent and rejected purely on the basis of the age alone. For the purposes of this case study, the presence of anomalously old illite ages within the general population of ages for the Magnus field is acknowledged.

The general trend for illite ages within the Magnus field, as with other fields in the East Shetland Basin, is a decrease in age down the oil column, with the younger ages occurring closer to the oil-water-contact. The youngest sampled ages occur in the water zone (Macaulay et al. 1992).

5.4 Modelling

Modelling studies per se have been widely applied to geological systems and are firmly established within the suite of analytical tools available to the petroleum geologist. Two predominant styles of regional modelling at the present are static models and basin models. Static models use a cross-section of the geology in question to investigate phenomena such as topographic drive through the subsurface at a particular moment in time (e.g. Garven 1989; Haszledine & McKeown 1995). Static models are suited to environments with a relatively constant structural framework.

Basin modelling codes have been developed to address a wide range of needs associated with geological time-scale basin wide simulations. Factors such as subsidence history, fault dynamics, and heat flow are calculated incrementally in order to forward model multi-phase fluid flow in an evolving geological framework. The co-dependent relationship between porosity, permeability, and fluid pressure, coupled with temperature change, form the basis of simulated water, oil and gas movements within the modelled system.

Magnus case study model - BasinMod® 2-D

The Magnus case study is conducted using BasinMod® 2-D, a basin modelling software package created by Platte River Associates, Inc, Denver, U.S.A (Platte River Associates 1995). A detailed discussion of the software follows below.

Model flexibility and solution space

For BasinMod® 2-D, the output from a model simulation is a unique solution dependent on the specific input values chosen for that run. As the basis for input values is at times uncertain, a suite of simulations for possible input values results in a range of possible solutions: a solution space – Figure 5.9. In practice, reasonable boundaries are set on the input variability in order to calculate the range of output. If the output range is not too great then the solution space defines the behaviour of the model. If the solution space is very large with respect to the cluster of observational data, this would tend to suggest that the model needs modification in order to adequately address the problem at hand (Neelamkavil, 1991). The smaller the error bars on input data, and more precise the algorithms employed, the smaller the solution space the model provides against which to test observed data. In essence, the smaller the solution space, the more likely the observed data will lie partially outside the solution space, implying either the model is inadequately simulating the system, or undisclosed errors are present in the comparative observational data set. A solution space that tightly encompasses comparative observation data provides a model solution that adequately simulates the system with respect to the observed data. Such a solution therefore supports the conceptual model underlying the code, but only to as high a degree of certainty as is present in the observed data set input and its range of uncertainty.

Model sensitivity

The importance of addressing the subject of model solution spaces is apparent when considering the sensitivity of models to specific variables. Depending on the algorithms employed within the code and the often commercially highly sensitive and confidential nature of algorithm execution, model solutions will be more sensitive to alterations for some variables with respect to others. As Darby (1995) demonstrates, the sensitivity of a model to parameter variation is determinable - Figure 5.10. The behaviour of a model with respect to input parameter variation, particularly with regard to uncalibrated and loosely calibrated data, is essential. This behaviour needs to be established in order to gain an understanding of how robust a given solution space is to such variations. This is certainly

the case at present, as the discipline of data collation is only just beginning to modify itself to the needs of petroleum system modelling. Hence even a geologically intensely investigated system such as the Northern North Sea is relatively poorly constrained when considering the sensitivity of model behaviour to specific parameters.

Model calibration and validation - oil and illite

The number of variables that are typically unconstrained or poorly constrained within petroleum systems and the complexity of the relationships governing model solutions when varying more than one variable simultaneously requires the modeller to prioritise calibration with respect to the nature of the study in question. The hypothesis underlying this case study is that fibrous illite diagenesis occurs at the time of oil accumulation in trap structures. With regard to this, the principal variables of interest pertain to the timing of maturation, charging and accumulation of hydrocarbons within the model. The primary aim of the modelling study is to calibrate the modelled petroleum system to the observed oil accumulation, vitrinite reflectance and hypothesised timing of oil generation. An additional aim is to calibrate the model to the hypothesised onset of oil accumulation as implied by illite ages for the Magnus field.

Pragmatic modelling - calibration

Basin modelling codes are primarily designed to simulate generic petroleum systems. The specific attributes of any case study and limitations related to the constraining data are likely to result in a degree of mismatch between the model solution and the conceptual expectation for the study as based on observed data. A model based on an oil field case study should as a first approximation show significant oil accumulation at the present day i.e. replicate the occurrence of the oil field. This simple calibration to an observed phenomenon is the foundation for a pragmatic resolution between the simulated system and the empirically constrained natural system. If all reasonable scenarios fail to adequately simulate the principal observations regarding the timing, location, temperature and pressure of the accumulation, the fundamental differences between the simulation and the observation should then be addressed with regard to model behaviour and possible shortfalls in the understanding of the natural system.

Illite ages and models - validation

Illite ages provide the principal comparative data set for this study. The experimental error bar on the absolute ages of the illite samples tends to be small relative to the geological time separation between significant events in the fluid flow dynamics of the basin as the petroleum system evolves through time. As a result illite diagenesis is potentially a useful validation parameter if the implicit assumptions relating oil accumulation to illite diagenesis are accepted. A number of studies have attempted to apply illite diagenesis to basin models. A brief review of the issues arising from previous studies follows below.

Illite age-validated basin modelling

Given the conjecture surrounding illite diagenesis, and the significance, if any, of the ages attributed to illite K-Ar ratios, it is reasonable to question the efficacy of using illite ages to validate events simulated by basin models. In recent years the shift in emphasis regarding the cause of illite diagenesis has been away from closed systems and prolonged equilibrium diagenetic alteration of clastic reservoirs (Harrison & Tempel 1993; Bjorlykke et al. 1992; Giles & Boer 1989). Open system, event-driven diagenesis in response to perturbations in the pore water fluid flow system is now the favoured explanation (Darby et al. 1997; Hogg et al. 1993; Haszeldine et al. 1992; Small 1992). The details of these publications are discussed at length at the beginning of chapter three. Furthermore, basin modelling studies integrating illite ages and quantitative studies relating oil emplacement with diagenesis have been published widely in the literature (e.g. Darby et al. 1995; Swarbrick 1994; Saigal et al. 1992). This basin modelling study investigates a fluid flow regime in a petroleum system where event-related diagenesis is thought to have occurred. The intention is not to 'fit' the modelled case study to a suite of illite ages and erroneously claim that one supports the other. The aim of this chapter is to challenge a commonly held hypothesis regarding illite diagenesis by testing the assumption that a basin model calibrated to illite age dates is feasible with regard to the timing of oil accumulation.

A principal criticism - experimental and geological error

A principal criticism concerning the use of illite ages as absolute values in modelling studies is the potential for error in the age itself. As discussed at length in chapter three, the two compound errors relating to illite ages are experimental and geological contamination. The former tends to be small enough not to be a significant factor when dealing with the levels of uncertainty of modelling results. The latter is a highly significant factor as contamination at the boundary of detection levels (5% feldspar) is high enough to alter the illite age beyond the resolution of the modelling results for event timings. However, if reasonable measures are taken to prevent and screen illite samples for contamination, as is evident in the two independent sources of illite data for this case study (Macaulay et al. 1991 and Emery et al 1993), correlation between simulated events and illite ages would prove significant.

Summary

Though neither the modelling of petroleum systems nor the phenomenon of fluid flow driven illite diagenesis are proven beyond doubt, the current interest in the relationship between these two distinct methods suggests that a basin modelling study specifically focused on illite diagenesis is apt and timely. This modelling case study performs simple simulations of the general petroleum system pertaining to the Magnus province. These simple models test the hypothesis that the timing of illite diagenesis is coincident with the significant changes in the petroleum system.

5.5 BasinMod® 2-D

It is worth considering the code used: BasinMod® 2-D Version 2.03. First developed in 1988 by Platte River Associates, BasinMod is a software tool specifically designed to dynamically model geological processes (Platte River Associates, 1995). Over the last decade BasinMod® has evolved in competition with other similar basin modelling codes to examine many of the complex non-linear processes associated with basin evolution.

A suitable code

BasinMod® 2-D is ideally suited to the investigation of a small-scale petroleum system that is adequately constrained within a two-dimensional cross section with respect to kitchen, migration pathway, trap structure and seal history. The Magnus case study was carefully chosen to meet the requirements of this style of modelling. However, the hypothesis under examination is whether or not model simulations reasonably indicate the timing of significant shifts in the basin evolution to the age of illite diagenesis in the oil field. To address this question it is important to consider the nascent methodology underlying the model architecture.

Methodology

The model simulates the motion of hydrocarbon phases, in addition to pore water flow, on the basis of source rock maturation in response to temperature change. However, the model relies primarily on the burial history of the section to calculate the porosity evolution and resultant pressure differentials and fluid movement within the section:

> *'The entire process is controlled by the reduction in pore space as a result of compaction; this pore space reduction is most affected by pressure.' (Platte River Associates, 1995)*

The independent variables, porosity and permeability, fundamentally control the evolution of the model simulation, and yet are poorly constrained for the shale-dominated stratigraphy of a basin (Oreskes et al. 1994). Even models that are calibrated with detailed present-day data are incapable of testing prediction and retrodiction scenarios with high levels of confidence as a result of this uncertainty in the input data. However, the dependent variables of kitchen maturation and trap accumulation are potentially calibrated by present-day observations and, are hypothetically constrained by the Magnus illite ages. Additionally, the Pressure-Volume-Temperature paradigm is intimately dependent on the porosity-permeability evolution of the modelled stratigraphy. Hence, the dependent variables related to hydrocarbon generation and accumulation can be indirectly constrained by model calibration to temperature, pressure and burial history, and are potentially validated by correlation with illite ages. If the simulation is empirically adequate with respect to independent variables and matches the timing of field charge to the illite ages the principal hypothesis stands. If the correlation requires values for independent variables that are not empirically reasonable and fail to match the calibration data, then the illite hypothesis is refuted.

Calculation method

The underlying conceptualisation of the model is evident in the calculation method use to simulate the system. Figure 5.11 illustrates the complex relationships and feedback between the different physical processes that make up the model. BasinMod 2-D consists of four integrated calculations: three iterative loops concerning compaction, temperature and fluid flow and a linear calculation concerning hydrocarbon maturation. All calculations are simultaneously resolved for each cell within the cell matrix for a single time-step in the model history. The role of each calculation is described below.

- the principal calculation loop simulates changes in porosity and permeability with time as the result of exponential compaction using a Sclater and Christie algorithm (Platte River Associates, 1995).

- the secondary calculation loop uses the resulting porosity to calculate heat flow and temperature.

- a third calculation loop combines the incremental changes in compaction and temperature to simulate Darcian fluid flow and estimate abnormal pressure.

- changes in the temperature are also used to calculate the time-temperature maturity evolution of source rocks in the model. This calculation, although only temperature dependent, modifies the next iterative loop regarding generation pressure, the addition of new hydrocarbon phases into the fluid system, and resultant hydrocarbon migration and accumulation.

These calculations for compaction, temperature and source rock maturation are resolved for all cells in the model grid for each time-step of the burial history, simulating the pressure differentials and flow of all fluid phases present at the start of the time step.

Parameters

In order to perform the above process, BasinMod® 2-D requires a suite of parameters. As table 5.1 illustrates, there are a number of such variables, each with either a range of settings or default values that have adjustable ranges depending on the requirements of the study in question. Where variables are poorly constrained with respect to the Magnus case study, values applicable to the general geological setting were chosen. These parameters form the basis for the first set of simulations.

Extrapolation

Assuming the quality of the input data and adequacy of the equations used to simulate the system, the conceptual model is the critique for the nature and timing of late diagenesis in Jurassic sandstone reservoirs of the Northern North Sea oil fields. Therefore, the model behaviour can only be used to evaluate the timing of significant accumulation with respect to the probable timing of illite diagenesis if the simulation is understood in the context of the underlying conceptual framework. It is on this basis that the model may be used to direct further research and predict the timing of late diagenesis in neighbouring oil fields subject to similar petroleum systems.

DEFAULT CALCULATION OPTIONS
Migration: Steady State
Expulsion: Saturation
Permeability: Power Law
Bottom Boundary: Closed

DEFAULT THERMAL PARAMETERS
Basement Heat Flow
Hydrocarbon mix
Present Day Surface Temp: 20 degC
Present Day Heat Flow: 64 mWm^-2

CALIBRATION CALCULATION OPTIONS
Migration: Transient
Expulsion: Pressure
Permeability: Modified Kozeny-Carman
Bottom Boundary: Closed

CALIBRATION THERMAL PARAMETERS
Transient Heat Flow
Hydrocarbon mix
Present Day Surface Temp: 5 degC
Present Day Heat Flow: 45 mWm^-2

DEFAULT PARAMETER VALUES

Lithology	iP (frac'n)	MD (g/cm^3)	K-C GS (mm)	QGS (mm)	QF (frac'n)	CCFoQ (fraction)	MTC (W/m*C)	MHC (kJ/m^3*C)	MTCA (ratio)	PRF (factor)	iVP (md)	KRF (factor)	IWS (frac'n)	FGF (factor)	PA (ratio)
Sandstone	0.45	2.64	0.5	0.5	0.9	0	4.4	2800	1	0.000175	30000	7	0.2	0.2	0.4
Siltstone	0.55	2.64	0.0156	0.005	0.5	0	2	2650	1	0.00023	100	6	0.4	0.3	0.2
Shale	0.6	2.6	0.0004	0.0001	0.25	0	1.5	2100	1	0.0003	10	6	0.4	0.8	0.2

CALIBRATION PARAMETER VALUES

Lithology	iP	MD	K-C GS	QGS	QF	CCFoQ	MTC	MHC	MTCA	PRF	iVP	KRF	IWS	FGF	PA
Sandstone	0.47	2.64	0.40312	0.41	0.82	0	3.758	2770	1	0.0004	9587	4.8	0.24	0.22	0.34822
Siltstone	0.55	2.64	0.0156	0.005	0.5	0	2	2650	1	0.00023	100	6	0.4	0.3	0.2
Shale	0.6	2.6	0.0004	0.0001	0.25	0	1.5	2100	1	0.00195	10	6	0.4	0.8	0.2

DIFFERENCE

Lithology	iP	MD	K-C GS	QGS	QF	CCFoQ	MTC	MHC	MTCA	PRF	iVP	KRF	IWS	FGF	PA
Sandstone	-0.02	0	0.09688	0.09	0.08	0	0.642	30	0	-0.000225	20413	2.2	-0.04	-0.02	0.05178
Siltstone	0	0	0	0	0	0	0	0	0	0	0	0	0	0	0
Shale	0	0	0	0	0	0	0	0	0	-0.00165	0	0	0	0	0

Key: iP - Initial Porosity, MD - Matrix Density, K-C GS - Koz-Car Grain Size, QGS - Quartz Grain Size, QF - Quartz Fraction, PA - Permeability Anisotropy, CCFoQ - Clay Coat Fraction on Quartz, MTC - Matrix Thermal Conductivity, MHC - Matrix Heat Capacity, MTCA - Matrix Thermal Conductivity Anisotropy, PRF - Porosity Reduction Factor, iVP - Initial Vertical Permeability, KRF - Permeability Reduction Factor, IWS - Initial Water Saturation, FG - Fracture Gradient

Table 5.1 A comparison of parameter values and options for both the default and calibration models.

5.6 Magnus Model

The model geometry is necessarily simplistic and the termination depth at the basal boundary shallow in order to keep calculation-run times short. However, the essential aspects of the petroleum system are all present in the two-dimensional model section. The modelled section is deliberately chosen to be perpendicular to the strike of the Magnus structure and regional grain in order to reduce the effect of fluid flow in the third spatial dimension, which is excluded by definition from the two-dimensional modelling software- Figure 5.12.

Wells on section

The model section is pinned by wells 211/12-1, 211/12-2, 211/13-3, 211/13-1 and 211/13-6. Well 210/10-1 is an assumed approximation of the stratigraphy and burial history for the deep Magnus Embayment – Appendix 5.1. The high-resolution stratigraphic data from the composite logs constrains the burial history over the structural highs and of the Magnus area. The occurrence of unconformities and the implicated but unconstrainable episodes of burial, hiatus and erosion compromise the accuracy of the burial history. The well logs, in conjunction with the interpreted seismic sections, allow for lateral extrapolation of the burial history into the two kitchen areas where no well data is available. Composite logs for the section wells are also used to constrain basic parameters such as lithology type, temperature and pressure conditions for the present-day reservoir, and allow for stratigraphic ties with the simplified model section.

Temporal and spatial division of the model

The model divides the section into cells, which make up rows and columns. Each cell contains a calculation node, with all the nodes defining the calculation grid for the section. BasinMod® 2-D is a finite difference model; the node calculation is located at the centre of each cell. The grid density varies throughout the section in response to a BasinMod® 2-D gridding algorithm, which gives a low-density grid in large uniform areas and a high grid density in areas of structural complexity, such as faults and unconformities. Grid density also varies stratigraphically to diminish the effect of mathematical grid artefacts during simulation. Model calculation times occur at the top and base of each stratigraphic unit, as well as at allocated time divisions within each unit. The spacing of such calculations is designed to focus calculation density on episodes of rapid change in burial history. This allows the operator to modify the complexity in response to hardware limitations and the precision required of the model simulation.

Scale and boundary conditions

The spatial scale for the model section is approximately 10 km deep x 100 km long. The temporal scale of the model is from the Recent to the early Mesozoic to allow simulation of present day conditions and fluid flow evolution simulation up to and immediately prior to the onset of the expected hydrocarbon movement. The spatial and temporal scales of the model are chosen to

encompass the geological system in question, while the placing the area and time of investigation - oil accumulation in the Magnus field - at the centre of the model away from boundary effects. Boundary conditions for the model are constrained at the base and top as closed and open respectively, with the exception of heat flux, which is an input variable for the base of the model, set to a value suitable for the East Shetland Basin. The lateral boundary conditions are closed to represent the closed nature of the system. These left and right boundary conditions are supported by the natural geometry of the system: lateral thinning of permeable Jurassic horizons in the deep half graben to the north west; and the closure of the Magnus petroleum province against the Penguin horst buttress to the south east – Figure 5.6.

5.7 Simulation series

The model section for the pilot study simulation is based on the regional seismic section for the Magnus Province, published by Emery et al. (1993), and a local well-tied section for the Penguin horst area produced by Shell UK (1995). Significant features comprising the system are the shallow and deep kitchen areas, the trap structure at the pivotal end of a rotated fault block, and the erosional unconformity capping the trap structure.

The system is modelled with a closed boundary to the left in accordance with the seismic section interpretation of syn-sedimentary lateral pinchout of permeable horizons to the northwest. The system is modelled as closed to the right, in accordance with data from Shell UK pertaining to the nature of the structural termination of the Magnus province against the Penguin block to the southeast.

The model reservoir unit was designated as being 'a good quality' reservoir sandstone to reflect the clean, massive Magnus Sandstone Member turbidite sandstones. Other modelled stratigraphic units in the Jurassic and Triassic were designated as being siltstones with the exception of the upper Jurassic mudstone source rocks. The two kitchen areas were designated as mudstones having a high Total Organic Content, at 9% , in order to represent the likely upper limit of organic content in the rich Kimmeridge Clay Formation mudstones thought to be the principal source rock in the region. The extensive presence of thick sequences of such a source rock is assumed given the unusual size and proximity and fields producing a relatively homogeneous crude oil in the East Shetland Basin. The thick Cretaceous-Tertiary-Quaternary sequences overlying the syn-rift and pre-rift lithologies of the Mesozoic were modelled as homogeneous shales in deference to the monotonous shale sequences logged for well 211/12-1.

The measurement locations within the model are standardised at selected nodes on the mesh to allow for comparison between separate simulation runs. The co-ordinates of the measurement locations, tabulated below, are relative to (0,0) - the upper left hand corner of the model section - Table 5.2.

Setting	*Location X,Z (m.)*	*Stratigraphy*	*Age*
Seal	5000, 2870	Barremian shale	124-141 Ma
Reservoir	5000, 2920	MSM sandstone	146-155 Ma
Reservoir datum	6500, 3050	MSM sandstone	146-155 Ma
Crest kitchen	5000, 3000	KCF2 shale (II 9%)	155-157 Ma
Shallow kitchen	14000, 4200	KCF1 shale (II 9%)	146-152 Ma
Deep kitchen	2500, 5400	KCF2 shale (II 9%)	155-157 Ma

Table 5.2 Measurement locations for the simulation series.

Simulation series one: pilot study

The first set of simulations is a simple attempt to model the system with default values for the poorly constrained variables. The aim is to assess the suitability of default parameter values as present in BasinMod® 2-D for the simulated Magnus system. Simulation series one results in minor adjustments to the model input. These adjustments are documented below in the order in which they occurred.

Grid density

The default model grid calculation has a low grid density of 7,832 unevenly distributed cells – Figure 5.13. This is an artefact of generic input settings. As a case-study specific model requires an effective grid density to ensure a stable simulation, the cell division options need to be changed to ensure the cell width is less than the stipulated maximum of 250 meters (Platte River Associates, 1995). This was achieved by increasing the *number of lateral cells* from 10 to 100. Additionally, in order to increase the cell density associated with sections of detailed stratigraphy, the cell *time interval* separation- the temporal cell division factor - is changed from 5 My to 20 My, and special time steps added – Figure 5.14. The latter modification is discretional and is used to maximise the model resolution at critical stratigraphic intervals. These alterations result in a more evenly distributed grid with more than twice the number of cells at 18,880. This marginally increases the run time of the model but is a prerequisite to stable model simulations.

Tuff adjustment

The default parameters – zero porosity and zero permeability for a BasinMod® 2-D modelled 'tuff' - effectively result in a basin-wide seal as soon as the tuff is deposited. This causes the simulation to become swamped with expelled gas from about 60 Ma onwards. Not only is this not observed in the field, it is highly unlikely with regard to the geology. Regionally widespread tuffaceous horizons in the North Sea, such as the Balder Tuff, are commonly perceived as highly weathered and friable units with porosity and permeability characteristics similar to a shale. As a result, in this model, the rock properties of the tuff were modified so that the event is simulated as having shale characteristics. Having highlighted this unexpected anomaly, the pilot study subsequently ceases to be gas prone in response to the modified tuff deposition.

Paleobathymetry

The model requires a paleobathymetry input to account for accommodation space during the post-rift Quaternary-Tertiary-Cretaceous events. An empirical value for regional paleobathymetric evolution is unobtainable due to the complexities of tectonic, eustatic and sedimentary interaction during the post-rift thermal sag phase of basin evolution. However, the apparent lateral variations in stratigraphic thickness and fault locations allow a reasonable estimation to be made. The simplest bathymetry that accounts for the two-dimensional variation in the thickness of these events was taken to be the present-day profile of the horizons reduced to an assumed minimum sea depth of 100 meters – Figure 5.15.

Migration

The setting for migration calculations is changed from *steady state* to *transient*. The *steady state* simulation is only an approximation and less able to resolve a model such as the Magnus model, which has rapid event changes e.g. the Quaternary-Tertiary-Cretaceous burial history and late Jurassic inversion (pers.comm. Platte River Associates, 2000). The *transient* option is more suited to the Magnus model.

Expulsion

The *pressure* option is chosen in favour of the *saturation* option as the *pressure* option calculates the timing of expulsion as a function of the generation pressure. The *saturation* method is dependent on an arbitrarily set threshold.

Permeability

BasinMod® 2-D provides two options: a *Power Law* calculation, using the Lerche method (Platte River Associates, 1998) to approximate the widely observed logarithmic relationship between porosity and permeability, dependent on the void ratio. The second option is the *Modified Kozeny-Carman* relationship. This slightly more sophisticated approximation is dependent on the lithology grain size and specific surface area. The *Modified Kozeny-Carman* option is selected as it is more effective at modelling tightly compacted rocks such as the shale units which dominate the Magnus burial history throughout the expected evolution of the hydrocarbon system.

The pilot study, simulation series one, results in a model that simulates the generation of hydrocarbon phases in a two-dimensional approximation of the Magnus system. However, the resultant accumulation history for the Magnus structure and generation timing of the shallow kitchen area differ from the observed and expected timing for the system – Figure 5.16. Additionally, the model output differs considerably from the observed present day porosity and permeability of the reservoir sandstone, as well as the observed temperature, pressure, and maturity for the oil field – Table 5.3, Figure 5.16. As a result, the pilot study as a first investigation, effectively establishes the basic premise for further modelling work. However, the pilot study fails to meet the criteria necessary to address the aims of this chapter, and so is unacceptable as a model solution to the Magnus system.

Observed/Expected data	*Pilot study output*	*Compliance*
Reservoir oil saturated at present day	Reservoir: gas saturated	No
Reservoir temperature: 240°F	Temperature: high @	No
Reservoir pressure: 6550 psi	Pressure: low @	No
Reservoir maturity, Ro: 0.7%	Maturity: high @	No
Reservoir poro-perm: 15%, 100 mD	Poro-perm: high @	No
Shallow kitchen generation at 70 Ma.	Generation: much earlier @	No

Table 5.3 Pilot study output versus observed- expected data for the Magnus field

Simulation series two: calibration

Simulation series two attempts to meet the aims of this chapter by calibrating the model output of the pilot study to the above measurements – Table 5.2. It is important to note that, although the present-day occurrence of a saturated reservoir within the Magnus structure is in itself a form of qualitative calibration, the accurate simulation of generation timing and accumulation history for the Magnus structure is not a contrived result. The simulation is entirely dependent on the quantitative calibration of the model to present day data reported from the Magnus oil field. It is the calibration of the model to this data that follows. The associated timing of oil generation and accumulation is dependent and arbitrary. The applied data set is tabulated below - Table 5.4.

Overpressure (Tertiary shale)	Unquantified (high)	900-1600 m.
Overpressure (Cretaceous shale)	Unquantified (high)	2800 m.
Pressure (reservoir datum)	6653 psi	3050 m.

Geothermal gradient	6.7°F/100 m.
Temperature (reservoir datum)	240°F @ 3050 m
Vitrinite reflectance	Ro 0.7 Kerogen type II max

Reservoir porosity	~ 10%-20%
Reservoir permeability	~82 md – 0.08 md

Table 5.4 Calibration data for the Magnus oilfield (After Shepherd et al. 1990)

Sandstone porosity and permeability calibration

The default model values for sandstone porosity and permeability are simulated as about 25% and 1000 mD respectively – Figure 5.17. These values are too high to meet the calibration constraints of 10-20% and 80 mD – Table 5.4.

The simulated porosity and permeability are respond to changes in the porosity reduction factor (PRF) and permeability reduction factor (KRF), used in BasinMod® 2-D – Figure 5.17. The default settings for all parameters relating to the model sandstone are also automatically adjusted in response to changes in the lithology mix. For example, with a default mix for the model sandstone of 100% sandstone, the *quartz fraction* parameter value is set at 90%. The Magnus sandstone, however, is observed as having a significant clay fraction. An adjustment in the lithology mix to a more geologically reasonable 80:20 sandstone:shale ratio causes the *quartz fraction* value to automatically adjust to 82% - Table 5.1.

An adjustment of the PRF value from 0.000175 to 0.0004, and KRF value from 7.0 to 4.8 results in a calibrated simulation – Figure 5.17. A further adjustment of the sandstone to an 80:20 sandstone:shale mix does not noticeably affect the calibrated porosity and permeability. However, note that the hydrocarbon accumulation history alters significantly in response to this adjustment, displaying a small accumulation at about 90 Ma, prior to the principal phase of saturation from 60 to 40 Ma – Figure 5.18.

Temperature and Vitrinite Reflectance calibration

The default heat flow and surface temperature settings for the model are too high, as indicated by simulated reservoir temperature and vitrinite reflectance values of 360°F, and 1.5% Ro respectively - Figure 5.19. A simple reduction in heat flow and surface temperature settings results in a calibrated model, - Figures 5.19, 5.20, and 5.21.

The *constant* heat flow for this calibrated model is geologically unreasonable, however, as the northern North Sea underwent significant extension during the late Jurassic to early Cretaceous. The simplest, geologically reasonable scenario is a *transient* heat flow model – Figure 5.22. The transient model hypothesis increases in heat flow during the late Jurassic to early Cretaceous extensional phase, approximately 160 –130 Ma, and then decreases throughout the late Cainozoic to the present day during the thermal sag phase of the basin history, as indicated by the thick accumulation of shale. A simple approximation of this scenario is the 'smooth spike' heat flow model – Figures 5.22 and 5.23. This 'smooth spike' model is poorly constrained with regard to the magnitude and timing of the maximum heat flow and the following rate of decline during the late Cainozoic. As a consequence, a suite of 'spiked' heat flow models were employed – Table 5.5. These speculative heat flow scenarios all resulted in calibrated simulations – Figures 5.25 to 5.31.

A comparison of the hydrocarbon behaviour for the constant heat flow model and the transient heat flow model highlights the distinct accumulation histories for the Magnus trap structure as a result of the change in heat flow input – Figures 5.24 and 5.25. The sensitivity of the calibrated Magnus model to variation in heat flow is discussed below in section 5.73.

HEAT FLOW TABLES

Default

Age (My)	HF (mWm^-2)
0	64
240	64

Calibration, constant

Age (My)	HF (mWm^-2)
0	46
240	46

Calibration, simple spike

Age (My)	HF (mWm^-2)
0	46
90	51
130	63.5
145	65
150	64
170	48
240	46

Smooth spike, medium (sms)

Age (My)	Heat flow (mWm^-2)
0	46
22	47
58	48.5
68	49
90	51
96	52
106	54.5
116	58
124	61.5
130	63.5
136	64.5
145	65
148	64.75
150	64
152	62
154	59
156	56
160	52
166	49
170	48
184	46.5
194	46.25
240	46

Higher Triassic heat flow (56), sms

Age (My)	Heat flow (mWm^-2)
0	46
22	47
58	48.5
68	49
90	51
96	52
106	54.5
116	58
124	61.5
130	63.5
136	64.5
145	65
148	64.9
150	64.5
152	63.6
154	62.2
156	60.7
160	58.8
166	57.4
170	56.9
184	56.2
194	56.1
240	56

Higher peak (80), sms

Age (My)	Heat flow (mWm^-2)
0	46
22	47
58	48.5
68	49
90	51
96	52
106	54.5
116	58
124	61.5
130	63.5
136	68.5
138	71
140	74
145	80
146	79.5
148	69
150	64
152	62
154	59
156	56
160	52
166	49
170	48
184	46.5
194	46.25
240	46

Table 5.5a Heat flow values for calibrated Magnus models and the related sensitivity analysis.

HEAT FLOW TABLES continued

Smooth spike, low

Age (My)	HF, low (mWm^-2)
0	46
30	46.25
56	46.25
70	46.5
80	47
90	48
100	50
112	54.5
116	56.5
130	63.5
136	64.5
145	65
148	64.75
150	64
152	62
154	59
156	56
160	52
166	49
170	48
184	46.5
194	46.25
240	46

Smooth spike, high

Age (My)	Heat flow (mWm^-2)
0	46
12	47
18	47.5
30	48.5
72	52
90	54
102	56
114	59
124	62
130	63.5
136	64.5
145	65
148	64.75
150	64
152	62
154	59
156	56
160	52
166	49
170	48
184	46.5
194	46.25
240	46

Alternative heat flow scenario

Age (My)	Heat flow (mWm^-2)
0	45
10	46
20	46
30	47
40	48
50	48
60	48
70	49
80	50
90	55
100	56
110	59
120	60
130	61
140	63
150	64
160	64
170	65
190	44
200	44
240	44

Alternative heat flow II

Age (My)	Heat flow (mWm^-2)
0	45
10	46
20	46
30	47
40	48
50	48
60	48
70	49
80	50
90	55
100	56
110	59
120	60
130	61
140	63
150	64
160	64
170	65
190	45
200	45
240	45

Table 5.5b Heat flow values for calibrated Magnus models and the related sensitivity analysis.

Pressure calibration

The default Magnus model pressure is low at 5911 psi – Figure 5.32. The simulated reservoir pressure is most sensitive to changes in the shale porosity reduction factor (PRF), as this directly affects the shale permeability and the related fluid flow in the simulated reservoir sandstone. There is considerable flexibility in the PRF input, as shale permeability is a poorly constrained parameter.

> *The relations [between porosity and permeability] are clearly complex and mathematically little understood.....Kozeny's equation is not truly quantitative and has no more than a general application to natural rock reservoirs.*
> (F.K. North 1990)

By general convention, the following permeability values are accepted for sedimentary rocks typically associated with hydrocarbon systems – see Table 5.6.

Qualitative description	*k-value (mD)*
Seal	10^{-4}- 0
Tight gas sand	0.1-0.001
Poor to fair reservoir sandstone	<1.0-15
Moderate reservoir sandstone	15-50
Good reservoir sandstone	50-250
Very good reservoir sandstone	250-1000
Excellent reservoir sandstone	>1000

Table 5.6 Permeability values for sedimentary rocks (after F.K. North, 1990).

With respect to shales, commonly accepted permeability values for compacted shale seals vary by orders of magnitude. Ranges from about 10^{-4} mD to 10^{-8} mD are quite common (F.K. North 1990). This uncertainty in the precise permeability of lithologies is of specific concern with regard to modelling shale units. Shale tends to dominate the burial history of North Sea petroleum systems and is the principal seal for the Magnus system. The pragmatic solution to this quandary is to adjust the shale PRF to a quantifiable and calibrated factor, which is sensitive to permeability, i.e. reservoir pressure. As long as the permeability value required for pressure calibration exists within accepted norms for the system then the calibration is deemed to be adequate.

The principal effect of a shale PRF alteration from the default value (0.0003), to the calibration value (0.0195), is a drop in the shale porosity and permeability - Figure 5.32. The simulated shale permeability value immediately overlying the sandstone - effectively the 'seal'- falls by over two orders of magnitude, with the porosity decreasing to 25% of the default value. The associated shift for parameters in the simulated sandstone record a significant alteration in porosity, permeability, temperature and vitrinite reflectance, as well as the desired shift in simulated pressure to

approximately 6650 psi. To summarise, a change in the shale PRF value from 0.0003 to 0.0195 results in a pressure-temperature-Ro calibrated simulation with suitable reservoir porosity and permeability matches for the present-day oil field – refer to Table 5.4. Additionally, note the significant change in the behaviour of the modelled hydrocarbon system with respect to both the shallow and deep kitchen areas and the Magnus accumulation history.

Calibration summary

The Magnus model is now calibrated with respect to the measured reservoir porosity, permeability, pressure, temperature and vitrinite reflectance. A comparison of the measured calibration data to the chosen calibration range and acceptable simulation output is shown in Figure 5.32b. The required alterations to input parameters and settings are summarised in Table 5.1. The resultant output for a calibrated simulation with respect to both the calibration parameters and the behaviour of the hydrocarbon system are shown in Figures 5.33 and 5.34.

Note that, although the model is calibrated to data for present day conditions from the Magnus oil field, the output also matches the following:

• the recorded bimodal overpressure in the Tertiary and Cretaceous section.

• the widely accepted timing of 70 Ma for the onset of oil migration from the shallow kitchen area.

• the K-Ar ages for diagenetic illite from the Magnus oil field, with respect to oil accumulation in the trap structure. Significantly, this correlation includes the oldest age in the data suite, supporting the view that this data point is a valid illite age, and not a contamination artefact of the destructive analytical procedure.

• a significant decrease in the shallow generation rate at about 40 Ma to 30 Ma, coincident with the youngest K-Ar ages for illite from the Magnus oil field.

The calibrated model also indicates that a deep kitchen area immediately to the northwest of the Magnus oil field may cause an early phase of oil to migrate through the Magnus structure at about 90 Ma. This would befit a deep Kimmeridge Clay Formation kitchen area in the Magnus Embayment, directly up-dip of the Magnus boundary fault, playing a significant role in the early history of the local petroleum system. It is worth noting that the justification for the depth and resultant generation timing of the proposed deep kitchen area is dependent on two points:

• the published sections for deep geometry and seismic reflectors in the area northwest of Magnus.

• the assumed occurrence of the regionally common KCF source rock.

Hence, the match between the simulated generation age in a deep kitchen area and the oldest illite ages is coincidental, rather than contrived, and as such supports the original hypothesis that illite ages and oil migration are intimately related. If the model proves to be robust with respect to sensitivity analysis, then this match provides a validation of the experimental technique and modelling approach.

The above simulation is not a unique solution to the Magnus model. The calibration ranges employed allow for a number of calibrated simulations that differ from each other, as already mentioned with regard to the heat flow input. The response of the model to input variation resulting in calibrated simulations is discussed below in the section on sensitivity analysis.

Simulation series three: sensitivity

The model is highly sensitive to the two principal aspects of the system that are poorly constrained i.e. permeability evolution, and the thermal evolution. With reasonable upper and lower limits set for the error bars on the dependant variables related to permeability, heat flow and surface temperature, it is possible to investigate the behaviour of the model within these limits.

Pressure sensitivity

The modelled reservoir pressure is highly sensitive to changes in the shale permeability. The shale permeability for the calibrated model is derived from a porosity reduction factor (PRF) of 0.00195. Changes in the PRF value establish the sensitivity of the model with respect to both the shale permeability and the reservoir pressure as well as the other associated calibration parameters. The sensitivity to changes in the shale PRF is also examined with regard to significant changes in the style and timing of hydrocarbon generation, expulsion and accumulation.

The reservoir datum pressure is empirically constrained as 6650 psi (X, Z location: 6500 m, 3050 m - *reservoir*). Allowing for a 5% error in this data point, the model is subjected to a sensitivity analysis with respect to the PRF over the pressure range 6325 psi – 6975 psi. PRF values ranging from 0.0015 to 0.0025, equivalent to 77% -128% of the *simulation series two* value, result in acceptable models with respect to all calibration data – Figure 5.35. The effect on shale permeability for this calibration range spans almost two orders of magnitude – Figure 5.36.

With regard to the hydrocarbon system, the modelled generation-expulsion behaviour appears little different for values within the PRF calibration range. However, the simulated accumulation of oil and gas in the Magnus trap structure is highly sensitive to this variation – Figure 5.37 and 5.38. In summary, the modelled kitchen behaviour is robust, whereas the accumulation behaviour is unstable.

Thermal sensitivity – heat flow scenarios

The thermal history of the model is constrained by the present day reservoir temperature and vitrinite reflectance. The respective ranges are:

- Reservoir temperature: 116°C +/- 6°C
- Vitrinite reflectance: 0.7% +/- 0.5%

The sensitivity of these parameters and the hydrocarbon system to variation in the heat flow input and surface temperature history is assessed below. The model is subjected to slight variations in the heat flow – Figure 5.23. These heat flow scenarios all result in calibrated models – Figures 5.24 to 5.31. The resultant hydrocarbon generation and expulsion for the deep kitchen area appear fairly robust to such changes – Figures 5.39 and 5.40. The shallow kitchen area generation and expulsion is slightly less robust – Figures 5.41 and 5.42. In contrast, the accumulation history for the Magnus trap structure is highly sensitive to variations in heat flow that result in calibrated simulations – Figure 5.43. The three accumulation modes are summarised below.

• an early, small accumulation – about 20% saturation – at about 88 My. This occurs in response to models where the heat flow in the Tertiary and Cretaceous is relatively high.

• an increasing accumulation, over 60-40 My, resulting in a stable, saturated reservoir. This mode occurs for both the relatively high and medium heat flow scenarios tested on the model

• a later accumulation over 40-20 My, resulting in a stable, saturated reservoir. This mode occurs in response to relatively low heat flow scenarios.

The instability of the early, small accumulation mode to changes in heat flow is illustrated by a small variation in the Triassic heat flow for the 'alternative' scenario - Figure 5.23. Note that, although the generation and expulsion behaviour for the two kitchen areas are effectively unchanged, the slight heat flow variation results in two distinct accumulation histories - Figures 5.30 and 5.31.

In summary, the model once again displays fairly robust and predictable behaviour with respect to generation and expulsion. The accumulation history, however, is quite unstable within the reasonable constraints established by the sensitivity analysis.

Thermal sensitivity – surface temperature scenarios

The calibrated simulations use a constant surface temperature of 5°C. This allows for reasonable heat flow values i.e. in excess of 40 mWm^{-2} at the present day, and increasing in the geological past. A palaeosurface temperature for the mid-Cretaceous – Tertiary – Quaternary (after Buchardt 1978) is used to test the model sensitivity to an alternative, transient surface temperature scenario. This results in a different saturation history and an increase in modelled temperature parameters – Figure 5.44. The high value for simulated vitrinite reflectance, as a result of palaeosurface temperature inclusion, requires the lowest temperature heat flow curve scenario in order to keep the model within calibration constraints – Figure 5.45. A calibrated simulation with a transient palaeosurface temperature results in an oil accumulation history of the 60-40 My mode, with an earlier gas accumulation at 80 My. The transient surface temperature doe not significantly alter the timing of the kitchen areas' generation and expulsion.

The favoured surface temperature model is a constant 4°C. Although ocean circulation has been restricted at times during the Cainozoic, and although the Shetland Basin's latitude has been tropical in the past, there is a possibility that the seafloor temperature has remained at a steady 4°C. This is possible as the maximum density of water occurs at this temperature. Hence, a cold dense layer of water may have insulated the sea floor from surface temperature variation.

In summary, the modelled hydrocarbon system is robust with regard to the timing of oil generation and expulsion from the two kitchen areas. However, the sensitivity analysis has exposed the accumulation history simulations as unstable with respect to reasonable variations in parameters controlling the simulated pressure and temperature conditions.

5.74 Simulation series four: extrapolation

The calibrated model is found to be robust with regard to the timing of oil generation and expulsion for the two kitchen areas. There are, however, two other potential kitchen areas associated with hydrocarbon systems related to the Magnus oil field.

• firstly, the model section also includes a shallower kitchen area to the south east of the Penguin horst block. This shallow Kimmeridge Clay unit, overlying a sandstone unit, is typical of shallow oil fields in the Brent province.

• secondly, as discussed earlier, the position of a deep kitchen area is assumed to be to northwest, immediately up-dip of the Magnus oil field, beyond the throw of the boundary fault. It is likely, however, that if such a kitchen area exists, it will deepen considerably to the northeast along the Magnus Embayment ramp, which eventually terminates in the much deeper More Basin. There is considerable potential for a deeper kitchen area to charge fields, such as Penguin, along the northern fringe of the East Shetland Basin.

The modelling can be extrapolated to investigate the behaviour of such potential kitchen areas for a simulation calibrated to the Magnus oil field. The model is adapted to simulate the timing of generation and expulsion for a deeper kitchen area by simply deepening the Kimmeridge Clay unit in the model-section's deep half graben – Figure 5.46. This is accomplished by thickening the stratigraphic unit immediately overlying the deep kitchen area. The model already includes a shallower kitchen area on the right flank of the section, in accordance with the original geological section – Figure 5.46.

The extrapolated model simulates that, for a deeper kitchen area, at a depth of 7000 meters, the timing of generation and expulsion would occur at about 125 My – Figure 5.47. For a shallower kitchen area, at a depth of about 3800 meters, although the simulated onset of generation is unaltered, expulsion would not occur until about 10-20 My – Figure 5.48.

5.8 A comparison of the simulation with Magnus illite ages

The comparison is excellent. A single model based on a simple along-dip section, and calibrated to present-day data from the Magnus oil field matches the simulated timing of oil accumulation in the trap structure to the complete population of illite ages. Although this calibrated model is sensitive to acceptable variation in the input parameters controlling pressure and temperature, the generation and expulsion histories for the two kitchen areas are stable. The kitchen area generation and expulsion, as robust aspects of the modelled hydrocarbon system, also match the illite age data set.

5.9 The Magnus model and Penguin illite ages

The field study yielded a wide range of illite ages for the four Penguin structures. The implications of the calibrated *Magnus model* and related extrapolations are considered for each of the structures.

• Penguin A - the calibrated simulation for the Magnus model indicates that hydrocarbons may have moved through the system at about 90 Ma. This is in accord with the ages recorded for the Penguin A structure. Generically, the Magnus and Penguin A structures are very similar. Their common geographical location, identical stratigraphic position and association to kitchen areas in the Magnus province and North Shetland Trough all suggest that the two fields are likely to have been exposed to the same hydrocarbon system. It would be reasonable, therefore, to expect that hydrocarbon-associated diagenesis resulting in fibrous illite would be similar in both.

• The Penguin B structure has the oldest illite ages for the study, at about 120 Ma. The extrapolated model simulates that a deeper kitchen area than the one included on the Magnus Model section, at a depth of about 7000 meters, may have been discharging hydrocarbons at about 125 My. This critical moment of hydrocarbon charge is a highly reasonable match for the hypothesised likely kitchen area responsible for Penguin B's gas condensate i.e. the More Basin, to the north of Penguin B. Well stratigraphy for 211/13- 1 indicates that the Lower Cretaceous is condensed to less than 30 metres. This would indicate that illite is growing in an environment where oil flow is possibly only retarded, or briefly retained, as opposed to trapped in the conventional sense.

• The bulk of the remaining ages in Penguin C, at 60 Ma and 90 Ma, conform to simulated timings for expulsion from the shallow Magnus province and deep North Shetland Trough kitchens, at a similar depth to that responsible for the present day Magnus oil field. However, these trap structures lie on the eastern flank of the Penguin B horst. This implies that charge to this structure probably originated in the Tampen Spur Embayment to the north-northeast. On the basis of the extrapolated simulation the youngest age measured for the Penguin field, 33 My, would be associated with a kitchen area deeper than 3800 meters and shallower than 4200 meters. The Extrapolation model simulation implies that the oldest age for the Penguin field, in Penguin D, 133 My, would require exposure to a hydrocarbon charge from a deep kitchen area to the North.

5.10 Interpretation with respect to East Shetland Basin data set

The bulk of the illite ages for the East Shetland Basin fall within the range: 70-40 My. The Magnus model implies that a shallow kitchen area is the generic kitchen area type for East Shetland basin illite diagenesis. The accumulation history for the model implies that the these structures have remained saturated, i.e. filled for the last 40 million years. The scatter of ages outside this range can be attributed to local kitchen areas that have matured slightly earlier or later than the generic kitchen, possibly as a result of local structural controls on the burial history of the source rock. The youngest age in the East Shetland Basin, at 17 Ma is in accordance with the Extrapolation model's indicated timing of expulsion for a kitchen area at about 3800 meters. The modelling study suggests that the absence of younger illite ages in the Northern North Sea and related illite diagenesis can be attributed to the absence of significant hydrocarbon charge to trap structures in the last 15 My.

5.11 Conclusion

In conclusion, the aims for this chapter have been met. Namely, a two-dimensional model of a proposed hydrocarbon system within the East Shetland Basin was constructed. The hydrocarbon system in question contained oil fields with proven fibrous-illite diagenesis. The modelled system was calibrated to independent variables from one of those oil fields. The resultant simulations for the calibrated model were assessed with regard to the generation, expulsion and accumulation of the petroleum system, and the sensitivity of the modelled was established with regard to pressure and temperature variation.

The model was found to be robust with regard to the timing of simulated hydrocarbon charges in the system. The model was also found to be unstable with regard to hydrocarbon accumulation history for the oil field on which the calibration was based. The various modes of accumulation presented by the unstable, calibrated simulations were characterised.

The behaviour of the *Magnus Model*, a simulated petroleum system within the East Shetland Basin, was then compared to illite ages from oil fields within the proposed system and also discussed within the context of illite ages for the region. The modelling suggests that there is good reason to support to the proposed hypothesis that fibrous illite diagenesis in oil fields is linked to the timing of hydrocarbon charges from local kitchen areas.

—

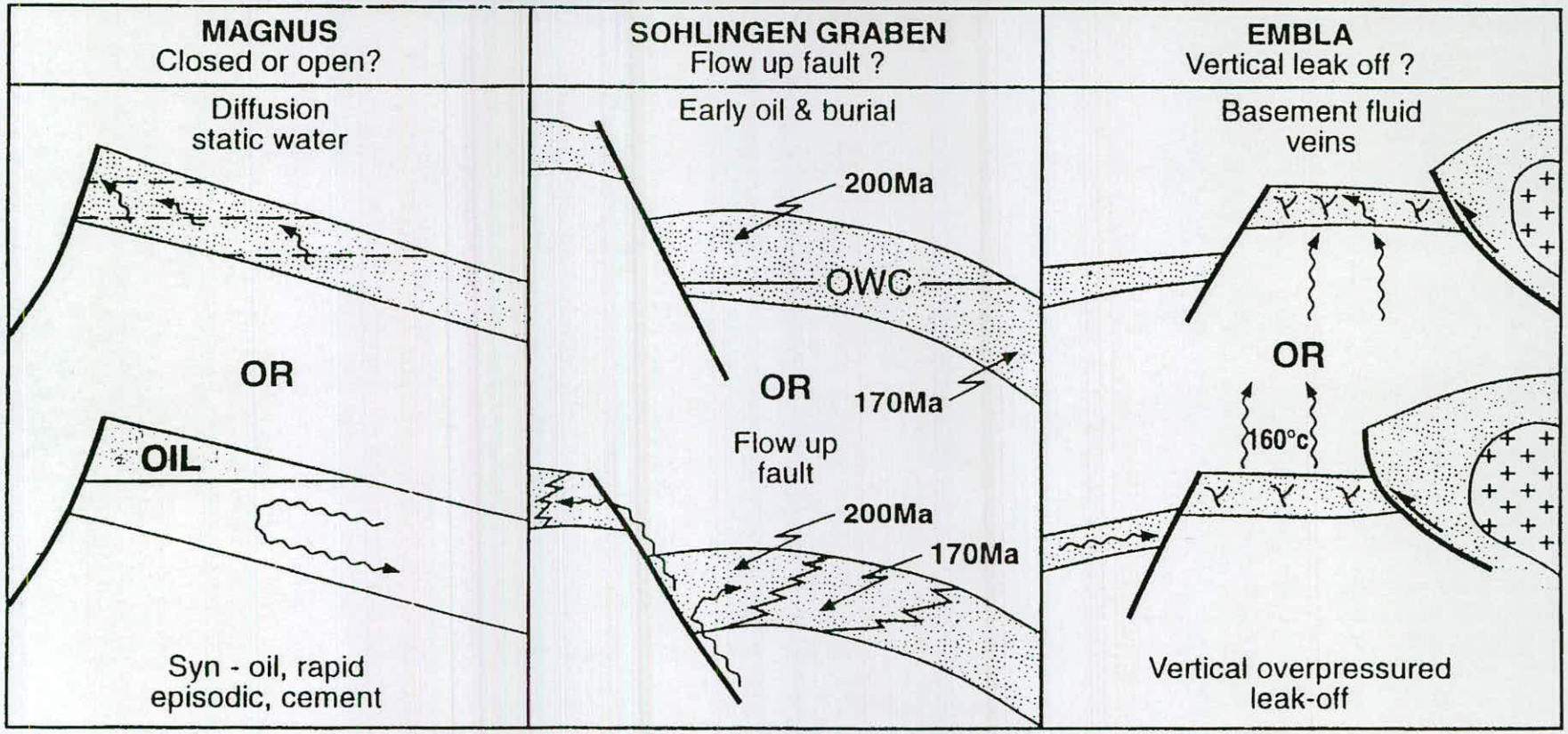

Figure 5.1 Three simple generic models for fluid-flow related illite diagenesis: water-oil mixing in open and closed systems; hot and exotic fluid invasion of oil fields along fault conduits; pressure-related vertical fluid expulsion. The first model correlates illite diagenesis with local oil incursion and accumulation at the trap structure; the second and third model associate illite diagenesis with regional changes in the hydrogeology i.e. maturation of source areas, generation of overpressure in deeper parts of the basin and tectonics

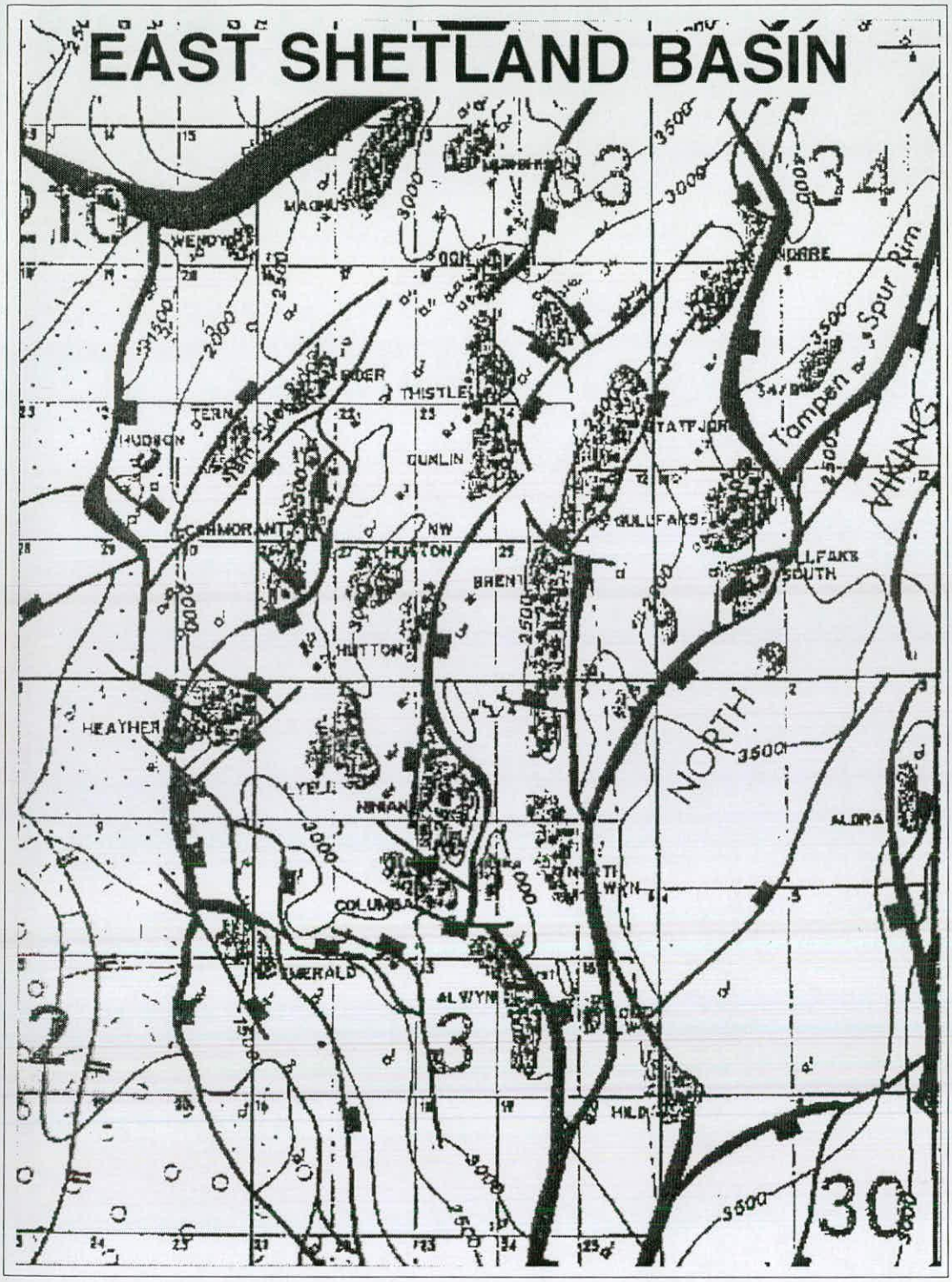

Figure 5.2 Geographically and geologically complex- the East Shetland Basin. A tapestry of oil fields, bifurcating faults, small intra-terrace basins and ramps underly the superficially simple arrangement of -north- northeast trending half grabens that deepen toward the axial Viking Graben.

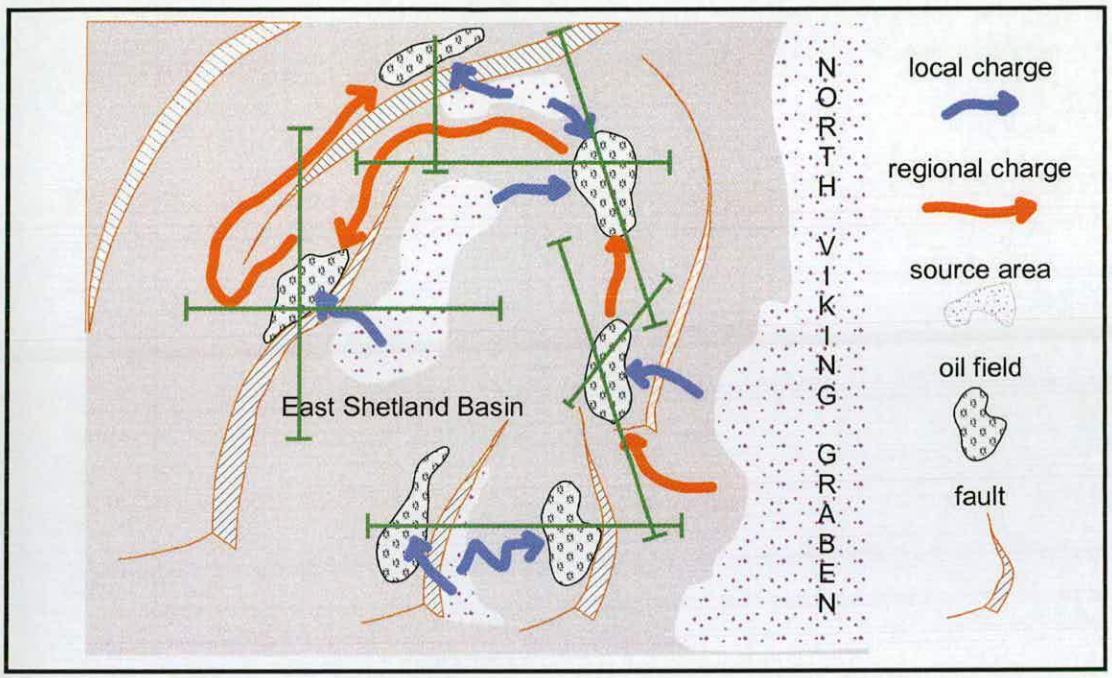

Figure 5.3 The concept of a hydrdynamic section. The schematic map shows a typical scenario in the East Shetland Basin. Regional seismic data is shot in straight lines, typically running parallel to or at a tangent to the general strkie direction. As the migration pathway arrows indicate, prospective fluid flow pathways may have a more complex relationship with the structure of the basin. A hydrodynamic section uses seismic sections to build up a hypothetical section along the proposed vector of fluid flow.

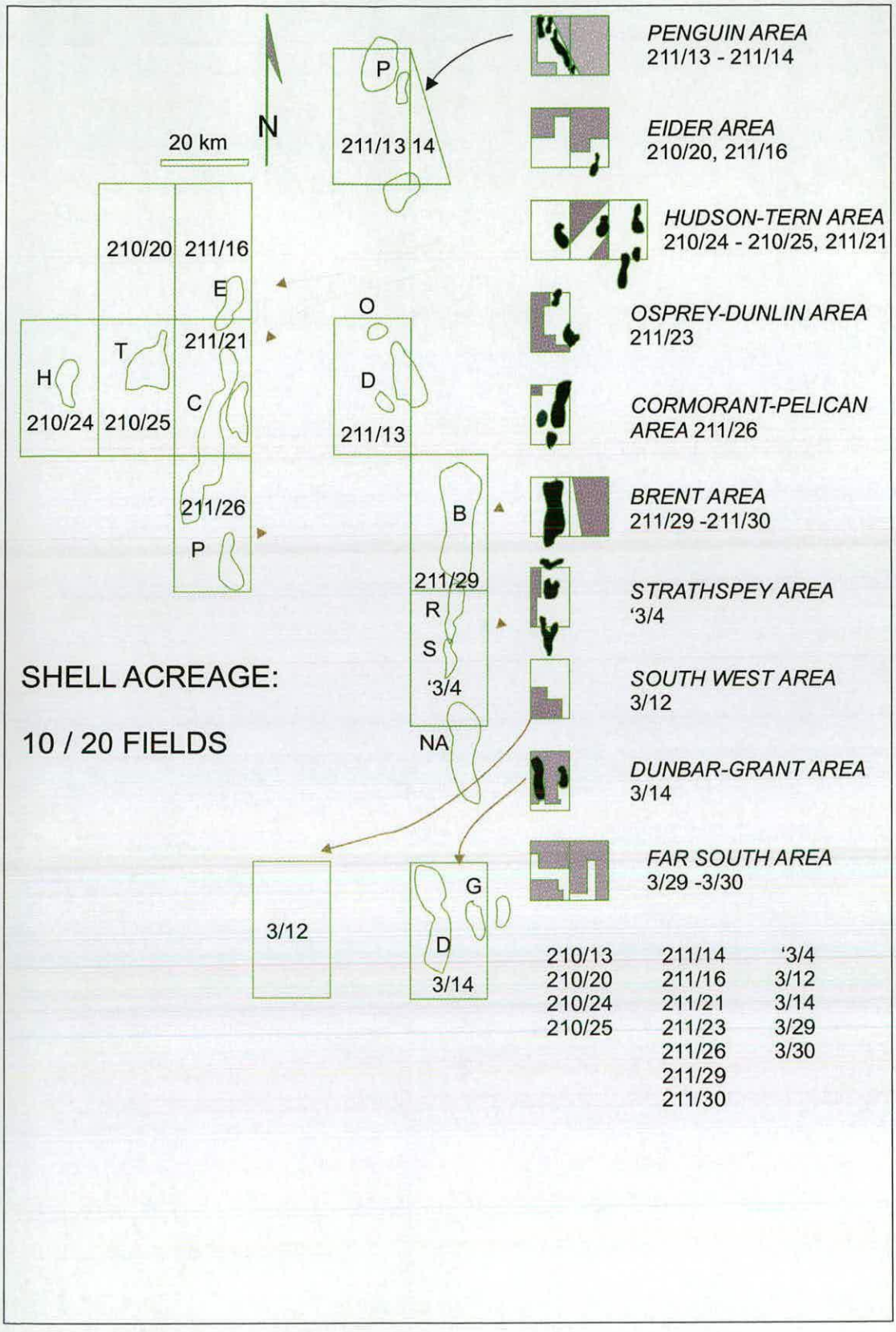

Figure 5.4 Shell acreage at the time of data acquisition. Shell UK is one of the largest operatives in the East Shetland Basin region, as evident by the fact that half of the twenty principal fields in the area are operated by the company.

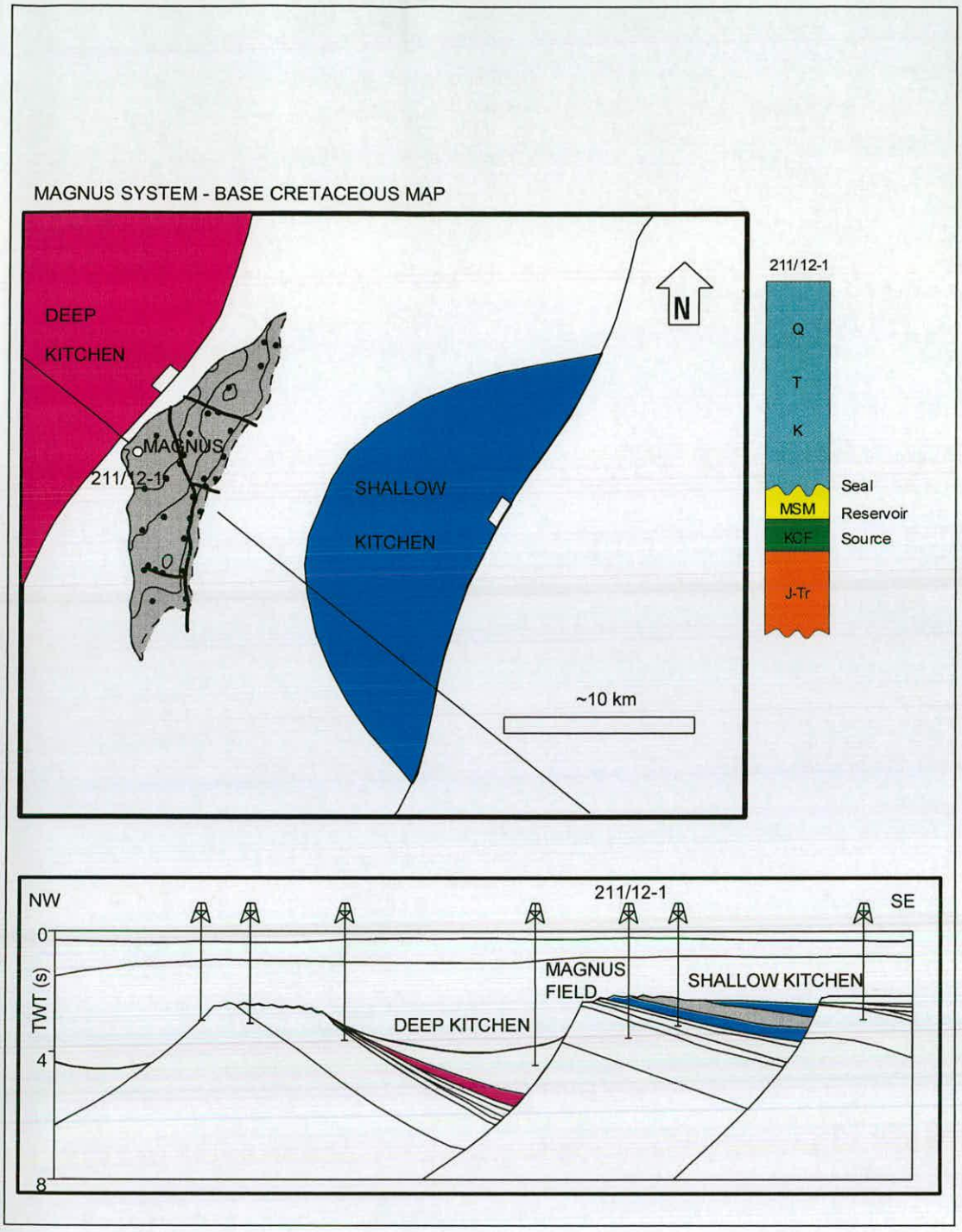

Figure 5.5 The Magnus system. The general relationship of the oil field to the two potential kitchen areas and major faults is shown in plan view and cross-section. A schematic stratigraphic column is also included, showing the basic supraposition of the important model elements of seal, reservoir and source rock. Note that the source rock, shown in green, is equivalent to the two depth representations for kitchen areas on the cross-section and map.

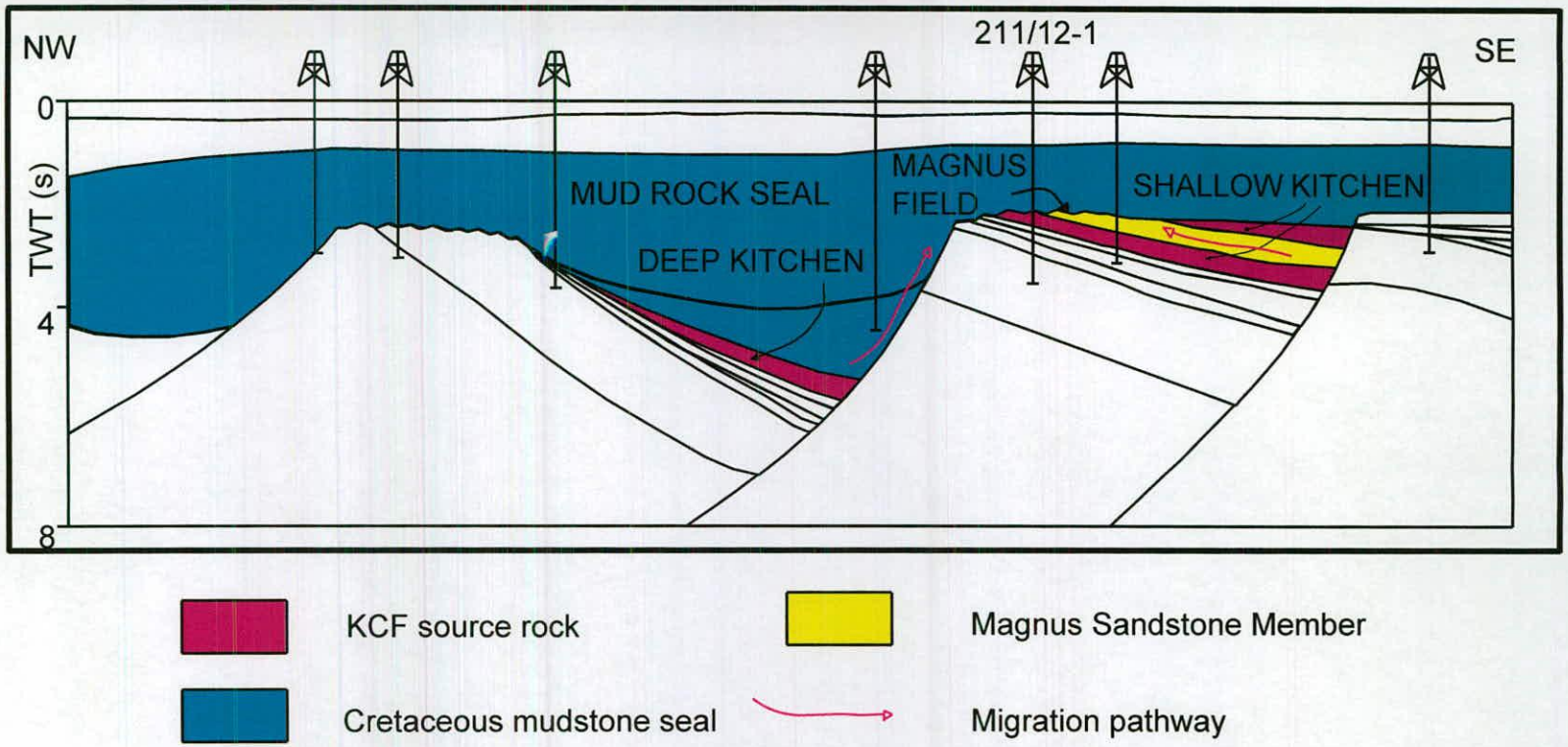

Figure 5.6 The Magnus system. Two Kimmeridge Clay Formation kitchen areas, labelled 'deep' and 'shallow' flank the eroded crestal area of a cantilever fault block, which marks the position of the oil field, Magnus. 211/12-1 marks the position of the discovery well on the section.

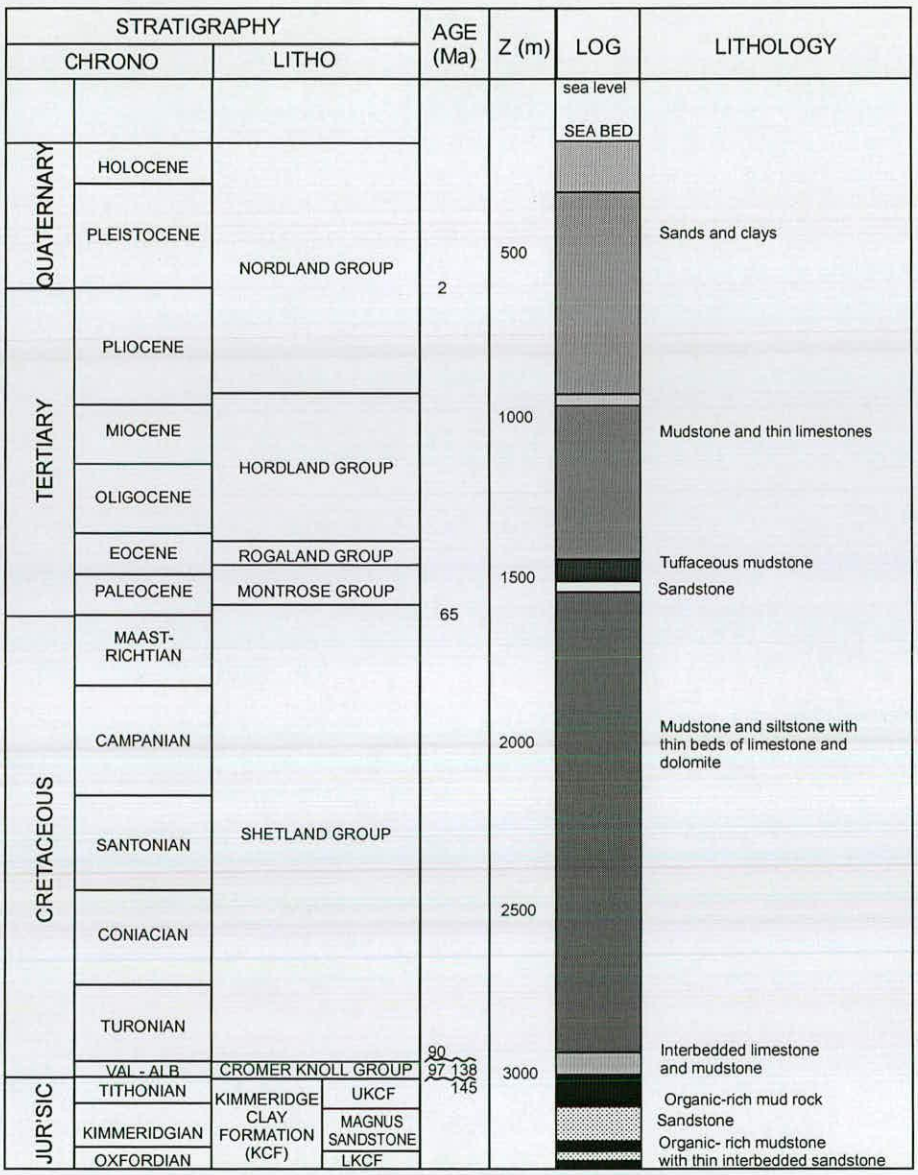

Figure 5.7 Magnus stratigraphy showing the relative thickness, significant ages and lithologies encountered in Magnus wells (after Shepherd *et al.* 1990).

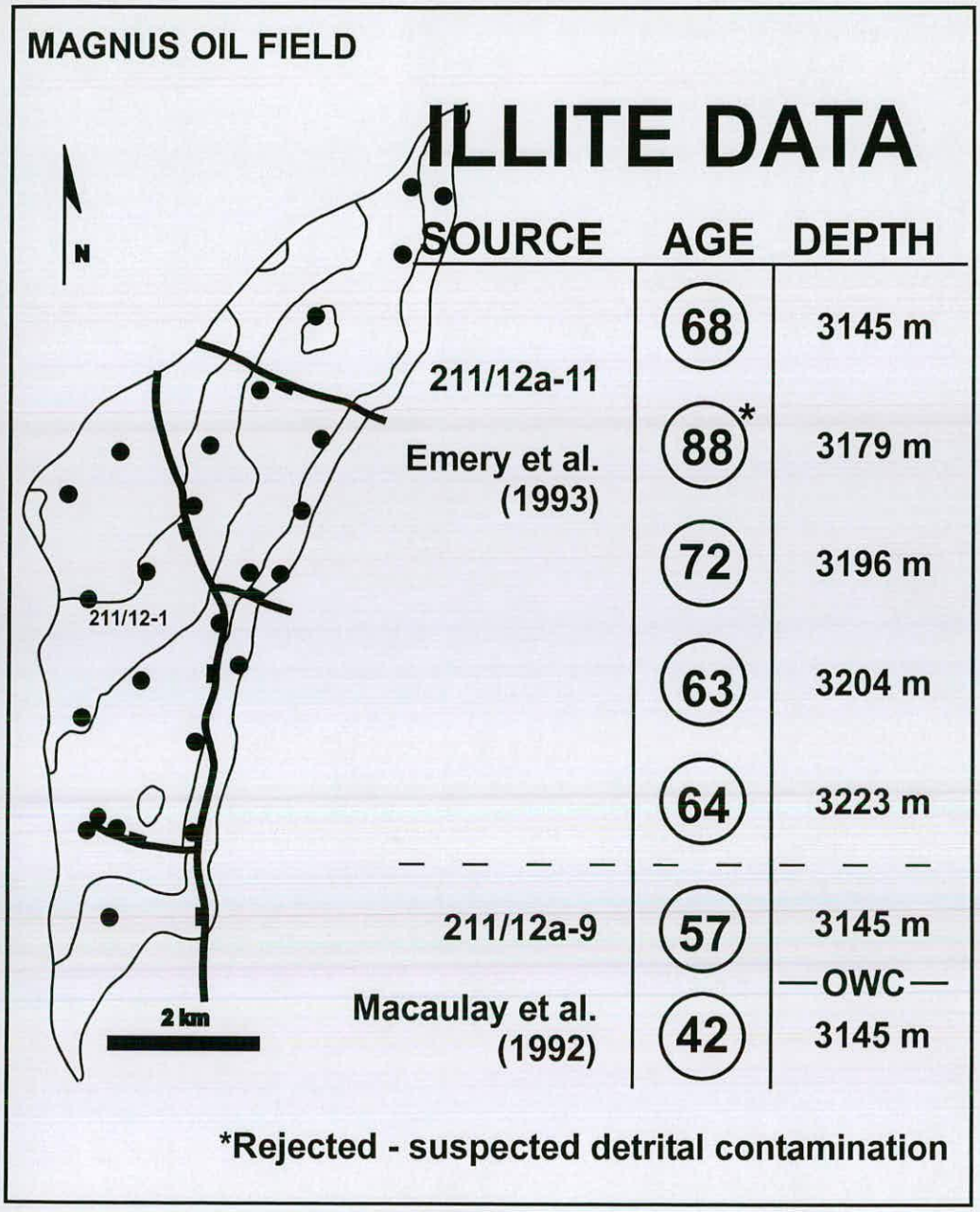

Figure 5.8 Illite ages for the Magnus oil field. The larger set, published by Emery *et al.* (1993), includes an illite age thought to be significantly older than expected ages for the field. As such, the age was rejected on grounds of suspected contamination. The illite ages for Magnus published by Macaulay *et al.* (1992) are suplemented by a further age in the doctoral thesis (Macaulay 1990).

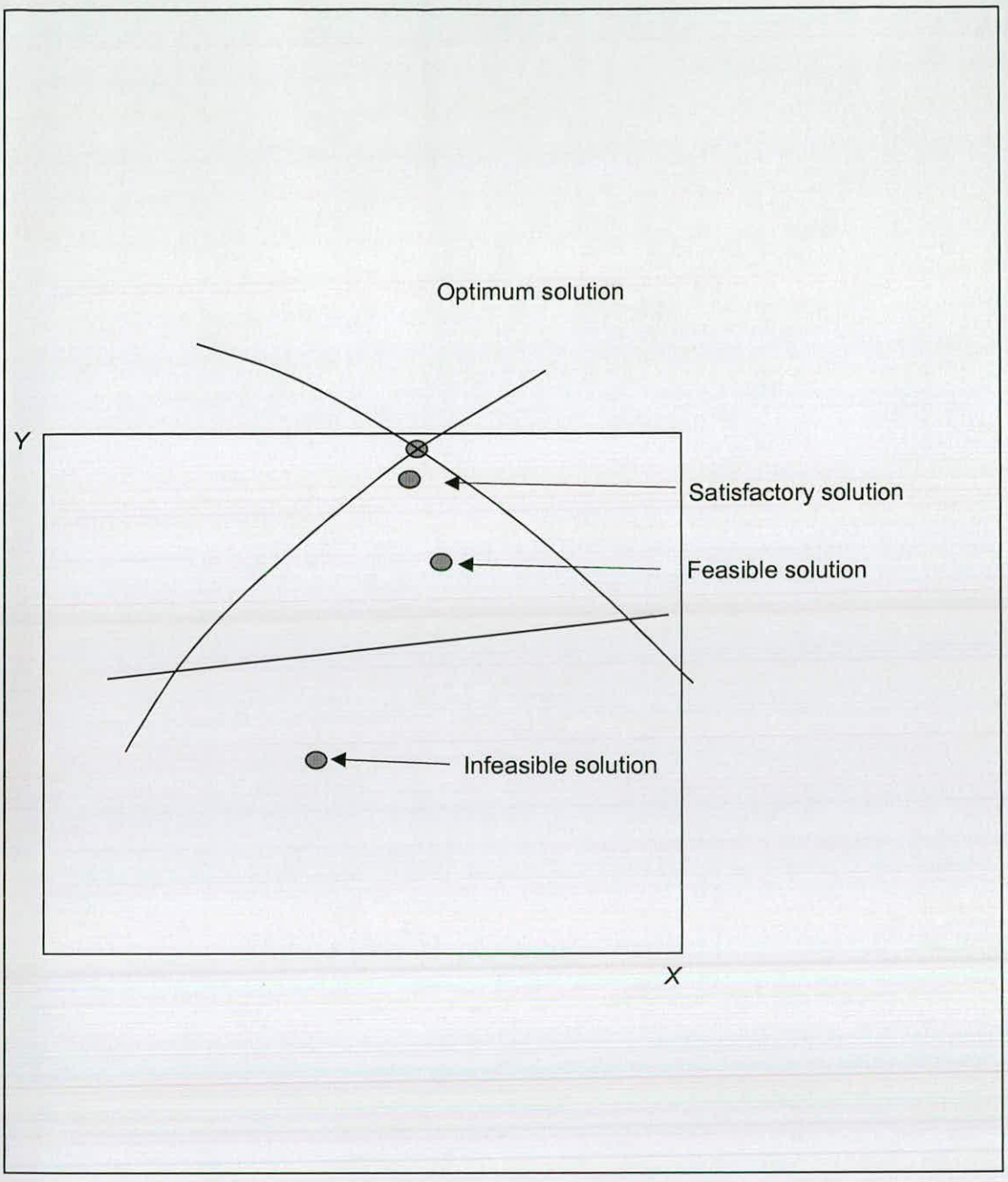

Figure 5.9 Solution spaces resulting from model simulations. Note that although the optimum solution is represented by a point, satisfactory and feasible solutions occupy a much larger, defined space. Most succesful natural system modelling studies are resolved in this space (from Neelamkavil 1991).

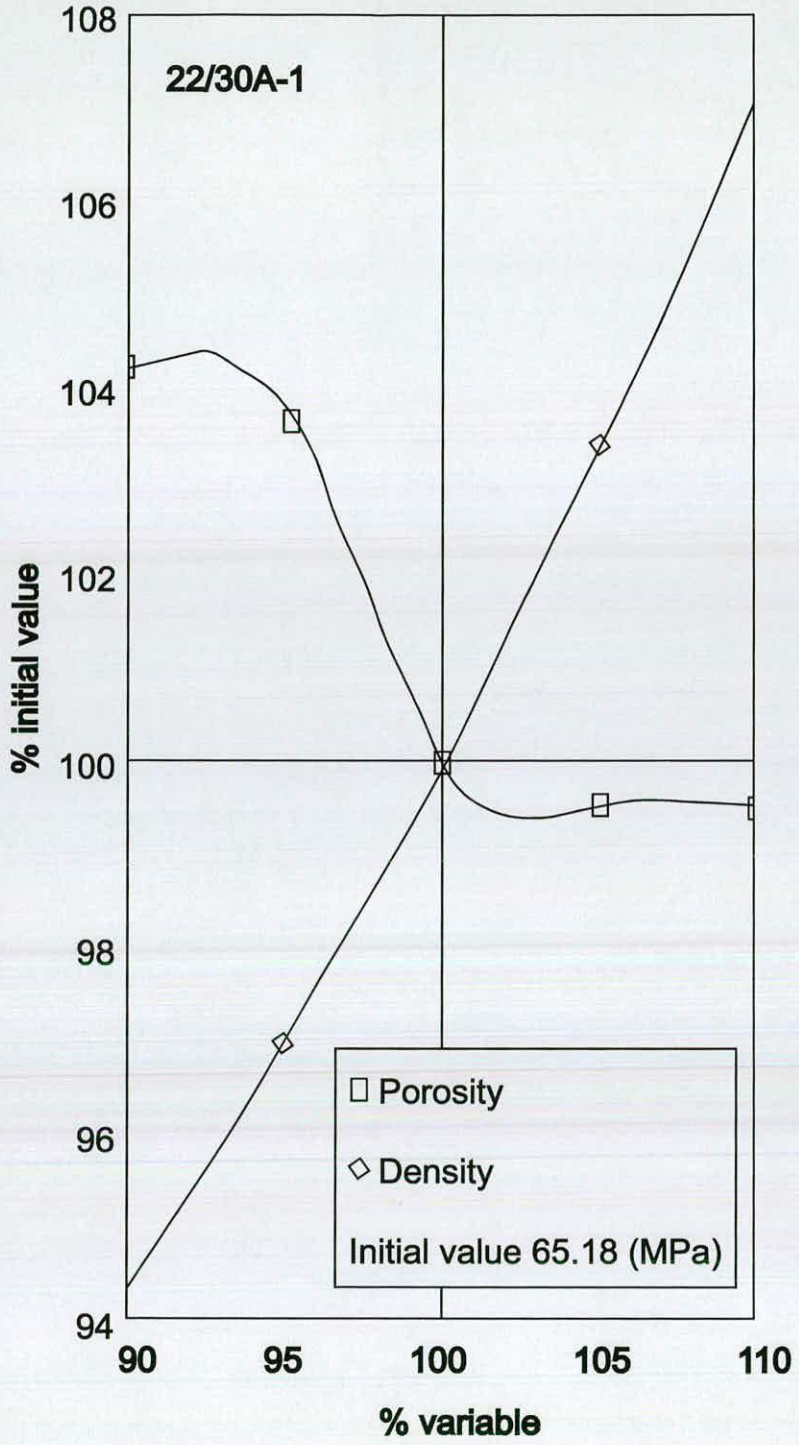

Figure 5.10 A sensitivity curve plot for a similar basin model study (Darby 1995). The sensitivity of a variable (x-axis) to variation in two input parameter values (y-axis) indicates the model is more sensitive to density variation than initial porosity with respect to pressure, the response variable.

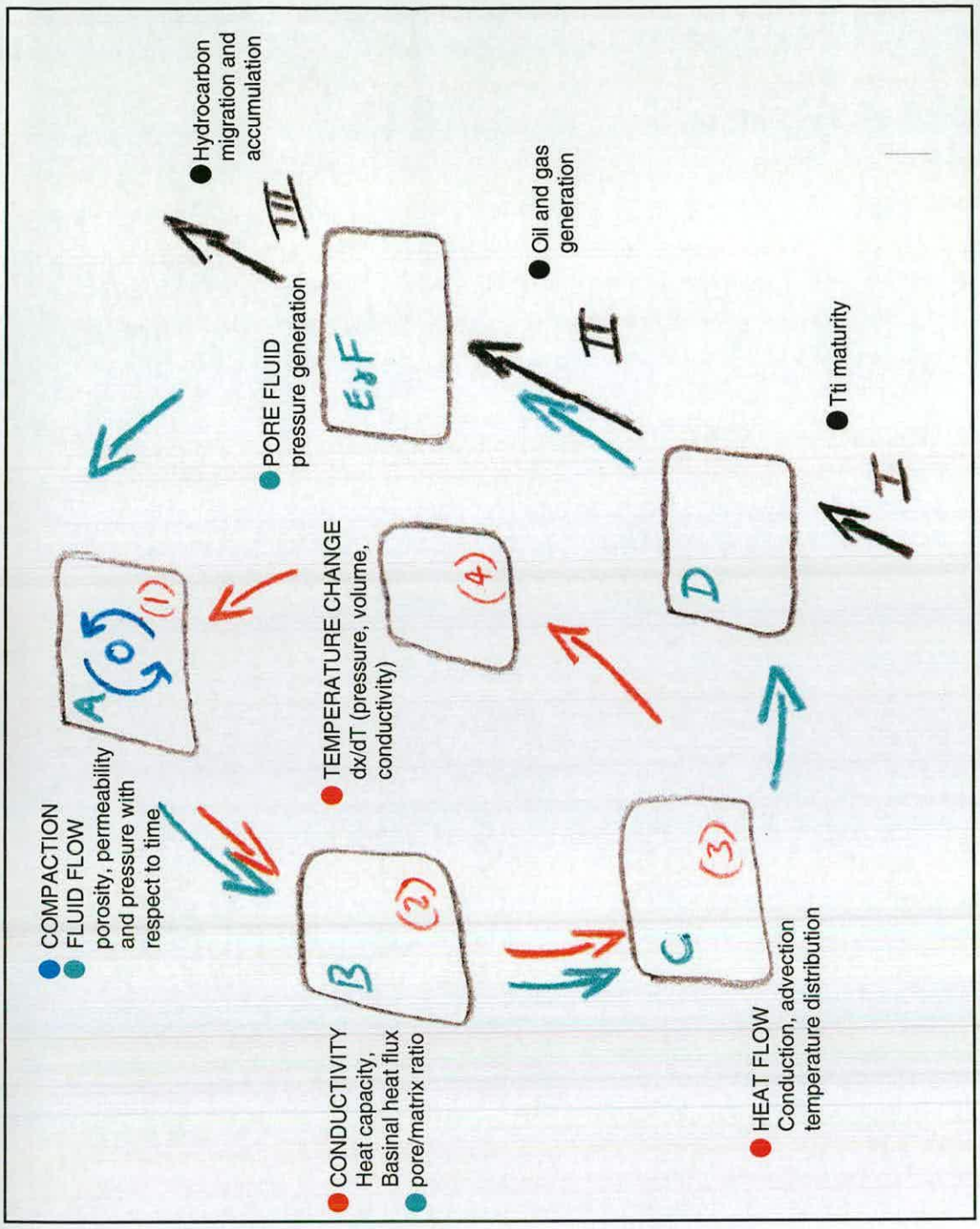

Figure 5.11 Calculation loops for BasinMod® 2-D (Platte River Associates 1998). This expression of the BasinMod® engine is more complex than the iterative loop described earlier –Chapter 2, Figure 2.8. The detailed diagram shown here demonstrates the primacy of compaction in the engine and the interdependency of compaction, fluid flow and thermodynamic loops. These three iterations combine with the non-iterative Time-temperature-index calculation for maturity to simulate the petroleum system as a whole. The underlying mathematics is presented in the appendices – Appendix 5.3.

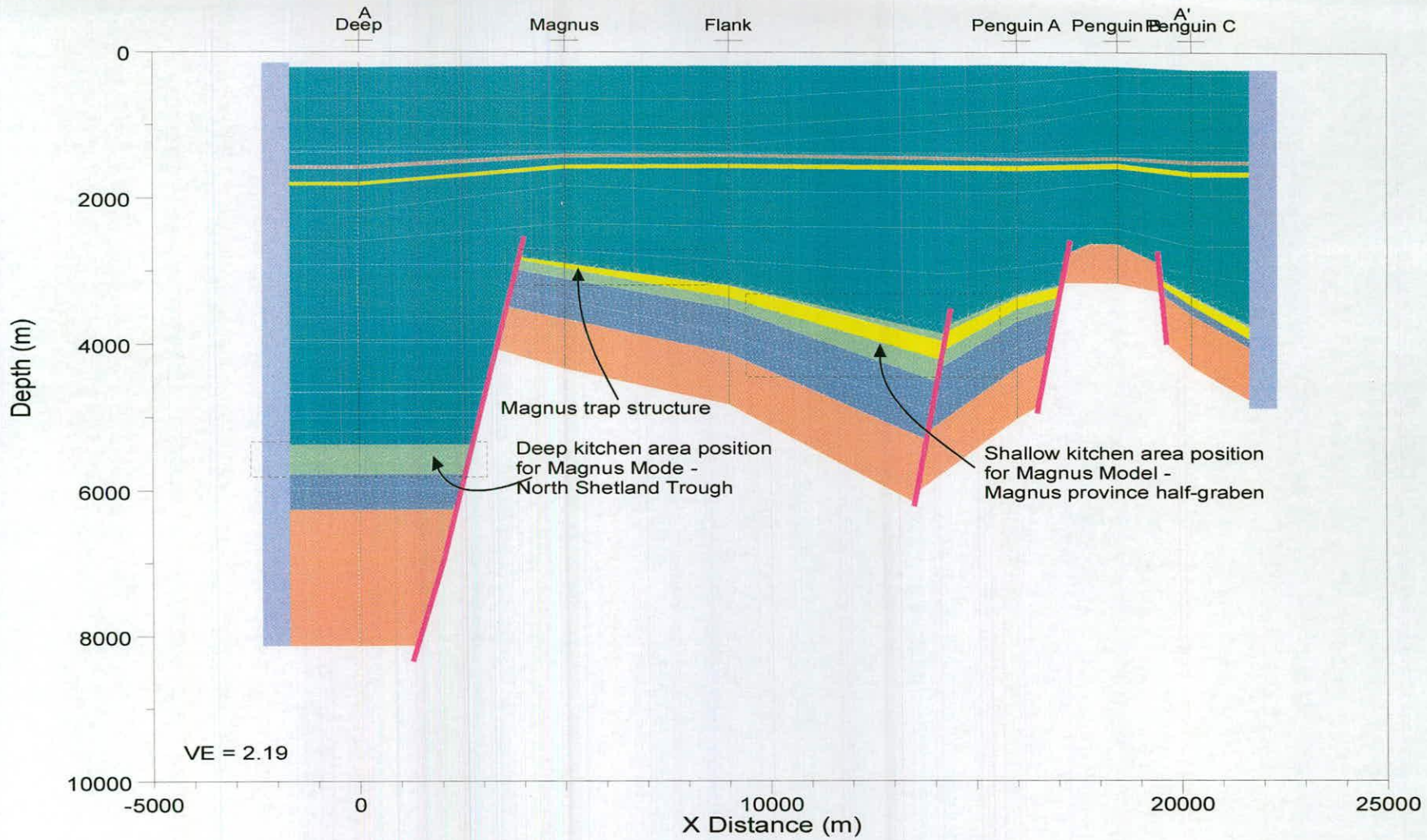

Figure 5.12 Magnus model - pilot study. The deep kitchen area lies in the North Shetland Trough at a depth of about 5400 meters. The shallow kitchen area lies to the east of the Magnus trap structure in the Magnus province half-graben. The position of stratigraphic wells pinning the section are denoted by field name.

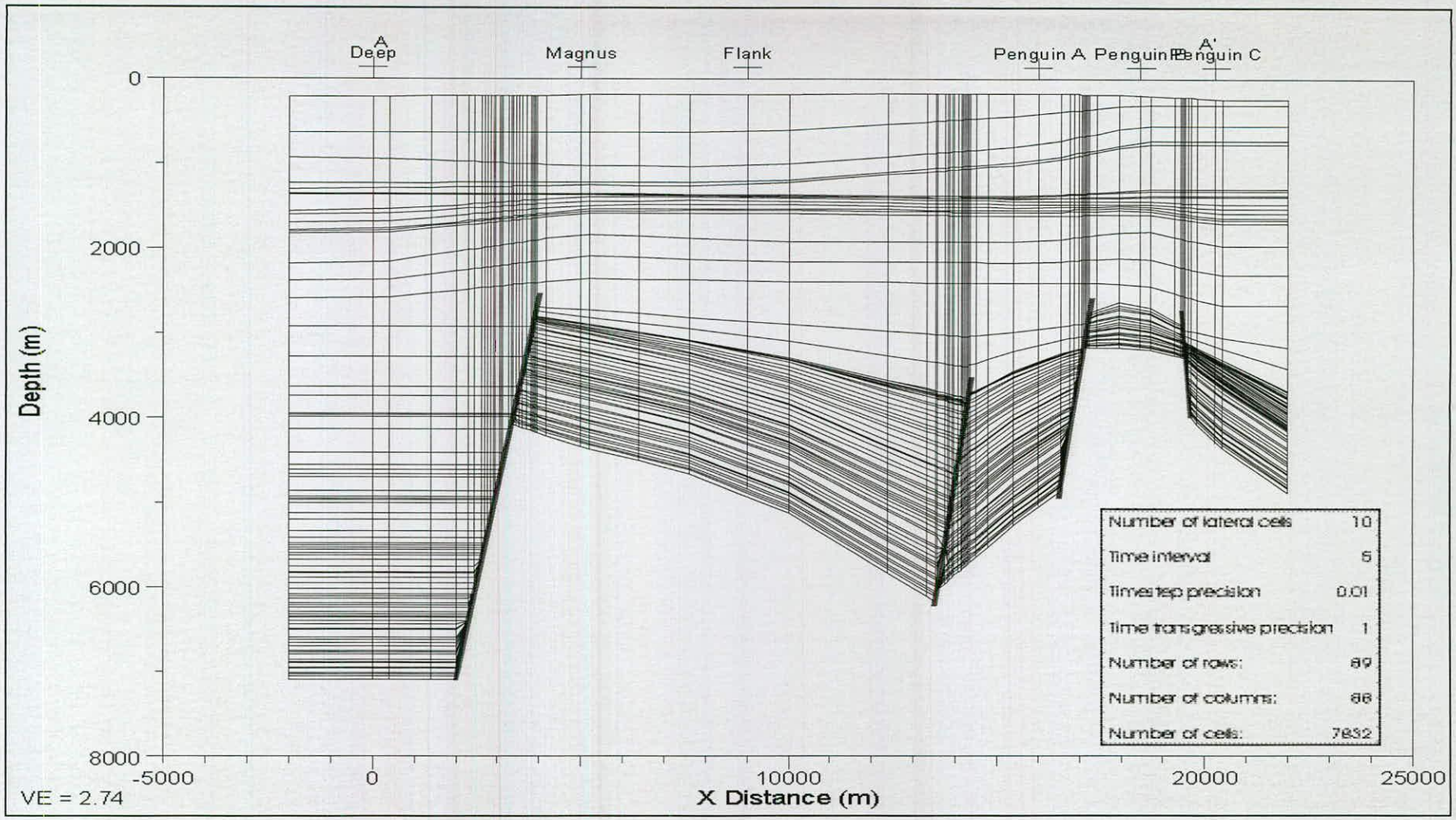

Figure 5.13 Cell coverage for the default model. The column density is controlled by the *number of lateral cells* input, faults and well positions; the row density by the *time interval* input and the model stratigraphy. The default matrix consists of 7832 cells.

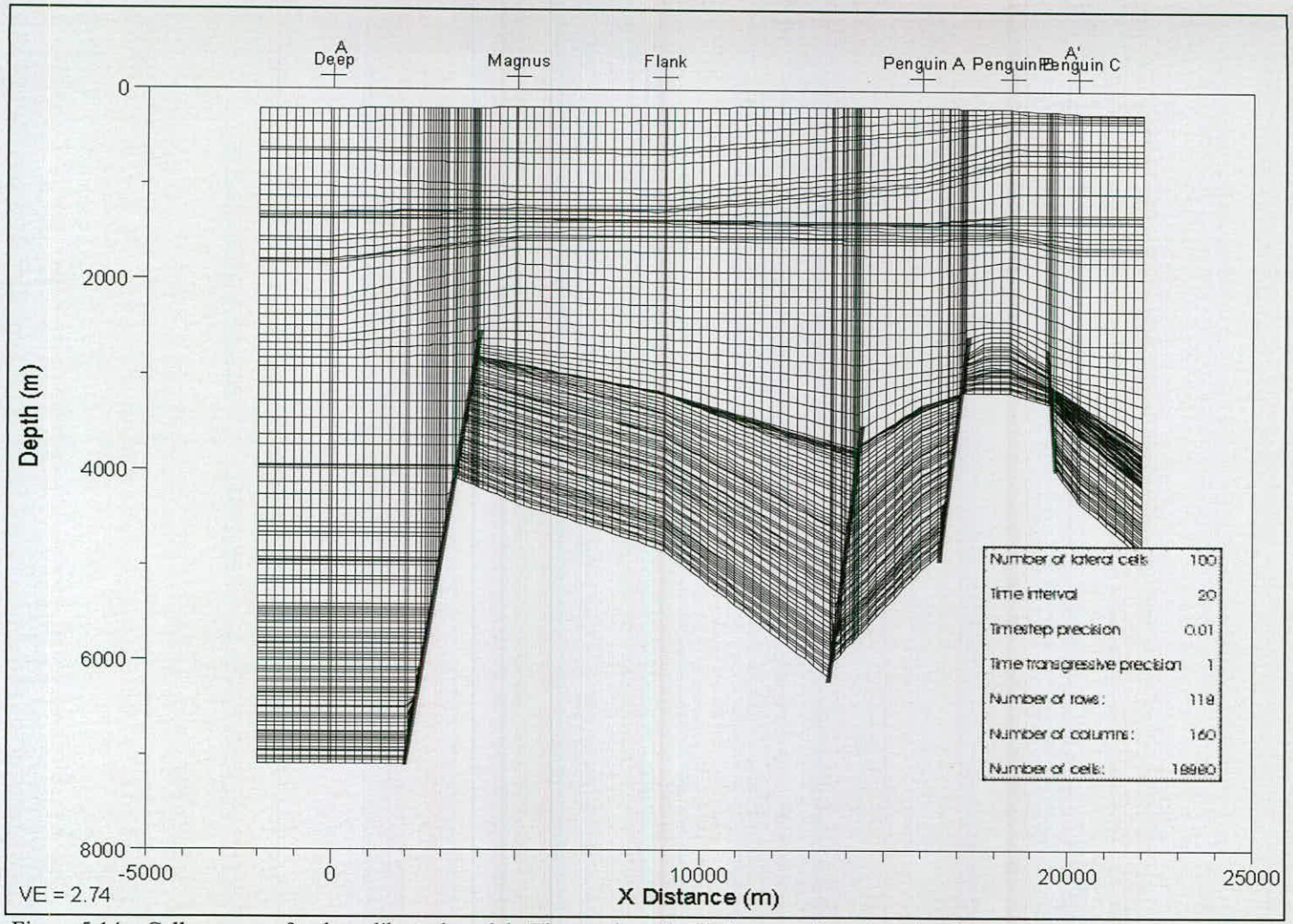

TIME STEPS	
No.	Age (My)
1	0.5
2	1
3	2
4	3
5	10
6	15
7	25
8	30
9	40
10	50
11	60
12	70
13	78
14	80
15	82
16	85
17	86
18	87
19	88.5
20	89
21	89.5
22	90
23	95
24	100
25	102
26	110
27	120
28	130
29	140

Figure 5.14 Cell coverage for the calibrated model. The number of cells is approximately twice that of the default model at 18,880. The added time steps have altered the row density. The *number of lateral cells* input has adjusted the number of columns.

PALEOBATHYMMETRY

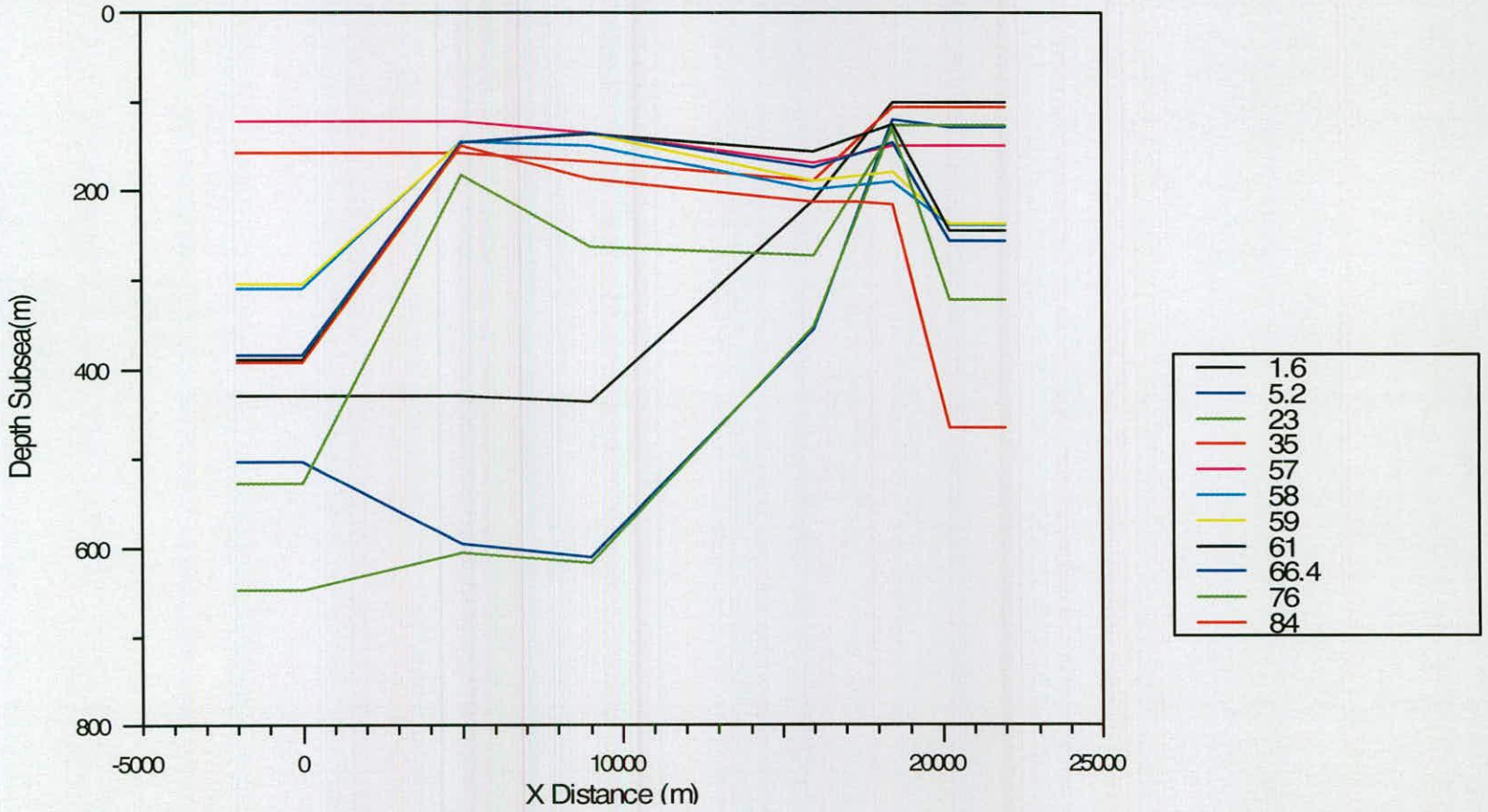

Figure 5-15 Assumed paleobathymetry for the Magnus model. The minimum sea depth is taken as 100 metres. The profiles are derived from present day profiles for the respective horizons.

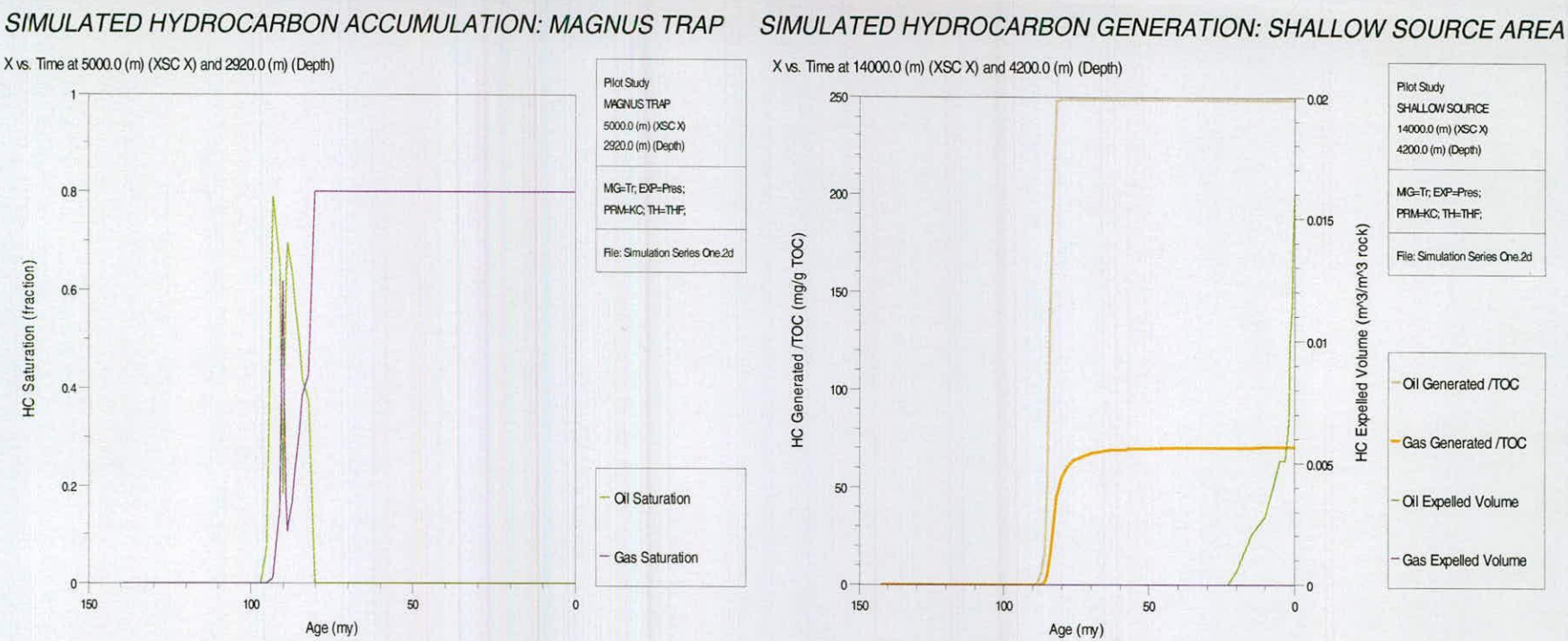

PDST 20 degC	Porosity	Permeability	Temperature	Pressure	Maturity, Ro
HF: 64 mWm^-2	(%)	(md)	(degC)	(psi)	(%)
Calibration (6500, 3050)	10-20	100	116	6550	0.7
Simulation (6500, 3050)	29	2535	207	5787	2.02

Figure 5.16 Output for the pilot study simulation, simulation series one. The simulated accumulation records an early phase of oil and gas saturation, 100-80 My, followed by a prolonged period of gas saturation to the present day. The simulated shallow source area generates oil and gas at about 90-80 My. Oil expulsion is much later at approximately 20-0 My. The values for simulated reservoir parameters, porosity, permeability, temperature and vitrinite reflectance are much higher than the calibration data while the simulated pressure is much lower.

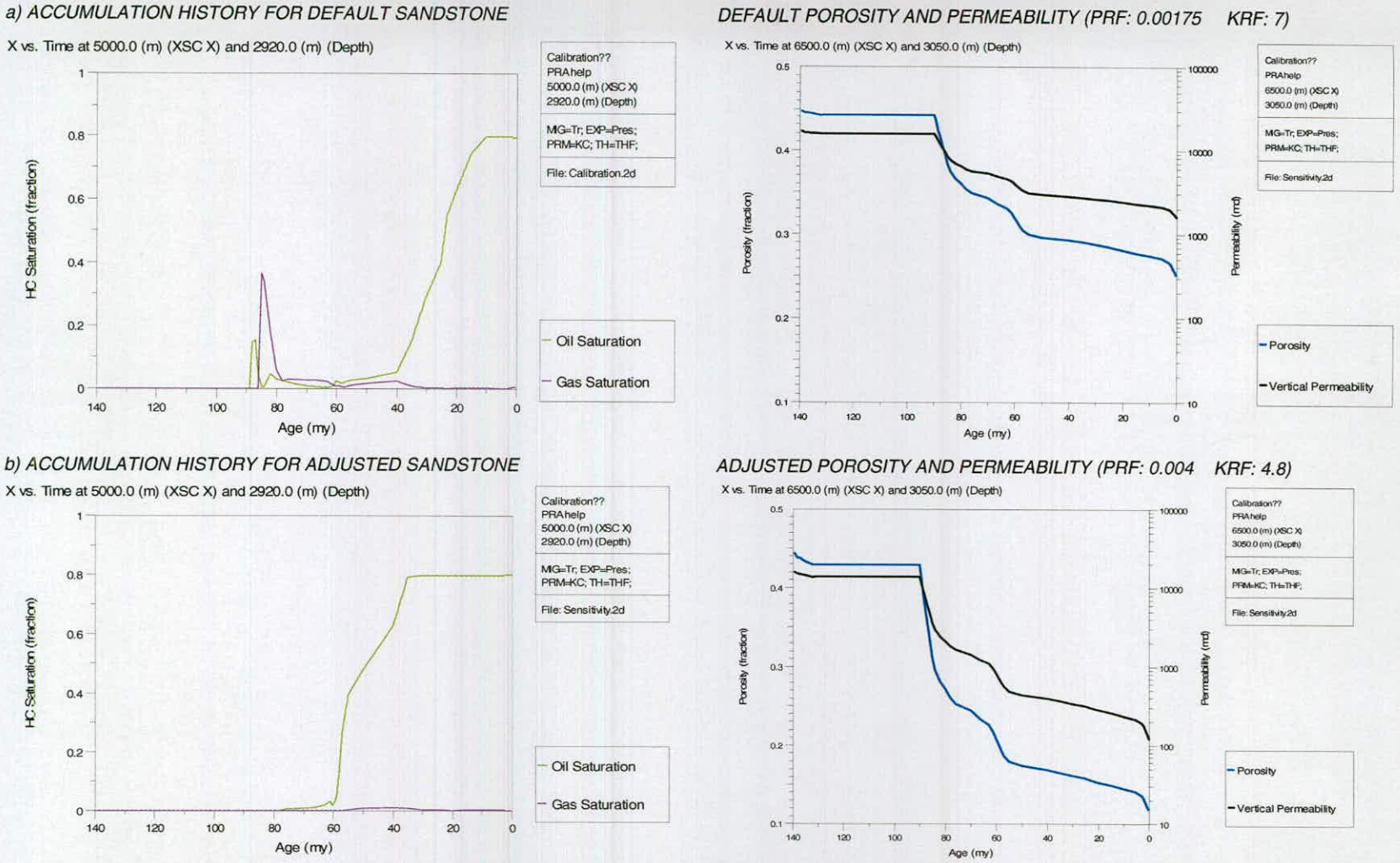

Figure 5.17 A comparison of the simulated hydrocarbon accumulation in the Magnus trap structure for different sandstone parameters: a) default values for the sandstone porosity reduction factor (PRF), and permeability reduction factor (KRF); b) adjusted PRF and KRF.

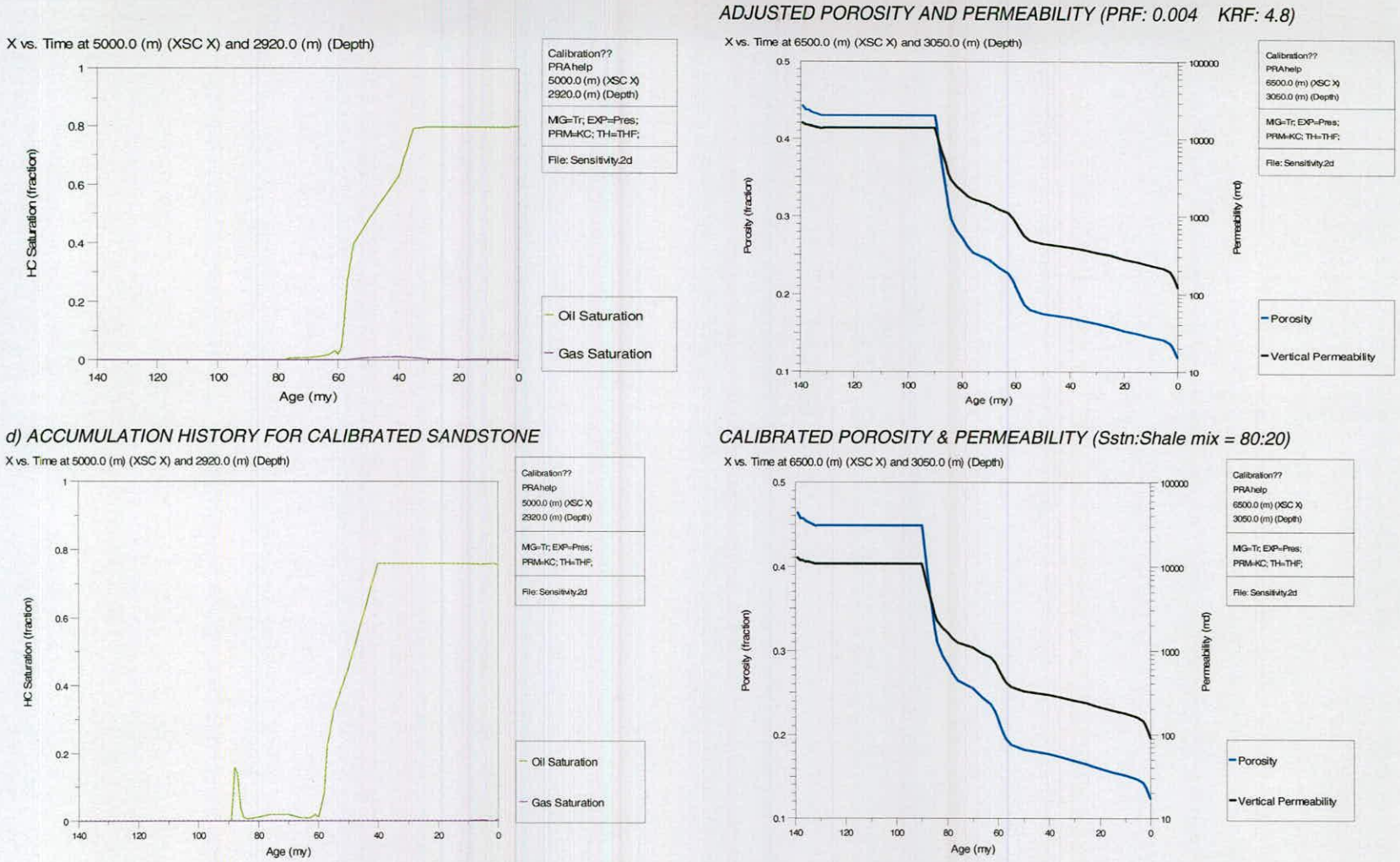

Figure 5.18 Simulated HC accumulation in the Magnus trap structure for a different sandstone mix: c) 100% sandstone with adjusted values for the porosity reduction factor (PRF), and permeability reduction factor (KRF); d) PRF and KRF as for 'c' but with an 80:20 sandstone:shale mix.

a) DEFAULT SURFACE TEMPERATURE AND HEATFLOW: 68 degF and 64 mWm^-2

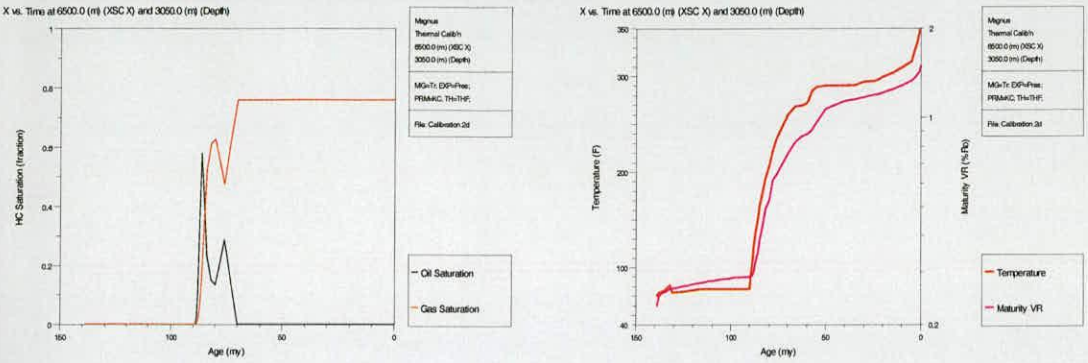

b) LOW SURFACE TEMPERATURE AND DEFAULT HEAT FLOW: 41 degF and 64 mWm^-2

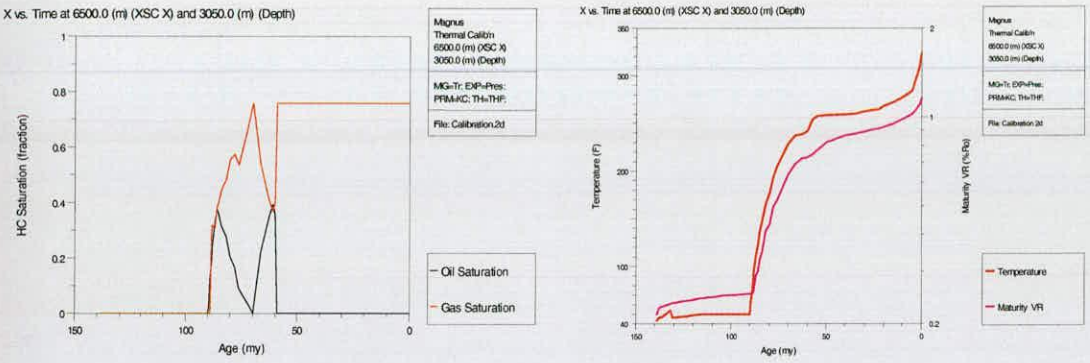

c) LOW SURFACE TEMPERATURE AND LOW HEATFLOW:* 41degF and 45 mWm^-2

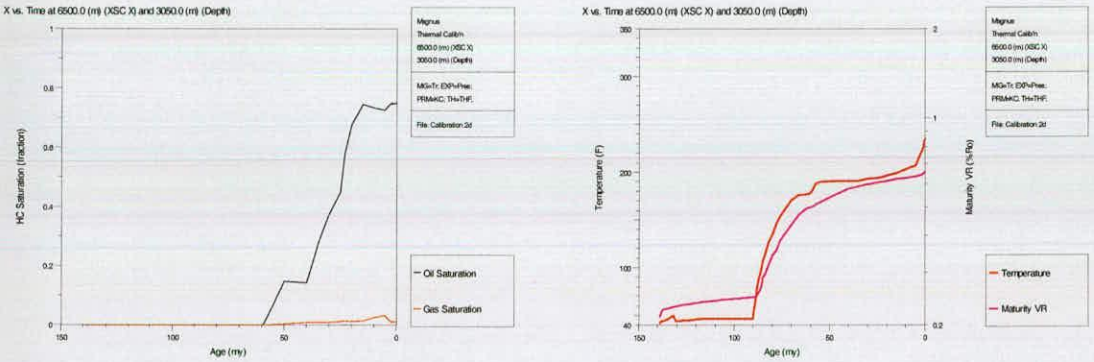

SIMULATED VALUES FOR RESERVOIR PARAMETERS

Calibration parameters	Porosity	Permeability	Temperature	Pressure	Maturity, Ro
Reservoir (6500, 3050)	(fraction)	(md)	(degF)	(psi)	(%)
Figure a - default	0.12	81	360	6533	1.5
Figure b - low surface temp	0.122	87	325	6591	1.2
Figure c* - low temp and HF	0.124	92	235	6654	0.66

*An improbable calibrated model, as the heat flow is likely to be higher in the past due to rifting.

Figure 5.19 Heat flow and surface temperature variation: their effect on reservoir saturation, temperature and maturity parameters. Figure 'c', the low heat flow and surface temperature simulation, qualifies as a calibrated model as all the reservoir parameters are within error.

DEFAULT SURFACE TEMPERATURE: 20 degC, constant

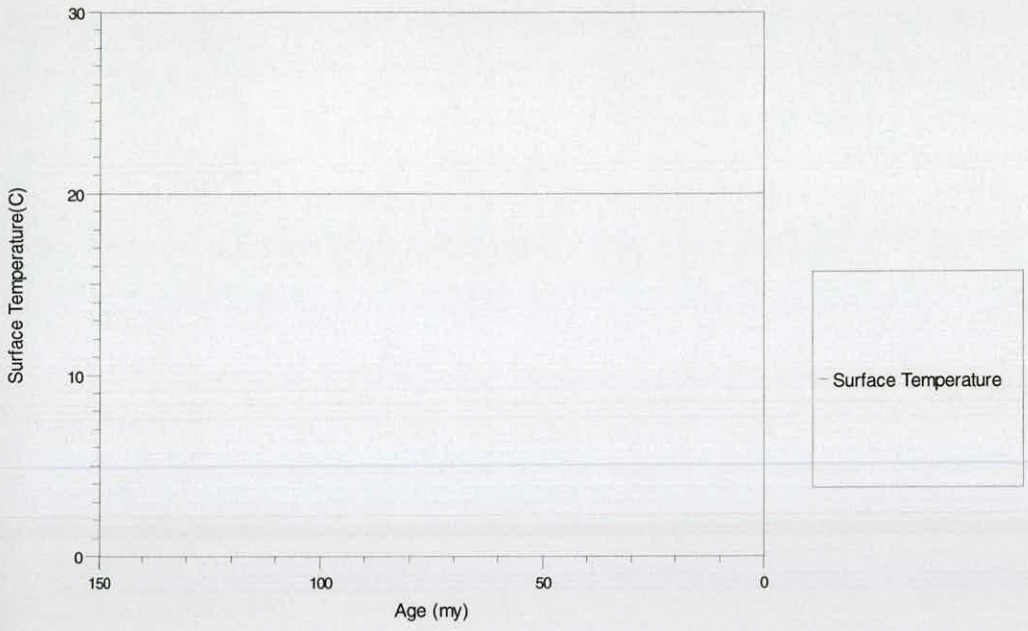

CALIBRATION SURFACE TEMPERATURE: 5 degC, constant

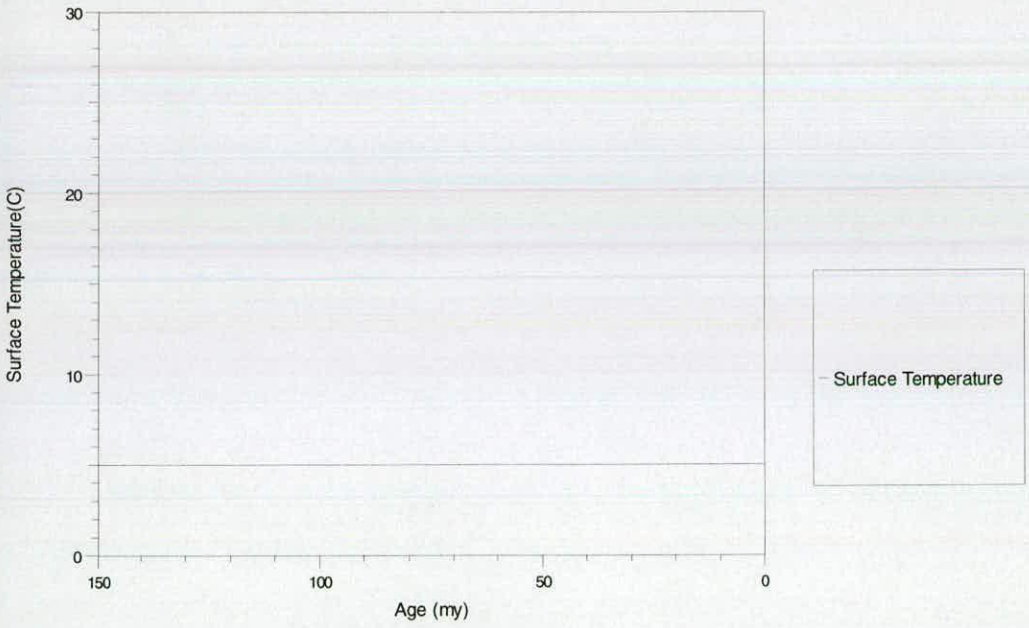

Figure 5.20 Surface temperature for both the default model and calibrated simulation.

DEFAULT HEAT FLOW: 64 mWm^-C, constant

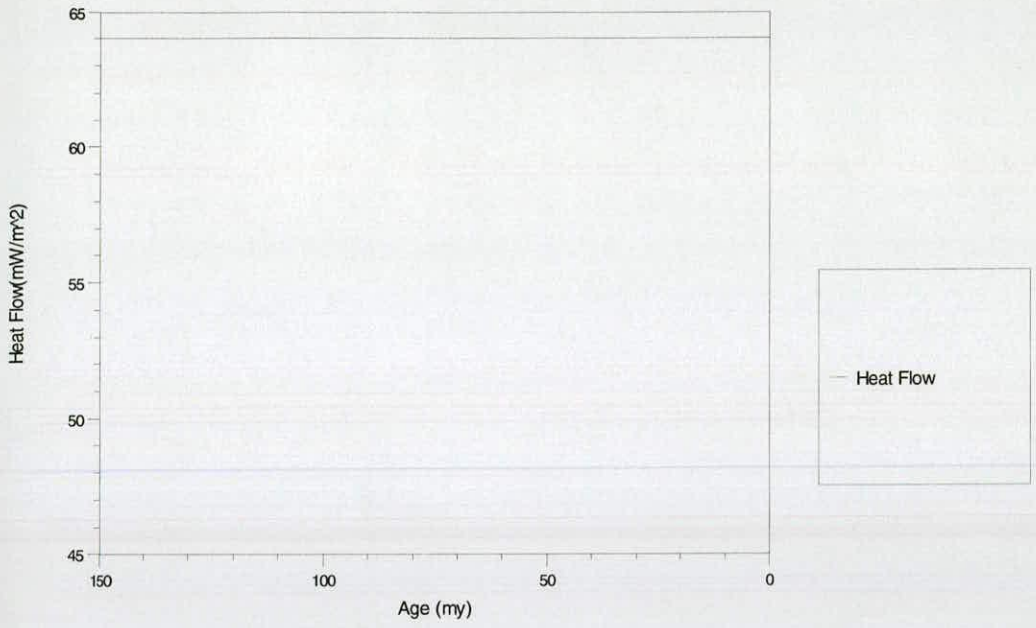

CALIBRATION HEAT FLOW: 46 mWm^-2, constant

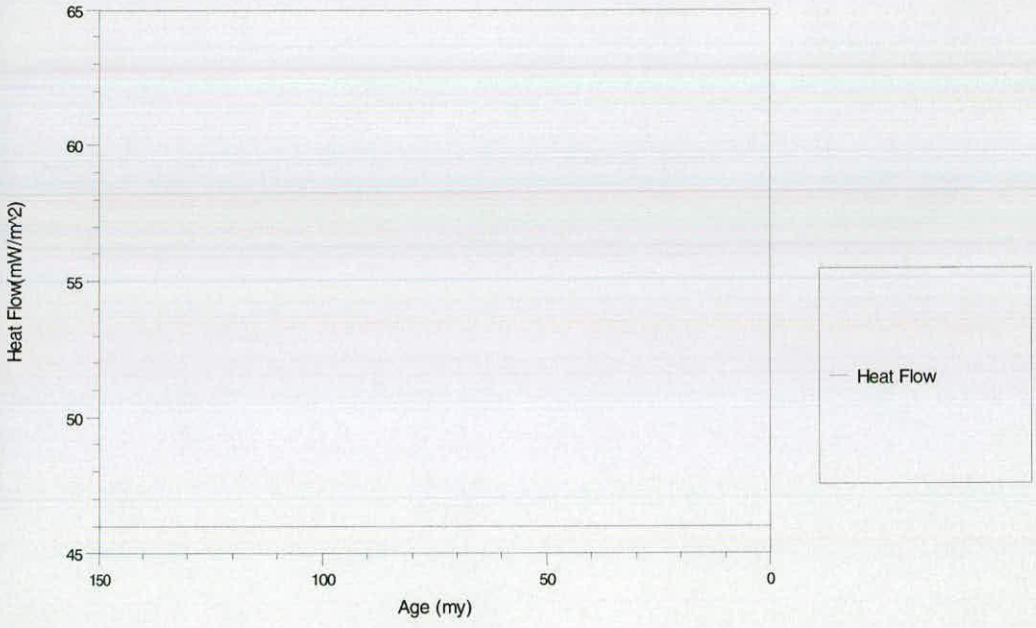

Figure 5.21 Heat flow for both the default model and the simplest calibrated simulation.

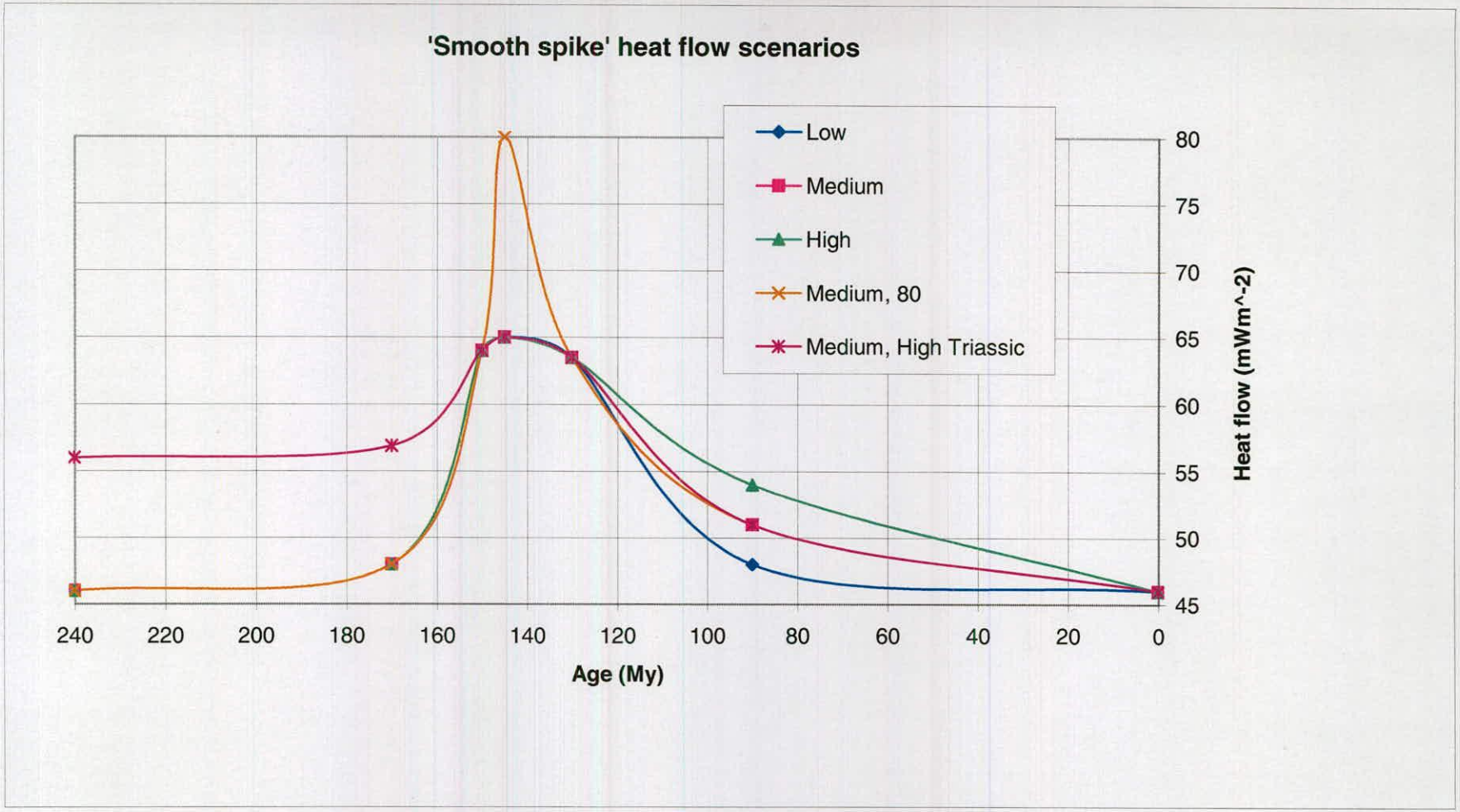

Figure 5.22 Transient heat flow scenarios for the Magnus model. The general shape and position of the 'smooth spike' is geologically reasonable. The magnitude and specific timing of heat flow change is an assumption.

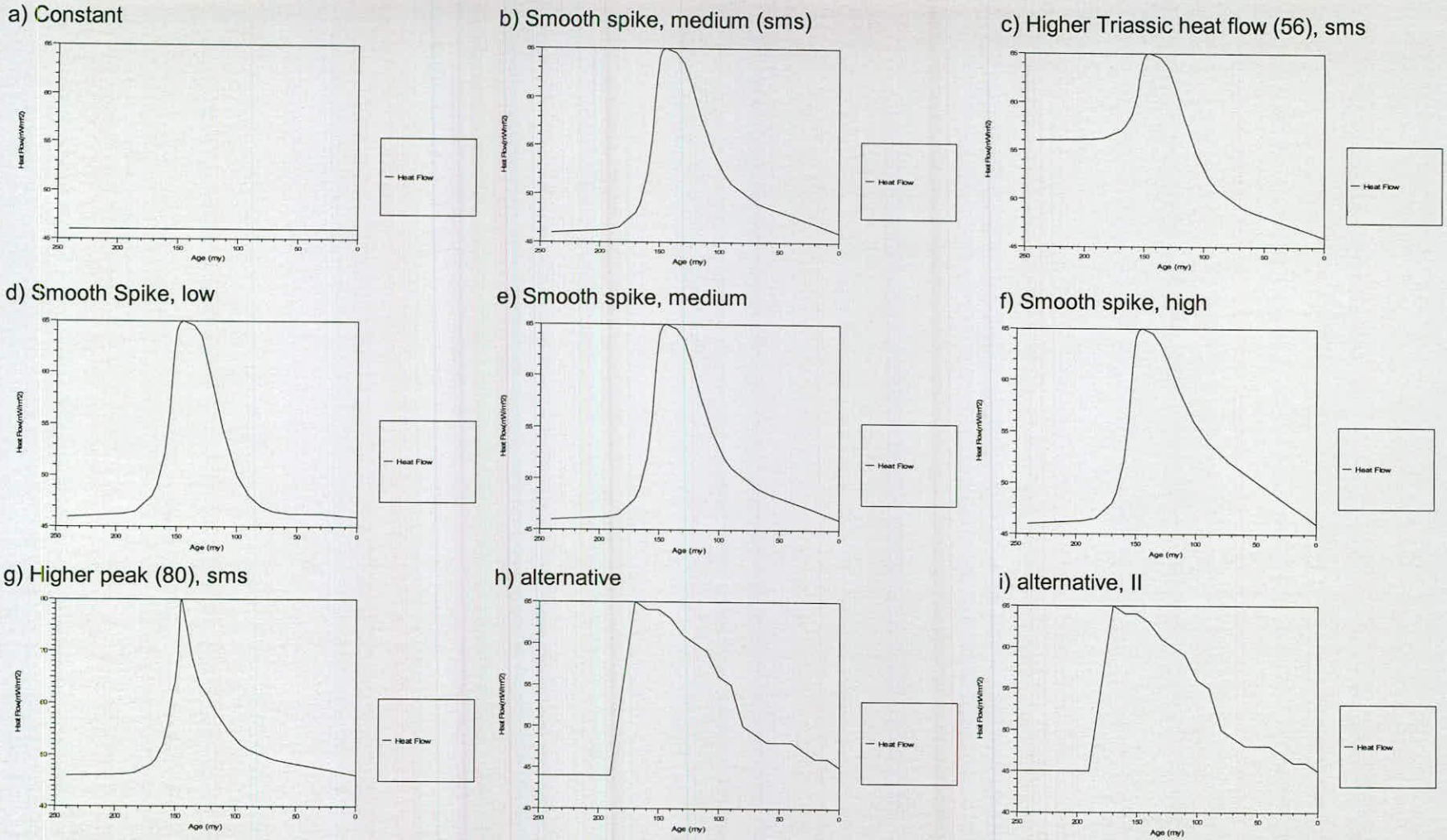

Figure 5.23 Heat flows resulting in a calibrated simulation. Figures a-b are used for model calibration. Figures c-g test the sensitivity of the model to variations in the simple heat flow scenario. Figures h-i are examples of alternative heat flow scenarios that indicate robust calibration.

HEAT FLOW: constant, 46 mWm^-2
SURFACE TEMPERATURE: constant, 5degC

HEATFLOW: constant

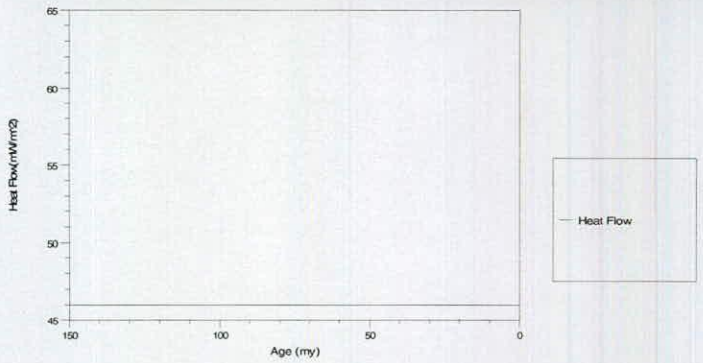

RESERVOIR: accumulation history and calibration parameters

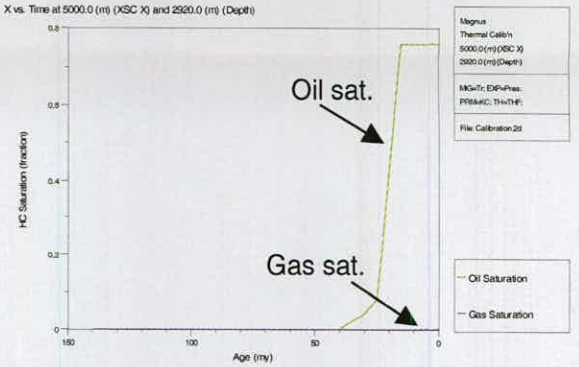

	Porosity	Permeability	Temperature	Pressure	Maturity, Ro
Res' Datum	12%	91 mD	115 degC	6649 psi	0.68%

DEEP SOURCE AREA: generation and expulsion

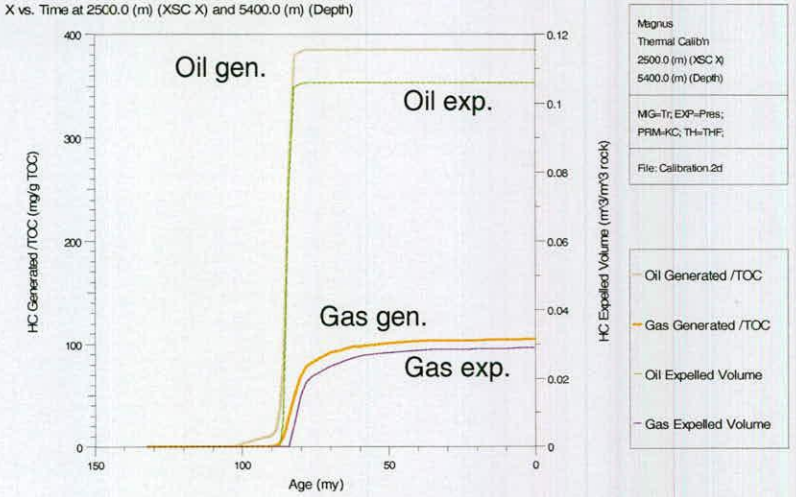

SHALLOW SOURCE AREA: generation and expulsion

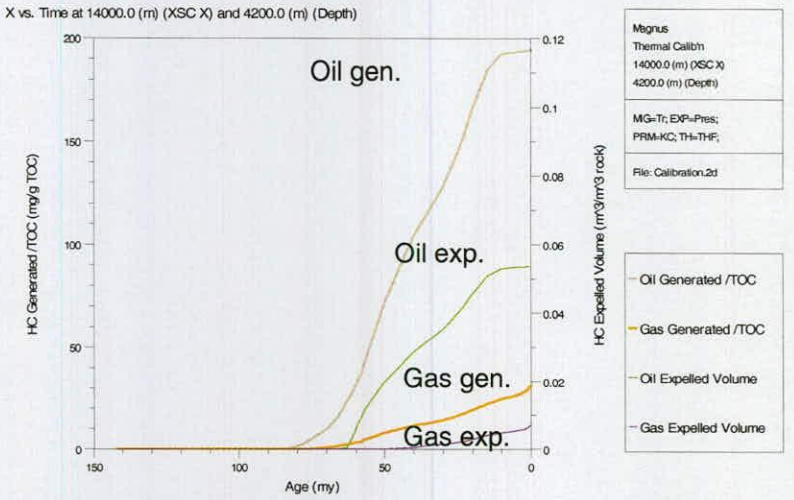

Figure 24 Modelled hydrocarbon response to heat flow and surface temperature parameters: the accumulation history for the Magnus, and related timing of generation and expulsion from the deep and shallow source areas. Simulated reservoir conditions for the present day calibration parameters are included.

HEAT FLOW: transient, 46-65 mWm^-2
SURFACE TEMPERATURE: constant, 5degC

HEATFLOW: smooth spike, medium

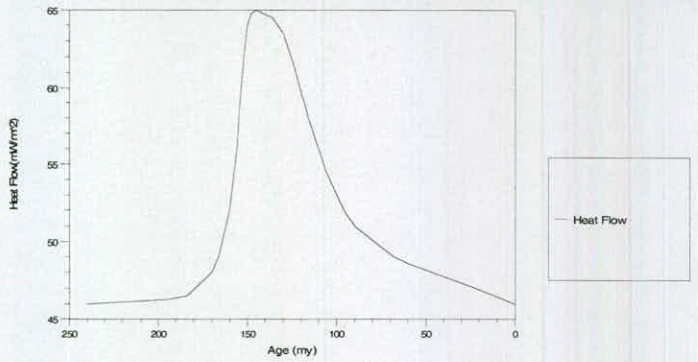

RESERVOIR: accumulation history and calibration parameters

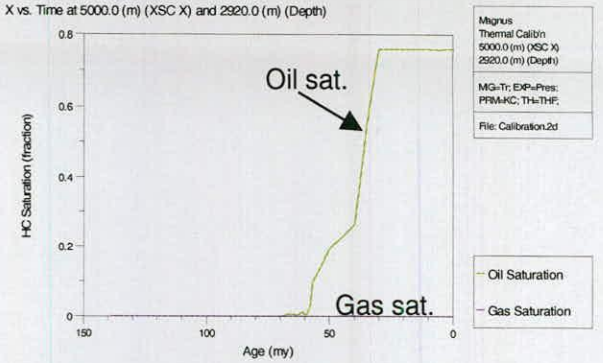

	Porosity	Permeability	Temperature	Pressure	Maturity, Ro
Res' Datum	12%	91	116	6646	0.69%

DEEP SOURCE AREA: generation and expulsion

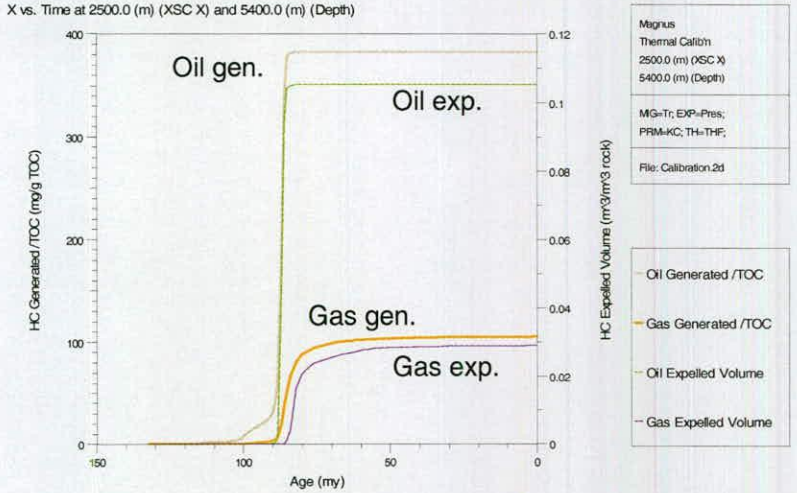

SHALLOW SOURCE AREA: generation and expulsion

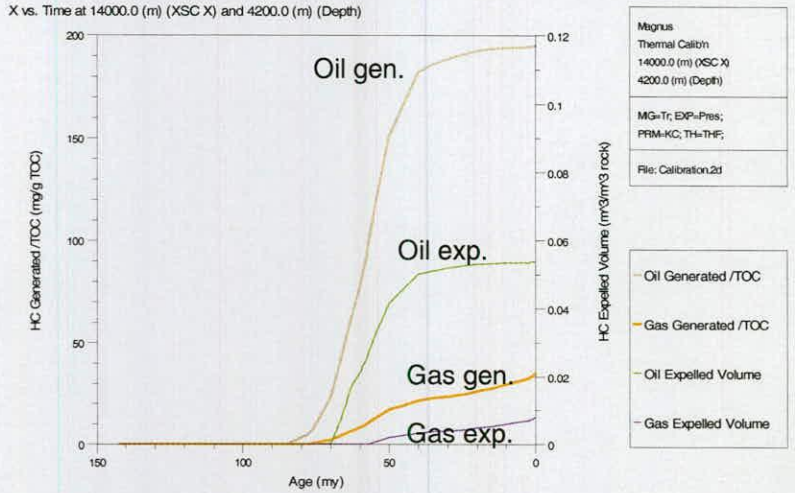

Figure 25 Modelled hydrocarbon response to heat flow and surface temperature parameters: the accumulation history for the Magnus, and related timing of generation and expulsion from the deep and shallow source areas. Simulated reservoir conditions for the present day calibration parameters are included.

HEAT FLOW: transient, 46-65 mWm^-2
SURFACE TEMPERATURE: constant, 5degC

HEATFLOW: high Triassic heat flow

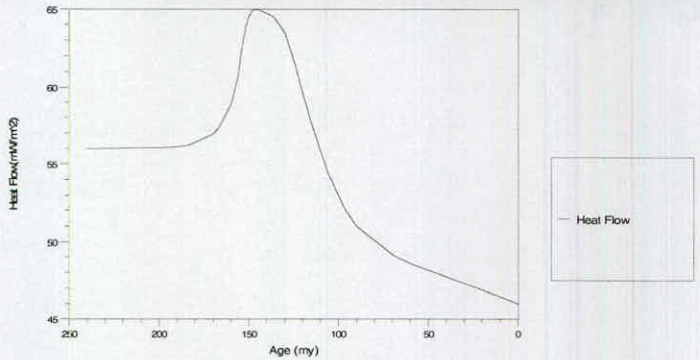

RESERVOIR: accumulation history and calibration parameters

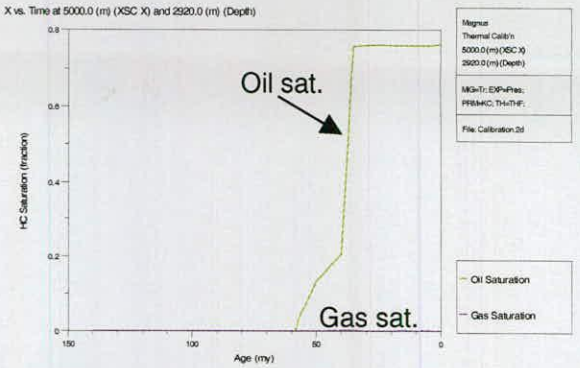

	Porosity	Permeability	Temperature	Pressure	Maturity, Ro
Res' Datum	12%	91	116	6646	0.69%

DEEP SOURCE AREA: generation and expulsion

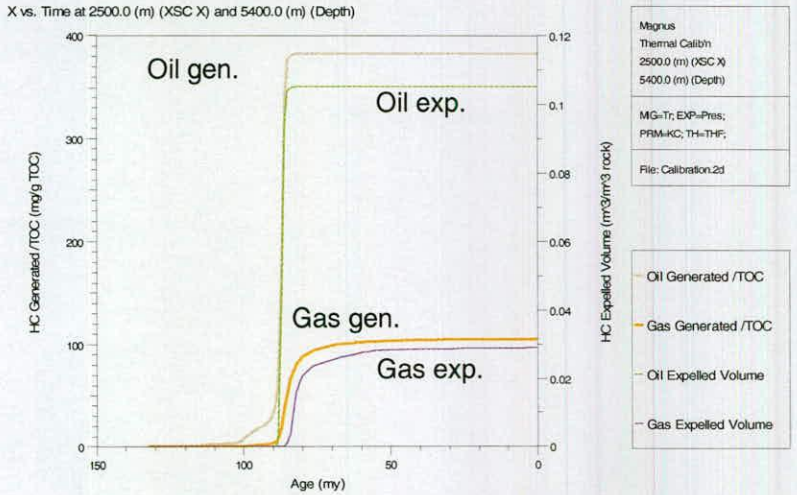

SHALLOW SOURCE AREA: generation and expulsion

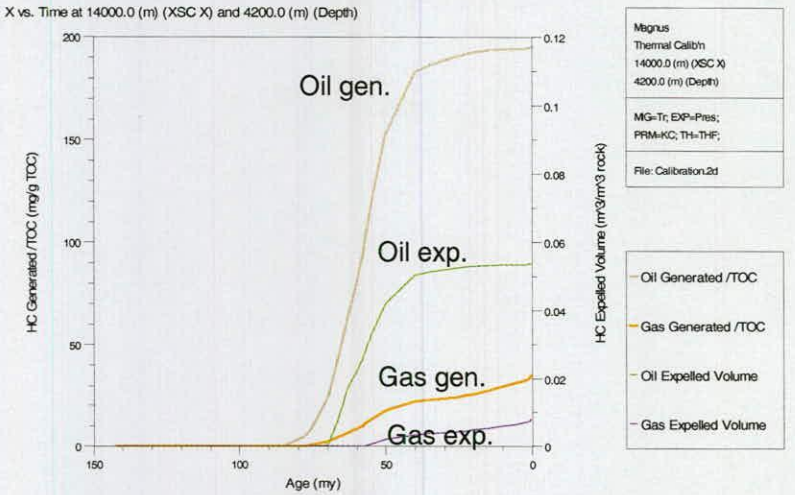

Figure 26 Modelled hydrocarbon response to heat flow and surface temperature parameters: the accumulation history for the Magnus, and related timing of generation and expulsion from the deep and shallow source areas. Simulated reservoir conditions for the present day calibration parameters are included.

HEAT FLOW: transient, 46-65 mWm^-2
SURFACE TEMPERATURE: constant, 5degC

HEATFLOW: smooth spike, low

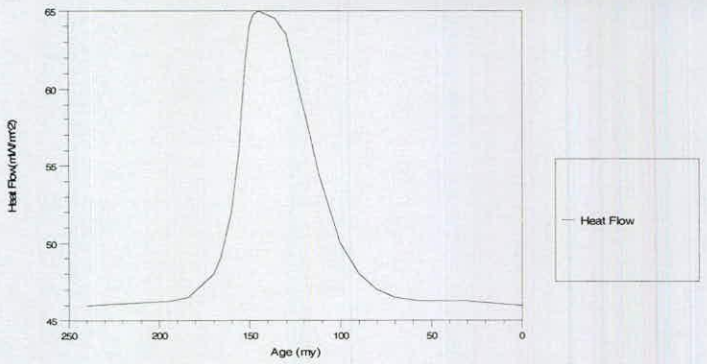

RESERVOIR: accumulation history and calibration parameters

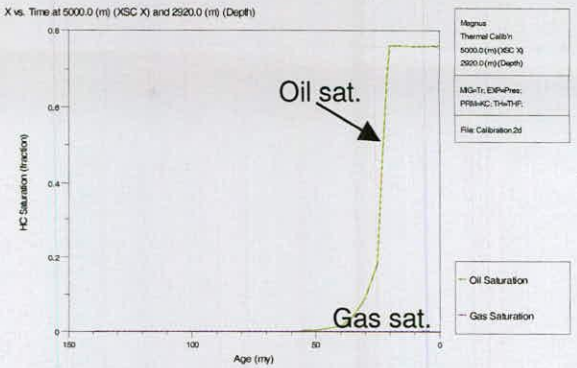

	Porosity	Permeability	Temperature	Pressure	Maturity, Ro
Res' Datum	12%	91 mD	115	6649	0.68%

DEEP SOURCE AREA: generation and expulsion

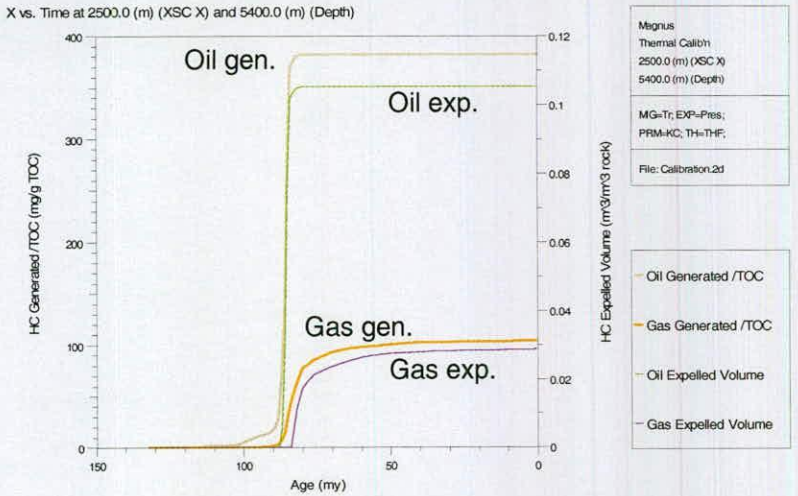

SHALLOW SOURCE AREA: generation and expulsion

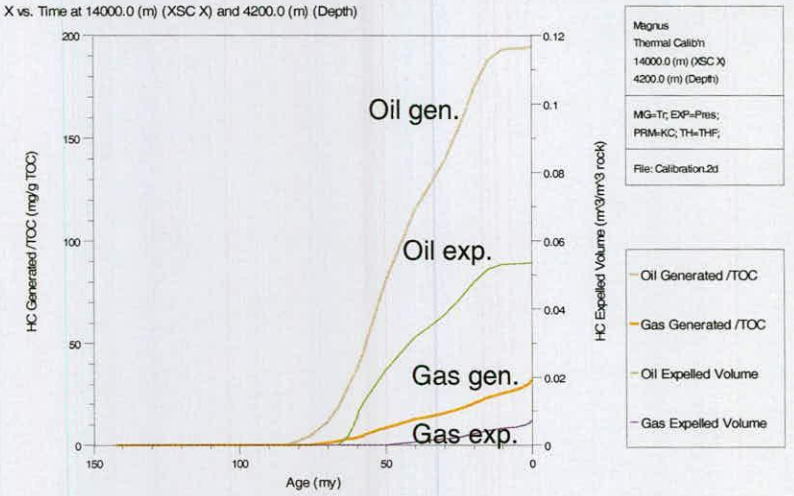

Figure 27 Modelled hydrocarbon response to heat flow and surface temperature parameters: the accumulation history for the Magnus, and related timing of generation and expulsion from the deep and shallow source areas. Simulated reservoir conditions for the present day calibration parameters are included.

e) *HEAT FLOW:* transient, 46-65 mWm^-2
SURFACE TEMPERATURE: constant, 5degC

HEATFLOW: smooth spike, high

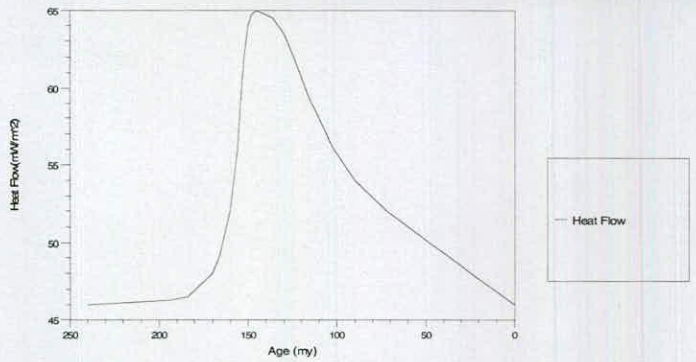

RESERVOIR: accumulation history and calibration parameters

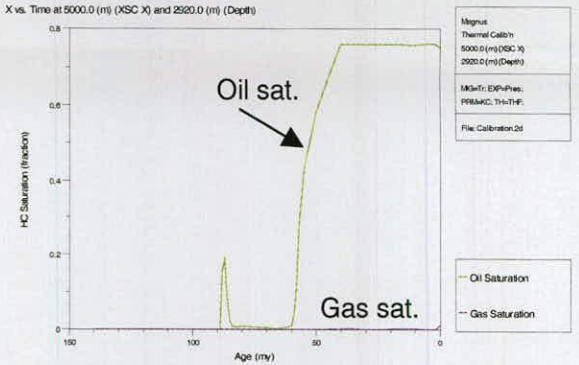

	Porosity	Permeability	Temperature	Pressure	Maturity, Ro
Res' Datum	12%	91	116	6643	0.70%

DEEP SOURCE AREA: generation and expulsion

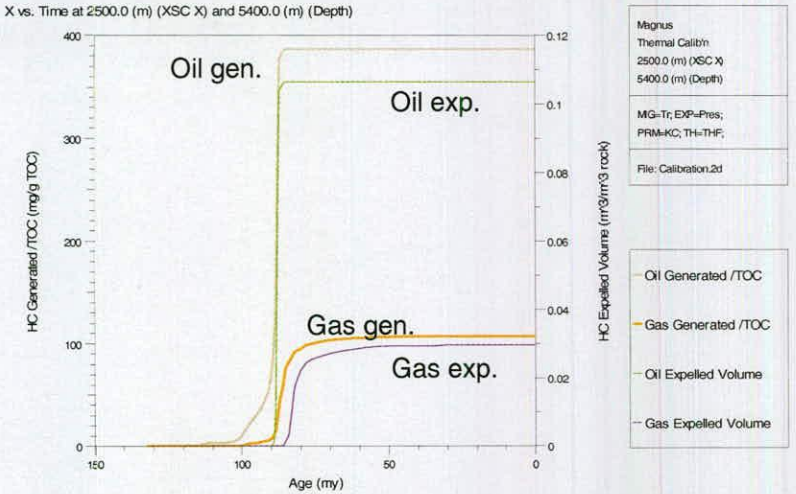

SHALLOW SOURCE AREA: generation and expulsion

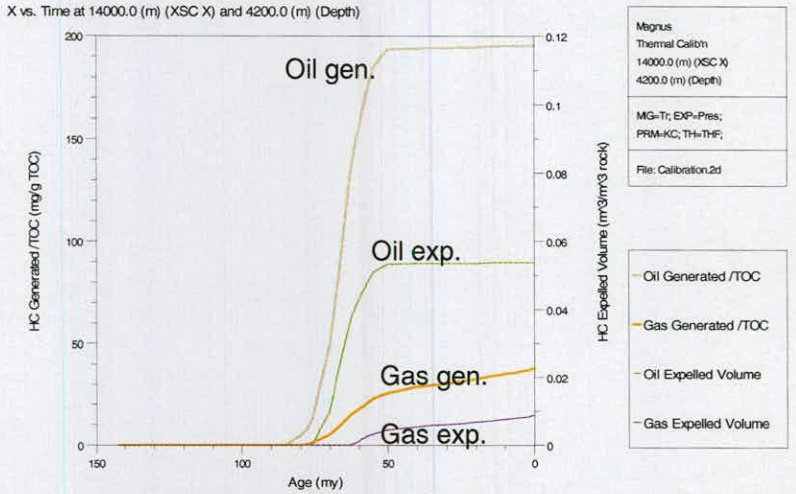

Figure 28 Modelled hydrocarbon response to heat flow and surface temperature parameters: the accumulation history for the Magnus, and related timing of generation and expulsion from the deep and shallow source areas. Simulated reservoir conditions for the present day calibration parameters are included.

HEAT FLOW: transient, 46-80 mWm^-2
SURFACE TEMPERATURE: constant, 5degC

HEATFLOW: high peak

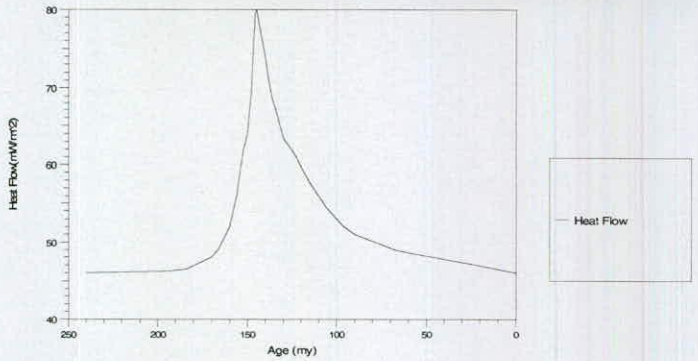

RESERVOIR: accumulation history and calibration parameters

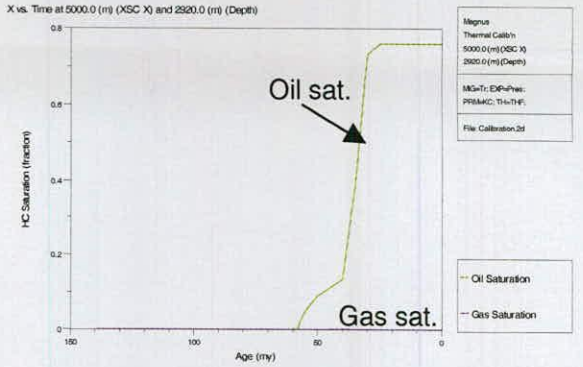

	Porosity	Permeability	Temperature	Pressure	Maturity, Ro
Res' Datum	12%	91 mD	116	6645	0.69%

DEEP SOURCE AREA: generation and expulsion

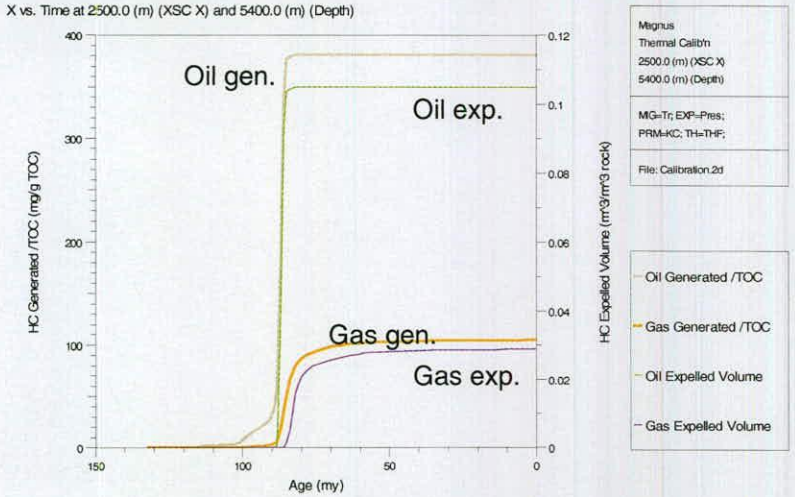

SHALLOW SOURCE AREA: generation and expulsion

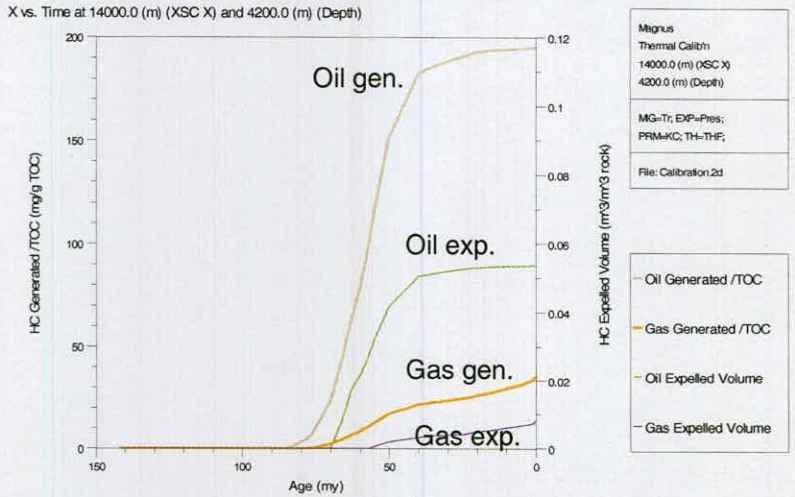

Figure 29 Modelled hydrocarbon response to heat flow and surface temperature parameters: the accumulation history for the Magnus, and related timing of generation and expulsion from the deep and shallow source areas. Simulated reservoir conditions for the present day calibration parameters are included.

HEAT FLOW: transient, 45-65 mWm^-2
SURFACE TEMPERATURE: constant, 5degC

HEATFLOW: alternative

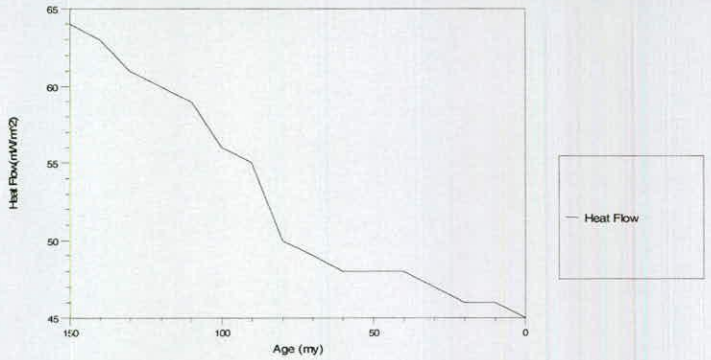

RESERVOIR: accumulation history and calibration parameters

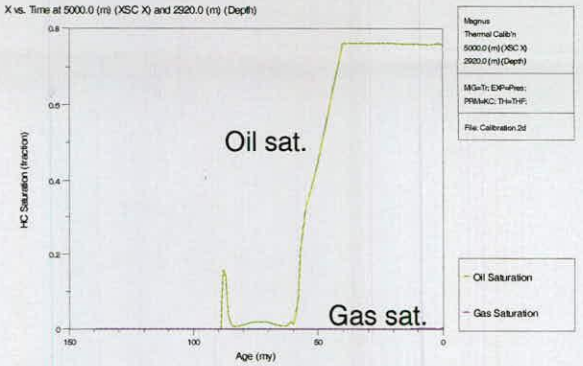

	Porosity	Permeability	Temperature	Pressure	Maturity, Ro
Res' Datum	12%	91 mD	113 degC	6648 psi	0.68%

DEEP SOURCE AREA: generation and expulsion

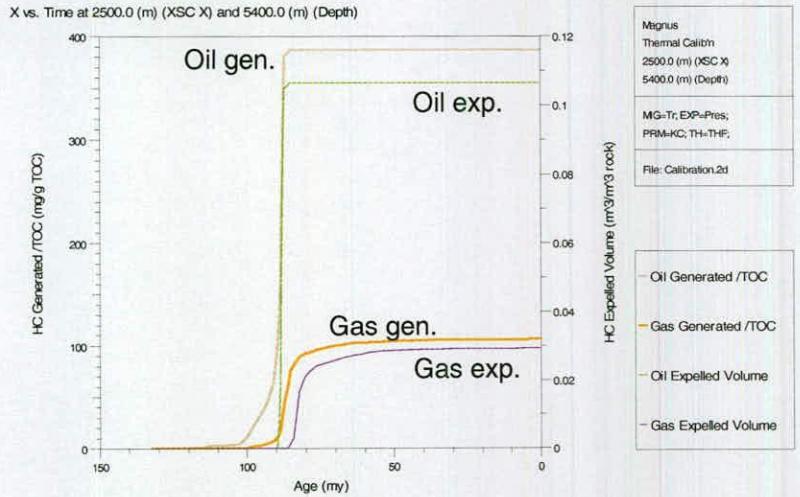

SHALLOW SOURCE AREA: generation and expulsion

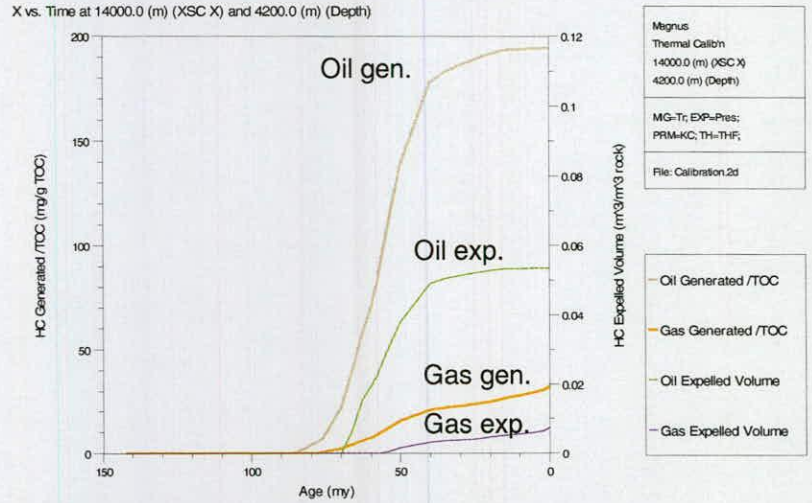

Figure 30 Modelled hydrocarbon response to heat flow and surface temperature parameters: the accumulation history for the Magnus, and related timing of generation and expulsion from the deep and shallow source areas. Simulated reservoir conditions for the present day calibration parameters are included.

HEAT FLOW: transient, 45-65 mWm^-2
SURFACE TEMPERATURE: constant, 5degC

HEATFLOW: alternative II

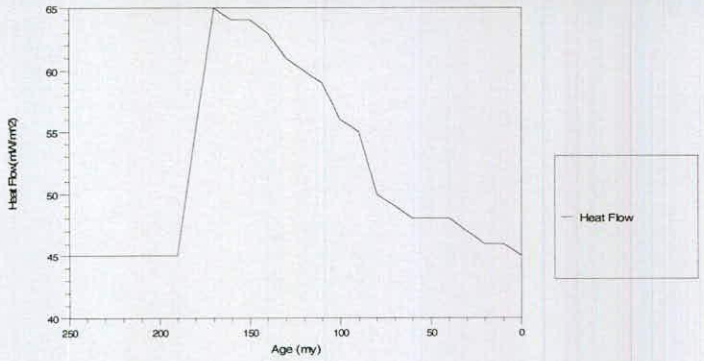

RESERVOIR: accumulation history and calibration parameters

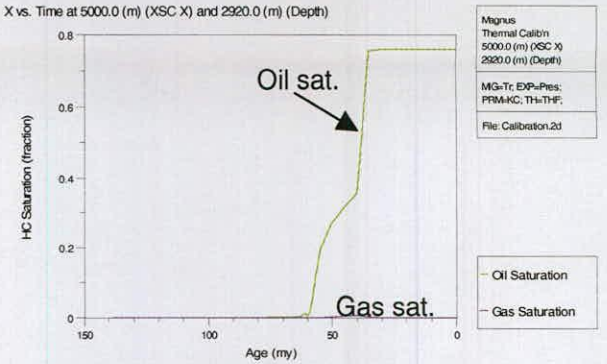

	Porosity	Permeability	Temperature	Pressure	Maturity, Ro
Res' Datum	12%	91	113	6648	0.68%

DEEP SOURCE AREA: generation and expulsion

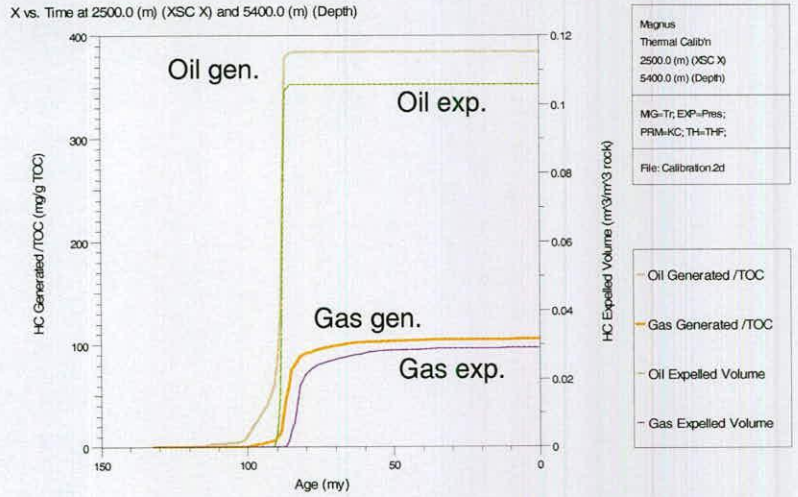

SHALLOW SOURCE AREA: generation and expulsion

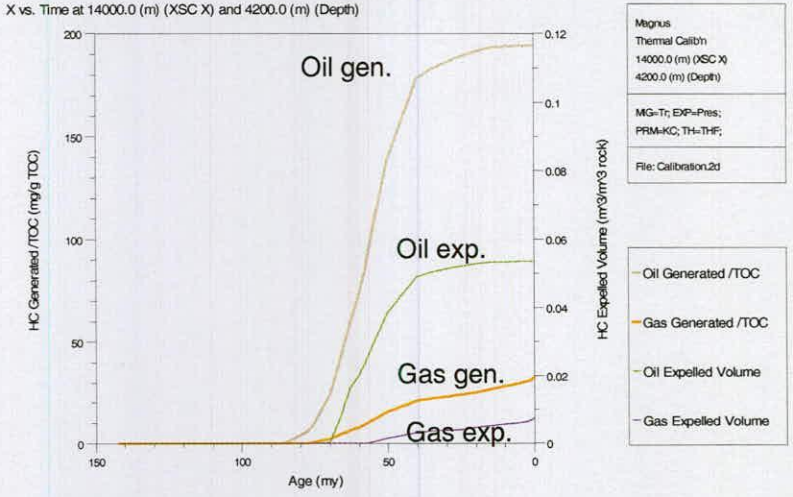

Figure 31 Modelled hydrocarbon response to heat flow and surface temperature parameters: the accumulation history for the Magnus, and related timing of generation and expulsion from the deep and shallow source areas. Simulated reservoir conditions for the present day calibration parameters are included.

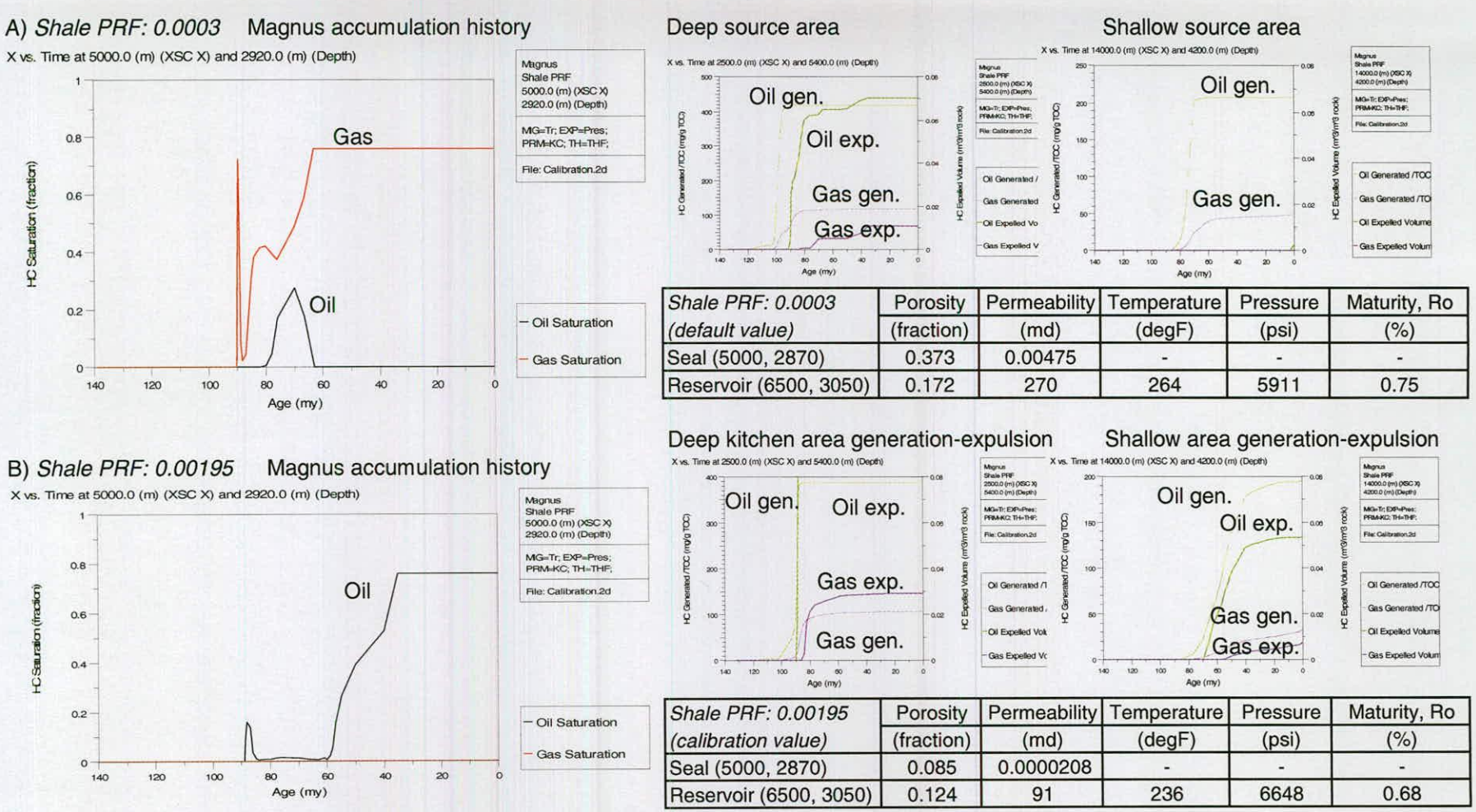

Shale PRF: 0.0003 (default value)	Porosity (fraction)	Permeability (md)	Temperature (degF)	Pressure (psi)	Maturity, Ro (%)
Seal (5000, 2870)	0.373	0.00475	-	-	-
Reservoir (6500, 3050)	0.172	270	264	5911	0.75

Shale PRF: 0.00195 (calibration value)	Porosity (fraction)	Permeability (md)	Temperature (degF)	Pressure (psi)	Maturity, Ro (%)
Seal (5000, 2870)	0.085	0.0000208	-	-	-
Reservoir (6500, 3050)	0.124	91	236	6648	0.68

Figure 32 The effect of Shale Porosity Reduction Factor (PRF) variation on simulated hydrocarbon behaviour for the Magnus model. Figure A is a calibrated simulation with the exception of the default PRF value, 0.0003 Figure B is a calibrated simulation with a much higher PRF, 0.0195. Note the difference in the kitchen areas; seal porosity and permeability; reservoir pressure response and the change in related reservoir parameters.

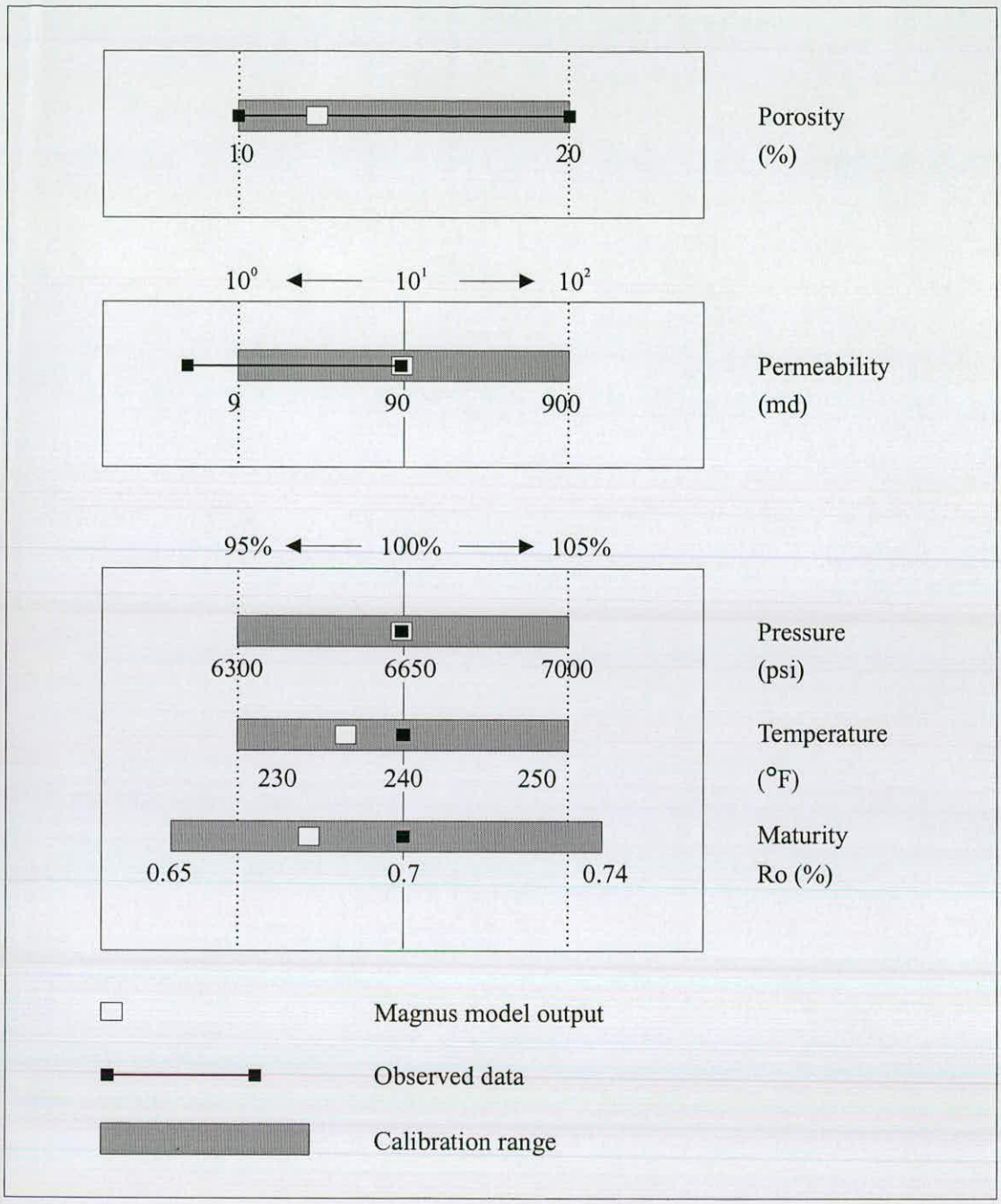

Figure 5.32b A comparison of output values for a calibrated Magnus model simulation with acceptable calibration ranges for measured parameters from the Magnus oil field. These results are satisfactory, falling close to optimum solutions as defined in Figure 5.9.

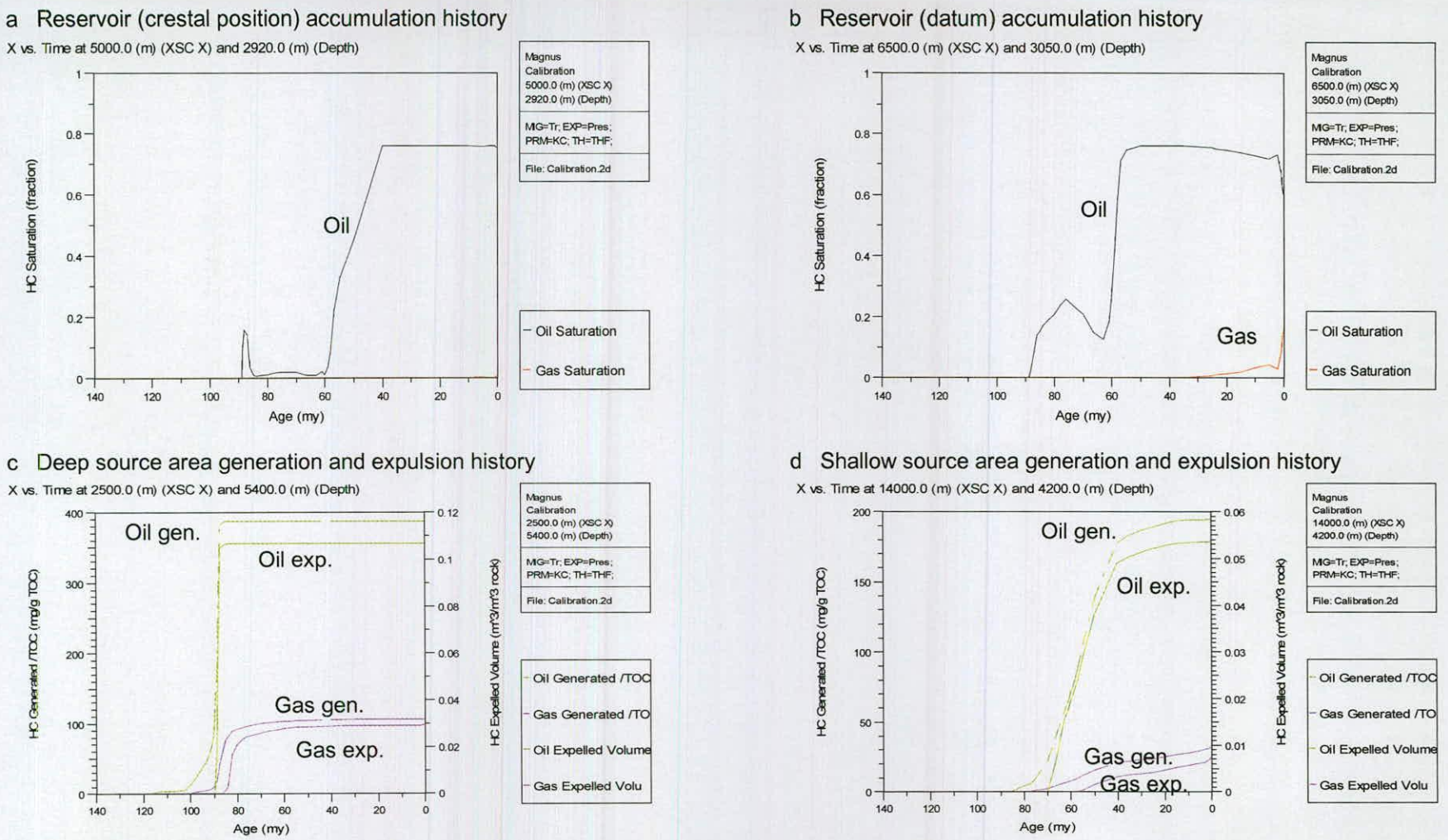

Figure 5.33 Simulated oil and gas behaviour for a fully calibrated Magnus model. Note the relationship between the bimodal oil accumulation history in the reservoir - figures *a* and *b*, and the distinct timings for oil generation and expulsion in the two source areas - figures *c* and *d*.

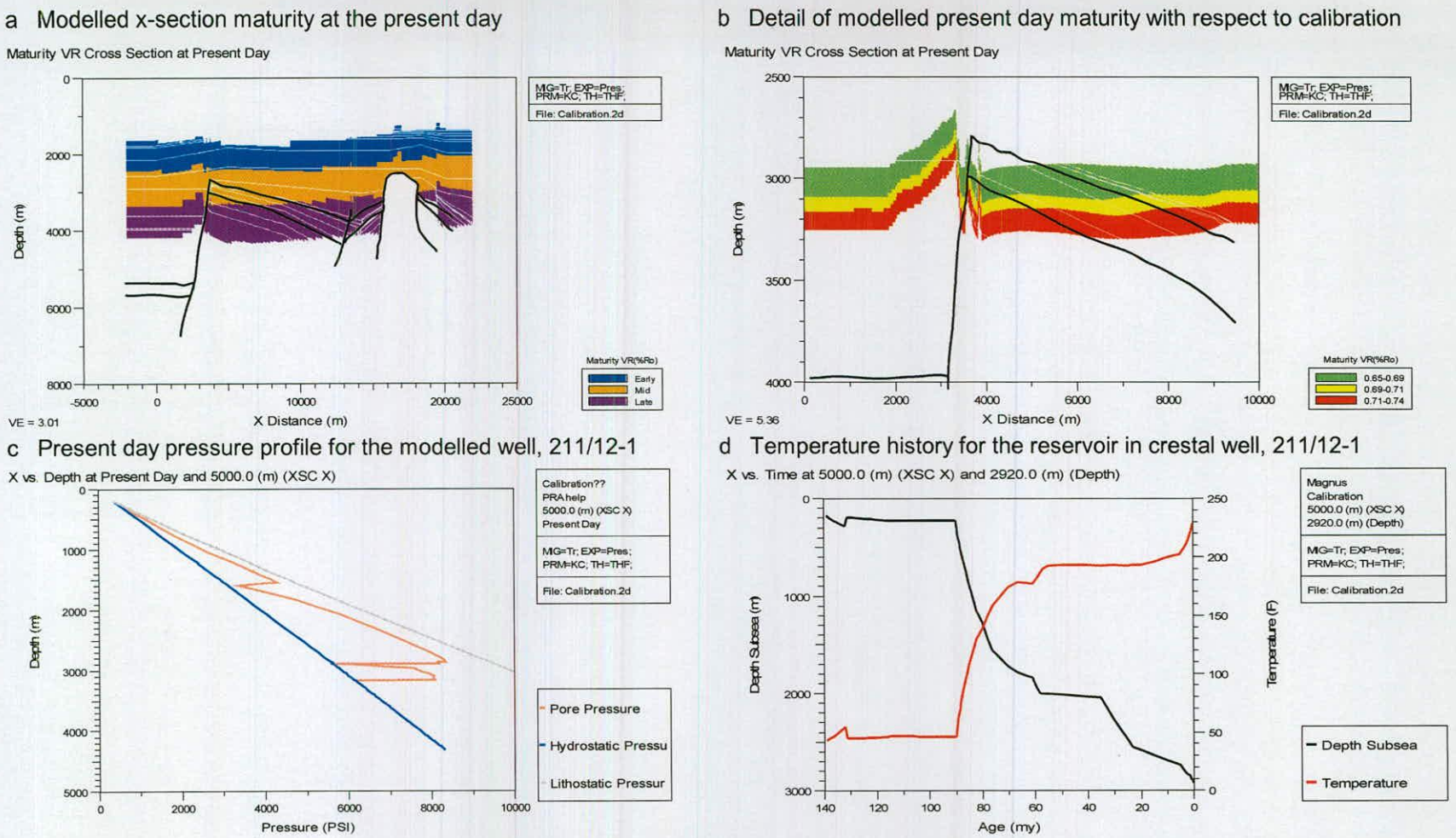

Figure 5.34 Simulated maturity, pressure and temperature output for a fully calibrated magnus model. Note the relationship between burial history and temperature evolution - figure *d*, the two overpressure peaks in the shale section - figure *c*, and the narrow band for simulated maturity, which relates to the error bar on the vitrinite reflection calibration point - figure *b*.

MODEL SENSIVITY TO SHALE PRF ALTERATION: calibrated reservoir parameters

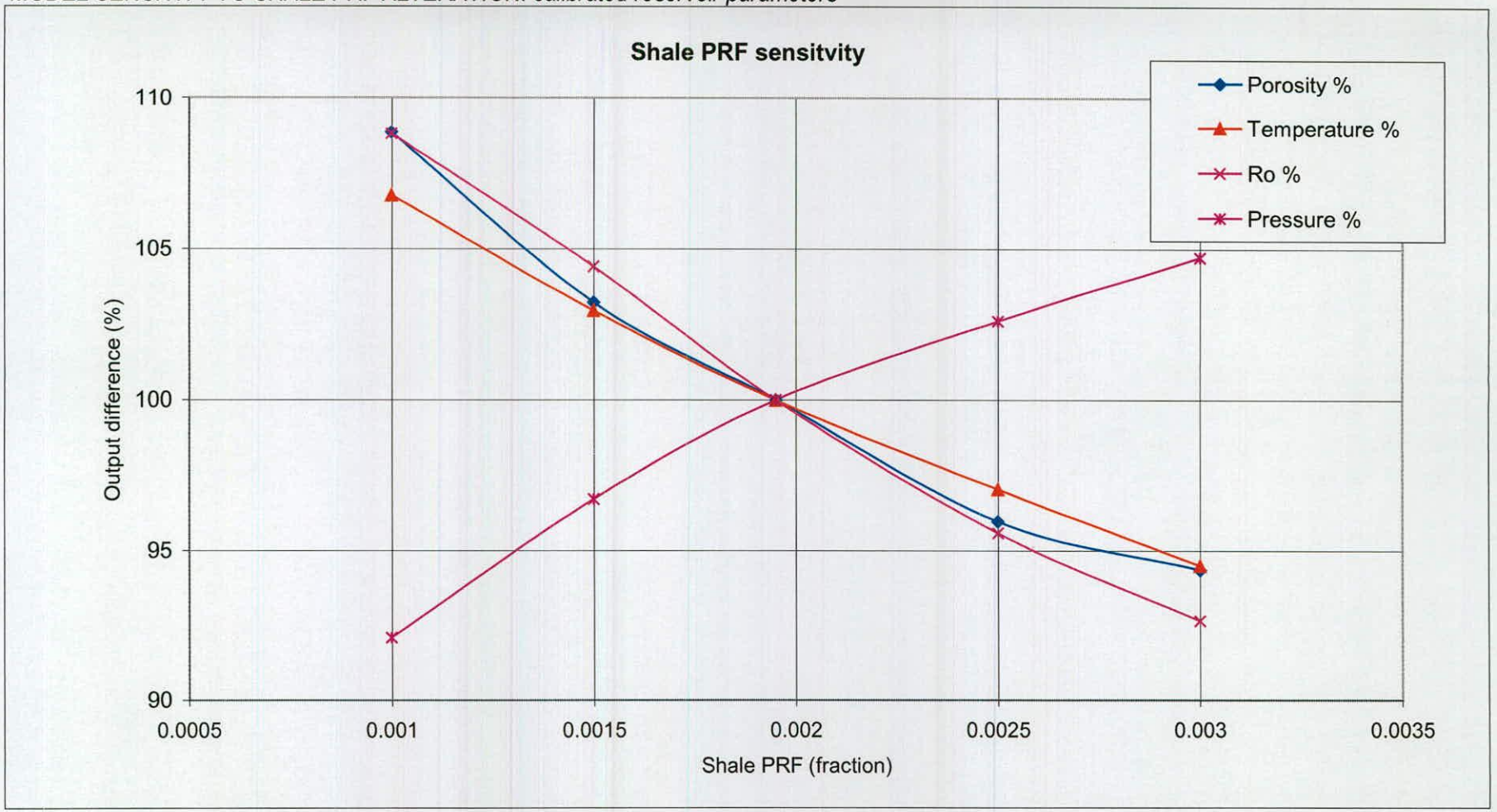

Figure 5.35 Model sensitivity to shale Porosity Reduction Factor (PRF). The curves crosses at the output values for a calibrated simulation, with a PRF value of 0.00195. The effect of PRF alteration on the ouptut parameters is shown in % difference from the original calibration.

MODEL SENSITIVITY TO SHALE PRF ALTERATION: shale and sandstone permeability

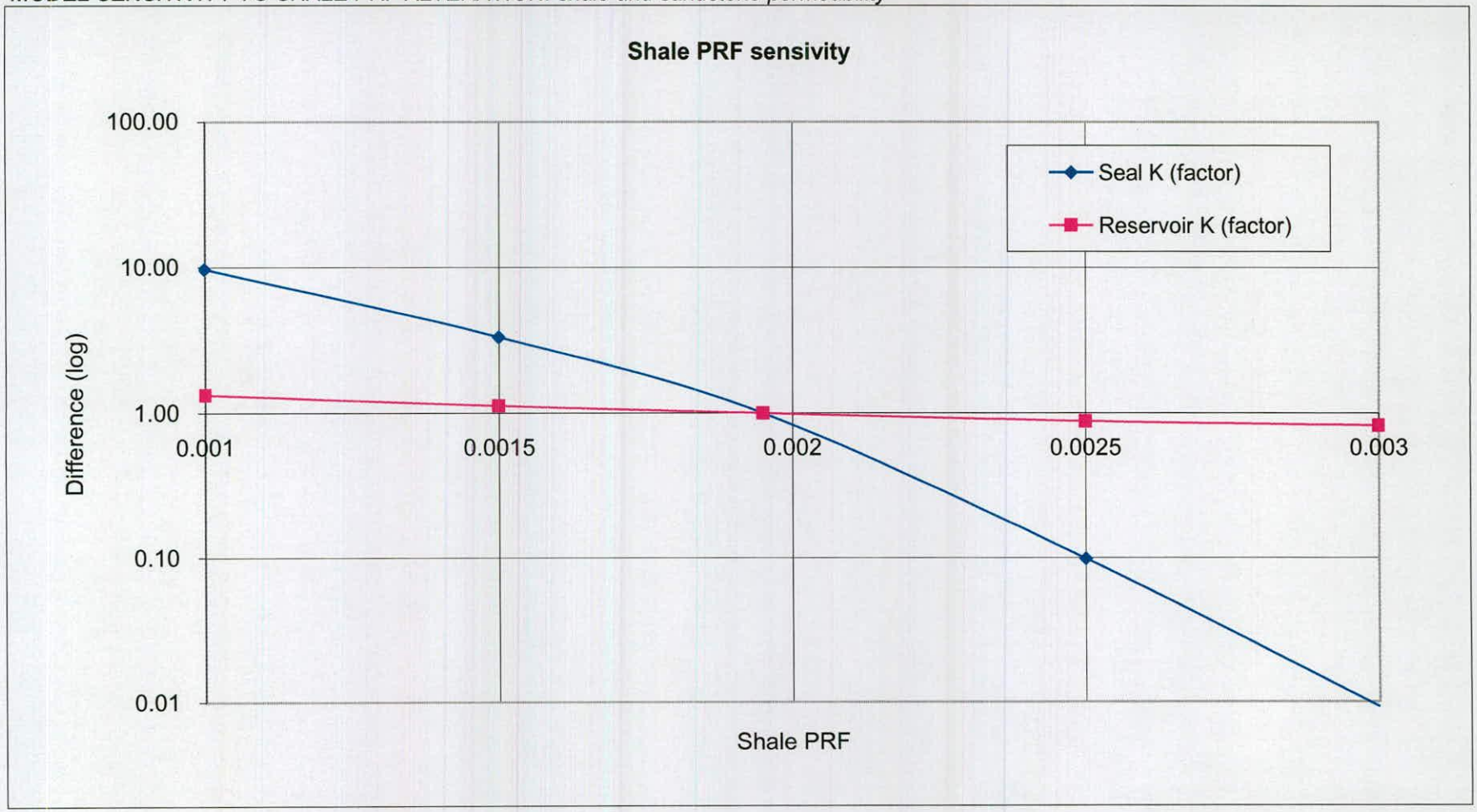

Figure 5.36 Model sensitivity to shale Porosity Reduction Factor (PRF). The curves crosses at the output values for a calibrated simulation, with a PRF value of 0.00195. The effect of PRF alteration on the ouptut is shown in orders of magnitude from the original calibration.

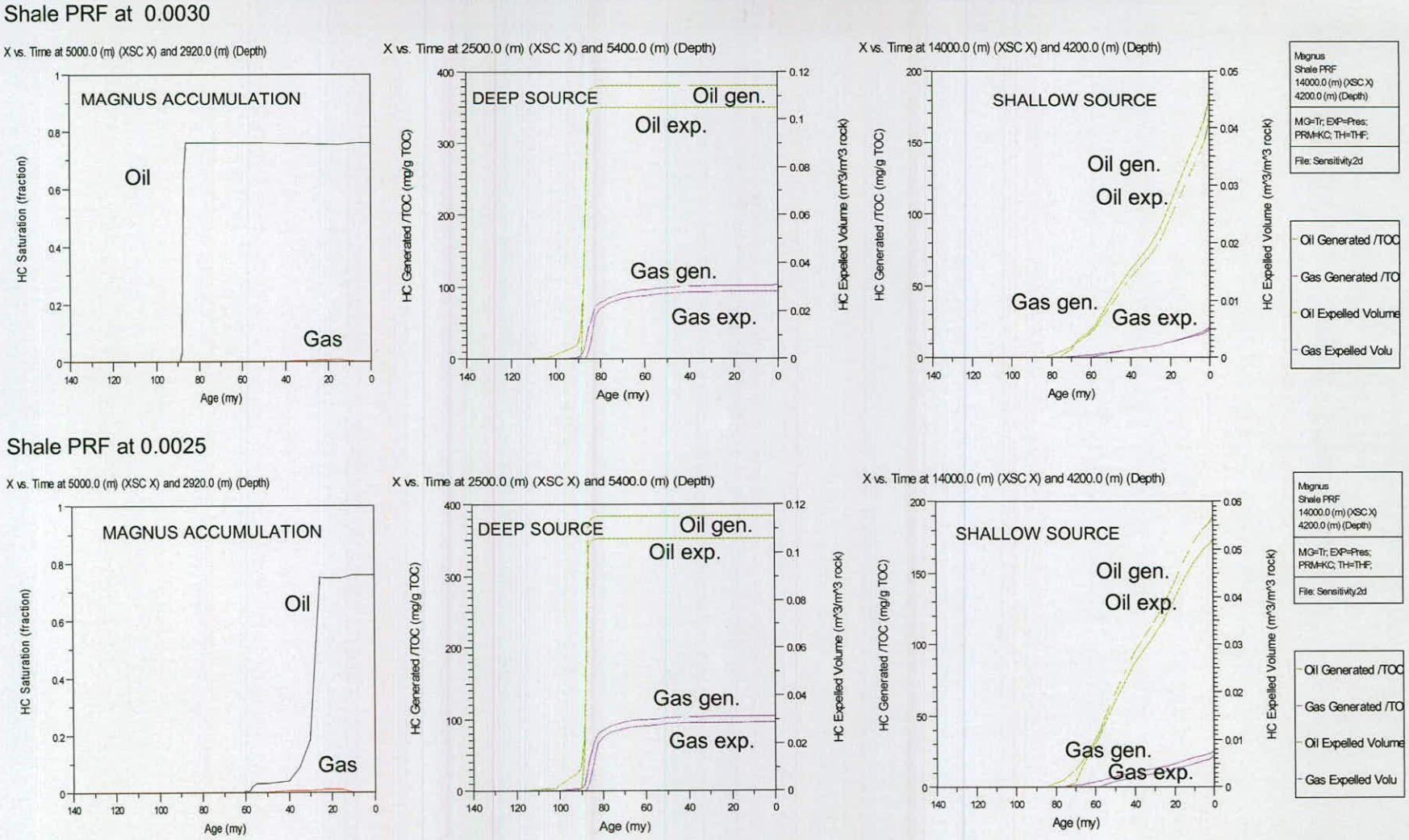

Figure 5.37 Model sensitivity - the effect of Shale Porosity Reduction Factor (PRF) variation on the hydrocarbon system

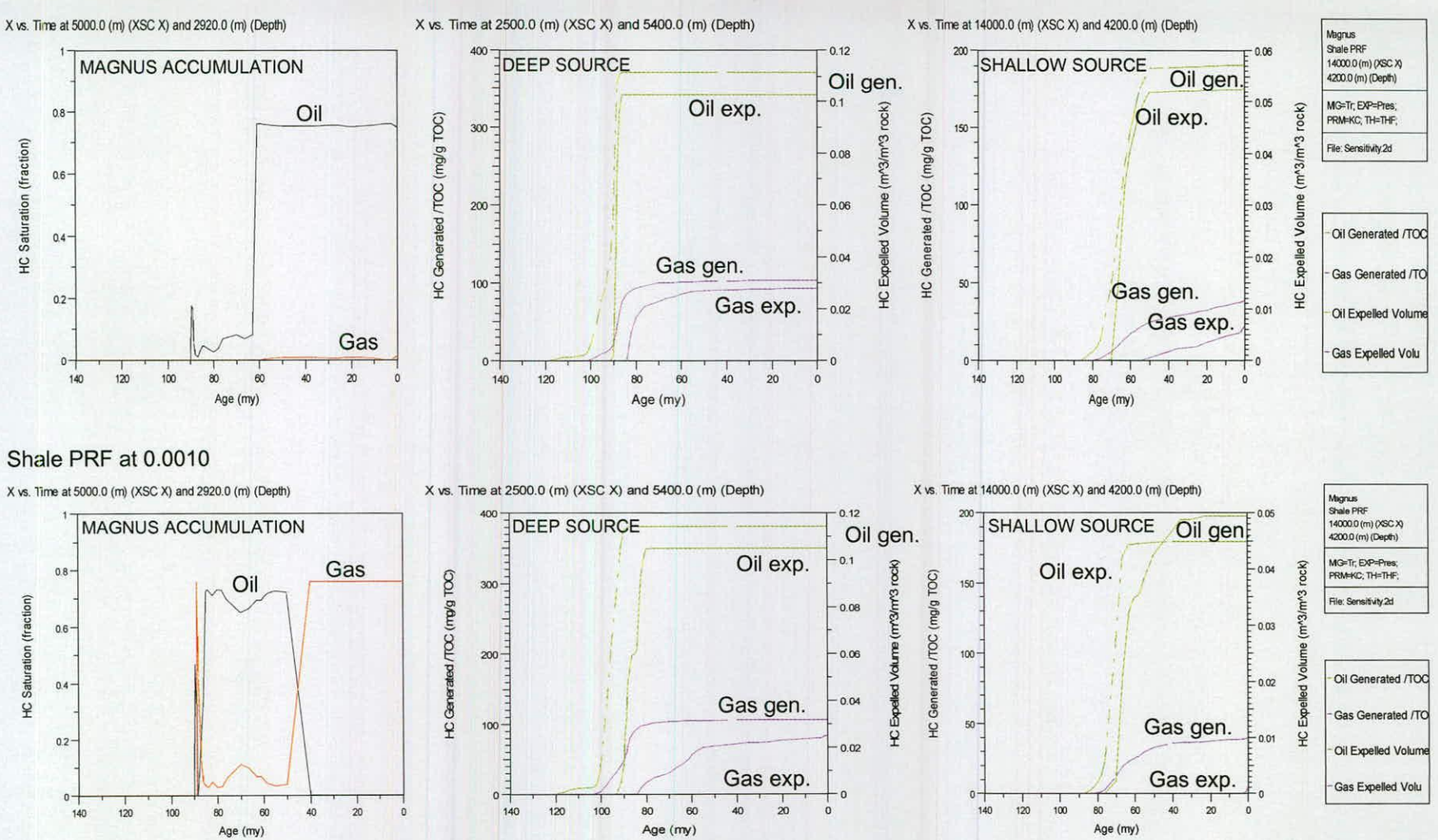

Figure 5.38 Model sensitivity: the effect of Shale Porosity Reduction Factor (PRF) variation on the simulated hydrocarbon system.

DEEP OIL GENERATION IN RESPONSE TO DIFFERENT HEAT FLOW MODELS

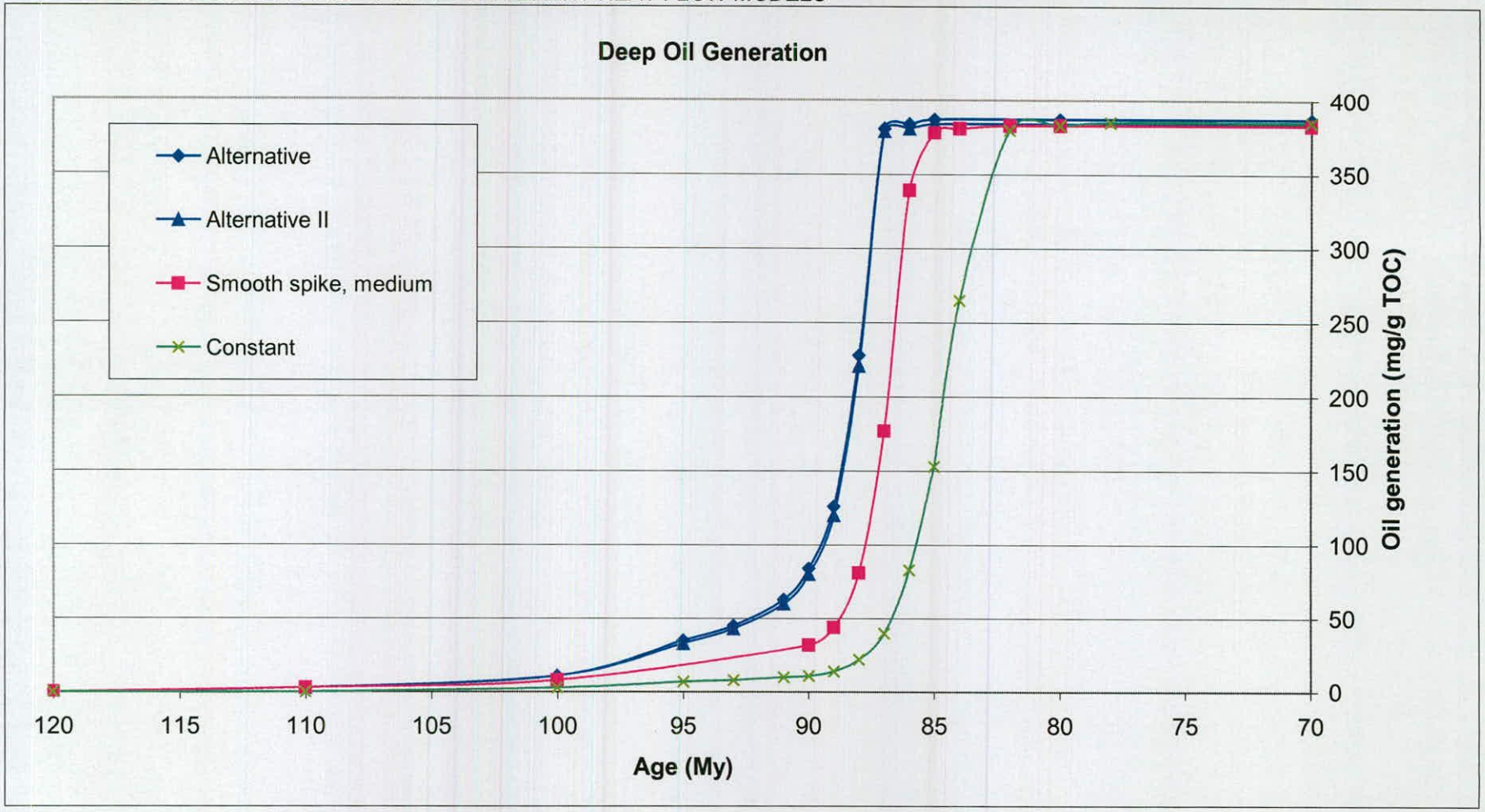

Figure 5.39 Deep oil generation for the Magnus model in response to different heat flow scenarios. The timing of oil generation for the deep source area occurs at about 95-85 My for all calibrated heat flow scenarios. In this respect, the model output is stable.

DEEP OIL EXPULSION IN RESPONSE TO DIFFERENT HEAT FLOW MODELS

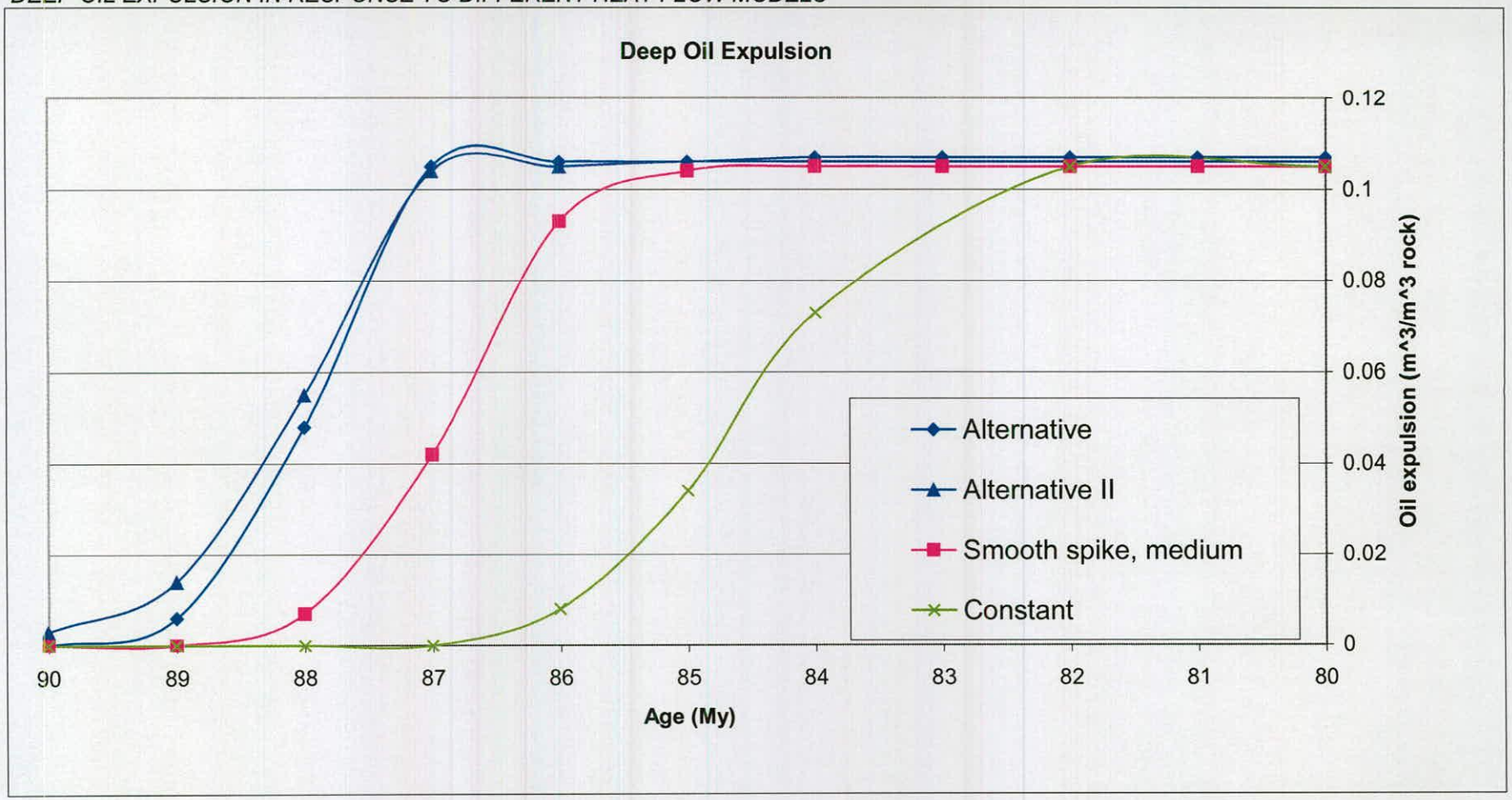

Figure 5.40 Deep oil expulsion for the Magnus model in response to different heat flow scenarios. The timing of oil expulsion for the deep source area occurs at about 90-86 My for all calibrated heat flow scenarios except 'Constant', which has a range of 86-82 My. The model output is stable with regard to the geologically reasonable heat flow scenarios.

SHALLOW OIL GENERATION IN RESPONSE TO DIFFERENT HEAT FLOW MODELS

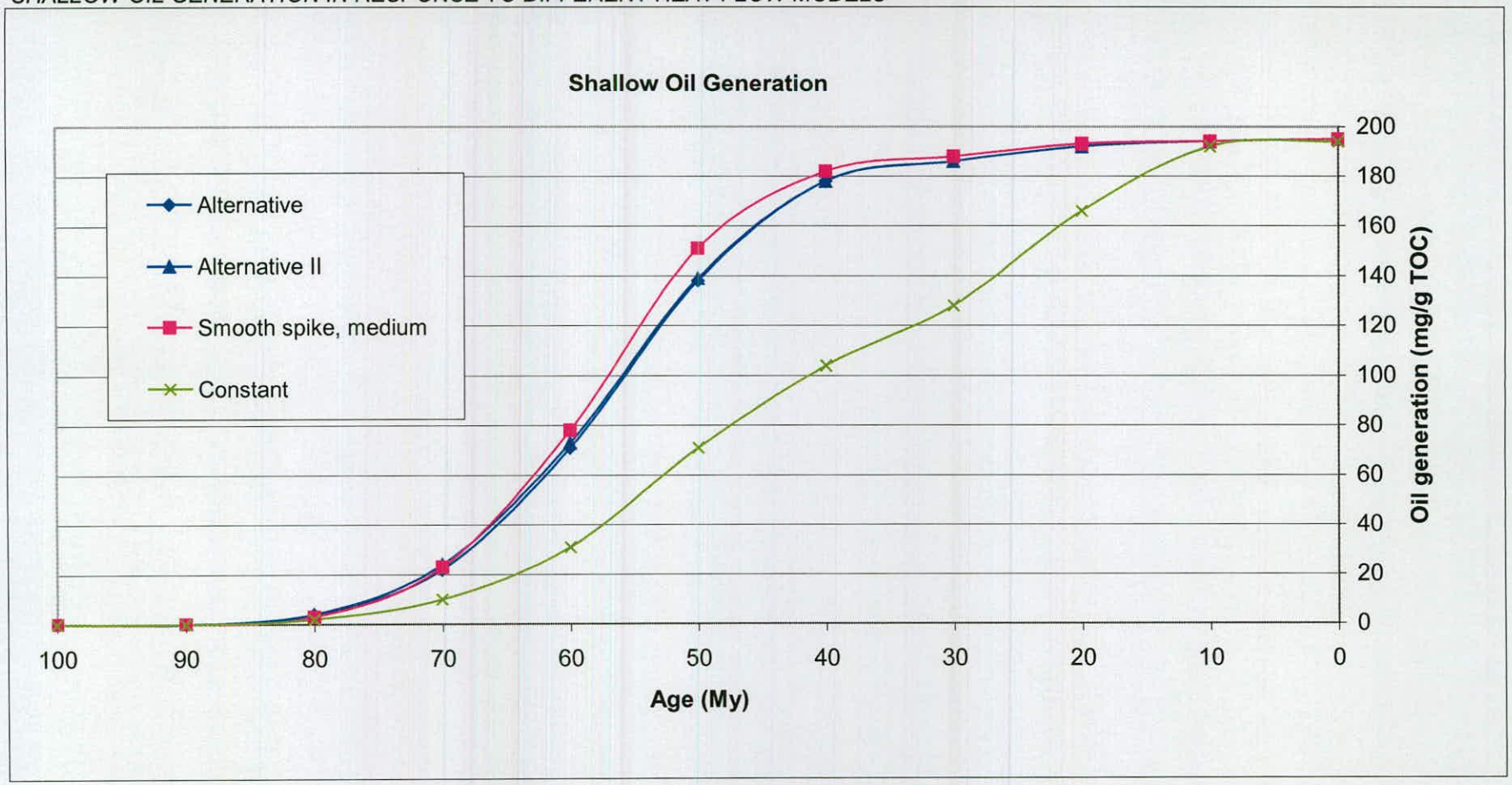

Figure 5.41 Shallow oil generation for the Magnus model in response to different heat flow scenarios. The timing of oil generation for the shallow source area occurs at about 80-40 My for all calibrated heat flow scenarios except 'Constant', which has a range of 80-10 My. The model output is stable with regard to the geologically reasonable heat flow scenarios.

SHALLOW OIL EXPULSION IN RESPONSE TO DIFFERENT HEAT FLOW MODELS

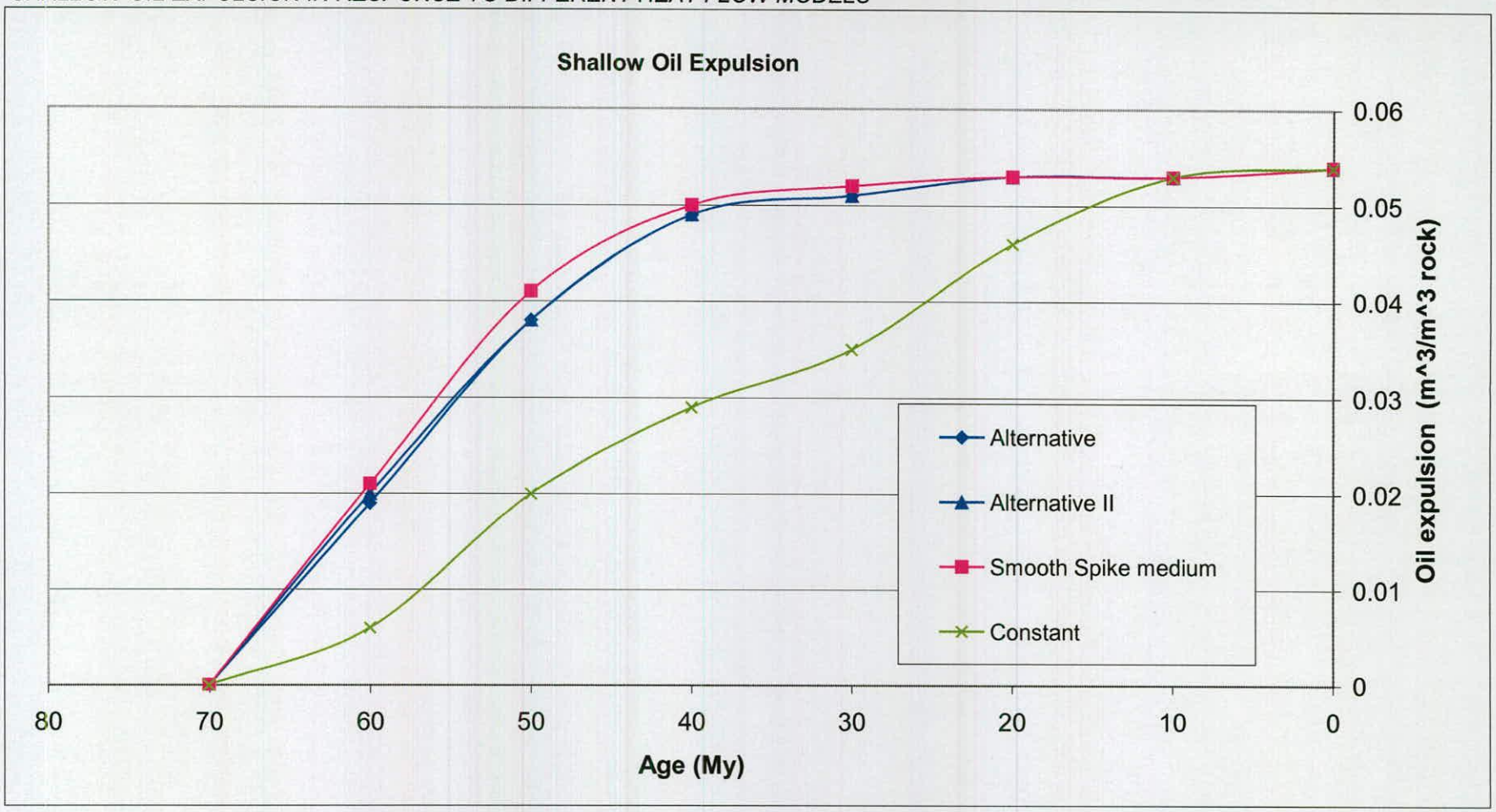

Figure 5.42 Shallow oil expulsion for the Magnus model in response to different heat flow scenarios. The timing of oil expulsion for the shallow source area occurs from 70-40 My for all calibrated heat flow scenarios except 'Constant', which has a range of 70-10 My. The model output is stable with regard to the geologically reasonable heat flow scenarios.

MODES OF ACCUMULATION FOR THREE TYPES OF HEAT FLOW MODEL

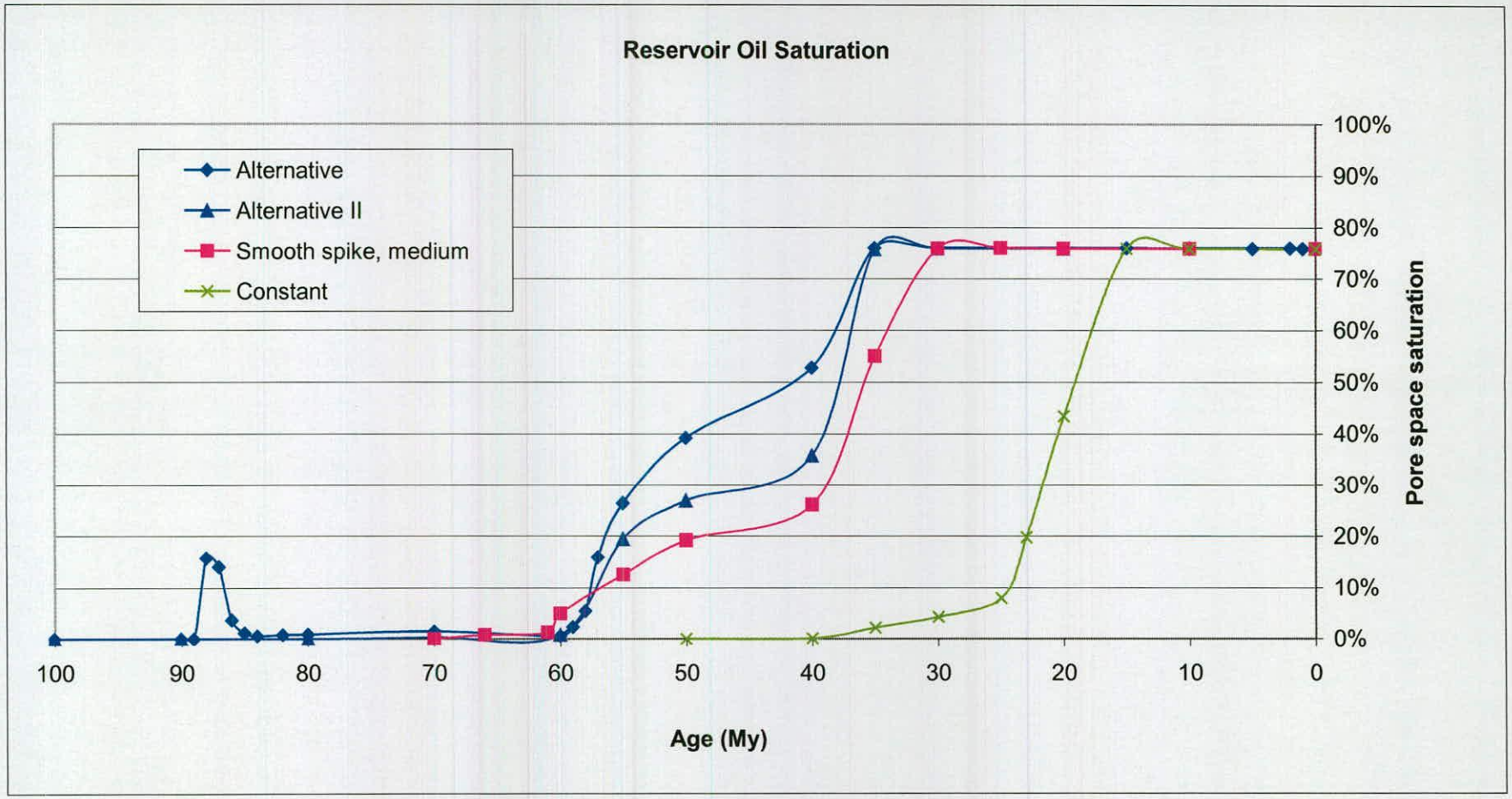

Figure 5.43 Modes of accumulation for the Magnus model. The simulation tends to saturate the Magnus trap structure at about 60-40 My. Calibrated simulations also display an earlier discreet phase of minor saturation, circa 88 My. A third mode related to low levels of heat flow results in saturation over the period 40-20 My.

HEAT FLOW: transient, 'alternative'
SURFACE TEMPERATURE: transient

SURFACE TEMPERATURE: transient (after Buchardt 1978)

RESERVOIR: accumulation history and calibration parameters

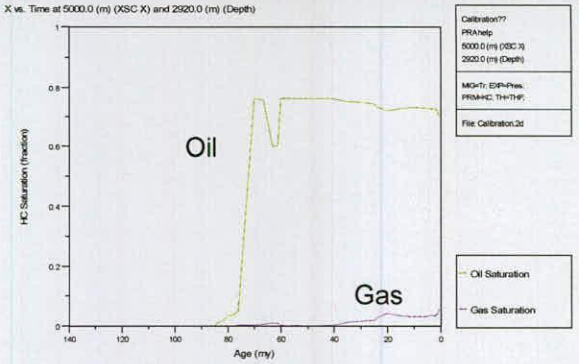

	Porosity	Permeability	Temperature	Pressure	Maturity, Ro
Res' Datum	12%	90 mD	116 degC	6634 psi	0.75%

DEEP SOURCE AREA: generation and expulsion

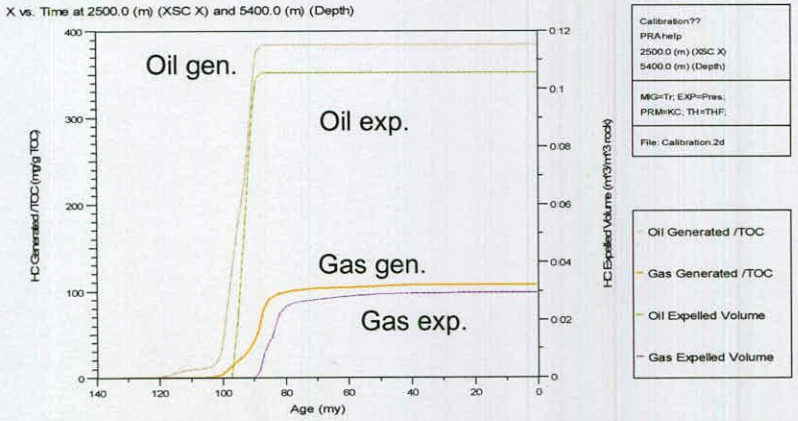

SHALLOW SOURCE AREA: generation and expulsion

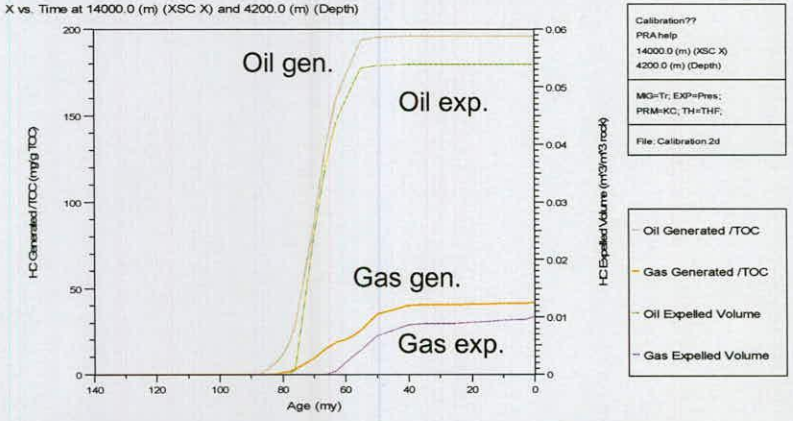

Figure 5.44 Modelled hydrocarbon response to a transient surface temperature input: the accumulation history for the Magnus is significantly altered. A value of 0.75% for the maturity parameter, Ro, is beyond the calibration range for the model. The paleosurface temperature input requires a lower heat flow to meet the calibration requirements.

HEAT FLOW: transient, 'smooth spike, medium'
SURFACE TEMPERATURE: transient

SURFACE TEMPERATURE: transient (after Buchardt 1978)

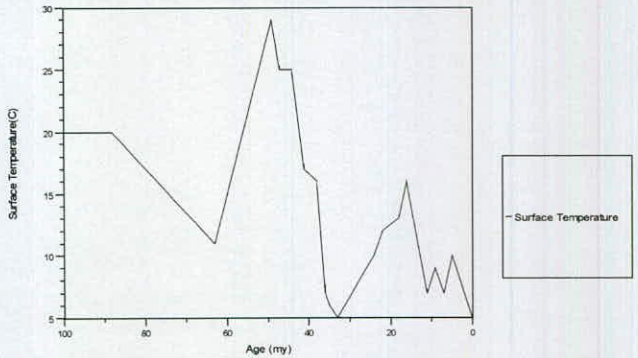

RESERVOIR: accumulation history and calibration parameters

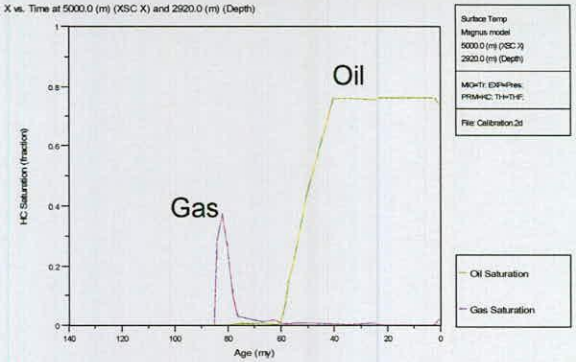

	Porosity	Permeability	Temperature	Pressure	Maturity, Ro
Res' Datum	12%	90 mD	118 degC	6635 psi	0.74%

DEEP SOURCE AREA: generation and expulsion

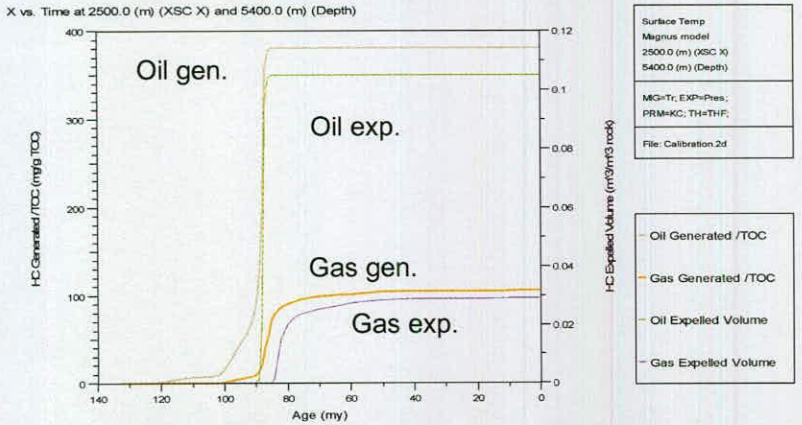

SHALLOW SOURCE AREA: generation and expulsion

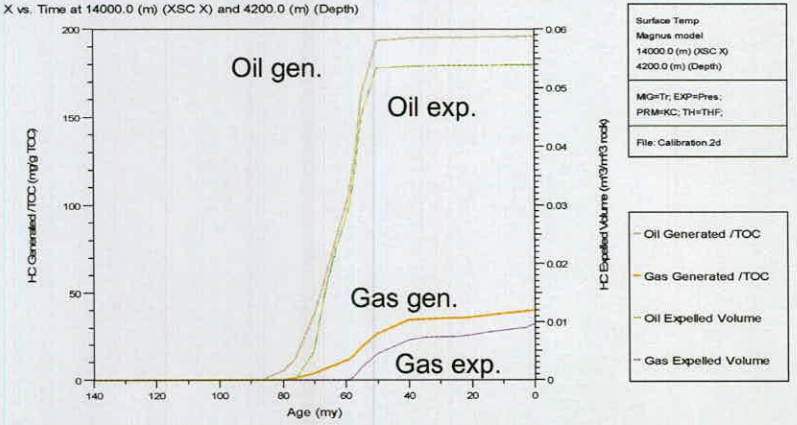

Figure 5.45 Modelled hydrocarbon response to a transient surface temperature input and the lowest heat flow scenario. The simulated value for Maturity, Ro, is just within the calibration range at 0.74% . This demonstrates the simulated accumulation history is sensitive to surface temperature input. The timing of generation and expulsion from the deep and shallow source areas is unaffected.

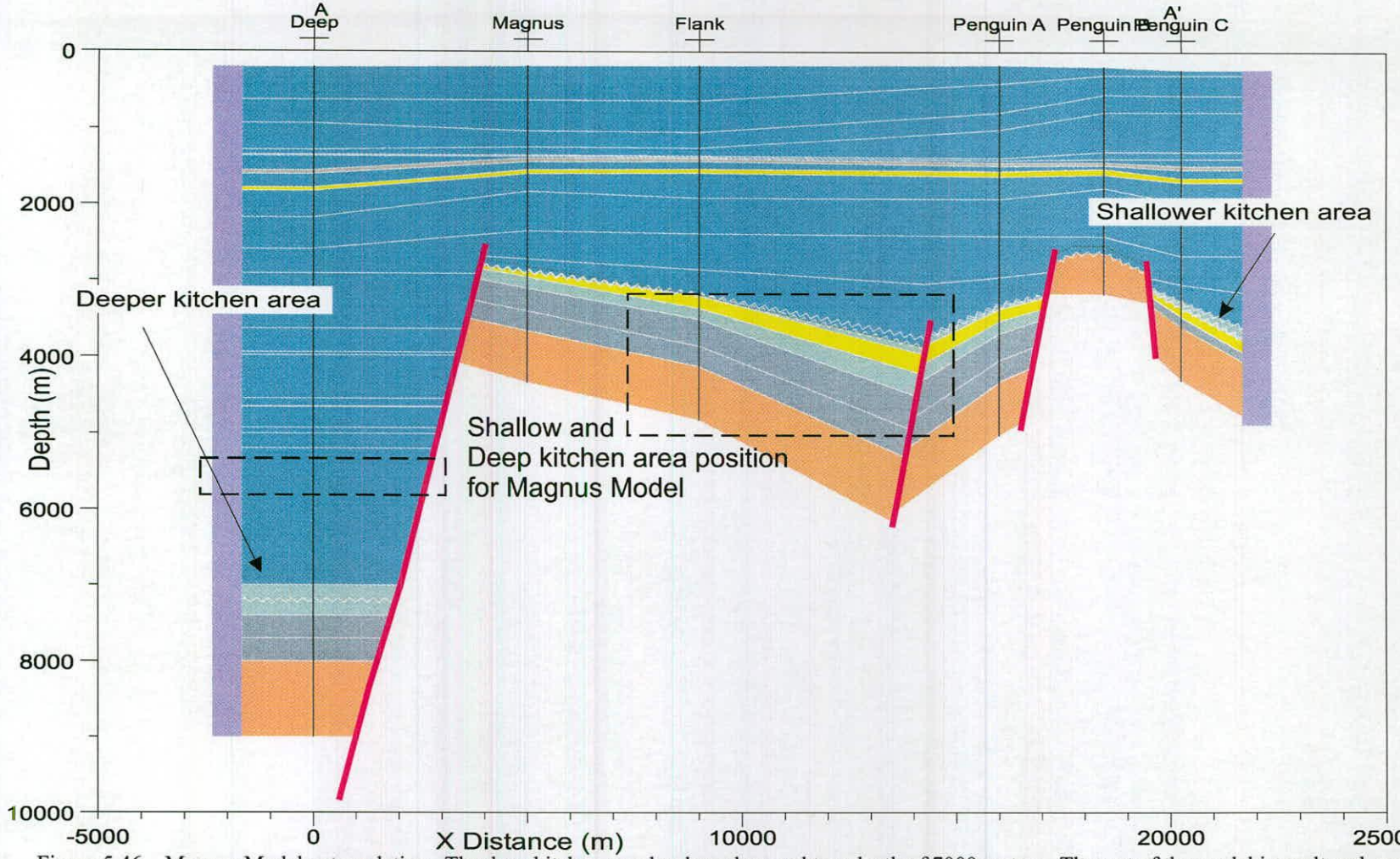

Figure 5.46 Magnus Model extrapolation. The deep kitchen area has been lowered to a depth of 7000 meters. The rest of the model is unaltered, and the general morphology of the section is retained. The new position of the deep kitchen area equates to a hypothetical kitchen area which is assumed to lie to the north-east, in the More Basin, out of the section upon which the model is based. The other extrapolated kitchen, to the east of the Penguin horst, represents the shallowest occurrence of Kimmeridge Clay likely to charge rift and pre-rift Mesozoic traps in the Northern North Sea.

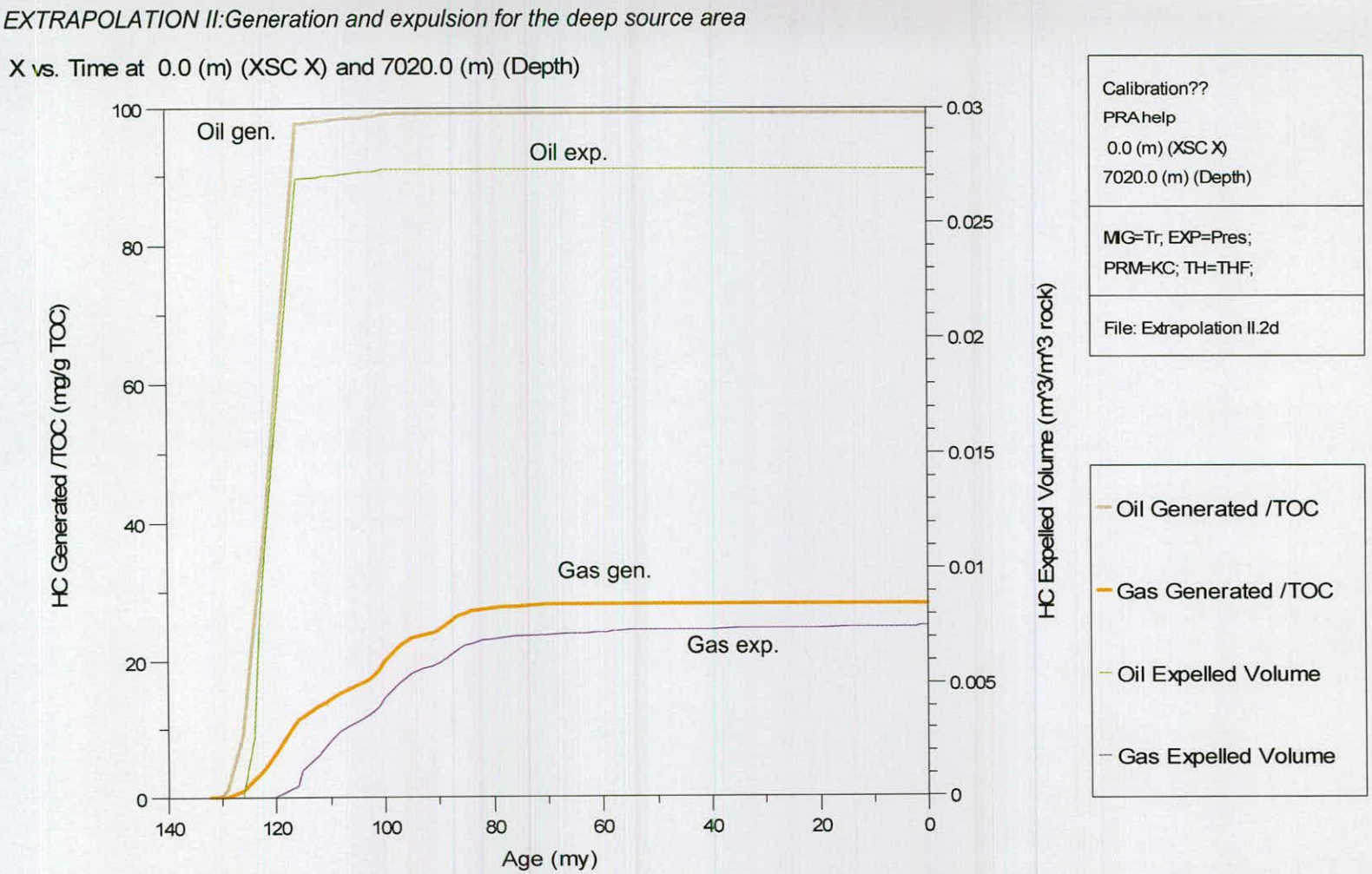

Figure 5.47 Extrapolation: simulated generation and expulsion for the deep source area. With the source area at a depth of 7000 meters, the onset of generation and expulsion occurs at about 125 My.

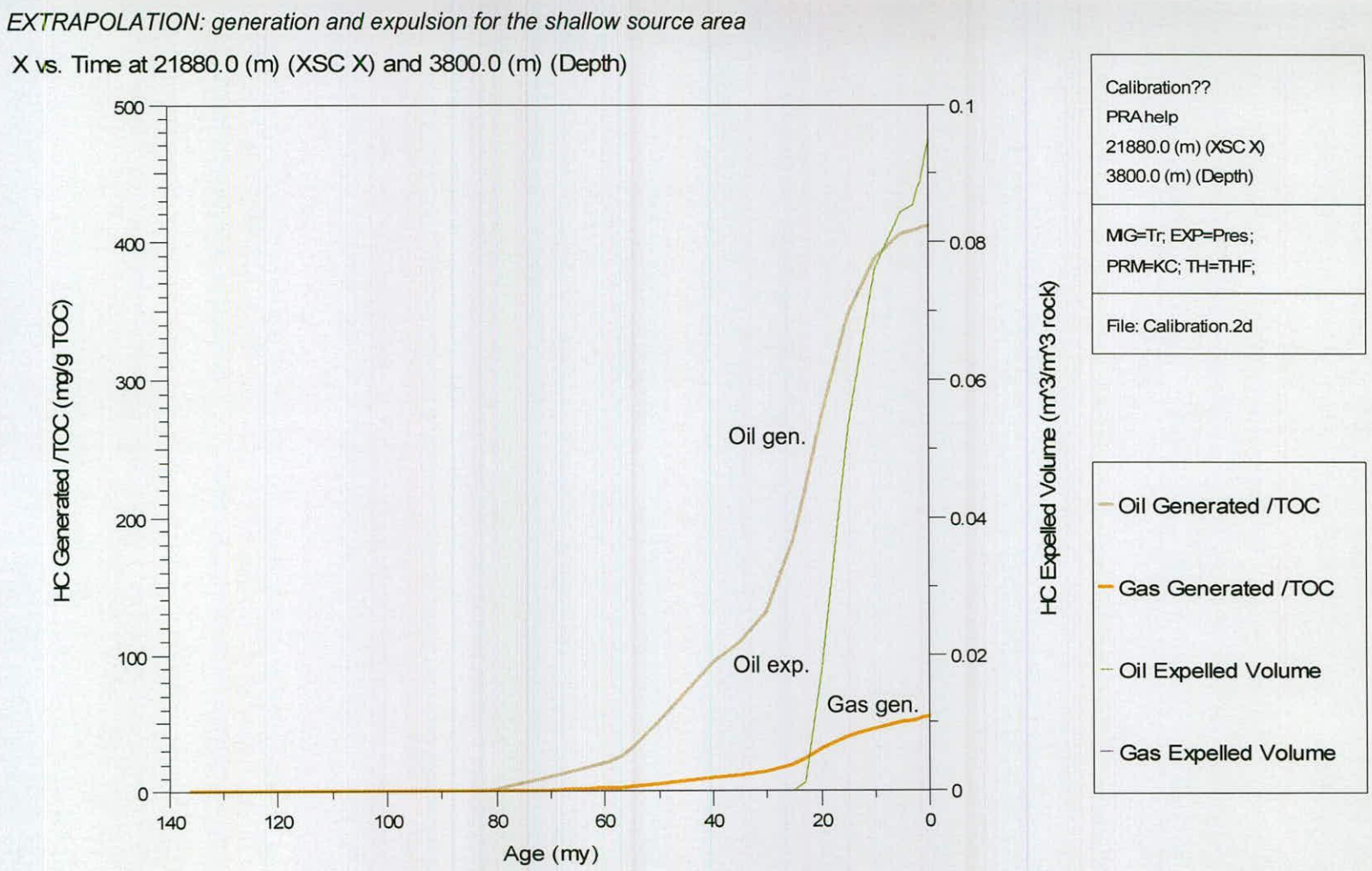

Figure 5.48 Extrapolation: simulated generation and expulsion for the shallow source area. With the source area at a depth of 3800 meters, the onset of generation is unchanged at about 80 My. However, the expulsion occurs at about 20 My.

Penguin field diagenesis and structural inversion
An alternative to hydrocarbon charge during the early Cretaceous

one need not increase, beyond what is
necessary, the number of entities required to
explain anything

This chapter presents an alternative and ultimately unsustainable hypothesis for unusually old illite diagenesis in the Penguin field area. This antithesis to the open system formulation of the null hypothesis depends on a highly unorthodox interpretation of the Penguin B horst structure.

6.0 Background

In retrospect, outcomes for the preceding research have been surprisingly coherent. In particular, there is a welcome correlation of petroleum system simulations, calibrated and extrapolated, as presented in chapter five, with experimentally obtained illite K-Ar ages for the Penguin and Magnus fields, as documented in chapter four. This validates the simple conceptual model proposed for illite diagenesis in chapter three i.e. fibrous illite diagenesis throughout the East Shetland Basin is indicative of the critical moment of hydrocarbon charge.

And so, both with regard to the small but complex arena of the Northern Group illite data, and more generally, in regard to the wider context of illite ages within the East Shetland Basin population, the results of this study have succeeded in explaining ages typical of the region. The research also resolves the anomalous and controversially old ages of the northwestern margins, as well as the long-standing conundrum concerning the absence of zero-age illite throughout the Northern North Sea.

Furthermore, this widely applicable model for illite diagenesis in the petroleum systems of the Northern North Sea has implemented a refinement of the original null hypothesis first proffered in the late 1970's. Sommer's original proposal (Sommer 1975) now stands on a much stronger footing with respect to issues concerning the underlying dynamics of illite precipitation, likely occurrence of the mineral, and reservations with respect to contamination and resolution of fibrous illite age data.

6.1 Aim and objective

This validation of Sommer's original work and refinement of the null hypothesis has perhaps been the most rewarding aspect of this Ph.D. However, it is worth noting that, prior to the basin modelling study, considerable effort was directed towards finding an alternative hypothesis, sympathetic to the closed system school of illite diagenesis, in order to explain the Penguin ages. It seems reasonable, therefore, to include a brief synopsis of the entertained antithesis i.e. a structural, burial history approach to resolving the Penguin isotopic data.

Consequently the objective of this short chapter is to present and consider an alternative approach to understanding illite diagenesis in the Penguin field implicit in a recently published structural study for the Northern North Sea area by Booth et al. (1992).

6.2 The antithesis - an alternative, burial history justification of the Penguin data

As stated above, the unusual and unexpected range of K-Ar ages for the Penguin field complex appeared unlikely to support a dynamic event-driven model of illite diagenesis and hydrocarbon charge. Expectations regarding the likely timing of oil migration in the area seemingly precluded the association of the oldest illite ages found in the Penguin B horst with fluid movement.

A burial history requirement

With the open system paradigm apparently untenable in light of the Penguin B data, the obvious alternative geological candidate for resolving the data appeared to be the closed system paradigm i.e. a thermodynamic control on the stability field of fibrous illite. The simplest relationship between thermodynamically dependent diagenesis and basin evolution tends to be burial history, as this is the principal temperature-factor within closed systems. As a consequence, a requirement of this alternative approach would be a highly unusual burial history for the Penguin B horst i.e. unusual enough to expose the Penguin B horst to the depths, and temperatures in excess of 80°C, required to enter the fibrous illite window as perceived by closed system advocates – Figure 6.1. The lack of evidence supporting this radical interpretation is considered in the following discussion.

Alignments and juxtapositions – a possibility

The implication that Penguin oil field was anomalous with regard to burial history struck a chord with the work of Booth et al. (1992). They proposed that the structure, though commonly portrayed as a horst on commercial seismic interpretations, was, in fact, an unusual inversion feature associated with uplift along reactivated lineaments in the Caledonian basement - the result of oblique shear during the onset of the North Atlantic opening. Certainly, maps of deep basement fault alignments, sutures and their juxtapositions, such as the recently published review by Doré & Lundin (1996), indicate that the field lies at the intersection of two major alignments, namely the Hitra and Tornquist - Figure 6.2.

The Booth interpretation

Booth and co-workers cite the deep basement fault trends in support of a highly unusual interpretation of regional seismic data for the Penguin field area –Figure 6.3. The section conforms to other widely accepted interpretations of the area with respect to the topographic profile of the Jurassic subcrop and geometry of the Mesozoic stratigraphy but deviates remarkably from convention in regard to the position, orientation, and sense of movement of the principal Penguin and Magnus faults. The most striking element of this new interpretation was the high-angle reverse fault associated with Penguin B. This implied that the trap structure formed not as the result of an extensional graben-horst-graben configuration, but in response to compression and inversion resulting in a pop-up or flower structure.

Implications

An initial consideration of this controversial model implied two attractive prospects. Firstly, that the Penguin B structure, with its errant ages, had undergone an unusual burial history – Figure 6.4 , neither apparent in its present day configuration, nor compatible with conventional reconstructions for the area – Figure 6.5. Secondly, Penguin inverted as a result of tectonic reconfiguration associated with the relocation of rifting to the west. Booth *et al.* (1992) do not commit to a specific timing, and so the proposed inversion is only constrained to have occurred during the Neocomian, i.e. 135 Ma –122 Ma. Both propositions seemed to indicate that the Penguin B horst may have experienced illite growth as a function of highly unusual burial. This would still be in accord with two of the basic premises of closed system diagenesis i.e. a thermodynamic threshold and a function of burial history.

6.3 Locally and regionally - a lack of supporting evidence

Consequently, for illite to grow in a closed system, driven by burial through a temperature threshold, the following geological conditions have to be met. Firstly, assuming a shallow closed-system threshold depth of 1,500 metres for illite diagenesis, equivalent to about 40°C - an optimistic assumption considering the rapid rates of burial required and previously mentioned high threshold temperature adhered to by closed system advocates - the Penguin area would have undergone this burial at around 120 Ma i.e. prior to the inferred rapid inversion and denudation that occurred shortly after entering the illite window. Additional assumptions require that the resultant illite was impervious to possible near-surface weathering during erosion, and that the structure resumed a more conventional burial history prior to 90 Ma, in order account for the oldest ages in the Magnus field and Penguin A field, as well as present day stratigraphy.

In an attempt to reconcile the Penguin isotopic data to this radical model of inversion and relict flower structures, a reappraisal of the local well stratigraphy, seismic profiles and commonly expounded tectonic models for the region was undertaken.

The regional profile

As can be seen from a conventionally derived cross-section - Figure 6.6, the Penguin horst is flanked by two apparently extensional graben features of similar depth. Secondly, the Penguin B feature, though slightly higher than the Magnus high and Snorre horst, is not extremely elevated relative to its neighbours. The apparent discrepancy with respect to depth on the section occurs to the west i.e. the depth of the North Shetland Trough, indicative of the North Atlantic opening and extensional stresses.

Local stratigraphy

A consideration of well stratigraphy for the Magnus province also indicates how unlikely a possibility compression is for the region during the Neocomian. In order to support the Booth *et al.* (1992) model, Penguin B needs to be overlain by a major unconformity instead of the minor Cretaceous unconformity apparently logged for the province - Figure 6.7. The occurrence of Lower Cretaceous in well 211/13-1 is crucial to this point. Secondly, the unconformity would have been highly erosional, and yet appears to have left no debris in the Lower Cretaceous and Coniacian mud-filled basin of the Magnus province. There is no apparent evidence of this denudation in the area - Figure 6.7.

3-D seismic

Furthermore, a recent evaluation of the original 2-D seismic line that runs through the Penguin B horst and well 211/13-3 on the Penguin B western flank, as provided by Shell UK (Shell UK 1998), revealed no evidence of the required fault geometries associated with flower structure inversions (pers comm., Underhill 2000). Indeed, the quality of this now effectively obsolete 2-D data was so poor in comparison to the intensive 3-D seismic surveys available for the field area, that there appeared to be no sufficient grounds for Booth *et al.* (1192) to use the 2-D data as evidence to support an unorthodox

view of tectonic activity in the area. A recent and comprehensive structural evaluation of the Penguin horst and western flank of the Penguin field area firmly supports the conventional view of the field area as extensional. Figure 6.8 is representative of a number of structural analyses by Al-Abry (2002), and is chosen as it is pinned to the same well as the Booth *et al.* (1992) section i.e. well 211/13-3.

While this tenuous structural model, derived from Booth *et al.* (1992) – Figure 6.4, is sympathetic to the oldest ages in Penguin B, it fails to address the complexity of the Penguin array, and relationship between the Magnus and Penguin fields. Furthermore the model sheds no light on the zero-age conundrum nor does it address the wider issues of the regional review. The limited implications and complexity of the model, coupled with a reliance on tenuous assumptions suggest that the antithesis is flawed in comparison to the null hypothesis – Figure 6.9.

6.4 Summary

The controversial views of Booth *et al.* (1992) were examined in an attempt to explain the Penguin B data. This alternative model invoked a highly unusual burial history for the Penguin horst and closed system illite diagenesis on the northwestern edge of the East Shetland Basin. This is a consequence of a premise of simple geochemistry in closed system formulations, namely that thermodynamics are a principal factor in determining the presence of fibrous illite in sandstones. This tenet of the closed system paradigm implies that old ages require old burial. As a consequence, Penguin B would need to have inverted and undergone 1.5 - 2.0 km of erosion during the early Cretaceous, despite no indication of subaerial exposure. If the Penguin B structure had experienced significant burial during the late Jurassic, then early Cretaceous inversion has to be inferred to explain both the lack of stratigraphic evidence and also the Cainozoic configuration. The evidence against this unusual interpretation of the Penguin B horst area is found to outweigh the merits of the study published by Booth *et al.* (1992), leaving the closed system antithesis as a convoluted, and ultimately unsupportable hypothesis. In this case, a complex fluid-charge history is preferred to complex geological phenomena.

6.5 Conclusion

The comprehensive match between the calibrated basin model presented in chapter five, and the Penguin illite ages presented in chapter four, provides a simple, yet successful validation of the null hypothesis in light of the model's calibrated output and extrapolated implications when considering the region as a whole. By judicious application of Occam's razor, the closed system antithesis is rejected in favour of the open system paradigm relating hydrocarbon charge from local kitchen areas to illite diagenesis in Northern North Sea oil fields. K-Ar ages for fibrous illite fractions extracted from oil field sandstones accurately constrain the critical moment of oil movement in small, locally sourced petroleum systems. The catastrophic null hypothesis stands.

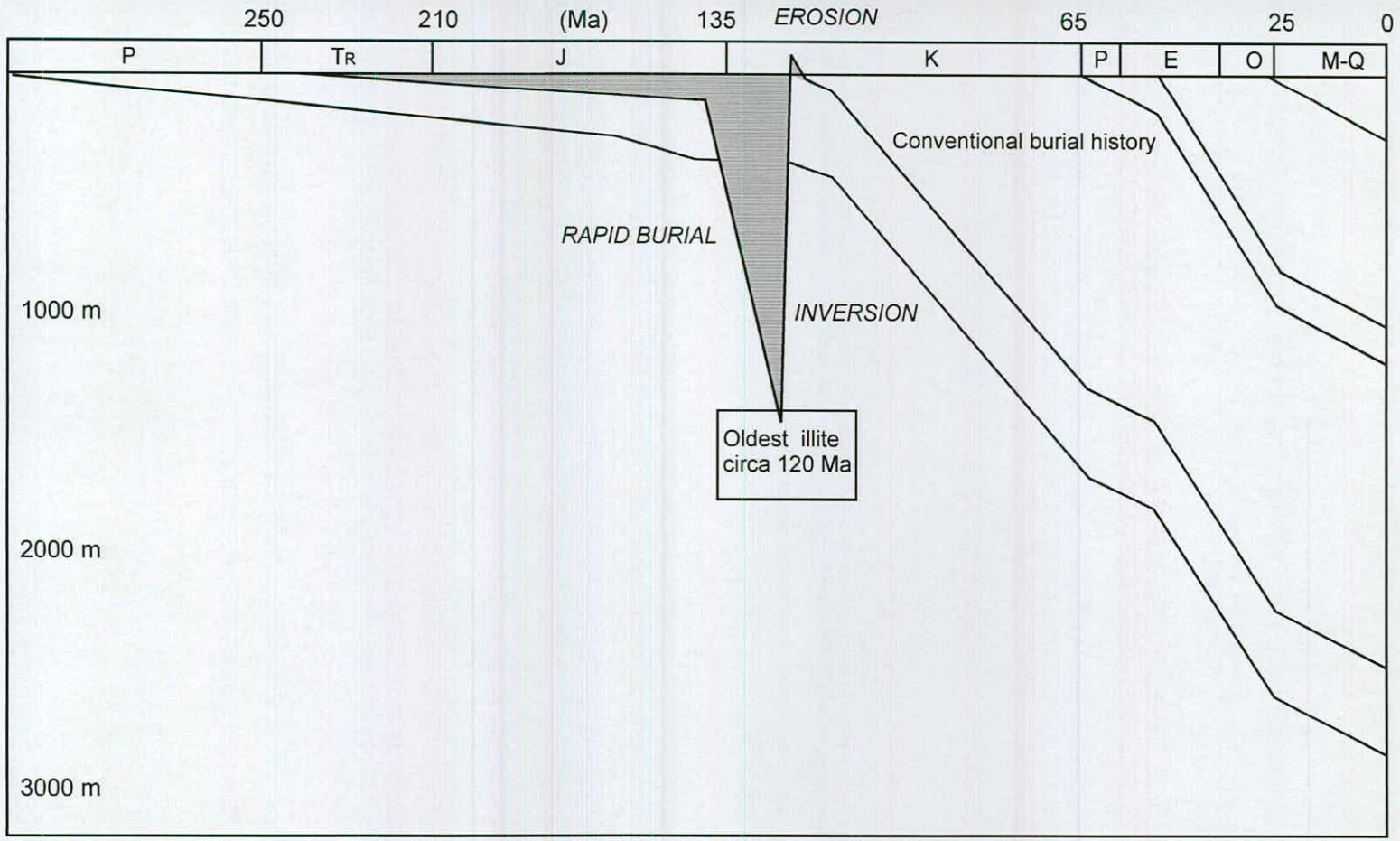

Figure 6.1 A burial history scenario for early burial and related illite diagenesis. The conventional burial history appears in the background. The shaded area indicates the extreme burial rate and inversion required to place the Penguin B reservoir in the likely window for early illite diagenesis at around 120 Ma, then return the structure to the surface to account for the present-day stratigraphy and seismic profile.

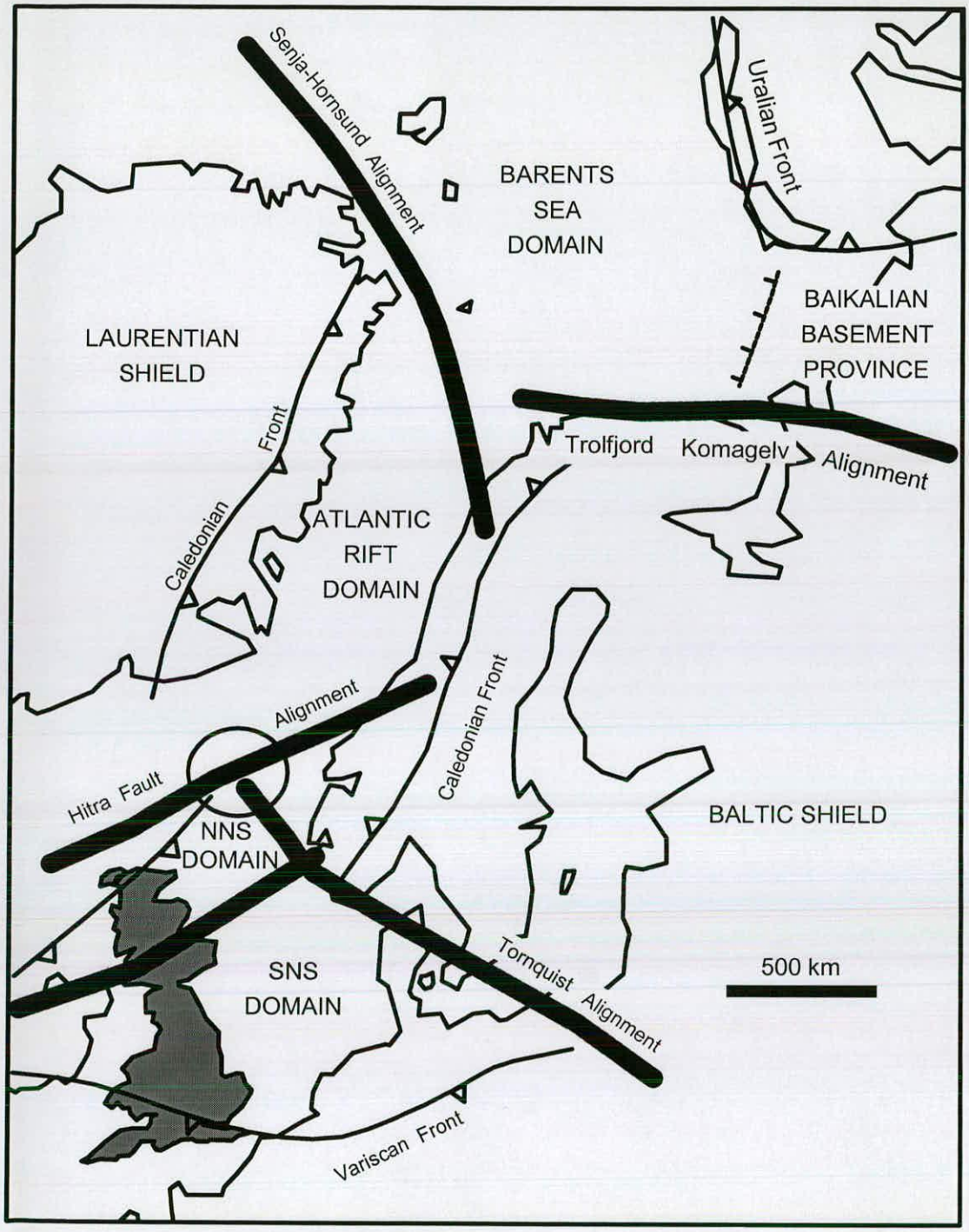

Figure 6.2 A regional picture of the north western European margin. A complex arrangement of plate fragments and fault alignments underlie the local tectonic response to regional stress fields. The Penguin area is circled at the probable junction between the Hitra Fault Alignment and the Tornquist alignment (after Doré & Lundin 1996).

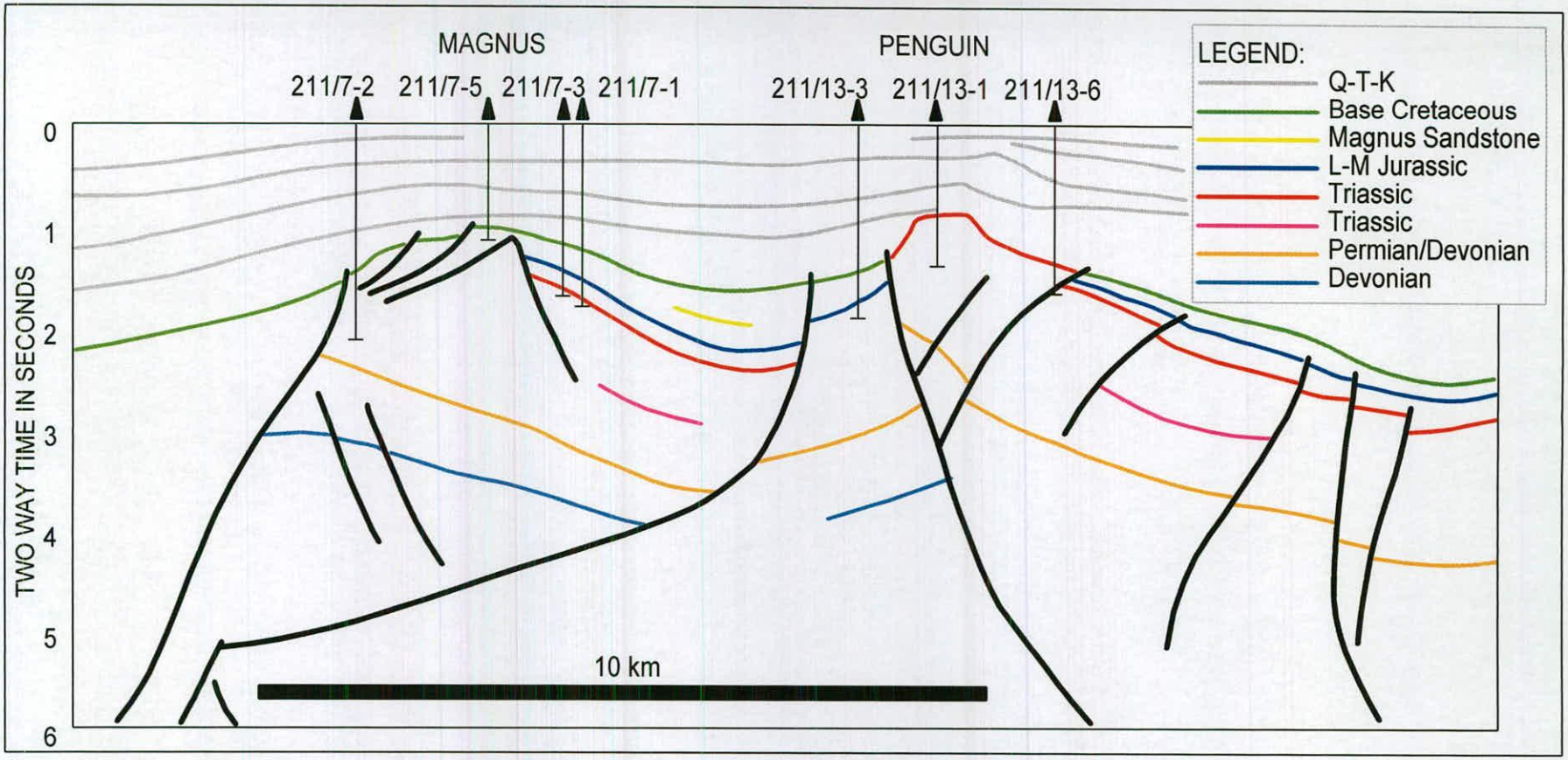

Figure 6.3 An unusual interpretation of the local structural styles associated with the Magnus and Penguin fields. Note the high-angle reverse fault underlying the Penguin B horst, and the associated detachment plane underlying the Magnus field. This unorthodox interpretation of the regional 2D seismic line implies that the Penguin B horst structure inverted, and underwent considerable uplift, probably during the earliest Cretaceous (after Booth, Stockley & Robbins 1992).

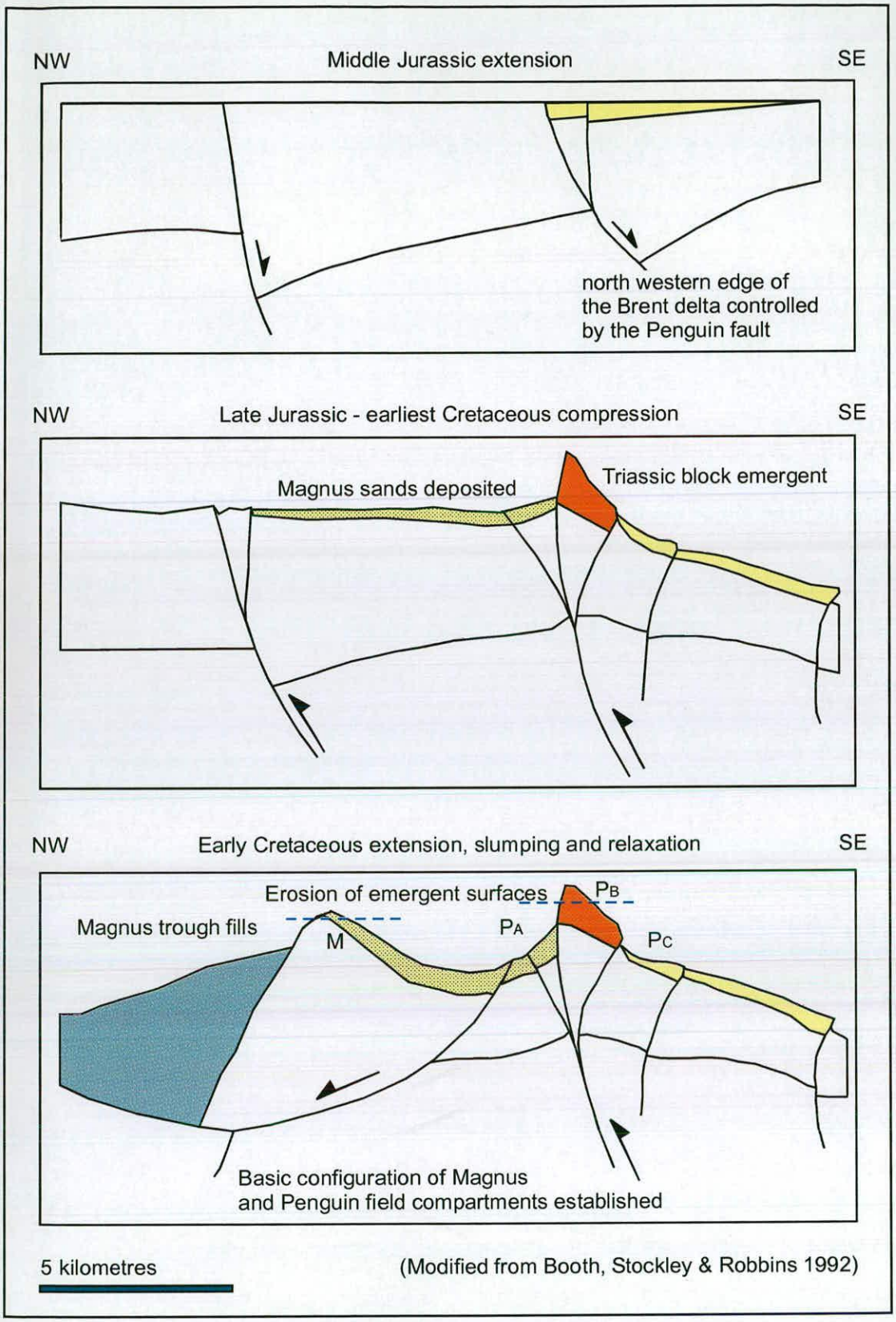

Figure 6.4 A hypothetical reconstruction of Magnus Province structural elements in response to a proposed period of compression and inversion at the end of the Jurassic and start of the Cretaceous by Booth, Stockley & Robbins (1992).

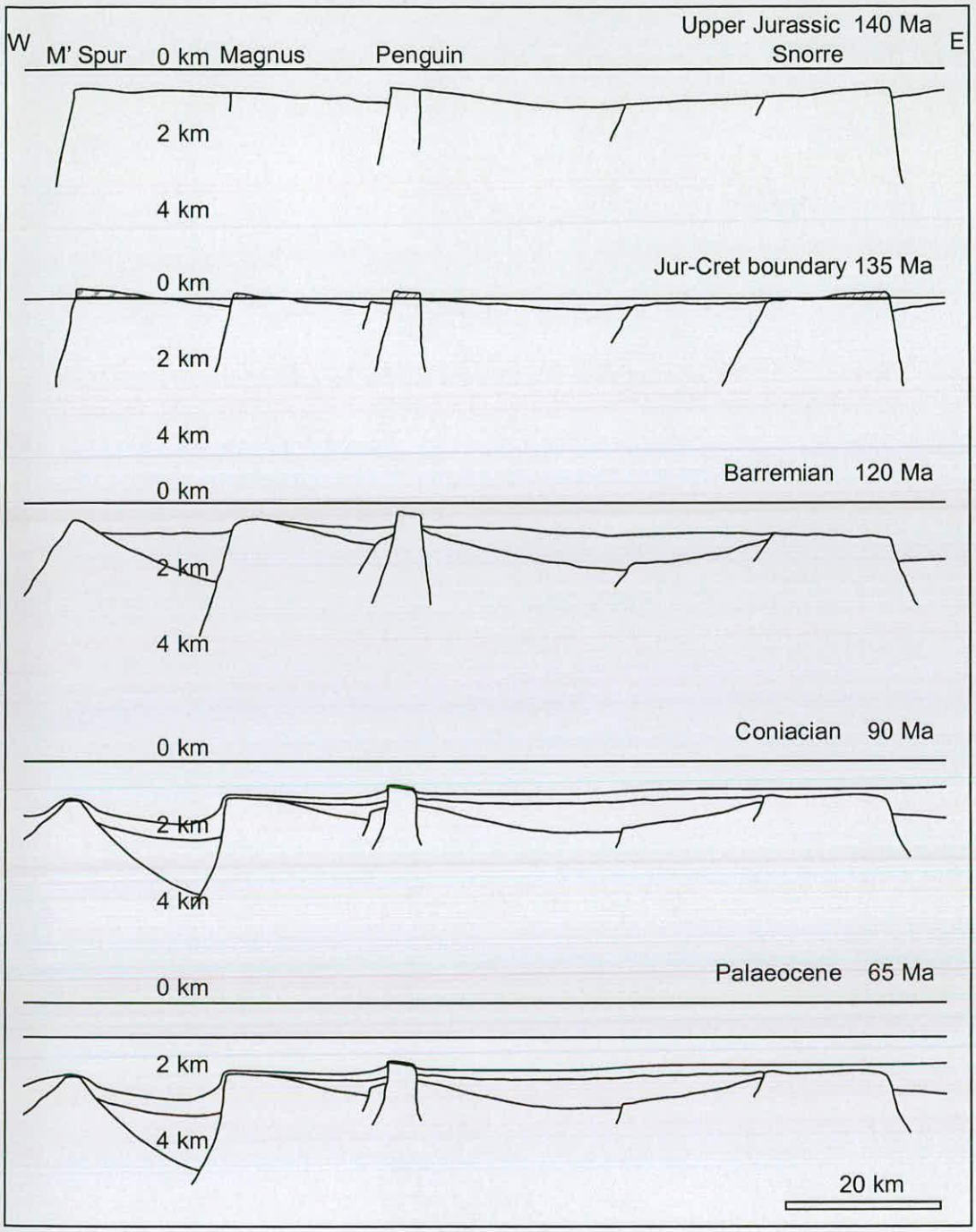

Figure 6.5 A conventional reconstruction model for the evolution of the northern margin of the East Shetland Basin. The Penguin horst develops in response to extensional stresses, resulting in half grabens to the west, and a wide graben to the east. The Magnus field is seen to be the result of failure in the large block to the west of the Penguin horst. The body of the data is taken from reconstructions provided by the CASE partner, Shell UK. The interpretation of the Magnus structure as a segmented half graben, failing at the end of the Jurassic was proposed by Underhill (pers. comm. 2001).

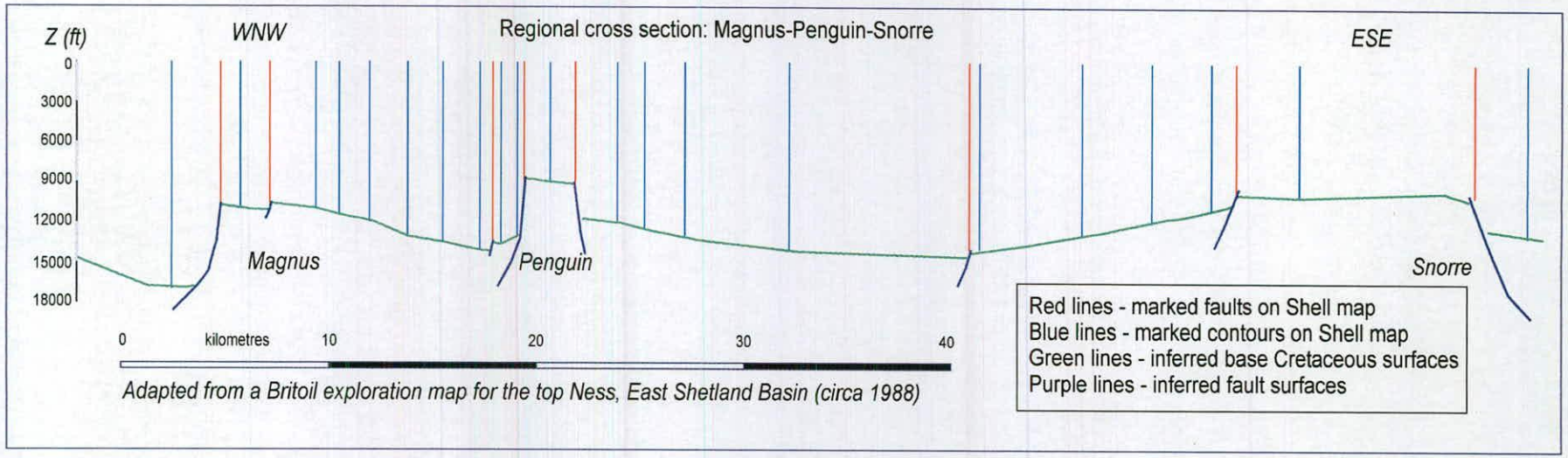

Figure 6.6 A regional section for the northern edge of the East Shetland Basin. The section comprises of the top Ness profile - a strong seismic reflection (Britoil 1988), and local structural maps including contoured depths for the base Cretaceous (Shell UK, 1995). These combine to place the Penguin horst block in a regional context. Note the similarity in depth of the basins that flank Penguin to the east and west, as well as the similar relief associated with both the Penguin horst and Snorre horst.

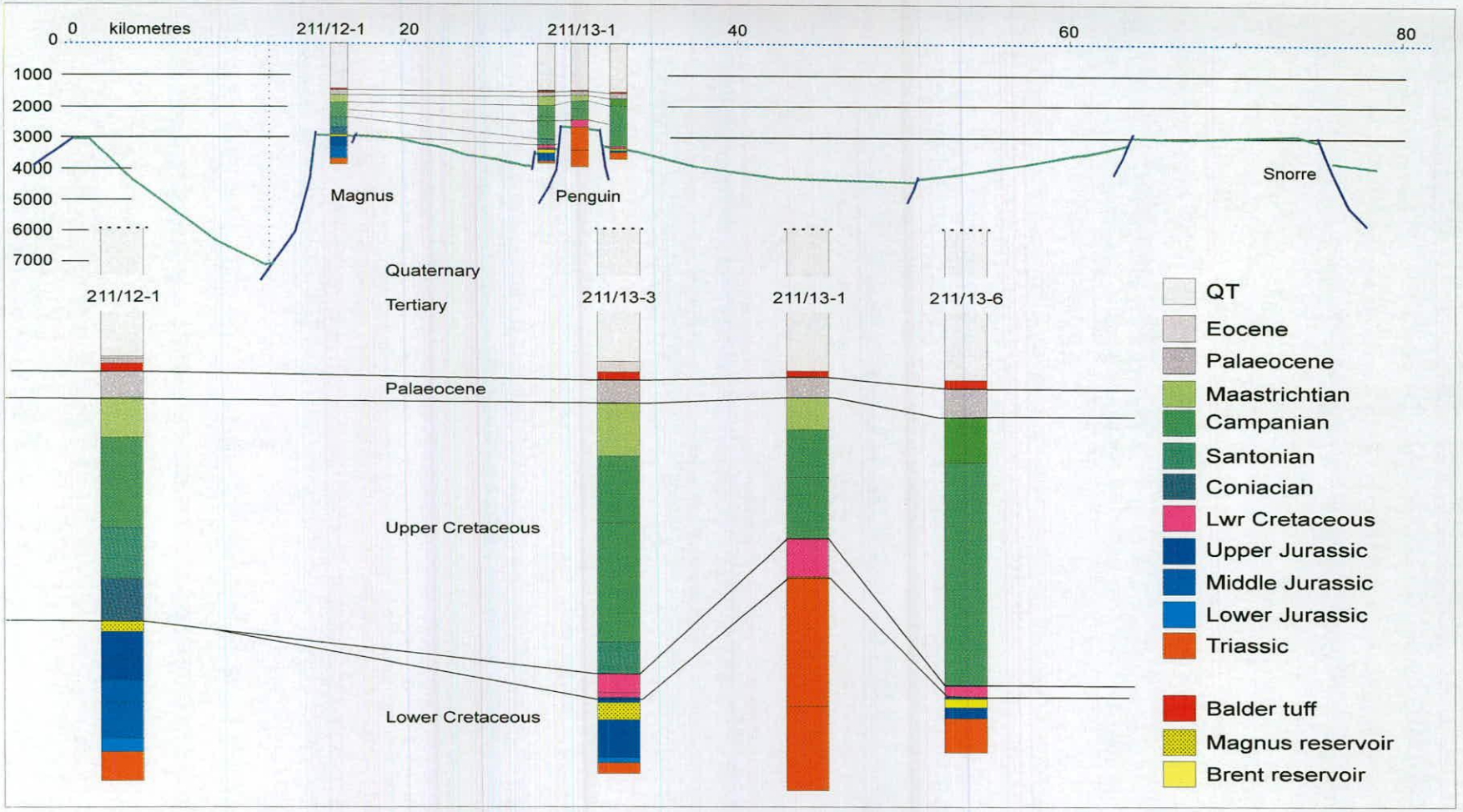

Figure 6.7 Stratigraphic well correlation for the Penguin B horst and Magnus Province (Shell UK, 1995). The resolution of stratigraphic horizons in the Cainozoic and Cretaceous are typically low. However, the section illustrates that while the principal Mesozoic phase of burial associated with these structures occurred during the Upper Cretaceous, all the structures appear to have a condensed Lower Cretaceous section, with the exception of the Magnus crest.

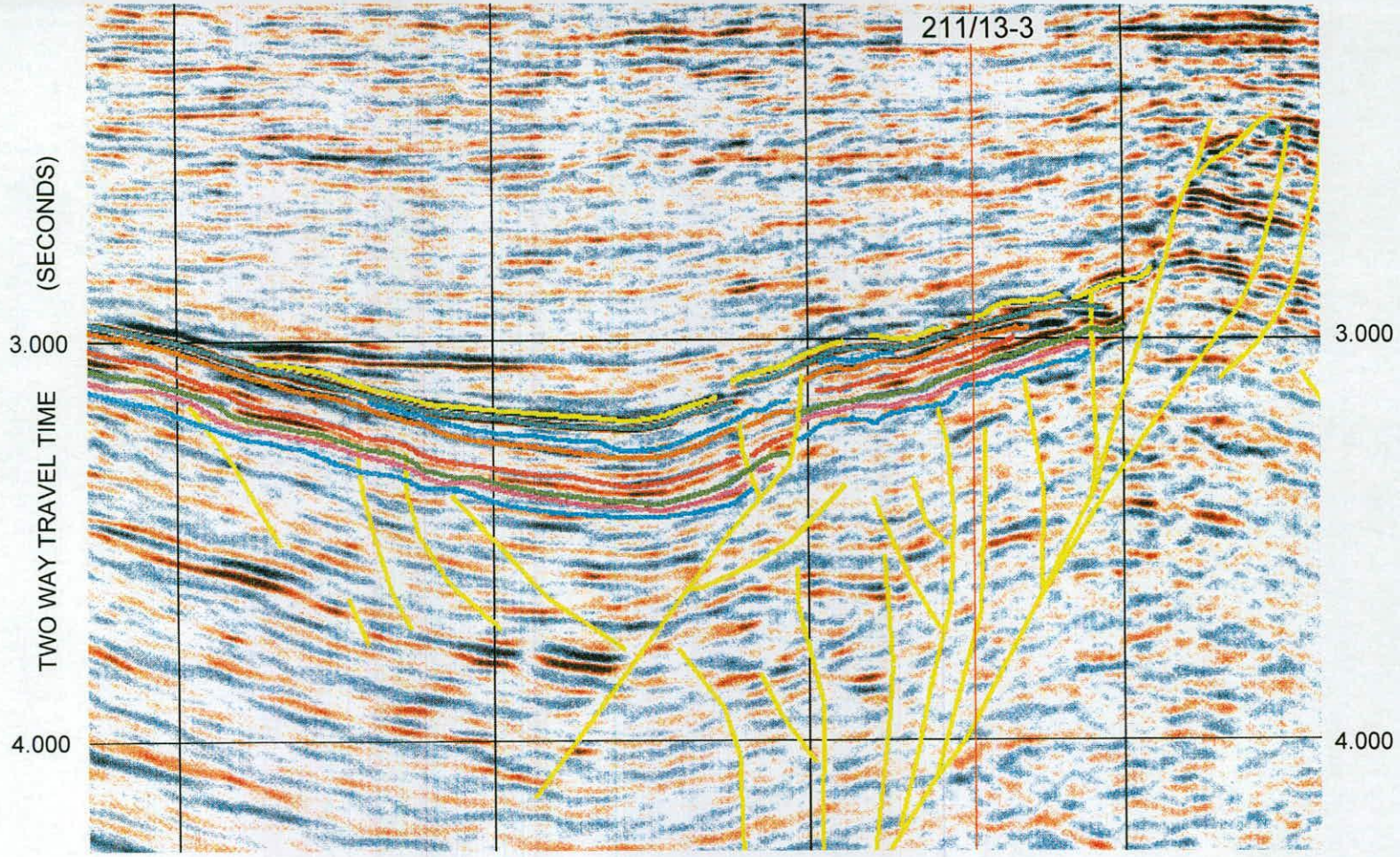

Figure 6.8 A recent interpretation of high-resolution 3-D seismic survey data for the Penguin field area, including the western flank of the Penguin B horst by Al-Abry (2002). Significant discontinuities, i.e. faults and stratigraphic boundaries, are shown in yellow. The structure appears to be typical of extensional configurations found throughout the East Shetland Basin. This interpretation was made after consideration of the Booth et al. Interpretation for the same structure. Both sections strike in similar directions and are pinned on the same well, 211/13-3.

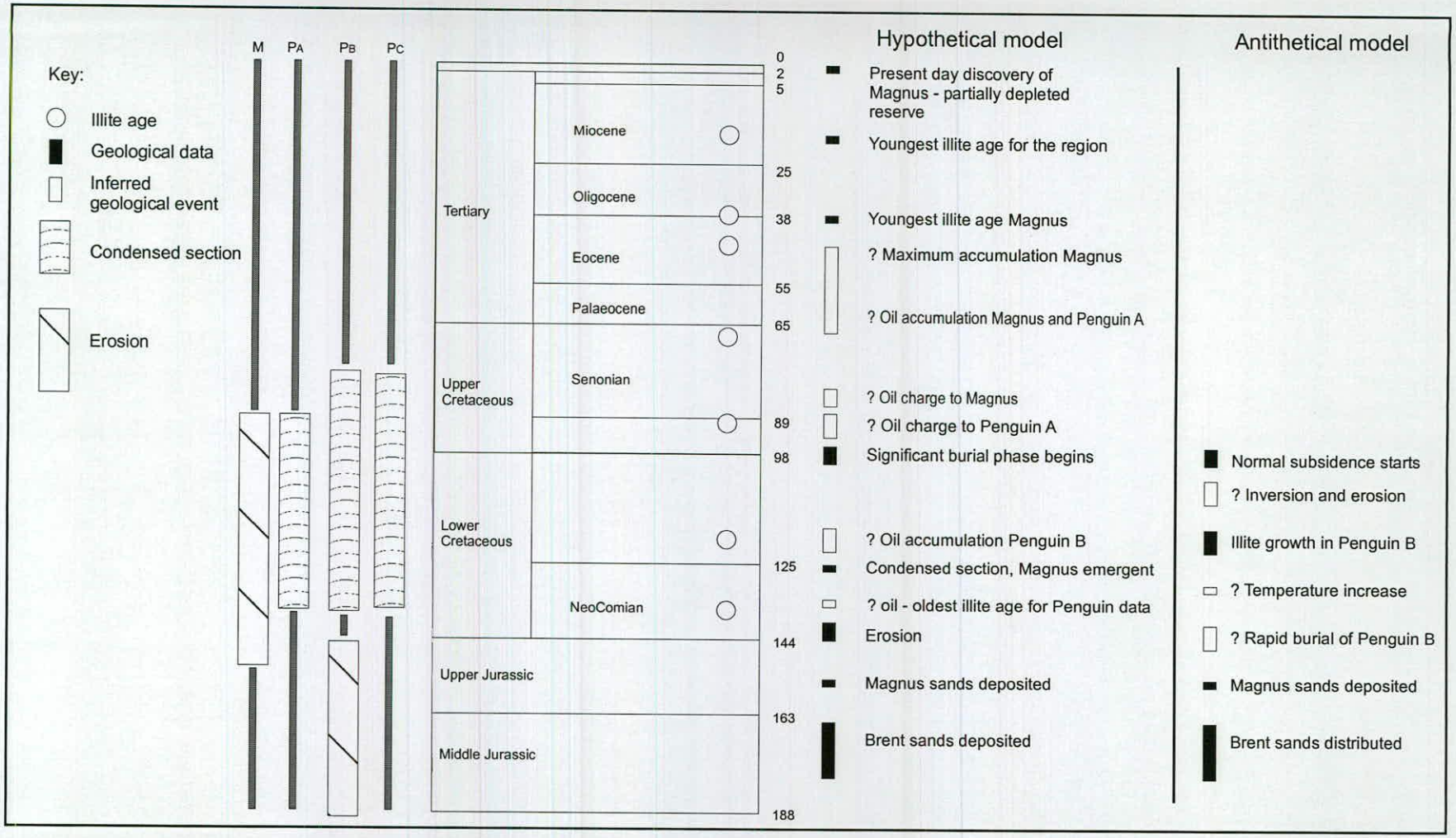

Figure 6.9 A correlation chart comparing the two competing models for illite diagenesis in the Magnus and Penguin fields. The geological data and implied geological events for the null hypothesis are far more comprehensive than the Penguin B-limited and earliest Cretaceous associations of the antithesis. The latter argument is dependent on a controversial and equivocal interpretation of obsolete seismic survey data for the Penguin field area.

The critical moment
A regional model associating hydrocarbon charge and fibrous illite diagenesis within the petroleum systems of the Northern North Sea

a fragment
like a universe
has to be entirely isolated
from the surrounding and be
complete in itself like
a porcupine

This chapter presents a new regional framework for the relationship between basinal fluid flow and fibrous illite diagenesis in Mesozoic sandstone oil reservoirs of the Northern North Sea, incorporating the implications of the petroleum system modelling, experimental petrology and regional geology outlined in chapters five, four and three respectively. The thesis closes with a review of the aims and consideration of potential further work arising from the research.

Tables

Figures

7.0 Aims and objectives

The previous three chapters have established a body of research relating to illite diagenesis and petroleum systems in the Northern North Sea. While the structure of the thesis emulates the progression of the study, covering the regional review, hypothesis formulation, sample selection, analysis, and resultant petroleum system modelling, this has tended to displace ephemeral but related research issues undertaken during the study to brief referrals in chapter interpretations and summaries.

Additionally, the linear and thematic architecture of the thesis, while hopefully providing the reader with a clear understanding of the research method, assumptions and philosophy implicit in the work, has restricted a more open discourse with regard to the general and inter-related aspects of the study.

Hence, it is the aim of this summary and concluding chapter to open up the discussion, in order to consider the findings of both the regional synthesis from chapter three and the parochial analytical and modelling studies of chapters four and five, in light of a general understanding resulting from the body of research, and with regard to interesting and pertinent aspects of other research areas. Hence, the objectives of the following chapter are as follows:

• to return to the main aspects of the thesis and reconsider the principal conjectures, dilemmas and resolutions as they occur in relation to each other and in hindsight of the overall study.

• to present the sustained null hypothesis, standing with respect to event-related open system diagenesis, and refined with regard to the dynamics and proximity of hydrocarbon charge in the basin.

• to present a coherent and original conceptual model of fibrous illite diagenesis as found in the petroleum systems of the Northern North Sea, and speculate on the potentially generic and predictive nature of this new paradigm for fibrous illite diagenesis.

In this regard, the following discussion presents a brief reconsideration of the three principal strands of research presented in this thesis, namely the regional Northern North Sea illite age review, the Penguin isotope analysis and the Magnus-Penguin petroleum system basin modelling.

The thesis closes with a brief summary of aims, principal findings and suggestions for further work.

7.1 The regional Northern North Sea illite pattern

The thesis opened with a brief literature review. On the basis of this, it was clear that despite a number of illite diagenesis studies within the Northern North Sea, considerable ambiguity and confusion remained with regard to the value and intrinsic meaning of potassium-argon illite ages.

However, it was also clear that a critical aspect of the debate hinged on the fluid dynamics of petroleum systems, an area that had seen considerable advances in computational simulation since the advent of studies in the region during the late 1970's and intense research effort during the early 1990's. As a consequence, this research attempted to resolve the dilemma between close system and open system positions by reviewing and synthesising the findings of twenty four oil field studies by fourteen published first authors into a coherent conceptual model for the Northern North Sea, as presented in chapter three. It was intended that this would provide the background necessary to select an incisive field area for isotope analysis, yielding useful additions to the pool of illite ages for the region, and providing the key elements for a two-dimensional modelling study within the region that would critique the illite-oil conjecture.

Sommer's legacy

In general, the published studies, and their associated ages are sympathetic to the earliest, seminal study by Sommer (1978). However, subtleties of the diagenetic system apparent amongst the various age arrays that comprised the pool of collective data resulted in considerable debate as to the validity and application of the original model. Positions regarding illite diagenesis and the K-Ar method had polarised and become trenchant towards the end of the last century, with studies by necessity remaining parochial in focus and interpretation. However, illite diagenesis clearly showed striking resemblances from field to field across the region, i.e. a pattern of ages decreasing with depth within fields yet age increase with depth amongst the basin-wide terraces of the Viking Graben. Superimposed on this simple pattern are reversals, errant ages, bimodality, suspect old ages, a lack of young ages, and regional modalities, all of which emerge from the regional synthesis and mapping of illite age data undertaken - Chapter three, Figure 3.16.

> *One of the three main diagenetic phases during the evolution of sand bodies of the Brent Formation, Viking Graben, is late illitization contemporaneous with the migration of hydrocarbons and associated water.... Migration is dated as probably occurring during Lower Eocene times. (Sommer 1978)*

So, while Sommer's initial findings continued to stand, and the data spread appeared sympathetic to an event-driven diagenetic paradigm related to oil charge, it was difficult firstly, to defend the position against closed system advocates, and secondly, distinguish between a regional model of fill-spill trapping and a smaller model of local kitchen area hydrocarbon charge-response. Researchers subsequent to Sommer had also failed to account for a lack of zero-age illite, and explain the widespread discrepancies underlying the generally concordant data pattern.

Complexity

This failure to accommodate complexity was further exasperated by new isotopic data for the Penguin field resulting from this study, as presented in chapter four. Not only were a wide range of modalities now present in a single field complex, but additional corroboration of Magnus data implied that

previous researchers may have been mistaken in their rejection of these ages as artefacts of contamination i.e. the oldest ages published at that time for the Northern North Sea coincided very well with new samples from the genetically related Penguin A structure – Chapter four, section 4.9.

The 90 Ma ages for Penguin A were palatable. However, the associated ages for the Penguin B structure were not. With ages of around 120 Ma, no conceptual model existed for fibrous illite diagenesis in the Northern North Sea which would defend such data suites against the obvious and fair criticism that the samples may have been contaminated by potassium-rich phases during the destructive analytical procedure – Chapter four, section 4.6. A comparison of the published East Shetland Basin age population with the new Penguin data presented in chapter four clearly illustrates the radical nature of this diverse and unusual array – Chapter 3, Figure 3.11; Chapter 4, Figure 4.23.

It is worth remembering that a commonplace, if somewhat understandable reliance of closed system advocates on invoking contamination in order to explain away unusually old potassium-argon ages had weakened the credibility of all illite ages presented – Chapter 3, Figure 3.3; Chapter 4, Figure 4.19. A second, similarly restrictive argument, denigrating illite age data on the basis of unquantifiable resolution issues was also widely cited. Hence the ease with which apparent, though subtle patterns in age arrays were deemed to be within error, allowing over-generalisations to mask the apparent discrepancies within most published studies. As a consequence, Sommer's original proposition became a vague and widely criticised model of illite growth as an unexplained response to some aspect of the generation-migration-trapping and accumulation of hydrocarbons. Workers in the field of illite diagenesis were in peril of becoming apologists for their own methods and hypercritical of challenges to the generally accepted orthodoxy of interpretation.

A catastrophic proposition

The regional review presented in chapter three attempted to approach the data in a balanced dispassionate and critical manner. Of the four arbitrary geographical groupings employed to manage the data set, the Northern Group was found to be most heterogeneous. This was to be further borne out by the augmentation of the area with new and diverse ages for the Penguin field complex, as discussed above. However, the overall pattern emergent from the map, frequency plots and depth comparisons, formed the basis for a critique and modification of Sommer's original findings in order to propose a null hypothesis for this study.

> *Fibrous, pore-filling diagenetic illite, as found in oil fields, is fundamentally a response to shifts in regional hydrodynamics and specifically the onset of oil migration within the petroleum system. As such, K-Ar illite ages record the onset of oil charge to a trap structure – Chapter 1, section 1.24.*

This was a classical, catastrophic proposition in style, and directly opposed to the uniformitarian view of closed system chemistry, dependent on thermodynamics, as currently supported by Bjorkum *et al.* (1998) and (Bjorlykke pers. comm. 2002) amongst others.

On consideration, the null hypothesis was found to contain two quite distinct, though complimentary positions - *illite diagenesis as a response to long range fill-spill migration;* and *illite diagenesis as a function of local kitchen area charge.* The first position perceived fibrous illite diagenesis in terms of a simple, generalised conceptual model for the region, consisting of three illite age fronts, or modalities, which decreased in age with distance from the Viking Graben. In this moot position the older ages and field-specific discrepancies could be resolved by dismissing all outliers as contaminated and acknowledging subtle contradictions as within the resolution of the method.

The alternative proposition, also dependent on hydrocarbon charge, attempted to conceptualise the associations between fibrous illite diagenesis and petroleum systems at a smaller scale and in response to relatively *short range migration* from intra-terrrace kitchen areas within the immediate locality of oil fields. These two cartoons of hydrocarbon charge - Chapter 3, Figure 3.17, being the parents of an event-driven diagenetic model of fibrous illite growth, became the inspiration for the two experimental studies that followed in chapter four and chapter five.

In order to further investigate the system and test this interpretation, it was decided to conduct a carefully chosen study that would not only fill a gap in analytically-derived ages for the East Shetland Basin, but also be amenable to two-dimensional modelling of the petroleum system. The perplexing diversity of illite ages in the geographical Northern Group and their association to apparently simple petroleum systems led the research towards an intensive sample strategy, targeting the Penguin field.

7.2 The Penguin field isotope analysis

The CASE partner, Shell UK, rejected the initial proposal for thirty samples on the basis of the total core length involved - approximately ten metres. However, a second bid resulted in ten samples representing all four major reservoir compartments of the Penguin field complex, A through to D, while also covering the Jurassic Brent and Magnus provinces, as well as the Triassic horst area.

Destructive analytical procedure

The samples were processed and analysed following a standard protocol for illite separation. Considerable care was taken to minimise the risk of contamination. Careful use of an adjustable crown mill, iterative sieving and removal of clay fractions, and a lengthy chemical-decontamination procedure yielded a set of high quality separates weighing less than a gram for each sample, one thousandth of the original rock mass.

Unusual K-Ar ages for Penguin illite aliquots

The quality of the suite of high-purity illite samples attained from the destructive analytical procedure was verified in detail by TEM and XRD analysis. These fractions resulted in a highly unusual suite of K-Ar ages for the region, though the body of data was largely in accord with the regional age spread, and local variation. On consideration of internal variance, the data array was geographically coherent, with each trap structure returning characteristic ages.

Penguin A, genetically related to the Magnus field and associated petroleum system, returned self-consistent ages of approximately 90 Ma. This correlated well with the oldest ages recorded for the Magnus field; ages which had been reported and rejected as unacceptably old, and therefore probably contaminated, by two independent studies (Macaulay et al.1992; Emery et al. 1993).

Penguin B further challenged the orthodoxy by consistently returning ages so old, at 120 Ma, that no accepted model for Northern North Sea diagenesis or petroleum system dynamics would support their inclusion in the general population. However, it was noted at the time that Penguin B had an unusual pedigree, not only with regard to the structural style, and regional location of the horst, but also by nature of the hydrocarbons encountered when appraised i.e. low API condensate - in contrast to the oil-wet fields that flank the horst to either side and occur throughout the East Shetland Basin. Condensate hydrocarbons are typical of over-mature petroleum systems, suggesting that the Penguin B horst was plumbed into the much deeper, proto-Atlantic basins to the North, such as the Møre Basin. As such, Penguin B was potentially a free agent with respect to the general North Sea paradigm.

The Brent Group structures, Penguin C and D exhibited bimodal and mid-range ages, 70 Ma to 30 Ma, typical of other fields in the Brent province, though once again the spectre of contamination appeared in the form of the oldest age in the Penguin array, at approximately 130 Ma, for Penguin D.

Contamination and controversy

Certainly, a consideration of the Penguin data array relative to published arrays for the region prompts obvious comparisons with the Liewig et al. (1987) 120 Ma-40 Ma suite from the Alwyn field, Southern Grouping – Chapter three, Figure 3.4. However, this comparison is easily refuted on closer inspection. Liewig et al. had a clear correlation between fraction size and age, highly suggestive of contamination. The data was also associated with a structurally simple field relative to the Penguin complex. Secondly, the Penguin data is locally, geographically coherent and self-consistent with respect to individual samples and well suites, showing similar ages for individual wells, and vitally, only a slight increase in age with size fraction, with the exception of one data point, though the structure in question has a separate sample that corroborates the exceptionally old age for illite diagenesis – Chapter four, Figure 4.23. Thirdly, the samples appeared to be of high purity when examined by TEM, and under careful scrutiny by ATEM, appeared to be virtually feldspar free when individual contaminant particles were analysed. Thus, the K-Ar data is considered to be authentic.

Intriguingly, considering the shallowness of some of the Penguin structures and their proximity to the youngest ages recorded for the Northern North Sea region, the data set failed to return unusually young ages, and certainly nothing indicative of zero-age illite. Despite this, the data set as a single field suite, when considered in the larger regional context of patterns established for the East Shetland Basin, and even in conjunction with the local field of Magnus, with its 70 Ma to 40 Ma primary suite, laid down a seemingly impossible challenge when considering the defence of the null hypothesis. On the face of it, relating the Penguin suite of ages to an event-driven petroleum system model for illite diagenesis seemed absurd. Indeed, the hope that such a model would extrapolate to explain not just fragments of a single data array but the whole pool, including the generalities of the regional pattern – Figure 7.1, complexities within individual fields, and the zero-age phenomenon seemed farcical. The new Penguin data set was open to dismissal as an artefact of contamination, and such was the initial response from sponsors and the wider scientific community on presentation of the K-Ar age data.

However, the local, geographical pattern of the Penguin suite, the Penguin A correlation with errant ages for the Magnus field, and TEM photographs of clean illite separates suggested the possibility that this highly unusual data set had an underlying geological integrity, signifying something quite out of the ordinary with respect to illite diagenesis and petroleum systems of the Northern North Sea. Furthermore, the same illite aliquots yielded a coherent and respectable suite of stable isotope values for oxygen and deuterium, which indicated reasonable temperatures for both illite diagenesis and the likely timing of hydrocarbon charge to the Penguin field structures – Chapter four, section 4.92.

7.3 The Magnus Model

A basin modelling study, as presented in chapter five, examined the output from an industry-standard two-dimensional modelling code for a generic petroleum system based upon the architecture, stratigraphy and boundary conditions of the Penguin and Magnus field areas, East Shetland Basin. A simple configuration, along dip of the Magnus terrace, encompassing a deep basin, the Magnus Embayment, to the westnorthwest, and shallow horst structure to the eastsoutheast was chosen as representative of the regional configurations between oil fields and local kitchen areas. In this respect the model study intended to shed light on the local variation to the null hypothesis, that fibrous illite grew in response to the critical moment of oil charge.

Great expectations

In light of the unusual K-Ar data extracted from the Penguin field study, expectations concerning the likely correlation between the simulation output and Magnus-Penguin isotopic data suites were low. In this respect, the model was only intended to meet the original aims and obligations of the PhD research as quickly and effectively as possible, without necessarily resolving the illite diagenesis conundrum. In hindsight, this parsimonious approach was advantageous in that model construction was simple, and calibration to observed parameters such as pressure, temperature, stratigraphy and vitrinite reflectance rigorously adhered to in the inevitable refinement of the multiple simulation

series. Such low expectations with regard to matching the full suite of local Penguin and Magnus illite ages meant that this data set remained independent of calibration considerations and as such, the Northern Group data suite retained its integrity as an independent parameter against which the model could be compared and ultimately tested.

Calibration and validation

The surprising output of the calibrated simulations, series two and series three - Chapter 5, sections 5.72 to 5.73, and the excellent correlation of these simulations with the local K-Ar suite for the Magnus and Penguin fields and aspects of the local and regional suites was an encouraging validation of null hypothesis, and clearly distinguished between local –charge and regional fill-spill variations. The former proposition is favoured and the latter rejected – Figure 7.2.

The calibrated basin model simulation for half graben, shallow-charge timings from the local Penguin-Magnus kitchen area match the orthodox K-Ar suite from Magnus field. Additionally, the local deep-charge kitchen area simulation provides an excellent match for the older ages in Magnus and all ages for the related Penguin A field area. This simple generic model, when calibrated to parameters associated with a specific petroleum system, independent of the diagenetic system, gives a comprehensive and robust simulation of the Magnus petroleum system that accurately corresponds to K-Ar ages, and the associated apparent timing of fibrous illite diagenesis throughout the Magnus province. This meets the criteria of a successful calibration and also provides an unexpected correlation with all isotopic data for the Magnus and the Penguin A fields. As a consequence, the working title of the *Magnus model* expanded to signify not just the field, but the whole province.

The Magnus Model also implied that the north end of Penguin C had been exposed to a hydrocarbon charge at around 70 Ma, from either the Magnus province half graben, or a kitchen area at about the same depth. A related implication, was that the slightly elevated Penguin D structure had been charged slightly later by a shallower kitchen area at around 35 Ma – both reasonable propositions. In other words the simplest interpretation of the calibrated simulation strongly suggested that illite diagenesis was an unambiguous response to the onset of hydrocarbon charge; that the principal controlling factor was the depth and burial history, not of the reservoirs, but the local kitchen area.

Extrapolation I - deeper

Perhaps just as surprising were the straightforward extrapolations of the calibrated model. The Penguin field data still seemed incongruous as a result of the exceptionally old ages recorded for the Penguin B field. However, as noted before, Penguin B appeared to be plumbed into the deeper proto-Atlantic basin to the North, the Møre Basin. As the Magnus Embayment progressively deepens to the northeast, before merging with the Møre Basin, it was a simple thematic leap to consider the effect on simulation output of changing the deep kitchen area. A reasonable estimation of the Møre Basin Kimmeridge Clay Formation source rock depth at around 7000 meters due north of Penguin B, along

the likeliest migration pathway, not only resulted in an extrapolated simulation of condensate expulsion from this deeper kitchen area at the present day, but also indicated that the critical moment of oil charge to the Penguin B horst occurred at approximately 120 Ma. This simple extrapolation of the Magnus Model correctly predicts the oldest and most unusual illite ages measured for the Northern North Sea. At the first attempt. The illite age is thought to signify the onset of oil migration at the critical moment of charge into the field, as the calibrated Magnus model matches the span of ages for the Magnus field to the duration of charge from the shallow Magnus province kitchen area.

Extrapolation II - shallower

The final variation on the calibrated model involved switching off the deep and shallow kitchen areas associated with the Magnus province in order to examine the thin and shallow remnant of Kimmeridge Clay Formation source rock included for the Brent province, situated on the Eastern flank of the Penguin horst, directly overlying the shallow Penguin C structure. This area highlights the timing and position of the shallowest kitchen areas likely to charge Mesozoic trap structures in the Northern North Sea. This area was originally included in the model as an artefact of ending the modelled section along dip and slightly further east of the last calibration well on the line, well 211/13-6.

Once again, the model remained calibrated to principal measured variables and stratigraphy. This time, however, the timing of generation and the onset of migration for this shallowest of kitchen areas provided an excellent match for the youngest age in the Northern Group, at 17 Ma; the youngest age in the Northern North Sea for that matter.

Calibration -shallow	*Calibration - deep*	*Extrapolation I -deeper*	*Extrapolation II -shallower*
70 Ma – 40 Ma	90 Ma	120 Ma	15 Ma

Table 7.1 Simulated critical moments for *Magnus Model* kitchens, Magnus-Penguin petroleum system

Zero-age problem resolved

The implication of the latter extrapolation is clear: the shallowest Mesozoic traps to have been drilled so far occur at this position; if these sandstones have been charged by local source rocks immediately overlying or down-dip of the structure, they are apparently exposed to a hydrocarbon charge no later than 15 Ma. In other words, assuming such structures are not plumbed into the deeper kitchen areas typical of the region, the very last opportunity for the onset of hydrocarbon charge would occur at about 15 Ma. No later. As a consequence, the extrapolation clearly indicates that 15 Ma is the youngest ceiling for both illite diagenesis and hydrocarbon charge in the region. No zero-age illite is to be found in Mesozoic sandstones. Once again, the principal control is the depth and burial history of source rocks in closely associated kitchen areas, and not the temperature of the trap sandstones.

A further independent validation of the model output and K-Ar illite ages is provided by the stable isotope data. The coherent and plausible geographical patterns of the radiogenic isotope data are

matched by similar patterns for the deuterium and oxygen data for the same aliquots – Chapter 4, Figures 4.25 and 4.26. Contamination would have distorted any coherent patterns in both sets of data, and made concordance between the two data sets highly unlikely. Additionally the temperatures, associated depths and likely timings of illite diagenesis indicated by the stable isotopes are in accord with the likely timing of early to late hydrocarbon charges for the Penguin trap structures.

The only obvious discrepancy between the model and the Penguin experimental data suite is the old Penguin D age. It is apt, in lieu of this, that contamination remains an issue. The risk to samples is no less fierce in light of a refined model for illite diagenesis. And yet, condensate occurs in the Penguin D trap structure, as it also occurs in Penguin B, implying a connection to the deep Møre basin and old oil charge. However, the age is still significantly older than the Penguin B suite at 135 Ma. It is an intriguing possibility that this small area of Penguin D was somehow plumbed into the deep Møre basin, and yet, the analytical procedure remains an uncertain aspect of this highly sensitive method.

7.4 Discussion

In retrospect, the surprisingly coherent outcome of the research, and in particular the welcome correlation of simulations, calibrated and extrapolated, for the modelling study presented in chapter five, in regard to both the Penguin and Magnus measured K-Ar ages as presented in chapter four, and more generally with respect to the geographical pattern of the wider Northern North Sea population presented in chapter three, has been the unifying aspect of this study – Figure 7.3. However, it is worth noting that at one time in the study considerable effort was directed towards finding an alternative antithesis to explain the Penguin ages, sympathetic to the closed system school of illite diagenesis. A brief synopsis of this distinct, and ultimately unsustainable, approach to resolving the Penguin isotopic data has been included in the text – Chapter 6. And so, the dominant conceptual model resulting from research undertaken for this thesis is as follows.

Oil and water - a petroleum system model for illite diagenesis

Diagenesis is generally perceived as a secondary consideration when attributing reservoir quality to basinal sandstones. However, despite the primacy of sedimentary input, depostional facies, grain size and sorting, diagenetic alteration remains a significant factor. Given that a reservoir sandstone is the prerequisite target of hydrocarbon exploration in the Northern North Sea, two vital controls on Northern North Sea reservoir quality and recoverable returns, as measured in barrels and dollars, are porosity and permeability damage by quartz overgrowths and fibrous illite diagenesis respectively.

Considerable expertise and time, therefore has been spent on understanding and predicting the occurrence of these two diagenetic phenomena. As part of that intellectual drive, it was the remit of this PhD to resolve the difficulties pertaining to an understanding of fibrous illite diagenesis in the petroleum systems of the Northern North Sea.

As discussed at length in the above passages, the body of research relating to this study clearly indicates that Sommer (1975, 1978) had a clear and valuable understanding of the relationship between a reservoir-damaging illite cement phase and oil field evolution. In one respect, the thesis stands as a validation of his original findings. However, it is also hoped that this study has managed to take his work on further, clarifying the precise nature of the relationship between petroleum system dynamics and fibrous illite diagenesis, in presenting a clear conceptual model of this unusual symbiosis between oil, water and a small, curiously formed crystal.

The new conceptual model clears the ground of numerous qualifications, criticisms and provisos that have dogged the illite age-dating technique for nigh on twenty years. A brief description of the new illite diagenesis paradigm follows, and a revised formulation of the original null hypothesis, incorporating the favoured variation, is formally documented below.

How it was – how it appears to be

Fibrous illite diagenesis in sandstone reservoirs of the Northern North Sea is an episodic phenomenon. The fibrous crystals appear to grow within the pore spaces of oil fields in direct response to the onset of hydrocarbon migration into the trap structure from locally maturing source rocks. In this respect, illite diagenesis is event-driven, and the resultant K-Ar illite ages accurately indicate the timing of this hydrocarbon charge, specific to a coupled trap structure and kitchen area. As a consequence, the permeability reduction that damages the possibility of oil recovery from a field occurs millions of years before industrial intervention, at the critical moment of hydrocarbon charge – Figure 7.3.

The crest of the trap structure tends to experience oil incursion and residence first, resulting in the oldest age. This is followed by a descending profile of decreasing ages which are highly likely to record the duration and extent of progressive filling within the oil field. A juxtaposition of small kitchen areas around a single structure, undergoing local variations in burial history, will result in multiple charges to the associated oil fields; this results in distinct phases of permeability damage. Present day subcrop maps of the East Shetland Basin give a reasonable indication of the complex and prolific juxtapositions of structural highs and intra-terrace kitchen areas – Figure 7.4.

The stability field of illite diagenesis, above 50°C appears to encompass most likely trap structure - kitchen area configurations on the Mesozoic terraces of the Viking Graben and Møre Basin, and as such is likely to have recorded the earliest onset of hydrocarbon charge in the region at around 120 Ma. Fibrous illite diagenesis is a sensitive indicator of local change in the dynamics of the Northern North Sea petroleum systems, accurately recording the last significant phase of fresh hydrocarbon charge amongst the shallow terrace areas at around 15 Ma. Five phases of illite growth and associated hydrocarbon charge are clearly distinguishable for the East Shetland Basin, at around 130-110 Ma, 90 Ma – 80 Ma, 70 Ma - 50 Ma, 45 Ma - 30 Ma; 25Ma to 15 Ma - Figure 7.5. These record the five principal episodes of hydrocarbon charge in the Northern North Sea petroleum systems – Table 7.2.

Shallows -ESB	*Mid terraces -ESB*	*Viking Graben*	*North Shetland Trough*	*More Basin*
15 Ma – 25 Ma	30 Ma –45 Ma	50 Ma –70 Ma	80 Ma –90 Ma	110 Ma –130 Ma

Table 7.2 Illite age profiles and inferred episodes of oil charge for the Northern North Sea

The null hypothesis

The episodic nature, parochial occurrence and variable timing of critical moments throughout the region account for the zero age illite conundrum, and equally address the subtle aspects of the regional review such as bimodality, age inversion and locally pervasive clusters, or modalities, in age arrays.

The far-reaching implications of such a model, the simplicity of its machinations, and potential complexity of possible outcomes, are all reliant on a simple set of assumptions implicit in the null hypothesis. These various facets combine to present a simple, yet effective conceptual model, complete in itself, and expressible in the null hypothesis stated below.

> *Fibrous illite diagenesis in the oil field reservoir sandstones of the Northern North Sea is a response to the onset of hydrocarbon charge from local kitchen areas. Potassium-argon ages for the finest fractions of illite obtained from such sandstones accurately indicates the critical moment of hydrocarbon charge to these trap structures.*

The hypothesis stands. The excellent match for the calibrated petroleum system simulations, the simple, yet successful extrapolation of the same basin model and its clear and lucid implications when considering the region as a whole all favour the catastrophic proposition. And so, in conclusion, the thesis has led to a clear vindication of the original null hypothesis and a useful refinement of the original formulation.

7.5 A review of aims and outcomes

The five principal aims of this research project were intended to distinguish between rival hypotheses for fibrous illite diagenesis – either as a closed system temperature-dependent phenomenon or an open system catastrophic response to oil charge. These are reviewed below.

• to review the geological context and occurrence of illite in the Northern North Sea by compiling maps, cross-sections and stratigraphic compilations of illite age data available in the public domain for the East Shetland Basin, Viking Graben and Norwegian Shelf.

• to formulate hypotheses of illite growth mechanisms in Jurassic sandstone reservoirs of the East Shetland Basin, and test these by the analysis and synthesis of data collated in the review of the Northern North Sea.

• to test the validity of predictions based on the Northern North Sea data synthesis by sampling and experimentally dating fibrous illite aliquots extracted from sandstone cores of reservoir compartments associated with an East Shetland Basin oil field, namely the Penguin field.

• to examine rival hypotheses of illite formation for the Penguin oil field, and computationally model the associated petroleum system, including the adjacent Magnus field.

• to synthesise the results of the petroleum system model, local experimental study, and regional data interpretation into an original conceptual model of the relationship between illite diagenesis and fluid flow history for the Northern North Sea.

Implications, conjectures and suggestions

These aims have been met, a new null hypothesis formulated and the general principles and premises of the study discussed at length in the preceding passages. It only remains to consider the implications and suggestions for further work arising from this research.

• The apparent accuracy of the illite ages with respect to the simulated timing of hydrocarbon charge to the Magnus and Penguin field structures implies that unknown kitchen areas and critical moments of hydrocarbon charge may be identified in prospective frontiers by measuring illite ages for sandstone cores extracted from successful wild cat wells at much shallower burial depths. Note that while a critical moment of oil charge is the favoured explanation for the pattern of illite ages in the Northern North Sea, this does imply that the event is instantaneous; the phrase refers to a geologically significant moment as event-related. As such, the critical moment hypothesis conforms to a neo-catastrophist view of episodic, event-related changes in petroleum systems, in stark contrast to the uniformitarian argument of closed system chemical evolution of petroleum basin sandstones.

• The occurrence of multiple ages in such wells would imply the occurrence of multiple charges, numerous kitchen areas and possibly numerous source rock depths in frontier basins. Oil charge to structurally high fields juxtaposed between local kitchen areas is likely to be multi-modal.

• Regional migration discrepancies, and associated fairway problems may be secondary considerations relative to the local configuration of small kitchen areas. Probability factors for prospectivity could be weighted accordingly.

• Field specific unimodal arrays of illite ages that show a coherent decrease in age with depth may be recording the precise timing of oil-water contact descent and duration of trap filling. This implication would allow a time-scale to be established for charge-associated quartz cementation and resultant porosity impairment in fields such as Miller, North Sea – see Marchand *et al.* (2000).

• Penguin A may have recorded unimodal ages, having retained the original oil charge, preventing a second episode of illite diagenesis. Magnus, by contrast, may record bimodality as it failed to retain the first oil charge and so underwent a second episode of oil accumulation.

• Despite the Penguin B trap structure being in close proximity to Penguin A, fibrous illite diagenesis, and related charging are discrete and independent of each other. By implication, the four structures in Penguin A, B, C and D appear to be plumbed into four separate kitchen areas. Faults are sealing, migration pathways are discrete and specific to each compartment. Generalised models of hydrocarbon charge even for small provinces may be misleading.

• Conjecture - the distribution of illite within an oil field and juxtaposition of different ages may be a artefact of first phase-second phase permeability pathways which will differ significantly with each new charge. In other words, early illite growth may be expected to grow and impede flow along the flow networks that had the best permeability at the time of migration. Such pathways may possibly show less mature diagenetic profiles than areas than areas of later illite growth.

• Conjecture - assuming that the micro-scale dynamics of illite growth are related to individual pores filling with oil and reaching a critical oil-water saturation and related chemistry, then the kinetics of water expulsion, and resultant illite diagenesis is likely to be exclusive to oil charge. Alternatively, the onset of local oil charge may possibly be associated with deep-water movement and related chemical changes in the pore spaces of the trap structure without implying the filling of individual pores with oil droplets. In other words, illite diagenesis may also result from significant perturbations in the system such as overpressure, exotic fluid migrations and tectonic events.

Either way, critical oil-water saturation and the related pore chemistry of sandstone formation waters is a controversial and specialised research field. While the thesis attempts to explain the regional 200 km pattern as a consequence of local 10 km scale basin dynamics within small sub-systems of the petroleum province, the meso-to-microscopic scale of cation supply and pore fluid dynamics are beyond the scope of this study. However, it does seem reasonable to conjecture that the origin of K^+ and Al^{3+} ions is to be found in the unstable, dissolving potassium feldspars evident in sampled sandstones. As such it is likely that cation transport is in solution and over short distances, at most one or two pore voids, from a corroding feldspar to the growing face of an illite fibre.

However, on the basis of apparent oil-water contact descent profiles and the observed morphology of illite i.e. occupying pore throats and interstitial spaces between grains, and absent from the central pore space occupied by oil droplets, the former conjecture, of pores filling with oil and fibrous illite growing in the remaining bound water in response to oil charge, is favoured over the latter. Is all.

—

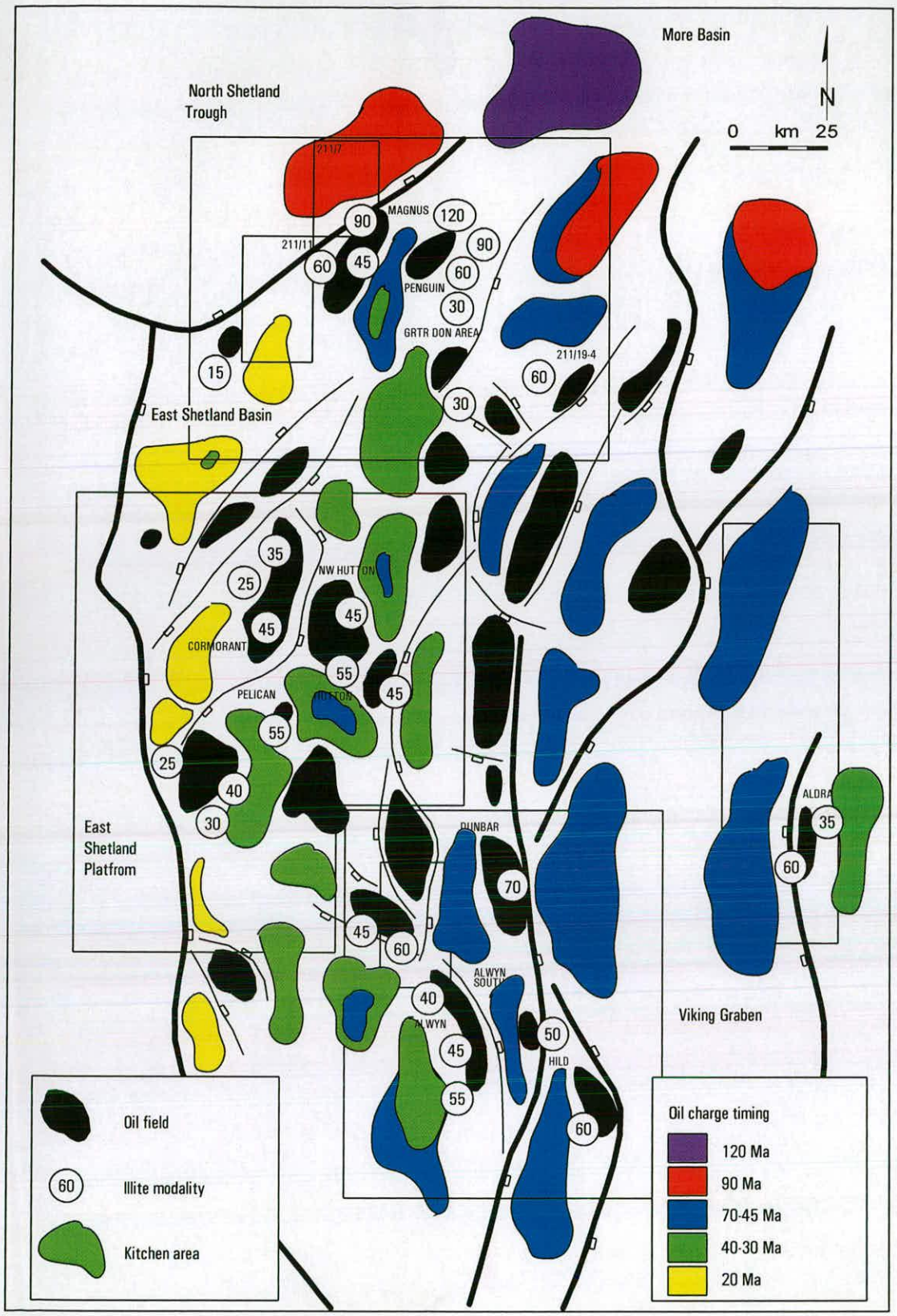

Figure 7.1 Critical moments - a map of hydrocarbon charge timing and illite age modalities for the Northern North Sea. The location, extent and timing of local kitchen areas as presented are thematic.

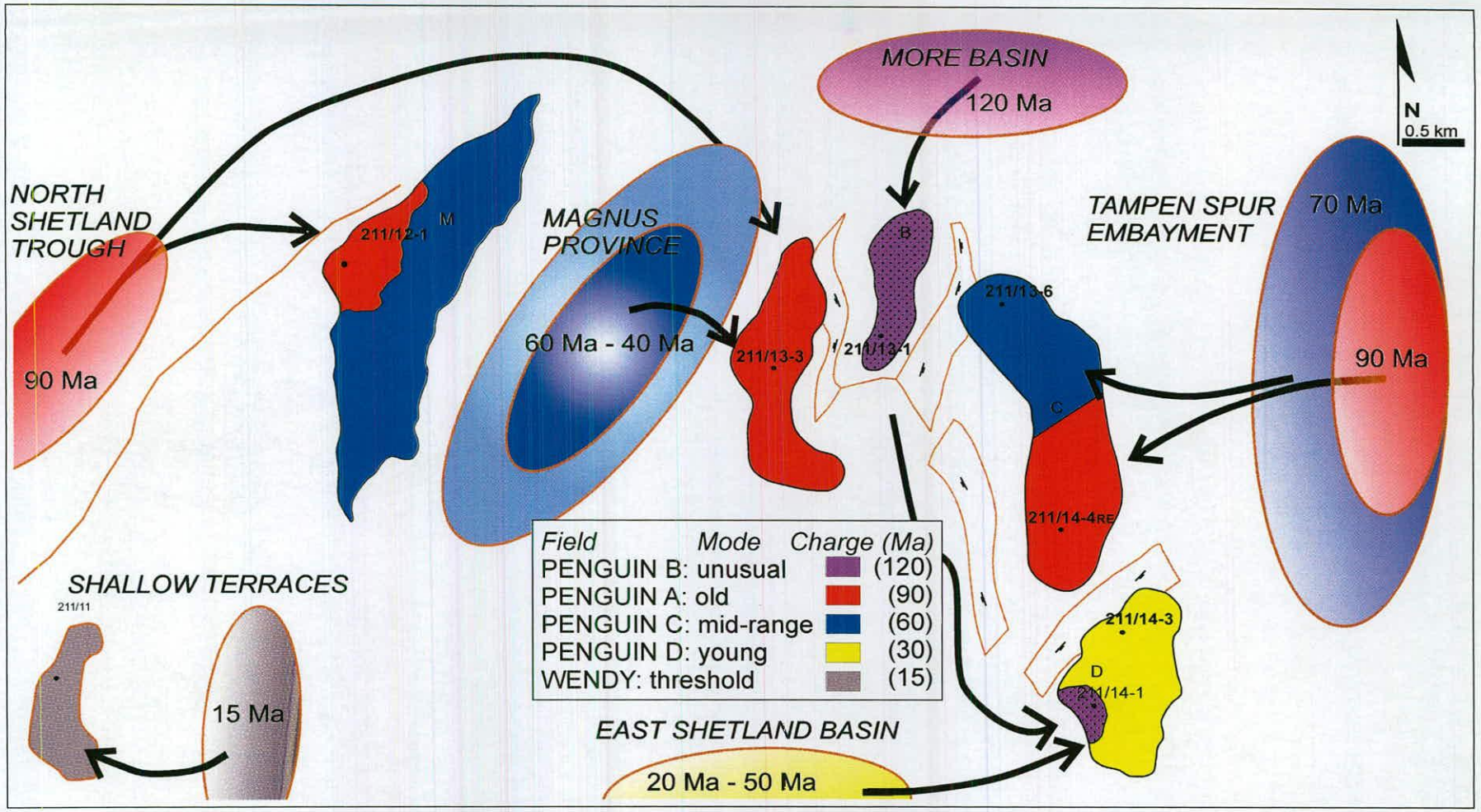

Figure 7.2 A model for oil charge from provincial kitchen areas for the Northern Group. This illustrates the juxtaposition of active kitchen areas and the closest geographical arrangement of the five principal modalities for the Northern North Sea. These various critical moments result in multiple charges and episodes of illite growth. While this conceptual model resembles an interpretation of illite data presented earlier - Chapter 4, Figure 4.30, the vital difference is that this version is fully supported by the independently calibrated *Magnus Model*.

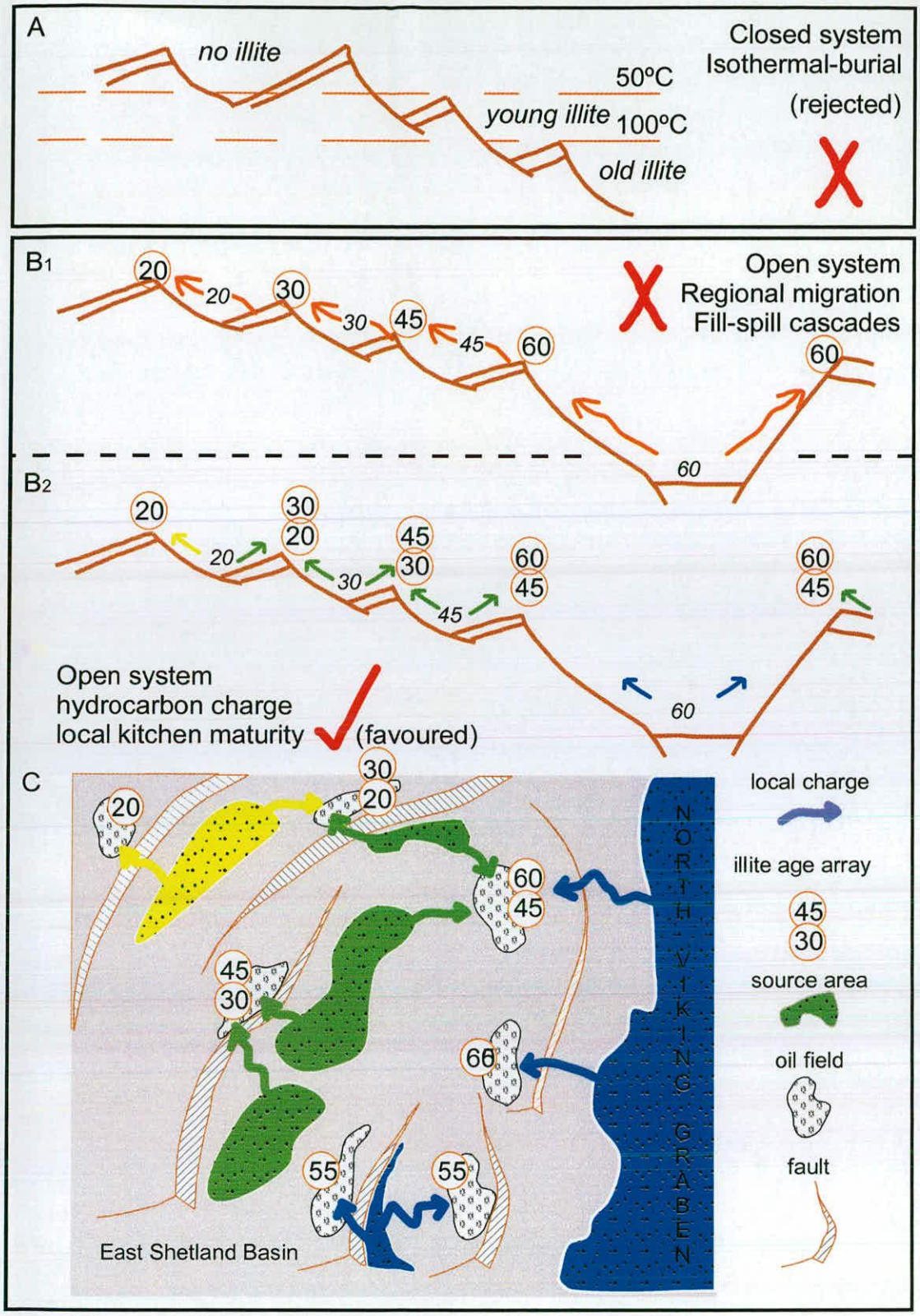

Figure 7.3 Simple hypothetical scenarios for illite diagenesis in oil fields. A - the closed system formulation, which is highly dependant on burial-related temperature thresholds, and fails to account for complexity in the data. B - two open system formulations. These differ in the nature and extent of hydrocarbon migration. C - a conceptual map of local charge and resultant illite ages for the area. The study has met the principal aim of discriminating between two opposing schools , rejecting the closed system proposition in favour of a local charge variation of the open system hypothesis.

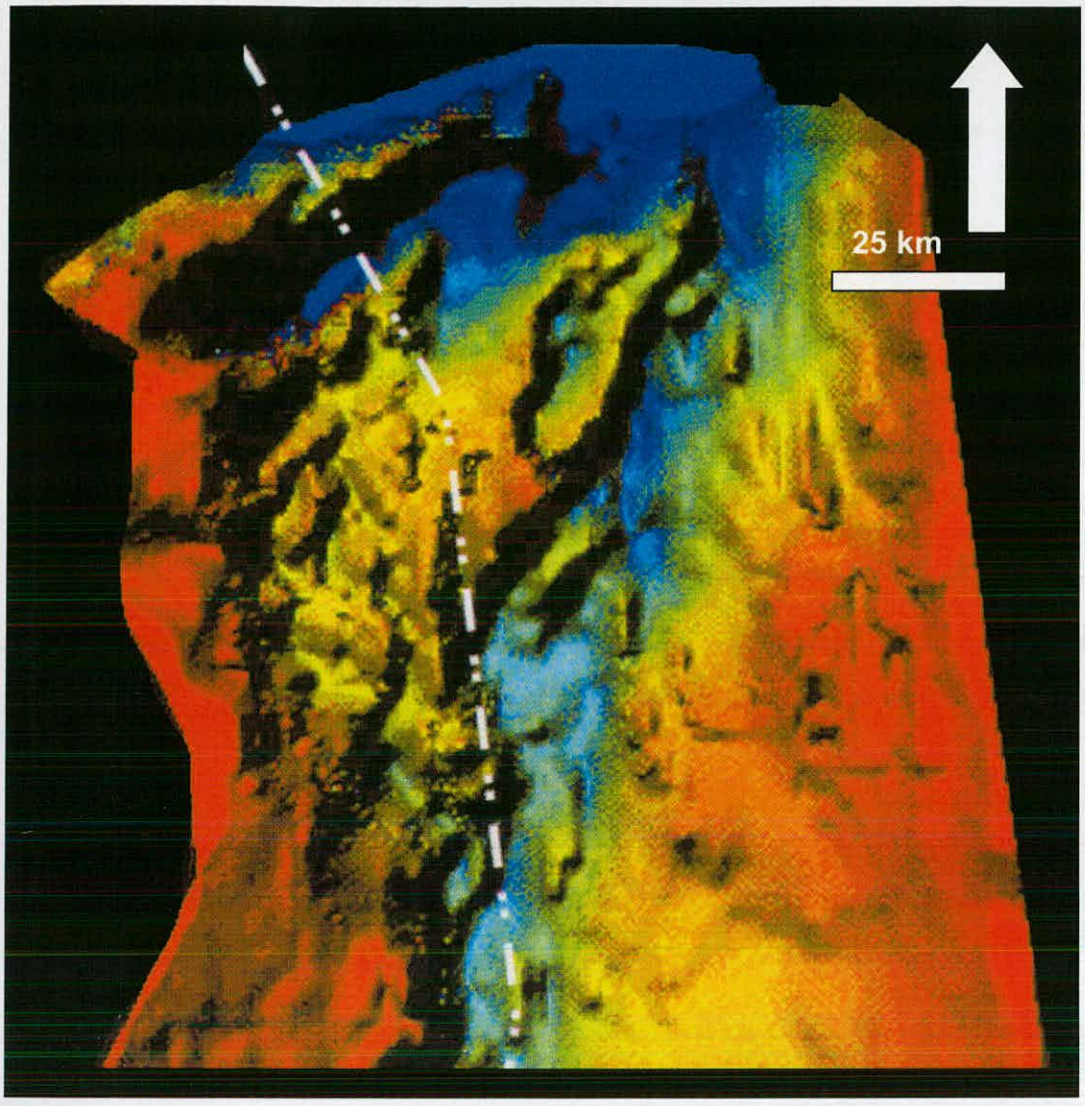

Figure 7.4 A 3-D relief map of the Viking Graben pre-Cretaceous subcrop. The illumination is from the west, the white arrow indicating true north. The stipled line represents the political boundary between British and Norwegian interests. The depth representation is a rainbow spectrum from shallow red on the platform to deep blue in the graben and northern embayments. The map gives a reasonable indication of the numerous local deeps that house the kitchen areas, resulting in multiple episodes of hydrocarbon charge (Shell UK, 1998).

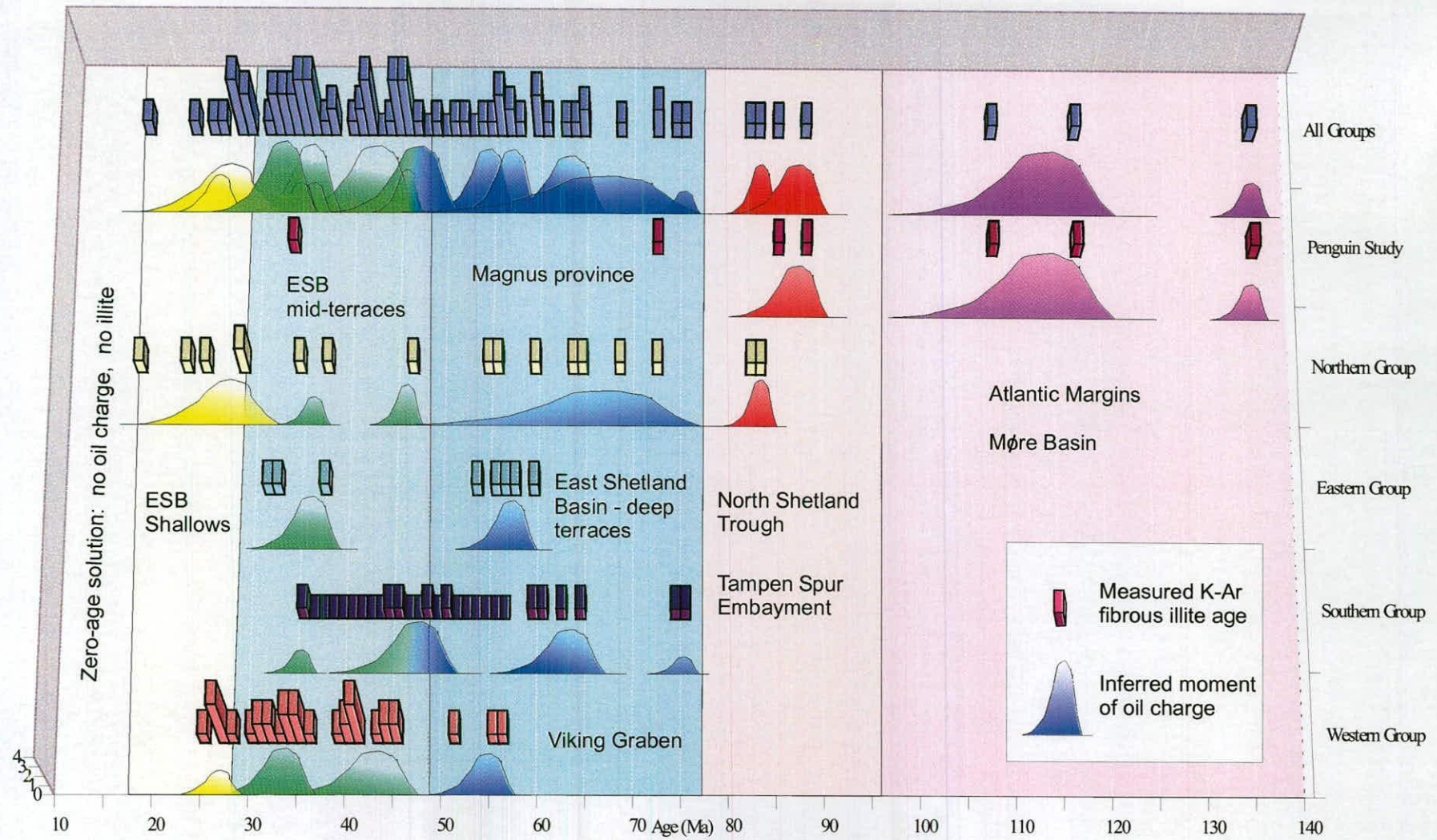

Figure 7.5 A histogram of measured illite ages and inferred episodes of hydrocarbon charge in the Northern North Sea. Fibrous illite records the critical moment.

Aagaard, P., Egeberg, P. K., Saigal G. C., Morad, S. & Bjørlykke, K. 1990. Diagenetic albitization of detrital K - feldspar in Jurasic, Lower Cretaceous and Tertiary clastic reservoir rocks from offshore Norway, II. Formation water, geochemistry and kinetic considerations. *Journal Sedimentary Petrology*, **60**, 575-581.

Andersen, T. B. 1991. A review and discussion of the stratigraphy and accretion history of the outboard terranes in the SW Norwegian Caledonides, *Terra Abstracts,* **4**, Blackwell Scientific.

Andrews-speed, C. P.; Oxburgh, E. Ron; Cooper, B. A. 1984. Temperatures and depth dependent heat flow in western North Sea, *American Association of Petroleum Geologists Bulletin*, **68**, 1764-1781.

Aronson, J. L. & Burtner R. L. 1983. K/Ar dating of illitic clays of Jurassic Nugget sandstone and timing of petroleum migration in Wyoming Overthrust Belt. *American Association of Petroleum Geologists Bulletin*, **67**, 414.

Audet, D. M., Fowler, A. C. 1992. A mathematical model for compaction in sedimentary basins. *Geophysical Journal International*, **110**, 577-590.

Badley, M. E., Price, J. D., Rambech dahl, C. & Agdestein, T. 1988. The structural evolution of the northern Viking Graben, *Journal of the Geological Society of London*, **145**, 455-472.

Barclay, S. A., Worden, R. H., Parnell, J., Hall, D. L. & Sterner, S. M. 2000. Assessment of fluid contacts and compartmentalisation in sandstone reservoirs using fluid inclusions: An example from the Magnus Oil Field, North Sea. *American Association of Petroleum Geologists Bulletin*, **84**, 489-504

Beach, A., Bird, T. & Gibbs, A.D. 1987. Extensional tectonics and crustal structure: deep seismic reflection data from the Northern North Sea Viking Graben. *In:* Coward, Dewey and Hancock (eds), *Extensional Tectonics*, Special Publication, Geological Society, London, **28**, 467-476.

Beard, D. C. & Weyl, P. K. 1973. Influence of texture on porosity and permeability of unconsolidated sand. *American Association Petroleum Geologists Bulletin*, **57**,349-369.

Bertram G. T. & Milton, N. J. 1989. Reconstructing basin evolution from sedimentary thickness; the importance of palaeobathymetric control with respect to the North Sea. *Basin Research*, **1**, 247-257.

Bethke, C. M., 1986. Inverse hydrologic analysis of the distribution and origin of Gulf Coast-type geopressured zones. *Journal of Geophysical Research*, **91**, 6535-6545.

Bethke, C.M. & Marshak, S. 1990. Brine migrations across North America - the plate tectonics of groundwater, *Annual Review Earth and Planetary Sciences,* **18**, 287-315.

Bjorkum, P. A., Oelkers, E. H., Nadeau, P. H., Walderhaug, O. & Murphy W. M. 1998. Porosity Prediction in Quartzose Sandstones as a Function of Time, Temperature, Depth, Stylolite Frequency, and Hydrocarbon Saturation. *American Association of Petroleum Geologists Bulletin*, **82**, 637-648.

Bjorlykke, K, Nedkvitine, T, Ramm, M & Saigal, GC. 1992. Diagenetic processes in the Brent Group (Middle Jurassic) reservoirs of the North Sea: an overview. *In:* Morton, A. C., Haszeldine, R. S., Giles, M. R. & Brown, S. (eds) *Geology of the Brent Group.* Geological Society, London. Special Publications, **61**, 263-287.
Booth, A., Stockley, F. J. & Robbins, J. A. 1992. Late Jurassic Structural Inversion in the North Viking Graben and East Shetland Basin, UK North Sea. *Energy Exploration and Exploitation*, **10**, 281-299.

Brennand, T. P., Van Hoorn, B. & James, K. H. 1990. Historical Review of North Sea Exploration. *In:* Glennie, K. W. (Ed) *Introduction to the Petroleum Geology of the North Sea.* 3rd Edition. Blackwell, 1-33.

Brint, J. F., Haszeldine, R. S., Hamilton, P. J. & Fallick, A. E. 1988. Isotope diagenesis and fluid movement in Brent sandstones, northern North Sea. In: *Clay Diagenesis in Hydrocarbon Reservoirs and Shales. Conference Abstracts. Clay Minerals Group. Mineralogical Society, Cambridge, UK, 2.*

Brodie J. & White N. 1994. Sedimentary basin inversion on the European continental shelf. *Geology*, **22**, 147-150.

Bryant, S., Cade, C. & Mellor D. 1993. Permeability prediction from geological Models. *American Association of Petroleum Geologists Bulletin*, **77**, 1338-1350.

Buchardt, B. 1978. Oxygen isotope palaeotemperatures from the Tertiary North Sea. *Nature*, **275**, 121-123.

Budding, M. C. & Inglin, H. F. 1981. A reservoir geological model of the Brent Sands in southern Cormorant. *Petroleum geology of the continental shelf of North-West Europe; Proceedings of the second conference*, 326-334.

Burrus, J., Kuhfuss, A., Doligez, B. & Ungerer, P. 1992. Are numerical models useful in reconstructing the migration of hydrocarbons? A discussion based on the Northern Viking Graben. *American Association of Petroleum Geologists, Bulletin*, **75**, 215-233.

Burrus, J., Osadetz, K.G., Wolf, S., Doligez, B., Visser, K., & Dearborn, D. 1996. A two-dimensional regional model of Williston hydrocarbon systems. *American Association of Petroleum Geologists, Bulletin*, **80**, 265-291.

Burst, J. F. 1969. Diagenesis of Gulf Coast clayey sediments and its possible relation to petroleum migration. *American Association of Petroleum Geologists Bulletin*, **53**, 73-93.

Clauer N, Zwingmann H & Chaudhuri S. 1996. Isotopic (K-Ar and oxygen) constraints on the extent and importance of the Liassic hydrothermal activity in western Europe. *Clay Minerals*, **31**, 301-318.

Coleman, M. L. 1999 *UK Petroleum Exploration Society of Great Britain Newsletter.* October, 12-17.

Cornford, C. 1990. Source rocks and Hydrocarbons of the North Sea. *In:* Glennie, K. W. (ed) *Introduction to the Petroleum Geology of the North Sea.* 3rd Edition. Blackwell, 294-361.

Cornford, C. 1994. Mandal-Ekofisk petroleum system in the Central Graben of the North Sea. *The petroleum system - from source to trap, American Association of Petroleum Geologists Memoir*, **60**, 537-571.

Coward, M. P. 1990. Caledonian framework. *In:* Brooks, J. & Hardman, R. F. P. (eds) *Tectonic events responsible for Britain's Oil and Gas Reserves. Geological Society, London, Special Publication*, **55**, 37-43.

Craig, H. 1961. Isotopic variations in meteoric waters. *Science*, **133**, 1702-1703.

Darby, D. 1995. Overpressure in the Central North Sea. *Ph. D. thesis, Department of Geology and Applied Geology, Glasgow University*, 157–167.

Darby D., Haszeldine R. S. & Couples G. D. 1996. Pressure cells and pressure seals in the UK Central Graben. *Marine and Petroleum Geology*, **13**, 865-878.

Darby, D., Wilkinson, M., Fallick, A. E. & Haszeldine, R. S. 1997. Illite dates record deep fluid movements in petroleum basins. *Petroleum Geoscience*, **3**, 133-140.

Darby, D., Haszeldine, R. S. & Couples, G. D. 1998. Central North Sea overpressures: insights into fluid flow from one and two dimensional basin modelling. *Geological Society, London, Special Publications*, **141**, 95-107.

Dawers, N.H., and Underhill, J.R. 2000. Fault interaction and linkage in syn-rift stratigraphic sequences: Late Jurassic, Statfjord East, Northern North Sea. *American Association of Petroleum Geologists Bulletin*, **84**, 45-64.

Davies, S. J., Dawers, N. H., Underhill, J. R. & Mcleod, A. E. 1999. Spatial and Temporal Evolution of Early syn-rift Deposition: Middle Jurassic Tarbert Formation, Northern North Sea. *In: Extended Abstract Volume, Sedimentary Environments of Offshore Norway - Palaeozoic to Recent, Norwegian Petroleum Society*,111-112.

De Segonzac, D. 1970. The transformation of clay minerals in diagenesis. *Sedimentology*, **15**, 281-346

Department of Trade & Industry, 1995. The Energy Report - *Oil & Gas Resources of the United Kingdom*, **2**, 204.

Dewers, T. & Ortoleva, P. 1994. Nonlinear dynamical aspects of deep basin hydrology: Fluid compartment formation and episodic fluid release, *American Journal of Science*, **294**, 713-755.

Doré, A. G. 1991. The structural foundation and evolution of Mesozoic seaways between Europe and the Artic. *Palaeogeography, Palaeoclimatology, Palaeoecology*, **87**, 441-492.

Emery, D., Myers, K. J., Young, R. 1990. Ancient subaerial exposure in sandstones. *Geology*, **18**, 1178-1181.

Emery D., Smalley P. C. & Oxtoby N. H. 1993. Synchronous oil migration and cementation in sandstones demonstrated by a description of diagenesis. *Philosophical Transactions of the Royal Society, A*, **344**, 115-125.

England,W. A. & Fleet, A. J. 1991. (eds.) Petroleum migration. *Geological Society, London,* **59**, 89-109.

Fallick, A. E., Macaulay, C. & Haszeldine, R. S. 1998. Clays revisited: stable and radiogenic isotope data reviewed. In: Mineral Diagenesis and Reservoir Quality - the Way Forward. Conference Abstracts. *Clay Minerals Group/Petroleum Exploration Society of Great Britian/London Petrophysical Society/Geological Society of London*, Cambridge, UK.

Fleming C. G. 1996. Modern day temperature field, Central Graben, North Sea: investigation of conduction and fluid advection. *Ph. D. thesis, Department of Geology & Applied Geology, Glasgow University*, 72-76.

Fleming, C. G., Haszeldine, R. S. & Couples, G. D. 1998. Thermal effects of fluid flow in steep fault zones. Geological Society, London, Special Publications, **147**, 217-229.
Garven G. 1989 A hydrogeologic model for the formation of the giant oil sands deposits of the western Canada sedimentary basin. *American Journal of Science*, **289**, 105-166.

Garven G., Ge, S., Person, M. A. & Sverjensky, D. A. 1993. Genesis of stratabound ore deposits in the Midcontinent basins of North America. *American Journal of Science*, **293**, 497-568.

Giles, M. R. & De Boer R. B. 1989. Secondary porosity: creation of enhanced porosities in the subsurface from the dissolution of carbonate cements as a result of cooling waters. *Marine and Petroleum Geology*, **6**, 261-269.

Glasmann, J. R., Lundegard, P. D., Clark, R. A., Penny, B. K. & Collins, I. D. 1989. Geochemical evidence for the history of diagenesis and fluid migration: Brent Sandstone, Heather Field, North Sea. *Clay Minerals*, **24**, 215-232.

Glasmann, J. R. 1992. The fate of feldspar in Brent Group reservoirs, North Sea: a regional synthesis of diagenesis in shallow, intermediate, and deep environments. *In:* Morton, A. C., Haszeldine, R. S., Giles, M. R., Brown, S. (eds*) Geology of the Brent Group*. Geological Society, London. Special Publications, **61**, 329-350.

Glennie, K. W. 1990. Introduction to the Petroleum Geology of the North Sea. 3rd Edition. Blackwells, 330-344.

Glennie K. W. 1998. Petroleum Geology of the North Sea: Basic Concepts Recent Advances, Blackwells, 463-547.

Goff J.C. 1983. Hydrocarbon generation and migration from Jurassic source rocks in the East Shetland Basin and Viking Graben of the northern North Sea. *Geological Society, London*, **140**, 445-474.

Grathoff, G. H., Moore, D. M., Hay, R. L. & Wemmer, K. 1995. Illite from Lower Paleozoic Shale Partings in the Illinois Basin: Mineralogy & K-Ar Age. *32nd annual Clay Mineral Society Meeting, Baltimore, Maryland.*

Hamilton, P. J., Blackbourn, G. A., McLachlan, W. A. & Fallick, A. E. 1987. Isotopic tracing of the provenance and diagenesis of Lower Brent Group sands: *In:* Brooks, J. & Glennie, K. (eds). *Petroleum Geology of North West Europe*. Graham & Trotman, London, 939-949.

Hamilton P. J., Kelley S., Fallick A. E. 1989. K-Ar dating of illite in reservoirs. *Clay Minerals*, **24**, 215-23.

Hancock, N. J. & Taylor, A. M. 1978. Clay mineral diagenesis and oil migration in the Middle Jurassic Brent Sand Formation. *Journal of the Geological Society of London*, **132**, 69-72.

Haq B. U., Hardenbol J. & Vail P. R. 1987 Chronology of Fluctuating Sea Levels since the Triassic (250 million years to present). *Science*, **235**, 1156-1167.

Harrison W. J. & Tempel R. N. 1993. Diagenetic pathways in sedimentary basins. *In:* Robinson A & Horbury A. (eds) *Paleohydrology and Diagenesis, American Association of Petroleum Geologists*, **36**, 69-86.

Haszeldine, R. S., Samson, I. M. & Cornford, C. 1984. Quartz diagenesis and convective fluid movements: Beatrice Oilfield, UK, North Sea. *Clay Minerals*, **19**, 391-402.

Haszeldine, R. S., Brint J. F., Fallick A. E., Hamilton P. J., & Brown S. 1992. Open and restricted hydrologies in Brent Group diagenesis: North Sea. *In:* Morton A. C., Haszeldine R. S., Giles, M. R. & BROWN S. (eds) *Geology of the Brent Group*. Geological Society Special Publication, **61**, 401-419.

Haszeldine R. S. & Mckeown C. 1995. A model approach to radioactive waste disposal. *Terra Nova*, **7**, 87-95.

Haszeldine, R.S., Macaulay, C. I., Marchand, A., Wilkinson, M., Graham, C. M., Cavanagh, A., Fallick, A. E., & Couples, G. D. 2000. Cementation fluids in hydrocarbon basins. *Journal of Geochemical Exploration*, **69**, 195-200.

Hogg, A. J. C., Sellier, E. & Jourdan, A. J. 1992. Cathodoluminescence of quartz cements in Brent Group sandstones, Alwyn South, UK North Sea. *In:* Morton A. C., Haszeldine R. S., Giles M. R. & Brown S. (eds) *Geology of the Brent Group*. Geological Society Special Publication, **61**, 421-440.

Hogg, A. J. C., Hamilton, P. J. & Macintyre R. M. 1993. Mapping diagenetic fluid-flow within a reservoir – K-Ar dating in the Alwyn area (UK North-Sea). *Marine and Petroleum Geology*, **10**, 279-294.

Hospers, J. & Ediriweera, K. K. 1991. Depth and configuration of the crystalline basement in the Viking Graben area, Northern North Sea, *Journal of the Geological Society, London*, **148**, 261-265.

Hossack, J. R. & Cooper, M. A. 1986. Collision tectonics in the Scandinavian Caledonides. *Geological Society Special Publications*, **19**, 287-304.

Jourdan, A., Thomas, M., Brevart, O., Robson, P., Sommer, F. & Sullivan, M. 1987. Diagenesis as the control of the Brent Sandstone reservoir properties in the Greater Alwyn area East Shetland Basin. *In:* Brooks, J. & Glennie, K. (eds) *Petroleum Geology of North West Europe*, Graham and Trotmann, 951-961.

Joy, A. M. 1993. The pattern of post-rift subsidence in the northern North Sea basin. *In:* Williams, G. D. & Dobb, A. (ed) *Tectonics and seismic sequence stratigraphy, Geological Society Special Publications*, **71**, 123-140.

Kantorowicz, J. 1984. The nature, origin and distribution of authigenic clay minerals from Middle Jurassic Ravenscar and Brent Group Sandstones. *Clay Minerals*, **19**, 359-375.

Karlsen, D. A., Nedkvitne,T., Larter,S. R. & Bjørlykke, K. 1993. Hydrocarbon composition of authigenic inclusions-application to petroleum reservoir filling history. *Geochemica et Cosmochemica Acta*, **57**, 3641-3659.

Kirk, R.H. 1980. Statfjord field - A North Sea Giant. *In:* Halbouty, M.T. (ed) *Giant Oil and Gas fields of the decade 1968-1978. American Association of Petroleum Geologists Memoir,* **30**, 95-116.

Klemperer, S. 1988. Crustal thinning and the nature of extension in the northern North Sea from deep seismic reflection profiling. *Tectonics*, **7**, 803-821.

Knag, G. O., South, D. & Spencer, A. M. 1995. Exploration trends in the Northern North Sea (60-62N). *In:* Hanslien, S. (ed.) *Petroleum exploration and Exploitation. NPF Special Publication*, **4**, 115-213.

Lander, R. H. & Walderhaug, O. 1999. Predicting porosity through simulating sandstone compaction and quartz cementation. *American Association of Petroleum Geologists Bulletin*, **83**, 433-449.

Larter, S.R., Taylor, P., Chen, M., Bowler, B., Ringrose, P. & Horstad, I. 1997. Secondary migration, visualising the invisible-what can geochemistry do? *In:* (Ed.) K. W. Glennie, *NW Europe's hydrocarbon Industry*, 137-143.

Larter, S.R., Bowler, B.F., Clarke, E., Wilson, C., Moffatt, B., Bennett, B., Yardley, G. & Carruthers, D. 2000. An experimental investigation of geochromatography during secondary migration of petroleum performed under subsurface conditions with a real rock. *Geochemical Transactions*, **9**, 103-147.

Lee, M. J., Aronson, J. L. & Savin, S. M. 1985. K/Ar dating of time of gas emplacement in Rotliegendes Sandstone. *American Association of Petroleum Geologists Bulletin*, **69**, 1381-1385.

Lee, M. J. & Hwang, Y. J. 1993. Tectonic evolution and structural styles of the East Shetland Basin. *In:* Parker , J. R. (Ed) *Petroleum Geology of Northwest Europe*, 1137-1149.

Lervik, K. S.; Spencer, A. M.; Warrington, G. 1989. Outline of Triassic stratigraphy and structure in the central and Northern North Sea. *In: Correlation in hydrocarbon exploration,* Graham & Trotman, 173-189.

Liewig, N., Clauer, N. & Sommer, F. 1987. Rb-Sr and K-Ar dating clay diagenesis in Jurassic sandstone oil reservoir, North Sea. *American Association of Petroleum Geologists Bulletin*, **71**, 1467-1474.

Liewig, N. & Clauer, N. 1998. K-Ar dating of texturally well-identified illite in a sandstone reservoir. *In: Mineral Diagenesis and Reservoir Quality - the Way Forward. Conference Abstracts. Clay Minerals Group/Petroleum Exploration Society of Great Britian/London Petrophysical Society/Geological Society of London*, Cambridge, UK.

Macaulay C. I. 1990. Clastic diagenesis and porefluid evolution: an isotopic study, Magnus oil field, North Sea. *Ph. D. thesis, Department of Applied Geology, University of Strathclyde.*

Macaulay, C. I., Haszeldine, R. S. & Fallick, A. E. 1992. Diagenetic porewaters stratified for at least 35 million years. *Bulletin of the American Association for Petroleum Geologists*, **76**, 1625-1634.

Macaulay, C. I., Fallick, A. E. & Haszeldine, R. S. 1993. Textural and isotopic variations in diagenetic kaolinite from the Magnus oil-field sandstones. *Clay Minerals*, **28**, 625-639.

Magara, K. 1987. Fluid flow due to sediment loading; an application to the Arabian Gulf region . *In: Fluid flow in sedimentary basins and aquifers*, Geological Society Special Publications, **34**, 19-28.

Magoon, L. B. & Dow, W. G. 1994. The system. *American Association of Petroleum Geologists*, **60**, 3-24.

Marchand, A. M. E., Haszeldine, R. S., Macaulay, C. I., Swennen, R. & Fallick, A. E. 2000. Quartz cementation inhibited by crestal oil charge: Miller sandstone, UK North Sea. *Clay Minerals*, **35**, 201-210.

Marsden, G., Roberts, A., Yielding, G. & Kusznir, N. J. 1990. Application of a flexural cantilever simple-shear/pure-shear model of continental lithosphere extension to the formation of the Northern North Sea Basin. *Tectonics of the North Sea Rift*, Oxford Science Publications, 240-261.

Matthews, J. C.; Velde, B. & Johansen, H. 1994. Significance of K-Ar age of authigenic illitic clay minerals in sandstones and shales from the North Sea. *Clay Minerals*, **29**, 379-389.

Mckenzie D. P. 1978. Some remarks on sedimentary basins. *Earth and Planetary Science Letters*, **40**, 25-32.

Mitchener, B. C., Lawrence, D. A., Partington, M. A. & Bowman, M. B. J. 1992. Brent Group: sequence stratigraphy and regional implications. *In:* Morton, A. C., Haszeldine, R. S., Giles, M. R., Brown, S. (eds*) Geology of the Brent Group*, Geological Society Special Publications, **61**, 45-80.

Mudford, B. S., Gradstein, F. M., Katsube, T. J. & Best, M. E, 1991, Modelling 1 D compaction - driven flow in sedimentary basins; a comparison of the Scotian Shelf, North Sea and Gulf Coast. *In:* W. A. England & A.J. Fleet (ed) *Petroleum Migration*. Geological Society Special Publication, **59**, 65-85.

Nadin, P. A.; Kusznir, N. J. 1995. Palaeocene uplift and Eocene subsidence in the northern North Sea basin from 2D forward and reverse stratigraphic modelling, Journal of the Geological Society of London, **152**, 833-848

Nadin, P. A., Kusznir, N. J. & Toth, J. 1995. Transient regional uplift in the early Tertiary of the northern North Sea and the development of the Iceland Plume, Journal of the Geological Society of London, **152**, 953-958.

Neelamkavil F. 1991. Computer Simulation and Modelling. John Wiley and Sons, London.

North, F. K. 1990. Petroleum Geology. Second Edition, Unwin Hyman, Boston, 216-217.

Oreskes N., Shraderfrechette K. & Belitz K. 1994. Verification, validation, and confirmation of numerical models in the earth sciences, *Science*, **263**, 641-646.

Osborne, M., Haszeldine, R. S., Fallick, A. E. 1994. Variation in kaolinite morphology with growth temperature in isotopically mixed porefluids, Brent Group, UK North Sea. *Clay Minerals*, **29**, 591-608.

Park, A. J. & Ortoleva, P. J. 1999. Enriched: Effects of compaction and diagenesis on the development of compartment seals. *American Association of Petroleum Geologists, Annual Meeting Expanded Abstracts*, A104.

Partington, M. A., Copestake, P., Mitchener, B. C. & Underhill, J. R. 1993. Biostratigraphic calibration of genetic stratigraphic sequences in the Hettangian to Ryazanian of the North Sea and adjacent areas. *In:* Parker, J. R. (ed) *Petroleum geology of Northwest Europe; 4th conference*, The Geological Society of London, 371-386.

Payne, D. F., Park, A. J. & Ortoleva, P. 1994. Modelling diagenetic reservoir modifications during basin evolution, offshore Norway. *American Association of Petroleum Geologists Meeting Abstracts*, 231.

Payne, D. F., Tuncay, K., Park, A., Comer, J. B. & Ortoleva, P. 1998. A reaction-transport-mechanical approach to modelling gas generation, overpressuring, and fracturing relationships; implications for the Cretaceous gas reservoirs of the Piceance Basin, Colorado. *American Association of Petroleum Geologists Bulletin*, **84**, 545-565.
Pegrum, R. M. & Spencer, A. M. 1991. Hydrocarbon plays, northern North Sea, *Geological Society*, **50**, 441-470.

Platte River Associates 1998. BasinMod□ 2-D for Windows; petroleum system software; document version 2.52. Platte River Associates Incorporated.
Purvis, K. 1995. Diagenesis of Lower Jurassic sandstones, Block 211/13 (Penguin area), UK northern North Sea. Marine and Petroleum Geology, **12**, 219-228.

Rattey, R. P. & Hayward, A. B. 1993. Sequence Stratigraphy of a failed rift system: the Middle Jurassic to Early Cretaceous basin evolution of the Central and Northern North Sea. In: Parker, J.R. (Ed) *Petroleum Geology of Northwest Europe Proceedings of the 4th Conference,* The Geological Society, 215-249.

Richards, P. C., Brown, S. & Dean, J. M. 1988. A new palaeogeographic reconstruction for the Middle Jurassic of the Northern North Sea, *Journal of Geological Society of London*, **145**, 883-886.

Richards, P. C., Lott, G. K., Johnson, H., Knox, R. W. O. & Riding, J. B. 1993. Jurassic of the central and Northern North Sea. *In:* Knox, R. W. O & Cordey, W. G. (eds) *Lithostratigraphic nomenclature of the UK North Sea.* British Geological Survey, Nottingham.

Roberts, D. G., Thompson, M. Mitchener, B., Hossack, J., Carmichael, S. & Bjørnseth, H. M. 1999. Palaeozoic to Tertiary rift and basin dynamics: mid-Norway to the Bay of Biscay – a new context in the deep water frontier. *In:* Fleet, A. J. & Boldy, S. A. R. (Eds*) Proceedings of the 5th Conference. Petroleum Geology of NW Europe*, 7-40.

Roberts, A., Yielding, G., Kusznir, N.J., Walker, I. & Dorn-Lopez, D. 1993. Mesozoic extension in the North Sea: Constraints from flexural backstripping, forward modelling and fault populations. *In:* Fleet, A. J. & Boldy, S. A. R. (Eds*) Proceedings of the 4th Conference. Petroleum Geology of NW Europe*, 1123-1136.

Roberts, A. M., Yielding, G., Kusznir, N. J., Walker, I. M. & Dorn-Lopez, D. 1995. Quantitative analysis of Triassic extension in the Viking Graben. *Journal of the Geological Society of London*, **152**, 15-26.

Saigal G. C., Bjorlykke K., & Larter S. 1992. The effects of oil emplacement - examples from the Fulmar reservoir sandstones, Central North Sea. *American Association of Petroleum Geologists Bulletin*, **76**, 1024-1033.

Shell UK. 1995. Unpublished structural section for the Penguin field area. North Sea, Shell UK, Aberdeen.

Shell UK. 1998. Unpublished map for the Northern North Sea area. North Sea, Shell UK, Aberdeen.

Shepherd M., Kearney C. J. & Milne J. H. 1990. Magnus Field. *In:* Beaumont E. A. & Foster N. H. (eds) *Structural Traps II: traps associated with tectonic faulting. American Association of Petroleum Geology*, 95-125.

Small J. S., Hamilton D. L. & Habesch S. 1992. Experimental simulation of clay precipitation within reservoir sandstones .2. illite formation and controls on morphology. *Journal of Sedimentary Petrology*, **62**, 520-529.

Smalley, P. C., Jablonski, D., Simpson, I. 1998. A process for predicting porosity and permeability in deep early Jurassic/Triassic targets, Australian North West Shelf. *Australian Petroleum Production and Exploration Association Journal*, **38**, 759-775.

Sommer, F. 1975. Histoire diagénétique d'une série gréseuse de Mer du Nord. Datation de l'intoduction des hydrocarbures. *Revue Institute francais Pétrole.* **30**, 729-741.

Sommer, F. 1978. Diagenesis of Jurassic sandstones in the Viking Graben. *Journal of the Geological Society, London*, **135**, 63-68.

Spencer, A. M. & Larsen, V. B. 1990. Fault traps in the Northern North Sea. *In:* Hardman, R. F. P. & Brooks, J. (eds) *Tectonic events Responsible for Britian's Oil and Gas Reserves.* Geological Society, London, Special Publications, **55**, 281-298.

Spencer, A. M. Birkeland, Ø., Knag, G. Ø. & Fredsted, R. 1999. Petroleum systems of the Atlantic margin of northwest Europe. *In:* Fleet, A. J. & Boldy, S. A. R. (Eds*) Proceedings of the 5th Conference. Petroleum Geology of NW Europe*, 231-246.

Srodon J. & Eberl D. D. 1984. Illite. Reviews of Mineralogy, 13: Micas. *Mineral Society of America*, 495-544.

Steel, R. J. 1993. Triassic-Jurassic megasequence stratigraphy in the northern North Sea; rift to post-rift evolution. *In:* Parker. J. R. (ed) *Petroleum geology of Northwest Europe; Proceedings of the 4th conference,* Geological Society of London, United Kingdom, 299-315.

Stewart, D. J., Schwander, M. & Bolle, L. 1995. Jurassic depositional systems of the Horda Platform, Norwegian North Sea: practical consequences of applying sequence sequence stratigraphic models, *In:* Steel, R. J (Ed.) *Sequence Stratigraphy on the Northwest European Margin NPF Special Publication,* **5**, 291-323.

Swarbrick, R. E. 1994. Reservoir diagenesis and hydrocarbon migration under hydrostatic palaeopressure conditions. *Clay Minerals*, **29**, 463-473.

Tucker, M. E. 1991. Sedimentary petrology – an introduction to the origin of sedimentary rocks. 2nd Edition.Blackwell, 209-210.

Underhill, J. R. & Partington, M. A. 1993. Jurassic thermal doming and deflation in the North Sea; implications of the sequence stratigraphic evidence. *In:* Parker, J. R. (ed) *Petroleum geology of Northwest Europe; Proceedings of the 4th conference*, The Geological Society of London, 337-345.

Weaver, C. E. 1960. Possible uses of clay minerals in the search for oil. *American Association of Petroleum Geologists Bulletin*, **44**, 1505-1518.

Whitaker, J. H. & Blanche, J. B. 1978. Diagenesis of part of the Brent Sand Formation (Middle Jurassic) of the Northern North Sea Basin. *Journal of the Geological Society of London*, **135**, 73-82.

White, N. 1989. Nature of lithospheric extension in the North Sea. *Geology*, **17**, 111-114.

White, N. & Latin, D. 1993. Subsidence analyses from the North Sea "triple-junction". *Journal of the Geological Society of London*, **150**, 473-488.

White N. J. & Mckenzie D. P. 1988. Formation of the 'Steer's Head' geometry of sedimentary basins by differential stretching of the crust and mantle, *Geology*, **16**, 250-253.

Wilkinson, M., Darby, D., Haszeldine, R. S. & Couples, G. D. 1997. Secondary porosity generation during deep burial associated with overpressure leak-off: Fulmar Formation, UKCS. *Bulletin of the American Association of Petroleum Geologists*, **81**, 803-813.

Wilkinson, M., Milliken, K. L. & Haszeldine, R. S. 2001. Systematic destruction of K-feldspars in deeply buried rift and passive margin sandstones. *Journal of the Geological Society*, **158**, 675-683.

Wilkinson, M., & Haszeldine, R.S. 2002. Fibrous Illite in Oilfield Sandstones - A Nucleation Kinetic Theory of Growth. *Terra Nova*, **14**, 56-60.

Williamson, M. A. & Smyth, C. 1992. Timing of gas and overpressure generation in the Sable Basin offshore Nova Scotia; implications for gas migration. *Bulletin of Canadian Petroleum Geology*, **40**, 151-169.

Worden R. H., Smalley, P. C. & Oxtoby N. H. 1998. Can oil emplacement prevent quartz cementation in sandstones? *Petroleum Geoscience*, **4**, 129-138.

Worden R. H. & Barclay, S. A. 2000. Internally-sourced quartz cement due to externally-derived CO2 in sub-arkosic sandstones, North Sea. *Journal of Geochemical Exploration* , **69**, 645-649.

Yielding, G., Badley, M. E. & Roberts, A. M. 1992. The structural evolution of the Brent Province. *In:* Morton, A. C., Haszeldine, R. S., Giles, M. R., Brown, S. (eds*) Geology of the Brent Group*, Geological Society Special Publications, **61**, 27-43.

Ziegler, K., Sellwood B. W. & Fallick A. E. 1994. Radiogenic and stable-isotope evidence for age and origin of authigenic illites in the Rotliegend, Southern North-Sea, *Clay Minerals*, **29**, 555-565.

Ziegler, P. A. 1982. *Geological Atlas of Western and Central Europe.* Elsevier, Amsterdam.

—

Appendix 3.1a – data related to published illite K-Ar ages for the Northern North Sea

Source	X/Y	Paper	Year	Field-Area	Well label	Depth (ft)	Depth (m)	Stratigraphy	Zone	Age (Ma)
		Brint et al.	1988	Thistle	'A'	*8694-9514*	2650-2900	Brent Group		
		Brint et al.	1988	Murchison	'B'	*8694-9514*	2650-2900	Brent Group		
		Emery et al.	1993	Magnus	211/12a-11	*10318*	3145	Magnus	oil	68
		Emery et al.	1993	Magnus	211/12a-11	*10430*	3179	Magnus	?water	88
		Emery et al.	1993	Magnus	211/12a-11	*10486*	3196	Magnus	?water	72
		Emery et al.	1993	Magnus	211/12a-11	*10512*	3204	Magnus	?water	63
		Emery et al.	1993	Magnus	211/12a-11	*10574*	3223	Magnus	?water	64
Giles et al.	Y	Giles et al.	1992	Tern	'I'	8350	2545	Etive		'-
Hamilton et al.	Y	Glasmann et al.	1989	Heather	-					
Hamilton et al.	Y	Glasmann et al.	1989	Heather	-	9750	*2972*	Broom		40
Glasmann	Y	Glasmann et al.	1989	Heather	-	*9843*	3000	Brent Group		41
Hamilton et al.	Y	Glasmann et al.	1989	Heather	-	10875	*3315*	Tarbert		40
Hamilton et al.	Y	Glasmann et al.	1989	Heather	-	10950	*3338*	Broom		51
Hamilton et al.	Y	Glasmann et al.	1989	Heather	-	11025	*3360*	Ness		31
Hamilton et al.	Y	Glasmann et al.	1989	Heather	-	11025	*3360*	Ness		34
Glasmann	Y	Glasmann et al.	1989	Heather	-	*11155*	3400	Brent Group		32
Hamilton et al.	Y	Glasmann et al.	1989	Heather	-	11175	*3406*	Etive		28
Hamilton et al.	Y	Glasmann et al.	1989	Heather	-	11175	*3406*	Etive		31

Appendix 3.1a – data related to published illite K-Ar ages for the Northern North Sea

Source	X/Y	Paper	Year	Field-Area	Well label	Depth (ft)	Depth (m)	Stratigraphy	Zone	Age (Ma)
Glasmann	Y	Glasmann et al.	1989	Heather	-	*11811*	3600	Brent Group		34
Hamilton et al.	Y	Glasmann et al.	1989	Heather	-	11850	*3612*	Broom		32
Hamilton et al.	Y	Glasmann et al.	1989	Heather	-	11850	*3612*	Tarbert		34
Hamilton et al.	Y	Glasmann et al.	1989	Heather	-	11850	*3612*	Tarbert		39
Hamilton et al.	Y	Glasmann et al.	1989	Heather	-	11925	*3635*	Etive		30
Glasmann	Y	Glasmann et al.	1992	Hild	-	*12795*	3900	Brent Group		60
Glasmann	Y	Glasmann et al.	1992	Hild	-	*12795*	3900	Brent Group		64
Glasmann	Y	Glasmann et al.	1989	Huldra		*12139*	3700	Brent Group		59
Glasmann	Y	Glasmann et al.	1989	Huldra		*12467*	3800	Brent Group		37
Glasmann	Y	Glasmann et al.	1989	Huldra		*13451*	4100	Brent Group		55
Glasmann	Y	Glasmann et al.	1989	Huldra		*13451*	4100	Brent Group		56
Glasmann	Y	Glasmann et al.	1989	Huldra		*13451*	4100	Brent Group		57
Glasmann	Y	Glasmann	1989	Hutton		*11483*	3500	Brent Group		45
Glasmann	Y	Glasmann	1989	Hutton		*12139*	3700	Brent Group		44
Glasmann	Y	Glasmann	1992	Oseberg		*9186*	2800	Brent Group	water	53
Glasmann	Y	Glasmann et al.	1989	Veslefrikk		*9514*	2900			31
Glasmann	Y	Glasmann et al.	1989	Veslefrikk		*9843*	3000			32
Glasmann	Y	Glasmann	1992	Viking Graben central		*14764*	4500	Brent Group		54
Glasmann	Y	Glasmann	1992	Viking Graben central		*14764*	4500	Brent Group		55
Glasmann	Y	Glasmann	1992	Viking Graben central		*14764*	4500	Brent Group		56

Appendix 3.1a – data related to published illite K-Ar ages for the Northern North Sea

Source	X/Y	Paper	Year	Field-Area	Well label	Depth (ft)	Depth (m)	Stratigraphy	Zone	Age (Ma)
Hamilton et al.	Y	Hamilton et al.	1992	'3/8	Well 2	12176	*3711*	Tarbert	oil	62
Hamilton et al.	Y	Hamilton et al.	1992	'3/8	Well 2	12308	*3751*	Etive	oil	45
Hamilton et al.	Y	Hamilton et al.	1992	'3/8	Well 1	13532	*4125*	Ness	oil	59
Hamilton et al.	Y	Hamilton et al.	1992	211/7	'	11243	*3427*	Tarbert	(residual oil)	36.5
Hamilton et al.	Y	Hamilton et al.	1992	211/11	'K'	11285	*3440*	Etive	water	24
Hamilton et al.	Y	Hamilton et al.	1992	211/11	'K'	11325	*3452*	Etive	water	17
Hamilton et al.	Y	Hamilton et al.	1987	Brent Province north				Rannoch		60-45
Hamilton et al.	Y	Hamilton et al.	1987	Brent Province north		x to x+109	x to x+33	Rannoch		59-46
Hamilton et al.	Y	Hamilton et al.	1992	Cormorant	211/26-CA30	9942	*3030*	Etive	water	36
Hamilton et al.	Y	Hamilton et al.	1992	Cormorant	211/26-CA30	9966	*3038*	Etive	water	147
Hamilton et al.	Y	Hamilton et al.	1992	Cormorant	211/26-CA30	9966	*3038*	Etive	water	41
Hamilton et al.	Y	Hamilton et al.	1992	Grtr Don Area	211/13- 'X'	11621	*3542*	Etive	oil	34
Hamilton et al.	Y	Hamilton et al.	1992	Grtr Don Area	211/13- 'X'	11621	*3542*	Etive	oil	28
Hamilton et al.	Y	Hamilton et al.	1992	Grtr Don Area	211/13- 'X'	11710	*3569*	Etive	oil	28
Hamilton et al.	Y	Hamilton et al.	1992	Grtr Don Area	211/13- 'X'	11710	*3569*	Etive	oil	22
Hamilton et al.	Y	Hamilton et al.	1992	NW Hutton	'Y'	12618	*3846*	Etive	water	35

Appendix 3.1a – data related to published illite K-Ar ages for the Northern North Sea

Source	X/Y	Paper	Year	Field-Area	Well label	Depth (ft)	Depth (m)	Stratigraphy	Zone	Age (Ma)
Hamilton et al.	Y	Hamilton et al.	1992	NW Hutton	'Y'	12618	*3846*	Etive	water	33
Hamilton et al.	Y	Hamilton et al.	1992	NW Hutton	'Y'	12467	*3800*	Ness	oil	45
Hamilton et al.	Y	Hamilton et al.	1992	NW Hutton	'Y'	12467	*3800*	Ness	oil	56
Hamilton et al.	Y	Hamilton et al.	1992	Pelican	Well C	10780	*3286*	Ness	oil	44
Hamilton et al.	Y	Hamilton et al.	1992	Pelican	Well C	10780	*3286*	Ness	oil	35
Hamilton et al.	Y	Hamilton et al.	1992	Pelican	Well C	10906	*3324*	Etive	oil	27
Hamilton et al.	Y	Hamilton et al.	1992	Pelican	Well B	11071	*3374*	Etive	oil	27
Hamilton et al.	Y	Hamilton et al.	1992	Pelican	Well A	11602	*3536*	Ness	oil	55
Hamilton et al.	Y	Hamilton et al.	1992	Pelican	Well A	11602	*3536*	Ness	oil	41
Hamilton et al.	Y	Hamilton et al.	1992	Pelican	Well A	11761	*3585*	Etive	oil	25
Hamilton et al.	Y	Hamilton et al.	1992	Penguin East Flank	'Z'	13322	*4061*	Tarbert	oil	54
Hamilton et al.	Y	Hamilton et al.	1987	Thistle/Murchison				Brent Group		
		Harris	1989	Hutton			3500	Brent Group		45
Hamilton et al.	Y	Haszeldine et al.	1992	Murchison	211/19-4	10202	3109	Rannoch		59
Glasmann	Y	Hogg	1989	Alwyn North			3700			74
	Y	Hogg et al.	1987	Alwyn South	3/14a-7-8-9		3552-3830	Brent Group		
Hamilton et al.	Y	Hogg et al.	1987	Alwyn South				Brent Group		45-56
Hamilton et al.	Y	Hogg	1989	Alwyn South				Brent Group		45-56
Glasmann	Y	Hogg	1989	Alwyn South			3600	Brent Group		48
Glasmann	Y	Hogg	1989	Alwyn South			3700	Brent Group		50

Appendix 3.1a – data related to published illite K-Ar ages for the Northern North Sea

Source	X/Y	Paper	Year	Field-Area	Well label	Depth (ft)	Depth (m)	Stratigraphy	Zone	Age (Ma)
Hamilton et al.	Y	Jourdan et al.	1987	Alwyn North	3/4-8; 3/9a-1-4			Brent Group		75
Hamilton et al.	Y	Jourdan et al.	1987	Alwyn North	'3/9-6			Brent Group		35-45
Hamilton et al.	Y	Jourdan et al.	1987	Alwyn North	'3/14-3-4-6-7-8-11;3/15-2-4			Brent Group		45-55
Hamilton et al.	Y	Jourdan et al.	1987	Alwyn South	'3/8-4;3/14-9-10-12			Brent Group		35-45
Hamilton et al.	Y	Liewig et al.	1987	Alwyn			3238-3470	Brent Group		
Hamilton et al.	Y	Liewig et al.	1987	Alwyn		10636	3242	Brent Group	oil / OWC	35
Hamilton et al.	Y	Liewig et al.	1987	Alwyn		10625	3239	Brent Group	oil / OWC	44
Hamilton et al.	Y	Liewig et al.	1987	Alwyn				Brent Group	oil / OWC	129-35
		Macaulay et al.	1992	Magnus	211/12a-9			Magnus	oil / OWC	57
		Macaulay et al.	1992	Magnus				Magnus	water / OWC	42
Hamilton et al.	Y	Scotchman et al.	1989	Hutton NW			3810-3963	Brent Group		49-39
Hamilton et al.	Y	Scotchman et al.	1989	Hutton NW			3810-3963	Brent Group	oil	av.43
Hamilton et al.	Y	Scotchman et al.	1989	Hutton NW			3810-3963	Brent Group	water	av.41
Hamilton et al.	Y	Sommer	1978	ESB	TOTAL-SNEAP			Brent Group		45-55
Glasmann		Thomas	1986	Heimdal	25/4-1-5		3179-3750	Brent Group		53
Glasmann		Thomas	1986	Heimdal			3400	Brent Group		53
Hamilton et al.	Y	Thomas	1986	'25/4	'25/4-1	10430-10600	3179-3231	Brent	oil	44-38
Hamilton et al.	Y	Thomas	1986	'25/4	'25/4-1	10780-11070	3286-3374	Statfjord	oil	62-44
Hamilton et al.	Y	Thomas	1986	'25/4	'25/4-5	12120-12220	3694-3725	Brent	water	52-40
Hamilton et al.	Y	Thomas	1986	'25/4	'25/4-5	12980-13170	3956-4014	Statfjord	water	40-28

Appendix 3.1b – further data related to published illite K-Ar ages for the Northern North Sea

Paper	Year	Field-Area	Well label	Age (Ma)	Bar +/-	Burial history	Temp. (C)	Size (µm)	K (wt%)	Ar40 (E-10 mol/gm)	Comments
Brint et al.	1988	Thistle	'A'								
Brint et al.	1988	Murchison	'B'								
Emery et al.	1993	Magnus	211/12a-11	68							
Emery et al.	1993	Magnus	211/12a-11	88							
Emery et al.	1993	Magnus	211/12a-11	72							
Emery et al.	1993	Magnus	211/12a-11	63							
Emery et al.	1993	Magnus	211/12a-11	64							
Giles et al.	1992	Tern	'I'	'-			<85				
Glasmann et al.	1989	Heather	-				80-130				
Glasmann et al.	1989	Heather	-	40							
Glasmann et al.	1989	Heather	-	41							
Glasmann et al.	1989	Heather	-	40							
Glasmann et al.	1989	Heather	-	51							
Glasmann et al.	1989	Heather	-	31				<0.1			
Glasmann et al.	1989	Heather	-	34							
Glasmann et al.	1989	Heather	-	32							
Glasmann et al.	1989	Heather	-	28				<0.1			
Glasmann et al.	1989	Heather	-	31							

Appendix 3.1b – further data related to published illite K-Ar ages for the Northern North Sea

Paper	Year	Field-Area	Well label	Age (Ma)	Bar +/-	Burial history	Temp. (C)	Size (µm)	K (wt%)	Ar40 (E-10 mol/gm)	Comments
Glasmann et al.	1989	Heather	-	34							
Glasmann et al.	1989	Heather	-	32							
Glasmann et al.	1989	Heather	-	34				<0.1			
Glasmann et al.	1989	Heather	-	39							
Glasmann et al.	1989	Heather	-	30							
Glasmann et al.	1992	Hild	-	60							
Glasmann et al.	1992	Hild	-	64							
Glasmann et al.	1989	Huldra		59							
Glasmann et al.	1989	Huldra		37							
Glasmann et al.	1989	Huldra		55							
Glasmann et al.	1989	Huldra		56							
Glasmann et al.	1989	Huldra		57							
Glasmann	1989	Hutton		45							
Glasmann	1989	Hutton		44							
Glasmann	1992	Oseberg		53	0.9		50-60				
Glasmann et al.	1989	Veslefrikk		31							
Glasmann et al.	1989	Veslefrikk		32							
Glasmann	1992	Viking Graben central		54							
Glasmann	1992	Viking Graben central		55							
Glasmann	1992	Viking Graben central		56							

Appendix 3.1b – further data related to published illite K-Ar ages for the Northern North Sea

Paper	Year	Field-Area	Well label	Age (Ma)	Bar +/-	Burial history	Temp. (C)	Size (µm)	K (wt%)	Ar40 (E-10 mol/gm)	Comments
Hamilton et al.	1992	'3/8	Well 2	62	1.4			<0.1	3.97	4.324	
Hamilton et al.	1992	'3/8	Well 2	45	1.1	Ro=0.62		<0.1	4.74	3.7032	
Hamilton et al.	1992	'3/8	Well 1	59	1.4	Ro=0.5		0.5-0.1	4.32	4.4986	
Hamilton et al.	1992	211/7	'	36.5	0.9	available	105	0.1-0.5	3.98	2.5428	intermediate
Hamilton et al.	1992	211/11	'K'	24	0.7	Ro<0.62	80+	<0.1	4.8	1.9982	cool
Hamilton et al.	1992	211/11	'K'	17	0.7	Ro<0.62	80+	<0.1	5.26	1.5925	cool
Hamilton et al.	1987	Brent Province north		60-45							
Hamilton et al.	1987	Brent Province north		59-46				<0.05			
Hamilton et al.	1992	Cormorant	211/26-CA30	36	0.8	Ro<0.62	75	<0.1	4.02	2.5283	
Hamilton et al.	1992	Cormorant	211/26-CA30	147	3			0.3-0.1	1.37	3.6113	
Hamilton et al.	1992	Cormorant	211/26-CA30	41	0.9			<0.1	3.72	2.6841	
Hamilton et al.	1992	Grtr Don Area	211/13- 'X'	34	0.9			0.3-0.1	6.23	3.7195	
Hamilton et al.	1992	Grtr Don Area	211/13- 'X'	28	1.1			<0.1	4.8	2.3157	
Hamilton et al.	1992	Grtr Don Area	211/13- 'X'	28	0.7	Ro=0.62	~100	0.3-0.1	5.9	2.9339	
Hamilton et al.	1992	Grtr Don Area	211/13- 'X'	22	0.7			<0.1	5.29	2.0325	
Hamilton et al.	1992	NW Hutton	'Y'	35	0.8			0.5-0.1	5.2	3.1426	

Appendix 3.1b – further data related to published illite K-Ar ages for the Northern North Sea

Paper	Year	Field-Area	Well label	Age (Ma)	Bar +/-	Burial history	Temp. (C)	Size (µm)	K (wt%)	Ar40 (E-10 mol/gm)	Comments
Hamilton et al.	1992	NW Hutton	'Y'	33	0.7	Ro=0.62	~100	<0.3	4.61	2.6718	
Hamilton et al.	1992	NW Hutton	'Y'	45	1			0.5-0.1	5.23	4.1588	
Hamilton et al.	1992	NW Hutton	'Y'	56	1.4	Ro=0.62	~100	<0.3	3.72	3.6693	
Hamilton et al.	1992	Pelican	Well C	44	1			0.5-0.1	4.64	3.5702	text is clearer than
Hamilton et al.	1992	Pelican	Well C	35	0.9			<0.1	4.55	2.7476	table (formatting)
Hamilton et al.	1992	Pelican	Well C	27	0.6	Ro=0.62	~100	0.3-0.1	6.03	2.8544	
Hamilton et al.	1992	Pelican	Well B	27	0.6			0.5-0.1	5.4	2.5754	
Hamilton et al.	1992	Pelican	Well A	55	1.39			0.5-0.1	4.54	4.4068	
Hamilton et al.	1992	Pelican	Well A	41	1.5			<0.1	3.98	2.8453	
Hamilton et al.	1992	Pelican	Well A	25	0.7	Ro=0.62	~100	0.5-0.1	5.95	2.5716	
Hamilton et al.	1992	Penguin East Flank	'Z'	54	1.4	R0=0.62	~100	<0.1	4.46	4.2575	
Hamilton et al.	1987	Thistle/Murchison									
Harris	1989	Hutton		45							
Haszeldine et al.	1992	Murchison	211/19-4	59				<0.1			
Hogg	1989	Alwyn North		74							
Hogg et al.	1987	Alwyn South	3/14a-7-8-9								
Hogg et al.	1987	Alwyn South		45-56				1.0-0.5			
Hogg	1989	Alwyn South		45-56				0.5-0.1			

Appendix 3.1b – further data related to published illite K-Ar ages for the Northern North Sea

Paper	Year	Field-Area	Well label	Age (Ma)	Bar +/-	Burial history	Temp. (C)	Size (µm)	K (wt%)	Ar40 (E-10 mol/gm)	Comments
Hogg	1989	Alwyn South		48							
Hogg	1989	Alwyn South		50							
Jourdan et al.	1987	Alwyn North	3/4-8; 3/9a	75			120	<0.2			
Jourdan et al.	1987	Alwyn North	'3/9-6	35-45				<0.2			
Jourdan et al.	1987	Alwyn North	'3/14-3-4-6-7-8-11;3/15-2-4	45-55				<0.2			
Jourdan et al.	1987	Alwyn South	'3/8-4;3/14-9-10-12	35-45			140	<0.2			hot fluids
Liewig et al.	1987	Alwyn					80-50				hot exotic fluids
Liewig et al.	1987	Alwyn		35	1			<0.6			
Liewig et al.	1987	Alwyn		44	2			<0.6			
Liewig et al.	1987	Alwyn		129-35				<0.6			contaminatio n
Macaulay et al.	1992	Magnus	211/12a-9	57							
Macaulay et al.	1992	Magnus		42							
Scotchman et al.	1989	Hutton NW		49-39							
Scotchman et al.	1989	Hutton NW		av.43							
Scotchman et al.	1989	Hutton NW		av.41							
Sommer	1978	ESB	TOTAL-SNEAP	45-55							

Appendix 3.1b – further data related to published illite K-Ar ages for the Northern North Sea

Paper	Year	Field-Area	Well label	Age (Ma)	Bar +/-	Burial history	Temp. (C)	Size (µm)	K (wt%)	Ar40 (E-10 mol/gm)	Comments
Thomas	1986	Heimdal	25/4-1-5	53							
Thomas	1986	Heimdal		53							
Thomas	1986	'25/4	'25/4-1	44-38							
Thomas	1986	'25/4	'25/4-1	62-44							
Thomas	1986	'25/4	'25/4-5	52-40							
Thomas	1986	'25/4	'25/4-5	40-28							

Appendix 3.2 – published illite K-Ar ages for the Northern North Sea by field area

Location	Author	Depth (ft)	Stratigraphy	Zone	Size (μm)	Age (Ma)
Brent Province north -ESB						
Brent Pr'nce -	Hamilton et al.	x to x+109	Rannoch	-	c'rse-fine	60-45
Brent Pr'nce -	Hamilton et al.	x to x+109	Rannoch	-	<0.05	59-46
ESB -	Sommer	-	Brent Group	-	-	45-55
Wendy-Magnus-Penguin-Don						
211/7- '	Hamilton et al.	11243	Tarbert	oil	0.1-0.5	36.5
'K'	Hamilton et al.	11285	Etive	water	<0.1	24
'K'	Hamilton et al.	11325	Etive	water	<0.1	17
211/12a-9	Macaulay et al.	10448	MSM	water	<0.1	55
211/12a-9	Macaulay et al.	10448	MSM	water	0.1-0.5	83
211/12a-9	Macaulay et al.	10704	MSM	water	0.1-0.5	46
211/12a-11	Emery et al.	*10318*	MSM	?oil	-	68
211/12a-11	Emery et al.	*10430*	MSM	?water	-	88
211/12a-11	Emery et al.	*10486*	MSM	?water	-	72
211/12a-11	Emery et al.	*10512*	MSM	?water	-	63
211/12a-11	Emery et al.	*10574*	MSM	?water	-	64
211/13- 'X'	Hamilton et al.	11621	Etive	oil	0.3-0.1	34
211/13- 'X'	Hamilton et al.	11621	Etive	oil	<0.1	28
211/13- 'X'	Hamilton et al.	11710	Etive	oil	0.3-0.1	28
211/13- 'X'	Hamilton et al.	11710	Etive	oil	<0.1	22
'Z'	Hamilton et al.	13322	Tarbert	oil	<0.1	54
Murchison-Thistle-Dunlin						
211/19-4	Haszeldine et al.	10202	Rannoch	-	<0.1	59
M'son/This -	Hamilton et al.	-	Brent Group	-	-	-
M'son/This -	Brint et al.	*8694-9514*	Brent Group	-	-	-
Tern-Eider-Cormorant						
Tern 'I'	Giles et al.	8350	Etive	-	-	-
211/26-CA30	Hamilton et al.	9942	Etive	water	<0.1	36
211/26-CA30	Hamilton et al.	9966	Etive	water	0.3-0.1	147
211/26-CA30	Hamilton et al.	9966	Etive	water	<0.1	41
Hutton-N.W.Hutton-Pelican-Heather						
Hutton -	Harris	-	Brent Group	-	-	45
Hutton -	Glasmann	*11483*	Brent Group	-	-	45
Hutton -	Glasmann	*12139*	Brent Group	-	-	44
N.W.Hutton-X	Hamilton et al.	12618	Etive	water	0.5-0.1	35
N.W.Hutton-X	Hamilton et al.	12618	Etive	water	<0.3	33

Appendix 3.2 – published illite K-Ar ages for the Northern North Sea by field area

Location	Author	Depth (ft)	Stratigraphy	Zone	Size (μm)	Age (Ma)
Hutton-N.W.Hutton-Pelican-Heather						
N.W.Hutton-X	Hamilton et al.	12467	Ness	oil	0.5-0.1	45
N.W.Hutton-X	Hamilton et al.	12467	Ness	oil	<0.3	56
Hutton -	Glasmann	*11483*	Brent Group	-	-	45
Hutton -	Glasmann	*12139*	Brent Group	-	-	44
N.W.Hutton-X	Hamilton et al.	12618	Etive	water	0.5-0.1	35
N.W.Hutton-X	Hamilton et al.	12618	Etive	water	<0.3	33
N.W.Hutton-X	Hamilton et al.	12467	Ness	oil	0.5-0.1	45
N.W.Hutton-X	Hamilton et al.	12467	Ness	oil	<0.3	56
N.W.Hutton-Y	Scotchman et al.	-	Brent Group	oil	-	av.43
N.W.Hutton-Y	Scotchman et al.	-	Brent Group	water	-	av.41
Well C	Hamilton et al.	10780	Ness	oil	0.5-0.1	44
Well C	Hamilton et al.	10780	Ness	oil	<0.1	35
Well C	Hamilton et al.	10906	Etive	oil	0.3-0.1	27
Well B	Hamilton et al.	11071	Etive	oil	0.5-0.1	27
Well A	Hamilton et al.	11602	Ness	oil	0.5-0.1	55
Well A	Hamilton et al.	11602	Ness	oil	<0.1	41
Well A	Hamilton et al.	11761	Etive	oil	0.5-0.1	25
Heather -	Glasmann et al.	9750	Broom	-	-	40
Heather -	Glasmann et al.	*9843*	Brent Group	-	-	41
Heather -	Glasmann et al.	10875	Tarbert	-	-	40
Heather -	Glasmann et al.	10950	Broom	-	-	51
Heather -	Glasmann et al.	11025	Ness	-	<0.1	31
Heather -	Glasmann et al.	11025	Ness	-	-	34
Heather -	Glasmann et al.	*11155*	Brent Group	-	-	32
Heather -	Glasmann et al.	11175	Etive	-	<0.1	28
Heather -	Glasmann et al.	11175	Etive	-	-	31
Heather -	Glasmann et al.	*11483*	Brent Group	-	-	27
Heather -	Glasmann et al.	11700	Etive	-	-	27
Heather -	Glasmann et al.	11775	Broom	-	-	35
Heather -	Glasmann et al.	*11811*	Brent Group	-	-	34
Heather -	Glasmann et al.	11850	Broom	-	-	32
Heather -	Glasmann et al.	11850	Tarbert	-	<0.1	34
Heather -	Glasmann et al.	11850	Tarbert	-	-	39
Heather -	Glasmann et al.	11925	Etive	-	-	30
Brent-Statfjord-Snorre-Gullfaks-Gullfaks.Sth						

Appendix 3.2 – published illite K-Ar ages for the Northern North Sea by field area

Location	Author	Depth (ft)	Stratigraphy	Zone	Size (μm)	Age (Ma)
Ninian-Columba						
Well 2	Hamilton et al.	12176	Tarbert	oil	<0.1	62
Well 2	Hamilton et al.	12308	Etive	oil	<0.1	45
Well 1	Hamilton et al.	13532	Ness	oil	0.5-0.1	59
Alwyn-Alwyn.Nth-Alwyn.Sth-Hild						
3/4 - 3/9-	Hogg	-	-	-	-	74
3/4-8; 3/9a-1-4	Jourdan et al.	-	Brent Group	-	<0.2	75
'3/9-6	Jourdan et al.	-	Brent Group	-	<0.2	35-45
'3/14-3-4-6-7-8-11;3/15-2-4	Jourdan et al.	-	Brent Group	-	<0.2	45-55
Alwyn -	Liewig et al.	-	Brent Group	-	-	-
Alwyn -	Liewig et al.	10636	Brent Group	OWC	<0.6	35
Alwyn -	Liewig et al.	10625	Brent Group	OWC	<0.6	44
Alwyn -	Liewig et al.	-	Brent Group	OWC	<0.6	129-35
'3/8-4;3/14-9-10-12	Jourdan et al.	-	Brent Group	-	<0.2	35-45
3/14a-7-8-9	Hogg et al.	-	Brent Group	-	-	-
Alwyn South -	Hogg et al.	-	Brent Group	-	1.0-0.5	45-56
Alwyn South -	Hogg	-	Brent Group	-	0.5-0.1	45-56
Alwyn South -	Hogg	-	Brent Group	-	-	48
Alwyn South -	Hogg	-	Brent Group	-	-	50
Hild -	Glasmann et al.	*12795*	Brent Group	-	-	60
Hild -	Glasmann et al.	*12795*	Brent Group	-	-	64
Huldra-Oseberg-Veslefrikk-Brage						
Huldra -	Glasmann et al.	*12139*	Brent Group	-	-	59
Huldra -	Glasmann et al.	*12467*	Brent Group	-	-	37
Huldra -	Glasmann et al.	*13451*	Brent Group	-	-	55
Huldra -	Glasmann et al.	*13451*	Brent Group	-	-	56
Huldra -	Glasmann et al.	*13451*	Brent Group	-	-	57
Oseberg-	Glasmann	*9186*	Brent Group	water	-	53
Veslefrikk -	Glasmann et al.	*9514*	-	-	-	31
Veslefrikk -	Glasmann et al.	*9843*	-	-	-	32

Appendix 3.2 – published illite K-Ar ages for the Northern North Sea by field area

Location	Author	Depth (ft)	Stratigraphy	Zone	Size (μm)	Age (Ma)
Heimdal-Emerald-Viking Graben-The South						
H'dal 25/4-1-5	Thomas	-	Brent Group	-	-	53
H'dal 25/4-1-5	Thomas	-	Brent Group	-	-	53
H'dal 25/4-1	Thomas	10430-10600	Brent	oil	-	44-38
H'dal 25/4-1	Thomas	10780-11070	Statfjord	oil	-	62-44
H'dal 25/4-5	Thomas	12120-12220	Brent	water	-	52-40
H'dal 25/4-5	Thomas	12980-13170	Statfjord	water	-	40-28
VG -	Glasmann	*14764*	Brent Group	-	-	54
VG -	Glasmann	*14764*	Brent Group	-	-	55
VG -	Glasmann	*14764*	Brent Group	-	-	56

Appendix 4.1 - petrographic analysis and point count data for the Penguin field, Northern North Sea.

PENGUIN A ID: thin section 1 (Magnus Province; Middle Jurassic submarine fan sandstone; feldspathic arkose; good reservoir; oil-wet.)
Well 211/13-3 Point count: 50x5 Porosity values as total rock volume percentage in red Mineral values as solid volume percentages in black

Depth 3439m	*Porosity*	Quartz	Plag	K-spar	Illite	Dolomite	Mica	2^ porosity	Kaolinite	Zircon	Calcite	TiO2	Sum
Red	*18*	44	16	22	6	6	4	2	0	0	0	0	100%
Orange	*16*	50	10	20	8	10	2	0	0	0	0	0	100%
Yellow	*21*	42	14	26	4	4	6	0	2	2	0	0	100%
Green	*22*	40	10	28	4	6	8	0	0	0	2	2	100%
Blue	*20*	36	14	30	6	2	10	0	0	0	2	0	100%
AVERAGE	*19*	42	13	25	6	6	6	0	0	0	1	0	100%

Notes - quartz-rich feldspathic arkose with about 20% porosity. 42% of the rock volume is quartz, 25% k-spar, 13% plagioclase; 6% mica, 6% dolomite; 6% illite. Poorly sorted, angular grains (0.5mm-0.05mm). Pore interconnectivity reasonable. Dolomite cement, with unstable margins and the presence of relict grain cavities, altered feldspars, and secondary porosity indicate early and late diagenetic events respectively. Generally clean, though presence of clays, kaolinite and illite on grain edges and occasioally pore-filling.

PENGUIN A ID: thin section 2 (Magnus Province; Mid Jur. turbidite sandstone; feldspathic arkose; good reservoir; oil-wet.)
Well 211/13-3 Point count: 50x5 Porosity values as total rock volume percentage in red Mineral values as solid volume percentages in black

Depth 3467m	*Porosity*	Quartz	Albite	K-spar	Illite	Dolomite	Mica	2^ porosity	Kaolinite	Zircon	Calcite	TiO2	Sum
Red	*12*	34	12	24	8	10	8	4	0	0	0	0	100%
Orange	*16*	36	18	24	8	8	2	4	0	0	0	0	100%
Yellow	*18*	28	16	32	4	4	10	2	2	0	2	0	100%
Green	*12*	30	18	26	2	6	8	6	2	0	2	0	100%
Blue	*16*	40	14	28	6	2	6	2	0	2	0	0	100%
AVERAGE	*15*	34	16	27	6	6	7	4	1	0	1	0	100%

Notes - essentially similar to the shallower sample, as described above. Clear quartz overgowths present. No large fluid inclusions. Porosity slightly lower and quartz content lower - stratigraphic or compactional? Signs of compaction - warped mica flakes, impacted qtz-on-qtz grain boundaries.

Appendix 4.1 - petrographic analysis and point count data for the Penguin field, Northern North Sea.

PENGUIN B ID: thin section 3 (Penguin province; Triassic continental sandstone; mixed arkose; moderate reservoir; condensate-wet.)
Well 211/13-1 Point count: 50x5 Porosity values as total rock volume percentage in red Mineral values as solid volume percentages in black

Depth 2686m	*Porosity*	Quartz	Albite	K-spar	Illite	Dolomite	Mica	2^ porosity	Kaolinite	Zircon	Calcite	Lithics	Sum
Red	*12*	24	18	22	6	4	6	6	4	0	0	10	100%
Orange	*13*	36	10	18	8	6	2	10	0	0	2	8	100%
Yellow	*18*	28	12	24	4	4	10	12	0	2	0	4	100%
Green	*12*	32	10	30	2	4	8	8	0	0	0	6	100%
Blue	*10*	36	14	22	6	2	10	4	0	0	4	2	100%
AVERAGE	*13*	31	13	23	5	4	7	8	1	0	1	6	100%

Notes - fine grained, mixed lithic-feldspathic arkose with about 13% porosity. 31% of the rock volume is quartz, 23% k-spar, 13% plagioclase; 7% mica; 4% dolomite; 5% illite. 6% lithics, notably polycrystalline qtz. Moderately sorted, angular grains (0.1mm-0.05mm). Pore interconnectivity low; dirty appearance due to common pore-filling clay cements.Relict grain cavities, altered feldspars, and secondary porosity common, indicating early and late diagenetic events respectively. Prevalent bitumen staining.

PENGUIN B ID: thin section 4 (Penguin province; Triassic continental sandstone; mixed arkose; moderate reservoir; condensate-wet.)
Well 211/13-1 Point count: 50x5 Porosity values as total rock volume percentage in red Mineral values as solid volume percentages in black

Depth 2855m	*Porosity*	Quartz	Albite	K-spar	Illite	Dolomite	Mica	2^ porosity	Kaolinite	Zircon	Calcite	Lithics	Sum
Red	*14*	26	14	24	8	2	10	8	0	0	0	8	100%
Orange	*10*	32	12	18	4	6	8	10	0	0	0	10	100%
Yellow	*10*	26	12	26	4	2	12	12	0	2	2	2	100%
Green	*12*	32	10	28	6	2	6	10	0	0	0	6	100%
Blue	*8*	36	12	22	6	6	6	8	0	0	0	4	100%
AVERAGE	*11*	30	12	24	6	4	8	10	0	0	0	6	100%

PENGUIN B ID: thin section 5 - second cut showing cementation feature
Well 211/13-1 (Penguin province; Triassic continental sandstone; mixed arkose; moderate reservoir; condensate-wet.)

Notes - thin section 4 similar in petrology to the shallower sample, thin section 3. Mica appears more prevalent. The second cut with obvious cementation feature appears to be a calcite cemented seam. No porosity in the seam and no bitumen present on one side of the seam.

Appendix 4.1 - petrographic analysis and point count data for the Penguin field, Northern North Sea.

PENGUIN C ID: thin section 6 (Brent province; Ness deltaic sandstone; feldspathic arkose; poor reservoir; oil-wet.)
Well 211/13-6 Point count: 50x5 Porosity values as total rock volume percentage in red Mineral values as solid volume percentages in black

Depth 3451m	*Porosity*	Quartz	Albite	K-spar	Illite	Dolomite	Mica	2^ porosity	Kaolinite	Zircon	Calcite	TiO2	Sum
Red	*12*	30	26	20	6	2	6	2	8	0	0	0	100%
Orange	*16*	36	22	12	6	0	12	6	4	0	0	2	100%
Yellow	*18*	28	34	16	8	4	8	2	0	0	0	0	100%
Green	*12*	30	24	18	8	2	4	8	2	0	2	2	100%
Blue	*16*	34	28	20	4	2	10	0	0	0	2	0	100%
AVERAGE	*15*	32	27	17	6	2	8	4	3	0	1	1	100%

Notes - mature feldpsathic arkose; grains appear subangular to rounded, med-fine; well sorted; plagioclase feldspar common; low porosity 5-10%; aligned mica flakes; stratigrpahic variation overprinted by compaction; porespace mostly filled with clay material; secondary porosity present within corroded feldspars.

PENGUIN C ID: thin section 7 (Brent province; Etive deltaic sandstone; feldspathic arkose; good reservoir; oil-wet.)
Well 211/14-4RE Point count: 50x5 Porosity values as total rock volume percentage in red Mineral values as solid volume percentages in black

Depth 3505m	*Porosity*	Quartz	Albite	K-spar	Illite	Dolomite	Mica	2^ porosity	Kaolinite	Zircon	Calcite	TiO2	Sum
Red	*18*	44	14	20	6	4	4	2	6	0	0	0	100%
Orange	*16*	52	10	20	8	0	2	0	8	0	0	0	100%
Yellow	*21*	44	14	24	4	4	6	0	2	2	0	0	100%
Green	*12*	36	12	26	2	6	8	6	2	0	2	0	100%
Blue	*16*	38	14	30	6	2	6	2	0	2	0	0	100%
AVERAGE	*17*	43	13	24	5	3	5	2	4	1	0	0	100%

Notes - quartz-rich feldspathic arkose with about 17% porosity. 43% of the rock volume is quartz, 24% k-spar, 13% plagioclase; 5% mica, 3% dolomite; 5% illite. Well sorted, sub-rounded grains (0.1mm-0.05mm). Impacted grains - compaction feature; quartz cement overgowths; pore interconnectivity good; generally clean, though presence of clays, kaolinite and illite on grain edges and occasioally pore-filling. Bitumen staining; few relict feldspar cavities, and secondary porosity ?late diagenetic event.

Appendix 4.1 - petrographic analysis and point count data for the Penguin field, Northern North Sea.

PENGUIN D ID: thin section 9 (Brent province; Etive deltaic sandstone; feldspathic arkose; good reservoir; oil-wet.)
Well 211/14-3 Point count: 50x5 Porosity values as total rock volume percentage in red Mineral values as solid volume percentages in black

Depth 3454m	*Porosity*	Quartz	Albite	K-spar	Illite	Dolomite	Mica	2^ porosity	Kaolinite	Zircon	Calcite	TiO2	Sum
Red	*14*	22	18	32	6	12	2	2	6	0	0	0	100%
Orange	*12*	36	14	20	4	10	2	2	12	0	0	0	100%
Yellow	*18*	30	10	28	4	8	10	4	4	0	2	0	100%
Green	*16*	30	12	26	6	12	8	0	6	0	0	0	100%
Blue	*16*	36	14	24	6	4	10	2	2	0	2	0	100%
AVERAGE	*15*	31	14	26	5	9	6	2	6	0	1	0	100%

Notes - medium grained, well sorted feldspathic arkose; sub-angular to sub-rounded grains,mica rich; mica in good condition; large secondary porosity void space. Polycrystalline quartz; relict feldspars; appears to have high albite content; rare zircons. Matures sandstone with good poroperm characteristics and evidence of late diagenetic alteration - kaolinite and illite overgrowths.

PENGUIN D ID: thin section 9 (Brent province; Etive deltaic sandstone; feldspathic arkose; good reservoir; oil-wet.)
Well 211/14-1 Point count: 50x5 Porosity values as total rock volume percentage in red Mineral values as solid volume percentages in black

Depth 3406m	*Porosity*	Quartz	Albite	K-spar	Illite	Dolomite	Mica	2^ porosity	Kaolinite	Zircon	Calcite	TiO2	Sum
Red	*16*	26	20	24	2	8	4	2	12	2	0	0	100%
Orange	*10*	38	14	26	0	8	2	2	10	0	0	0	100%
Yellow	*20*	34	10	28	6	12	4	0	6	0	0	0	100%
Green	*14*	34	14	32	2	10	8	0	0	0	0	0	100%
Blue	*12*	36	12	20	6	14	6	4	2	0	0	0	100%
AVERAGE	*14*	34	14	26	3	10	5	2	6	0	0	0	100%

Notes - similar to the other etive sandstones documented above; compacted with extensive grain-to-grain contact; medium,fine grain tending to sub-angular; reasonable connectivity; pores appear open with obvioud diagenetic rims of quartz, illite and kaolinite; feldspars are commonly altered; rare lithics of polycrystalline quartz; bitumen stained.

Appendix 4.2 - Transmission Electron Microscope analysis

MISR - Macaulay Institute of Scientific Research
Aberdeen - (midsummer, World Cup) - June/July 1998

Penguin clay separates - TEM photography at 100 kV
12 ranked samples for purity assessment and selection

-purity assessment: qualitative, on basis of illite morphologies versus irregular and non-illite morphologies.

- selection criteria: representative samples for further Analytical Transmission Electron Microscope (ATEM) work i.e. quantitative analysis of morphotypes at Aberdeen University ATEM facility.

Operator: Martin Roe Assistant: Andrew Cavanagh

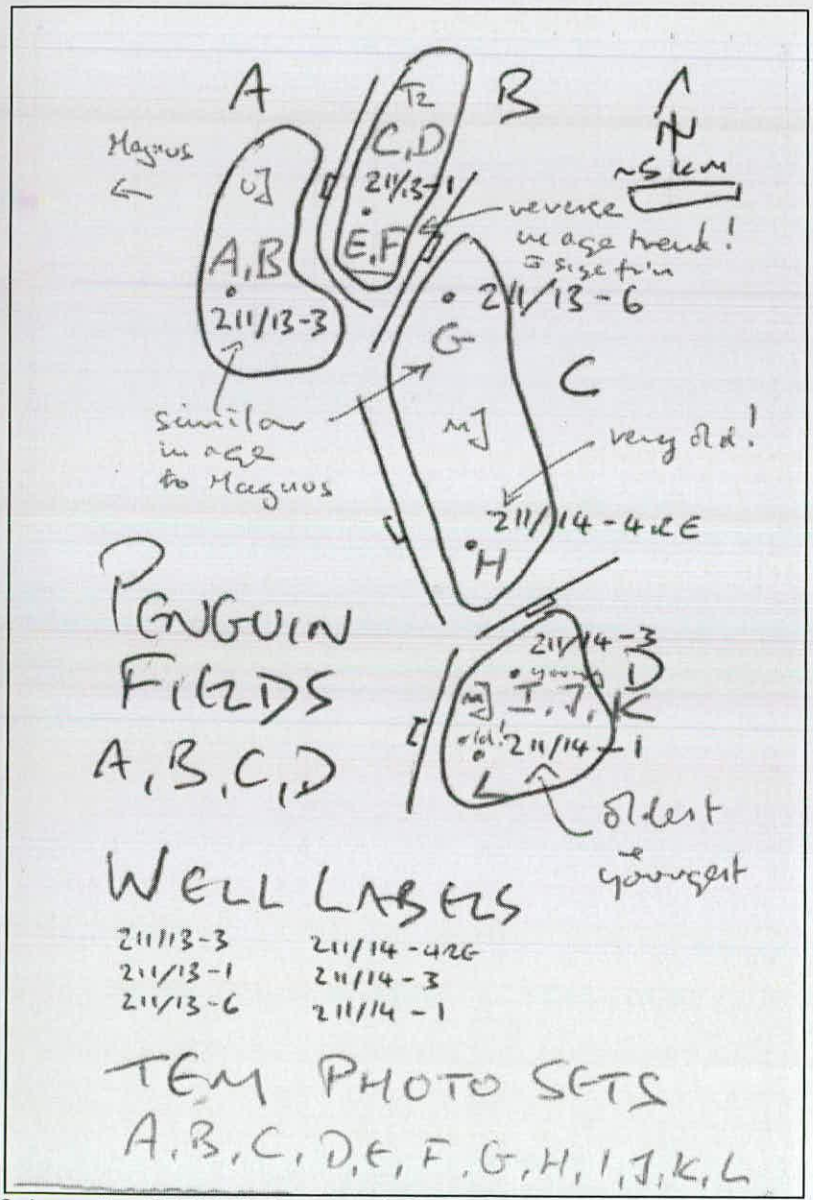

Schematic of TEM photo sets relating to Penguin fields

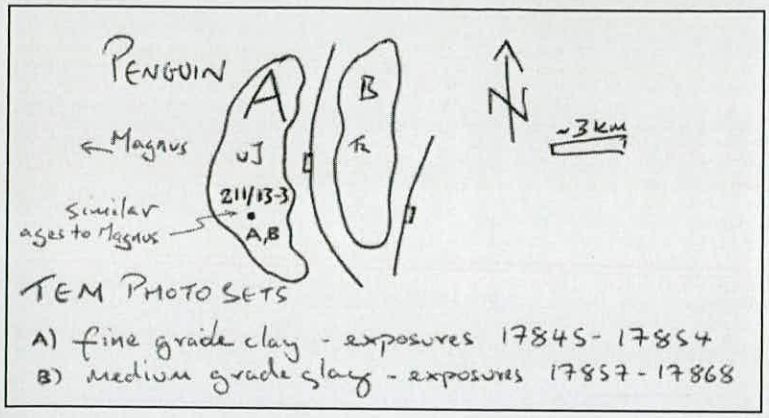

Set A	Set B
17845	17857
17846	17859
17849	17861
17850	17862
17851	17863
17852	17864
17853	17865
17854	17868

Schematic of TEM photo sets, A and B, relating to the Penguin A field

TEM photo set A	Penguin A	Clay fraction: 0.1<μm<0.5
Sample ID: P4 (A)	211/13-3	Age: 90 Ma
Separation ID: AJC-XRD6	3439 m	dD: no data
TEM rank: 3	MSM, oil wet	dO: 15.1

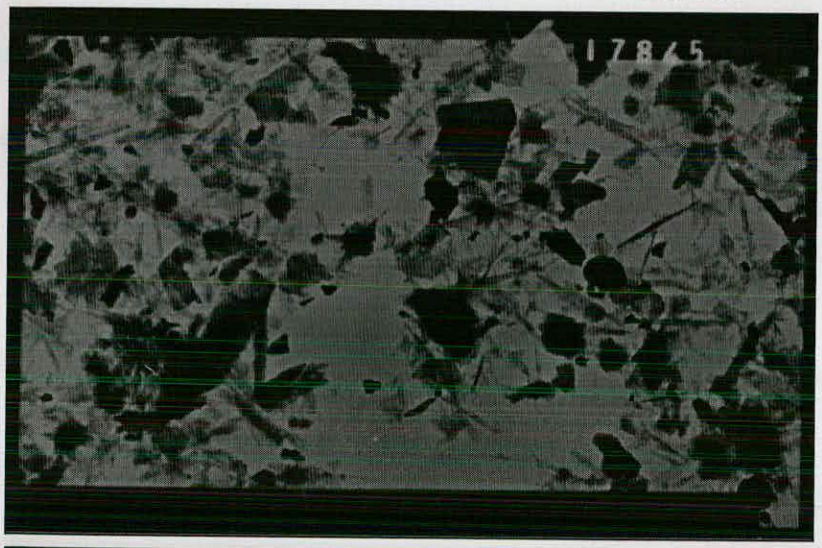

Set A	Mag'n
17845	**6k**
17846	15k
17849	15k
17850	15k
17851	15k
17852	15k
17853	30k
17854	40k

Scale bar: 5μm

Set A	Mag'n
17845	6k
17846	**15k**
17849	15k
17850	15k
17851	15k
17852	15k
17853	30k
17854	40k

Scale bar: 2μm

TEM photo set A
Sample ID: P4 (A)
Separation ID: AJC-XRD6
TEM rank: 3

Penguin A
211/13-3
3439 m
MSM, oil wet

Clay fraction: 0.1<µm<0.5
Age: 90 Ma
dD: no data
dO: 15.1

Ap'x 4.2

Set A	Mag'n
17845	6k
17846	15k
17849	**15k**
17850	15k
17851	15k
17852	15k
17853	30k
17854	40k

Scale bar: 2µm

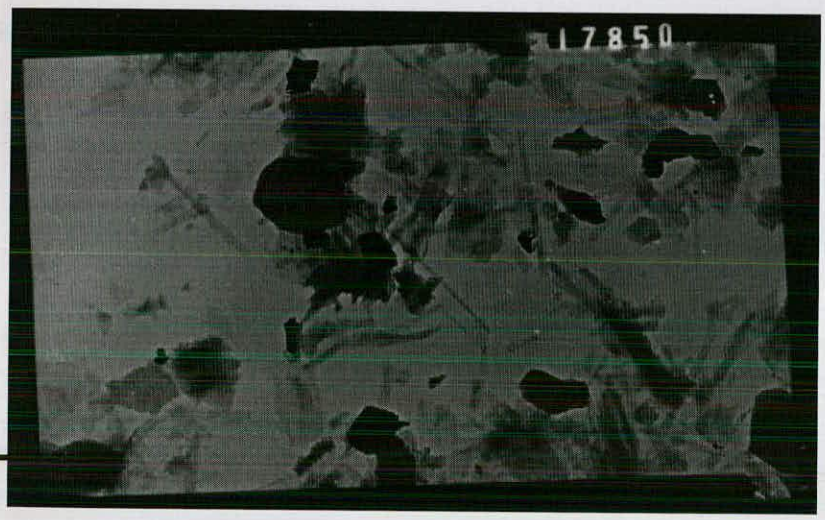

Set A	Mag'n
17845	6k
17846	15k
17849	15k
17850	**15k**
17851	15k
17852	15k
17853	30k
17854	40k

Scale bar: 2µm

Set A	Mag'n
17845	6k
17846	15k
17849	15k
17850	15k
17851	**15k**
17852	15k
17853	30k
17854	40k

Scale bar: 2µm

TEM photo set A
Sample ID: P4 (A)
Separation ID: AJC-XRD6
TEM rank: 3

Penguin A
211/13-3
3439 m
MSM, oil wet

Clay fraction: 0.1<µm<0.5
Age: 90 Ma
dD: no data
dO: 15.1

Ap'x 4.2

Set A	Mag'n
17845	6k
17846	15k
17849	15k
17850	15k
17851	15k
17852	**15k**
17853	30k
17854	40k

Scale bar: 2µm

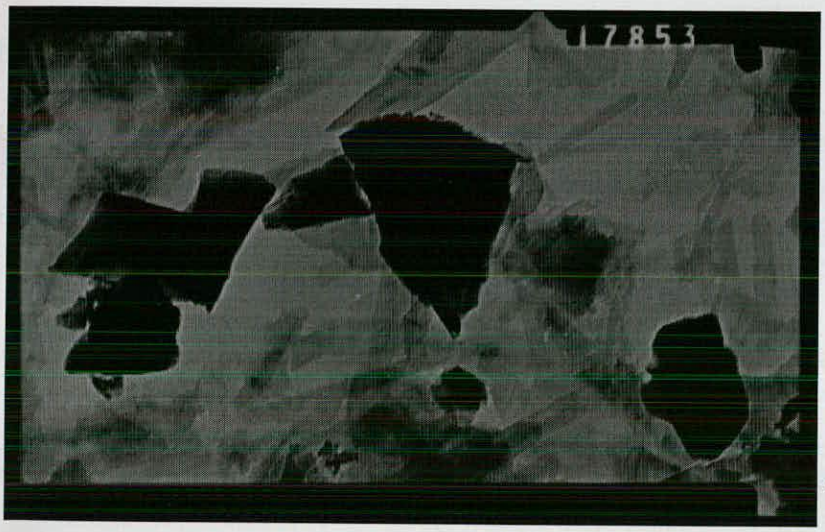

Set A	Mag'n
17845	6k
17846	15k
17849	15k
17850	15k
17851	15k
17852	15k
17853	**30k**
17854	40k

Scale bar: 1µm

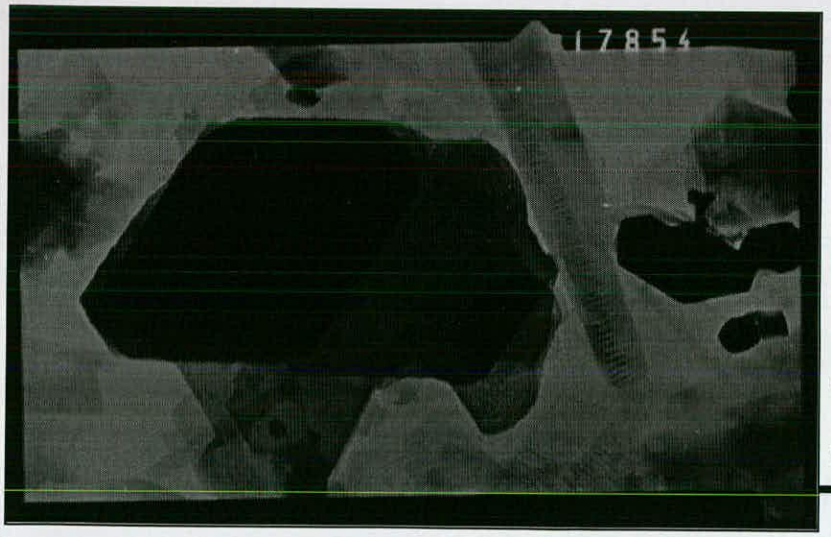

Set A	Mag'n
17845	6k
17846	15k
17849	15k
17850	15k
17851	15k
17852	15k
17853	30k
17854	**40k**

Scale bar: 1µm

TEM photo set B
Sample ID: P4 (A)
Separation ID: AJC-XRD5
TEM rank: 4

Penguin A
211/13-3
3439 m
MSM, oil wet

Clay fraction: 0.5<µm<1.0
Age: 98 Ma
dD: -55
dO: 14.9

Ap'x 4.2

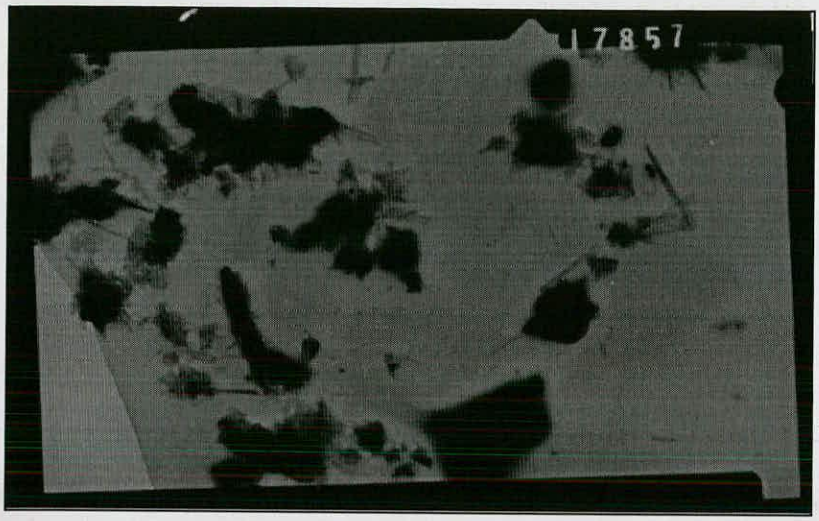

Set B	Mag'n
17857	**15k**
17859	15k
17861	15k
17862	15k
17863	15k
17864	15k
17865	40k
17868	3k

Scale bar: 2µm

Set B	Mag'n
17857	15k
17859	**15k**
17861	15k
17862	15k
17863	15k
17864	15k
17865	40k
17868	3k

Scale bar: 2µm

Set B	Mag'n
17857	15k
17859	15k
17861	**15k**
17862	15k
17863	15k
17864	15k
17865	40k
17868	3k

Scale bar: 2µm

TEM photo set B
Sample ID: P4 (A)
Separation ID: AJC-XRD5
TEM rank: 4

Penguin A
211/13-3
3439 m
MSM, oil wet

Clay fraction: 0.5<µm<1.0
Age: 98 Ma
dD: -55
dO: 14.9

Ap'x 4.2

Set B	Mag'n
17857	15k
17859	15k
17861	15k
17862	**15k**
17863	15k
17864	15k
17865	40k
17868	3k

Scale bar: 2µm

Set B	Mag'n
17857	15k
17859	15k
17861	15k
17862	15k
17863	**15k**
17864	15k
17865	40k
17868	3k

Scale bar: 2µm

Set B	Mag'n
17857	15k
17859	15k
17861	15k
17862	15k
17863	15k
17864	**15k**
17865	40k
17868	3k

Scale bar: 2µm

TEM photo set B	Penguin A	Clay fraction: 0.5<μm<1.0	Ap'x 4.2
Sample ID: P4 (A)	211/13-3	Age: 98 Ma	
Separation ID: AJC-XRD5	3439 m	dD: -55	
TEM rank: 4	MSM, oil wet	dO: 14.9	

Set B	Mag'n
17857	15k
17859	15k
17861	15k
17862	15k
17863	15k
17864	15k
17865	**40k**
17868	3k

Scale bar: 1μm

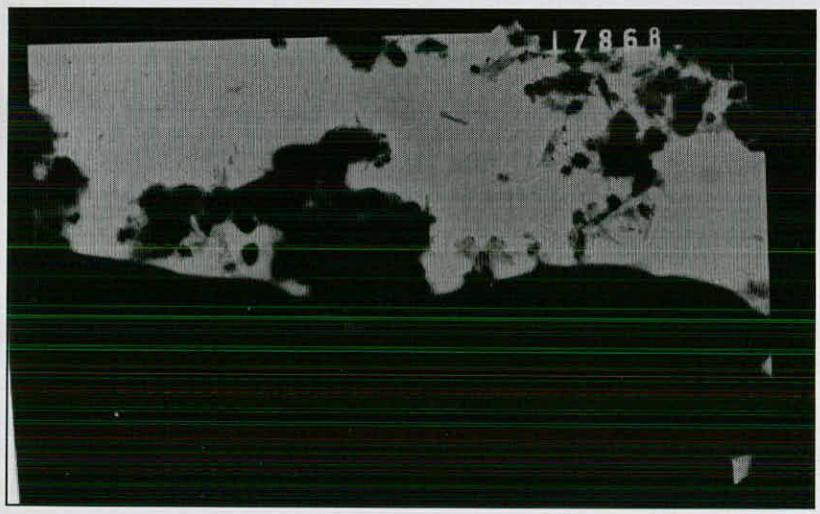

Set B	Mag'n
17857	15k
17859	15k
17861	15k
17862	15k
17863	15k
17864	15k
17865	40k
17868	**3k**

Scale bar: 10μm

TEM photo sets, C and D, for Penguin field B

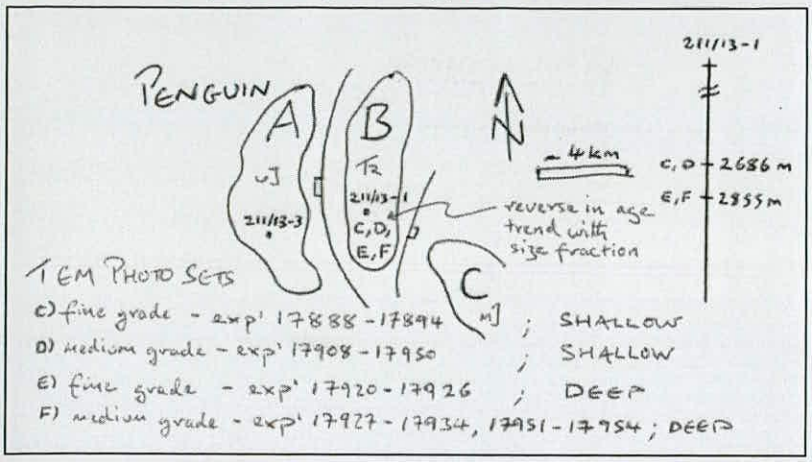

Set C	Set D
17888	17908
17889	17910
17890	17911
17891	17912
17892	17913
17893	17914
17894	17950

Schematic of TEM photo sets, C to F, relating to the Penguin B field

TEM photo set C	Penguin B	Clay fraction: 0.1<μm<0.5
Sample ID: P9 (B)	211/13-1	Age: 117 Ma
Separation ID: AJC-XRD18	2686 m	dD: -53
TEM rank: 7	Triassic, condensate	dO: 14.2

	Mag'n
17888	**6k**
17889	30k
17890	30k
17891	30k
17892	30k
17893	30k
17894	50k

Scale bar: 5μm

Set C	Mag'n
17888	6k
17889	**30k**
17890	30k
17891	30k
17892	30k
17893	30k
17894	50k

Scale bar: 1μm

TEM photo set C
Sample ID: P9 (B)
Separation ID: AJC-XRD18
TEM rank: 7

Penguin B
211/13-1
2686 m
Triassic, condensate

Clay fraction: 0.1<µm<0.5
Age: 117 Ma
dD: -53
dO: 14.2

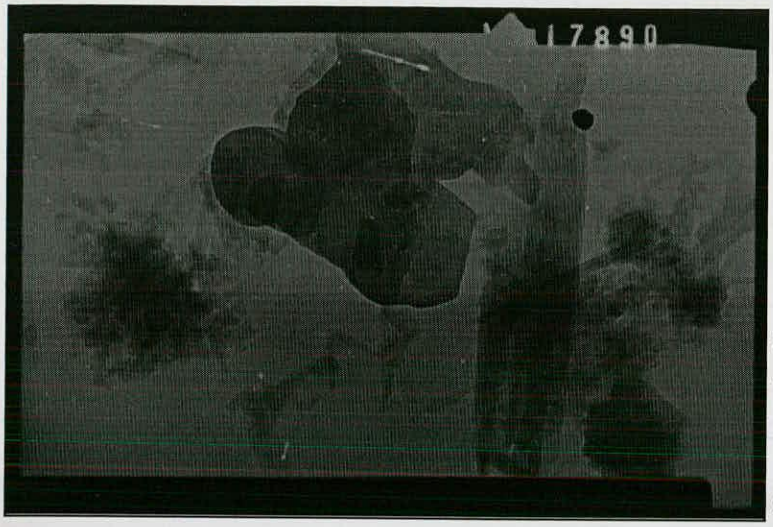

Set C	Mag'n
17888	6k
17889	30k
17890	**30k**
17891	30k
17892	30k
17893	30k
17894	50k

Scale bar: 1µm

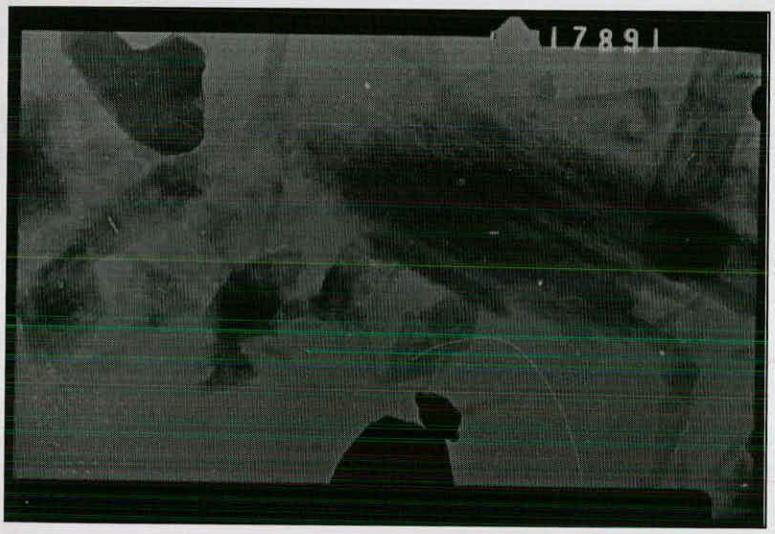

Set C	Mag'n
17888	6k
17889	30k
17890	30k
17891	**30k**
17892	30k
17893	30k
17894	50k

Scale bar: 1µm

Set C	Mag'n
17888	6k
17889	30k
17890	30k
17891	30k
17892	**30k**
17893	30k
17894	50k

Scale bar: 1µm

TEM photo set C
Sample ID: P9 (B)
Separation ID: AJC-XRD18
TEM rank: 7

Penguin B
211/13-1
2686 m
Triassic, condensate

Clay fraction: 0.1<µm<0.5
Age: 117 Ma
dD: -53
dO: 14.2

Set C	Mag'n
17888	6k
17889	30k
17890	30k
17891	30k
17892	30k
17893	**30k**
17894	50k

Scale bar: 1µm

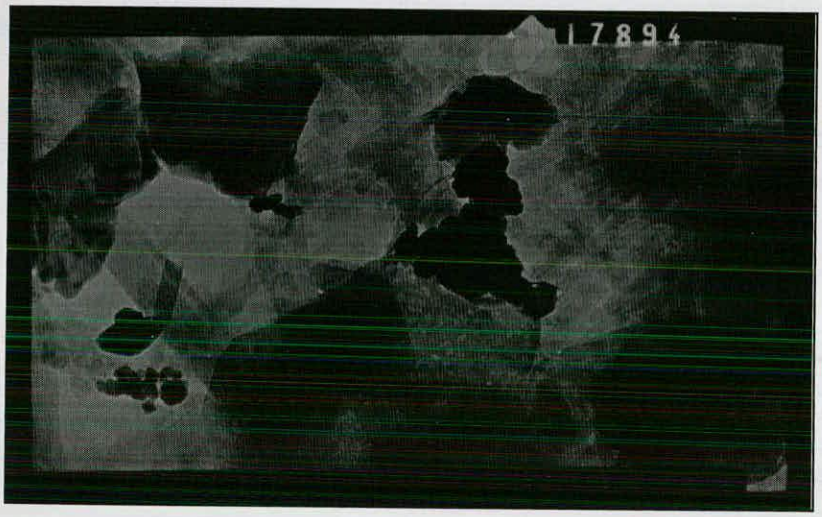

Set C	Mag'n
17888	6k
17889	30k
17890	30k
17891	30k
17892	30k
17893	30k
17894	**50k**

Scale bar: 0.5µm

TEM photo set D
Sample ID: P9 (B)
Separation ID: AJC-XRD17
TEM rank: 9

Penguin B
211/13-1
2686 m
Triassic, condensate

Clay fraction: 0.5<µm<1.0
Age: 127 Ma
dD: -52
dO: 16.2

Set D	Mag'n
17908	**6k**
17910	15k
17911	15k
17912	15k
17913	15k
17914	25k
17950	15k

Scale bar: 5µm

Set D	Mag'n
17908	6k
17910	**15k**
17911	15k
17912	15k
17913	15k
17914	25k
17950	15k

Scale bar: 2µm

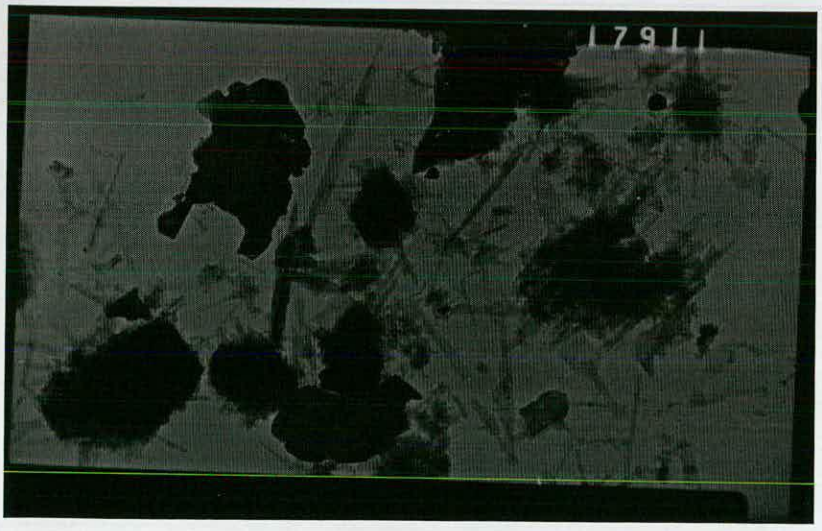

Set D	Mag'n
17908	6k
17910	15k
17911	**15k**
17912	15k
17913	15k
17914	25k
17950	15k

Scale bar: 2µm

TEM photo set D | Penguin B | Clay fraction: 0.5<µm<1.0
Sample ID: P9 (B) | 211/13-1 | Age: 127 Ma
Separation ID: AJC-XRD17 | 2686 m | dD: -52
TEM rank: 9 | Triassic, condensate | dO: 16.2

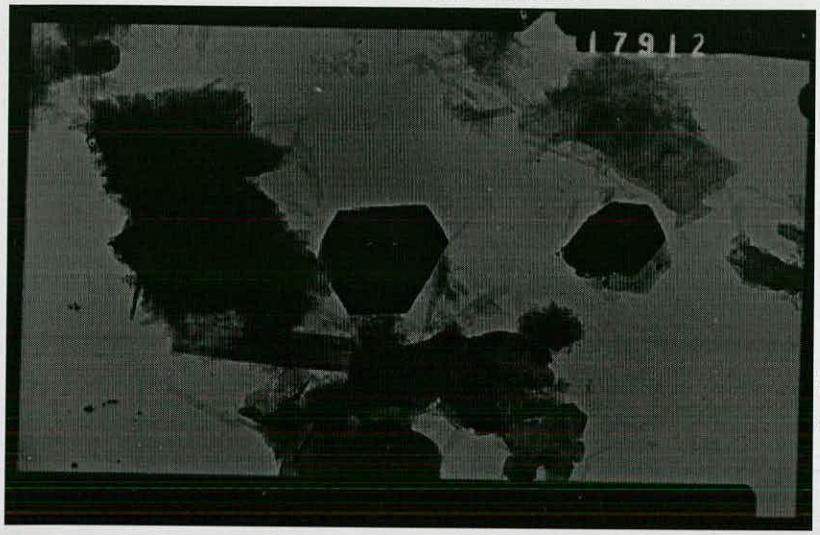

Set D	Mag'n
17908	6k
17910	15k
17911	15k
17912	**15k**
17913	15k
17914	25k
17950	15k

Scale bar: 2µm

Set D	Mag'n
17908	6k
17910	15k
17911	15k
17912	15k
17913	**15k**
17914	25k
17950	15k

Scale bar: 2µm

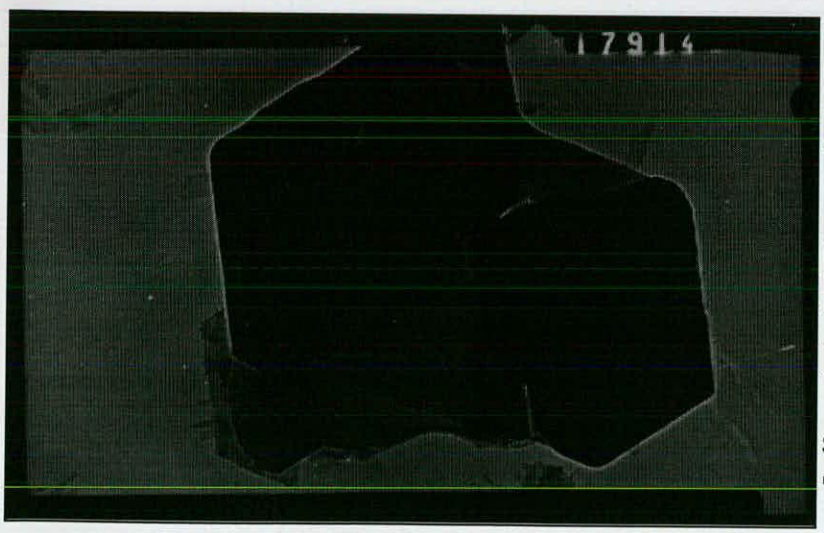

Set D	Mag'n
17908	6k
17910	15k
17911	15k
17912	15k
17913	15k
17914	**25k**
17950	15k

Scale bar: 1µm

TEM photo set D
Sample ID: P9 (B)
Separation ID: AJC-XRD17
TEM rank: 9

Penguin B
211/13-1
2686 m
Triassic, condensate

Clay fraction: 0.5<µm<1.0
Age: 127 Ma
dD: -52
dO: 16.2

Set D	Mag'n
17908	6k
17910	15k
17911	15k
17912	15k
17913	15k
17914	25k
17950	**15k**

Scale bar: 2µm

TEM photo sets, E and F, for Penguin field B

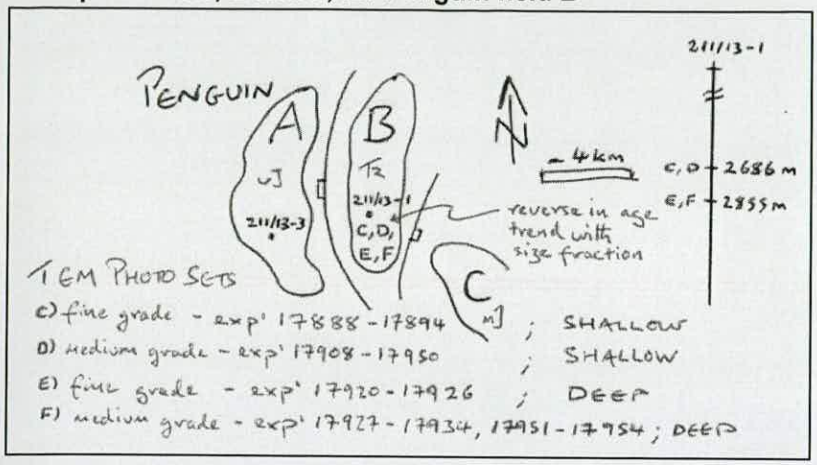

Set E	Set F
17920	17927
17921	17928
17922	17930
17923	17931
17924	17932
17925	17933
17926	17934
	17951
	17952
	17953
	17954

Schematic of TEM photo sets, C to F, relating to the Penguin B field

TEM photo set E	Penguin B	Clay fraction: 0.1<μm<0.5
Sample ID: P7 (B)	211/13-1	Age: 108 Ma
Separation ID: AJC-XRD15	2855 m	dD: -55
TEM rank: 10	Triassic, conden	dO: 14.6

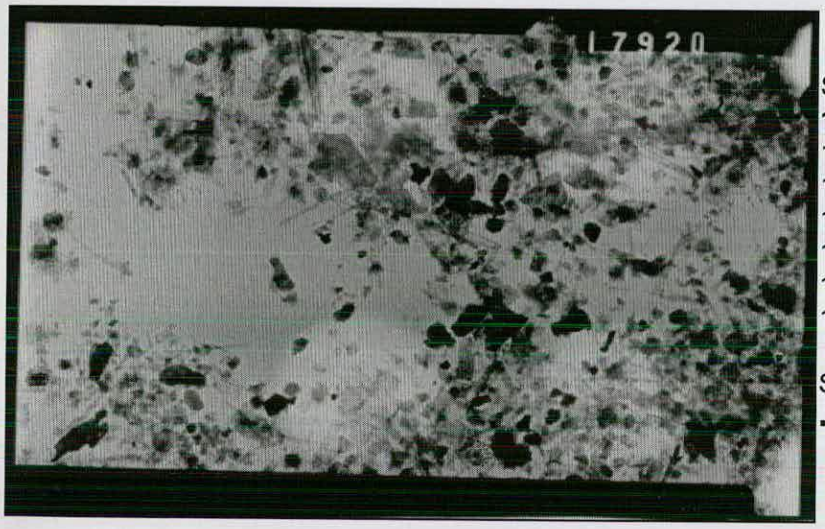

Set E	Mag'n
17920	**6k**
17921	15k
17922	25k
17923	25k
17924	25k
17925	25k
17926	80k

Scale bar: 5μm

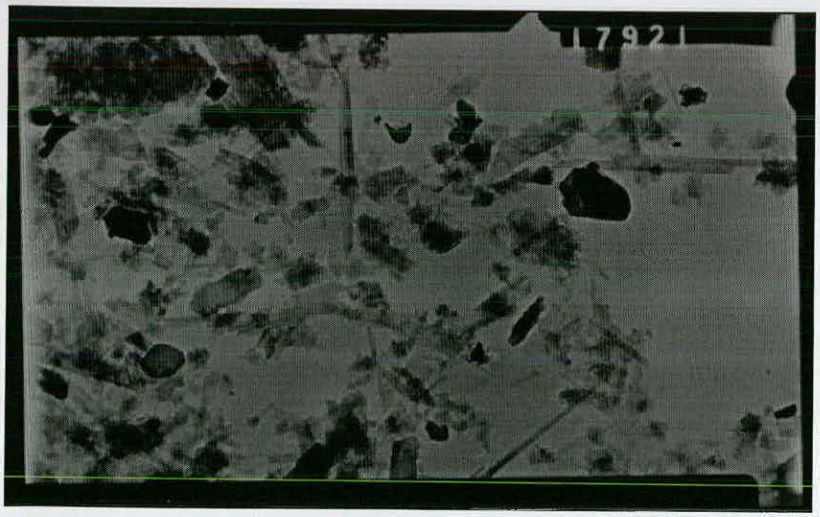

Set E	Mag'n
17920	6k
17921	**15k**
17922	25k
17923	25k
17924	25k
17925	25k
17926	80k

Scale bar: 2μm

TEM photo set E
Sample ID: P7 (B)
Separation ID: AJC-XRD15
TEM rank: 10

Penguin B
211/13-1
2855 m
Triassic, condens

Clay fraction: 0.1<µm<0.5
Age: 108 Ma
dD: -55
dO: 14.6

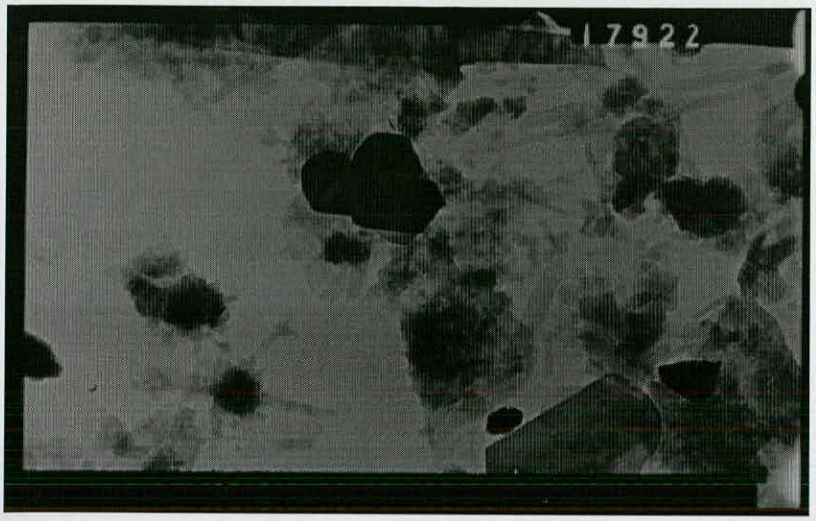

Set E	Mag'n
17920	6k
17921	15k
17922	**25k**
17923	25k
17924	25k
17925	25k
17926	80k

Scale bar: 1µm

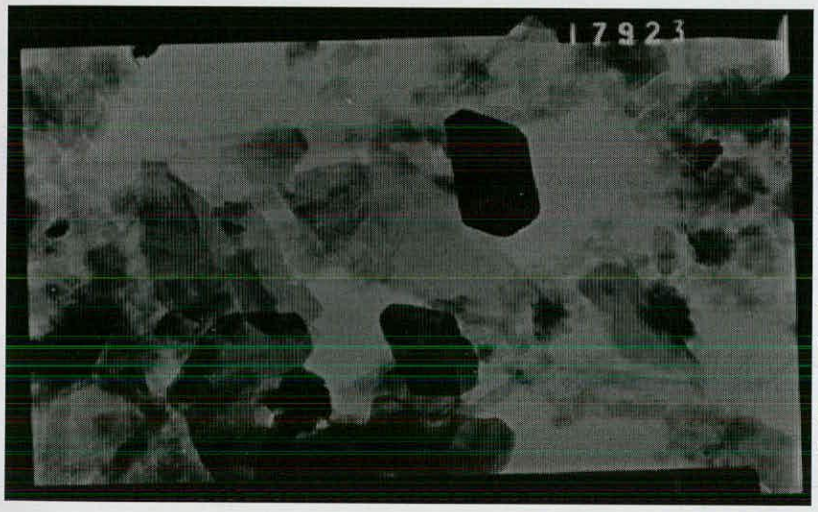

Set E	Mag'n
17920	6k
17921	15k
17922	25k
17923	**25k**
17924	25k
17925	25k
17926	80k

Scale bar: 1µm

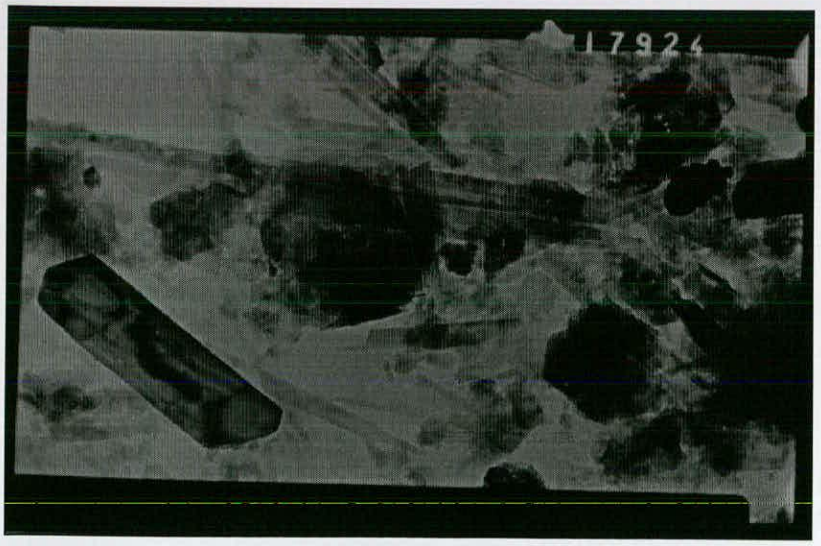

Set E	Mag'n
17920	6k
17921	15k
17922	25k
17923	25k
17924	**25k**
17925	25k
17926	80k

Scale bar: 1µm

TEM photo set E
Sample ID: P7 (B)
Separation ID: AJC-XRD15
TEM rank: 10

Penguin B
211/13-1
2855 m
Triassic, condensate

Clay fraction: 0.1<µm<0.5
Age: 108 Ma
dD: -55
dO: 14.6

Set E	Mag'n
17920	6k
17921	15k
17922	25k
17923	25k
17924	25k
17925	**25k**
17926	80k

Scale bar: 1µm

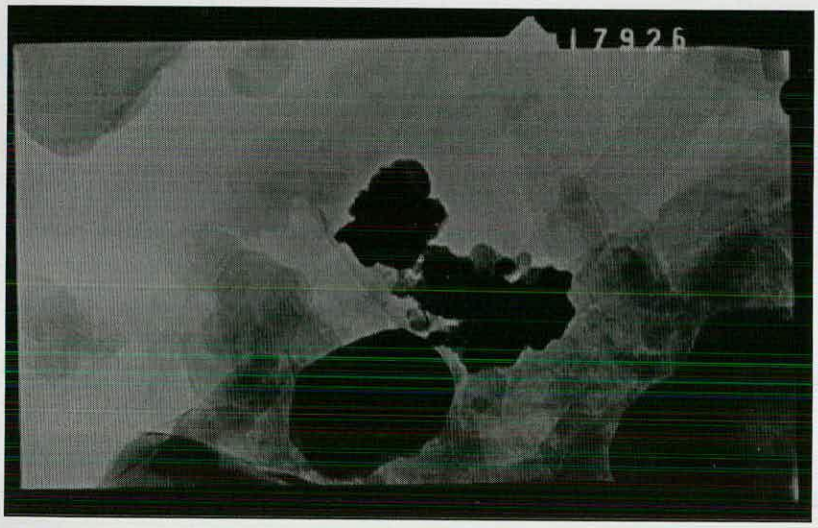

Set E	Mag'n
17920	6k
17921	15k
17922	25k
17923	25k
17924	25k
17925	25k
17926	**80k**

Scale bar: 0.25µm

TEM photo set F
Sample ID: P7 (B)
Separation ID: AJC-XRD14
TEM rank: 11

Penguin B
211/13-1
2855 m
Triassic, condensate

Clay fraction: 0.5<µm<1.0
Age: 80 Ma
dD: -52
dO: 15.7

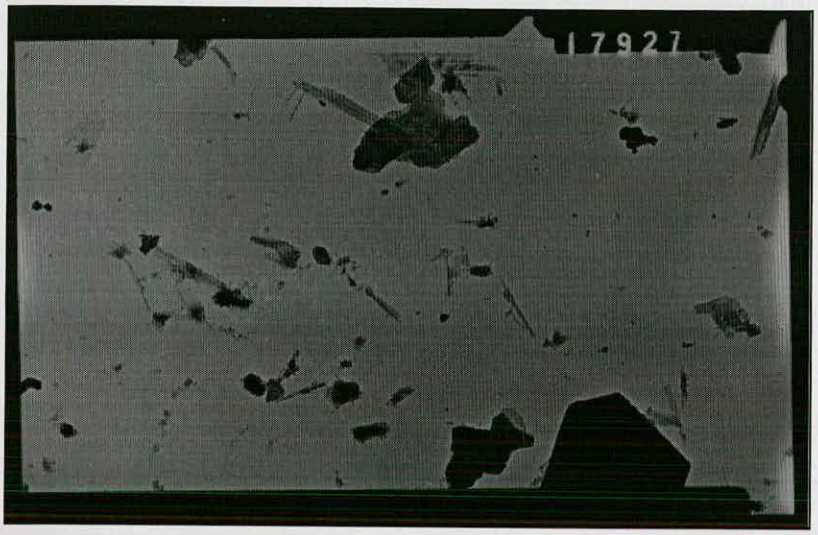

Set F	Mag'n
17927	**6k**
17928	30k
17930	10k
17931	10k
17932	10k
17933	10k
17934	10k
17951	10k
179....	

Scale bar: 5µm

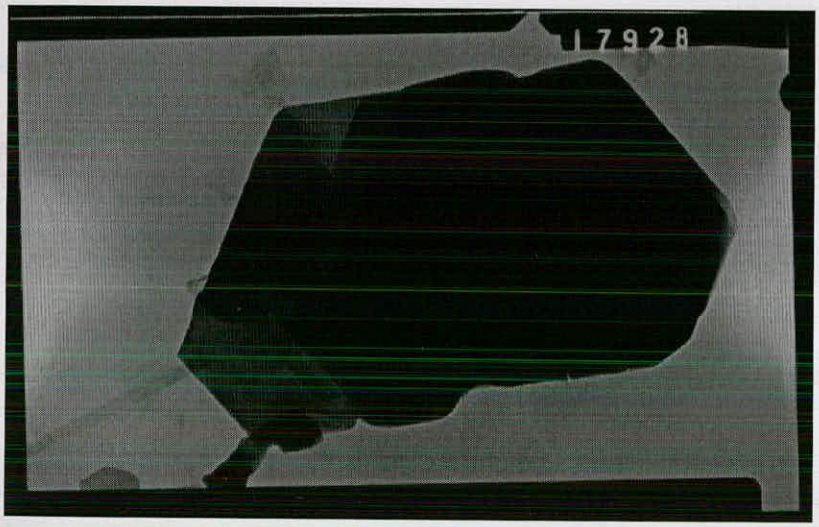

Set F	Mag'n
17927	6k
17928	**30k**
17930	10k
17931	10k
17932	10k
17933	10k
17934	10k
17951	10k
179....	

Scale bar: 1µm

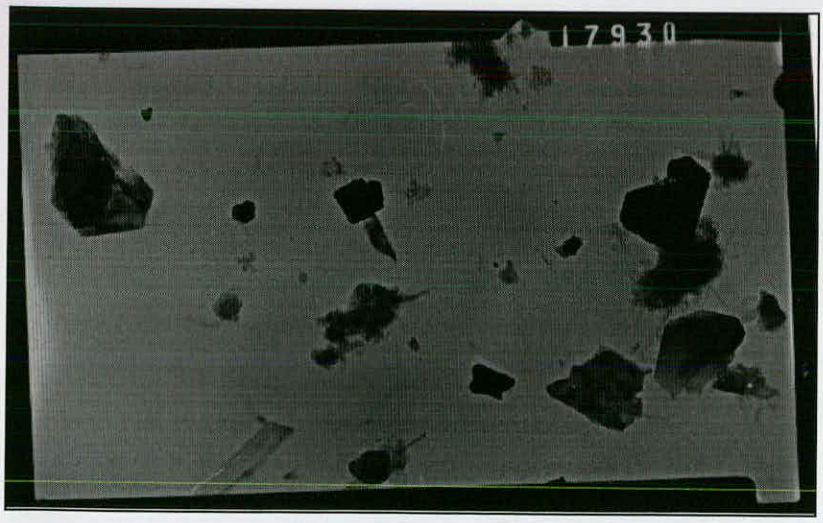

Set F	Mag'n
17927	6k
17928	30k
17930	**10k**
17931	10k
17932	10k
17933	10k
17934	10k
179....	

Scale bar: 2µm

TEM photo set F
Sample ID: P7 (B)
Separation ID: AJC-XRD14
TEM rank: 11

Penguin B
211/13-1
2855 m
Triassic, condensate

Clay fraction: 0.5<μm<1.0
Age: 80 Ma
dD: -52
dO: 15.7

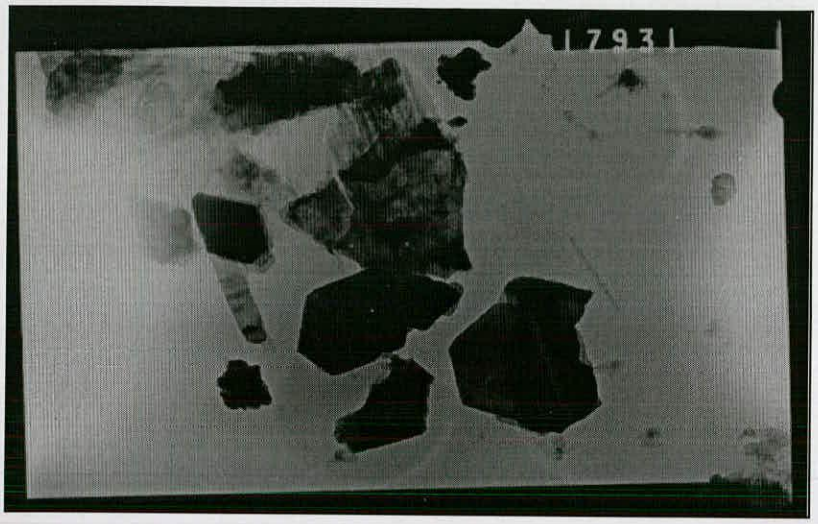

Set F	Mag'n
17930	10k
17931	**10k**
17932	10k
17933	10k
17934	10k
17951	10k
17952	10k
179...	

Scale bar: 2μm

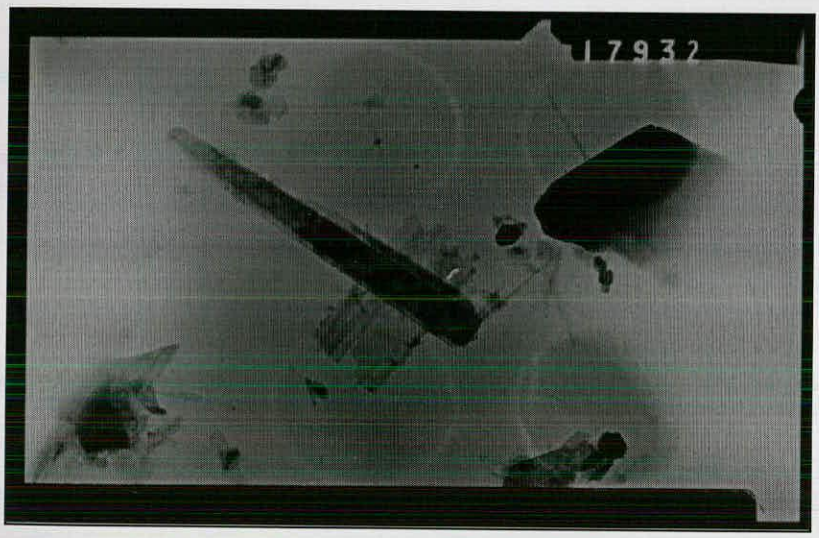

Set F	Mag'n
17930	10k
17931	10k
17932	**10k**
17933	10k
17934	10k
17951	10k
17952	10k
179...	

Scale bar: 2μm

Set F	Mag'n
17930	10k
17931	10k
17932	10k
17933	**10k**
17934	10k
17951	10k
17952	10k
179...	

Scale bar: 2μm

TEM photo set F
Sample ID: P7 (B)
Separation ID: AJC-XRD14
TEM rank: 11

Penguin B
211/13-1
2855 m
Triassic, condensate

Clay fraction: 0.5<µm<1.0
Age: 58 Ma
dD: -52
dO: 13.8

Set F	Mag'n
17930	10k
17931	10k
17932	10k
17933	10k
17934	**10k**
17951	10k
17952	10k
179...	

Scale bar: 2µm

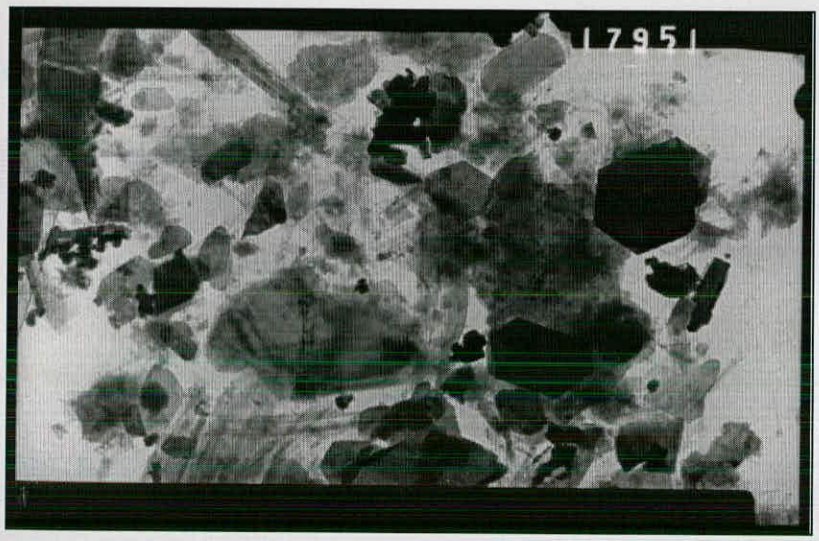

Set F	Mag'n
17930	10k
17931	10k
17932	10k
17933	10k
17934	10k
17951	**10k**
17952	10k
179...	

Scale bar: 2µm

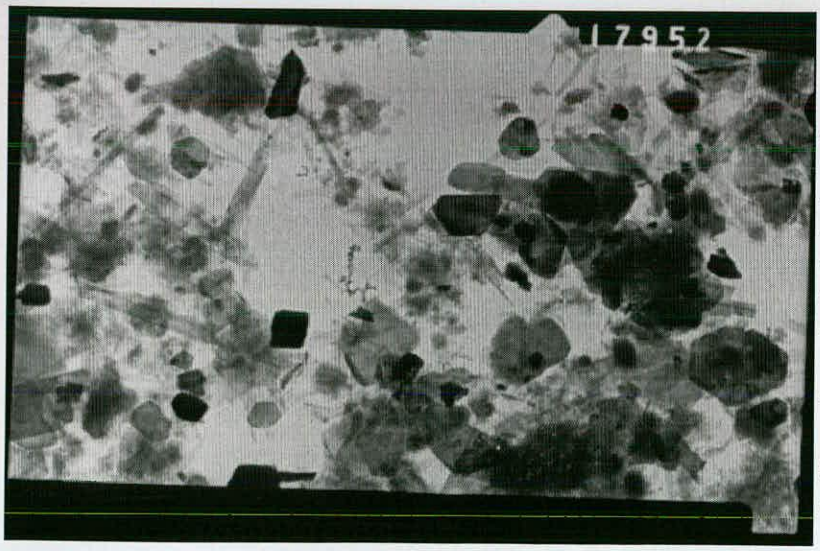

Set F	Mag'n
17930	10k
17931	10k
17932	10k
17933	10k
17934	10k
17951	10k
17952	**10k**
179...	

Scale bar: 2µm

TEM photo set F
Sample ID: P7 (B)
Separation ID: AJC-XRD14
TEM rank: 11

Penguin B
211/13-1
2855 m
Triassic, condensate

Clay fraction: 0.5<µm<1.0
Age: 58 Ma
dD: -52
dO: 13.8

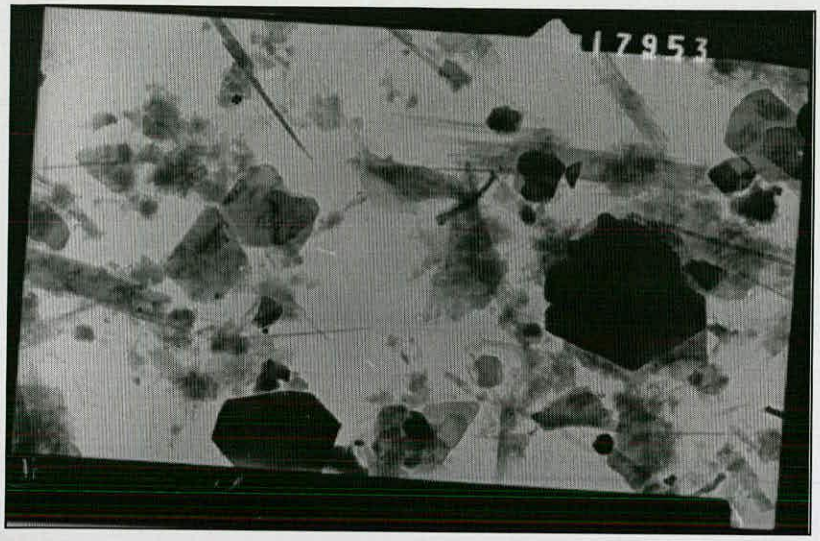

Set F	Mag'n
17932	10k
17933	10k
17934	10k
17951	10k
17952	10k
17953	**10k**
17954	10k

Scale bar: 2µm

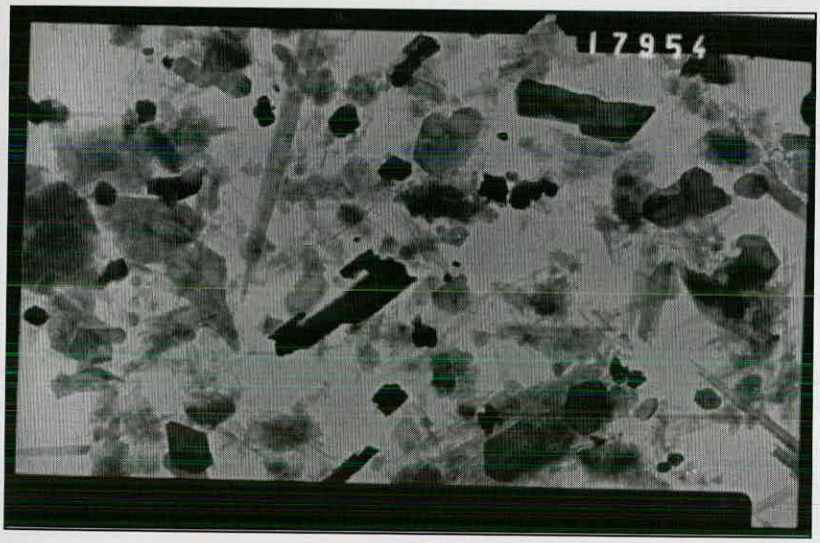

Set F	Mag'n
17932	10k
17933	10k
17934	10k
17951	10k
17952	10k
17953	10k
17954	**10k**

Scale bar: 2µm

TEM photo sets, G and H, for Penguin field C

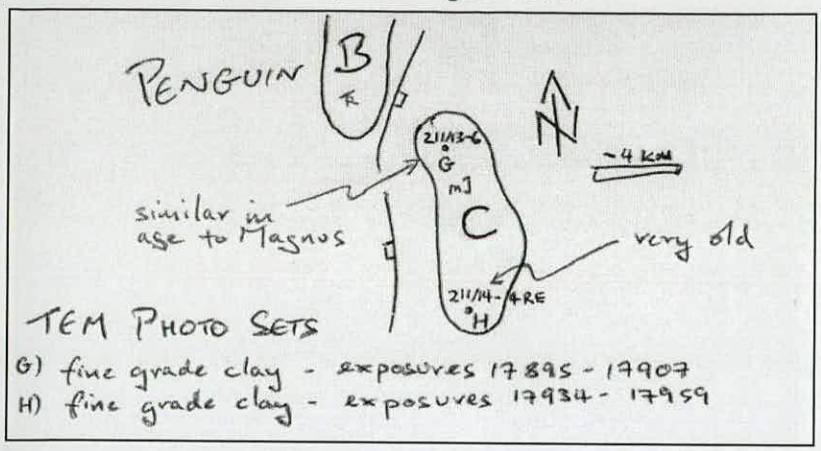

Set G	Set H
17895	17935
17896	17936
17897	17937
17898	17938
17899	17939
17901	17941
17906	17955
17907	17956
	17957
	17958

Schematic of TEM photo sets, G and H, relating to the Penguin C fie 17959

TEM photo set G	Penguin C	Clay fraction: 0.1<μm<0.5
Sample ID: P10 (C)	211/13-6	Age: 71 Ma
Separation ID: AJC-XRD21	3451 m	dD: -53
TEM rank: 8	Rannoch, oil wet	dO: 15.3

Set G	Mag'n
17895	**8k**
17896	15k
17897	15k
17898	15k
17899	15k
17901	15k
17906	30k
17907	30k

Scale bar: 2μm

Set G	Mag'n
17895	8k
17896	**15k**
17897	15k
17898	15k
17899	15k
17901	15k
17906	30k
17907	30k

Scale bar: 2μm

TEM photo set G
Sample ID: P10 (C)
Separation ID: AJC-XRD21
TEM rank: 8

Penguin C
211/13-6
3451 m
Rannoch, oil wet

Clay fraction: 0.1<μm<0.5
Age: 71 Ma
dD: -53
dO: 15.3

Set G	Mag'n
17895	8k
17896	15k
17897	**15k**
17898	15k
17899	15k
17901	15k
17906	30k
17907	30k

Scale bar: 2μm

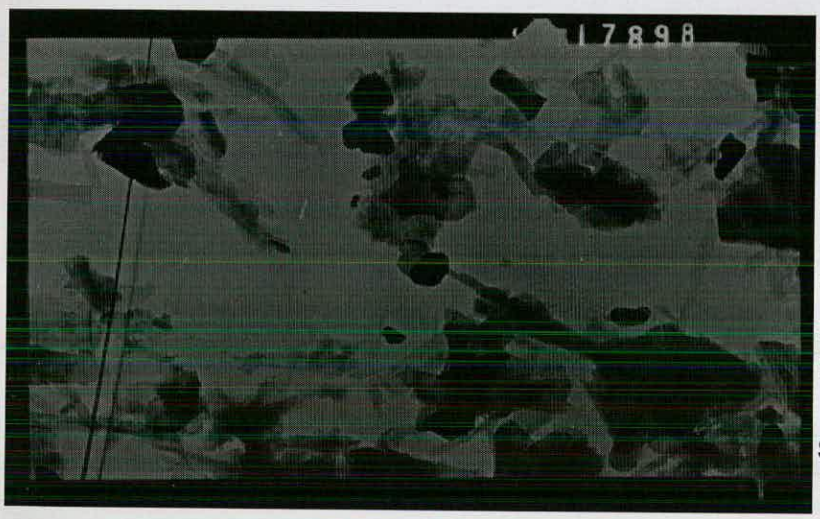

Set G	Mag'n
17895	8k
17896	15k
17897	15k
17898	**15k**
17899	15k
17901	15k
17906	30k
17907	30k

Scale bar: 2μm

Set G	Mag'n
17895	8k
17896	15k
17897	15k
17898	15k
17899	**15k**
17901	15k
17906	30k
17907	30k

Scale bar: 2μm

TEM photo set G
Sample ID: P10 (C)
Separation ID: AJC-XRD21
TEM rank: 8

Penguin C
211/13-6
3451 m
Rannoch, oil wet

Clay fraction: 0.1<µm<0.5
Age: 71 Ma
dD: -53
dO: 15.3

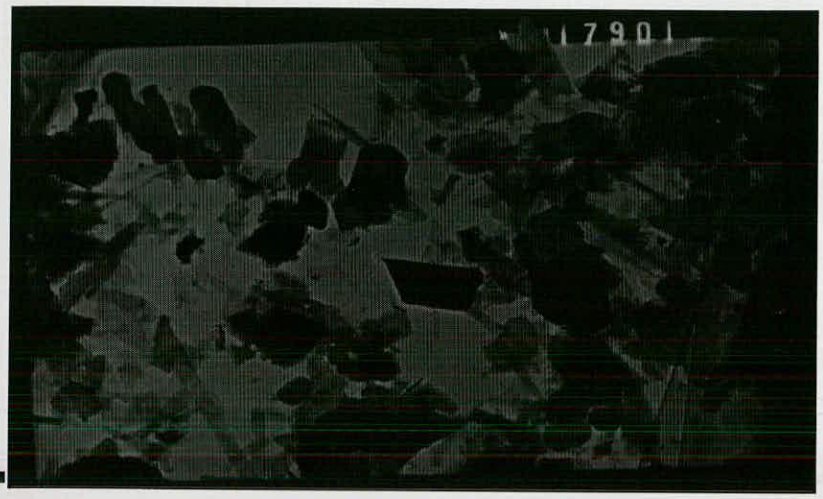

Set G	Mag'n
17895	8k
17896	15k
17897	15k
17898	15k
17899	15k
17901	**15k**
17906	30k
17907	30k

Scale bar: 2µm

Set G	Mag'n
17895	8k
17896	15k
17897	15k
17898	15k
17899	15k
17901	15k
17906	**30k**
17907	30k

Scale bar: 1µm

Set G	Mag'n
17895	8k
17896	15k
17897	15k
17898	15k
17899	15k
17901	15k
17906	30k
17907	**30k**

Scale bar: 1µm

TEM photo set H | Penguin C | Clay fraction: 0.5<μm<1.0

Sample ID: P2 (C) | 211/14-4RE | Age: 130 Ma

Separation ID: AJC-XRD3 | 3505 m | dD: -52

TEM rank: 12 | Etive, oil wet | dO: 13.8

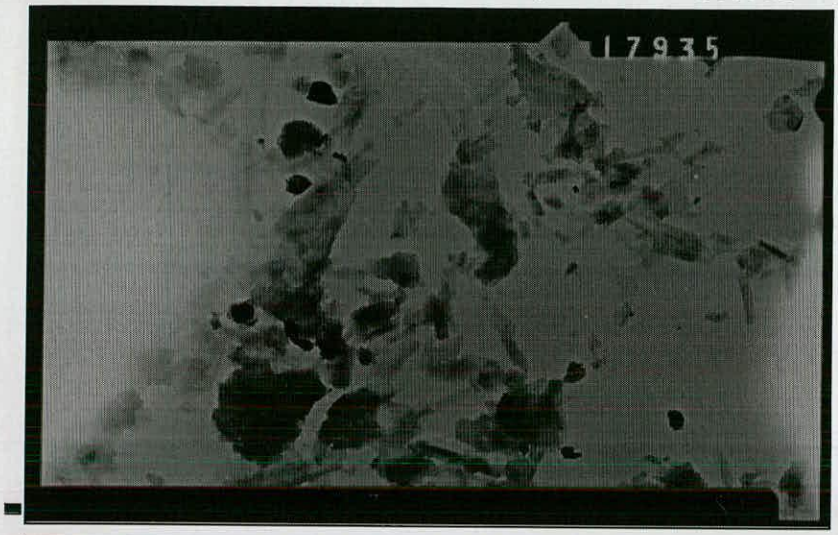

Set H	Mag'n
17935	**10k**
17936	10k
17937	10k
17938	10k
17939	10k
17941	60k
17955	6k
179....	

Scale bar: 2μm

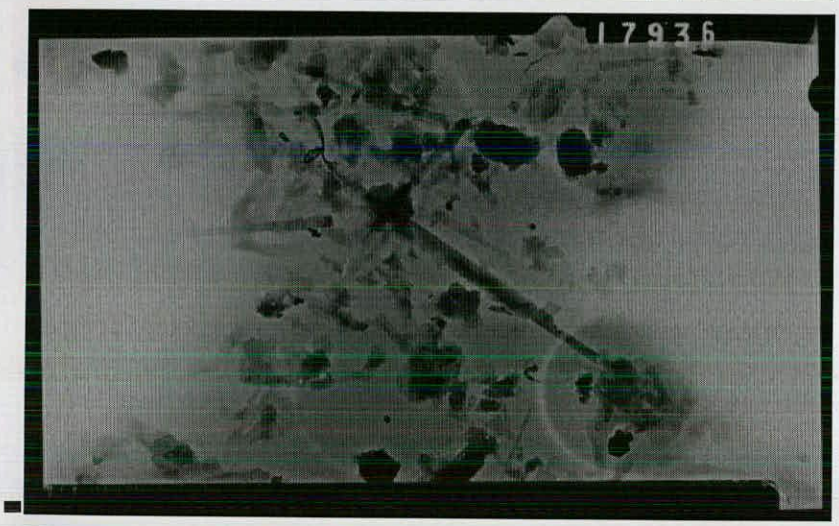

Set H	Mag'n
17935	10k
17936	**10k**
17937	10k
17938	10k
17939	10k
17941	60k
17955	6k
179....	

Scale bar: 2μm

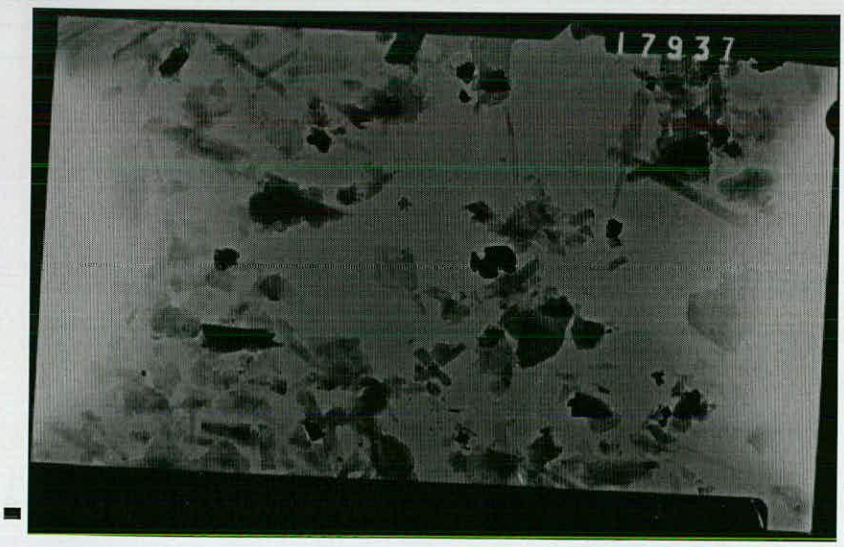

Set H	Mag'n
17935	10k
17936	10k
17937	**10k**
17938	10k
17939	10k
17941	60k
17955	6k
179....	

Scale bar: 2μm

TEM photo set H	Penguin C	Clay fraction: 0.5<μm<1.0
Sample ID: P2 (C)	211/14-4RE	Age: 130 Ma
Separation ID: AJC-XRD3	3505 m	dD: -52
TEM rank: 12	Etive, oil wet	dO: 13.8

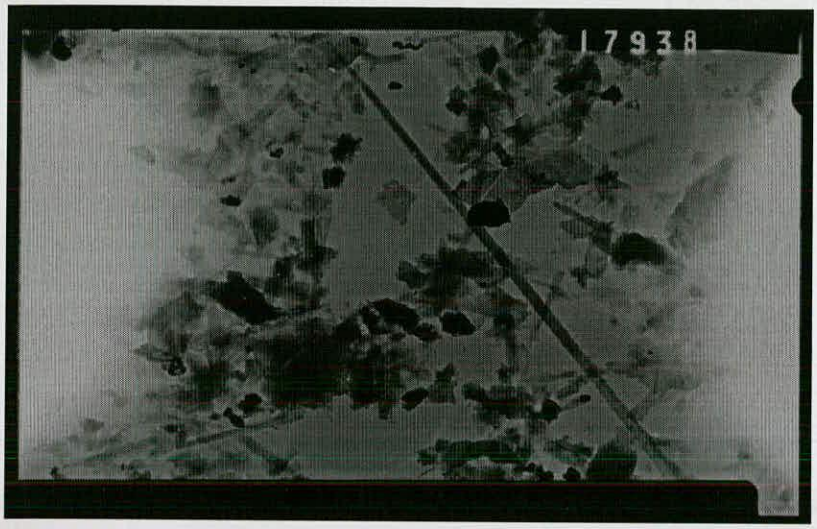

Set H	Mag'n
17935	10k
17936	10k
17937	10k
17938	**10k**
17939	10k
17941	60k
17955	6k
179....	

Scale bar: 2μm

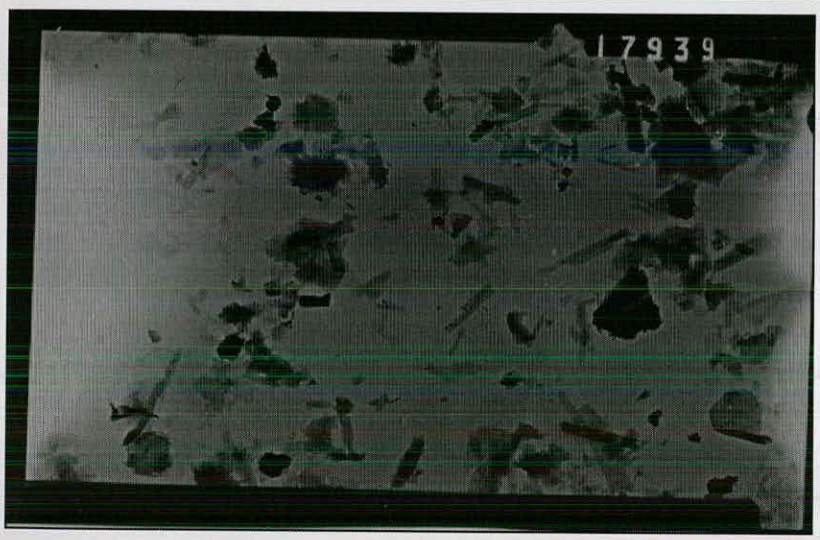

Set H	Mag'n
17935	10k
17936	10k
17937	10k
17938	10k
17939	**10k**
17941	60k
17955	6k
179....	

Scale bar: 2μm

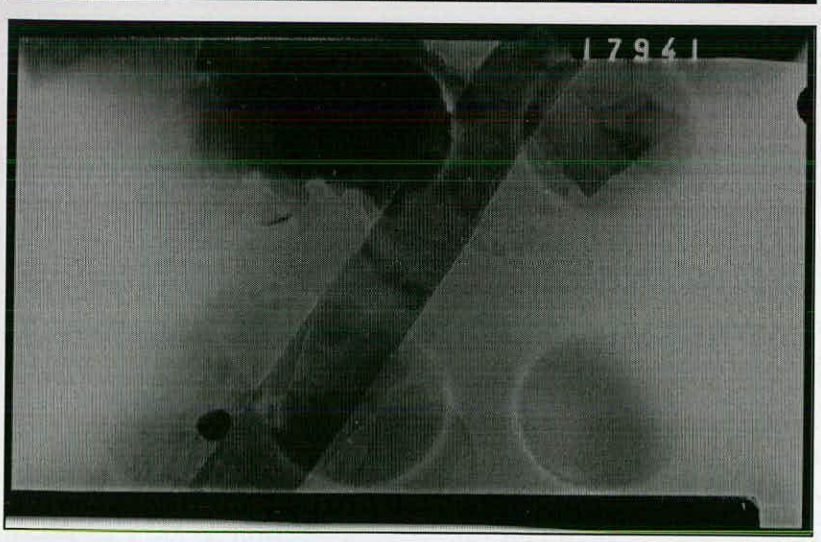

Set H	Mag'n
17935	10k
17936	10k
17937	10k
17938	10k
17939	10k
17941	**60k**
17955	6k
179....	

Scale bar: 0.5μm

TEM photo set H	Penguin C	Clay fraction: 0.5<μm<1.0
Sample ID: P2 (C)	211/14-4RE	Age: 130 Ma
Separation ID: AJC-XRD3	3505 m	dD: -52
TEM rank: 12	Etive, oil wet	dO: 13.8

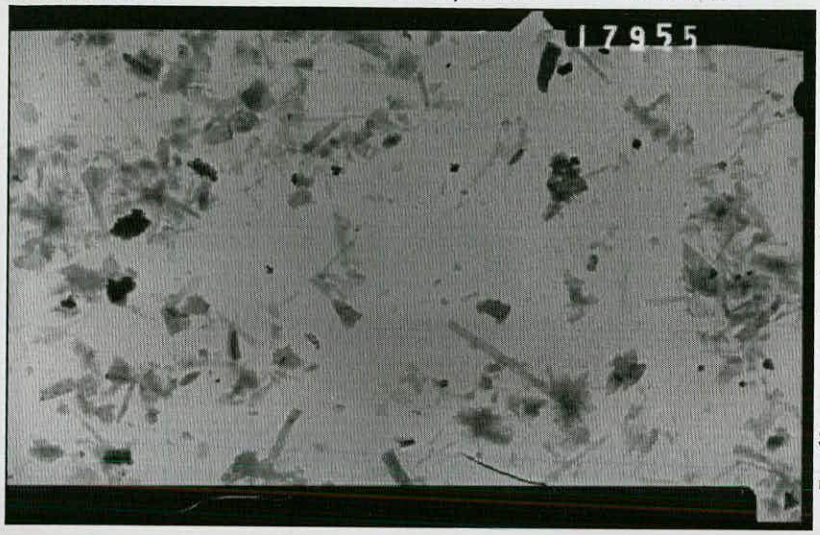

Set H	Mag'n
17939	10k
17941	60k
17955	**6k**
17956	10k
17957	10k
17958	10k
17959	10k

Scale bar: 4μm

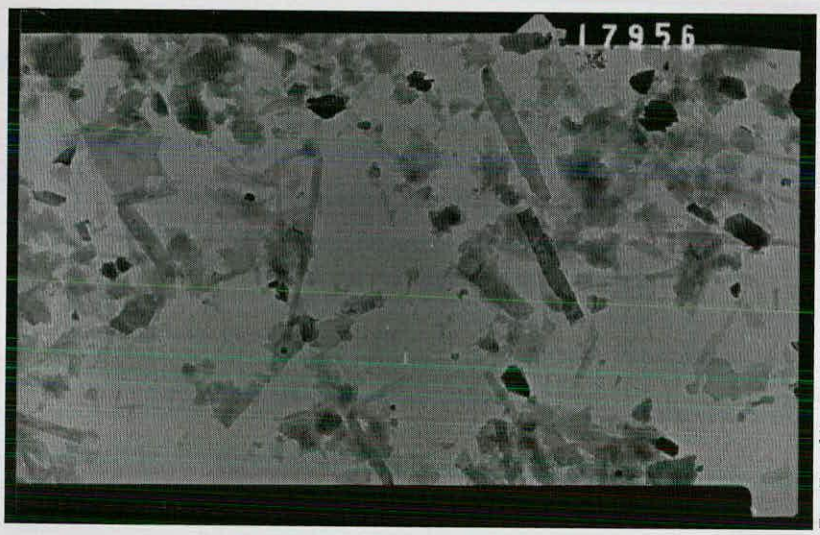

Set H	Mag'n
17939	10k
17941	60k
17955	6k
17956	**10k**
17957	10k
17958	10k
17959	10k

Scale bar: 2μm

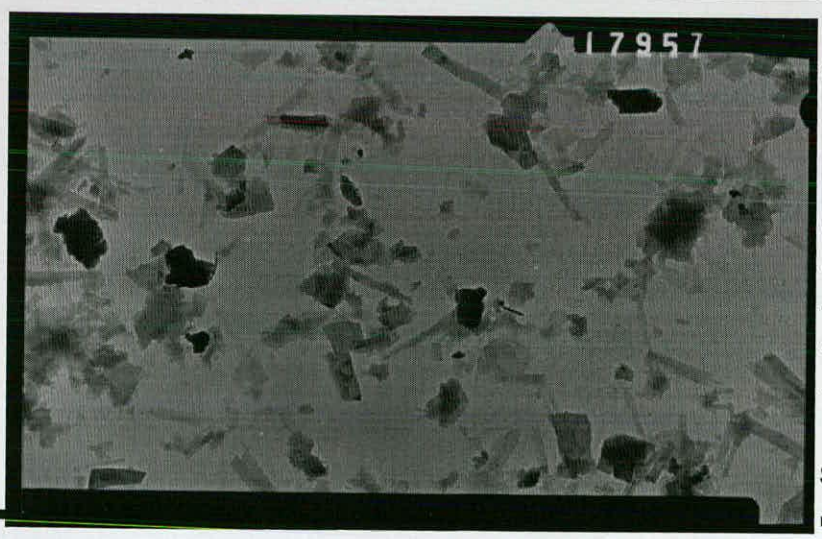

Set H	Mag'n
17939	10k
17941	60k
17955	6k
17956	10k
17957	**10k**
17958	10k
17959	10k

Scale bar: 2μm

TEM photo set H	Penguin C	Clay fraction: 0.5<μm<1.0
Sample ID: P2 (C)	211/14-4RE	Age: 130 Ma
Separation ID: AJC-XRD3	3505 m	dD: -52
TEM rank: 12	Etive, oil wet	dO: 13.8

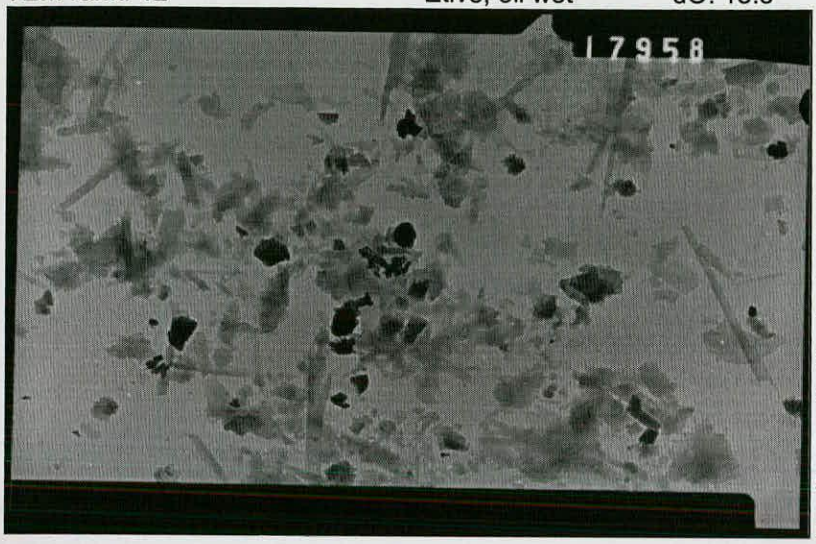

Set H	Mag'n
17939	10k
17941	60k
17955	6k
17956	10k
17957	10k
17958	**10k**
17959	10k

Scale bar: 2μm

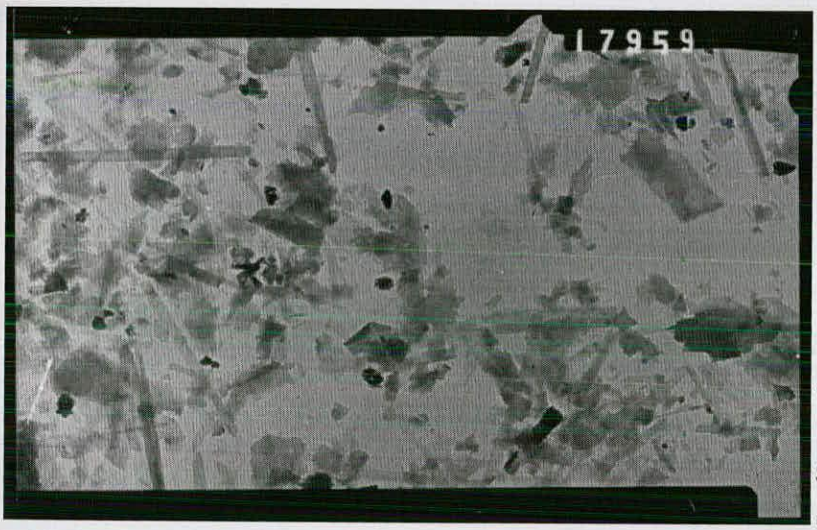

Set H	Mag'n
17939	10k
17941	60k
17955	6k
17956	10k
17957	10k
17958	10k
17959	**10k**

Scale bar: 2μm

TEM photo sets, I,J,K and L, for Penguin field D

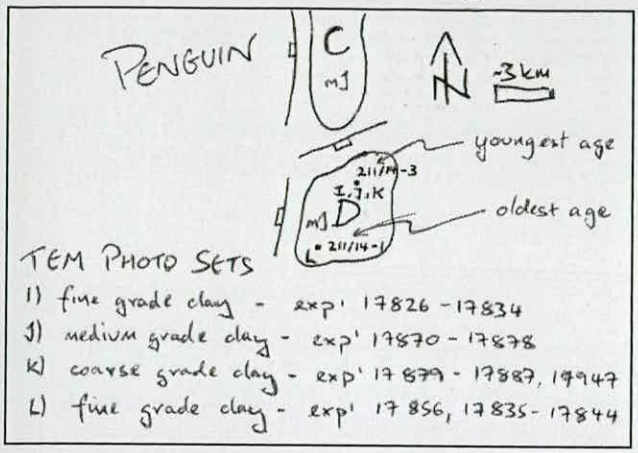

Set I	Set J	Set K	Set L
17826	17870	17879	17856
17827	17871	17880	17835
17828	17872	17881	17836
17829	17873	17883	17837
17830	17874	17884	17838
17832	17875	17885	17839
17833	17878	17886	17840
17834		17887	17842
		17947	17844

Schematic of TEM photo sets, I, J K and L, relating to the Penguin D field

TEM photo set I	Penguin D	Clay fraction: 0.1<μm<0.5
Sample ID: P11 (D)	211/14-3	Age: 34 Ma
Separation ID: AJC-XRD24	3454 m	dD: no data
TEM rank: 1	Etive, oil wet	dO: 13.6

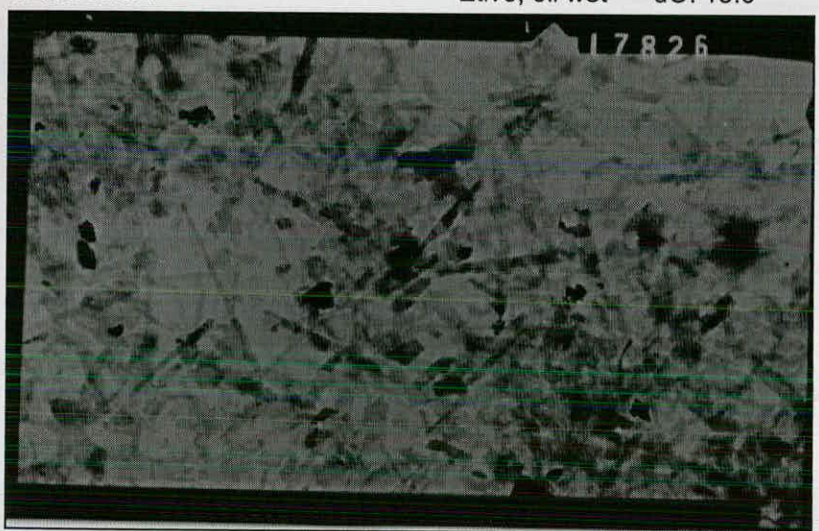

Set I	Mag'n
17826	**6k**
17827	15k
17828	15k
17829	15k
17830	15k
17832	50k
17833	50k
17834	50k

Scale bar: 4μm

Set I	Mag'n
17826	6k
17827	**15k**
17828	15k
17829	15k
17830	15k
17832	50k
17833	50k
17834	50k

Scale bar: 2μm

TEM photo set I	Penguin D	Clay fraction: 0.1<μm<0.5
Sample ID: P11 (D)	211/14-3	Age: 34 Ma
Separation ID: AJC-XRD24	3454 m	dD: no data
TEM rank: 1	Etive, oil wet	dO: 13.6

Set I	Mag'n
17826	6k
17827	15k
17828	**15k**
17829	15k
17830	15k
17832	50k
17833	50k
17834	50k

Scale bar: 2μm

Set I	Mag'n
17826	6k
17827	15k
17828	15k
17829	**15k**
17830	15k
17832	50k
17833	50k
17834	50k

Scale bar: 2μm

Set I	Mag'n
17826	6k
17827	15k
17828	15k
17829	15k
17830	**15k**
17832	50k
17833	50k
17834	50k

Scale bar: 2μm

TEM photo set I | Penguin D | Clay fraction: 0.1<μm<0.5

Sample ID: P11 (D) | 211/14-3 | Age: 34 Ma

Separation ID: AJC-XRD24 | 3454 m | dD: no data

TEM rank: 1 | Etive, oil wet | dO: 13.6

Set I	Mag'n
17826	6k
17827	15k
17828	15k
17829	15k
17830	15k
17832	**15k**
17833	50k
17834	50k

Scale bar: 2μm

Set I	Mag'n
17826	6k
17827	15k
17828	15k
17829	15k
17830	15k
17832	50k
17833	**50k**
17834	50k

Scale bar: 2μm

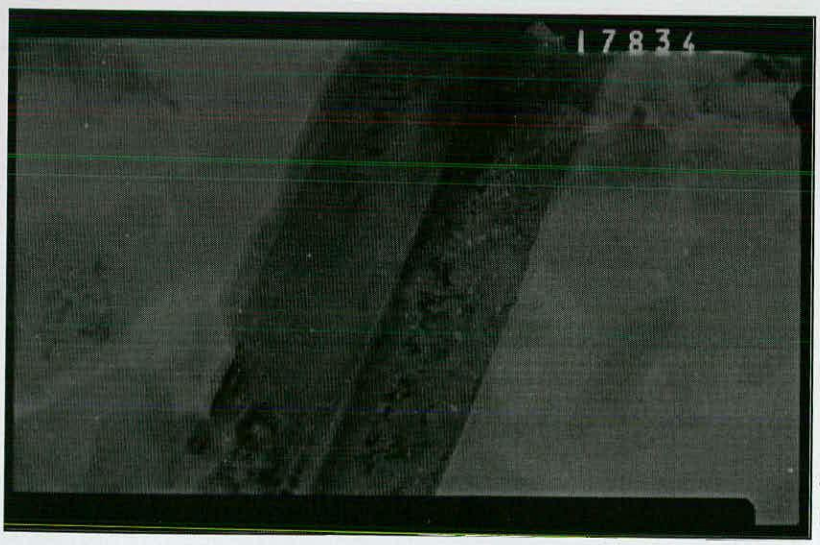

Set I	Mag'n
17826	6k
17827	15k
17828	15k
17829	15k
17830	15k
17832	50k
17833	50k
17834	**50k**

Scale bar: 2μm

TEM photo set J | Penguin D | Clay fraction: 0.5<μm<1.0

Sample ID: P11 (D) | 211/14-3 | Age: 47 Ma

Separation ID: AJC-XRD23 | 3454 m | dD: -55

TEM rank: 5 | Etive, oil wet | dO: 12.9

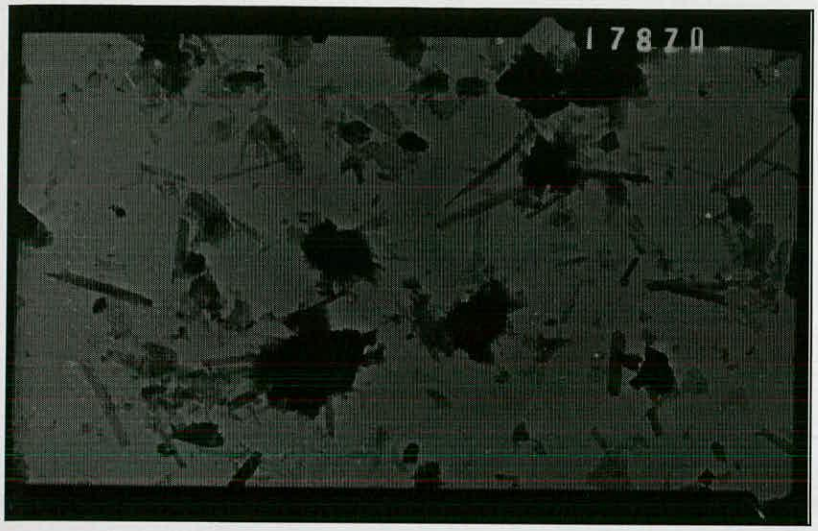

Set J	Mag'n
17870	**6k**
17871	15k
17872	15k
17873	15k
17874	25k
17875	15k
17878	15k

Scale bar: 4μm

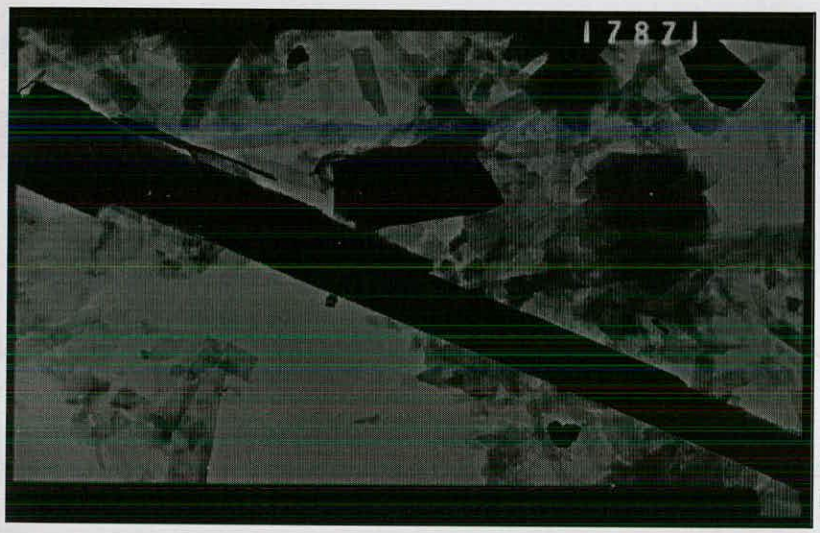

Set J	Mag'n
17870	6k
17871	**15k**
17872	15k
17873	15k
17874	25k
17875	15k
17878	15k

Scale bar: 2μm

Set J	Mag'n
17870	6k
17871	15k
17872	**15k**
17873	15k
17874	25k
17875	15k
17878	15k

Scale bar: 2μm

TEM photo set J
Sample ID: P11 (D)
Separation ID: AJC-XRD23
TEM rank: 5

Penguin D
211/14-3
3454 m
Etive, oil wet

Clay fraction: 0.5<µm<1.0
Age: 47 Ma
dD: -55
dO: 12.9

Set J	Mag'n
17870	6k
17871	15k
17872	15k
17873	**15k**
17874	25k
17875	15k
17878	15k

Scale bar: 2µm

Set J	Mag'n
17870	6k
17871	15k
17872	15k
17873	15k
17874	**25k**
17875	15k
17878	15k

Scale bar: 1µm

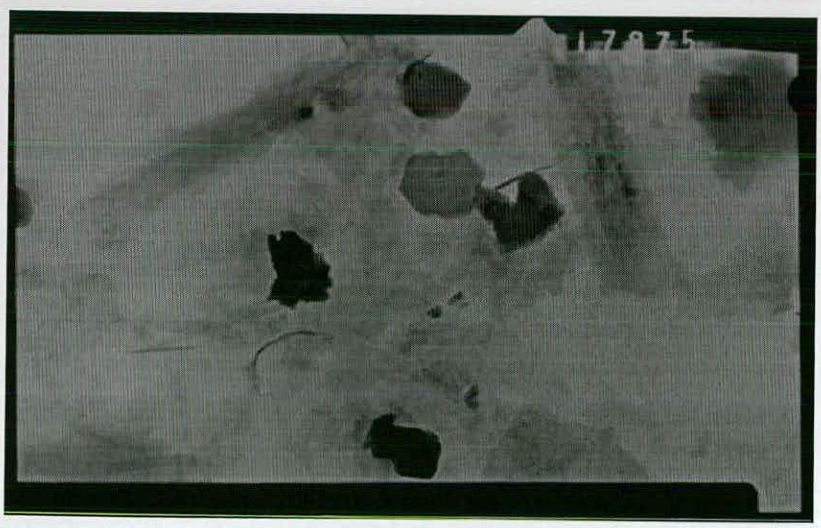

Set J	Mag'n
17870	6k
17871	15k
17872	15k
17873	15k
17874	25k
17875	**15k**
17878	15k

Scale bar: 2µm

TEM photo set J
Sample ID: P11 (D)
Separation ID: AJC-XRD23
TEM rank: 5

Penguin D
211/14-3
3454 m
Etive, oil wet

Clay fraction: 0.5<µm<1.0
Age: 47 Ma
dD: -55
dO: 12.9

Set J	Mag'n
17870	6k
17871	15k
17872	15k
17873	15k
17874	25k
17875	15k
17878	**15k**

Scale bar: 2µm

TEM photo set K
Sample ID: P11 (D)
Separation ID: AJC-XRD22
TEM rank: 6

Penguin D
211/14-3
3454 m
Etive, oil wet

Clay fraction: 1.0<µm<2.0
Age: 76 Ma
dD: -66
dO: 12.3

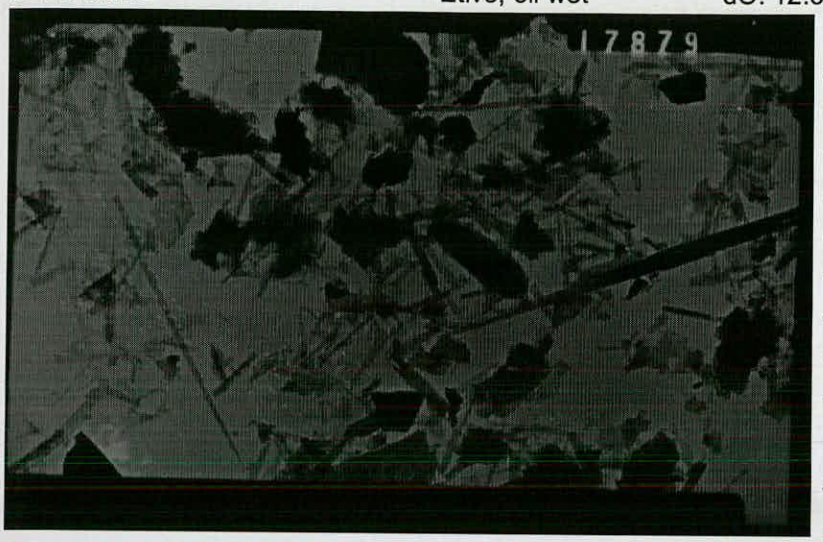

Set K	Mag'n
17879	**6k**
17880	15k
17881	15k
17883	15k
17884	15k
17885	15k
17886	15k
178...	

Scale bar: 4µm

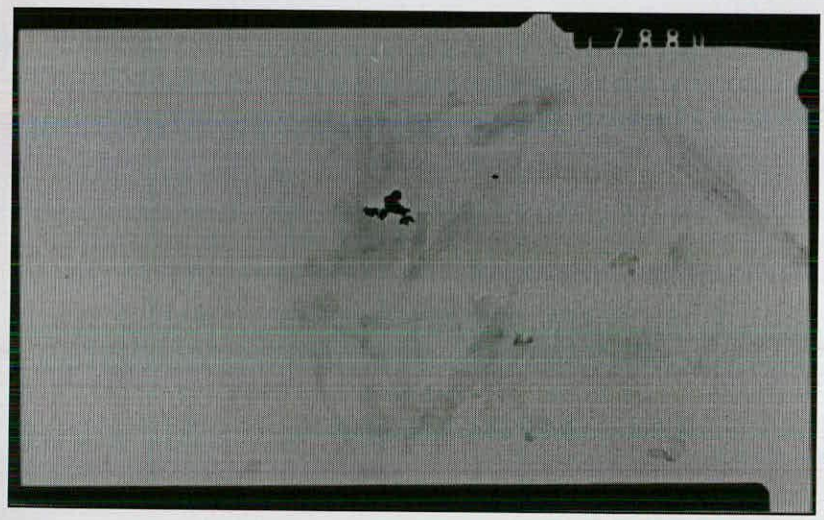

Set K	Mag'n
17879	6k
17880	**15k**
17881	15k
17883	15k
17884	15k
17885	15k
17886	15k
178...	

Scale bar: 2µm

Set K	Mag'n
17879	6k
17880	15k
17881	**15k**
17883	15k
17884	15k
17885	15k
17886	15k
178...	

Scale bar: 2µm

TEM photo set K
Sample ID: P11 (D)
Separation ID: AJC-XRD22
TEM rank: 6

Penguin D
211/14-3
3454 m
Etive, oil wet

Clay fraction: 1.0<µm<2.0
Age: 76 Ma
dD: -66
dO: 12.3

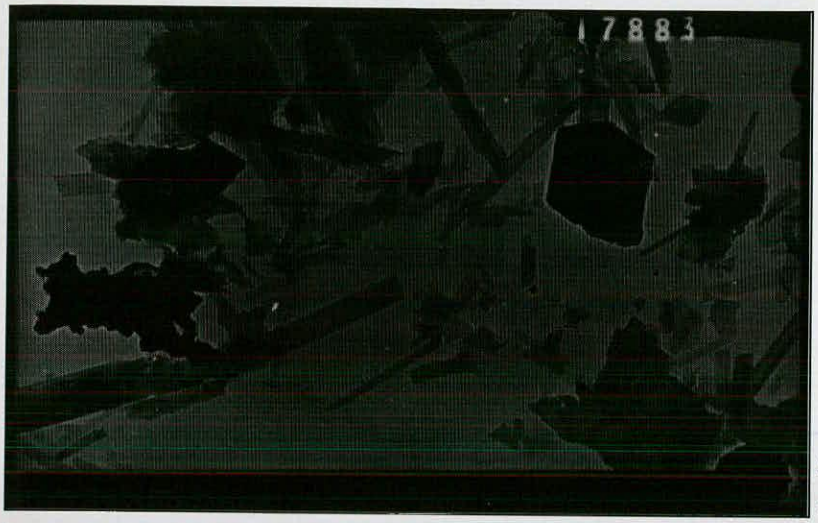

Set K	Mag'n
17879	6k
17880	15k
17881	15k
17883	**15k**
17884	15k
17885	15k
17886	15k
178...	

Scale bar: 2µm

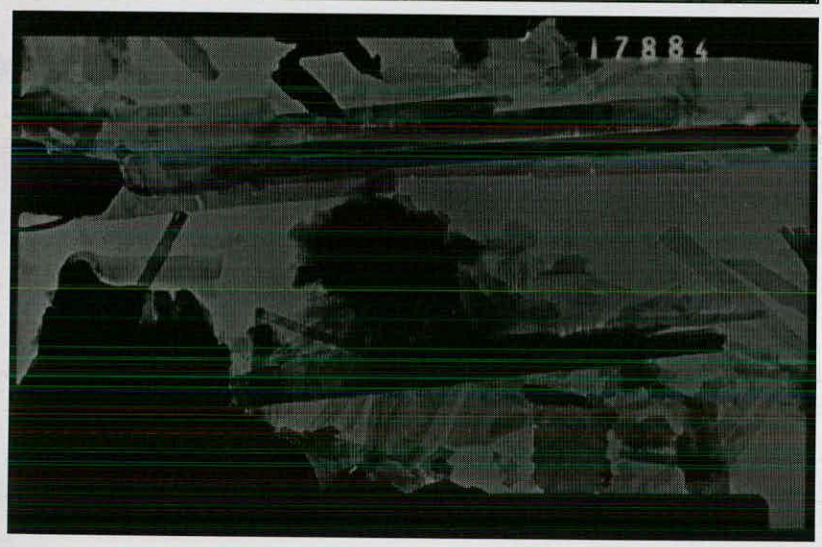

Set K	Mag'n
17879	6k
17880	15k
17881	15k
17883	15k
17884	**15k**
17885	15k
17886	15k
178...	

Scale bar: 2µm

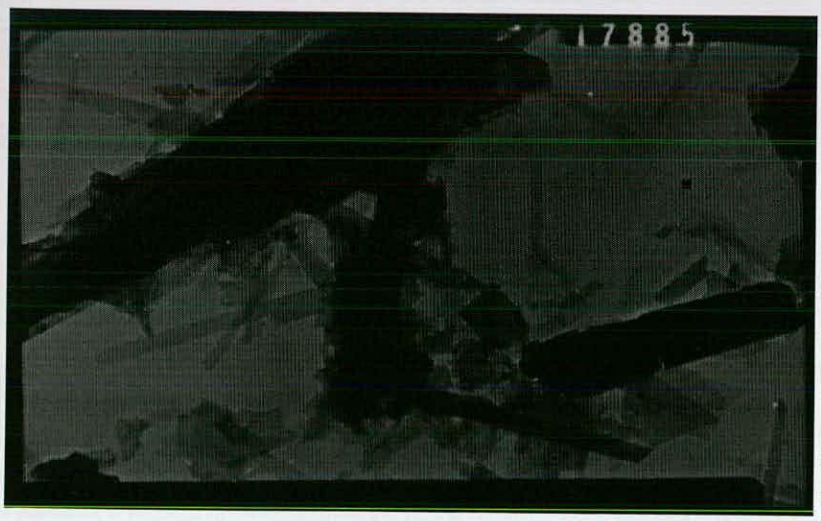

Set K	Mag'n
17879	6k
17880	15k
17881	15k
17883	15k
17884	15k
17885	**15k**
17886	15k
178...	

Scale bar: 2µm

TEM photo set K
Sample ID: P11 (D)
Separation ID: AJC-XRD22
TEM rank: 6

Penguin D
211/14-3
3454 m
Etive, oil wet

Clay fraction: 1.0<µm<2.0
Age: 76 Ma
dD: -66
dO: 12.3

Set K	Mag'n
17880	15k
17881	15k
17883	15k
17884	15k
17885	15k
17886	**15k**
17887	40k
17947	15k

Scale bar: 2µm

Set K	Mag'n
17880	15k
17881	15k
17883	15k
17884	15k
17885	15k
17886	15k
17887	**40k**
17947	15k

Scale bar: 0.5µm

Set K	Mag'n
17880	15k
17881	15k
17883	15k
17884	15k
17885	15k
17886	15k
17887	40k
17947	**15k**

Scale bar: 2µm

TEM photo set L | Penguin D | Clay fraction: 0.1<μm<0.5

Sample ID: P6 (D) | 211/14-1 | Age: 145 Ma

Separation ID: AJC-XRD12 | 3406 m | dD: no data

TEM rank: 2 | Etive, condensate | dO: 13.4

Set L	Mag'n
17856	**6k**
17835	30k
17836	15k
17837	15k
17838	15k
17839	15k
17840	15k
178...	

Scale bar: 4μm

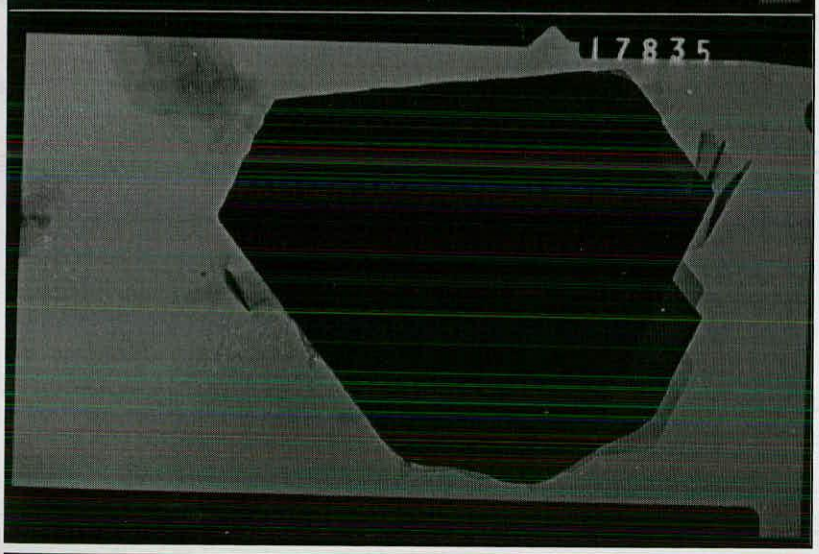

Set L	Mag'n
17856	6k
17835	**30k**
17836	15k
17837	15k
17838	15k
17839	15k
17840	15k
178...	

Scale bar: 1μm

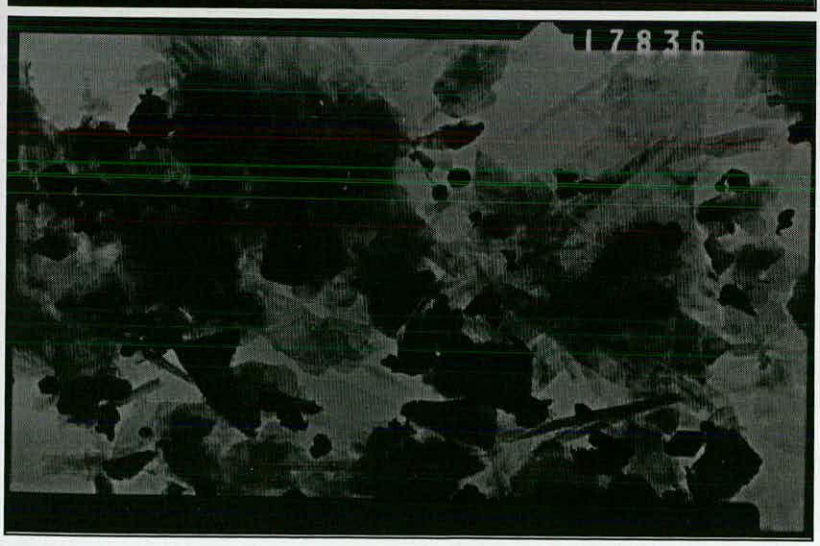

Set L	Mag'n
17856	6k
17835	30k
17836	**15k**
17837	15k
17838	15k
17839	15k
17840	15k
178...	

Scale bar: 2μm

TEM photo set L | Penguin D | Clay fraction: 0.1<μm<0.5

Sample ID: P6 (D) | 211/14-1 | Age: 145 Ma

Separation ID: AJC-XRD12 | 3406 m | dD: no data

TEM rank: 2 | Etive, condensate | dO: 13.4

Set L	Mag'n
17856	6k
17835	30k
17836	15k
17837	**15k**
17838	15k
17839	15k
17840	15k
178...	

Scale bar: 2μm

Set L	Mag'n
17856	6k
17835	30k
17836	15k
17837	15k
17838	**15k**
17839	15k
17840	15k
178...	

Scale bar: 2μm

Set L	Mag'n
17856	6k
17835	30k
17836	15k
17837	15k
17838	15k
17839	**15k**
17840	15k
178...	

Scale bar: 2μm

TEM photo set L
Sample ID: P6 (D)
Separation ID: AJC-XRD12
TEM rank: 2

Penguin D
211/14-1
3406 m
Etive, condensate

Clay fraction: 0.1<µm<0.5
Age: 145 Ma
dD: no data
dO: 13.4

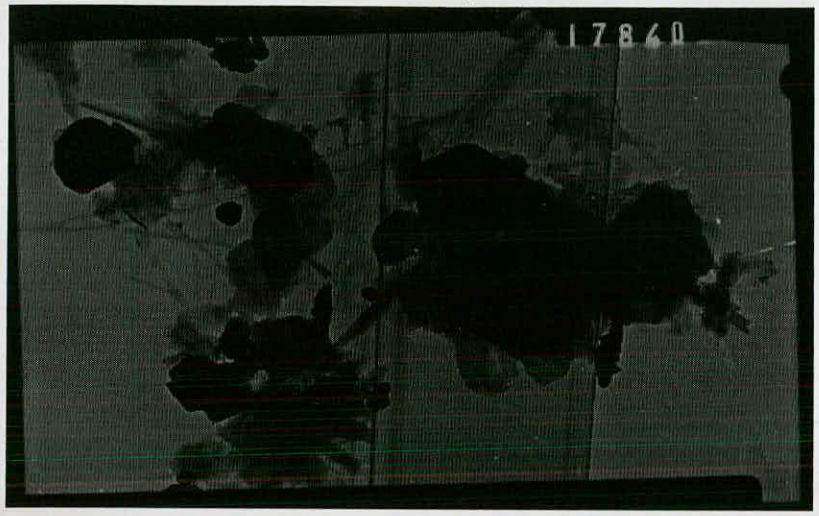

Set L	Mag'n
17835	30k
17836	15k
17837	15k
17838	15k
17839	15k
17840	**15k**
17842	200k
17844	50k

Scale bar: 2µm

Set L	Mag'n
17835	30k
17836	15k
17837	15k
17838	15k
17839	15k
17840	15k
17842	**200k**
17844	50k

Scale bar: 0.1µm

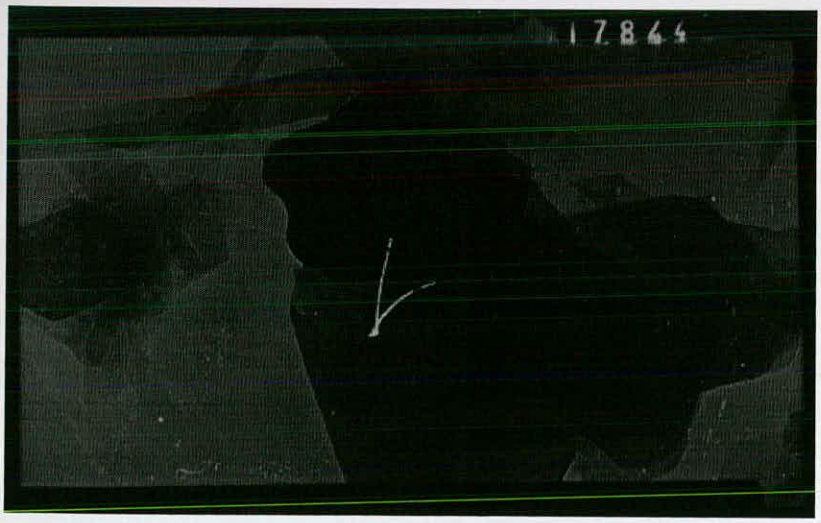

Set L	Mag'n
17835	30k
17836	15k
17837	15k
17838	15k
17839	15k
17840	15k
17842	200k
17844	**50k**

Scale bar: 0.5µm

Appendix 5.1 Deep well - North Shetland Trough

Event	*Type*	*Age (Ma)*	*Well top (m)*
Quaternary	F	1.6207	
Pliocene	F	5.2	629
Miocene	F	23	934
Oligocene	F	35	1298
Eocene	F	57	1358
Palaeocene 1	F	58	1371
Tuff	F	59	1559
Palaeocene 2	F	61	1605
Palaeocene 3	F	66.4	1788
Maastrichtian	F	76	1833
Campanian	F	84	2178
Santonian	F	88	2592
Coniacian	F	90	2915
Turonian	F	93	3632
Cenomanian	F	100	3941
Albian 1	F	104	3982
Albian 2	F	108	4546
Aptian	F	115	4650
Barremian	F	122	4656
Hauterivian	F	126	4924
Valanginian	F	131	5003
Berriasian	F	132	5198
KCF 1	F	138	5323
KCF2-H	H	142	
KCF2	F	149	5499
Dogger	F	178	5662
Lias	F	208	6077
Triassic	F	240	6389

Magnus well (211/12-1)

Event	*Type*	*Age(Ma)*	*Well top (m)*
Quaternary	F	1.6	190
Pliocene	F	5.2	629
Miocene	F	23	1026
Oligocene	F	35	1255
Eocene	F	57	1358
Palaeocene 1	F	58	1371
Tuff	F	59	1394
Palaeocene 2	F	61	1446
Palaeocene 3	F	66.4	1546
Maastrichtian	F	76	1596
Campanian	F	84	1831
Santonian	F	88	2349
Coniacian	F	90	2718
Barremian-H	H	115	
Barremian	F	131	2880
KCF1-E	E	132	
AAA	D	138	
KCF1	F	142	2895
KCF 2	F	149	2957
Dogger	F	178	3101
Lias	F	208	3401
Triassic	F	240	3656

Flank well (211/12-2)

Event	*Type*	*Age(Ma)*	*Well top (m)*
Quaternary	F	1.6	181
Pliocene	F	5.2	635
Miocene	F	23	1040
Oligocene	F	35	1267
Eocene	F	57	1367
Palaeocene 1	F	58	1384
Tuff	F	59	1399
Palaeocene 2	F	61	1436
Palaeocene 3	F	66.4	1536
Maastrichtian	F	76	1585
Campanian	F	84	1913
Santonian	F	88	2386
Coniacian	F	90	2856
Barremian-H	H	115	
Barremian	F	131	3176
KCF1-E	E	132	
AAA	D	135	
KCF1	F	138	3192
MSM	F	142	3200
KCF 2	F	149	3361
Dogger	F	178	3505
Lias	F	208	3855
Triassic	F	240	4121

Appendix 5.1 Penguin A well (211/13-3)

Event	*Type*	*Age (Ma)*	*Well top (m)*
Quaternary	F	1.6	171
Pliocene	F	5.2	410
Miocene	F	23	785
Oligocene	F	35	1001
Eocene	F	57	1388
Palaeocene 1	F	58	1418
Tuff	F	59	1448
Palaeocene 2	F	61	1488
Palaeocene 3	F	66.4	1556
Maastrichtian	F	76	1624
Campanian	F	84	1922
Santonian	F	88	2412
Coniacian	F	90	2952
Barremian-H	H	115	
Barremian	F	131	3306
KCF1-H	H	135	
KCF1	F	138	3330
MSM	F	142	3368
KCF 2	F	149	3520
Dogger	F	178	3687
Lias	F	208	4037
Triassic	F	240	4323

Penguin B well (211/13-1)

Event	*Type*	*Age(Ma)*	*Well top (m)*
Quaternary	F	1.6	189
Pliocene	F	5.2	300
Miocene	F	23	550
Oligocene	F	35	776
Eocene	F	57	1306
Palaeocene 1	F	58	1400
Tuff	F	59	1440
Palaeocene 2	F	61	1479
Palaeocene 3	F	66.4	1525
Maastrichtian	F	76	1596
Campanian	F	84	1781
Santonian	F	88	2415
Triassic-E	E	88.5	
H	D	115	
G	D	138	
F	D	142	
E	D	149	
D	D	155	
C	D	157	
B	D	178	
A	D	208	
Triassic	F	240	2633

Penguin C well (211/13-6)

Event	*Type*	*Age(Ma)*	*Well top (m)*
Quaternary	F	1.6	231
Pliocene	F	5.2	300
Miocene	F	23	559
Oligocene	F	35	776
Eocene	F	57	1306
Palaeocene 1	F	58	1400
Tuff	F	59	1488
Palaeocene 2	F	61	1536
Palaeocene 3	F	66.4	1645
Maastrichtian	F	76	1706
Campanian	F	84	1970
Santonian	F	88	2665
Coniacian	F	90	3042
Barremian-H	H	115	
Barremian	F	131	3276
KCF1-H	H	135	
KCF1	F	138	3338
KCF2-H	H	142	
KCF2	F	149	3349
Dogger	F	178	3356
Lias	F	208	3470
Triassic	F	240	3602

Appendix 5.2 *BasinMod® 2-D table for itemised events in the Magnus model*

Event	*Lithology*	*Kerogen*	*%TOC*	*Colour*
Quaternary	Shale			White
Pliocene	Shale			White
Miocene	Shale			White
Oligocene	Shale			White
Eocene	Shale			White
Paleocene 1	Shale			White
Tuff	Igneous			Red
Palaeocene 2	Shale			White
Palaeocene 3	Sandstone			Yellow
Maastrichtian	Shale			White
Campanian	Shale			White
Santonian	Shale			White
Coniacian	Shale			White
Triassic-E	Siltstone			White
Coniacian	Shale			White
Coniacian	Shale			White
Triassic-E	Siltstone			White
Coniacian	Shale			White
Coniacian	Shale			White
EOTWF	Sandstone			Grey
PBW	Sandstone			Grey
PBE	Sandstone			Grey
H	Siltstone			White
Barremian-H	Shale			White
Barremian-H	Shale			White
Barremian-H	Shale			White

Appendix 5.2 BasinMod® 2-D table for itemised events in the Magnus model

Event	*Lithology*	*Kerogen*	*%TOC*	*Colour*
Turonian	Shale			White
PHG	Sandstone			Grey
Cenomanian	Shale			White
Albian 1	Shale			White
Albian 2	Shale			White
Aptian	Shale			White
Barremian	Shale			White
Barremian	Shale			White
G	Siltstone			White
Barremian	Shale			White
Barremian	Shale			White
Hauterivian	Shale			White
Valanginian	Shale			White
KCF1-E	Shale	Type II (Espitalie '88 Viking Graben)		Dark grey
KCF1-H	Shale	Type II (Espitalie '88 Viking Graben)	9	Magenta
KCF1-H	Shale	Type II (Espitalie '88 Viking Graben)	9	Magenta
Berriasian	Shale			White
AAA	Shale	Type II (Espitalie '88 Viking Graben)	9	Magenta
KCF 1	Shale	Type II (Espitalie '88 Viking Graben)	9	Green
KCF1	Shale	Type II (Espitalie '88 Viking Graben)	9	Green
KCF1	Shale	Type II (Espitalie '88 Viking Graben)	9	Green
KCF1	Shale	Type II (Espitalie '88 Viking Graben)	9	Green
F	Siltstone			White
MSM	Sandstone			Yellow
KCF2-H	Shale	Type II (Espitalie '88 Viking Graben)	9	Magenta
KCF2-H	Shale	Type II (Espitalie '88 Viking Graben)	9	Magenta
MSM	Sandstone			Yellow
E	*Siltstone*			*White*

Appendix 5.2 BasinMod® 2-D table for itemised events in the Magnus model

Event	Lithology	Kerogen	%TOC	Colour
KCF2	Shale	Type II (Espitalie '88 Viking Graben)	9	Green
KCF2	Shale	Type II (Espitalie '88 Viking Graben)	9	Green
Event	*Lithology*	*Kerogen*	*%TOC*	*Colour*
KCF 2	Shale	Type II (Espitalie '88 Viking Graben)	9	Green
KCF 2	Shale	Type II (Espitalie '88 Viking Graben)	9	Green
D	Siltstone			White
Dogger	Siltstone			White
Dogger	Siltstone			White
Dogger	Siltstone			White
Dogger	Siltstone			White
C	Siltstone			White
B	Siltstone			White
A	Siltstone			White
Lias	Siltstone			White
Lias	Siltstone			White
Lias	Siltstone			White
Lias	Siltstone			White
Triassic	Siltstone			White
Triassic	Siltstone			White
Triassic	Siltstone			White
Triassic	Siltstone			White
Triassic	Siltstone			White

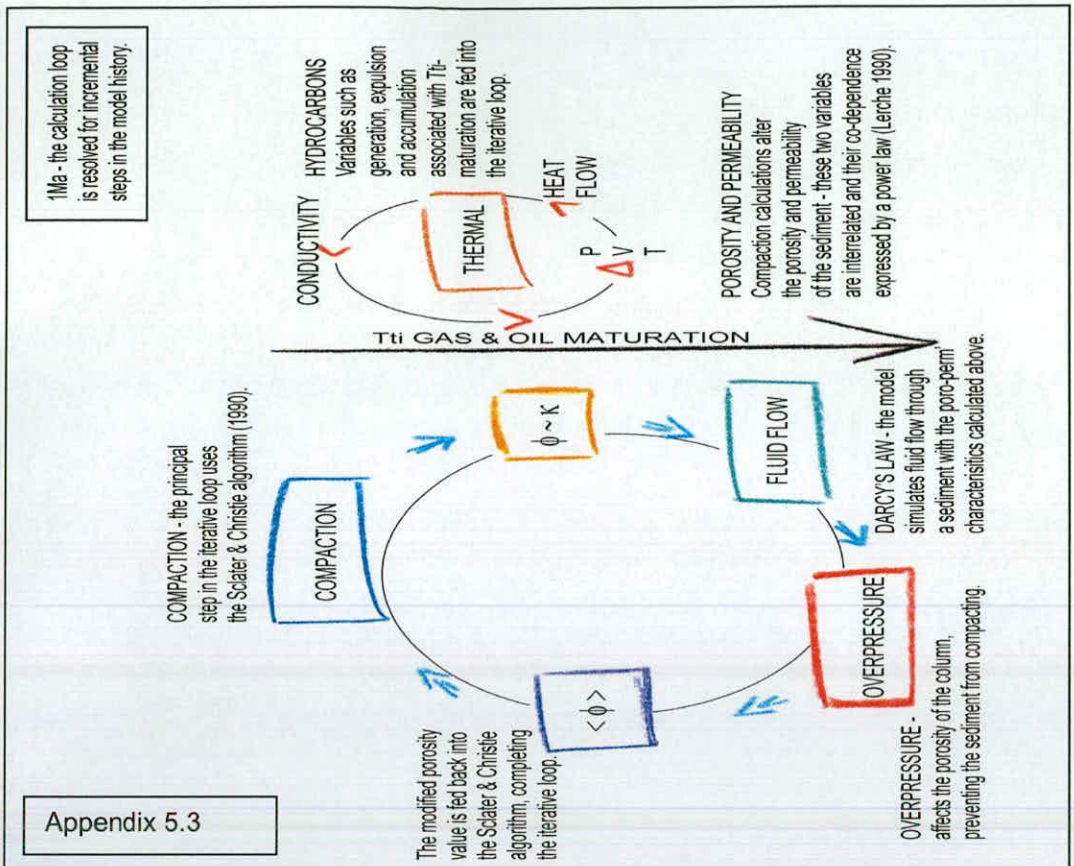

OVERPRESSURE (Lerche 1990)

$$\delta H/\delta t = \delta H/\delta t|_c + \delta H/\delta t|_a + \delta H/\delta t|_f + Q_H$$

H = enthalpy
t = time
Q_H = internal heat source
c = conduction
a = advection
f = convection

COMPACTION (Sclater & Christie 1990)

$$\rho = \rho_{sc} \cdot \exp[\beta(P - 0.1) - \alpha(T - 25)] \text{ kgm}^{-3}$$

ρ = density
ρ_{sc} = 0.001 kgm^{-3} (standard P & T)
P = pressure (Mpa)
T = temperature
α = 5×10^{-4} C^{-1} (constant)
β = 4.3×10^{-4} Mpa (constant)

FLUID FLOW (DARCY'S LAW)

$$v = -\frac{K}{\mu}\frac{\delta P}{\delta l}$$

v = rate of fluid movement
K = permeability
μ = fluid viscosity
P = excess hydrostatic pressure
L = distance

POROPERM POWER LAW (Lerche 1990)

$$K = K_* \left(\frac{\phi}{\phi_*}\right)^B$$

K = average surface permeability
K_* = initial surface permeability
ϕ = porosity
B = permeability reduction factor